Biotransformation of Santalene Derivatives from Indian Sandalwood: *Santalum album*

THESIS SUBMITTED

TO

UNIVERSITY OF PUNE

FOR THE DEGREE

OF

DOCTOR OF PHILOSOPHY

IN

BIOTECHNOLOGY

BY

Mr. PANKAJ PANDHARINATH DARAMWAR

UNDER THE GUIDANCE OF

Dr. H. V. THULASIRAM

DIVISION OF ORGANIC CHEMISTRY

CSIR-NATIONAL CHEMICAL LABORATORY

PUNE - 411 008, INDIA.

MAY 2014

Dr. H. V. Thulasiram
Principal Scientist,
Chemical-Biology Unit,
Division of Organic Chemistry,
CSIR-National Chemical Laboratory,
Pune 411 008.

+91 20 2590 2478
hv.thulasiram@ncl.res.in

CERTIFICATE

This is to certify that the work presented in the thesis entitled **"Biotransformation of Santalene Derivatives from Indian Sandalwood: *Santalum album*"** submitted by **Mr. Pankaj P. Daramwar**, was carried out by the candidate at CSIR-National Chemical Laboratory, Pune, under my supervision. Such materials as obtained from other sources have been duly acknowledged in the thesis.

May 2014

Dr. H. V. Thulasiram
(Research Supervisor)

CANDIDATE'S DECLARATION

I hereby declare that the thesis entitled **"Biotransformation of Santalene Derivatives from Indian Sandalwood: *Santalum album*"** submitted for the award of degree of ***Doctor of Philosophy*** in Biotechnology to the 'University of Pune' has not been submitted by me to any other university or institution. This work was carried out by me at CSIR-National Chemical Laboratory, Pune, India. Such materials as obtained from other sources have been duly acknowledged in the thesis.

Mr. Pankaj P. Daramwar
(Research student)
Division of Organic Chemistry,
CSIR-National Chemical Laboratory,
Pune- 411 008.

May 2014
Pune.

Dedicated to My Beloved
Aai, Papa and Sisters

Acknowledgements

This thesis has been built up from the inspiration, advices, support, love, strength and encouragement provided by all my well wishers. First and foremost, I express my deep sense of gratitude to my research guide Dr. Thulasiram H. V. for his able guidance, constant support, valuable suggestions, encouragement and inspiration rendered to me during my research career. I thank him for introducing me to this exciting field of 'biotransformation and biosynthesis' that helped me develop skills and knowledge in this multidisciplinary scientific domain. I am grateful for his immense support throughout the past years.

I am also grateful to Director, NCL, Pune, and Head, Organic Chemistry Division for giving me an opportunity to work in this institute and making all the facilities available for my research work. I owe my earnest regards to Dr. Jomon Joseph, Prof. Pal J. K and Dr. Gopi H. N. for evaluating my progress reports and presentations. I extend my sincere thanks to Dr. Srinivas Hotha, Dr. D. S. Reddy, Dr. S. Dhanasekaran, Dr. M. J. Kulkarni, Dr. A. P. Giri, Dr. Moneesha Fernandes, Dr. M. Muthukrishnan, Dr. C. V. Ramana, Dr. N. P. Aragade, Dr. U. R. Kalkote, Dr. P. K. Tripathi, Dr. N. N. Joshi, Dr. R. A. Joshi and Dr. S. P. Chavan for their help and suggestions during this research work. Help rendered by the members of IR and microanalysis (Dr. P. L. Joshi and group), mass spectroscopy (Dr. Shanthakumari and group), NMR (Dr. Rajmohanan and group) and X-ray analysis (Mr. Rajesh Gonade) for characterization of compounds is also acknowledged. I wish to thank all the divisional members and staff of SAO for the timely help I received from them.

I duly acknowledge Council of Scientific and Industrial Research, New Delhi for financial support in terms of CSIR-Junior Research Fellowship and Senior Research Fellowship.

My labmates have been a continuous source of support and scientific suggestions during my stay in this lab. A wonderful company of Mrs. Swati with her sisterly support and scientific suggestions during hard times is a must mention. A special thanks to Prabhakar, Priyadarshini, Dr. Sharanbasappa and Vaibhav for their significant scientific contributions, advice and moral support

during my research project. I am thankful to all my present and past labmates including Saikat, Nilofer, Dipesh, Harshal, Krithika, Atul, Devdutt, Avinash, Aarthy, Ajay, Balaji, Fayaj, Pruthaviraj, Uttara, Rani, Anurag, Ramesha, Rahul, Rincy, Sonia, Dr. Prasad, Dr. Anirban, Dr. Manoj, Dr. Mohan, Debu, Ashwini, Trushna, Radha, Vijayshree, Rajashree, Aradhana, Rohil, Ashish, Krunal, Bhagyashree, Sneha, Arundhati, Hemant and Sarika.

I am indebted to a great backing from my senior colleagues, Dr. Bapu, Dr. Namdev, Dr. Deepak S., Dr. Sudhir, Dr. Nilkanth, Dr. Abasaheb, Deepak J., Ankush, Dr. Sane, Dr. Kedar, Dr. Prasad, Dr. Manmath, Dr. Suleman, Pankaj Bhole, Dr. Vishwas, Dr. Bande, Dr. Shankar, Dr. Narayan, Dr. Vrushali, Dr. Manoj, Dr. Nagendra, Dr. Pandurang, Dr. Ganesh, Dr. Sachin, Dr. Khirud, Dr. Madhuri, Dr. Rajesh, Dr. Prasanna, Dr. Swaroop, Dr. Nishant, Dr. Rahul, Dr. Bharat, Dr. Pitambar, Dr. Avadhoot, Dr. Sachin, Dr. Kishor, Dr, Lalit, Dr. Puspesh, Dr. Sujit, Dr. Debashish and Dr. Abhishek. Great friends at NCL will be an asset throughout life and their company was most cherishable. Though, it is difficult to make a mention of each and every one, I can't forget the suppot from Sandeep, Mangesh, Dr. Nilesh, Dr. Kiran, Dr. Dhanaraj, Chinmay, Majid, Bhausaheb, Atul, Pradeep, Shekhar, Dr. Digambar, Milind, Dnyaneshwar, Govinda, Dr. Venu, Dr. Anand, Pradeep, Prakash, Abhijeet, Dr. Bharmana, Suresh, Dr. Seema, Dr. Namrata, Dr. Partha, Krishanu, Rahul, Mangesh, Manoj, Anjan, Tanaya, Richa, Gauri, Prashant, Dr. Mandeep, Brijesh, Shweta, Arati, Rubina and Jagadeesh. Their cheerful company added a lighter mode to life.

My college friends who motivated me to pursue a career in research, Sanket, Advait, Avadhoot, Dipayan, Shefali, Shweta, Dr. Prajakta, Dr. Aditi, Daryl, Dr. Arvind, Valmik, Dr. Brinda, Deepali, Yogesh, Mahesh, Sampat, Barku, Prashant, Dev, Chandu, and Mahadev and many of my school friends who possibly can't be mentioned individually.

I am highly obliged to my teachers and mentors, who have been a tremendous source of inspiration. The people who helped me achieve my goals and shape my career: Dr. Chitale, Dr. Kaulgud, Dr. Kondedeshmukh, Dr. Pardeshi, Dr. Tadake, Dr. Nandedkar, Dr. Mahamulkar, Dr. Deogadkar, Dr. Pol, Dr. Wadia, Dr. Dhavale, Dr. Kusurkar, Dr. Kulkarni, Dr. Lokhande, Dr.

Waghmode and Dr. (Mrs.) Shinde. I thank them for their magnificent teaching and sharing of knowledge.

I pay high regards and respect to my parents Shri Pandharinath and Smt. Shobha for their blessings, unconditional love, care, sacrifice and encouragement, without which this work would not have been possible. I extend heartiest thanks to my dear sisters, Dr. Preeti and Dr. Pooja, brothers-in-law, Dr. Preshit and Dr. Suyog and all the family members for their love, and of course an ever-lasting support. Their encouragement and adjustment on several fronts has made it possible for me to complete this work. Finally, I am grateful to the eternal, almighty Lord Ganesha, for giving me patience, strength, energy and determination to complete my Ph. D. research in the best possible manner and for guiding my path of life.

with many thanks,

Pankaj P. Daramwar.

Contents

List of Research Publications

- Transformation of (±)-lavandulol and (±)-tetrahydrolavandulol by a fungal strain *Rhizopus oryzae*.
  Pankaj P. Daramwar, Raju Rincy, Siddiqui Niloferjahan, Ramakrishnan Krithika, Arvind Gulati, Amit Yadav, Rakesh Sharma, Hirekodathakallu V. Thulasiram *Bioresour. Technol.*, **2011**, *115*, 70.

- Preparative separation of α- and β-santalenes and (*Z*)-α- and (*Z*)-β-santalols using silver nitrate-impregnated silica gel medium pressure liquidchromatography and analysis of sandalwood oil.
  Pankaj P. Daramwar, Prabhakar Lal Srivastava, Balaraman Priyadarshini and Hirekodathakallu V. Thulasiram *Analyst*, **2012**, *137*, 4564.

- Biocatalyst mediated regio- and stereo-selective hydroxylation and epoxidation of (*Z*)-α-Santalol.
  Pankaj P. Daramwar, Prabhakar Lal Srivastava, Swati P. Kolet, Hirekodathakallu V. Thulasiram *Org. Biomol. Chem.*, **2014**, *12*, 1048.

- Mechanistic Insights in Biosynthesis of Santalane, Bergamotane and Curcumene type sesquiterpenes.
  Pankaj P. Daramwar, Prabhakar Lal Srivastava, Hirekodathakallu V. Thulasiram.
  (Manuscript under preparation).

- Fungi mediated regio- and stereo-selective hydroxylation of 1,8-Cineole.
  Pankaj P. Daramwar, Hirekodathakallu V. Thulasiram.
  (Manuscript under preparation).

Symposia Attended/Poster/Oral Presentations:

- Attended and presented poster in the international conference Biotrans 2011, held at Sicily, Italy.
- Attended and presented poster in the National level Symposium: 'CRSI' 2009, held at National Chemical Laboratory, Pune.
- Attended and presented poster in the International level Symposium: "INSA" 2009 held at National Chemical Laboratory, Pune.
- Posters presented on Science Day at NCL from 2009 to 2012.

Abbreviations

Å	Angstrom
ACN	Acetonitrile
AcOH	Acetic acid
aq.	Aqueous
b.p.	Boiling point
Calc.	calulated
Cat.	Catalytic/catalyst
CH_2Cl_2	Dichloromethane
Conc.	Concentrated
COSY	Correlation Spectroscopy
DEPT	Distortionless Enhancement by Polarization Transfer
DIBAH	Di-isobutyl aluminium hydride
DI	De-ionized
1D	One Dimensional
2D	Two Dimensional
DMAP	N,N-Dimethyl amino pyridine
EDTA	Ethylenediaminetetraacetic acid
EtOH	Ethanol
EtOAc	Ethyl acetate
g	Gram
h	Hour/s
HIV	Human Immuno Difficiency Virus
HPLC	High Performance Liquid Chromatography
HMBC	Heteronuclear Multiple Bond Correlation Spectroscopy
HSQC	Heteronuclear Single Quantum Coherence Spectroscopy
Hz	Hertz
IBX	2-Iodoxy benzoic acid
IR	Infra red
L	Liter
LC-MS	Liquid Chromatography-Mass Spectrometry
MeOH	Methanol
MF	Molecular formula

mg	Milligram
MHz	Megahertz
min	Minute/s
M	Molar
µL	Microliter
µM	Micromolar
mL	Milliliter
mM	Millimolar
mm Hg	millimeters of Mercury
mmol	Millimoles
m.p.	Melting point
MS	Mass spectrometry
MW	Molecular weight
NCIM	National collection of industrial microorganisms
n-BuLi	*n*-Butyl lithium
NCS	N-Chloro succinimide
NMR	Nuclear Magnetic Resonance
NOESY	Nuclear Overhauser Effect Spectroscopy
Obs.	Observed
ppm	Parts per million
Pet-ether	Petroleum ether
R_f	Retention factor
RP	Reversed Phase
rt	Room temperature
s	Second
TBDMS	Tertiary butyl dimethyl silyl
TBAF	Tetra n-butyl ammonium fluoride
THF	Tetrahydrofuran
$Ti(O\text{-}^{i}Pr)_4$	Titanium tetra isopropoxide
TLC	Thin layer chromatography
Ts	*p*-Toluene sulphonyl
UV-Vis	Ultraviolet-Visible

Abstract

Biotransformation of Santalene Derivatives from Indian Sandalwood, *Santalum album*.

Thesis has been divided into three chapters:

Chapter 1: Isolation, Purification and Quantification of Santalenes from Indian Sandalwood, *Santalum album*.

Section 1.1: Introduction: Indian Sandalwood, *Santalum album*.

This section briefly describes classification of sandalwood, in general, with emphasis on Indian sandalwood, *Santalum album*.[1] The extraction methods of sandalwood oil and its commercial and biological importance are also discussed. The phytochemical constitution of the oil[2-5] and the biosynthesis of major components of oil, α- and β-santalols,[6,7] and their pharmaceutical applications[8-12] are described. A short discussion on argentation chromatography explains its application in separation science.[13-15]

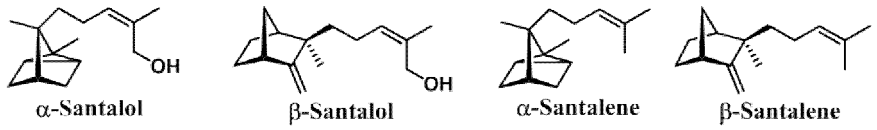

α-Santalol β-Santalol α-Santalene β-Santalene

Scheme 1: Components of Sandalwood oil.

Section 1.2: Preparative separation of α- and β-santalenes and (*Z*)-α- and (*Z*)-β-santalols using silver nitrate-impregnated silica gel medium pressure liquid chromatography.

Analysis of the GC chromatogram of sandalwood oil, both commercial and extracted from sandalwood of Pune region, indicated that the santalol content [(*Z*)-α-santalol (**1**), (*Z*)-β-santalol (**2**) and (*Z*)-*epi*-β-santalol (**3**), and (*Z*)-α-*exo*-bergamotol (**4**)] was >80% and rest of the minor components constituted α-santalene (**5**), β-santalene (**6**), *epi*-β-santalene (**7**), (*Z*)-α-bisabolol (**8**), (*E*,*E*)-farnesol (**9**), (*E*)-nuciferol (**10**), (*Z*)-lanceol (**11**), *exo*-α-bergamotene (**12**), and α-curcumene (**13**). The terpene fraction of sandalwood oil (KSDL) contained the sesquiterpene hydrocarbons (**5**, **6**, **7**, and **12**) upto 65%, and santalols, constituted a minor portion.[7]

From the terpene fraction (20 g), santalenes (10.6 g), and santalols (9.4 g) could be separated using silica gel column chromatography. Further attempts for quantitative purification of santalol congeners (α- and β-) using conventional techniques such as column chromatography, distillation at atmospheric and reduced pressures and derivatization of santalols to their corresponding esters with achiral and chiral acids did not show any separation of the two components. On thin layer chromatography with normal silica gel (0% silver nitrate), both santalene (R_f values 0.91, system I: hexane) and santalol (R_f 0.71, system III: dichloromethane) congeners migrated as a single spot with different developing systems (Fig. 1). When silver nitrate coated silica gel TLC plates were used, both α- and β-santalenes and (*Z*)-α- and (*Z*)-β-santalols separated well with developing solvent systems II (hexane: ethyl acetate, 98.5: 1.5) and IV (CH_2Cl_2: methanol, 98.5: 1.5), respectively (Fig. 1). This formed the basis for development of MPLC method with silver nitrate impregnated silica gel for the quantitative separation of α- and β-santalenes and (*Z*)-α- and (*Z*)-β-santalols.

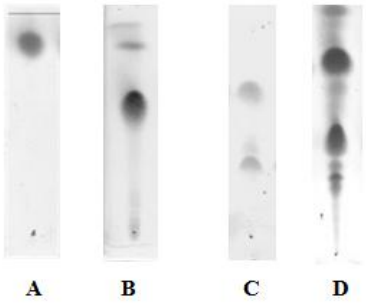

Figure 1. Santalenes and santalols on uncoated TLC plate (A), (B); and on $AgNO_3$ (5% in methanol) coated silica gel TLC plates (C) and (D), respectively.

Purification of hydrocarbon mixture (2 g) using silver nitrate impregnated silica gel medium pressure liquid chromatography (MPLC) with hexane as the eluent yielded fractions containing pure components, α-santalene (**5**, 0.48 g), β-santalenes (0.78 g). The β-santalene fraction obtained from the column contained both β-santalene (**6**) and *epi*-β-santalene (**7**) in a ratio of 58:42 (Fig. 2). These compounds were characterized based on various spectral data and the spectra were consistent with those reported in literature.[16]

Further, purification of sesquiterpene alcohol mixture (2 g) using silver nitrate impregnated silica gel MPLC with CH_2Cl_2 as eluent yielded of (*Z*)-α-santalol (**1**, 1.16

g), (*Z*)-β-santalols (0.52 g). The GC and GCMS analyses indicated that, the fraction obtained for (*Z*)-β-santalol contained both (*Z*)-β-santalol (**2**) and (*Z*)-*epi*-β-santalol (**3**) in the ratio of 87:13 (Fig. 3).[7] These alcohols were characterized based on various spectral studies, which agreed with the literature.[17,18]

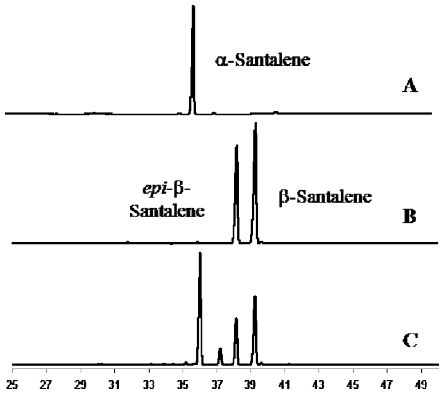

Figure 2. GC traces of purified santalenes from Sandalwood oil. **A**: α-santalene; **B**: *epi*-β-santalene and β-santalene; **C**: Sandalwood oil.

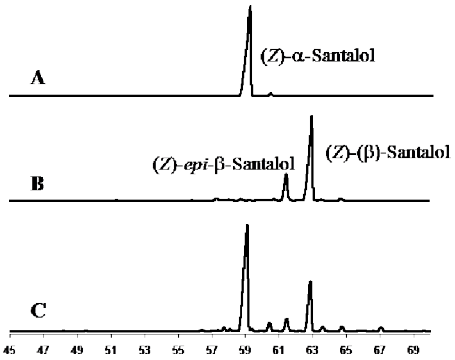

Figure. 3. GC traces of purified alcohols from Sandalwood oil. **A**: (*Z*)-α-santalol; **B**: (*Z*)-*epi*-β-santalol and (*Z*)-β-santalol; **C**: Sandalwood oil.

Section 1.3: Quantification of Santalene derivatives from Sandalwood oil and its adulteration study.

Sandalwood oil is often adulterated, the common adulterants being castor oil, cedarwood oil and low-grade oil from other sandalwood species. In this section we have demonstrated gas chromatography quantification method to assess the percentages of these santalols. Limits of quantification (LoQ) relative to FID detector were measured for eight important constituents of heartwood oil of *S. album* using serial dilutions of the stock solutions of (*Z*)-α-santalol (**1**), (*Z*)-β- and *epi*-β-santalols (**2** and **3**), (*Z*)-α-*trans*-bergamotol (**4**), α-bisabolol (**9**), (*Z*)-lanceol (**12**), (*E*,*E*)-farnesol (**10**), α-santalene (**5**) and β- and *epi*-β-santalenes (**6** and **7**). A ten points calibration curve was constructed for all these compounds and the regression coefficients were found to be 0.999 for all the constituents measured. All these compounds showed different FID detector responses as evidenced by different values for the slope and intercepts of the calibration curve drawn for every compound. Using these standard curves, GC-FID quantification studies were carried out under similar conditions for commercial sandalwood oil and deliberate adulteration with known quantities of paraffin oil, coconut oil, and ethylene glycol. As

anticipated, the measurements were in accordance with the content of the sesquiterpene alcohols in adulterated sandalwood oil.

Chapter 2: Biotransformation of (*Z*)-α-Santalol Derivatives.

Section 2.1: Introduction: Biotransformation.

This section briefly explains about the biotransformation process, with some of the examples of biotransformation of acyclic and cyclic terpenoids.

Section 2.2: Microbial biotransformation of (*Z*)-α-Santalyl acetate:

We have studied the biotransformation of (*Z*)-α-santalyl acetate (**2**) using *M. piriformis* to yield quantitative transformation of **2** in to four metabolites through de-acetylated compound (*Z*)-α-santalol (**1**) (Scheme 2).[19]

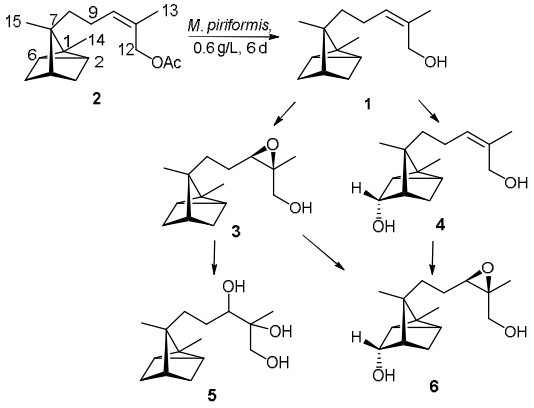

Scheme 2. Pathway for biotransformation of (*Z*)-α-santalyl acetate (**2**) with *M. piriformis*.

Substrate concentration of 0.6 g/L with an incubation period of 6 days was optimized from the substrate concentration and time course experiments. Large scale fermentation of **2** with *M. piriformis* yielded a neutral fraction (1.1 g).

Elution of the column with ethyl acetate/hexane (3:47) gradient, afforded **1** which was evidenced from GC and GC-MS analyses and co-injection with authentic (*Z*)-α-santalol. ^{1}H and ^{13}C NMR signals for **1** were assigned by 2D NMR spectral analysis (Scheme 3) and the spectral data were in complete agreement with that reported in literature.

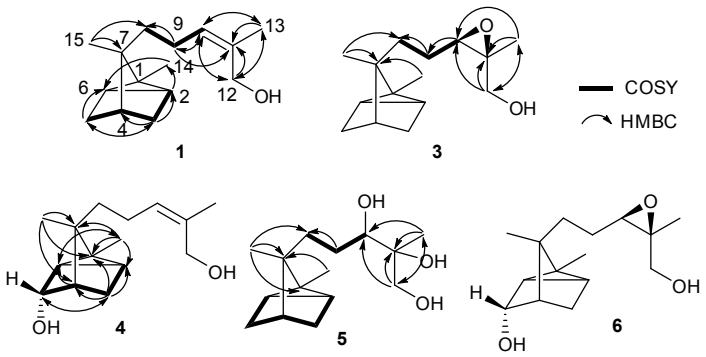

Scheme 3. Characterization of metabolites (**1**, **3**-**6**) by 2D NMR spectral analyses.

Further elution of the column with ethyl acetate/hexane gradients yielded metabolites **3**, **4**, **5**, and **6**. The purified metabolites were characterized using GC-MS, HRMS, ^{1}H, ^{13}C, DEPT and 2D (COSY, NOESY, HMBC, HSQC) NMR techniques. Four novel metabolites were characterized as 10,11-cis-β-epoxy-α-santalol (**3**), 5α-hydroxy-(Z)-α-santalol (**4**), 10,11-dihydroxy-α-santalol (**5**) and 5α-hydroxy-10,11-*cis*-β-epoxy-α-santalol (**6**). (Scheme 3). Further, the stereochemistry of newly introduced epoxy functionality was confirmed by Sharpless asymmetric epoxidation (SAE) of **1** using (+)-diethyl tartrate (DET) or (-)-DET which are known to introduce β-epoxide or α-epoxide, respectively.

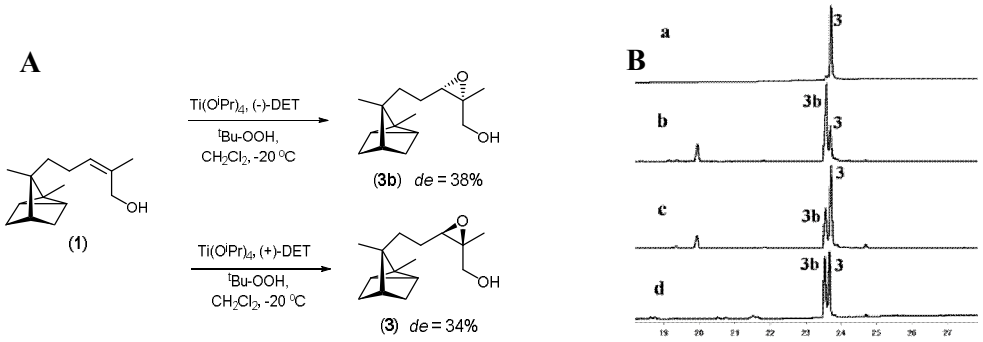

Figure 5: (**A**) Synthesis of **3b** (38% de) with (-)-DET and **3** (34% de) with (+)-DET, according to SAE methodology. (**B**) GC traces of (a) 10,11-*cis*-β-epoxy-α-santalol (**3**) obtained from biotransformation of (*Z*)-α-santalyl acetate with *M. piriformis*. Synthesized 10,11-*cis*-epoxy-α-santalols with (b) (-)-DET, (c) (+)-DET, (d) *m*CPBA.

Time course experiments carried out with **2** revealed complete transformation of the substrate (**2**) into various metabolites (**1**, **3**-**5**) within 5 days of incubation period. GC profiles of total metabolites formed at different time intervals indicated that at the

end of 6 days, **5** was obtained as the major product (38%) (Fig.6). Biotransformation pathway was established by incubating metabolite **3** with resting cells.[19]

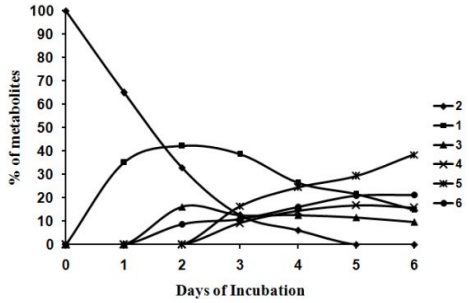

Figure 6: Time course study of the biotransformation of (*Z*)-α-santalyl acetate (**2**) with *M. piriformis*: (■) (*Z*)-α-santalol (**1**); (♦) (*Z*)-α-santalyl acetate (**2**); (▲) 10,11-*cis*-β-epoxy-α-santalol (**3**); (×) 5α-hydroxy-(*Z*)-α-santalol (**4**); (*) 10,11-dihydroxy-α-santalol (**5**); (●) 5α-hydroxy, 10,11-*cis*-β-epoxy-α-santalol (**6**).

Further, for kinetic resolution of epoxides (*cis*-α or *cis*-β), **1** was subjected to epoxidation with *m*CPBA that delivered diastereomeric mixture of epoxy-α-santalols. A range of commercially available lipases were screened for kinetic resolution of the diastereomeric epoxy-α-santalols [R_t 23.54 min and 23.67 min; HP-Chiral (20% β-cyclodextrin) column] by selective acetylation in presence of vinyl acetate, an acyl donor, in hexane. Promising results were obtained with Amano PS lipase from *B. cepacia* when acetylation of β-epoxide (**3**) was kinetically favored over α-epoxide (**3b**) with oxirane moiety remaining intact (Fig. 7).

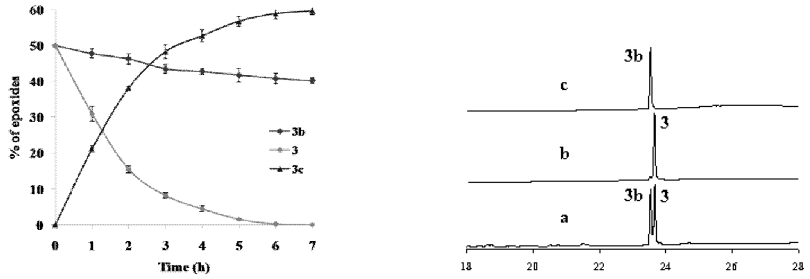

Figure 7 (A): Time course study plot of kinetic resolution of 10,11-*cis*-epoxy-α-santalol diastereomers by Amano PS lipase from *B. cepacia* for 7 h; (▲) 10,11-*cis*-epoxy-α-santalyl acetate (**3c**), (●) 10,11-*cis*-β-epoxy-α-santalol (**3**), (♦) 10,11-*cis*-α-epoxy-α-santalol (**3b**). **(B)** GC traces for (**a**) racemic-10,11-*cis*-epoxy-α-santalol (**3**+**3b**), (**b**) **3**, (c) **3b**.

The progress and selectivity of acetylation of epoxy-alcohol diastereomeric mixture (**3** + **3b**) was monitored by analyzing the aliquots drawn at every 1h over a period of 7h. Incubation of diastereomeric epoxide with lipase for 6h furnished α-epoxide (**3b**) with >99% de (40% yield). On the other hand, when the reaction was quenched at 2h, β-epoxy-α-santalyl acetate (39%) was obtained which on deacetylation with LiOH furnished **3** with 96% de (Fig. 7).

Chapter 3: Mechanistic Insights in Biosynthesis of Santalenes and analogous Sesquiterpenes.

Section 3.1: Introduction: Terpenes and Terpene Synthases.

This section explains the role of terpenes in nature[20] and use of deuterium labeled substrates to elucidate the mechanistic insights in biosynthetic pathways.[21-23]

Section 3.2: Synthesis of deuterated diphosphate substrates:

Different sets of enzymatic assays of *SaSS* with the synthesized substrate (*E*,*E*)-FPP (**14**) or the enzymatically generated **14** from chain elongation reaction of IPP with DMAPP or GPP in presence of *SaFDS*, generated the products **1-6** with similar ratios. This section delineates the biosynthesis of deuterated analogues of farnesyl diphosphate with labels at C1, C2, C4, C5, C6 and C13 from chain elongation reactions of un/labeled IPP and un/labeled GPP catalyzed by *SaFDS*.

Synthesis of [4,4-$^2H_2$]-Isopentenyl diphosphate ([4,4-$^2H_2$]-11):

Synthesis of **[4,4-$^2H_2$]-11** was initialized from commercially available 4-hydroxybutanone (**24**). Compound **24** was protected as *tert*-butyldimethylsilyl ether (**25**) and the carbonyl moiety was subjected to Wittig olefination in presence of *n*-BuLi with trideuteriomethyl-triphenylphosphonium iodide which itself was synthesized from trideuteriomethyl iodide and triphenylphosphine. The resultant dideuterated olefin **[4,4-$^2H_2$]-26** was deprotected followed by tosylation to provide **[4,4-$^2H_2$]-17**. The tosylate group was substituted by diphosphate on reacting with tris-tetrabutylammonium diphosphate salt (**15**) in CH_3CN. Further purifications according to well documented procedure by Davisson *et al*. delivered **[4,4-$^2H_2$]-11** (Scheme 4).

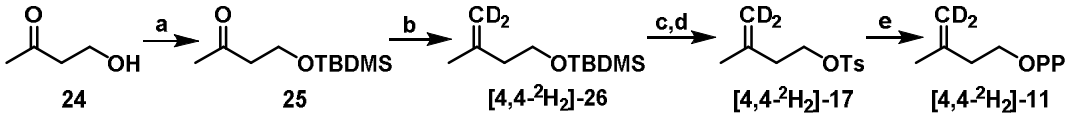

Scheme 4. *Reagents and conditions*: a) TBDMS-Cl, Et_3N, CH_2Cl_2, 0 °C to rt, 3 h, 91%; b) PPh_3CD_3I, *n*-BuLi, THF, 0 °C to rt, 2 h, 78%; c) TBAF, 0 °C to rt, 1 h; d) CaH_2, DMAP, Ts-Cl, CH_2Cl_2, 0 °C to rt, 2 h, 74%; e) $[N(n\text{-}Bu)_4]_3P_2O_7H$, CH_3CN, rt, 2h, 49%.

Synthesis of [2,2-$^2H_2$]-Isopentenyl diphosphate ([2,2-$^2H_2$]-11):

Dideuteration at α-position was achieved by stirring **27** with D_2O for 24 h to give **[2,2-$^2H_2$]-27**. Reduction followed by silyl protection of primary hydroxy group and oxidation of secondary hydroxy afforded [**2,2-$^2H_2$]-25**. Further, synthesis of **[2,2-$^2H_2$]-11** was followed using similar steps as in scheme 4. (Scheme 5).

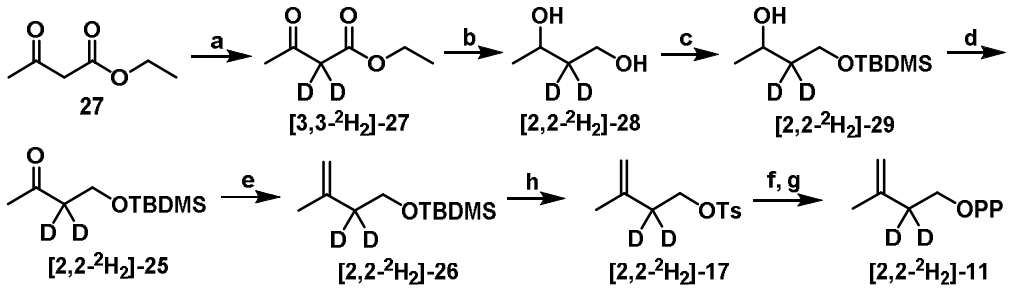

Scheme 5. *Reagents and conditions*: a) D_2O, rt, 24 h, 2 times, 92%; b) DIBAH, CH_2Cl_2, 0 °C to rt, 5 h, 76%; c) TBDMS-Cl, Et_3N, CH_2Cl_2, 0 °C to rt, 2 h, 88%; d) Dess-Martin periodinane, CH_2Cl_2, 3 h, 91%; e) PPh_3CH_3I, *n*-BuLi, THF, 0 °C to rt, 2 h, 72%; f) TBAF, THF, 0 °C to rt, 1 h; g) CaH_2, DMAP, Ts-Cl, CH_2Cl_2, 0 °C to rt, 3 h, 89%; h) $[N(n\text{-}Bu)_4]_3P_2O_7H$, CH_3CN, rt, 2 h, 31%.

Synthesis of [5,5,5-$^2H_3$]-Isopentenyl diphosphate ([5,5,5-$^2H_3$]-11):

Propylene glycol (**30**) was selectively mono-protected to its silyl ether **31** followed by oxidation of the other hydroxy group to an aldehyde **32**. The aldehyde **32** was methylated with Grignard reagent, trideuteriomethylmagnesium bromide (CD_3MgBr) to fetch **[1,1,1-$^2H_3$]-29** that was again subjected to oxidation to yield **[1,1,1-$^2H_3$]-25**. Synthesis of **[2,2-$^2H_2$]-11** was followed as described in scheme 4. (Scheme 6).

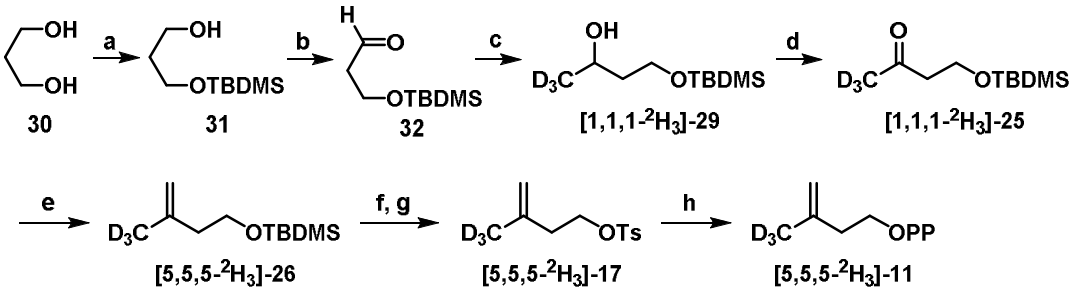

Scheme 6. *Reagents and conditions*: a) TBDMS-Cl, Et_3N, CH_2Cl_2, 0 °C to rt, 3 h, 91%; b) IBX, ethyl acetate, reflux, 4 h, 91%; c) CD_3MgBr, THF, 0 °C to rt, 2 h, 67%; d) IBX, ethyl acetate, reflux, 4 h, 92%; e) PPh_3CH_3I, *n*-BuLi, THF, 0 °C to rt, 2 h, 70%; f) TBAF, THF, 0 °C to rt, 1 h; g) CaH_2, DMAP, Ts-Cl, CH_2Cl_2, 0 °C to rt, 3 h, 77% over two steps; h) $[N(n\text{-}Bu)_4]_3P_2O_7H$, CH_3CN, rt, 2 h, 39%.

Synthesis of [4,4,5,5,5-$^2H_5$]-Isopentenyl diphosphate ([4,4,5,5,5-$^2H_5$]-11):

Intermediate **[1,1,1-$^2H_3$]-25** (Scheme 6) was utilized in the synthesis of **[4,4,5,5,5-$^2H_5$]-11**. Trideuteriomethyl ketone, **[1,1,1-$^2H_3$]-25** was subjected to a series of reactions identical to that of **25** in Scheme 4.

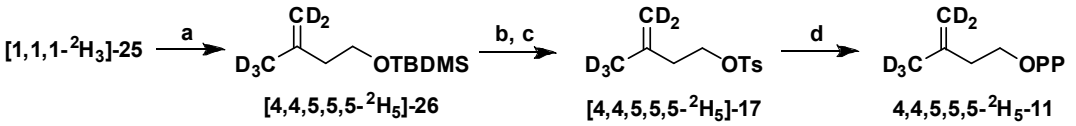

Scheme 7: *Reagents and conditions*: a) PPh_3CD_3I, n-BuLi, THF, 0 °C to rt, 2 h, 78%; b) TBAF, THF, 0 °C to rt, 2 h; c) CaH_2, DMAP, TsCl, CH_2Cl_2, 0 °C to rt, 3 h, 82%; d) $[N(n\text{-}Bu)_4]_3P_2O_7H$, CH_3CN, rt, 2 h, 34%.

Synthesis of [1,1-$^2H_2$]-Geranyl diphosphate ([1,1-$^2H_2$]-13):

Synthesis of **37** was accomplished by a series of oxidation-reduction procedures from Geraniol (**20**). It was oxidized to citral (**21**), followed by reduction with $LiAlD_4$ to yield **[1-$^2H_1$]-20**. One more cycle of oxidation-reduction with PDC and $LiAlD_4$, respectively was carried out with **[1-$^2H_1$]-20** to yield **[1,1-$^2H_2$]-20**. Chlorination of **[1,1-$^2H_2$]-20** to halide **[1,1-$^2H_2$]-21** followed by diphosphorylation in presence of **15** yielded **[1,1-$^2H_2$]-13** (Scheme 8).

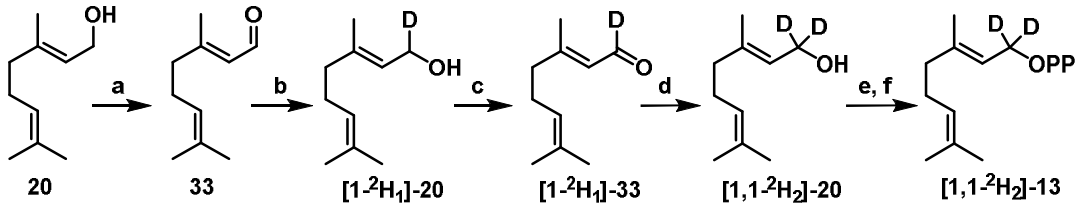

Scheme 8: *Reagents and conditions*: a) IBX, ethyl acetate, 75 ^{o}C, 3 h, 96%; (b) $LiAlD_4$, THF, -40 ^{o}C, 2 h, 92%; (c) PDC, CH_2Cl_2, rt, 2 h, 81%; (d) $LiAlD_4$, THF, -40 ^{o}C, 2 h, 87%; e) NCS, $(CH_3)_2S$, CH_2Cl_2, -30 °C to rt, 3 h, 90.4%; f) $[N(n\text{-}Bu)_4]_3P_2O_7H$, CH_3CN, rt, 2 h, 64%

Synthesis of [1,1-$^2H_2$]-Farnesyl diphosphate ([1,1-$^2H_2$]-14):

Following an identical sequence of reactions as applied in the synthesis of **[1,1-$^2H_2$]-13**, synthesis of dideuterated product, [1,1-$^2H_2$]-farnesyldiphosphate (**[1,1-$^2H_2$]-14**) was carried out from (*E*,*E*)-Farnesol (**22**).

Biosynthesis of deuterated analogues of (*E*,*E*)-FPP (14):

Farnesyl diphosphate synthase (*FDS*), belonging to prenyltransferase class of enzymes catalyses the head to tail condensation (chain elongation reaction) of dimethylallyl diphosphate (DMAPP) and geranyl diphosphate (GPP) with isopentenyl diphosphate (IPP) to deliver the linear product (*E*,*E*)-FPP. (Scheme 10).

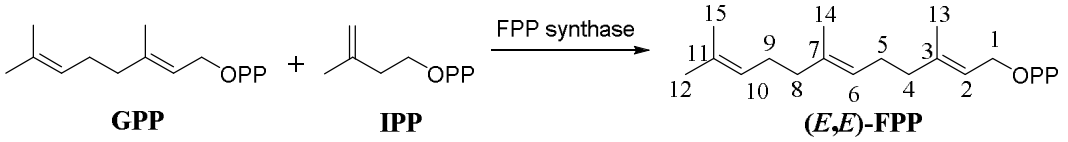

Scheme10: Biosynthesis of (*E*,*E*)-FPP.

In a similar way, *SaFDS*[24] isolated from sandalwood, was utilized in the biosynthesis of differentially labeled (*E*,*E*)-FPP analogues by the condensation of the above synthesized labeled substrates (IPP with GPP or DMAPP) (Scheme 11).

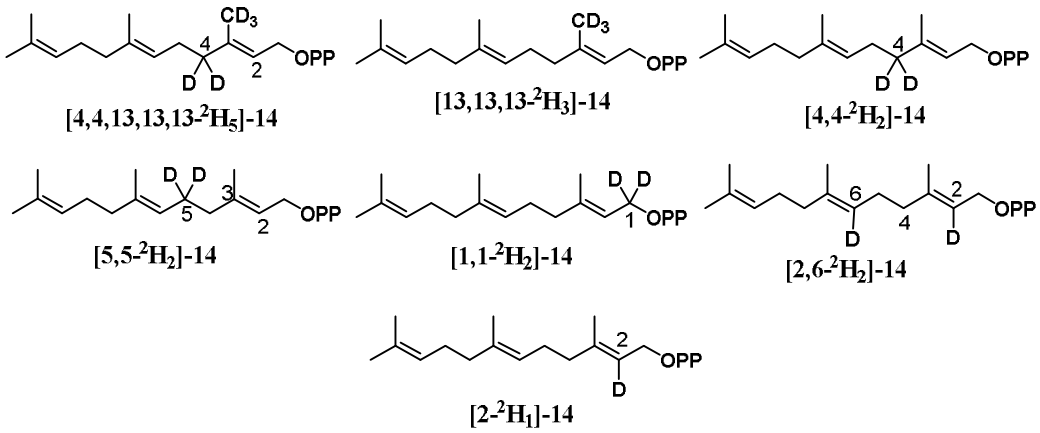

Scheme 11: Deuterium labeled (*E*,*E*)-FPP analogues.

Section 3.3: Mechanistic Insights for Biosynthesis of Santalenes, Bergamotenes, Curcumenes and analogous sesquiterpenes.

Santalum album Santalene Synthase (*SaSS*) isolated from the interface of heartwood and sapwood of *S. album* catalyzes biosynthesis of six sesquiterpene hydrocarbons, α-santalene (**1**, 41%), β-santalene (**2**, 29.4%), *epi*-β-santalene (**3**, 4.3%), *exo*-α-bergamotene (**4**, 22.5%), *exo*-β-bergamotene (**5**, 2.2%) and (*E*)-β-farnesene (**6**, 0.7%), when incubated with **14** (Scheme 12). Other variants of this enzyme produced by site directed mutagenesis of the amino acid residues around the catalytic site emanated other bi- and mono-cyclic sesquiterpenes, identified as, *endo*-α-bergamotene (**7**), β-curcumene (**8**), γ-curcumene (**9**) and α-zingiberene (**10**).[24] To investigate the mechanistic insights in the biosynthetic pathways of these sesquiterpenes (**1**-**10**), deuterium labeled analogues of **14** (Scheme 11) were incubated with *SaSS* enzymes. Formation of the labeled products was monitored by GC-MS analysis and the ratios of products induced by kinetic isotope effects (KIE) were determined from GC analysis.

Biosynthesis of Santalenes (1, 2 and 3) and *exo*-α-Bergamotene (4):

An initial step in the biosynthesis of santalenes is Mg^{2+} assisted ionization of the allylic diphosphate substrate, (*E*,*E*)-FPP (**14**), from C1 to get the charged diphosphate anion and the farnesyl carbocation (at C1) that subsequently isomerizes to its tertiary counterpart, nerolidyl cation (**I**). Free rotation around C2-C3 bond forms *cisoid* nerolidyl cation which undergoes facile C1-C6 *endo*-anti cyclization to form bisabolyl cation (**II**),[25] which further experiences C7-C2 closure leading to bergamotyl cation

(**III**). The cation **III** thereupon goes through one more carbocationic intermediate (**IV**) before forming santalyl cation (**V**) with a carbocation on C3, which forms a branching point in the biosynthesis of α-santalene (**1**) and β-santalene (**2**).

When **[4,4-$^2H_2$]-14** was incubated with *SaSS*, the molecular ion $[M]^+$ for **1** and **4** shifted from *m*/*z* 204.1 (unlabeled products in control experiments) to *m*/*z* 205.1, thereby indicating an increment of 1 *amu* in the labeled products. GC-MS analysis of labeled analogues of **1** and **4** obtained from incubation of other analogues of **14** labeled at C1, C2, C5, C6 and C13 with *SaSS* resulted in the retention of all the deuteriums. Incubation of **[13,13,13-$^2H_3$]-14** with *SaSS*, showed a shift of molecular ion, $[M]^+$ from *m/z* 204.1 to *m/z* 206.1 indicating loss of a deuterium from C13 in the formation of **[13,13-$^2H_2$]-2**.

On replacing the substrate **14** with **[4,4-$^2H_2$]-14** in the enzymatic assay with *SaSS*, product ratio [**1**/**2**], decreased from 1.56 to 0.76 and a KIE, $[(\mathbf{1}/\mathbf{2})^H/(\mathbf{1}/\mathbf{2})^D]$ of 2.05 was consistent with the cleavage of C-D bond at C4 in the formation of **1**. On the other hand, when **14** was replaced with **[13,13,13-$^2H_3$]-14**, the product ratio **[2/1]**, decreased from 0.65 to 0.23 with a KIE, $[(\mathbf{2}/\mathbf{1})^H/(\mathbf{2}/\mathbf{1})^D]$= 2.89 that was in good agreement with the formation of **[13,13-$^2H_2$]-2**. In a similar way, when *SaSS* incubations with **14** were replaced by **[4,4-$^2H_2$]-14**, the product ratio [**4**/**2**] decreased from 1.01 to 0.42 with a KIE, $[(\mathbf{4/2})^H/(\mathbf{4/2})]^D$= 2.39 observed due to cleavage of C-D bond at C4 in the formation of **4**.

From these results, it could be observed that the cation **VB** converts into **1** when new C3-C4 sigma bond is formed by subsequent loss of a proton from C4, whereas loss of a proton from C13 forms **2** (Scheme 12). Also, loss of a proton at C4 from **III**, forms C3-C4 π-bond leading to the formation of **4**.

Biosynthesis of *epi*-β-santalene (**3**) from **14** can be proposed in two ways. First pathway could be traversed through epimerization of **II** to **IIA** following a free, low-energy rotation about C6-C7 and further cyclization to the *epi*-santalyl cation (**VA**), pursuing the intermediates (**IIIA** and **IVA**) formed through a similar reaction cascade as followed in the biosynthesis of **2**. The other way could be through two consecutive methyl shifts from the intermediate **V** (Scheme 12). The GC-MS analysis of **3** was same as that of **2** indicating loss of a proton from C13 in the formation of **3**. Within the experimental errors, incubations of all deuterated analogues of **14** resulted in the formation of **3** at the same levels, as observed in control experiments with *SaSS*. From

these results, allowed rotation about C6-C7 bond gave rise to the *epi*-isomer and justified the prevalence of pathway-1, while eliminating the possibility of pathway-2 in the formation of **3**

Biosynthesis of *exo*-β-Bergamotene (5) and *endo*-α-Bergamotene (7):

The biosynthesis of *exo*-β-bergamotene (**5**) originates from the bergamotyl cation (**III**) that follows loss of a proton from C13 to quench the carbocation at C3, with a formation of exocyclic C3-C13 π-bond. A single point mutant of *SaSS*, by replacing arginine at 474 with leucine, produced **4** (74.7%) and **5** (25.3%), on incubation with **14**. Incubations of **[13,13,13-^{2}H$_3$]-14** with *SaSS* as well as with a mutant enzyme R474L-*SaSS* produced **[13,13-^{2}H$_2$]-5** containing two deuterium atoms, as seen by shift of the molecular ion $[M]^+$ from *m*/*z* 204.1 to *m*/*z* 206.2. The deuterated analogues of **5** obtained from incubation of **14** labeled at C1, C2, C4, C5 and C6 with *SaSS* enzymes retained all the deuterium atoms. When **14** was replaced with **[13,13,13-^{2}H$_3$]-14** in the enzymatic assays with R474L-*SaSS* mutant, the ratio **[5/4]** decreased from 0.34 to 0.09 revealing a KIE, $[(\mathbf{5}/\mathbf{4})^H/(\mathbf{5}/\mathbf{4})]^D$= 3.72. These results indicate the formation of **5** and **4** through deprotonation of **III** at C13 and C4, respectively (Scheme 12).

Biosynthesis of **7** is proposed to proceed through *endo*-bisabolyl cation (**IIA**) which initially experiences a free rotation around C6-C7 from **II**. Cation **IIA** subsequently undergoes C2-C7 closure to produce *endo*-bergamotyl cation (**IIIA**) with a carbocation at C3. Further, **IIIA** encountered deprotonation from C4 to result in the final product **7** with a C3-C4 π-bond. A single point mutant of *SaSS*, by replacing tyrosine at 539 with tryptophan (Y539W) produced **4** (32.2%), **5** (24.1%), **7** (22.0%) along with other sesuiterpenes, on incubation with **14**. Incubation of **[4,4-^{2}H$_2$]-14** and **[4,4,13,13,13-^{2}H$_5$]-14** with Y539W-*SaSS*-mutant resulted in **[4-^{2}H]-7** and **[4,13,13,13-^{2}H$_4$]-7**, which exhibited a shift of molecular ion peak $[M]^+$ from *m*/*z* 204.1 to *m*/*z* 205.1 and *m*/*z* 208.1, respectively. Incubations with other analogues of **14** labeled at C1, C2, C5, C6 and C13 resulted in the retention of all the deuterium labels. When the substrate **14** was replaced with [**4,4-^{2}H$_2$]-14**, GC analysis of the assay products revealed a decrease in the ratio **[7**/**5**] from 0.91 to 0.37 demonstrating a KIE, $[(\mathbf{7}/\mathbf{5})^H/(\mathbf{7}/\mathbf{5})]^D$= 2.45. These results indicate that **III** and **IIIA** are interconvertible through **II** with C6-C7 bond rotations, while the sesquiterpene **7** is formed through deprotonation at C4 of **IIIA** (Scheme 12).

Biosynthesis of Monocyclic sesquiterpenes (8, 9, and 10):

A single point mutant of *SaSS*, by replacing isoleucine at 422 with alanine (I422A) produced monocyclic sesquiterpene products, β-curcumene (**8**, 64.3%), γ-curcumene (**9**, 13.6%), and α-zingiberene (**10**, 1.7%), along with other sesuiterpenes, on incubation with **14**. Biosynthesis of these monocyclic sesquiterpenes is proposed through carbocation **IIB**, which experiences hydride shifts followed by proton loss from specific centers. In the enzymatic assays of I422A-*SaSS* mutant, when the substrate **14** was replaced with **[5,5-^{2}H$_2$]-14**, the $[M]^+$ at *m/z* 204.1 shifted to *m/z* 205.2, and the product ratio [**8**/**9**] decreased from 4.71 to 2.47 with a KIE, $[\mathbf{8}/\mathbf{9}]^H/[\mathbf{8}/\mathbf{9}]^D$= 1.91, indicating elimination of a deuterium from C5 due to creation of a C5-C6 π-bond in the formation of **8** (Scheme 12). On the other hand, replacement of **14** with **[1,1-^{2}H$_2$]-14**, the $[M]^+$ at *m/z* 204.1 shifted to *m/z* 205.1, and the product ratio [**9**/**8**] decreased from 0.21 to 0.08 with a KIE, $[\mathbf{9}/\mathbf{8}]^H/[\mathbf{9}/\mathbf{8}]^D$= 2.52, indicating elimination of a deuterium from C1 due to creation of a C1-C6 π-bond in the formation of **9** (Scheme 12).

Incubations of **[5,5-^{2}H$_2$]-14** with I422A-*SaSS* mutant generated **[5,5-^{2}H$_2$]-10** with $[M]^+$ at *m/z* 206.1 indicating presence of two deuterium atoms, while incubations with **[4,4-^{2}H$_2$]-14** resulted in **[4-^{2}H$_1$]-10** with $[M]^+$ at *m/z* 205.1 containing only one deuterium, which supported the deprotonation from C4. These results indicate that in biosynthesis of **10**, the *exo*-bisabolyl cation undergoes hydride shift from C1 to C7 along with the shift of π-electron density from C2-C3 to form C1-C2 π-bond generating a carbocation at C3. Ultimate deprotonation from C4 immediately follows to form a new C3-C4 π-bond generating **10** (Scheme 12).

Biosynthesis of acyclic sesquiterpene, (*E*)-β-Farnesene (6):

Transoid conformers of nerolidyl cation obtained from (*E*,*E*)-FPP, cannot undergo 1,6-cyclization due to remoteness of the reacting centers, but suffer deprotonation yielding acyclic and 1,4-eliminated products like (*E*)-β-farnesene (**6**) (Scheme 12). A single point mutant of *SaSS*, by replacing leucine at 427 with alanine (L427A) produced **1** (9.5%), **4** (57.3%), and **6** (33.2%), on incubation with **14**. Incubation of **14** with the mutant L427A-*SaSS* delivered **6** with $[M]^+$ at *m/z* 204.1, while that with **[13,13,13-^{2}H$_3$]-14** a shift of $[M]^+$ to *m/z* 206.2, indicating presence of two deuterium atoms, but elimination of a deuterium from C13 when C3-C13 π-bond was formed.

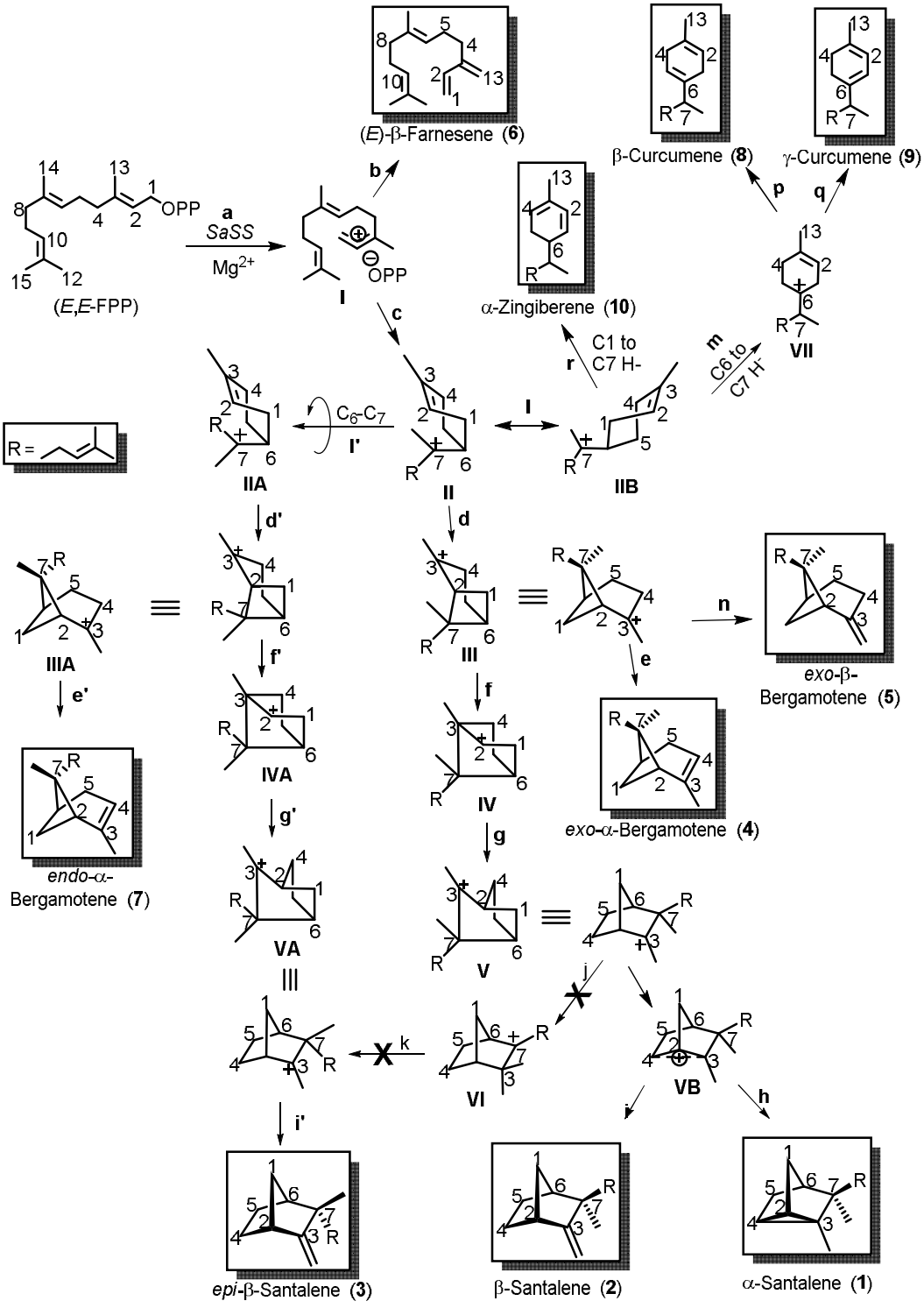

Scheme 12. Proposed mechanism for biosynthesis of sesquiterpenes.

References:

(1) Harbaugh, D. T.; Baldwin, B. G. *Am. J. Bot.* **2007**, *94*, 1028-1040.
(2) Kim, T. H.; Ito, H.; Hatano, T.; Takayasu, J.; Tokuda, H.; Nishino, H.; Machiguchi, T.; Yoshida, T. *Tetrahedron* **2006**, *62*, 6981-6989.
(3) Baldovini, N.; Delasalle, C.; Joulain, D. *Flavour Frag. J.* **2011**, *26*, 7-26.
(4) Kim, T. H.; Ito, H.; Hatano, T.; Hasegawa, T.; Akiba, A.; Machiguchi, T.; Yoshida, T. *J. Nat. Prod.* **2005**, *68*, 1805-1808.
(5) Kim, T. H.; Ito, H.; Hayashi, K.; Hasegawa, T.; Machiguchi, T.; Yoshida, T. *Chem. Pharm. Bull.* **2005**, *53*, 641-644.
(6) Erligmann, A. *Int. J. Aromather.* **2001**, *11*, 186-192.
(7) Daramwar, P. P.; Srivastava, P. L.; Priyadarshini, B.; Thulasiram, H. V. *Analyst* **2012**, *137*, 4564-4570.
(8) Dwivedi, C.; Guan, X. M.; Harmsen, W. L.; Voss, A. L.; Goetz-Parten, D. E.; Koopman, E. M.; Johnson, K. M.; Valluri, H. B.; Matthees, D. P. *Cancer Epidem. Biomar.* **2003**, *12*, 151-156.
(9) Dwivedi, C.; Valluri, H. B.; Guan, X.; Agarwal, R. *Carcinogenesis* **2006**, *27*, 1917-1922.
(10) Bommareddy, A.; Hora, J.; Cornish, B.; Dwivedi, C. *Anticancer Res.* **2007**, *27*, 2185-2188.
(11) Misra, B. B.; Dey, S. *Phytomedicine* **2013**, *20*, 409-416.
(12) Paulpandi, M.; Kannan, S.; Thangam, R.; Kaveri, K.; Gunasekaran, P.; Rejeeth, C. *Phytomedicine* **2012**, *19*, 231-235.
(13) Barrett, C. B.; Dallas, M. S. J.; Padley, F. B. *Chem. Ind.* **1962**, 1050-1051.
(14) Morris, L. J. *Chem. Ind.* **1962**, 1238-1240.
(15) Stevens, P. J. *J. Chromatogr. A* **1968**, *36*, 253-258.
(16) Oppolzer, W.; Chapuis, C.; Dupuis, D.; Guo, M. *Helv. Chim. Acta* **1985**, *68*, 2100-2114.
(17) Schlosser, M.; Zhong, G. F. *Tetrahedron Lett.* **1993**, *34*, 5441-5444.
(18) Christenson, P. A.; Willis, B. J. *J. Org. Chem.* **1979**, *44*, 2012-2018.
(19) Daramwar, P. P.; Srivastava, P. L.; Kolet, S. P.; Thulasiram, H. V. *Org. Biomol. Chem.* **2014**, *12*, 1048-1051.
(20) Gershenzon, J.; Dudareva, N. *Nat. Chem. Biol.* **2007**, *3*, 408-414.
(21) Thulasiram, H. V.; Erickson, H. K.; Poulter, C. D. *J. Am. Chem. Soc.* **2008**, *130*, 1966-1971.
(22) Thulasiram, H. V.; Poulter, C. D. *J. Am. Chem. Soc.* **2006**, *128*, 15819-15823.
(23) Cane, D. E.; Prabhakaran, P. C.; Salaski, E. J.; Harrison, P. H. M.; Noguchi, H.; Rawlings, B. J. *J. Am. Chem. Soc.* **1989**, *111*, 8914-8916.
(24) Srivastava, P. L., University of Pune, 2014.
(25) Cane, D. E. *Accounts Chem. Res.* **1985**, *18*, 220-226.

Chapter 1

Isolation, Purification and Quantification of Santalenes and Santalols from Indian Sandalwood, *Santalum album*

Section 1.1.

Introduction:

Indian Sandalwood

'*Santalum album*'.

NCL parking area. Courtesy: Dr. Thulasiram H. V.

1.1.1 Classification, taxonomy and regional distribution:

Sandalwood is a general name given to a small group of parasitic trees in the genus *Santalum*, family *Santalaceae*. The taxonomic classification and molecular phylogeny of *Santalum* genus has been reviewed[1] and inferred to consist of 18 species which are xylem-tapping root hemi-parasites.[2,3] Members of the genus *Santalum* are scattered over broad regions of India, China, West Indies, Indonesia, Australia, New Guinea, Hawaii, Vanuatu, New Caledonia and many South-Pacific islands and are characteristic to the regions. It is distributed as far southeast as the Juan Fernandez Islands, only 600 miles off the coast of Chile, and as far northwest as the Bonin Islands, 600 miles south of Honshu, Japan.[4-6] Sandalwoods are slow growing, root-parasitic trees[7] meaning they derive water and some vital nutrients from surrounding trees with the help of root connections called 'haustoria'.[8-11] The host plants differ depending on the *Santalum* species. True Sandalwood is obtained from different *Santalum* species of different origins,[12] of which only three are exploited commercially, *viz*.

a) *Santalum album* L., also known as Indian Sandalwood or East Indian Sandalwood, which is majorly found growing in the parts of India, Sri Lanka, Indonesia (*viz*. Timor, Celebes and Sumbawa) and northern Australia.

b) *S. austrocaledonicum* Vieill., found only in the New Caledonian and Vanuatu archipelagos,

c) *S. spicatum* (R. Br.) A. DC, widespread in the arid areas of southwestern Australia.

Indian Sandalwood or East Indian Sandalwood also known as sandalwood (commercial name), botanically known as '*Santalum album*' belonging to the *Santalaceae* family, is a small to medium-sized, evergreen tree and attains a height of 60-65 feet. It is majorly found growing in the parts of India, Sri Lanka, and Indonesia and also cultivated in Australia. In India, populations are more concentrated in the southern region, especially Karnataka (Mysore, Coorg), Tamil Nadu (Chennai), Maharashtra and Kerala. It generally occurs at the altitudes of 2000-3000 feet. It is a hemi-root parasitic plant and can parasitize over 300 species from grass to another sandal plant.[13,14] Soon after germination of the seed, the roots attach themselves to those of nearby grasses, herbs, bushes, and undergrowth in general, obtaining nutrients by means of the haustorium and finally causing the host plant to perish. It depends on various hosts like *Cassia siamea, Pongamia glabra* and *Lantana*

acuminata. *S. album* thrives in well-drained loamy soil, preferably on slopes of hills exposed to the sun. It requires a minimum of 20-25 inches rainfall per year. The finest wood grows in driest region, particularly on red or stony ground while on rocky ground the tree often remains small but gives the highest yield of oil.[15]

S. album is a small evergreen glabrous tree. The trunk of sandalwood is divided into two parts, the sapwood white and odorless, which is an external portion below the bark and the heartwood, yellowish brown, strongly scented, which is the internal core. The heartwood is described as astringent, bitter, moderately hard, heavy, durable, yellow or brown in appearance, with an oily texture and is an exquisite material for carving intricate designs.[16]

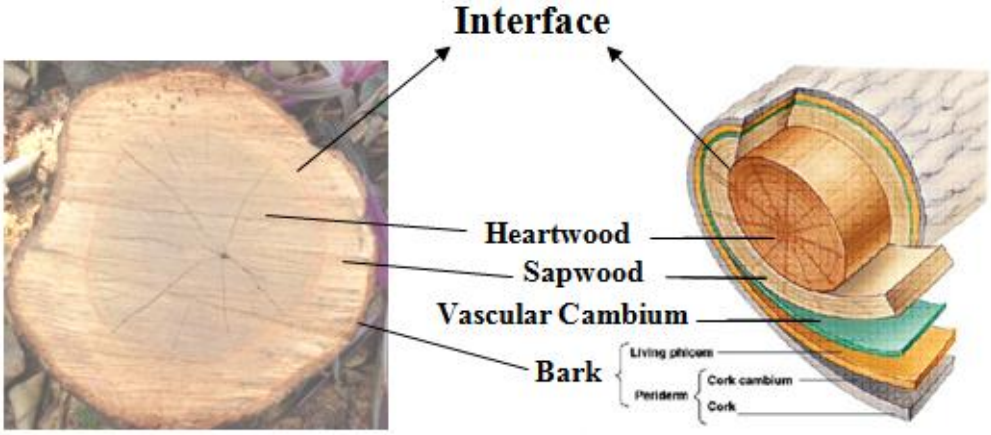

NCL parking area. Courtesy: Dr. Thulasiram H. V.

Figure 1.1.1. Cross-section of sandalwood

The formation of oil takes place at the transition zone of sapwood and heartwood and is deposited in the heartwood, which is mainly dead tissue (Figure 1.1.1). The heartwood is almost absent in the early age of the tree and its formation generally starts only after 10-13 years of age, but what triggers this process has not been identified. The occurrence of heartwood varies and after a certain age most of the root part also becomes heartwood, however in the stem it highly varies from place to place as the external factors remain responsible for it. It can range from 90% of the stem wood to a negligible amount, or be absent depending on the age of the tree. Natural varieties of Indian Sandalwood take 60 to 80 years to yield highest quality and quantity of oil. The cost of sandalwood is dependent on its oil content, which is subsequently dependent on the age and girth of the

heartwood. In a tree, the oil content is maximum in the root and next in the stem at the base of the tree and gradually decreases towards the apex of the tree. Similarly, the heartwood at the core is denser with oil and the oil content decreases towards the periphery.

1.1.2. Historical and commercial importance:

Sandalwood (*Santalum album* L.) is a valuable tree associated with Indian culture and is named as '*Chandana*' (in Sanskrit) in Indian mythology. Its heartwood is highly in demand since ancient days for its fragrant properties that made it useful for carving, decoratives, rituals, incense manufacture, oil extraction, holy practices such as *homa-havana*, and many more. *S. album* is considered the pride of India and is one of the most valuable trees in the world.[17] The use of sandalwood is mentioned from the ages of '*Ramayana*' (around 2000 B.C.) in Indian mythology. Aroma of the oil and the wood is esteemed by people belonging to three major religions of the world - Hinduism, Buddhism and Islam. For more than 5000 years, India has been the traditional leader of sandalwood oil production.[18] The trade of sandalwood from India is dated back to the beginning of trading in India. Its use in toiletries was mentioned in Buddhist Jataka stories in 7th century B.C.[16] Mauryan dynasty in 3rd century B.C. also mentions the use of this precious wood. Most of the geographic distribution of sandalwood in Deccan India overlapped with the regime of Vijayanagara dynasty which was ruled by its famous king Krishnadevaraya in early 16th century.[19] It is said that the richness of this dynasty with natural resources like sandalwood, spices, diamonds and other precious stones provided an important source of economy with which the empire could trade for guns and horses with Arabs and Europeans to build its own military strength and become a powerful kingdom. Later in the 18th century, Tipu Sultan, who ruled the kingdom of Mysore, declared sandalwood as the 'Royal tree' and took over sandalwood trade of the state on monopoly basis. The later kings of Mysore region continued this tradition and brought the trade and disposal of sandalwood under jurisdiction. From last six decades, trade of sandalwood has been replaced by government owned sandalwood extraction factories as well as craft industries. Nalwadi Krishnaraja Wodeyar (1884–1940) (aka Krishnaraja Wodeyar IV), whose period of sovereignty is often described as the 'Golden Age of Mysore', was instrumental in conceiving the idea of starting a sandalwood oil factory. As an impact of outbreak of World war-I, demand of

sandalwood decreased resulting in discontinuation of its export and compiling of huge unsold stocks. During the visit of Maharaja of Mysore to the Forestry Department at Sankey road in Bengaluru in 1916, he put forth an idea of extraction of oils from these huge stocks. He, after seeking advice from the scientists, established Sandalwood oil distillery in the vicinity of Sankey Tank, Malleswaram, Bengaluru, which was later, shifted to Mysore and eventually became the renowned 'Government Sandalwood Oil Factory'.

For the past 40 years, the production of wood has continued to diminish due to several factors such as uncontrolled felling, smuggling, illegal poaching and spike disease. Despite being State-controlled, it is difficult to estimate production due to fraud. However, it is thought that production is in the range of 3000 to 6000 tons of wood per year. According to Chana,[20] the wood has its main centers of production in Karnataka (Mysore) and Tamil Nadu (Chennai), also over 90% of the world's sandalwood output is from India. The Food and Agriculture Organization of the United Nations reports an estimated 40 tons per annum over the period of 1987 to 1993 (Anonymous 1995). Indonesia, the world's second largest producer of *S. album* products, produced an average of 15 tons of oil per annum for the same period.[21] From 1995 to 2005, Indonesia provided the bulk of *S. album* products to the world markets, while India's production levels fell significantly due to scarcity and legislated resource protection. In March 2006, the highest auction price in India for cleaned *S. album* logs was Aus$ 105,400 per ton (Source: Tropical Forestry Services Pty. Ltd., Australia).

1.1.3. Economic status:

The demand for high quality sandalwood and its oil has been ever-increasing, because of their extensive use in broad spectrum of fields ranging from perfumes, handicrafts to cosmetics, medicines and so on. It being a slow-growing tree that further requires 60-80 years of growth for harvest of good quality heartwood that can yield maximum quantity of oil, is not able to meet the market's rising demand. Excessive harvesting without replenishment of this invaluable resource has substantially reduced the sandalwood industry, resulting in global shortage and soaring of market prices.[22] Its cost is increasing steeply in domestic as well as international markets due to a significantly decreased supply,[23] which is exemplified from the auction prices of the scented wood declared by

Government of Karnataka, which increased from Rs. 1.553 million /tonne in 2004 to Rs. 3.557 million /tonne in 2009.[24] Over 70 years ago, nearly 90% of the natural sandalwood populations occurred in the southern part of Karnataka and northern part of Tamil Nadu.[25] In Karnataka, sandalwood populations have reduced to sparse and devoid of larger girth; mature trees have been nearly vandalized.[26] Apart from illegal harvesting and smuggling, spike disease that caused heavy economic losses, also add up to the depletion of the native sandalwood reserves. Spike disease has proved to be a major affliction for sandalwoods, as it compelled the Karnataka government to cut 700,000 sandalwood trees in the State of Mysore and 350,000 in the erstwhile Coorg State during the period 1903-1916 by the application of arsenical solution.[27] The other reasons of paucity of sandalwood include forest fires, absence of adequate number of seed-bearing trees, lack of established plantations and heavy demand by the 'Sandalwood Oil Factory'. As a result, in 1997 Indian Sandalwood has been listed on the International Union for Conservation of Nature (IUCN) threatened species' red list. According to a survey, supplies of good quality sandalwoods in India may be depleted in as little as five years which demands some serious measures to be adopted to save this endangered species from extinction.

1.1.4. Sandalwood oil utility and methods of extraction:

1.1.4.1. Sandalwood oil and its uses:

Sandalwood is among the oldest known perfumery material and is highly valued worldwide for its fragrant heartwood. The highest value sandalwood is used for carving religious statues and objects, handicrafts, art, and decorative furniture. Larger basal pieces and roots are preferred for carving. In Hawai, sandalwood was sometimes used to make musical instruments such as the musical bow.[28,29] It is used in handicraft industry to make a wide variety of artifacts such as boxes, cabinet panels, jewel cases, combs, picture frames, hand fans, pen holders, card cases, letter openers and bookmarks. Carved images of gods and mythological figures have high demand in the market and are also displayed in museums. Sandalwood is considered as sacred and is used for burning in certain Hindu and Buddhist rituals, religious ceremonies and during meditation and prayers. The beige-colored paste obtained by grinding of this scented wood is used as an ointment to apply on forehead and

other body parts, as it functions as a coolant by dissipating heat and also as a beauty aid. Wood powder is used to make incense sticks.

It is no wonder that sandalwood is the second most expensive wood in the world, next to the African Blackwood (*Dalbergia melanoxylon*) and continues to increase in price each year. Indian Sandalwood, *S. album* also known as 'True Sandalwood' yields highest quality and quantity of oil as compared to the other aromatic heartwood bearing and oil yielding sandalwood species. Sandalwood oil is obtained by steam distillation of heartwood powder, is expensive and sold by weight. The typical values of oil yield from *S. album* are 6-7% (w/w).[30,31] Extractable oil yield can vary from zero to nearly 9% (w/w) from within one tree.[32] *S. yasi* from Fijiis is reported to yield about 5% oil, *S. austrocaledonicum* around 3-5%, and *S. spicatum* around 2%.[33] Sandalwood oil is a blend of mono and sesquiterpenoids of which, santalols (α- and β-), the mono-hydroxylated sesquiterpenes constitute major part and also decide the odor and consequently the quality of the oil. The value of the tree is due to its oil content and the superiority of the oil pertains with the percentage of sesquiterpene alcohols, which in turn are dependent on the age of the tree. The varieties of oils containing more than 90% santalols are considered to be of the highest quality.[34] To produce commercially valuable sandalwood with high levels of fragrance oils, harvested *S. album* have to be at least 40 years of age, but 80 or above is preferred. However, inferior sandalwood produced from trees at 30 years of age can still fetch a decent price due to increasing market demand. Depending upon their age, trees can be empirically classified as young or mature, but the oil content may differ from tree to tree at the same age.

(i) Young trees (height less than 10 m, girth less than 50 cm and heartwood diameter 0.5-2 cm) have heartwood with 0.2-2 % oil content, which has 85% santalols, 5% acetates and 5% santalenes.

(ii) Mature trees (height 15-20 m, girth 0.5-1 m and heartwood diameter 15-20 cm) have heartwood with oil content of 2-6.2%, which has over 90% α-santalol,[25] 3-5% acetates and 3% santalenes.[35]

Sandalwood oil extracted from the heartwood, has a multitude of uses in daily life as well as in medicine, as it possesses characteristic smell and medicinal properties. Sandalwood oil is a pale yellow to yellow viscous liquid, possessing sweet, fragrant,

persistent, spicy, warm, woody, milky and nutty notes. These properties of the oil are due to α-santalol and β-santalol, which are the major sesquiterpenes, but the α-isomer predominates. It is used as a fixative and highly valued in the perfumery, cosmetics and pharmaceutical industry; especially, for certain delicate scents those are extremely rare and fragile. Sandalwood oil serves as an ingredient and is added in ample amounts in most of the heavy or oriental perfumes. Most Indian *attars* use this oil as the base because of its inherent capacity to absorb most of the ethereal notes of other whole herbs or flowers, as it can enhance their perfumery status and stability. Being popular as the most precious perfumery material since ancient times, sandalwood oil has still retained its importance, popularity and demand in perfume industry. It is used in aromatherapy as it relieves stress. US-FDA, Flavor and Extract Manufacturers' Association, Council of Europe and Joint FAO/WHO Expert Committee on Food Additives have approved the use of sandalwood oil as food ingredient.[36] It is used as a flavoring substance in frozen dairy desserts, candy, pan masala, baked food, gelatin, puddings and also in alcoholic and non-alcoholic beverages at use levels generally below 0.001% (10 ppm) except in hard candy. The highest maximum use level for sandalwood oil in food products is approximately 90 ppm. Sandalwood oil is generally used as a natural flavoring substance or in conjunction with other flavor ingredients.

Sandalwood oil has been mentioned in Indian system of medicine (Ayurveda), Chinese and Tibetan medicinal systems for its therapeutic effects[18] and has acquired an important place in the indigenous system of medicines. In Ayurveda, sandalwood oil is largely used as a demulcent, diuretic and mild stimulant.[37] It is used in the treatment of common colds, bronchitis, fever, dysentery, piles, scabies and infection of the urinary tract, inflammation of the mouth and pharynx, liver and gall-bladder complaints and as an expectorant, stimulant, carminative, digestive and as a muscle relaxant.[36] A recently conducted *in vitro* study has shown that sandalwood oil is effective on methicillin-resistant *Staphylococcus aureus* (MRSA) and antimycotic-resistant *Candida* species.[38] In another study, a crude methanolic extract as well as isolated compounds of sandalwood oil (α-, β-santalol and their derivatives) showed promising anti-bacterial activity against the antibiotic resistant strain of *Helicobacter pylori*, a Gram-negative bacterium which is strongly linked to the development of duodenal, gastric and stomach ulcers and is also a risk factor in the

development of gastric cancer.[39] The anti-bacterial properties of five extracts (*in vitro* samples, that is, callus, somatic embryo and seedlings, and *in vivo* samples from leaves of non-oil yielding young and oil-yielding matured trees) were compared with sandalwood oil by screening against nine Gram-negative and five Gram-positive bacterial strains by disc diffusion, agar spot and TLC bioautography methods. Minimum inhibitory concentration (MIC) for sandalwood oil was determined to be in the range of 0.078–5 μg/mL for most of the test micro-organisms screened, but also revealing that the Gram-negative bacterium *Pseudomonas fluorescens* and the Gram-positive bacterium *Micrococcus flavus* being resistant to it.[40] Among the extracts screened, the somatic embryo extracts showed the strongest anti-bacterial activity comparable only with sandalwood oil and matured tree leaves' extract. F. Benencia *et al*. have demonstrated that sandalwood oil possessed dose-dependent anti-viral activities against HSY-l and HSY-2, more significant against HSY-l.[41] It was concluded that the oil was not virucidal, thus indicating that it affected the replication of the virus in treated cells. Recent data have shown that sandalwood oil exerts a modulatory influence on mouse hepatic glutathione *S*-tranferase (GST) activity. Mice orally fed with the oil, exhibited an increase in GST activity in time- and dose-responsive manners. In addition, an increase in acid-soluble sulphydryl levels in the hepatic tissue of these mice was also observed, suggesting a possible chemopreventive action of sandalwood oil against carcinogenesis.[42] Additionally, Palamara *et al*.[43] have reported an anti-viral activity of glutathione, which inhibit the *in vitro* replication of HSV-1. Thus, it can be speculated that the anti-viral activity of sandalwood oil against HSV could be an indirect effect of its reported modulatory influences on cellular glutathione *S*-transferase (GST) activities and acid- soluble sulphydryl levels. Sandalwood oil elevates pulse rate, skin conductance level and systolic blood pressure and brings about higher ratings of attentiveness and mood in humans.[44] Kulkarni *et al*. demonstrated anti-hyperglycemic and anti-hyperlipidemic effect of pet ether extract of *S. album* oil in streptozotocin induced diabetic rats.[45] Treatment of diabetic rats with the *S. album* fraction for 60 days demonstrated reduction in blood glucose level by 140 mg/dl. Metformin treated group showed a decrease in blood glucose by 70 mg/dl, as against an increase in diabetic control group by 125 mg/dl. Total cholesterol (TC), low-density lipoprotein (LDL) and triglyceride (TG) levels were decreased by 22, 31 and 44%, respectively, in treated diabetic rats,

whereas, cardio-protective, high-density lipoprotein (HDL) increased by 46%. In case of Metformin, the values were 11, 29 and 15% respectively, while HDL increased by 7%. Significant improvement in atherogenic index from 267 to 139% was observed in treated rats.

1.1.4.2. Methods of Extraction:

Sandalwood oil is extracted from the heartwood (in stem and roots) of the sandalwood tree. At the time of harvest, all of the commercially utilized sandalwoods are pulled from the ground along with roots, the upper limbs are cut and bark removed. The logs obtained are dressed to get rid of the sapwood, which is devoid of any oil and thus has very little economic importance. The logs are chopped into chips and billets, and further ground to a powder, which is subjected to down-stream processing. Oil is harvested from the heartwood powder by several techniques, which have their own advantages over the other.

A) Steam distillation:

The ground wood is distilled by either hydro- or steam-distillation to produce neat oil. Hydro-distillation is done with Clevenger's apparatus, wherein the plant material is boiled along with water and essential oil is distilled out with steam. In steam-distillation, steam is passed through plant material, to distill the oil with steam. The oil that floats on water is then separated.

B) Solvent extraction:

The sandalwood powder is soaked in organic solvents such as *n*-hexane, methanol, and ethyl acetate and agitated for several hours. The mass is then filtered out and the solvent extract is concentrated to get the oil.

C) Supercritical liquid CO_2 extraction:

Extraction by means of carbon dioxide in the supercritical state (SFE) is a good technique for the production of essential oils from plant material. Conventional processes such as distillation and solvent extraction often require additional steps, and are usually inferior to CO_2 with respect to selectivity. In addition, the lower temperature in the SFE avoids thermal degradation; also the low water content limits hydrolytic processes. Therefore, volatile oils obtained by SFE are devoid of fatty acids, resins, waxes and coloring matters normally present in vegetable matter and co-extracted by

conventional solvent extraction, and exhibit a scent more similar to the original source.[46] Compressed CO_2 is safe, non-toxic, non-combustible, inexpensive and its critical temperature and pressure are not high, 31.06 °C and 73.825 bar.[47] As reported by B. Marongiu *et al*., the main difference between oil obtained from SFE and hydro-distillation (HD) of *S. album* was the content of required oxygenated compounds, which were higher in the SFE product (95.8 vs 86.9%), from the identical sources.

1.1.5. Santalol biosynthesis:

Sandalwood oil is a perfect blend of mono- and sesqui-terpenoids, which are secondary metabolites biosynthesized by plants. The major constituents of sandalwood oil are the hydroxylated sesquiterpenes such as (*Z*)-α-santalol, (*Z*)-α-bergamotol, (*Z*)-β-santalol and (*Z*)-*epi*-β-santalol. Other minor sesquiterpenes, which are detected from GC-EI-MS analysis of the oil, are (*Z*)-lanceol, (*E*)-nuciferol and precursor hydrocarbons such as, α-santalene, *exo*-α-bergamotene, *epi*-β-santalene, β-santalene, β-curcumene, α-curcumene, γ-curcumene and β-bisabolene.

Sesquiterpenes constitute a class of natural products, which are formed from the acyclic diphosphate precursor, farnesyl diphosphate (FPP), which in turn is formed by repetitive head to tail (also called 'regular') condensation of three isoprenoid units [one unit of dimethylallyl diphosphate (DMAPP) and two units of isopentenyl diphosphate (IPP)]. The first committed step in the biosynthesis of santalenes involves ionization of FPP and concomitant cyclization of the resulting carbocation in presence of santalene synthase (*SaSS*). These sesquiterpene hydrocarbons undergo hydroxylation at *cis*-methyl group of side chain, which is catalyzed by cytochrome P450, monooxygenase systems to form santalols (Scheme 1.1.1). Enzymes involved in the biosynthesis of santalenes and santalols are expressed at the transition zone of heartwood and sapwood. Mechanism involved in cyclization of FPP to several sesquiterpenes including santalenes has been described in detail in Chapter 3 of this thesis.

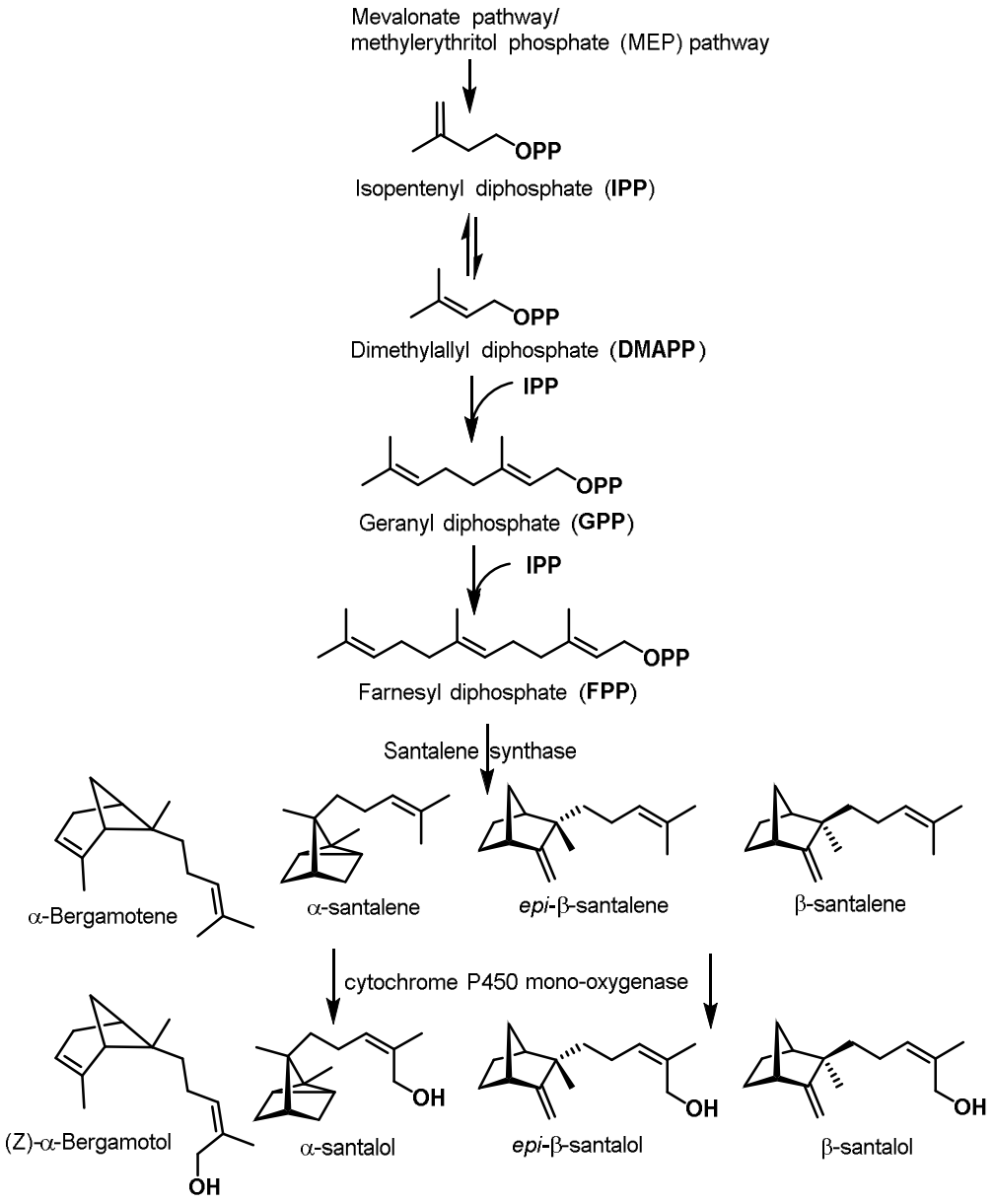

Scheme 1.1.1. Biosynthesis of sesquiterpenoid alcohols in sandalwood.

1.1.6. Pharmaceutical importance of Santalols and their derivatives:

1.1.6.1. Biological importance of α-santalol and β-santalol:

(*Z*)-α-Santalol constitutes 50-60% of the terpene content in sandalwood oil from a well matured tree and is an active component responsible for the fragrance and medicinal properties exhibited by the oil. Studies reported that topical application of (*Z*)-α-santalol (5%, w/v) showed significant chemo-preventive effects on 7,12-dimethylbenzanthracene

(DMBA)-initiated and 12-*O*-tetradecanoylphorbol-13-acetate (TPA)-promoted skin cancer development, and inhibited ornithine decarboxylase (ODC) activity and DNA synthesis induced by TPA in both CD-1 and SENCAR mice.[48] Furthermore, (*Z*)-α-santalol (5%, w/v) application significantly inhibited UVB-initiated and TPA-promoted, DMBA-initiated and UVB-promoted, and UVB-initiated and UVB-promoted skin tumorigenesis in SKH-1 hairless mice, and also suppressed UVB-caused induction of epidermal ODC activity in SKH-1 mice.[49] Dose-response experiment indicated that 5% of (*Z*)-α-santalol (w/v) application resulted in a relatively higher inhibition of skin tumorigenesis induced by UVB in SKH-1 mice.[50] Both *in vivo* and *in vitro* models suggested that one of the possible mechanisms of its chemo-preventive effects is related to induction of apoptosis through both extrinsic and intrinsic pathways.[51,52] Zhang *et al*. studied effects of (*Z*)-α-santalol in G2/M phase arrest and described detailed mechanisms of G2/M phase arrest by this agent. The data demonstrated that treatment with (*Z*)-α-santalol resulted in a concentration- and time- dependent inhibition of cell viability on A431 cells and UACC-62 cells as determined by MTT assay. Treatment with (*Z*)-α-santalol (50 μM) for 12 h did not significantly decrease cell viability of A431 and UACC-62 cells. However, flow cytometric analysis of cell cycle distribution revealed that (*Z*)-α-santalol (50-75 μM) from 6 h to 24 h treatment led to a 49%-285% and 71%-306% induction of G2/M phase in A431 cells and UACC-62 cells, respectively, as compared to control cells. These findings indicated that G2/M phase cell cycle arrest induced by (*Z*)-α-santalol treatment may be one of the mechanisms which resulted in a decrease of cell viability in A431 and UACC-62 cells after (*Z*)-α-santalol treatment.[53]

As mentioned previously, (*Z*)-α-santalol showed moderate cytotoxic activities against HL-60 cells, but exhibited negligible effect on TIG-3 cell growth even at a concentration of 40 μM.[54] Effects of (*Z*)-α- and (*Z*)-β-santalols on selected CNS parameters were studied by Okugawa H. *et al*.[55] On intraperitoneal (*i.p.*), oral and/ or intracerebroventricular (*i.c.v.*) administration to mice, (*Z*)-α-santalol showed better effects on hypothermia and reduction in spontaneous locomotor activity than (*Z*)-β-santalol, while (*Z*)-β-santalol had better analgesic activity than (*Z*)-α-santalol. Both compounds produced the same effects on hexobarbital-induced sleeping time by *i.p.* administration (50 mg/kg) that was almost the same as that of Nitrazepam at 5 mg/kg. (*Z*)-α- and (*Z*)-β-santalols

reduced both Methamphetamine and Apomorphine-induced activities. However, hypnosis, muscle relaxation, reversal of reserpine-induced hypothermia and anti-convulsive effects were not produced by (*Z*)-α- and (*Z*)-β-santalols in mice.

The *in vivo* anti-hyperglycemic and anti-oxidant experiments were conducted in alloxan-induced diabetic and D-galactose mediated oxidative stress induced male Swiss albino mice models, respectively, by Misra B. B. *et al*.[56] Administration (*i.p.*) of (*Z*)-α-santalol (100 mg/kg BW) and sandalwood oil (1 g/kg BW) for a week, modulated parameters such as body weight, blood glucose, serum bilirubin, liver glycogen, and lipid peroxides content to normoglycemic levels in the alloxan-induced diabetic mice. Similarly, administration of (*Z*)-α-santalol (100 mg/kg BW, *i.p.*) and sandalwood oil (1g/kg BW, *i.p.*) for two weeks altered parameters such as serum amino transferases, alkaline phosphatase, bilirubin, superoxide dismutase, catalase, free sulfhydryl, protein carbonyl, nitric oxide, liver lipid peroxide contents, and antioxidant capacity in D-galactose mediated oxidative stress induced mice. It was also observed that the other terpene components of sandalwood oil had synergistic effects on the beneficial activity exhibited by (*Z*)-α-santalol, thus demonstrating an enhanced activity with the traditionally used natural resource.

The anti-influenza A/HK (H3N2) virus activity of (*Z*)-β-santalol was evaluated in MDCK cells and the effect of (*Z*)-β-santalol on synthesis of viral mRNAs was investigated.[57] (*Z*)-β-Santalol was investigated for its anti-viral activity against influenza A/HK (H3N2) virus using a cytopathic effect (CPE) reduction method. It exhibited anti-influenza A/HK (H3N2) virus activity of 86% with no cytotoxicity at the concentration of100 μg/mL, by reducing the formation of a visible CPE. Oseltamivir, marketed anti-viral drug, also showed moderate antiviral activity of about 83% against influenza A/HK (H3N2) virus at the concentration of 100 μg/mL.

1.1.6.2. Phytochemicals from *S. album*:

The oil of *S. album* shows a complex mixture of closely related terpenoids consisting of over 12 mono- and 90 sesqui-terpenoids.[12,58,59] Good quality sandalwood oil extracted from a matured tree contains the major components, (*Z*)-α-santalol (50- 55 %), and (*Z*)-β-santalol (25-30 %),[60] when the total sesquiterpenoid alcohol content is >90%. Apart from these sesquiterpenes, several minor compounds belonging to different classes have been isolated

and reviewed in literature.[12] Derivatives of santalols are reported to exhibit more potent pharmaceutical activities in comparison to their precursors.

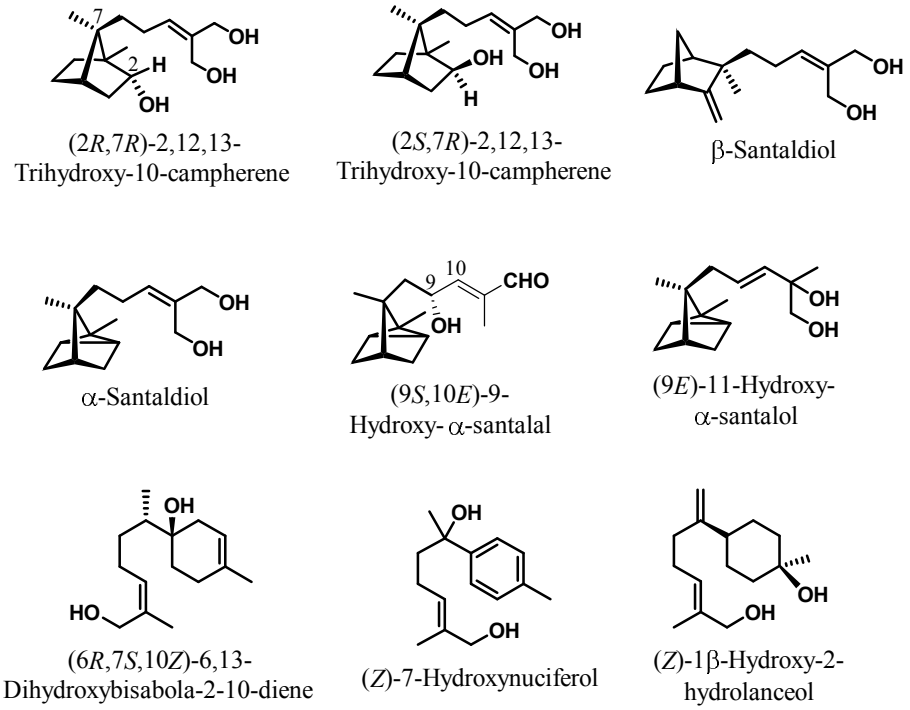

Figure 1.1.2. Sesquiterpenoids exhibiting various biological activities isolated from sandalwood.

Kim *et al*.[58] studied the antitumor effects of the purified constituents from *S. album* of Indian origin *in vitro* and *in vivo*. The inhibitory effects of the isolates on EBV-EA activation induced by 12-*O*-tetradecanoylphorbol-13-acetate (TPA), which is a short-term *in vitro* screening method frequently used to survey possible antitumor promoters in nature were assessed. (2*R*,7*R*)-2,12,13-Trihydroxy-10-campherene, (2*S*,7*R*)-2,12,13-trihydroxy-10-campherene and β-santaldiol among the tested compounds showed a remarkable inhibitory effect on EBV-EA activation with 63.9, 62.3 and 61.8% inhibition, respectively, at a concentration of 500 mol ratio/TPA, preserving high cell viability. These activities were comparable to (-)-epigallocatechin gallate (EGCG), which is a well-known anti-tumor promoting polyphenol from green tea[61] and was used as a positive control in the assay. *In vivo* studies on suppression of two-stage mouse skin carcinogenesis induced by 7,12-dimethylbenz-anthracene (DMBA) as an initiator and TPA as a promoter, (2*R*,7*R*)-2,12,13-

trihydroxy-10-campherene, β-santalol and β-santaldiol showed potent activities. In comparison to the controls, where 100% of the mice bore papillomas after 10 weeks of promotion, treatment of above three santalol derivatives along with the initiator and promoter reduced the percentages of tumor-bearing mice to 33.4–46.7% even at 15 weeks. Among these compounds, (2*R*,7*R*)-2,12,13-Trihydroxy-10-campherene had the most potent activity, reducing the incidence to 86.6% over 20 weeks (Figure 1.1.2).

Anti-*Helicobacter pylori* activities of santalol derivatives isolated from sandalwood were tested against the antibiotic resistant strain TS281 by Ochi T. *et al*.[39] From the MIC values of all isolated sesquiterpenes tested, (*Z*)-α-santalol, (*Z*)-β-santalol and α-santaldiol proved to be potent against tested strain with α-santaldiol being the most potent (Figure 1.1.2).[39]

Matsuo *et al*. evaluated the isolated α-santalol derivatives for their cytotoxicity against HL-60 tumor cells and TIG-3 normal cells.[54] (9*S*,10*E*)-9-hydroxy-α-santalal showed cytotoxicity against HL-60 cells as high as cis-platin, with an IC_{50} value of 2.2 ± 0.23 μM, whereas (*Z*)-α-santalol, α-santaldiol, and (9*E*)-11-hydroxy-α-santalol showed moderate cytotoxicities against HL-60 cells with IC_{50} values of 13.8 ± 0.97 μM,11.1 ± 0.19 μM and 21.3 ± 0.51 μM, respectively (Figure 1.1.2). These compounds had negligible effects on TIG-3 cell growth even at a sample concentration of 40 μM.

1.1.7. Purification techniques of Santalols and quality assessment:

As previously discussed, (*Z*)-α-santalol, (*Z*)-α-*trans*-bergamotol, (*Z*)-*epi*-β-santalol and (*Z*)-β-santalol constitute >90% of the total terpene content of sandalwood oil, whereas, the sesquiterpene hydrocarbon precursors, α-santalene, α-bergamotene, *epi*-β-santalene and β-santalene form a minor portion of the oil (~ 5%). Of these, (*Z*)-α- and (*Z*)-β-santalol are accountable for fragrance and medicinal properties demonstrated by the oil. These two sesquiterpene alcohols exhibit closely matching physical properties due to similarity in skeleton, geometry of the olefin and stereochemistry around all the chiral centers, which make quantitative separation of these two isomers a tedious task. Conventional techniques such as column chromatography and distillation methods did not provide promising results in the separation of santalenes and santalols. Sandalwood oil obtained from sandalwood by previously mentioned methods is subjected to various techniques for isolation and

purification of santalenes and santalols. Generally, α- and β-santalenes and (*Z*)-α- and (*Z*)-β-santalols are separated by repeated fractional distillation. In fractional distillation, extreme care has to be taken to regulate the temperature, else the two sesquiterpene hydrocarbons and alcohols show a tendency of distilling as a constant boiling mixture.[62] Further, if the fractionating column is inefficient, the separation of the two isomers will not be effective. Vacuum distillation of sandalwood oil was carried out by Dwivedi C. *et al*. to obtain a fraction containing (*Z*)-α-santalol (boiling point 95°C at 0.5 mm Hg) in major, which was ascertained by GC-MS data and boiling point determinations.[48] The fraction contained ~61% (*Z*)-α-santalol and ~28% of another isomer, thus demonstrating only partial purification of (*Z*)-α-santalol. Successive purification techniques were applied by Okugawa H. *et al*. for above purification.[55] The crushed sandalwood was extracted with benzene, which was subsequently chromatographed over silica gel using benzene-ethyl acetate (20:1) to give three fractions. Fraction no. 2 (300 mg) was subjected to HPLC separation to afford (*Z*)-α-santalol (155 mg; 1.2%) and (*Z*)-β-santalol (76 mg; 0.6%), using *n*-hexane-diethyl ether (100:17.5) at 1.5 mL/min on μ-Bondasphere (19mm × 150 mm) column with detection at UV 226 nm. Kim T. H. *et al*. partitioned the methanolic extract of sandalwood chips to get a fraction containing terpenes.[58,63] This was further fractionated over silica gel using a stepwise gradient of *n*-hexane/ ethyl acetate. A fraction eluting at *n*-hexane/ ethyl acetate, 3:2 was subjected to reversed phase preparative HPLC using 40% CH_3CN to yield partially purified terpene alcohols which were further purified by preparative normal phase HPLC to get the required compounds, but, with poor yields. Modern techniques such as preparative HPTLC were also employed for a small-scale purification of santalols.[56] In spite of the sophistication of the techniques employed, quantitative purification of santalol congeners still remains an unexplored territory. Therefore, development of a method for quantitative separation and purification of (*Z*)-α- and (*Z*)-β-santalols and santalenes need attention.

Over the past few years, natural *S. album*[17,64] resources around the world continue to decline due to complex cultivation requirements, long growth periods and continuous harvesting (particularly from illegal poaching and smuggling), combined with limited plantation. Contradictorily, the demands and prices of sandalwood continue to increase, thereby promoting the adulteration of the original stocks with low quality oils from related

sandalwood species. With such a change in the source materials, there is a continuing demand for methods to determine the quality of heartwood and oil products. The most obvious of the quality factors to be monitored are heartwood oil yields and levels of santalols in the oil. Accurate determination of sandalwood oil yield and quality is an important part of its international trade, since these factors decide its market value. Sandalwood oil, being an important export commodity is highly sought after in international market, and tends to be adulterated by various adulterants which do not alter the odour of the oil; common adulterants being low grade cost-effective, viscous oils and synthetic or semi-synthetic substitutes such as Sandalore.[34,65] The frequent adulterants reported include castor oil, cedarwood oil and low-grade oil from 'sandalwood' species other than *S. album*.[34] The most common adulterant is the castor oil (botanical name *Ricinus communis* of the family *Eurphorbiacae*). Adulteration of sandalwood oil is a serious problem for regulatory agencies and oil suppliers. As per the directives and norms laid down by various competent authorities such as, ISO, good quality sandalwood oil should not contain lower than 90% (w/w) of (free) alcohols, calculated as santalols; in particular, (*Z*)-α-santalol falling in the range of 41–55%, while (Z)-β-santalol in 16-24% range.[66]

There have been various techniques developed and recommended, of which every method has its own advantages over the other. Acetylation methods described to quantify the santalol content of sandalwood oil, generally lack specificity and accuracy and cannot distinguish among the santalol isomers. There is an increasing demand for the development of a new, rapid, and non-destructive method instead of traditional, time consuming and expensive analysis techniques. Application of Near Infrared (NIR) spectroscopy combined with chemometric techniques for determination of authenticity of the oil and for a very precise estimation of extent of adulteration of sandalwood oil with a common adulterant castor oil has been described by Saji Kuriakose *et al*.[67] Multivariate analyses like Principal Component Regression (PCR)[68] and Partial Least Square Regression (PLSR)[69] have been applied to NIR spectrometry for quantitative analysis to extract vital information through non-destructive methods.

Sandalwood oil can also be evaluated by gas chromatography (GC) coupled simultaneously or separately with FID (flame ionization detector) and MS (mass

spectroscopy) detectors. Howes *et al*.[70] reported a qualitative analysis of several trade samples of sandalwood oil, made available from market and different exporters. Relative percentages of santalols were determined from the integration of GC-FID responses to assess the quality of all the samples and identification of the peaks was supported from MS data. But the technique used was relative and did not specify about the quantitative santalol contents of oils and is therefore not very reliable as the adulterants used in the marketed samples may not necessarily resolve from the desired peaks and thus will not give an exact extent of contamination present in the adulterated oil sample. In another attempt to quantify the santalol content in sandalwood oil, Danilo Sciarrone *et al*.[71] applied a multidimensional gas chromatography (MD-GC) equipped with simultaneous flame ionization detector and mass spectrometry (FID/MS) to the analysis of a series of sandalwood oils of different origin. This approach was used to resolve all the components of the oil and to determine LoD (MS) and LoQ (FID) values of (*E*,*E*)-farnesol that was considered as the representative of all the oxygenated sesquiterpenes present in the oil considering the unavailability of other standard compounds in the market. A four-point standard graph of (*E*,*E*)-farnesol was constructed which was used to quantify the santalol contents of all the oil samples analyzed. Shellie *et al*. used GC × GC–FID and GC×GC–MS (a time-of-flight system) for the characterization of eight important constituents, namely (*Z*)-α-santalol, *epi*-α-bisabolol, (*Z*)-α-*trans*-bergamotol, *epi*-β-santalol, (*Z*)-β-santalol, (*E*,*E*)-farnesol, (*Z*)-nuciferol, and (*Z*)-lanceol.[72] Quantitative analysis method is advantageous over the qualitative approach as an exact concentration of santalols can be estimated and the oil can be graded according to the norms of standard organizations. We, in our current work have constructed the calibration curves of the purified major components of the oil and developed an efficient, feasible GC-based method to determine the adulteration of sandalwood oils.

1.1.8. Silver nitrate adsorbed on silica gel - efficient stationary phase for purification of olefins:

Olefin containing substances possess an interesting property to form compounds of relatively low stability with halogens and metal ions, which are appropriately termed as "addition" or "coordination" compounds. The examples of compounds belonging to the

coordination type are the complex salts of hydrocarbons with aluminium and ferric chlorides, the loose addition compounds of olefins with hydrogen bromide, of the type $C_2H_4 \cdot HBr$; with zinc chloride, of the type $C_5H_{10} \cdot ZnC1_2$ and the addition compounds of aromatic hydrocarbons with nitro compounds. Due to their complex forming properties, metal ions such as Cu (I), Ag (I), and Hg (II) salts are used for absorbing olefins.[73] Lucas H. J. and co-workers[74] extensively studied the complexation between silver ion and a number of unsaturated compounds by the distribution method and concluded that complex formation with aqueous silver ion is a general property of compounds possessing an olefin. Silver ions (Ag^+) were derived from either silver perchlorate, or silver nitrate. From different experiments conducted, it was found that the complex forming reactions were rapid and reversible in all cases studied. In an experiment to crystallize silver olefin complex, dicyclopentadiene was melted and stirred up with silver perchlorate to give white solid which was recrystallized from ethanol. The crystals exhibited slow darkening in light that proved the complexation of Ag^+ with the olefin. Reversible nature of this complex was demonstrated when practically the entire combined hydrocarbon was steam-distilled off easily. A structure was proposed for the ethylenic silver ion complex, according to which the ethylenic compound occupied one of the two coordination positions of silver by acting as the donor of an electron pair. A covalence joined the silver atom to one of the two carbon atoms, and a partial positive charge appeared on the other. Resonance involving two such bonded forms and an unbonded form was believed to account for the stability of the complex. Influence of structure of olefin on the silver complex was also studied, when it was concluded that the more buried the olefin is in a carbon chain of a compound, lesser is the value for K_0, where, K_0 is an equilibrium constant that signifies the stability of the silver-olefin complex. Thus, influence of structure on the stabililty of the complex was observed to be steric in nature. Nichols *et al*.[75] studied the argentation constants of methyl oleate (*cis*-isomer) and methyl elaidate (*trans*-isomer) for partitioning between isooctane as one phase and aqueous methanol as the other and concluded that the *cis*-isomer exhibited a greater argentation constant than the *trans*-isomer. Accordingly, it was recognized that a distribution of this type could be used as a basis for the separation of *cis*- and *trans*-isomers as well as for the separation of saturated and unsaturated fatty acid esters, in particular, or olefinic compounds, in general.

From above studies, it can be concluded that silver ions show differential affinity for olefins as they form association products or donor-acceptor π-complexes of weak interactions, wherein, organic compounds containing vinyl groups function as electron donors, and Ag^+ ions as electron acceptors. These interactions are developed by electron donation from the double bond to the vacant *s*-orbital of the silver ion, followed by donation of *d*-orbital electrons from the metal ion to the anti-bonding orbitals of the olefins.[74,76,77] Because the symmetry of these orbitals is not correct for interaction, these bonds are distinct, much weaker than those established in the formation of covalent bonds, unstable in nature, involve smaller heats of interaction and are in equilibrium with the free components.[78] The interactions proved to be favourable in chromatographic techniques as the original organic compound remained unaffected at the end of the separation and thus could be easily recovered in its original state. Silver ions are adsorbed on a solid support such as silica, which is inherently used in chromatographic separations, to result in 'argentized silica' and is used in 'argentation chromatography'. The technique of adsorbing Ag^+ ions on silica particles has evolved over a period of time and the Ag^+ adsorbed silica has been widely explored in separation methods such as thin layer chromatography (TLC), flash chromatography, medium pressure liquid chromatography (MPLC), high pressure liquid chromatography (HPLC), gas chromatography (GC), solid phase extraction (SPE) and is very well documented in literature. Argentation chromatography is being extensively utilized in separations of versatile classes of compounds such as steroids, pheromones, terpenes, fatty acids and their esters, lipids, metabolites, natural product and synthetic intermediates. Argentation chromatography can be used for the separation of geometrical isomers, and compounds with differences in unsaturations.

Thin layer chromatography (TLC) on silica gel impregnated with $AgNO_3$ was first used by Barrett *et al.*[79] and by Morris[80] to distinguish between saturated and unsaturated compounds. It was successively employed by several others for the separation of terpenes such as caryophyllene and β-selinene which are difficult to be separated by normal silica gel layers.[81] Sesquiterpenes and monoterpenes play a major role in flavours and fragrance industry and every component has its own characteristic odour. The isomers of a compound may have entirely distinct notes and therefore need purification before being used in a blend in fragrance industry. Thin layer chromatography of sesquiterpenes on silica gel-

silver nitrate, in conjunction with gas-liquid chromatography (GLC), has established its importance in the study of essential oils, both in identification of various components and analysis of their purity. Comparisons of retention capabilities of silver nitrate to silver perchlorate adsorbed silica, with and without gypsum, have been undertaken with a number of terpenes.[82] The results suggest that use of the perchlorate counter-ion in the absence of gypsum is the optimum combination for terpene separation. Gupta *et al*.[81] have reported an individual R_f study of the related compounds using specially prepared silver nitrate coated silica. Steroids,[83] sterol acetates[84] and their synthetic intermediates[85] were also separated by this method on the basis of their degree of unsaturation. Morris[80] and de Vries succeeded in separating methyl esters of oleic acid, linoleic acid and linolenic acid, which differed in the number of olefins. Furthermore, *cis-trans* isomers such as methyl oleate and methyl elaidate and their corresponding epoxy and hydroxy esters were also separated. The fractionation of synthetic mixtures of triglycerides and of natural oils and fats on silver nitrate plates, using eluting solvent mixture, such as carbon tetrachloride-chloroform-ethanol, was described by Barrett *et al*.[79] Since naturally occurring sterol mixtures or oils are composed of saturated, mono-, di-, and polyunsaturated sterols, silver nitrate adsorbent layers proved as a powerful tool in the analysis of steroids. Identification of steroids from snail's body was performed by the use of argentation TLC and other bonded phases that resulted in distinct bands for every steroid as compared to the earlier studies in which sterols were determined only as a single, mixed fraction when analyzed on normal phase silica gel layers.[86] Semi-preparative separation of fatty acid methyl esters (FAMEs) using two-dimensional TLC was achieved wherein, a part of layer was impregnated with urea (first dimension of development) and second part with $AgNO_3$ (second dimension). The FAMEs were separated according to the structure of the chain (branched) and also on the basis of number ofolefins.[87] Organic reactions which involve reduction of C=C double bonds or formation of geometric isomers are difficult to be monitored by normal silica TLC, as usually the separation among reaction components is poor and requires the application of more sophisticated techniques such as GC, HPLC or NMR. Silver nitrate coated TLC, although not capable of quantifying the results, can be used qualitatively as a quick and easy tool to govern such reactions.

On similar lines, the concept of argentation chromatography has been extended to quantitative separations using HPLC and MPLC methods which effect the separations yielding pure compounds on preparative scale. The separation of geometrical isomers is often difficult to achieve on a preparative scale using unmodified silica phase, when the acquisition of a single pure isomer may be important. In synthetic organic chemistry, it is difficult to synthesize the olefins (C=C) with absolute stereo-specificity and often result in a mixture of geometric isomers, separation of which is a tedious and time-consuming process. In synthetic organic chemistry, the *cis* and *trans* congeners of an intermediate exhibit different reactivity and selectivity, especially in case of compounds which are to undergo cyclization, and therefore arises the need to separate them before proceeding to subsequent steps. The substrates incubated with enzymes in biological assays must be pure isomers and must have a stereochemistry identical to that of the natural isomer, as the unnatural substrates either may not fit the active site pocket or may yield a different set of products.[88] In the field of insect pheromones in particular, isomer purity can be of highest concern and small amounts of contamination by an unnatural isomer may strongly modify the insect response. HPLC in the silver ion mode has been adapted for the analysis of positional and geometrical isomers of fatty acids, and especially for the determination of *trans* unsaturation in fats and oils,[89] for geometrical isomers of unsaturated acetates, aldehydes, hydrocarbons[90] and pheromones.[91]

The sequence of elution of geometric isomers was not consistent in argentation chromatography and was observed as a function of co-ordination of hindered olefins around the silver ions. As observed by Evershed R. P. *et al*., (*E*)-isomers eluted before (*Z*)-isomers in cases of 8-heptadecene, 9-nonadecene and (*E*)-7-methyl-6-nonen-3-one, but the trend had reversed for farnesenes, where the (*Z*)-isomers eluted prior to the (*E*)- in both the cases *viz*., (*Z*,*E*), (*E*,*E*) and (*E*,*Z*), (*Z*,*Z*) that covered the separation of all possible isomers of farnesenes.[92] Even in case of separation of farnesol isomers using preparative 1% silver nitrate silica TLC plate developed with hexane: ethyl acetate: methanol: acetone (7:1:1:1), demonstrated by Thulasiram *et al*., (*Z*,*E*)-farnesol showed lower retention (R_f = 0.40) in comparison to its all trans congener, (*E*,*E*)-farnesol (R_f = 0.30).[93] Argentation flash chromatography was applied for the separation of 13 olefinic mixtures, containing 32 steroids and triterpenoids on silica impregnated with $AgNO_3$ (10%).[94]

A general procedure for preparation of $AgNO_3$ coated silica gel employed for TLC, MPLC and HPLC, involves following steps:

i) A specific ratio of $AgNO_3$ to silica gel is decided and required quantities are weighed.

ii) $AgNO_3$ solution is prepared by dissolving it in distilled water or acetonitrile to which silica gel (230-400 mesh or grade-G) is added and is stirred well to make uniform slurry. Some authors have suggested grinding this mixture in a mortar.

iii) For TLC, this slurry is applied onto the plates by means of an applicator to make layers of uniform thickness. The plates are then dried at 110-150 °C in hot air oven for 1-2 h. These plates must be used within 2-3 days after its preparation or should be stored in dark to prevent them from turning brown, as a consequence of oxidation of Ag^+ ions which may decrease its activity. In another procedure, TLC plates pre-coated with silica gel were developed once with an aqueous solution of $AgNO_3$ (2.0 g) in distilled water (5 mL) and subsequently dried and activated by keeping in hot oven, as above.[94]

iv) For MPLC and preparative HPLC uses, above slurry is first dried by removing most of the water in vacuum on rotary evaporator and then dried at elevated temperatures (110-150 °C) to get dry silica coated with silver nitrate which is then used to pack the columns. In an alternative method of argentation, silica was impregnated with silver nitrate by passing 250 mL of a 0.5% (w/w) solution of $AgNO_3$ in methanol through a pre-packed dry silica column and then recycling 500 mL more of this solution overnight at the same rate. The column was finally rinsed by passing 200 mL of methanol.[95] The phases prepared with above method did not retain Ag^+ ions when most of it eluted out with successive passage of methanolic solution and thus produced less efficient columns for resolution of olefins. Fairly good results were obtained when $AgNO_3$ solution was prepared in acetonitrile instead of methanol. A minimum amount of acetonitrile was used for dissolving silver nitrate, and the solution was injected into the column followed by washing of column with *n*-hexane. Quantitative retention of silver salt on the silica gel surface could be achieved.[96]

Argentation chromatography has found some of the interesting applications in a variety of fields. It has been applied in 'solid-phase extraction' (SPE) technique for the separation of volatile aliphatic and aromatic hydrocarbons from crude oils and the versatility of the SPE method has been demonstrated by B. Bennett *et al*.[97] using a light

crude oil from the North Sea and a heavy crude oil from Orcutt field (Monterey, California, U.S.A.). Considering the volatility of aliphatic hydrocarbons, this method has been found to be advantageous in terms of recovery of the volatile fraction over column chromatography method as the later required solvent evaporation at certain stage, whereas, SPE frits could be easily washed with suitable solvent without evaporation of the volatiles. In argentation chromatography, the percentage of silver nitrate to silica gel varies from 2% to 40% (w/w) depending on the nature and difficulty of the separation among the compounds to be analyzed. In most of the cases, improvement in separation was observed with increase in percentage of $AgNO_3$ except a few, where it was unaffected. However, balancing a high cost of $AgNO_3$ with desired effective separation, the ratio generally ranged from 5% to 20%, although many authors have claimed repeated use of the same column without affecting the desired separation. Reusability of the stationary phase enhances economic viability of the process.

Section 1.2.

Preparative Separation of α- and β-Santalenes and (*Z*)-α- and (*Z*)-β-Santalols using Silver nitrate-Impregnated Silica gel Medium Pressure Liquid Chromatography

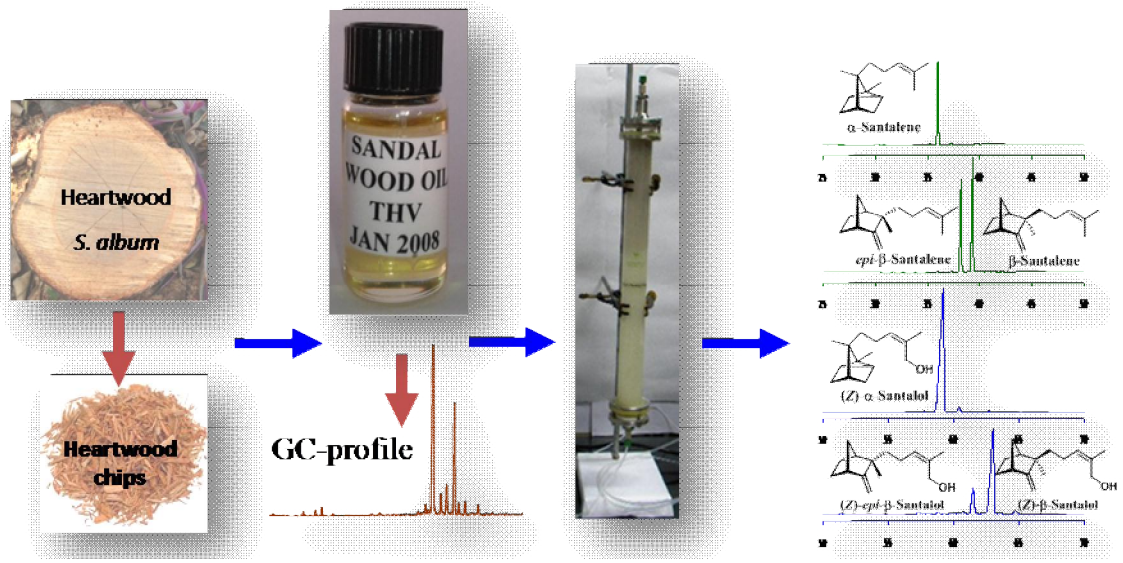

1.2.1. Rationale for present work:

The Indian sandalwood, *Santalum album* is known worldwide for its pleasant woody fragrance. The essential oil of sandalwood is widely used in aromatherapy, as an anti-depressant, anti-inflammatory, anti-fungal, astringent, sedative, insecticide, antiseptic and in sacred unguents.[36,42,98-101] The genes responsible for santalene biosynthesis are expressed at the transition zone of the sapwood and heartwood of *S. album*. The first committed step in santalol biosynthesis involves cyclization of farnesyl diphosphate (FPP) by santalene synthase to yield α- and β-santalenes, which will be converted to santalols by enzymes from cytochrome P450 system. The sesquiterpene alcohols (*Z*)-α-santalol (**1**) and (*Z*)-β-santalol (**2**) (Scheme 1.2.1) together constitute over 80% of heartwood oil obtained from the well matured tree.[102] Both **1** and **2** are responsible for most of the biological activities of the oil and have attracted increasing attention for their neuroleptic properties and chemo-preventive effects *in vitro* and *in vivo* bioassay systems.[39,49,50,52,58,98,103] Although several syntheses[104-110] of **1** and **2** are known, they are not economically viable and hence sandalwood oil remains as the sole source for these sesquiterpene alcohols. Attempts of purification of these sesquiterpenoids by conventional techniques such as fractional distillation or even modern techniques such as repeated extraction, column chromatography, gel-permeation chromatography and HPLC in a sequential manner did not yield quantitative results.[58,59,63] As such there is no efficient method reported so far, and therefore demands an effective methodology for the separation of santalenes and santalols. This work describes a quantitative separation of α-, β-santalenes and (*Z*)-α-, (*Z*)-β-santalols using preparative MPLC with $AgNO_3$ impregnated silica gel as the stationary phase and hexane and dichloromethane as mobile phases, respectively.

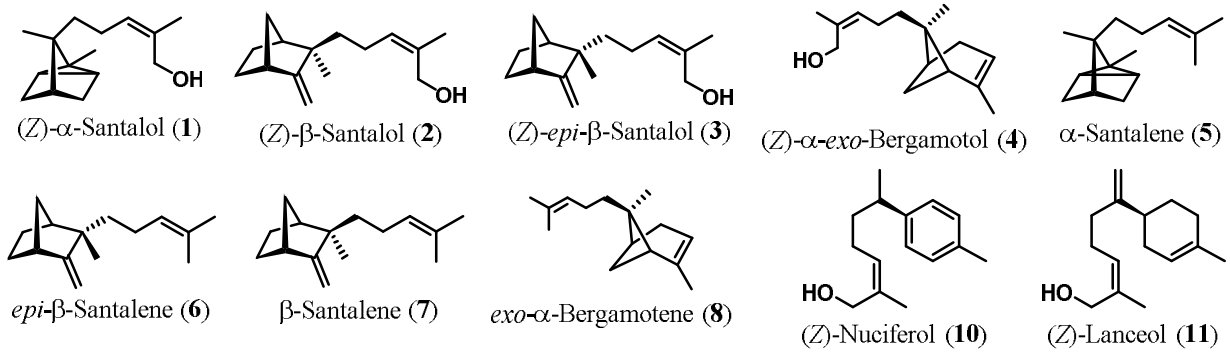

Scheme 1.2.1. Sesquiterpenes from sandalwood oil.

1.2.2. Present Work:

Indian Sandalwood, *Santalum album* is commercially exploited and highly acclaimed globally for its fragrant heartwood and the oil extracted from it. It is a small to medium-sized tree and yield of heartwood oil varies with the age, and is higher in older trees. The content of oil in a particular tree is also dependent on section of the tree; while it is highest in roots (~10 %), it decreases towards the tip. Sandalwood oil is a rich blend of mono- and sesquiterpenoids, which render it a typical pleasant, woody odour. These components form a complex mixture making the analysis and further purification of individual compounds an exhaustive task.

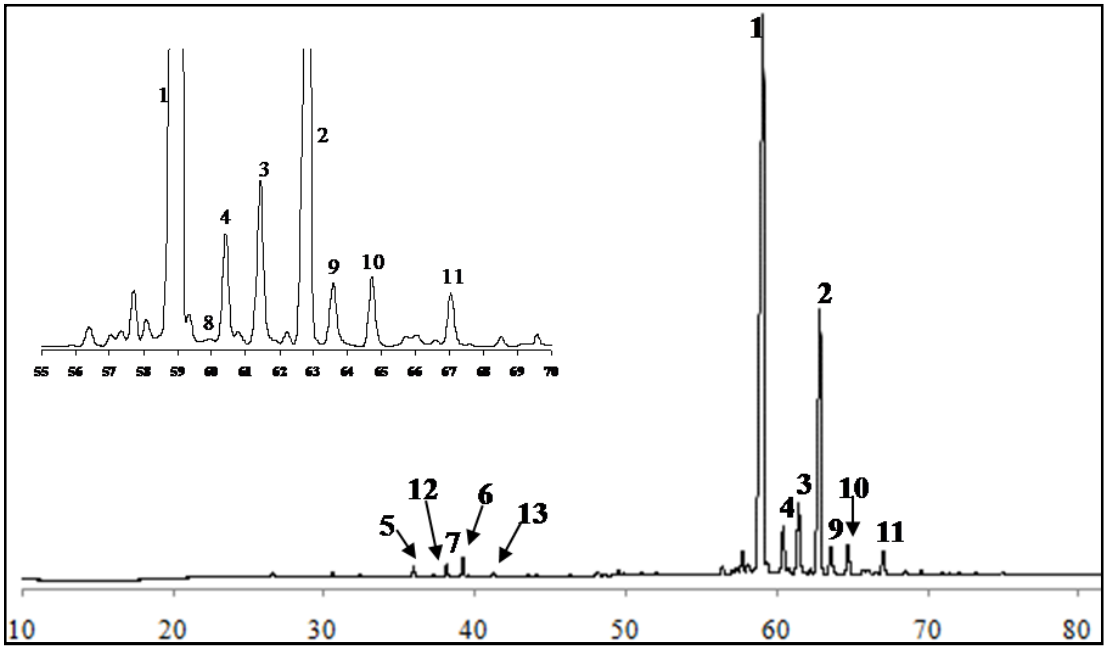

Figure 1.2.1. GC-FID traces of sandalwood oil using a HP-5 capillary column (30 m × 0.32 mm × 0.25 µm, J & W Scientific). Peak identification: **1**: (*Z*)-α-Santalol, **2**: (*Z*)-β-Santalol, **3**: (*Z*)-*epi*-β-Santalol, **4**: (*Z*)-*exo*-α-Bergamotol, **5**: α-Santalene, **6**: β-Santalene, **7**: *epi*-β-Santalene, **8**: (-)-α-Bisabolol, **9**: (*E*,*E*)-Farnesol, **10**: (*E*)-Nuciferol, **11**: (*Z*)-Lanceol, **12**: *exo*-α-Bergamotene, **13**: α-Curcumene.

Analysis of the GC chromatogram of sandalwood oil indicated that the santalol content [(*Z*)-α-santalol (**1**), (*Z*)-β-santalol (**2**) and (*Z*)-*epi*-β-santalol (**3**), and (*Z*)-α-*exo*-bergamotol (**4**)] was >80% (Table 1.2.1) and rest of the minor components constituted α-

santalene (**5**), β-santalene (**6**), *epi*-β-santalene (**7**), (*Z*)-α-bisabolol (**8**), (*E*,*E*)-farnesol (**9**), (*E*)-nuciferol (**10**), (*Z*)-lanceol (**11**), *exo*-α-bergamotene (**12**), and α-curcumene (**13**), (Figure 1.2.1). The terpene fraction was also analysed under identical conditions and was observed to contain the sesquiterpene hydrocarbons (**5**, **6**, **7**, and **12**) upto 65%, whereas the hydroxylated sesquiterpenes, santalols, constituted a minor portion (Figure 1.2.2). Sciarrone *et al*. successfully applied a multi-dimensional gas chromatographic system (MD-GC), equipped with simultaneous flame ionization and mass spectrometric detection (FID/MS) to the analysis of a series of sandalwood oils of different origin. In their investigation, they approximated (*E*,*E*)-farnesol as the representative of all sesquiterpene alcohols constituting the oil, to measure 'limits of detection' (LoD) relative to the MS detector and 'limits of quantification' (LoQ) relative to the FID detector, while emphasizing the use of multi-dimensional GC technique for better resolution of (*E*,*E*)-farnesol from santalols. In the present work, a method is developed to resolve all the terpene components of sandalwood oil using a simple set-up with a very routinely used GC-column, HP-5, installed in a GC coupled to FID, and ruled out the necessity of MD-GC to resolve the peaks in sandalwood oil.

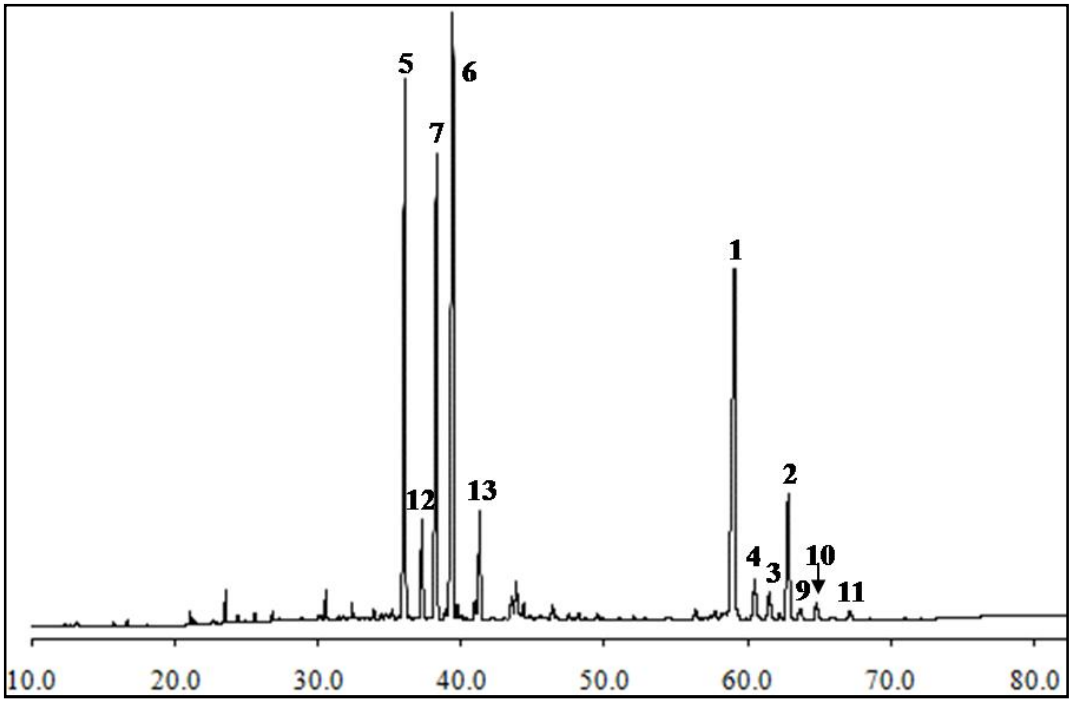

Figure 1.2.2. GC-FID traces of Sandalwood oil terpene fraction using HP-5 capillary column (30 m × 0.32 mm × 0.25 µm, J & W Scientific).

All the peaks of interest are resolved to base line and are confirmed by co-injection with the standards as well as by GC-MS analysis, under identical parameters. The oil extracted from the plants with heartwood formation of about 2 inches found at NCL campus, Pune (as explained in experimental section) was also analysed by GC-FID and was compared with that of the commercial sample. On comparison, both the samples were found to have similar total content of hydroxylated sesquiterpenes.

Table 1.2.1. Comparison of components of commercial Sandalwood oil (KSDL) and oil extracted from heartwood of sandalwood (Pune region). Components are arranged serially according to their retention time (R_t) in GC.

Sr. no.	Compounds	R_t (min)	Sandalwood oil (KSDL)	Sandalwood extract (Pune region)
1.	α-Santalene (**5**)	35.92	0.51 %	1.31 %
2.	(*Z*)-α-Bergamotene (**12**)	37.20	0.18 %	0.26 %
3.	*epi*-β-Santalene (**7**)	38.12	0.71 %	1.37 %
4.	β-Santalene (**6**)	39.20	1.11 %	1.84 %
5.	(*Z*)-α-Santalol (**1**)	59.31	54.24 %	49.19 %
6.	(*Z*)-α-*trans*-Bergamotol (**4**)	60.53	3.34 %	8.49 %
7.	(*Z*)-*epi*-β-Santalol (**3**)	61.57	4.95 %	3.79 %
8.	(*Z*)-β-Santalol (**2**)	63.03	19.20 %	25.26 %
9.	(*E*,*E*)-Farnesol (**9**)	63.79	2.10%	0.66%

After analysis of the oil samples, next task was the quantitative purification of individual components, for their structural characterization and application in further work. Although, several syntheses[104-110] are known for α- and β-santalenes and santalols, they are not economically viable due to lengthy synthetic procedures, poor yields and low enantiomeric purity of the products. Hence, sandalwood oil remains as the sole source for these sesquiterpene alcohols as large quantity of oil can be extracted from the trees and the natural isomers of the sesquiterpenes can be obtained. GC and GCMS analyses of the

commercial sandalwood terpene fraction contained the sesquiterpene hydrocarbons, α- and β-santalenes as the major components.

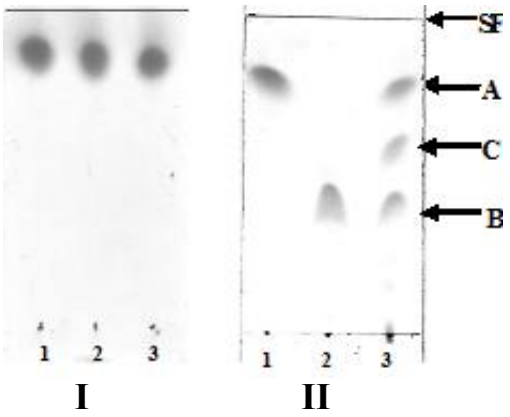

Figure 1.2.3. Thin-layer chromatography of α-santalene (**5**) (lane 1), β-santalene (**6**) (lane 2) and terpene hydrocarbons mixture (lane 3) on (**I**) normal silica gel (0% $AgNO_3$) and (**II**) silica gel impregnated with 5% $AgNO_3$, developed in hexane and hexane / ethyl acetate (9.85:0.15, v/v), respectively. On normal silica gel, α-santalene (**5**) (lane 1), β-santalene (**6**) (lane 2) and terpene hydrocarbons mixture (lane 3) migrated as a single spot (R_f 0.91). On 5% silver nitrate impregnated silica gel, α-santalene (**5**, R_f 0.92) (lane 1) and β-santalene (**6**, R_f 0.52) (lane 2) separated into spots A and B with *exo*-α-bergamotene (**12**) as spot C (R_f 0.73) (lane 3). The solvent front (SF) is shown on chromatogram.

The terpene fraction (20 g) was loaded on to a 100-200 mesh silica gel column (as described in experimental section) and sesquiterpene hydrocarbons could be eluted from the column using hexane, which on concentration under reduced pressure yielded terpene hydrocarbons (10.6 g). The column was further eluted with 10% ethyl acetate in hexane to obtain the sesquiterpene alcohols (9.4 g). Purification of sesquiterpenes was a difficult task, as α- and β-santalenes on one hand and α- and β-santalols on the other, possessed similar physical and chemical properties attributing to the very close structural similarities.

Efforts to individually purify α- and β-santalenes and (*Z*)-α- and (*Z*)-β-santalols from the above hydrocarbon or alcohol mixtures, respectively, using column chromatography with various column sizes and normal silica gel with varied particle sizes did not yield any fractions with pure α- or β-santalenes and (*Z*)-α- or (*Z*)-β-santalols. On

thin layer chromatography with normal silica gel, both santalene (R_f values 0.91, system I) and santalol (R_f 0.71, system III) congeners migrated as a single spot with different developing systems attempted (Figures 1.2.3 and 1.2.4). Taking advantage of their close boiling points, distillations at atmospheric as well as reduced pressures were carried out, but fractions with desired purity could not be obtained. Santalol benzoates could be separated by HPLC just to base line on reverse phase (C-18) analytical column, when eluted with methanol, but the separation was not sufficient for preparative HPLC and thus a quantitative separation could not be achieved.

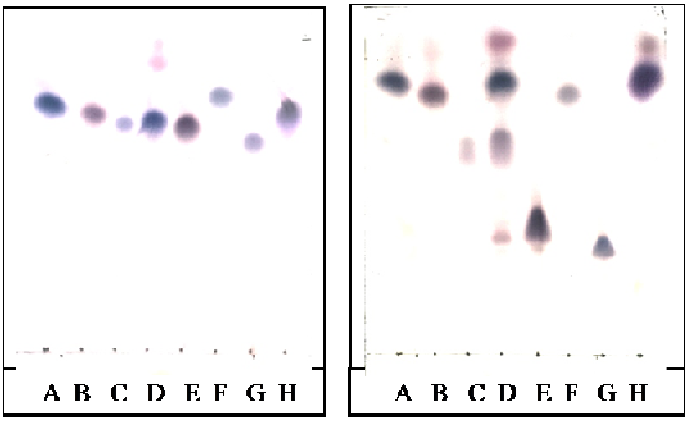

Figure 1.2.4. Thin-layer chromatography of (*Z*)-α-santalol (**1**) (A), (*Z*)-α-*trans*-bergamotol (**4**) (B), (*Z*)-β-santalol (**2**) (C), sandalwood oil (D), (*Z*)-lanceol (**11**) (E), α-bisabolol (**8**) (F), (*E*,*E*)-farnesol (**9**) (G) and (*Z*)-nuciferol (**10**) (H) on (**I**) normal silica gel (0% $AgNO_3$) developed in CH_2Cl_2 and on (**II**) silica gel impregnated with 5% $AgNO_3$ developed in 1.5% methanol in CH_2Cl_2. On normal silica gel sesquiterpenoid alcohols, from sandalwood terpene alcohol mixture (A-H) migrated as a single spot. On 5% $AgNO_3$ impregnated silica gel, (*Z*)-α-santalol (**1**, R_f 0.77), (*Z*)-α-*trans*-bergamotol (**4**, R_f 0.64), (*Z*)-β-santalol (**2**, R_f 0.39), (*Z*)-lanceol (**11**, R_f 0.25), α-bisabolol (**8**, R_f 0.73), (*E*,*E*)-farnesol (**9**, R_f 0.19) and (*Z*)-nuciferol (**10**, R_f 0.79) (lanes A-H, respectively) separated into different spots.

Various achiral esters such as acetates, benzoates, succinates and chiral esters with *N*-methyl proline, (*R*)-*O*-acetyl mandelic acid, (+)-(*S*)-Camphor sulphonic acid were synthesized and the separations were monitored on silica gel G-coated TLC plates

developed with different solvent systems that resulted in single spots for all the resultant products. The sesquiterpene alcohol mixture containing **1** and **2** as major components, when oxidized to their corresponding aldehydes using 'Swern oxidation' protocol, did show marginal difference in the R_f values on TLC, but exhibited poor stability when separated by column chromatography, and subsequently degraded with further processing.

Lucas and Nichols[74,75] studied the complexation of silver ions with alkenes and utilized silver nitrate for complexation, recrystallization and argentation chromatography, wherein, silver ions were adsorbed on the surface of silica gel particles. Different procedures in the preparation of silver nitrate coated silica and its applications in different areas of separation science are discussed in previous section. This technique of separation is often used to separate geometrical isomers of small molecules such as lipids, fatty acids, terpenoids and steroids, and is based on the interaction of Ag^+ ions with π-electrons of the double bonds.[93,111-113] Since, santalene and santalol congeners had different number of double bonds, these were expected to be separated easily using argentation chromatography. Consequently, when silver nitrate coated silica gel TLC plates were used, both **1** and **2** as well as **5** and **6** separated well with developing solvent systems II and IV, respectively (Figures 1.2.3 and 1.2.4). This formed the basis for development of MPLC method with silver nitrate impregnated silica gel as the stationary phase, for the quantitative separation of **1** and **2**, and **5** and **6**. In argentation chromatography, choice of solvent system made significant alterations in the separation of santalols, as they showed lesser separation with pet ether/ ethyl acetate system in comparison to system IV. 2 g of above hydrocarbon mixture consisting of **5** and **6** as major components was loaded on to a preparative MPLC column (as described in the experimental section). The column was eluted with hexane at a flow rate of 7.5 mL/ min and 10 mL fractions were collected till most of the hydrocarbons eluted from the column. The fractions were analyzed by silver nitrate impregnated silica gel TLC as well as by GC. The fractions containing pure **5** or **6** were pooled separately and concentrated. From 2 g of crude hydrocarbon mixture, 0.48 g of **5** (R_f 0.92, system II; R_t 35.92 min), 0.78 g of β-santalenes and 0.52 g of mixture of α- and β-santalene were obtained. The β-santalene fraction obtained from the column contained both **6** (R_f 0.52, system II; R_t 39.20 min) and **7** (R_f 0.52, system II; R_t 38.12 min) in the ratio of 58:42 (Figure 1.2.5). *Exo*-α-bergamotene (**12**) was obtained as a minor component on repetitive

purifications of the sesquiterpenes mixture eluted from the column. These compounds were characterized based on various spectral data (experimental section, Appendix 1) and the spectra were consistent with those reported previously.[114]

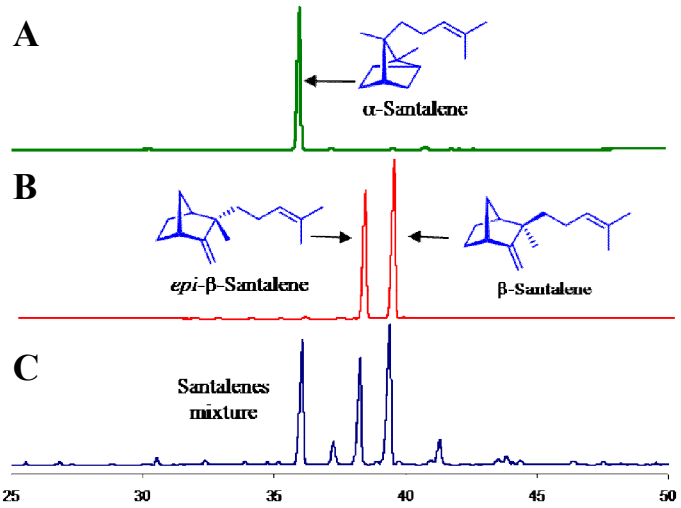

Figure 1.2.5. GC-FID traces of the purified santalenes from terpene fraction of Sandalwood oil. **A**: α-santalene (**5**); **B**: *epi*-β-santalene (**7**) and β-santalene (**6**); **C**: Sandalwood oil.

Further, 2 g of sesquiterpene alcohol mixture containing (*Z*)-α- and (*Z*)-β-santalols as the major components was subjected to the silver nitrate impregnated silica gel MPLC (as described in the experimental section) and the fractions (8 mL) were collected using dichloromethane (CH_2Cl_2) as eluent at a flow rate of 7.5 mL/ min. After TLC and GC analyses, the fractions containing pure sesquiterpene alcohols were pooled separately and concentrated. (*Z*)-α-*trans*-bergamotol (**4**) and (*Z*)-lanceol (**11**) were purified by repeated column chromatography. From 2 g of crude sesquiterpene alcohol mixture, 1.16 g of **1** (R_f 0.77, system IV; R_t 59.31 min), 0.52 g of **2** (R_f 0.39, system IV; R_t 63.03 min), 0.28 g of mixture of **1** and **2**, and minor quantities of **4** (R_f 0.64, system IV; R_t 60.53 min) and **11** (R_f 0.24, system IV; R_t 67.33 min) were obtained. GC and GCMS analyses indicated that, the fraction obtained for (*Z*)-β-santalol contained both **2** (R_f 0.39, system IV; R_t 63.03 min) and **3** (R_f 0.39, system IV; R_t 61.57 min) in the ratio of 87:13 (Figure 1.2.6). These alcohols were characterized based on various spectral studies (experimental section, Appendix 1) and the spectral data agreed with earlier reports.[110,115] The intensity of interactions between

sesquiterpenes and silver ions was dependent on the number of olefin groups present in the compounds and was directly proportional to the later. Sesquiterpenoids **1**, **2** and **11** possessing one, two and three olefins respectively, showed increasing retention trend on silver nitrate coated silica TLC plates, that was demonstrated from their decreasing R_f values 0.77, 0.39 and 0.24, respectively. Although, **4** and **2** possessed same number of double bonds, the later had lesser R_f value which highlighted another important fact that, these interactions were also dependent on the substitutions on the olefin, that is the steric environment around olefins. Similar pattern of elution was also observed in argentation column chromatography. Santalols or santalenes were completely eluted from the column with CH_2Cl_2 or hexane, respectively and the column was washed, equilibrated with three column volumes of appropriate solvents. The same silica packing could be used for next batch of purification that reduced the consumption of $AgNO_3$ coated silica gel and broadened the applicability of this process by making it economically viable for regular usage and for scale-up requirements. Argentation chromatography has proved a valuable technique for qualitative analysis as well as quantitative purification of terpenoids from sandalwood oil.

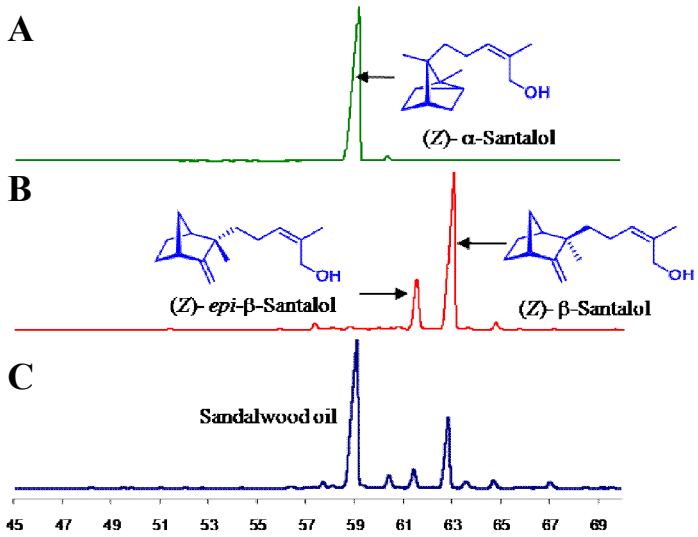

Figure 1.2.6. GC-FID traces of the purified alcohols from Sandalwood oil. **A**: (*Z*)-α-santalol (**1**); **B**: (*Z*)-*epi*-β-santalol (**3**) and (*Z*)-β-santalol (**2**); **C**: Sandalwood oil.

Section 1.3.

Quantification of Santalene derivatives from Sandalwood oil and its adulteration study.

The purified terpenoids find a variety of applications in perfumery, medicine, toxicology studies, cosmetics and quality control of sandalwood oil. Indian sandalwood oil due to its unique fragrance and medicinal properties is highly recognized and has always been in high demand in Indian as well as in international markets. The rising demand is a cause for its inflating price which in turn results from the depletion of natural resources due to uncontrolled felling, poor planning and management in plantation of newer strands, theft and smuggling, and spike disease. Due to rising demands, the cost of original stocks of sandalwood oil and its products has continuously showed a sharply rising trend. But, these higher prices are not affordable for the consumers. This creates a pressure on the suppliers and sellers as they have to find a way out to match the demands of the consumers with the rising market trends. The suppliers who are expected to maintain the high quality of their product, despite the reduced supply, find it difficult to cope up with the situation and resort to alternative ways, such as adulteration of the original products. The materials which are commonly used as adulterants in Indian sandalwood oil are low grade oils from other *Santalum* species, castor oil, cedarwood oil, and other viscous oils which do not significantly affect the original odour of sandalwood oil but can easily form a blend with it. Therefore, easy and quick methods need to be developed which can detect the level of adulteration and can keep a check on the quality of sandalwood oils marketed by several brands. Different methods employed for inspection of quality of sandalwood oil are reported in literature and are discussed previously.

In the present study, calibration curves for all the purified components of sandalwood oil *viz*., (*Z*)-α-santalol (**1**), (*Z*)-β-santalol (**2**) and (*Z*)-*epi*-β-santalol (**3**), (*Z*)-α-*trans*-bergamotol (**4**), α-santalene (**5**), β-santalene (**6**) and *epi*-β-santalene (**7**), (-)-α-bisabolol (**8**), (*E*,*E*)-farnesol (**9**), and (*Z*)-lanceol (**11**) were constructed. A ten point straight line graph was obtained for all the above mentioned sesquiterpenes when a constant volume from the serial dilutions of their standard stocks was injected in GC, and the FID responses for each component were plotted against the concentrations injected. All these compounds showed different FID detector responses as evidenced by different values for the slopes and intercepts of the calibration curves drawn for each compound. Using these standard curves the GC-FID quantification studies were carried out in similar conditions for commercial sandalwood oil and deliberate adulteration of commercial sandalwood oil with known

quantities of paraffin oil, coconut oil, and ethylene glycol (Table 1.2.2, Appendix 1). As anticipated, the measurements were in accordance with the content of the sesquiterpene alcohols in adulterated sandalwood oil and the percentage errors were within 5%.

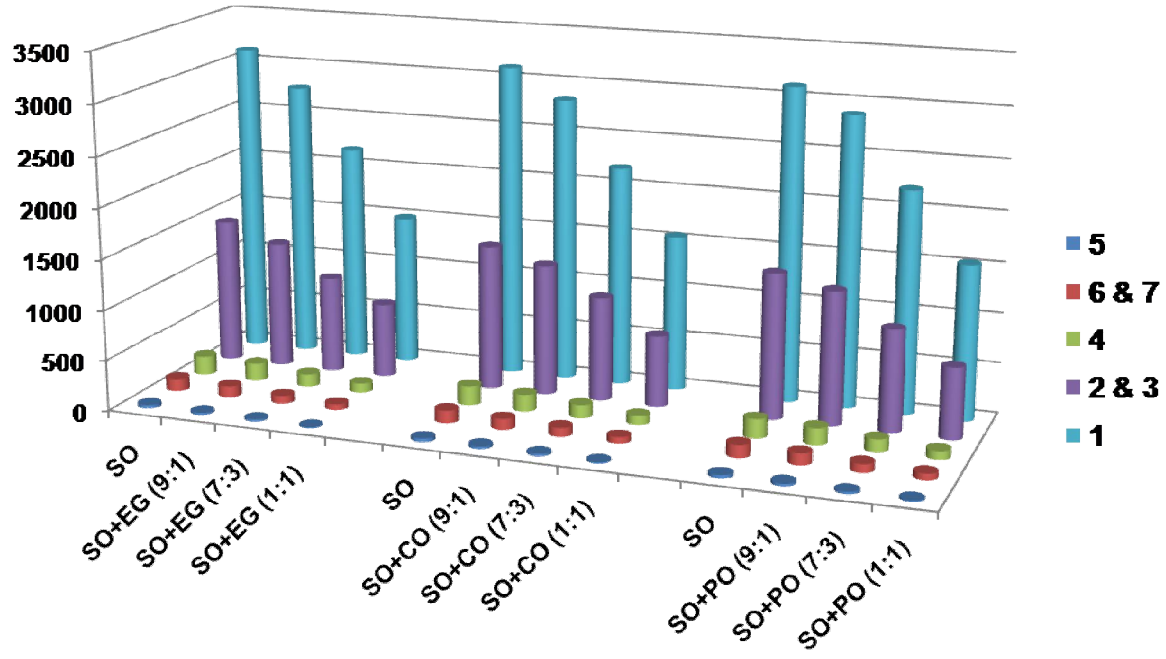

Figure 1.2.7. Quantification of adulterated samples of sandalwood oil.

Key: α-Santalol (**1**), β-Santalol (**2**), *epi*-β-Santalol (**3**), (*Z*)-α-*trans*-bergamotol (**4**), α-santalene (**5**), β-santalene (**6**) and *epi*-β-santalene (**7**); **SO**: Sandalwood oil, **EG**: Ethylene glycol, **CO**: Coconut oil, **PO**: Paraffin oil.

1.2.3. Summary and Conclusion:

The present study clearly demonstrated the method for separation of α- and β-santalenes and (*Z*)-α- and (*Z*)-β-santalols, (*Z*)-α-*trans*-bergamotol and (*Z*)-lanceol using preparative medium pressure liquid chromatography (MPLC) with silver nitrate impregnated silica gel as the stationary phase and hexane and dichloromethane as mobile phases, respectively. The method developed, enabled the quantitative separation of (*Z*)-α- and (*Z*)-β-santalols, which are responsible for most of the biological activities observed with sandalwood oil. Standard linear graphs were constructed for eight important sesquiterpenes of heartwood oil of *S. album* using GC analysis of serial dilutions of the stock standard solutions. It was also demonstrated that the quality of commercial sandalwood oil can be assessed for the content of individual sesquiterpene alcohols regulated by Australian Standard (AS2112-2003), International Organization for Standardization ISO 3518:2002 (E) and the European Union (E. U.).

1.2.4. Experimental:

1.2.4.1. Samples and chemicals:

Silver nitrate was purchased from Sigma-Aldrich. Silica gel, silica gel G-coated TLC plates (0.25 mm) and all the solvents were purchased from Merck. Heartwood samples of 15-20 year old sandalwood trees (NCL campus, Pune) were collected with the help of a wood-borer. Heartwood powder was extracted with methanol; organic layer was filtered, concentrated and analysed by GC and GC-MS. Commercial Sandalwood oil and terpene fraction were procured from KSDL, Mysore, Karnataka.

1.2.4.2. Bulk separation of sesquiterpene hydrocarbons from alcohols:

Commercial Sandalwood oil (20.5 g) was subjected to simple column chromatography over silica gel (100-200 mesh, 425 g) and was eluted with hexane till most of these sesquiterpene hydrocarbons eluted. The column was further eluted gradually with ethyl acetate-hexane (8: 92) to obtain oil (15.5 g) which contained mainly sesquiterpene alcohols.

1.2.4.3. Silver nitrate coated silica gel medium pressure liquid chromatography:

The preparative MPLC column (i.d. = 36 mm, height = 460 mm; Buchi catalog no. 17981) was filled with 50 g uncoated silica gel (230-400 mesh) and then with 200 g of silver nitrate impregnated silica gel. Nitrogen pressure was applied to pack the column and to remove dead volume. The column was washed and equilibrated with three column volumes of dichloromethane (CH_2Cl_2) at a flow rate of 20 mL/min, using a peristaltic pump (Figure 1.8).

1.2.4.4. Chromatography:

GC analyses were carried out on an Agilent 7890 instrument equipped with a hydrogen flame ionization detector and HP-5 capillary column (30 m × 0.32 mm × 0.25 mm, J & W Scientific). Nitrogen was used as carrier gas for GC analysis at a flow rate of 1 mL/min. Initially, the column temperature was maintained at 60 °C for 2 min, followed by a temperature gradient from 60 °C to 120 °C at 2 °C/min and held constant for 5 min at 120 °C, then raised to a temperature of 150 °C at 1 °C/min and finally to a temperature of 200 °C with a 5 °C/min rise and maintained for10 min at 200 °C. The injector and detector

temperatures were maintained at 250 °C and operated in split mode (split ratio1: 10). GC-MS was performed on an Agilent 5975C mass selective detector interfaced with an Agilent 7890A gas chromatograph. GC-MS analyses were performed under similar conditions using a HP-5-MS capillary column (30 m × 0.32 mm × 0.25 mm, J & W Scientific) and helium as the carrier gas (mobile phase).

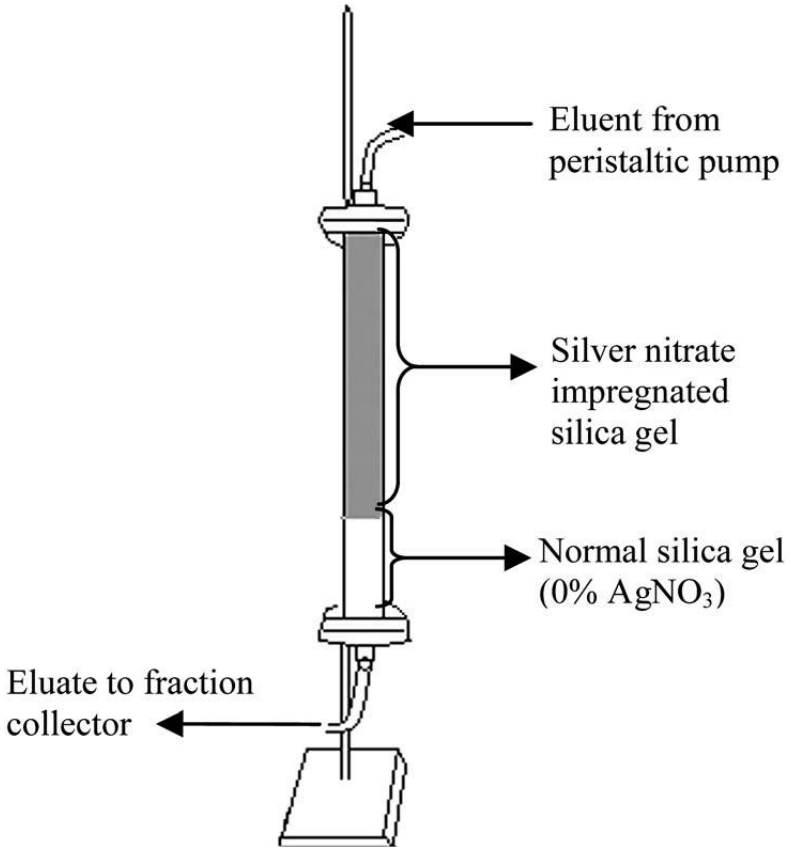

Figure 1.2.8. Schematic representation of silver nitrate impregnated silica gel column used for the separation of santalols and santalenes.

Thin-layer chromatography (TLC) was performed on silica gel G-coated plates (0.25 mm for analytical) developed with hexane (system I), hexane-ethyl acetate (98.5 : 1.5; system II), dichloromethane (system III), and dichloromethane-methanol (98.5 : 1.5; system IV). Compounds were visualized by spraying with a solution of 3.0% anisaldehyde, 2.8% H_2SO_4, and 2% acetic acid in ethanol followed by heating for 1-2 min. Argentized silica gel G-coated plates (0.25 mm) were prepared by dipping the plates in a methanolic solution of $AgNO_3$ (5%, w/v) and dried in hot air oven at 80 °C for 5 min to dry out from methanol. Silver nitrate coated silica gel (230-400 mesh) for column chromatography was

prepared by adding the silica gel to methanolic silver nitrate (5%, w/v) solution. The slurry was dried under reduced pressure on a rotary evaporator and then in hot air oven at 80 °C for 1 hour to obtain dry silver nitrate coated silica gel for column chromatography. This was either immediately used or stored for future use, in a container protected from light.

1.2.4.5. Spectral studies:

Infrared (IR) spectra were recorded on a Shimadzu FTIR 8400 spectrophotometer. High resolution mass spectra (HRMS) were recorded on an MSI auto-concept UK with ionization energy 70 eV and on Waters make QTOF (Synapt-HDMS). Boiling points were determined using a Buchi M560 apparatus. ^{1}H and ^{13}C nuclear magnetic resonance (NMR) spectra were recorded on Bruker DRX-500 (500 MHz), Bruker AC-200 (200 MHz) spectrometers. Chemical shifts are reported in parts per million, with respect to tetramethylsilane (TMS) as the internal standard. The spectral data for α-santalene, β-santalene, *exo*-α-bergamotene, (*Z*)-α-santalol, (*Z*)-β-santalol, (*Z*)-α-*trans*-bergamotol and (*Z*)-lanceol are as follows:

(*Z*)-α-Santalol (1):

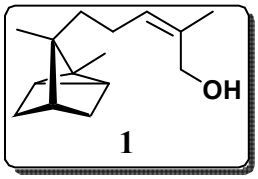

1

[α]$_D$ +17.9 ($CHCl_3$, *c* = 2.65), reported $[\alpha]_D$ = +17.20 ($CHCl_3$, *c* = 0.8)[116]; **IR** ($CHCl_3$, cm^{-1}): ν_{max} 3399, 2945, 1676; **^{1}H NMR** (500 MHz, $CDCl_3$): δ 5.32 (t, *J* = 7.43 Hz, 1H), 4.15 (s, 2H), 1.97 (m, 2H), 1.80 (d, *J* = 1.10Hz, 3H), 1.56 (m, 4H), 1.24 (m, 2H), 1.14 (m, 1H), 1.06 (t, *J* = 10.73 Hz, 2H), 1.00 (s, 3H), 0.83 (s, 3H); **^{13}C NMR** (125 MHz, $CDCl_3$): δ 133.6 (C_2), 129.5 (C_4), 61.6 (C_1), 45.8 (C_7), 38.1 (C_{12}), 34.9 (C_{13}), 31.5 (C_{11}), 30.9 (C_5), 27.3 (C_8), 22.9 (C_6), 21.2 (C_9), 19.5 (C_{10}), 19.4 (C_3), 17.5 (C_{14}), 10.6(C_{15}); **GC-EI-MS**: *m/z* 220.2 $[M]^+$, 202.2, 187.2, 159.1, 133.1, 121.1, 107.1, 94.1 (100%), 93.1, 91.1, 79.1, 67.1; **HRMS:** Calcd. for $C_{15}H_{22}$ $[M\text{-}H_2O]^+$: 202.1716 found: 202.1724; **B. P.**: 300.1 °C to 302.6 °C.

(*Z*)-(β + *epi*-β)-Santalol (2 and 3):

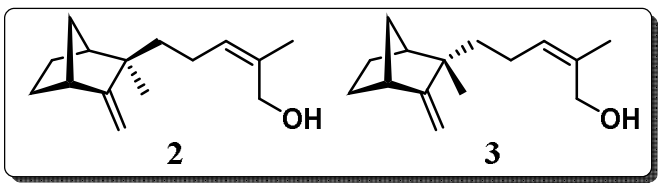

2 **3**

IR ($CHCl_3$, cm^{-1}): ν_{max} 3363, 2963, 1651, 1455; **^{1}H NMR** (400 MHz, $CDCl_3$): δ 5.29 (t, *J* = 7.28 Hz, 1H),

4.74 (s, 1H), 4.46 (s, 1H), 4.14 (bs, 2H), 2.67 (bs, 1H), 2.10 (s, 1H), 1.96-2.08 (m, 1H), 1.79 (s, 3H), 1.63-1.67 (m, 3H), 1.37-1.44 (m, 2H), 1.17-1.27 (m, 4H), 1.04 (s, 3H); **^{13}C NMR** (100 MHz, $CDCl_3$): δ 166.2 (C_2), 133.9 (C_{13}), 129.0 (C_4), 99.7 (C_{14}), 61.6 (C_1), 46.8 (C_{11}), 44.7 (C_7), 44.6 (C_8), 41.5 (C_6), 37.1 (C_{12}), 29.6 (C_{10}), 23.7 (C_9), 23.2 (C_5), 22.6 (C_{15}), 21.2 (C_3); **GC-EI-MS**: *m/z* 220.2 $[M]^+$, 202.2, 189.2, 161.1, 147.1, 133.1, 122.1, 94.1 (100%), 93.1, 79.1, 67.1; **B. P.**: 289.5 °C to 292.3 °C.

(*Z*)-α-*trans*-Bergamotol (4):

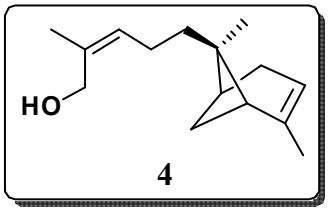

4

IR ($CHCl_3$, cm^{-1}): ν_{max} 3327, 2925, 1449, 1439, 1010; **[α]$_D$** -45.4 ($CHCl_3$, *c* = 2.0); **^{1}H NMR** (200 MHz, $CDCl_3$): δ 5.37 (t, *J* = 7.1 Hz, 1H), 5.22 (m, 1H), 4.17 (bs, 2H), 1.97-2.36 (m, 6H), 1.82 (m, 2H), 1.63-1.68 (m, 6H), 1.23-1.29 (m, 1H), 1.18 (d, *J* = 8.47 Hz, 3H), 0.83 (s, 3H); **^{13}C NMR** (50 MHz, $CDCl_3$): δ 144.2 (C_{11}), 133.8 (C_2), 128.9 (C_4), 116.4 (C_{10}), 61.2 (C_1), 45.2 (C_{12}), 41.0 (C_7), 38.9 (C_{13}), 38.8 (C_8), 31.5 (C_6), 31.1 (C_9), 23.3 (C_5), 22.9 (C_{15}), 21.1 (C_{14}), 17.3 (C_3); **GC-EI-MS**: *m/z* 220.1 $[M]^+$, 202.2, 187.2, 159.1, 145.1, 132.1, 119.1, 93.1 (100%), 79.1, 55.1; **B. P.**: 312.5 °C to 313.6 °C.

α-Santalene (5):

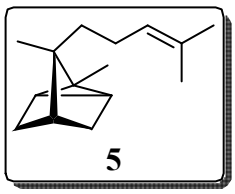
5

[α]$_D$ +14.99 ($CHCl_3$, *c* = 2.12); **IR** ($CHCl_3$, cm^{-1}): ν_{max} 2942, 1644; **^{1}H NMR** (400 MHz, $CDCl_3$): δ 5.12 (m, 1H), 1.83-1.95 (m, 2H), 1.68 (s, 3H), 1.61 (s, 3H), 1.59 (m, 3H), 1.11-1.26 (m, 2H), 1.02-1.07 (m, 3H), 0.99 (s, 3H), 0.83 (s, 3H); **^{13}C NMR** (100 MHz, $CDCl_3$): δ 130.8 (C_2), 125.5 (C_4), 45.8 (C_7), 38.1 (C_9), 34.5 ($C_{11/13}$), 31.5 ($C_{13/11}$), 31.0 (C_6), 27.4 (C_8), 25.7 ($C_{10\ \&\ 12}$), 23.2 (C_5), 19.5 ($C_{15\ \&\ 3}$), 17.5 (C_1), 10.7 (C_{14}); **GC-EI-MS**: *m/z* 204.2 $[M]^+$, 189.2, 161.2, 148.2, 133.1, 121.1, 107.1, 94.1 (100%), 93.1, 79.1, 67.1; **HR-EI-MS:** Calcd. for $C_{15}H_{24}$, 204.1878, found 204.1864; **B. P.**: 251.4 °C to 253.2 °C.

(β + *epi*-β)-Santalene (6 and 7):

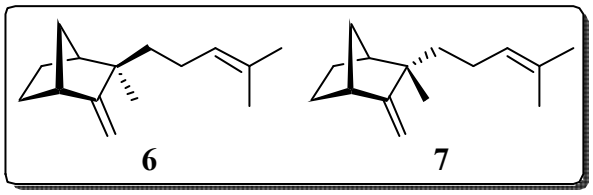
6 7

IR ($CHCl_3$, cm^{-1}): ν_{max} 2962, 1654, 1458; **^{1}H NMR** (400 MHz, $CDCl_3$): δ 5.08-5.15 (m, 1H), 4.73 (s, 1H), 4.47 (s, 1H), 2.67 (m,

1H), 1.83-2.14 (m, 3H), 1.57-1.69 (m, 9H), 1.37-1.46 (m, 2H), 1.15-1.28 (m, 3H), 1.02-1.05 (s, 3H); **^{13}C NMR** (100 MHz, $CDCl_3$): δ 166.9 and 166.5 (C_{13}), 131.1 and 131.0 (C_2), 125.0 (C_4), 99.4 and 99.2 (C_{14}), 46.8 and 46.7 (C_{11}), 45.2 and 44.5 (C_8), 44.9 and 44.7 (C_7), 41.2 and 39.1 (C_6), 37.1 (C_{12}), 29.7 and 29.1 (C_{10}), 25.7 and 25.7 (C_3), 24.0 and 23.6 (C_9), 23.7 (C_5), 22.6 and 25.2 (C_{14}), 17.6 and 17.5 (C_1); **GC-EI-MS**: *m/z* 204.2 $[M]^+$, 189.2, 161.1, 147.1, 133.1, 122.1, 107.1, 94.1 (100%), 79.1, 67.1; **B. P.**: 261.4 °C to 262.6 °C.

***Exo*-α-Bergamotene (12):**

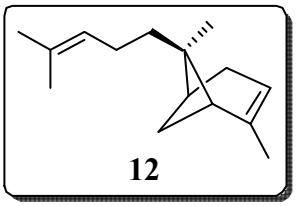

12

^{1}H NMR (500 MHz, $CDCl_3$): δ 5.20-5.22 (m, 1H), 5.17 (tquin, *J* = 1.22, 7.02 Hz, 1H), 2.30-2.34 (m, 1H), 2.22-2.27 (m, 1H), 2.11-2.17 (m, 2H), 1.94-2.01 (m, 3H), 1.70 (brs, 3H), 1.66 (q, *J* = 1.8 Hz, 3H), 1.63 (brs, 3H), 1.59-1.64 (m, 2H), 1.17 (d, *J* = 8.54 Hz, 1H), 0.83 (s, 3H)[117]; **^{13}C NMR** (125 MHz, $CDCl_3$): δ 144.5 (=C), 130.9 (=C), 125.3 (=CH), 116.5 (=CH), 45.4 (-CH), 41.1 (-C-), 38.9 (-CH), 38.6 ($-CH_2$), 31.6 ($-CH_2$), 31.2 ($-CH_2$), 25.7 ($-CH_3$), 23.8 ($-CH_2$), 23.0 ($-CH_3$), 17.6 ($-CH_3$), 17.4 ($-CH_3$);[118] **GC-EI-MS:** *m/z* 204.2 $[M]^+$, 189.1, 161.1, 147.1, 133.1, 119.0 (100%), 107.1, 93.0, 69.1, 55.0; **HR-EI-MS:** Calcd. for $C_{15}H_{24}$, 204.1878, found 204.1877.

(*Z*)-Lanceol (11):

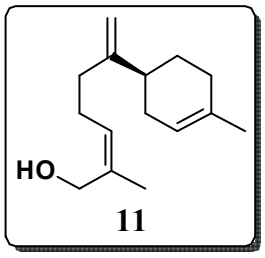

11

[α]$_D$ -72.7 ($CHCl_3$, *c* = 2.0); **IR** ($CHCl_3$, cm^{-1}): ν_{max} 3366, 2923, 1670, 1603, 1410; **^{1}H NMR** (200 MHz, $CDCl_3$):δ 5.40 (m, 1H), 5.31 (t, *J* = 7.1 Hz, 1H), 4.78 (s, 1H), 4.72 (d, *J* = 1.39 Hz, 1H), 4.13 (bs, 2H), 1.83-2.23 (m, 9H), 1.80 (d, *J* = 1.2 Hz, 3H), 1.65 (bs, 3H), 1.35-1.56 (m, 1H), 1.21-1.26 (m, 1H); **^{13}C NMR** (50 MHz, $CDCl_3$): δ 153.9 (C_7), 134.5 (C_{11}), 133.8 (C_2), 128.1 (C_{12}), 120.7 (C_4), 107.5 (C_{14}), 61.6 (C_1), 39.8 (C_8), 34.9 (C_6), 31.4 (C_{10}), 30.7 (C_9), 28.3 (C_{13}), 26.3 (C_5), 23.4 (C_{15}), 21.2 (C_3); **GC-EI-MS**: *m/z* 220.2 $[M]^+$, 202.2, 187.2, 174.1, 159.1, 134.1, 119.1, 105.1, 93.1 (100%), 79.0, 67.0; **B. P.**: 327.2 °C to 328.7 °C.

Appendix 1

Appendix 1 Index

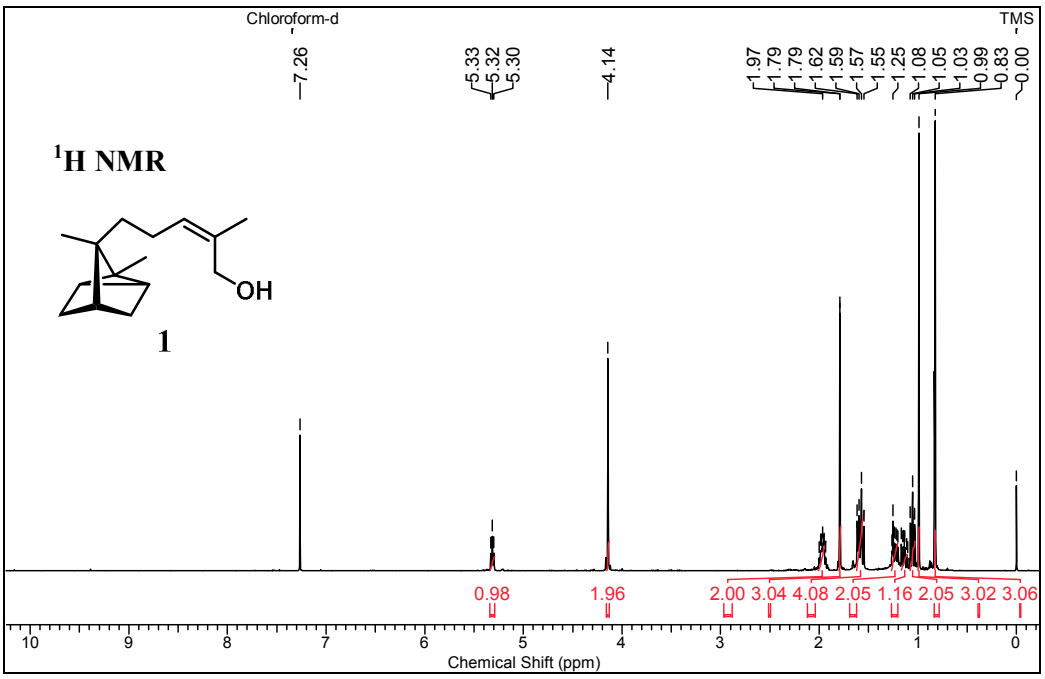
Chloroform-d
TMS
7.26
5.33
5.32
5.30
4.14
1.97
1.79
1.79
1.62
1.59
1.57
1.55
1.25
1.08
1.05
1.03
0.99
0.83
0.00
^{1}H NMR
OH
1
0.98
1.96
2.00 3.04 4.08 2.05 1.16 2.05 3.02 3.06
Chemical Shift (ppm)

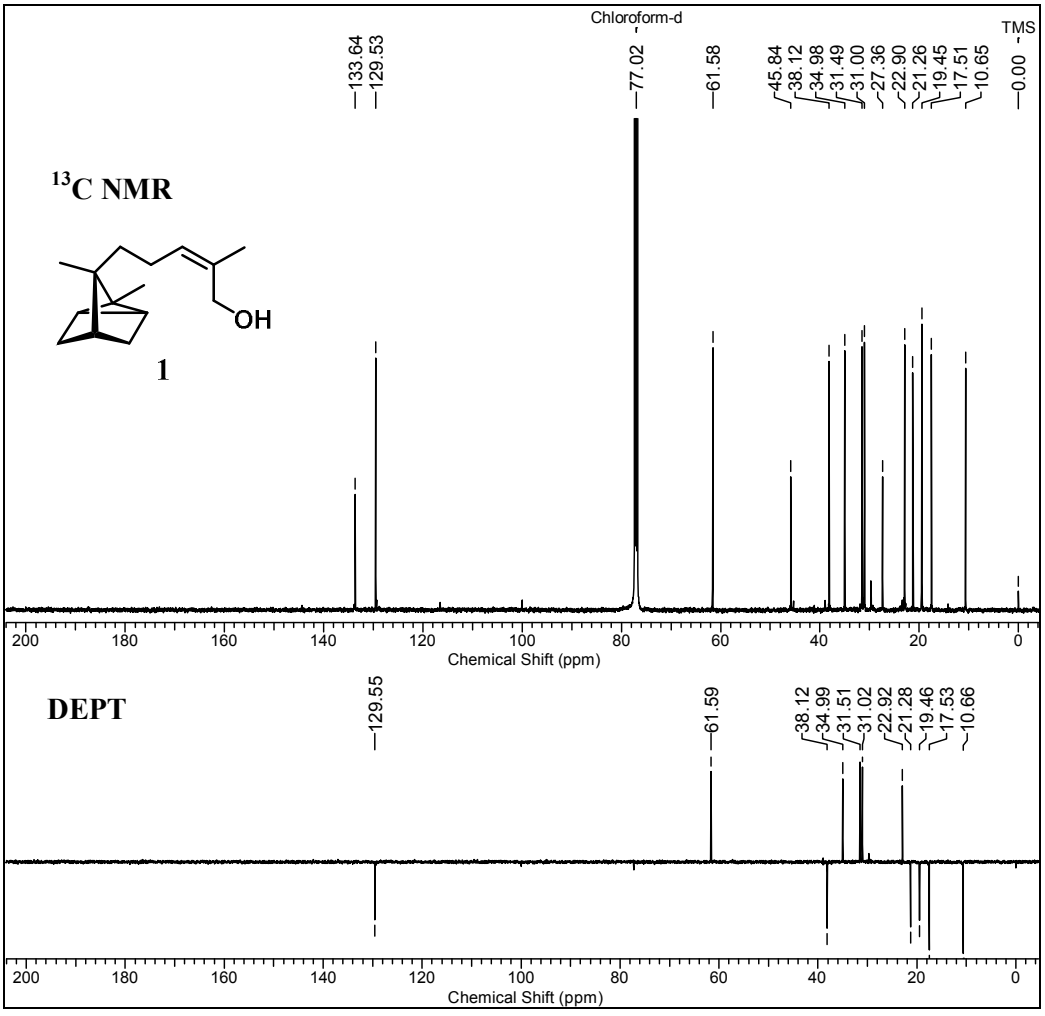
Chloroform-d
TMS
133.64
129.53
77.02
61.58
45.84
38.12
34.98
31.49
31.00
27.36
22.90
21.26
19.45
17.51
10.65
0.00
^{13}C NMR
OH
1
Chemical Shift (ppm)
DEPT
129.55
61.59
38.12
34.99
31.51
31.02
22.92
21.28
19.46
17.53
10.66
Chemical Shift (ppm)

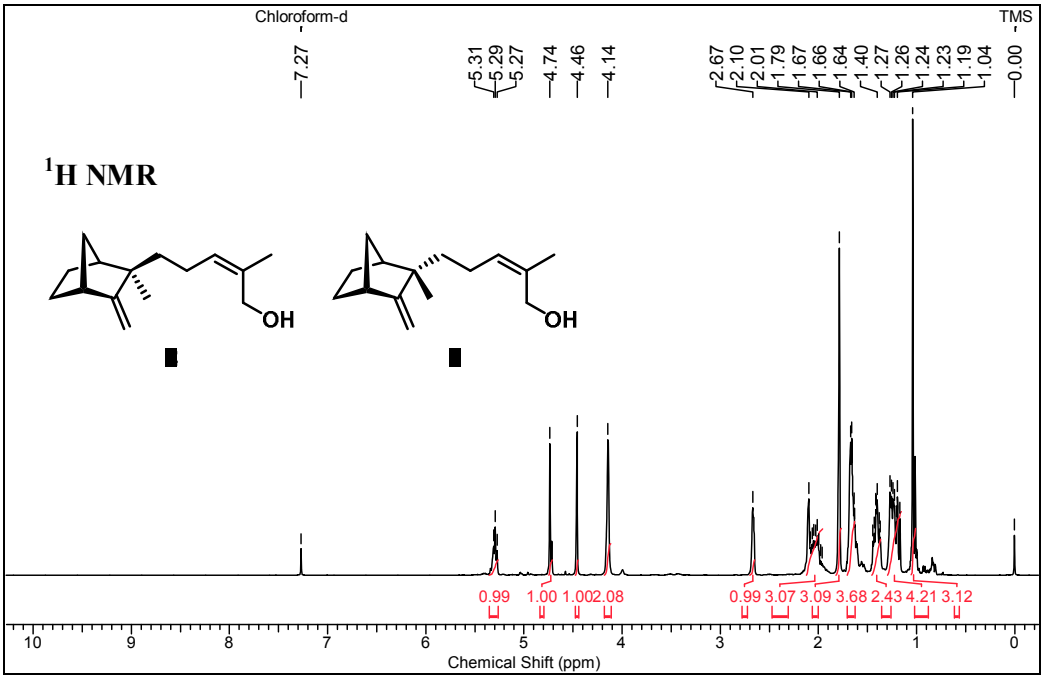
Chloroform-d
TMS
7.27
5.31
5.29
5.27
4.74
4.46
4.14
2.67
2.10
2.01
1.79
1.67
1.66
1.64
1.40
1.27
1.26
1.24
1.23
1.19
1.04
0.00
1H NMR
OH
OH
0.99 1.00 1.00 2.08
0.99 3.07 3.09 3.68 2.43 4.21 3.12
Chemical Shift (ppm)

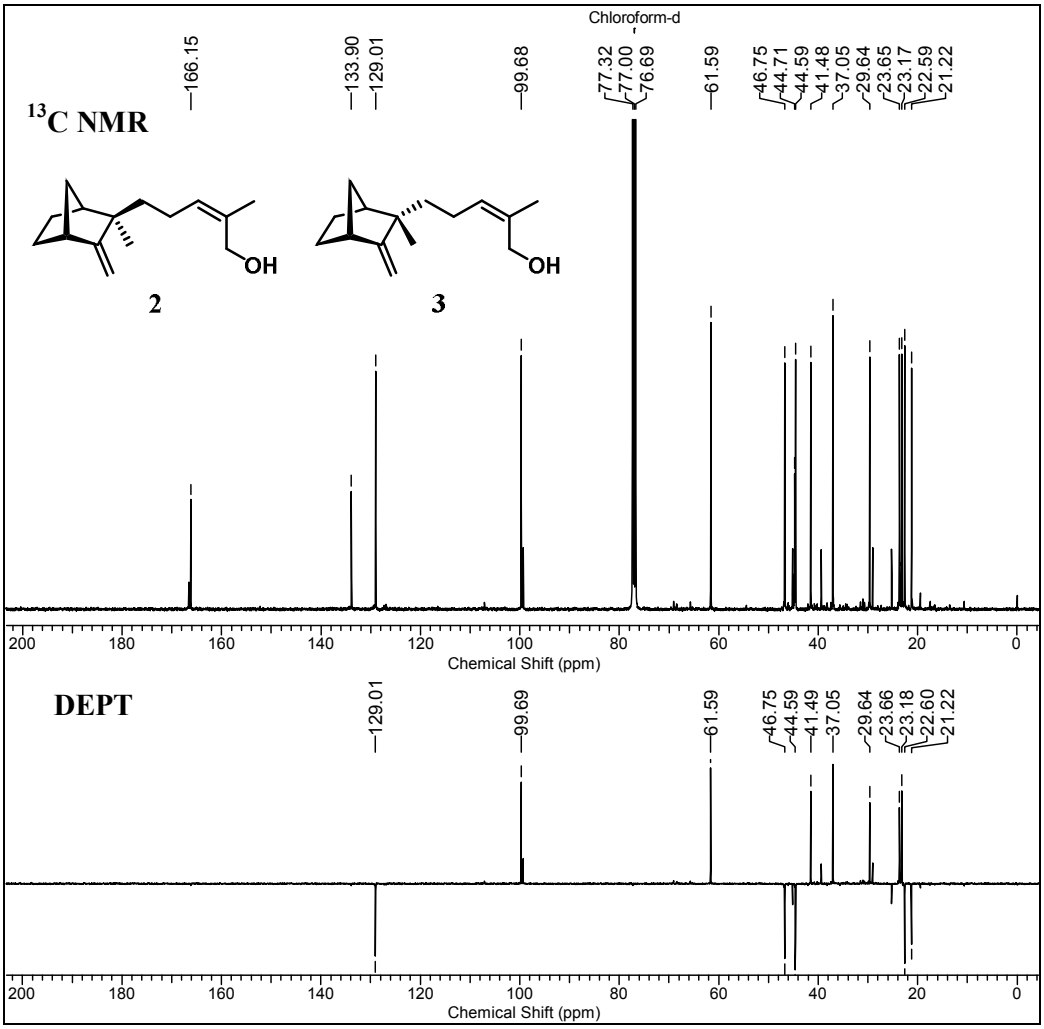
Chloroform-d
166.15
133.90
129.01
99.68
77.32
77.00
76.69
61.59
46.75
44.71
44.59
41.48
37.05
29.64
23.65
23.17
22.59
21.22
13C NMR
OH
OH
2
3
Chemical Shift (ppm)
DEPT
129.01
99.69
61.59
46.75
44.59
41.49
37.05
29.64
23.66
23.18
22.60
21.22
Chemical Shift (ppm)

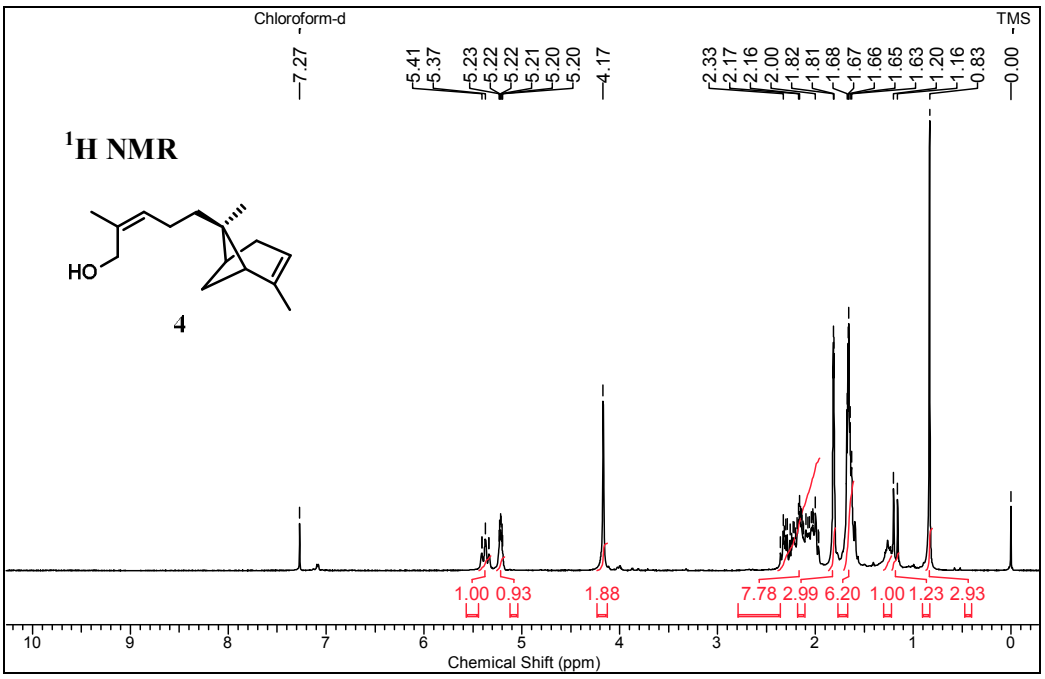
Chloroform-d
TMS
7.27
5.41
5.37
5.23
5.22
5.22
5.21
5.20
5.20
4.17
2.33
2.17
2.16
2.00
1.82
1.81
1.68
1.67
1.66
1.65
1.63
1.20
1.16
0.83
0.00
1H NMR
HO
4
1.00 0.93 1.88 7.78 2.99 6.20 1.00 1.23 2.93
Chemical Shift (ppm)

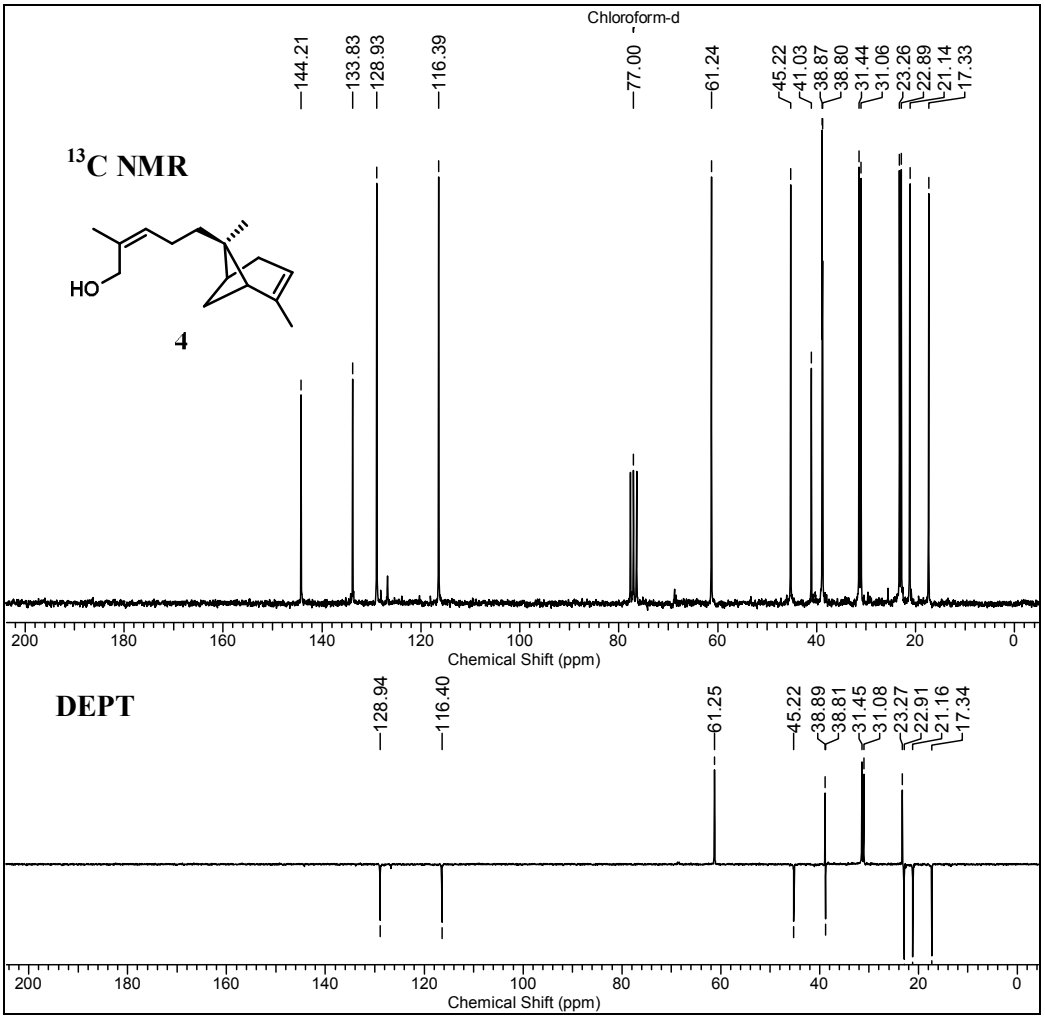
Chloroform-d
144.21
133.83
128.93
116.39
77.00
61.24
45.22
41.03
38.87
38.80
31.44
31.06
23.26
22.89
21.14
17.33
13C NMR
HO
4
Chemical Shift (ppm)
DEPT
128.94
116.40
61.25
45.22
38.89
38.81
31.45
31.08
23.27
22.91
21.16
17.34
Chemical Shift (ppm)

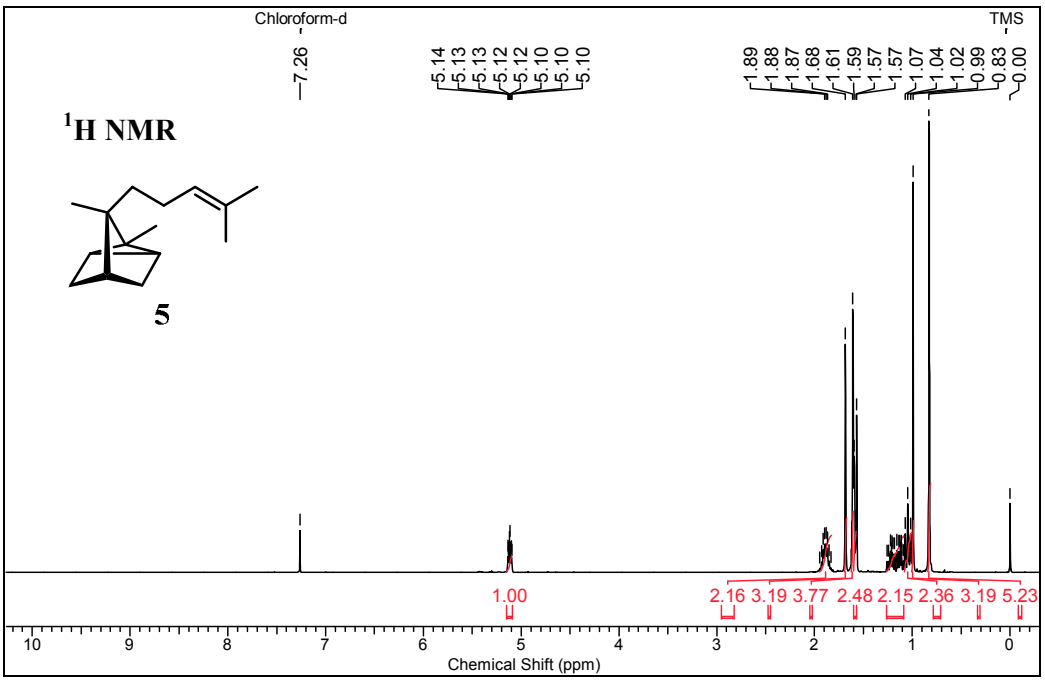
Chloroform-d
TMS
7.26
5.14 5.13 5.13 5.12 5.12 5.10 5.10 5.10
1.89 1.88 1.87 1.68 1.61 1.59 1.57 1.57 1.07 1.04 1.02 0.99 0.83 0.00
1H NMR
5
1.00
2.16 3.19 3.77 2.48 2.15 2.36 3.19 5.23
Chemical Shift (ppm)

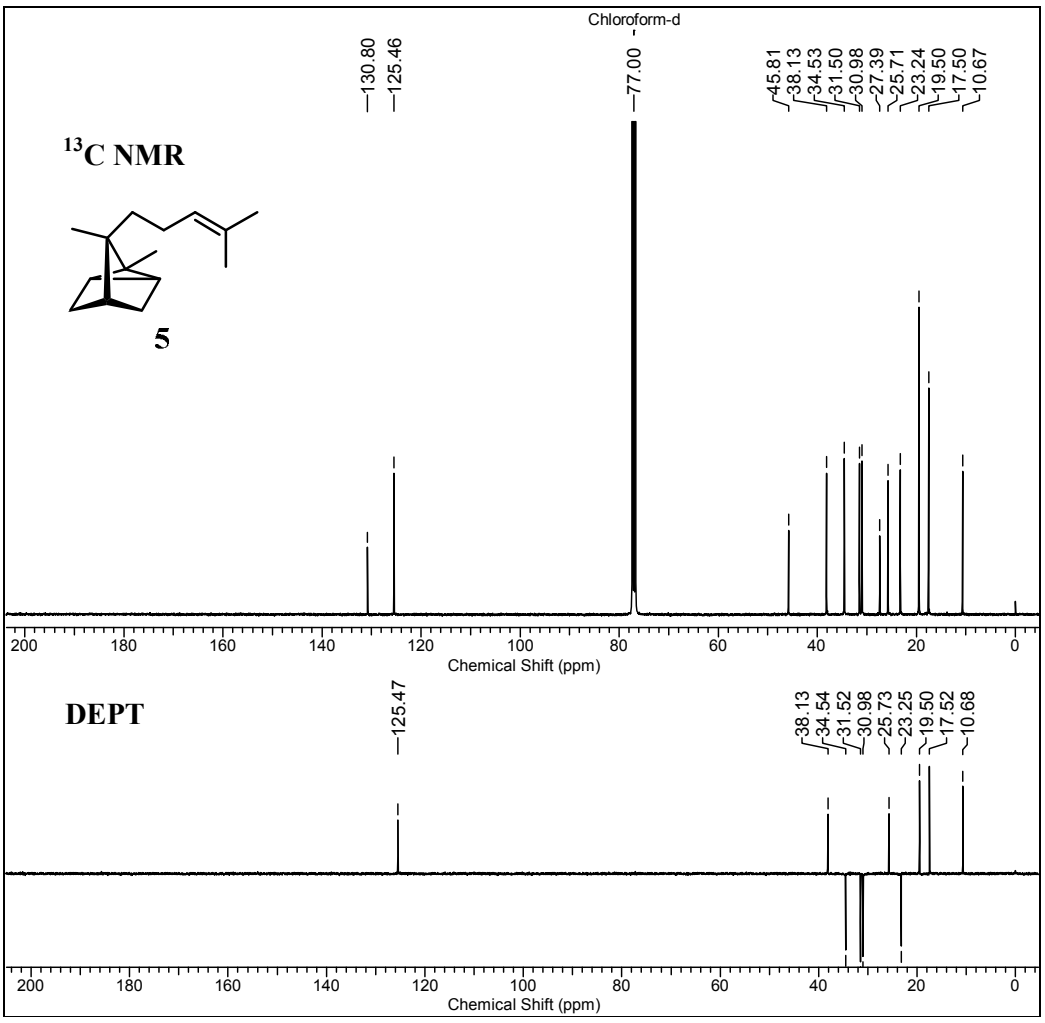
Chloroform-d
130.80 125.46
77.00
45.81 38.13 34.53 31.50 30.98 27.39 25.71 23.24 19.50 17.50 10.67
13C NMR
5
Chemical Shift (ppm)
DEPT
125.47
38.13 34.54 31.52 30.98 25.73 23.25 19.50 17.52 10.68
Chemical Shift (ppm)

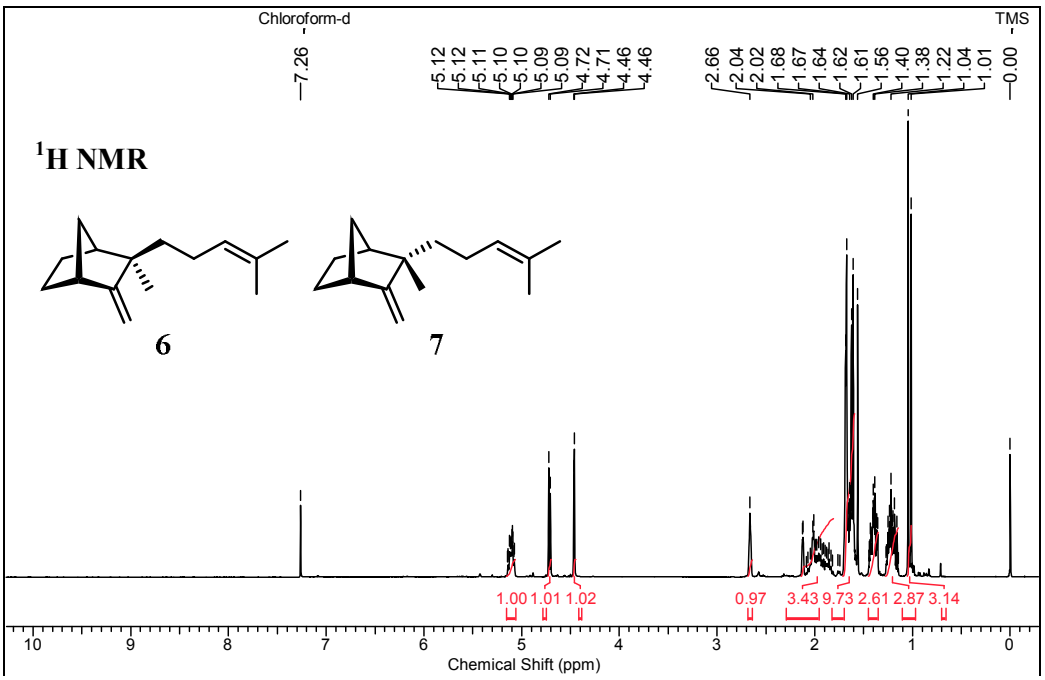
Chloroform-d
TMS
7.26
5.12 5.12 5.11 5.10 5.10 5.09 5.09 4.72 4.71 4.46 4.46
2.66 2.04 2.02 1.68 1.67 1.64 1.62 1.61 1.56 1.40 1.38 1.22 1.04 1.01
0.00
1H NMR
6
7
1.00 1.01 1.02
0.97 3.43 9.73 2.61 2.87 3.14
Chemical Shift (ppm)

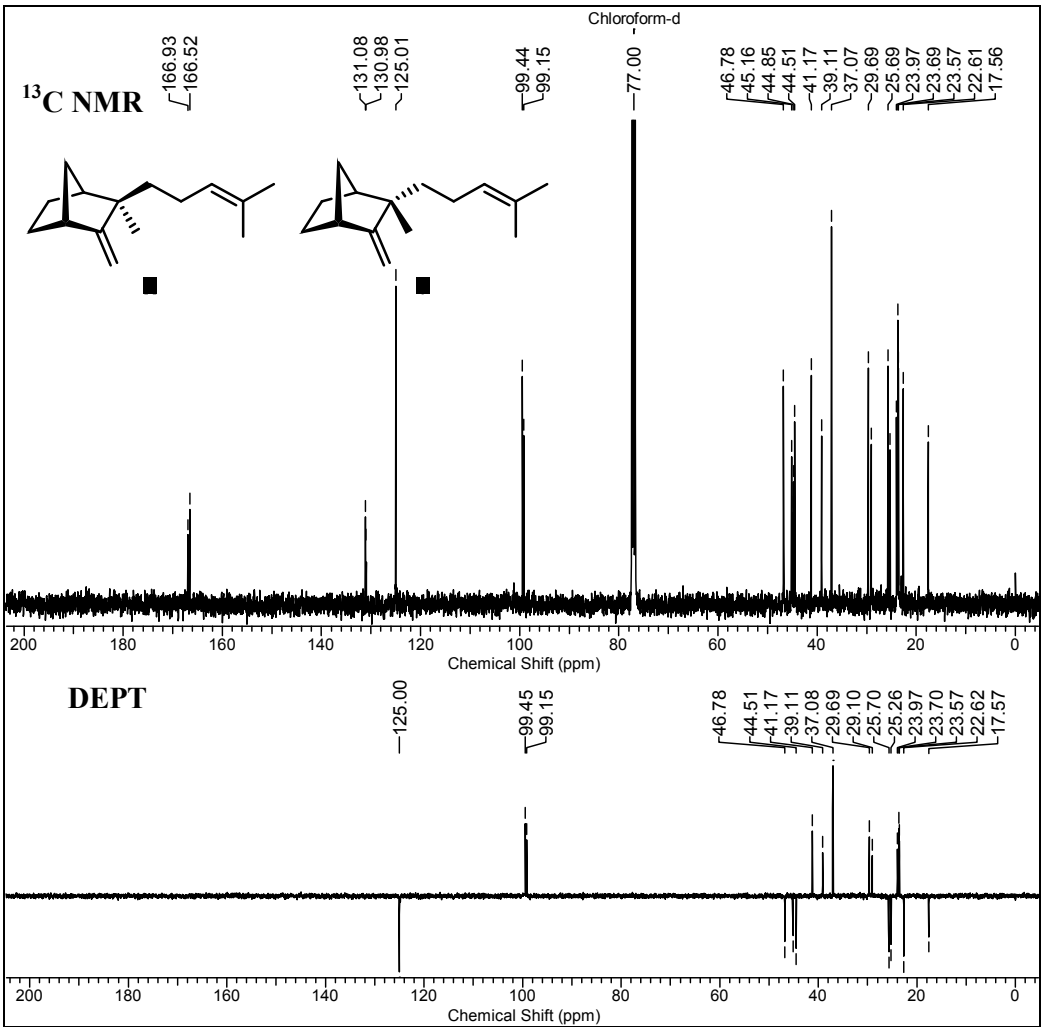
13C NMR
166.93 166.52
131.08 130.98 125.01
99.44 99.15
Chloroform-d
77.00
46.78 45.16 44.85 44.51 41.17 39.11 37.07 29.69 25.69 23.97 23.69 23.57 22.61 17.56
Chemical Shift (ppm)
DEPT
125.00
99.45 99.15
46.78 44.51 41.17 39.11 37.08 29.69 29.10 25.70 25.26 23.97 23.70 23.57 22.62 17.57
Chemical Shift (ppm)

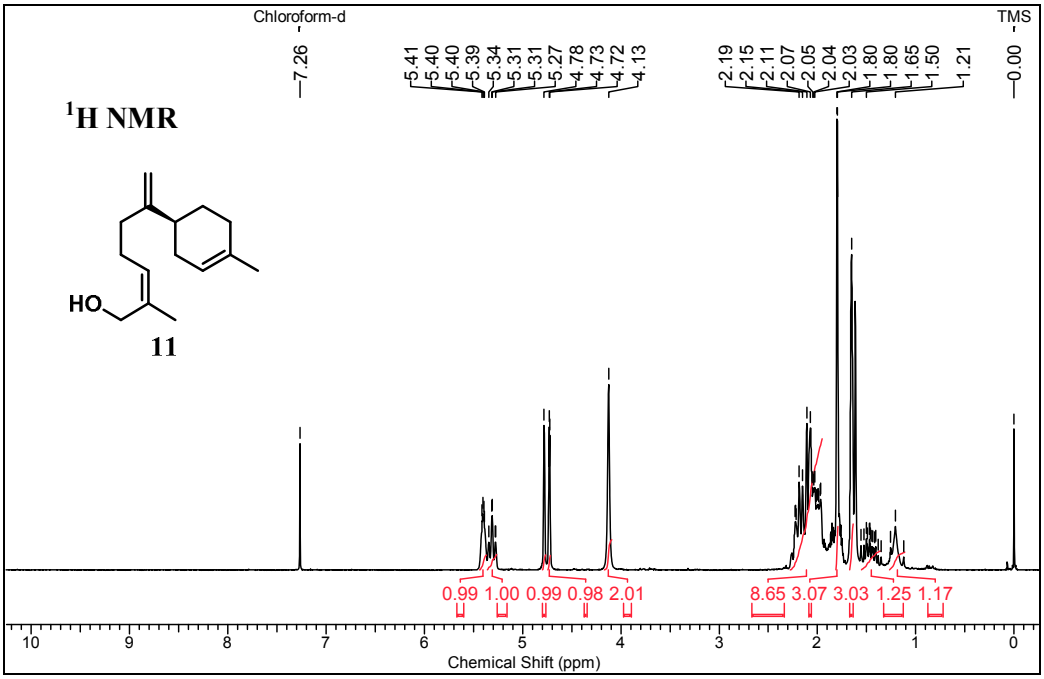
Chloroform-d
TMS
7.26
5.41
5.40
5.40
5.39
5.34
5.31
5.31
5.27
4.78
4.73
4.72
4.13
2.19
2.15
2.11
2.07
2.05
2.04
2.03
1.80
1.80
1.65
1.50
1.21
0.00
1H NMR
HO
11
0.99 1.00 0.99 0.98 2.01
8.65 3.07 3.03 1.25 1.17
Chemical Shift (ppm)

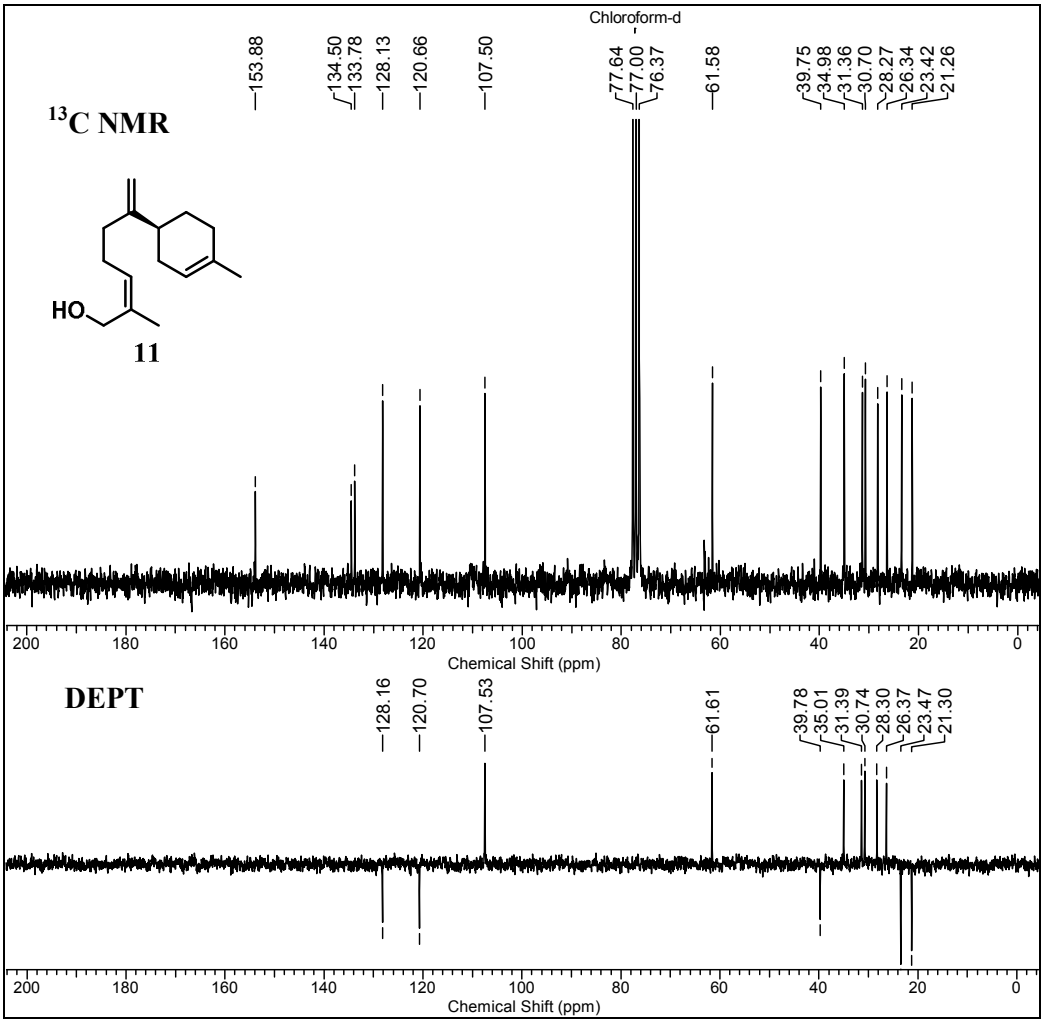
Chloroform-d
153.88
134.50
133.78
128.13
120.66
107.50
77.64
77.00
76.37
61.58
39.75
34.98
31.36
30.70
28.27
26.34
23.42
21.26
13C NMR
HO
11
Chemical Shift (ppm)
DEPT
128.16
120.70
107.53
61.61
39.78
35.01
31.39
30.74
28.30
26.37
23.47
21.30
Chemical Shift (ppm)

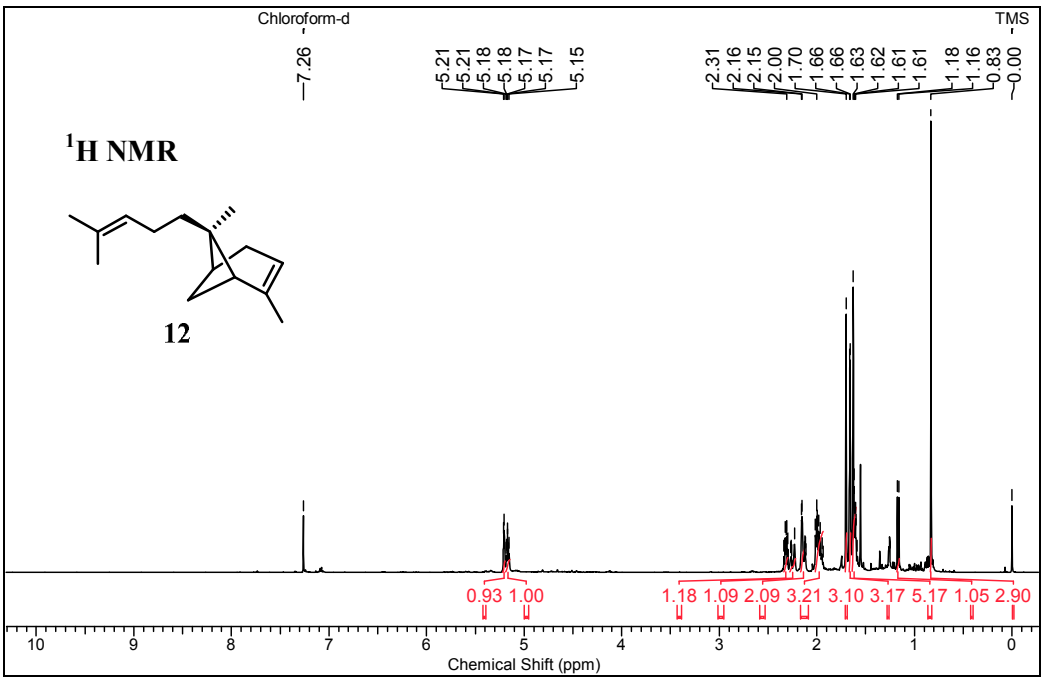
Chloroform-d
TMS
7.26
5.21 5.21 5.18 5.18 5.17 5.17 5.15
2.31 2.16 2.15 2.00 1.70 1.66 1.66 1.63 1.62 1.61 1.61 1.18 1.16 0.83 0.00
^{1}H NMR
12
0.93 1.00
1.18 1.09 2.09 3.21 3.10 3.17 5.17 1.05 2.90
Chemical Shift (ppm)

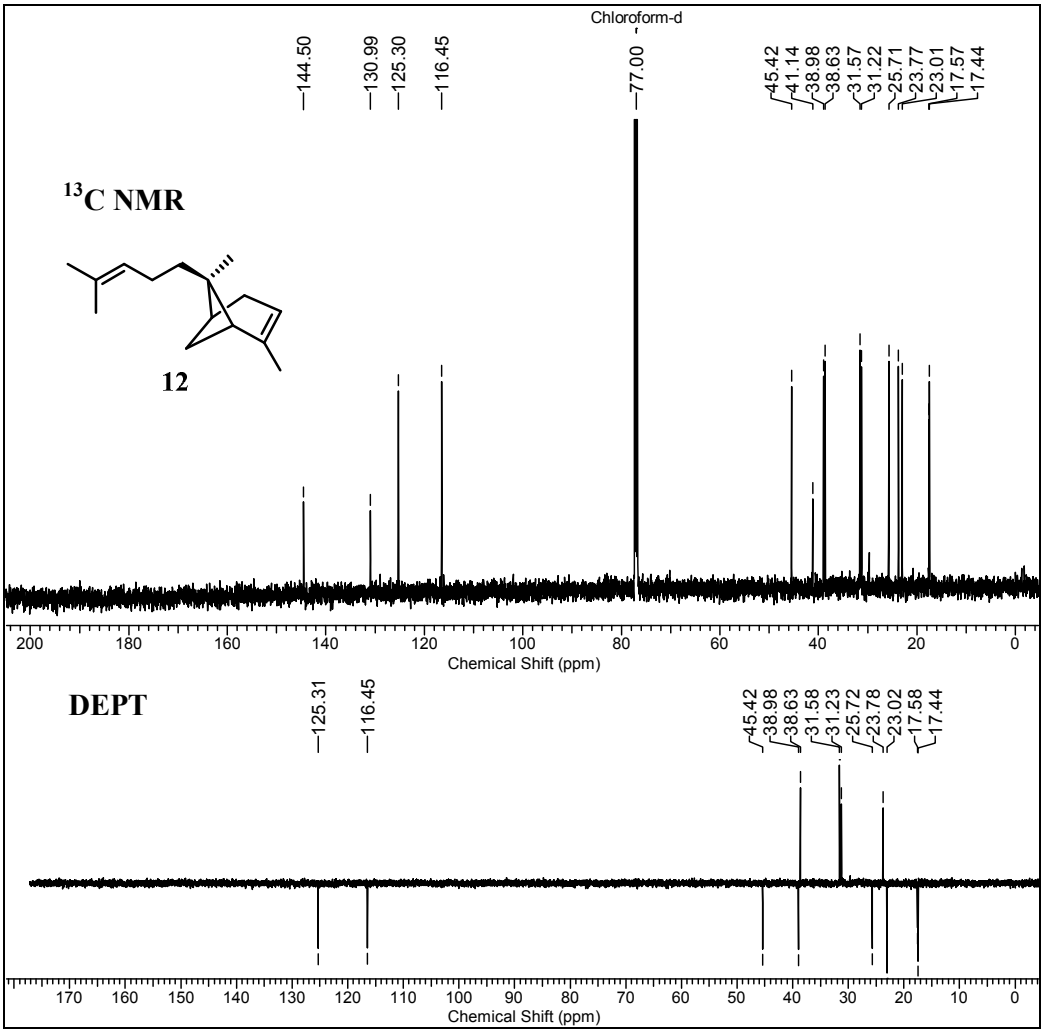
Chloroform-d
144.50
130.99
125.30
116.45
77.00
45.42 41.14 38.98 38.63 31.57 31.22 25.71 23.77 23.01 17.57 17.44
^{13}C NMR
12
Chemical Shift (ppm)
DEPT
125.31
116.45
45.42 38.98 38.63 31.58 31.23 25.72 23.78 23.02 17.58 17.44
Chemical Shift (ppm)

GC traces for co-injections of purified sesquiterpene components with Sandalwood oil:

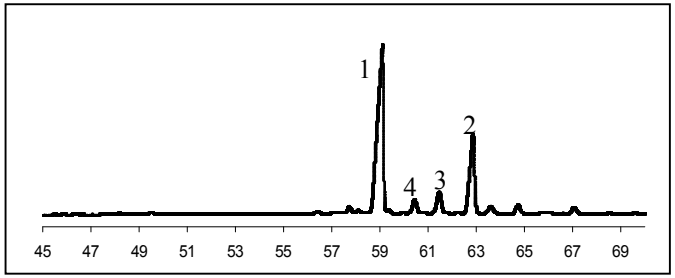

A) Sandalwood oil

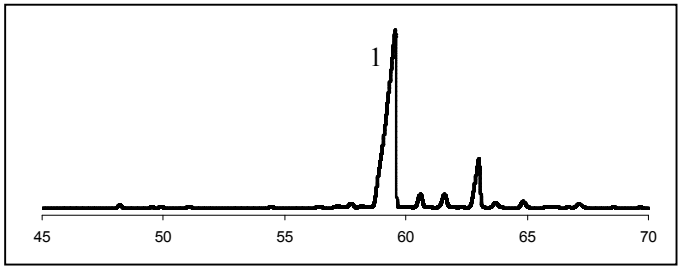

B) Co-injection of (*Z*)-α-Santalol (**1**) with Sandalwood oil

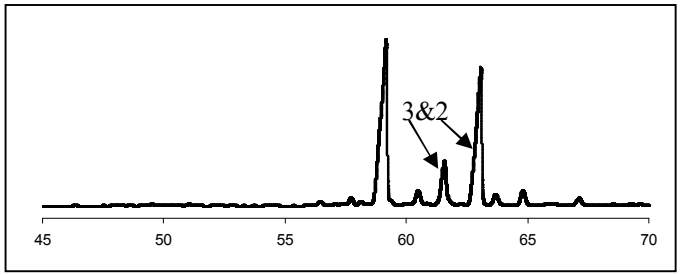

C) Co-injection of (*Z*)-(β + *epi*-β)-Santalol (**2&3**) with Sandalwood oil.

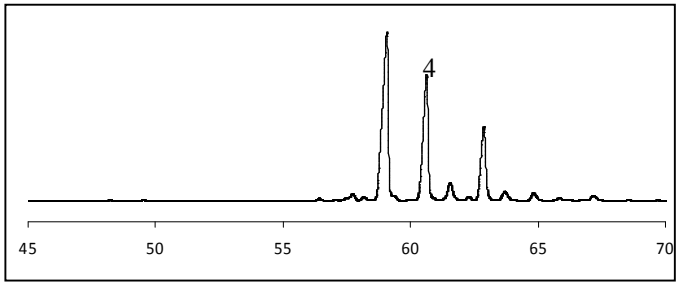

D) Co-injection of (*Z*)-α-*trans*-Bergamotol (**4**) with Sandalwood oil

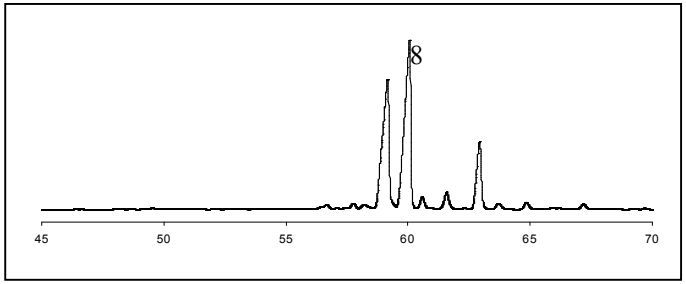

E) Co-injection of (-)-α-Bisabolol (**8**) with Sandalwood oil

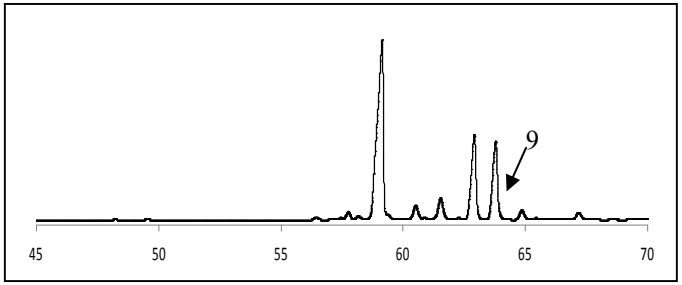

F) Co-injection of (*E*,*E*)-Farnesol (**9**) with Sandalwood oil

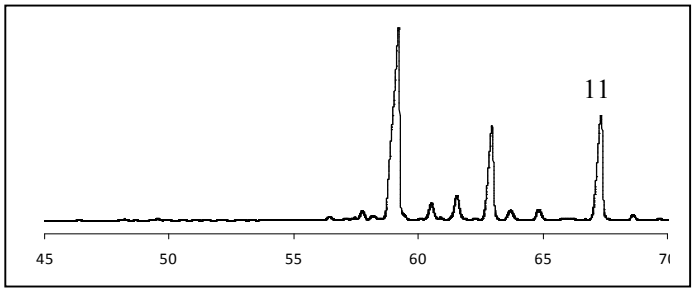

G) Co-injection of (*Z*)-Lanceol (**11**) with Sandalwood oil

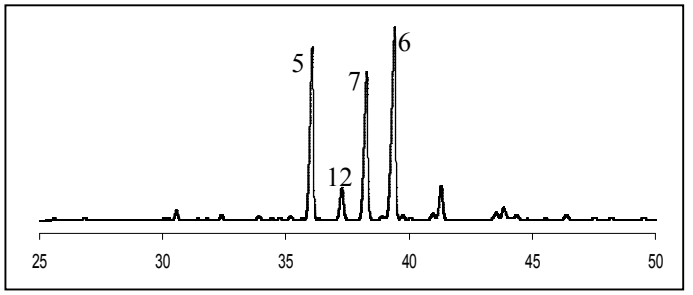

H) Santalenes mixture

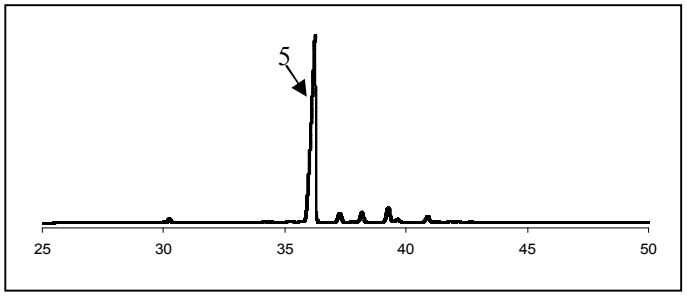

I) Co-injection of α-Santalene (**5**) with Sandalwood oil

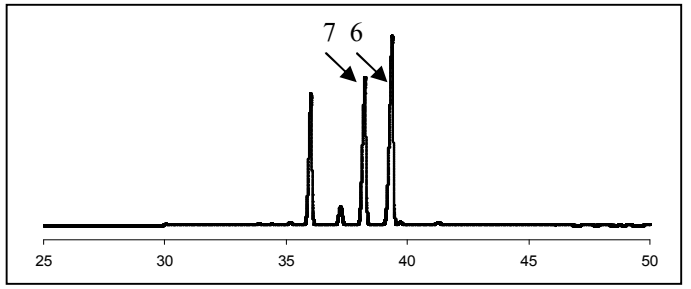

J) Co-injection of (β+ *epi*-β)-Santalene (**6&7**) with Sandalwood oil.

Standard graphs of purified sesquiterpenes of sandalwood oil:

A) **(*Z*)-α-Santalol (1):**

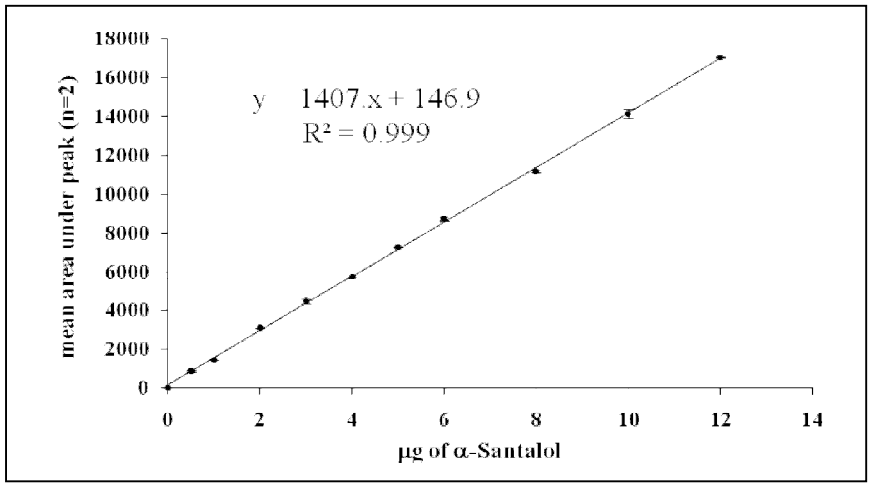

B) (*Z*)-(β+ *epi*-β)-Santalol (2 & 3):

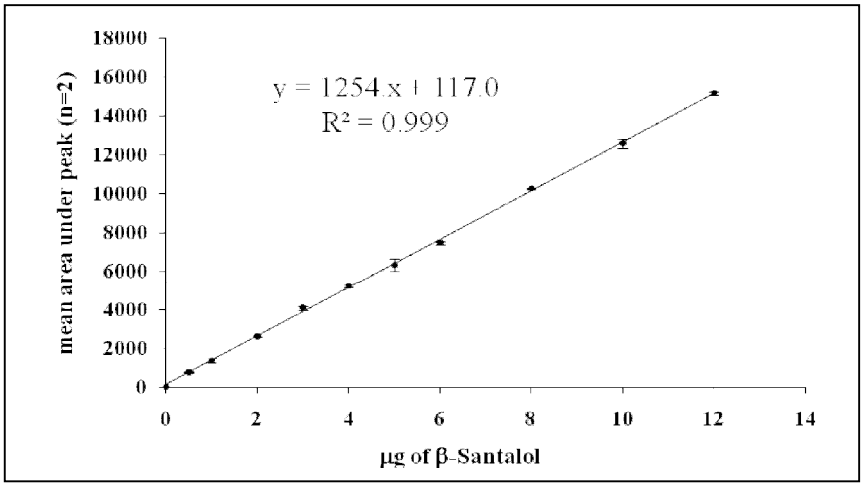

C) (*Z*)-α-trans-Bergamotol (4):

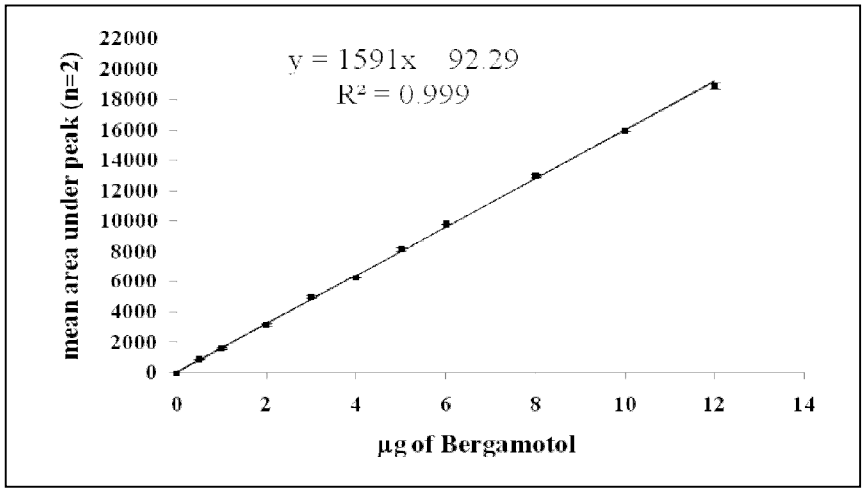

D) α-Santalene (5):

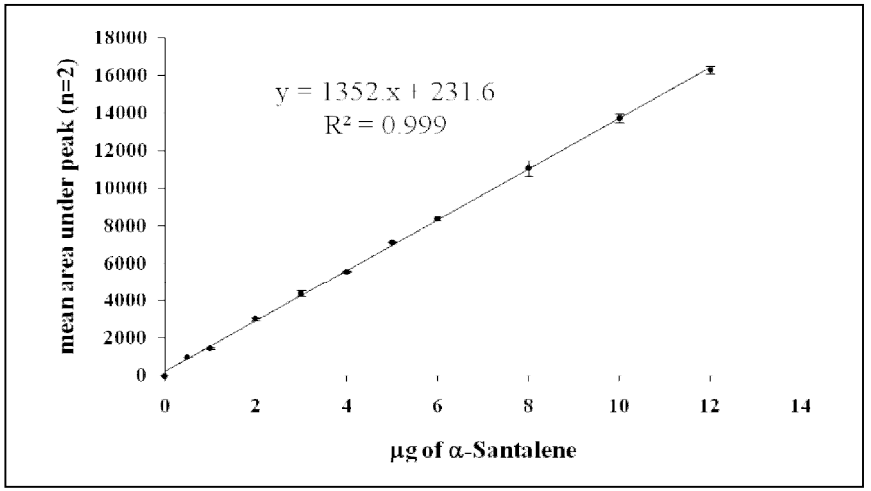

E) (β+ *epi*-β)-Santalene (6 & 7):

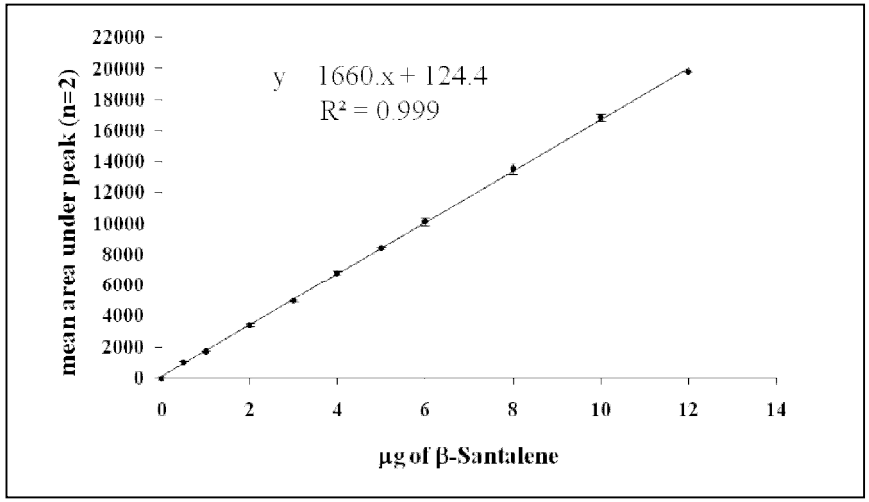

F) (-)-α-Bisabolol (8):

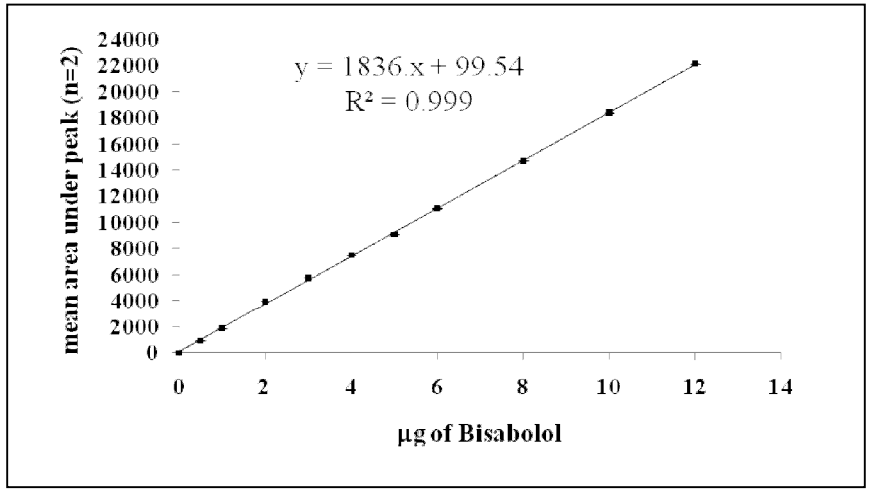

G) (*E*), (*E*)-Farnesol (9):

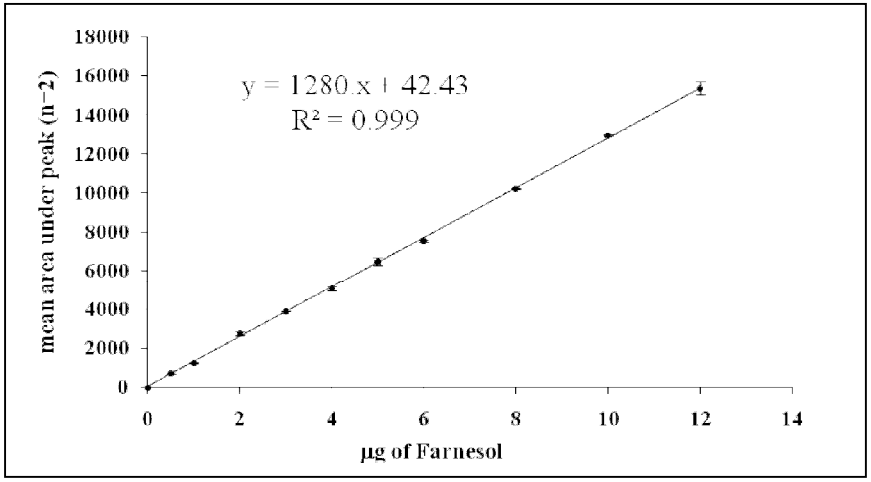

H) (*Z*)-Lanceol (11):

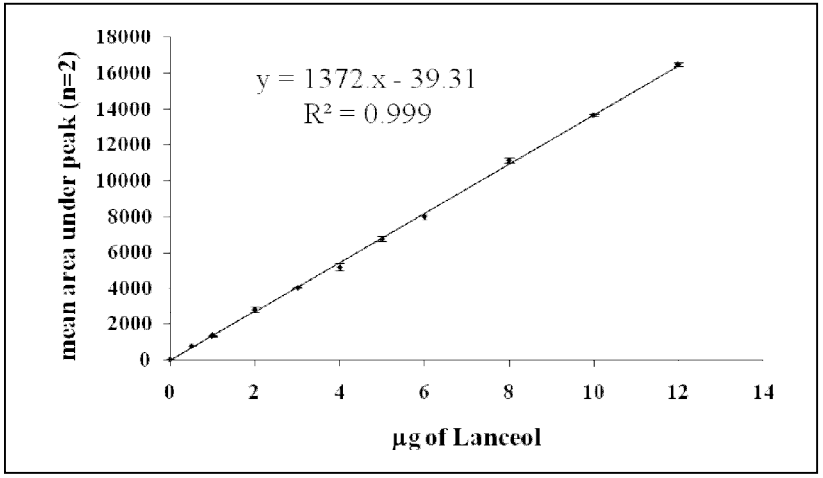

Table 1.2.2: Adulteration study of sandalwood oil (KSDL) with coconut oil, liquid paraffin and ethylene glycol.

Sr. No.	Composition	Area of α-Santalol	Area of (β + *epi*-β)-Santalol	Expected value of α-Santalol (mg)	Observed value of α-Santalol (mg)	Expected value of (β+*epi*-β)-Santalol (mg)	Observed value of (β+*epi*-β)-Santalol (mg)	% error in α-Santalol	% error in (β+*epi*-β)-Santalol
1	MSW : Coconut Oil (9:1)	3200.9	1460.6	2.17	2.17	1.05	1.07	0.03	2.04
		3156.4	1415.0	2.17	2.14	1.05	1.04	1.43	1.42
2	MSW : Coconut Oil (7:3)	2558.8	1171.1	1.68	1.71	0.81	0.84	2.04	3.78
		2470.7	1153.8	1.68	1.65	0.81	0.83	1.69	2.07
3	MSW : Coconut Oil (1:1)	1821.9	842.7	1.20	1.19	0.58	0.58	0.79	0.22
		1816.0	868.9	1.20	1.19	0.58	0.60	1.14	3.38
1	MSW : Paraffin (9:1)	3105.7	1474.5	2.17	2.10	1.05	1.08	3.09	3.10
		3171.7	1439.2	2.17	2.15	1.05	1.05	0.93	0.42
2	MSW : Paraffin (7:3)	2485.2	1122.2	1.68	1.66	0.81	0.80	1.08	1.04
		2515.3	1158.7	1.68	1.68	0.81	0.83	0.20	2.56
3	MSW : Paraffin (1:1)	1825.3	842.7	1.20	1.19	0.58	0.58	0.59	0.22
		1859.9	868.9	1.20	1.22	0.58	0.60	-1.46	-3.38

1	MSW : Ethylene glycol (9:1)	3163.4	1399.2	2.17	2.14	1.05	1.02	1.20	2.62
		3127.6	1404.4	2.17	2.12	1.05	1.03	2.37	2.23
2	MSW : Ethylene glycol (7:3)	2525.8	1104.0	1.68	1.69	0.81	0.79	0.64	2.83
		2462.7	1099.4	1.68	1.65	0.81	0.78	2.03	3.28
3	MSW : Ethylene glycol (1:1)	1804.3	866.2	1.20	1.18	0.58	0.60	1.84	3.01
		1837.9	853.2	1.20	1.20	0.58	0.59	0.15	1.22

1.4. References:

(1) Harbaugh, D. T.; Baldwin, B. G. *Am. J. Bot.* **2007**, *94*, 1028-1040.

(2) Hamilton, L. a. C., C.E In *Proceedings of the Symposium on Sandalwood in the Pacific*; In: Hamilton, L. and Conrad, C.E., ed. ed. Tech. Rep. PSW-122, Pacific Southwest Research Station, Forest Service, U.S., 1990.

(3) Barrett, D. R. a. F., J.E.D. In *Sandalwood seed nursery and Plantation Technology*; In: Gjerum, L., Fox, J.E.D. and Ehrhart, Y., ed. ed. FAO, Suva, Fiji, 1995; Vol. Field Document No. 8. (RAS/92/361):3-23.

(4) van Balgooy, M. M. J. In *Santalum*; In C.G.G.J. Van Steenis and M.M.J. Van Balgooy [eds.] ed.; Blumea, Leyden, Netherlands: 1966; Vol. vol. 5, p 136-137.

(5) van Balgooy, M. M. J.; Blumea 6 ed. 1971, p 1-222.

(6) van Balgooy, M. M. J., P.H. Hovenkamp, and P.C. van Welzen In *The origin and evolution of Pacific Island biotas, New Guinea to eastern Polynesia: patterns and processes*; In A. Keast and S.E. Miller [eds.] ed.; SPB Academic Publishing, Amsterdam, Netherlands: 1996, p 191-213.

(7) Tennakoon, K. U.; Cameron, D. D. *Can. J. Bot.* **2006**, *84*, 1608-1616.

(8) Loneragan, O. W. 1990.

(9) Radomiljac A., M. J. A. *Nitrogen-fixing and non-nitrogen-fixing woody host influences on the growth of the root hemi-parasite Santalum album L.*; ACIAR: Canberra, 1998.

(10) Radomiljac, A. M.; McComb, J. A.; Pate, J. S. *Ann. Bot.* **1999**, *83*, 215-224.

(11) Kushan U. Tennakoon, D. D. C. *Can. J. Botany* **2006**, *84*, 1608-1616.

(12) Baldovini, N.; Delasalle, C.; Joulain, D. *Flavour Frag. J.* **2011**, *26*, 7-26.

(13) Rai, S. N. In *USDA Forest Service Gen. Tech. Rep. PSW-122* 1990, p 66-71.

(14) Thomson, L. A. J. In *Species Profiles for Pacific Island Agroforestry*; April 2006 ed. 2006; Vol. ver 2.1, p 1-21.

(15) Rakesh K. Sindhu, U., Ashok Kumar, Sahil Arora *Int. J. PharmTech. Res.* **2010**, *2*, 914-919.

(16) Srinivasan, V. V., Sivaramakrishnan, V. R., Rangaswamy, C. R., Ananthapadmanabha, H. S. and Shankaranarayana, K. H.; ICFRE, Ed. Dehradun, 1992.

(17) Fox, J. E. *Biologist* **2000**, *47*, 31-34.

(18) Hansda, R.; Food and Agriculture Organizations Regional Office, B., Ed. 2009, p 89.

(19) Ganeshaiah, K. N.; Shaanker, R. U.; Vasudeva, R. *Curr. Sci.* **2007**, *93*, 140-146.

(20) Chana, J. S. *Int. J. Aromather.* **1994**, *6*, 11-13.

(21) Coppen, J. J. W. In *Flavours and fragrances of plant origin*; Nations, F. a. A. O. o. t. U., Ed. 1995, p 53-58.

(22) Kumar, A. N. A.; Joshi, G.; Ram, H. Y. M. *Curr. Sci.* **2012**, *103*, 1408-1416.

(23) Subasinghe, S. M. C. U. P. *J. Trop. For. Environ.* **2013**, *3*, 1-8.

(24) Dhanya, B.; Syam, V.; Seema, P. *J. Trop. Agri.* **2010**, *48*, 1-10.

(25) Rai, S. N. In *Proceedings of the Symposium on Sandalwood in the Pacific*; In L. Hamilton and C. E. Conrad [eds.] ed. Honolulu, Hawaii, USA, 1990, p 66-71.

(26) Swaminathan, M. H.; Hosmath, B. J.; Mallesha, B. B. In *Sandal and Its Products* 1998, 3-5.
(27) Rajan, B. K. C. *Ten Forest Products*; Jaya Publications, 1992.
(28) Buck, P.; Bishop Museum: Honolulu, 1964; Vol. Publication 45.
(29) Krauss, B. H. *Plants in Hawaiian Culture*; University of Hawai'i Press, Honolulu, 1993.
(30) Shankaranarayana K.H., P. K. In *Indian perfumer* 1987; Vol. 31, p 211-214.
(31) Verghese J., S. T. P., Balakrishnan K.V. *Flavour Frag. J.* **1990**, *5*, 223-226.
(32) Jones, C. G.; Ghisalberti, E. L.; Plummer, J. A.; Barbour, E. L. *Phytochemistry* **2006**, *67*, 2463-2468.
(33) Applegate GB, C. J., et al. In *In 'Proceedings of the Symposium on Sandalwood in the Pacific* (US Forest Service: Honolulu, Hawaii), 1990.
(34) Anonis, D. P. In *Perfumer and Flavorist* 1998; Vol. 23, p 19-24.
(35) McKINNELL, F. H. In *Proceedings of the Symposium on Sandalwood in the Pacific*; In L. Hamilton and C. E. Conrad [eds.] ed. Honolulu, Hawaii, USA, 1990, p 19-25.
(36) Burdock, G. A. a. C., I. G. *Food Chem. Toxicol.* **2008**, *46*, 421–432.
(37) Pande, M. C. In *Medicine and Surgery* 1977; Vol. 17, p 13-16.
(38) Warnke, P. H. e. a. *J. Carnio Maxillofacial Surg.* **2009**, *37*, 392-397.
(39) Ochi, T.; Shibata, H.; Higuti, T.; Kodama, K.; Kusumi, T.; Takaishi, Y. *J. Nat. Prod.* **2005**, *68*, 819-824.
(40) Misra, B. B.; Dey, S. *Lett. Appl. Microbiol.* **2012**, *55*, 476-486.
(41) Benencia, F.; Courreges, M. C. *Phytomedicine* **1999**, *6*, 119-123.
(42) Banerjee, S.; Ecavade, A.; Rao, A. R. *Cancer Lett.* **1993**, *68*, 105-109.
(43) Palamara, A. T.; Perno, C. F.; Ciriolo, M. R.; Dini, L.; Balestra, E.; Dagostini, C.; Difrancesco, P.; Favalli, C.; Rotilio, G.; Garaci, E. *Antivir. Res.* **1995**, *27*, 237-253.
(44) Heuberger, E.; Hongratanaworakit, T.; Buchbauer, G. *Planta Medica* **2006**, *72*, 792-800.
(45) Kulkarni, C. R.; Joglekar, M. M.; Patil, S. B.; Arvindekar, A. U. *Pharm. Biol.* **2012**, *50*, 360-365.
(46) Bruno Marongiu, A. P., Silvia Porcedda and Enrica Tuveri *Flavour Frag. J.* **2006**, *21*, 718-724.
(47) Angus S, A. B., De Reuck M, Altunin VV, Gadeskii OG, Chapela GA, Rowlinson JS; International Thermodynamic Tables of the Fluid State, C. D., Ed.; Pergamon Press: Oxford: 1983.
(48) Dwivedi, C.; Guan, X. M.; Harmsen, W. L.; Voss, A. L.; Goetz-Parten, D. E.; Koopman, E. M.; Johnson, K. M.; Valluri, H. B.; Matthees, D. P. *Cancer Epidem. Biomar.* **2003**, *12*, 151-156.
(49) Dwivedi, C.; Valluri, H. B.; Guan, X.; Agarwal, R. *Carcinogenesis* **2006**, *27*, 1917-1922.
(50) Bommareddy, A.; Hora, J.; Cornish, B.; Dwivedi, C. *Anticancer Res.* **2007**, *27*, 2185-2188.
(51) Arasada, B. L.; Bommareddy, A.; Zhang, X.; Bremmon, K.; Dwivedi, C. *Anticancer Res.* **2008**, *28*, 129-132.
(52) Kaur, M.; Agarwal, C.; Singh, R. P.; Guan, X. M.; Dwivedi, C.; Agarwal, R. *Carcinogenesis* **2005**, *26*, 369-380.

(53) Zhang, X.; Chen, W.; Guillermo, R.; Chandrasekher, G.; Kaushik, R. S.; Young, A.; Fahmy, H.; Dwivedi, C. *BMC research notes* **2010**, *3*, 220-220.
(54) Matsuo, Y.; Mimaki, Y. *Phytochemistry* **2012**, *77*, 304-311.
(55) Okugawa, H.; Ueda, R.; Matsumoto, K.; Kawanishi, K.; Kato, A. *Phytomedicine* **1995**, *2*, 119-126.
(56) Misra, B. B.; Dey, S. *Phytomedicine* **2013**, *20*, 409-416.
(57) Paulpandi, M.; Kannan, S.; Thangam, R.; Kaveri, K.; Gunasekaran, P.; Rejeeth, C. *Phytomedicine* **2012**, *19*, 231-235.
(58) Kim, T. H.; Ito, H.; Hatano, T.; Takayasu, J.; Tokuda, H.; Nishino, H.; Machiguchi, T.; Yoshida, T. *Tetrahedron* **2006**, *62*, 6981-6989.
(59) Kim, T. H.; Ito, H.; Hayashi, K.; Hasegawa, T.; Machiguchi, T.; Yoshida, T. *Chem. Pharm. Bull.* **2005**, *53*, 641-644.
(60) Erligmann, A. *Int. J. Aromather.* **2001**, *11*, 186-192.
(61) Yoshizawa, S. H., H.; Fujiki, H.; Yoshida, T.; Okuda, T.; Sugimura, T. *Phytother. Res.* **1987**, *1*, 1190-1195.
(62) Guha, P., Bhattacharya, S. C. *J. Indian Chem. Soc.* **1944**, *21*, 261.
(63) Kim, T. H.; Ito, H.; Hatano, T.; Hasegawa, T.; Akiba, A.; Machiguchi, T.; Yoshida, T. *J. Nat. Prod.* **2005**, *68*, 1805-1808.
(64) Radomiljac, A. M., Ananthapadmanabho,H.S., Welbourn, R.M., Satyanarayana Rao, K. In *ACIAR Proceedings* Australian Centre for International Agricultural Research, Canberra: 1998; Vol. No. 84.
(65) Naipawer, R. E. In *Flavors and Fragrances, A World Perspective, Proceedings of the 10th International Conference of Essential Oils*; B. M. Lawrence, M., B. D., Willis, B. J., Ed.; Elsevier: Amsterdam, 1988, p 805.
(66) II ed.; ISO 3518:2002(E), 2002-03-01: Geneva, Switzwerland, 2002.
(67) Kuriakose, S.; Thankappan, X.; Joe, H.; Venkataraman, V. *Analyst* **2010**, *135*, 2676-2681.
(68) Marjoniemi, M. *Appl. Spectrosc.* **1992**, *46*, 1908-1911.
(69) Guiteras, J.; Beltran, J. L.; Ferrer, R. *Anal. Chim. Acta* **1998**, *361*, 233-240.
(70) Howes, M. J. R.; Simmonds, M. S. J.; Kite, G. C. *J. Chromatogr. A* **2004**, *1028*, 307-312.
(71) Sciarrone, D.; Costa, R.; Ragonese, C.; Tranchida, P. Q.; Tedone, L.; Santi, L.; Dugo, P.; Dugo, G.; Joulain, D.; Mondello, L. *J. Chromatogr. A* **2011**, *1218*, 137-142.
(72) Shellie, R.; Marriott, P.; Morrison, P. *J. Chromatogr. Sci.* **2004**, *42*, 417-422.
(73) Eberz, W. F.; Welge, H. J.; Yost, D. M.; Lucas, H. J. *J. Am. Chem. Soc.* **1937**, *59*, 45-49.
(74) Winstein, S.; Lucas, H. J. *J. Am. Chem. Soc.* **1938**, *60*, 836-847.
(75) Nichols, P. L. *J. Am. Chem. Soc.* **1952**, *74*, 1091-1092.
(76) Dewar, J. S. *B. Soc. Chim. Fr.* **1951**, *18*, C71-C79.
(77) Janak, J.; Jagari, Ä., Z.; Dressler, M. *J. Chromatogr. A* **1970**, *53*, 525-530.
(78) Guha, O. K.; JanÃ¡k, J. *J. Chromatogr. A* **1972**, *68*, 325-343.
(79) Barrett, C. B.; Dallas, M. S. J.; Padley, F. B. *Chem. Ind.* **1962**, 1050-1051.
(80) Morris, L. J. *Chem. Ind.* **1962**, 1238-1240.
(81) Gupta, A. S.; Dev, S. *J. Chromatogr. A* **1963**, *12*, 189-195.

(82) Prasad, R. S.; Gupta, A. S.; Dev, S. *J. Chromatogr. A* **1974**, *92*, 452-453.
(83) Bennett, R. D.; Heftmann, E. *J. Chromatogr. A* **1962**, *9*, 359-362.
(84) Copius-Peereboom, J. W.; Beekes, H. W. *J. Chromatogr. A* **1965**, *17*, 99-113.
(85) Stevens, P. J. *J. Chromatogr. A* **1968**, *36*, 253-258.
(86) Jarusiewicz, J.; Sherma, J.; Fried, B. *J. Liq. Chromatogr. Relat. Technol.* **2005**, *28*, 2607-2617.
(87) Rezanka, T. *J. Chromatogr. A* **1996**, *727*, 147-152.
(88) Faraldos, J. A.; O'Maille, P. E.; Dellas, N.; Noel, J. P.; Coates, R. M. *J. Am. Chem. Soc.* **2010**, *132*, 4281-4289.
(89) Christie, W. W.; Breckenridge, G. H. M. *J. Chromatogr. A* **1989**, *469*, 261-269.
(90) Heath, R. R. T., J.H.; Doolittle, R.E.; Proveaux, A. T. *J. Chromatogr. Sci.* **1975**, *13*, 380-382.
(91) Heath, R. R. T., J.H.; Doolittle, R.E.; Duncan, J.H. *J. Chromatogr. Sci.* **1977**, *15*, 10-13.
(92) Evershed, R. P.; Morgan, E. D.; Thompson, L. D. *J. Chromatogr.* **1982**, *237*, 350-354.
(93) Thulasiram, H. V.; Poulter, C. D. *J. Am. Chem. Soc.* **2006**, *128*, 15819-15823.
(94) Li, T.-S.; Li, J.-T.; Li, H.-Z. *J. Chromatogr. A* **1995**, *715*, 372-375.
(95) Heftmann, E.; Saunders, G. A.; Haddon, W. F. *J. Chromatogr. A* **1978**, *156*, 71-77.
(96) Morita, M.; Mihashi, S.; Itokawa, H.; Hara, S. *Anal. Chem.* **1983**, *55*, 412-414.
(97) Bennett, B.; Larter, S. R. *Anal. Chem.* **2000**, *72*, 1039-1044.
(98) Dwivedi, C.; Maydew, E. R.; Hora, J. J.; Ramaeker, D. M.; Guan, X. M. *Eur. J. Cancer Prev.* **2005**, *14*, 473-476.
(99) Hongratanaworakit, T.; Heuberger, E.; Buchbauer, G. *Planta Medica* **2004**, *70*, 3-7.
(100) Jirovetz, L.; Buchbauer, G.; Denkova, Z.; Stoyanova, A.; Murgov, I.; Gearon, V.; Birkbeck, S.; Schmidt, E.; Geissler, M. *Flavour Frag. J.* **2006**, *21*, 465-468.
(101) So, P. L.; Tang, J. Y.; Epstein, E. H. *Expert Opin. Inv. Drug.* **2010**, *19*, 1099-1112.
(102) Christenson, P. A.; Secord, N.; Willis, B. J. *Phytochemistry* **1981**, *20*, 1139-1141.
(103) Chilampalli, S.; Zhang, X. Y.; Fahmy, H.; Kaushik, R. S.; Zeman, D.; Hildreth, M. B.; Dwivedi, C. *Anticancer Res.* **2010**, *30*, 777-783.
(104) Buchbauer, G.; Stappen, I.; Pretterklieber, C.; Wolschann, A. *Eur. J. Med. Chem.* **2004**, *39*, 1039-1046.
(105) Corey, E.; Kirst, H.; Katzenellenbogen, J. *J. Am. Chem. Soc.* **1970**, *92*, 6314-6320.
(106) Fehr, C.; Magpantay, I.; Arpagaus, J.; Marquet, X.; Vuagnoux, M. *Angew. Chem. Int. Edit.* **2009**, *48*, 7221-7223.
(107) Monti, H.; Corriol, C.; Bertrand, M. *Tetrahedron Lett.* **1982**, *23*, 5539-5540.
(108) Pianowski, Z.; Rupnicki, L.; Cmoch, P.; Stalinski, K. *Synlett* **2005**, 900-904.
(109) Sato, K.; Miyamoto, O.; Inoue, S.; Honda, K. *Chem. Lett.* **1981**, 1183-1184.
(110) Schlosser, M.; Zhong, G. F. *Tetrahedron Lett.* **1993**, *34*, 5441-5444.
(111) Durrani, A. A.; Garrett, A.; Johnson, R. A.; Sood, S. K.; Tyman, J. H. P. *J. Liq. Chromatogr. Relat. Technol.* **2002**, *25*, 1543-1559.
(112) Kagan, I. A.; Rimando, A. M.; Dayan, F. E. *J. Agric. Food Chem.* **2003**, *51*, 7589-7595.

(113) Yong, K. W. L.; Jankam, A.; Hooper, J. N. A.; Suksamrarn, A.; Garson, M. J. *Tetrahedron* **2008**, *64*, 6341-6348.
(114) Oppolzer, W.; Chapuis, C.; Dupuis, D.; Guo, M. *Helv. Chim. Acta* **1985**, *68*, 2100-2114.
(115) Christenson, P. A.; Willis, B. J. *J. Org. Chem.* **1979**, *44*, 2012-2018.
(116) Azeez, S. A.; Nelson, R.; Prasadbabu, A.; Rao, M. S. *Afr. J. Biotechnol.* **2009**, *8*, 2943-2947.
(117) Alizadeh, B. H.; Kuwahara, S.; Leal, W. S.; Men, H. C. *Biosci. Biotech. Bioch.* **2002**, *66*, 1415-1418.
(118) Snider, B. B.; Beal, R. B. *J. Org. Chem.* **1988**, *53*, 4508-4515.

Chapter 2

Biotransformation of (*Z*)-α-Santalyl Derivatives

Section 2.1.

Introduction:

Biotransformation

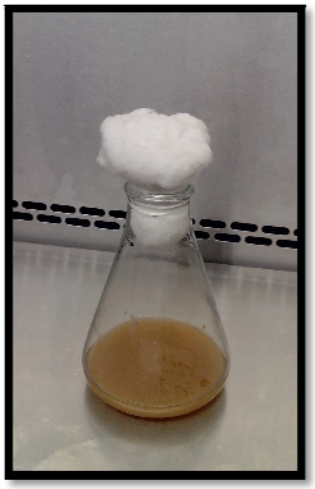

Fungal culture.

'Biotransformation' is a broad term assigned to modification of organic molecules, chemical substances, nutrients, amino acids, toxins, and drugs to their derivatives (in some cases also called as 'secondary metabolites') by introduction or elimination of one or more functional groups mediated by biocatalysts such as fungi, bacteria, algae, yeast and plant cultured cells or by isolated enzymes in their native or modified forms. In case of biocatalyst mediated transformation of xenobiotics to CO_2, NH_4^+ or H_2O, the process is called 'biomineralization'.

2.1.1. History of Biotransformation

Throughout the times of mankind, microorganisms have gathered a remarkable social and economic status. The history of utilization of microbial catalysts in the production and preservation of foods and beverages dates back to primitive culture of humans, even when existence of the former was unknown. While the Sumerians and Babylonians practised the brewing of beer before 6000 BC, Egyptians used yeast for baking bread. Vinegar production, perhaps the oldest and best known example of microbial oxidation, dates back to around 2000 BC. However, knowledge of the production of chemicals such as alcohols and organic acids through fermentation is relatively recent and the first reports in the literature only appeared in the second half of the 19th century. The rational application of these early techniques could come only after the scientific practice of organic chemistry and microbiology had begun. Only in the later part of 17th century, Dutch microscopist, Antony von Leeuwenhoek became the first person to recognize the existence of microbes.[1] The discovery of new microscopic life was the foundation for experimental biology as a basis for the development of the biotransformations. Louis Pasteur, in 1858, laid a landmark in biocatalysis setting the stage for modern day enzymatic kinetic resolution of racemates, when he demonstrated the resolution of tartaric acid with a culture of the mould *Penicillium glaucum*, leading to the consumption of (+)-tartaric acid and a simultaneous enrichment of the (-)-enantiomer. Eduard Buchner in 1897 reported the successful fermentation of sugar to lactic acid and ethanol by cell free yeast extract, which precluded the necessary requirement of living cells for biological alterations.[2] Pasteur discovered that all fermentative processes are the result of microbial activity and the individual microbial species are responsible for discrete chemical alteration of selected substrates. These earliest scientific experiments were called as the "birth of microbiology". As time elapsed, greater advances added knowledge to the fundamental studies. In the first half of the 20th century scientists in

academia and industry learned how to use whole cells, cell extracts, or partially purified enzymes in various biocatalytic processes. Demonstration of microbial catalysis of the regio- and stereoselective oxidative hydroxylation of steroids, as first in the early 1950s by such pharmaceutical companies as Upjohn, Schering, Pfizer, and Merck set the beginning for the present day research and technology in biotransformation processes.

In recent years, the most significant development in the field of synthetic organic chemistry has been the application of biological systems to chemical reactions. Reactions catalyzed by whole cell biocatalysts and enzyme systems have displayed far greater specificities than the more conventional organic reactions. Displaying a great potential and versatility, microbial transformations have dominated applications in a wide variety of processes such as, manufacturing of foods,[3] flavors and perfumery,[4] synthesis of pharmaceutically active components,[5] organic reactions leading to novel biologically active derivatives,[6] fermentations, beverages, and biodegradation of pesticides, pollutants, pharmaceuticals,[7] dyes and xenobiotics. One of the important aspects of microbial system is their broad substrate specificity, which empowers them with an ability to carry out wide variety of reactions such as oxidation, reduction, hydrolysis, hydroxylation, dehydration, condensation, isomerization, rearrangement, etc. The versatile nature of microorganisms have enabled chemists to use them as supplement to some of the steps / processes involved in the chemical synthesis of various pharmacologically important compounds. In microbial conversion, microorganisms replace organic reagents that carry out various functional group inter-conversions to form metabolites, which serve different functions in living systems.

In the present times, biotransformation of steroids and terpenoids is being tremendously sought after in industrial production of some of the vital drug intermediates.[8-10] In 1952, Murray and Peterson first patented the process for 11α-hydroxylation of progesterone by *Rhizopus* species, which initiated the utility of industrially viable microbial processes for the synthesis of different biologically active complex molecules.[11] Thousands of microbial transformations involving different types of reactions with organic compounds and natural products have now become known, some of them proving to be very useful in synthetic organic chemistry. Biocatalysis in industrial applications has not only delivered the products with greater chemoselectivity, regioselectivity and stereoselectivity, but have also helped to cut the costs of the final products drastically by reducing the intermediate steps required for synthesis.[12]

2.1.2. Advantages of Biocatalysts:

Microbial transformations are versatile, covering many reactions such as, (i) oxidation, (ii) reduction, (iii) hydrolysis, (iv) dehydration and condensation, (v) degradation, (vi) formation of C-C or hetero atom bonds, (vii) isomerization and rearrangements. The biotransformation of organic compounds by microorganisms is considered an economical and ecologically viable technology. In addition, it is a useful tool for the structural modification of bioactive natural products and the study of natural product metabolism.[13,14] Several advantages in selecting microbial reactions as a rational supplement to chemical synthesis are the following:

1. Activation of unreactive centers:

   Microbial reactions can be used to attack positions in the molecules which are not normally affected by chemical methods because of lack of activation or, require a number of intermediate synthetic stages to impart chemical accessibility. Oxygen functionality or other substituents can be introduced stereospecifically and regiospecifically or altered with a possible formation of optically active centers.

2. Catalysis of multiple reactions:

   Several reactions can be combined in one fermentation step and actually programmed to occur in a specific sequence, if a suitable microorganism with a number of appropriate enzyme systems can be used. Modern techniques leading to development of engineered cells have enhanced the importance of these processes.

3. Green processes:

   The conditions under which microbial reactions take place are mild. Hence, compounds that are sensitive to heat, acid, and base become amenable to such transformations.

4. Microbial synthesis also has advantages in the preparation of optically active compounds, since chemical synthesis leads to racemic mixtures that must subsequently be resolved. It displays selectivity in the reactions as below:

   i) Chemoselectivity:

      Biocatalysts are particular towards a single type of functional group and other sensitive functionalities which would otherwise be affected in synthetic reactions remain intact and unaffected. As a result, reaction course is cleaner and the products are free from impurities which omit laborious purification procedures.

   ii) Regioselectivity and Diastereoselectivity:

Due to their complex quaternary structure, enzymes/ biocatalysts can distinguish between functional groups which are located in different regions of the same substrate molecule.

iii) Enantioselectivity:

As all enzymes are made from L-amino acids, they create chiral environment when in contact with the chiral substrates. They recognize chirality of the substrates upon formation of substrate-enzyme complex. Thus, a prochiral substrate may be transformed into an optically active product through a desymmetrization process and both enantiomers of a racemic substrate usually react at different rates, affording a kinetic resolution. On the other side, the principles of asymmetric synthesis employ chiral auxiliaries in catalytic and sometimes stoichiometric amounts, which are often expensive, not recoverable from the reaction media, and in turn increase the cost of the overall process.

5. It is often cheaper to use a biocatalyst for the preparation of an organic compound than to synthesize it chemically. Above all, the processes mediated by microbes are eco-friendly and so these processes produce minimum environmental pollution unlike processes mediated by chemical reagents.
6. Industrially scalable:

Biocatalytic processes can be scaled up from shake flask to industrial levels in large fermentors. This aspect in particular has attracted the attention of industrial and synthetic chemists and biologists for the production of pharmaceuticals.

Hence, it is not surprising to note that several of the medicinally and commercially important molecules including steroids hormones are now produced on a large scale by microbial processes. Above features collectively prove the superiority of biocatalytic processes over use of conventional synthetic organic chemistry tools. However, biocatalytic processes suffer from a few drawbacks:

1. Biocatalysts display their highest catalytic activity in water. The water solubility of hydrophobic substrates can be overcome by using additives such as tween, cyclodextrin, which may improve solubility of the substrates. Biphasic transformations or ionic liquids may also be employed.
2. Selection of an appropriate biocatalyst for a particular process may require screening of many cultures, but can be rationalized.

Depending on the type and scale of reaction and the requirement of co-factors, whole cells or isolated enzymes can be employed in biotransformation. In recent times,

with the advancements in technology, it has become easy to produce and purify the enzymes on higher scales. Nowadays, many pure enzymes in various forms (immobilized, lyophilized) are commercially available for specific type of reactions. Enzymes thus modified are relatively more stable, easy to use and yield single product. But depending on the type of reaction, supplementary co-factors may be required which limit the applications of pure enzymes over whole cell. Enzymatic processes may be substituted with whole cell transformations where fungi, bacteria, yeasts and algae are employed as reagents. Microbial transformations produce more than one product depending on the substrate used, but are easy to be scaled up and often cheaper to be used, than isolated enzyme systems. Nature and number of products, and incubation times can be varied by screening more number of cultures. Substrate concentrations can be standardized for an individual culture to prevent inhibitions. Biotransformation of a natural or synthetic substrate can yield the products with new functionalities or entirely new scaffolds, which may have an entirely new spectrum of unexplored biological activities.

2.1.3. The process of microbial transformation:

A) Organism:

Microbes are living organisms which synthesize multiple enzymes for their survival and normal functioning. When incubated with the substrate of interest, they may produce one or more, or sometimes, no products. Therefore, in microbial transformation, it often becomes necessary to screen several cultures for the desired conversion. Selection of an appropriate culture forms the primary requirement. Screening of a microorganism constituting the required enzyme can be done by random screening, enrichment procedure or may be based on some earlier analogies, where some of the cultures are reported to constitute the enzyme/s of interest. Procedures of random screening involve incubating the substrate with a large number of cultures and analysis of the reaction mixture for presence of the product after uniform time intervals. The organism that would test positive, yielding the desired product with maximum substrate conversion is selected for further investigation. In enrichment procedure, soil samples are continuously supplemented with large amount of substrate, together with water and additional nutrients so as to make only those microbes survive from a vast pool of those which

can adapt to the confining environment. These organisms are isolated by plating technique and further used for transformation.

B) Sterile conditions:

Sterility must be maintained because contamination can suppress the desired reaction, induce the formation of faulty conversion products or cause total substrate breakdown. Fermentation media is sterilized by autoclaving it before use.

C) Aeration and stirring:

For efficient aerobic microbial transformation, adequate oxygen supply must be made available to cells. Sterile air is obtained by passing it through sterile filters before allowed to enter the reaction container. The complete reaction mass must be continuously agitated so as to maintain the homogeneity and uniform transformation.

D) Substrate homogeneity:

In these processes, solubility and rate of diffusion of organic substrate (generally hydrophobic) in aqueous media are the rate-limiting steps. Emulsifiers such as Tween, water miscible solvents of low toxicity (ethanol, acetone, DMF, DMSO), cyclodextrin or biphasic ionic liquids may help to solubilize the poorly soluble compounds.

E) Product isolation:

The end product of transformation reactions are usually extra cellular and may occur in either dissolved form or suspended form. Depending on the solubility of the products, recovery can be performed by precipitation, adsorption on ion-exchangers, extraction with appropriate organic solvents or for volatile substances, by direct distillation from the reaction media. Product isolation is usually followed by the qualitative analysis, and purification of the products employing conventional techniques such as silica gel column chromatography, distillation or sophisticated techniques such as GC, MPLC, and HPLC.

2.1.4. Biotransformation of Sesquiterpenes:

2.1.4.1. Acyclic sesquiterpenes:

Sesquiterpenes are the natural products belonging to a broad class of 'Terpenoids', also known as 'isoprenoids' and are built of 3 isoprene units (15 carbon atoms). Acyclic sesquiterpenes are widely distributed in nature and are biosynthetic precursors of cyclic sesquiterpenoids present in living organisms. The fundamental sesquiterpene acyclic unit, (*E*,*E*)-farnesyl diphosphate [(*E*,*E*)-FPP], is biosynthesized in nature by dissociative electrophilic alkylation of a hemiterpene unit isopentenyl diphosphate (IPP) with the carbocation derived from one unit of geranyl diphosphate (GPP) or sequential condensation of two IPP units with carbocation from one unit of dimethylallyl diphosphate (DMAPP). The acyclic diphosphate precursor (FPP) undergoes cyclization in presence of specialized enzymes called 'terpene cyclases' which are present in living systems. Hydrolysis of the diphosphate ester bond in (*E*,*E*)-FPP releases (*E*,*E*)-farnesol. In chapter-3, biosynthesis of sesquiterpenes has been discussed in detail.

2.1.4.1.1. Biotransformation of (*E*,*E*)-farnesol:

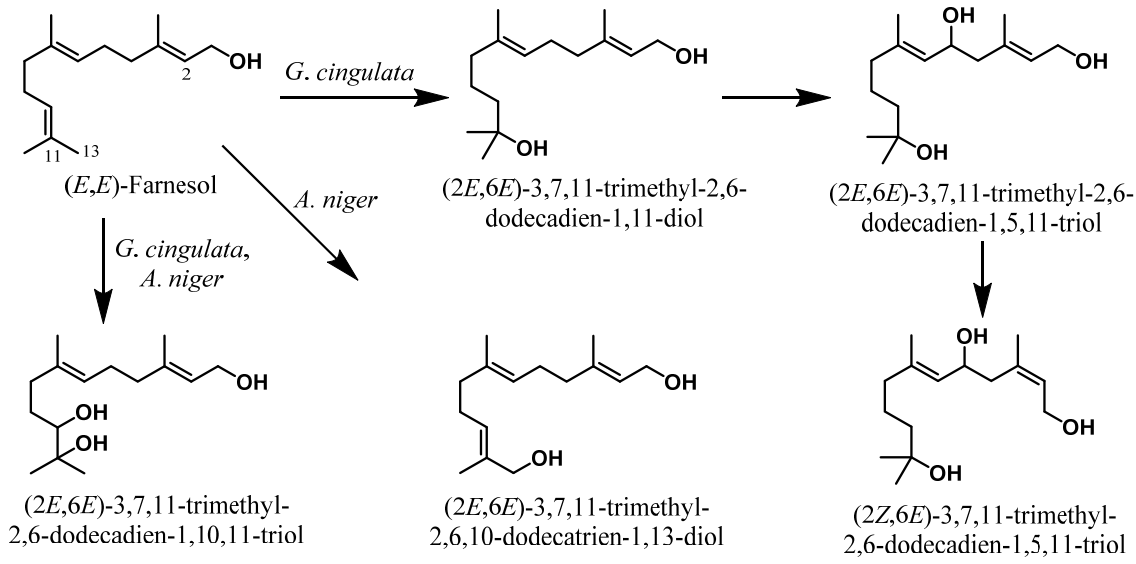

Scheme 2.1.1. Transformation of (*E*,*E*)-farnesol mediated by fungal cultures.

Biotransformation of (*E*,*E*)-farnesol was studied with several fungal cultures to yield higher oxygenated and in some cases isomerized products. It was transformed into (2*Z*,6*E*)-farnesol by *Helminthosporium sativum*[15] and to (2*E*,6*E*)-3,7,11-trimethyl-2,6-dodecadien-1,10,11-triol and (2*E*,6*E*)-3,7,11-trimethyl-2,6,10-dodecatrien-1,13-diol by *Aspergillus niger*.[16] Miyazawa M. *et al*. have reported the transformation of (*E*,*E*)-

farnesol to (2*E*,6*E*)-3,7,11-trimethyl-2,6-dodecadien-1,11-diol, (2*E*,6*E*)-3,7,11-trimethyl-2,6-dodecadien-1,5,11-triol, (2*Z*,6*E*)-3,7,11-trimethyl-2,6-dodecadien-1,5,11-triol and (2*E*,6*E*)-3,7,11-trimethyl-2,6-dodecadien-1,10,11-triol[17] (Scheme 2.1.1).

2.1.4.1.2. Biotransformation of nerolidol:

Miyazawa *et al*. speculated if it would be possible to produce new cyclic terpenoids or synthetic precursors of bioactive compounds from acyclic terpenoids by microbial transformation that would be valuable for synthetic organic chemistry. They studied the biotransformation of acyclic sesquiterpenoids, (±)-*cis*-nerolidol by plant pathogenic fungus, *Glomerella cingulata*.[18]

The effect of geometry of C=C double bond on the mode of microbial transformation of (*E*)- and (*Z*)-nerolidol was examined with a fungus *G. cingulata*. On biotransformation, both the isomers were mainly oxidized at the remote double bond, but with markedly different metabolites. With the *cis*-isomer, epoxidation of the remote double bond and subsequent hydrolysis presented (*Z*)-3,7,11-trimethyl-1,6-dodecadien-3,10,11-triol as the major metabolite,[18] whereas, with *trans*-isomer, hydration of the remote double bond was the main pathway to give (*E*)-3,7,11-trimethyl-l,6-dodecadien-3,11-diol as the major metabolite and only small amount of (*E*)-3,7,11-trimethyl-1,6-dodecadiene-3,10,11-triol was obtained.[19] This difference in product formation between (*Z*)-form and (*E*)-form of the substrate by the fungus was explained by influence of *Z/E* configuration of the substrate (Scheme 2.1.2).

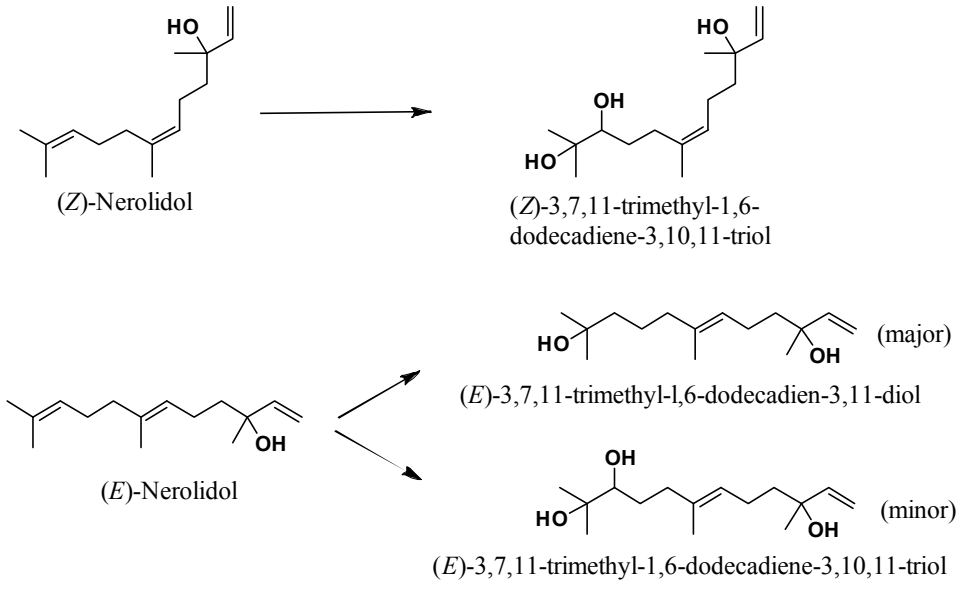

Scheme 2.1.2. Microbial transformation of (*E*)- and (*Z*)-nerolidol with *G. cingulata*.

(*E*)-Nerolidol was microbially transformed to Caparrapidiol and many other oxidized derivatives by five kinds of *Fusarium* strains and some of these are shown in scheme 2.1.3.[20] As reported by Abraham W. R., of the 100 cultures screened, only *Fusarium* species which is an economically important soil-borne plant pathogenic genus, could exhibit the biotransformation of (*E*)-nerolidol. A series of reactions such as epoxidations, hydroxylations and cyclizations led to many of the metabolites which were not known until then, and possessed novel structures including di-tetrahydrofuranes, which helped in deriving the absolute stereochemistry of hydroxylated derivatives of Caparrapidiol.

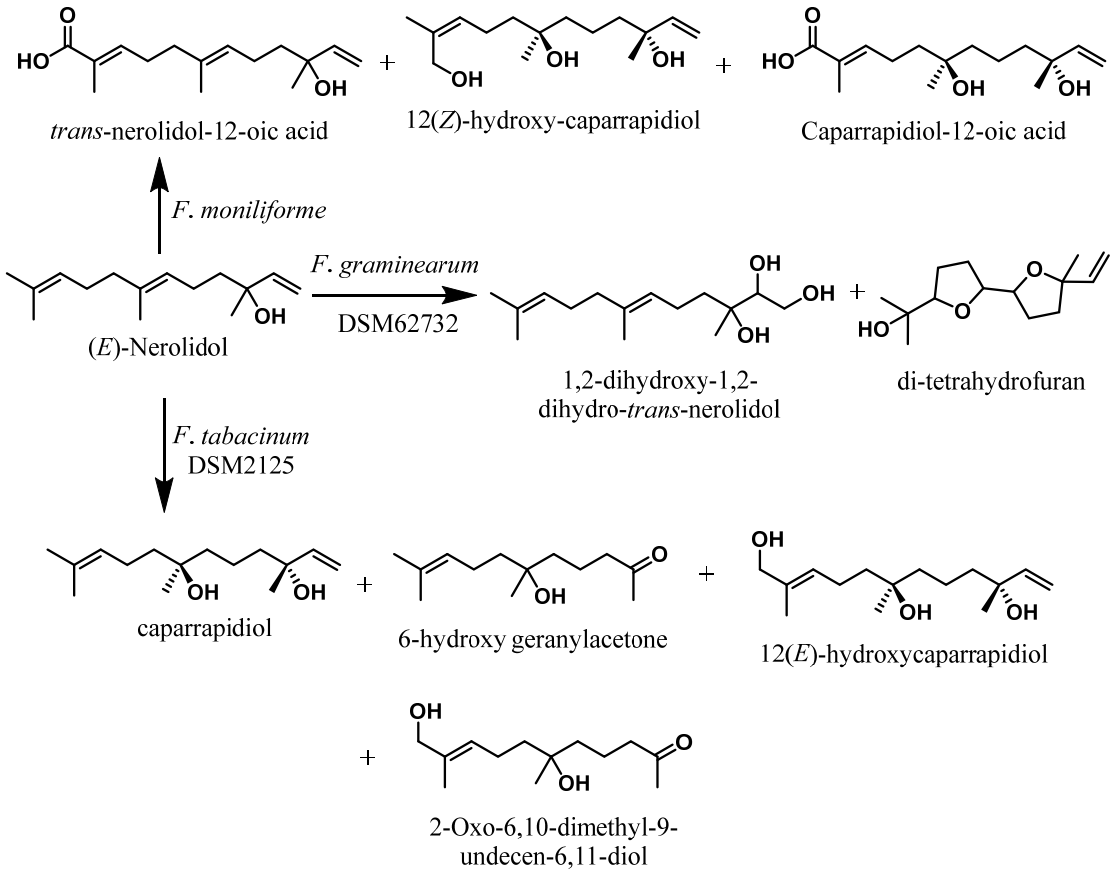

Scheme 2.1.3. Biotransformation of (*E*)-nerolidol with various *Fusarium* species.

2.1.4.2. Cyclic sesquiterpenes:

2.1.4.2.1. Biotransformation of cyclonerodiol:

Cyclonerodiol has been isolated from the fungi, *Myrothecium* sp., *Trichothecium reseum*, *Gibberella fujikuroi*, *Fusarium culmorum*, and *Trichoderma koningii* as the plant growth regulatory active constituent.[21] Li *et al*. studied the mode of

biotransformation of cyclonerodiol with two marine-derived strains, an ascomycete, *Penicillium* sp. (MFAac49) and an actinomycete, *Streptomyces* sp. Fermentation of cyclonerodiol with *Penicillium* sp. followed by extraction of the metabolites with ethyl acetate and subsequent purifications yielded one glycoside, which was characterized as cyclonerodiol mannopyranoside. On the other hand, incubation of cyclonerodiol with *Streptomyces* sp. furnished two oxidised metabolites which were purified and characterized as 10(*Z*)-15-hydroxycyclonerodiol and 10(*E*)-12-hydroxycyclonerodiol (Scheme 2.1.4). When examined for the effect of these compounds on the viability of HeLa cells, cyclonerodiol and 10(*Z*)-15-hydroxycyclonerodiol exhibited an IC_{50} value of 172.1 μM and 145.7 μM, respectively.[21]

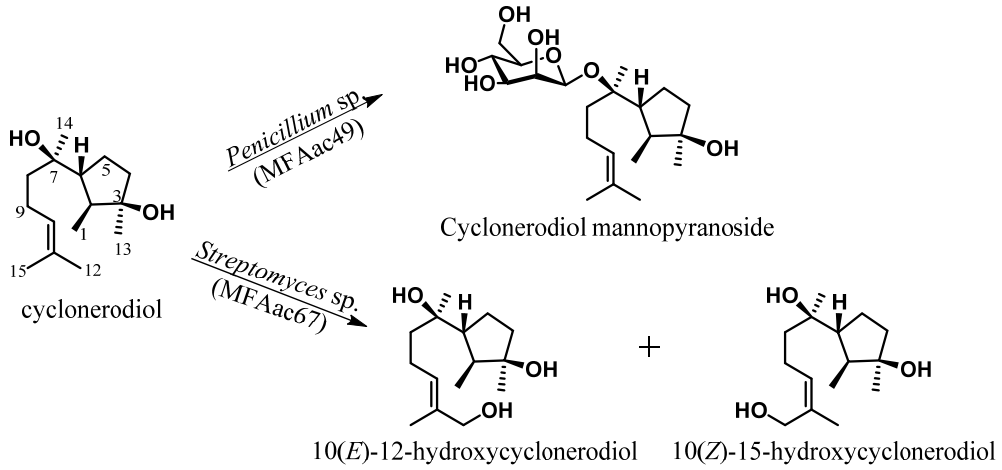

Scheme 2.1.4. Biotransformation of Cyclonerodiol by *Penicillium* and *Streptomyces* sp.

2.1.4.2.2. Biotransformation of Zerumbone:

Zerumbone, a humulenoid sesquiterpene possessing a flexible skeleton structure was isolated from wild ginger (*Zingiber zerumbet* Smith) by hydro-distillation.[22] Zerumbone and its derivatives have been reported to exhibit anti-inflammatory and anti-tumor-promoting activity.[23,24] Biotransformation of zerumbone was examined by Sakamaki *et al*. using suspension cultured cells of *Caragana chamlagu* (Leguminosae) to generate zerumbone epoxide as the intermediate product, preferentially. The intermediate further underwent enantioselective reduction of one of the olefins to form two reduced products, which were identified as (2*R*,3*R*,7*R*)-2,3-epoxy-9-humulen-8-one and (2*R*,3*S*,7*R*)-2,3-epoxy-9-humulen-8-one (Scheme 2.1.5).[25]

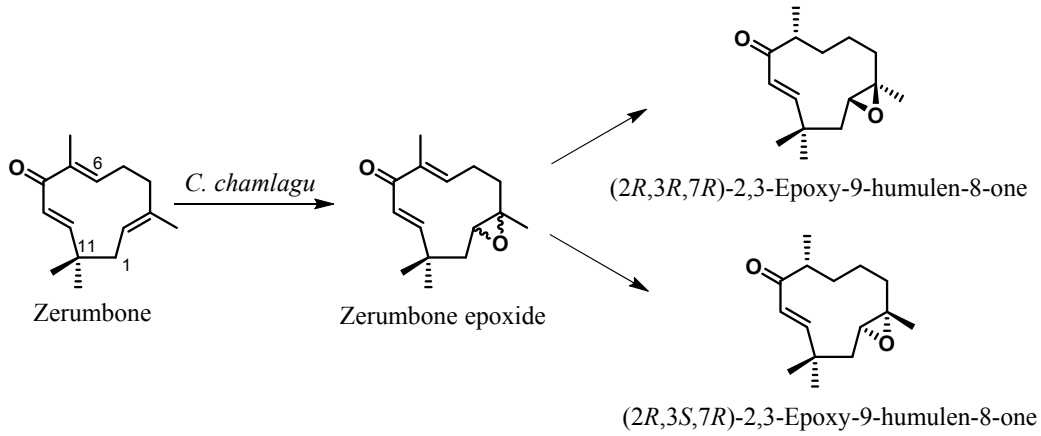

Scheme 2.1.5. Biotransformation of Zerumbone with cultured cells of *C. chamlagu*.

2.1.4.2.3. Biotransformation of Curdione:

Sesquiterpenes such as Curcumol and Curdione which are the major ingredients of *Rhizoma curcumae*, play important roles in Chinese Traditional Medicine. Their microbial transformation by *Cunninghamella elegans* AS 3.2028 was studied that resulted in stereoselective epoxidation at the double bond of Curcumol yielding 10*S*,14-epoxycurcumol as the major metabolite (>99% de), with no detectable 10*R*,14-epoxycurcumol. Epoxidation also occurred at the double bond of Curdione, generating both (1*S*,10*S*)- and (1*R*,10*R*)-1,10-epoxycurdione. The diastereomeric excess (de) of the (*S*)-diastereomer was 27% (Scheme 2.1.6).[26]

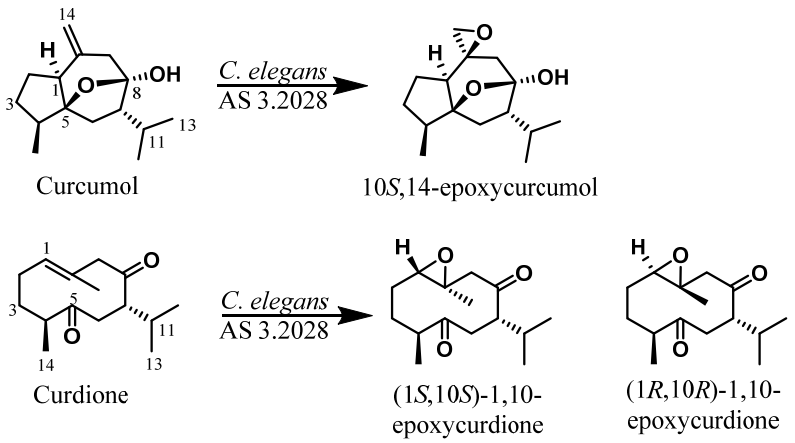

Scheme 2.1.6. Stereoselective epoxidation of Curcumol and Curdione by *Cunnighamella elegans* AS 3.2028.

2.1.4.2.4. Biotransformation of Tagitinin C:

An unusual and an unexpected biotransformation of Tagitinin C with *Aspergillus terreus* MT 5.3 was obtained to form 1-methoxy-3-hydroxy-3,10β-4,5α-diepoxy-8β-isobutyroyloxygermacr-11(13)-en-6α,12-olide as the sole metabolite (Scheme 2.1.7).[27] Tagitinin C is a sesquiterpene lactone (STL) belonging to a large group of natural products found mainly in plants of the family *Asteraceae*. It occurs in the glandular trichomes of the leaves and inflorescences of Mexican sunflower (*Tithonia diversifolia* Hemsl. A. Gray, *Asteraceae*) and shows anti-inflammatory, and anti-feedant activities, and thus is a promising compound for further research into its mechanisms of action in different targets. However, due to the toxicity of STLs, their use for pharmaceutical purposes remains to be a point of concern; therefore, some of their derivatives those may have lower toxic effects and improved pharmacological activities need to be obtained. Biotransformation of STLs can be an attractive alternative for the above problem that can yield new derivatives with desired properties and can establish *in vitro* models to predict mammalian metabolites. According to the literature, the main enzymatic reactions of STLs those are able to be catalyzed by *Aspergillus* species are hydrogenation, hydroxylation, reduction, and acetylation.

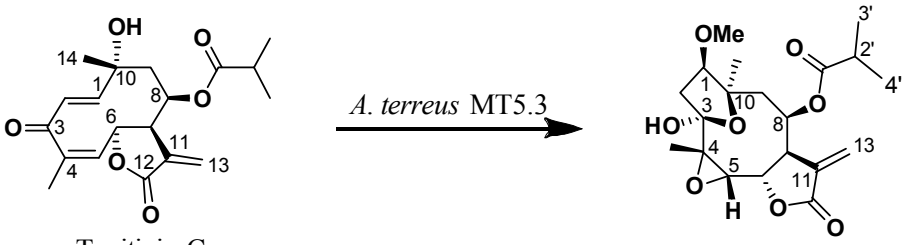

Tagitinin C

1-methoxy-3-hydroxy-3,10 β-4,5α-diepoxy-8β-isobutyroyloxygermacr-11(13)-en-6 α,12-olide

Scheme 2.1.7. Biotransformation of Tagitinin C with *A. terreus* MT 5.3.

From structural elucidation of the metabolite formed, reactions occurred on the substrate could be explained as, epoxidation between C4 and C5; a methoxy group added at C1, reduction of ketone at C3, and a C3-C10 ether bridge formed in the 10-membered ring of the substrate, but the exocyclic double bond at C11-C13 was preserved (Scheme 2.1.7). The metabolite could also be isolated from a rinse extract of the inflorescences of Brazilian population of Mexican sunflower *T. diversifolia* by Ambrosio S R *et al*. While the chemical structure of the metabolite was already known,

it was not obtained as a product from microbial biotransformation. The metabolite indicated that the *Aspergillus* strain used in this work was able to catalyze chemical reactions that mimicked those which occur inside the glandular trichomes from the inflorescences of *T. diversifolia* and could be used as an alternative source for production of the metabolite. However, the structural modifications brought about by biotransformation in Tagitinin C did not improve or decrease the cytotoxic activity of the metabolite in HL-60 cells in comparison to the substrate.

2.1.4.2.5. Biotransformation of Caryophyllene oxide:

Caryophyllene oxide was fermented with many fungal cultures to afford 9 metabolites which were identified as its oxidized derivatives (Scheme 2.1.8).[28] Incubation of (-)-caryophyllene oxide with *Cephalosporium aphidicola* yielded two metabolites, (1*R*,4*R*,5*R*,9*S*)-4,5-dihydroxycaryophyllan-8(13)-ene formed by epoxide hydrolase enzyme which is also present in eukaryotic cells, and (1*S*,4*R*,5*R*,8*S*,9*S*)-clovane-5,9-diol. These compounds were also isolated as secondary metabolites from the neutral fraction of the dried pods of the medicinal plant *Sindora sumatrana*.[29] When caryophyllene oxide was incubated with *Macrophomina phaseolina*, two metabolites with primary hydroxy groups (hydroxylated at geminal methyl groups) were obtained which were identified as (1*R*,4*R*,5*R*,9*S*,11*R*)-4,5-epoxycaryophyllan-8(13)-en-15-ol and (1*R*,4*R*,5*R*,9*S*,11*S*)-4,5-epoxycaryophyllan-8(13)-en-14-ol. Incubation of the substrate with *Aspergillus niger*, *Fusarium lini*, and *Gibberella fujikuroi* yielded one metabolite each as (1*R*,4*R*,5*R*,8*S*,9*S*,13*S*)-caryolane-5,8,13-triol, (1*R*,3*R*,4*R*,5*R*,8*S*,9*S*)-4,5-epoxy-caryophyllan-3,13-diol and (1*S*,4*R*,5*R*,8*S*,9*S*)-clovane-5,9,12-triol, respectively. All the metabolites along with the substrate were tested for butyrylcholinesterase (BChE) inhibition activity when it was observed that the later 4 metabolites showed a stronger inhibitory activity against the BChE enzyme as compared to the substrate. (1*R*,4*R*,5*R*,9*S*,11*S*)-4,5-epoxy-caryophyllan-8(13)-en-14-ol was found to exhibit potency similar to galanthamine HBr (IC_{50} 10.9 *vs* 8.5 μM). Structural changes in the transformed products played a significant role in terms of butyrylcholinesterase enzyme inhibition. Opening of the epoxide ring of the substrate into a *trans*-diol increased the inhibitory potential (IC_{50} = 44.01 ± 0.2 μM) of (1*R*,4*R*,5*R*,9*S*)-4,5-dihydroxy-caryophyllan-8(13)-ene. Hydrogen bonding of the hydroxylated groups with amino acid

residues in the active site of BChE is a potentiating factor for the enzyme inhibitor complex and resulted in the higher inhibitory activity of the metabolite.

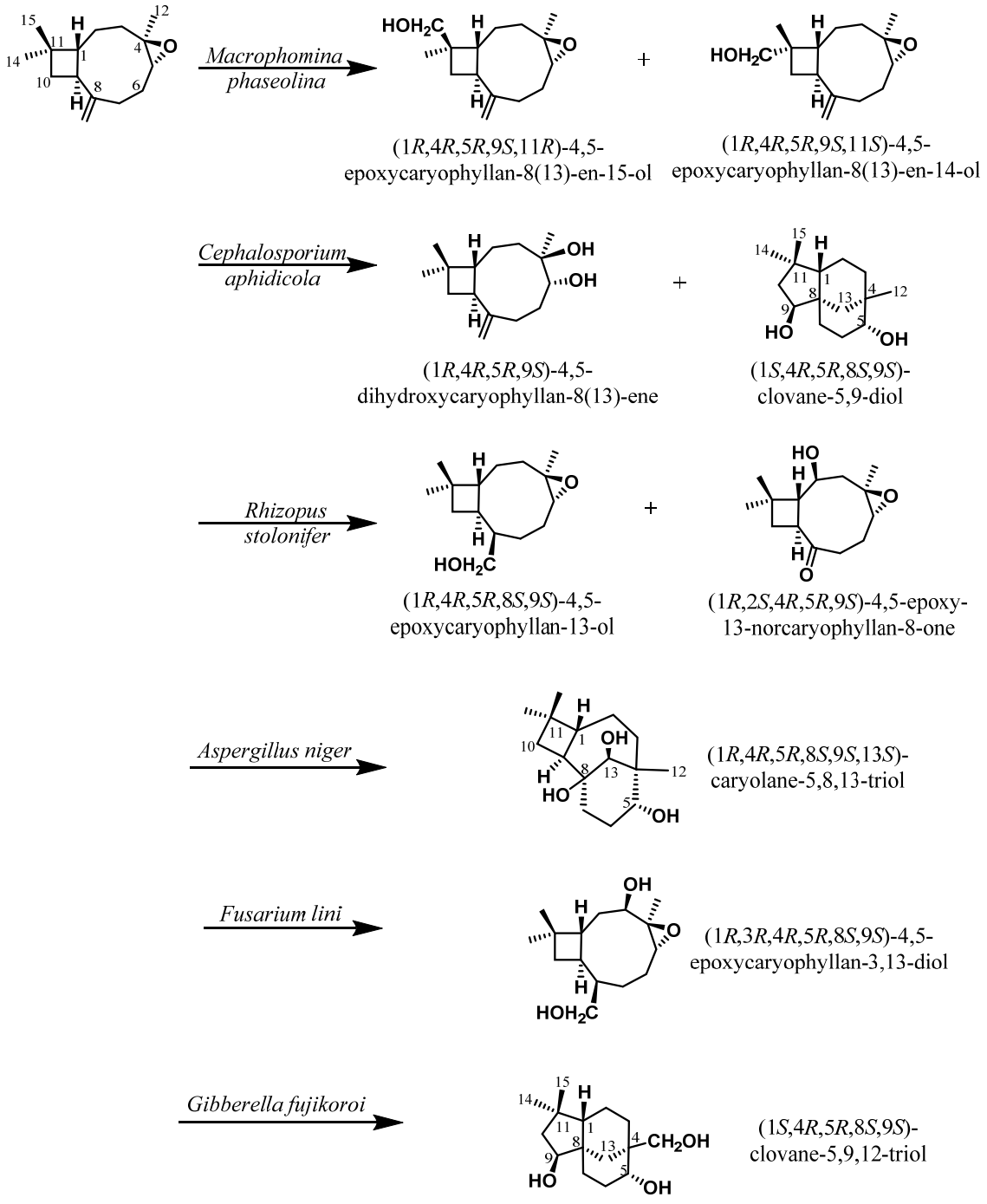

Scheme 2.1.8. Biotransformation of (-)-Caryophyllene oxide with different fungal cultures.

2.1.4.2.6. Biotransformation of aromadendrane type sesquiterpenoids:

(+)-Aromadendrene, (-)-allo-aromadendrene and (+)-ledene are sesquiterpene hydrocarbons with an aromadendrane skeleton. Miyazawa *et al*. investigated for the biotransformation of these sesquiterpenoids with *Aspergillus wentii*.[30] (+)-Aromadendrene on incubation with *A. wentii* produced only one metabolite, which was identified as (-)-(10*S*,11*S*)-10,13,14-trihydroxyaromadendrane. Incubation of (-)-allo-Aromadendrene achieved two metabolites which were characterized as (+)-(1*S*,11*S*)-1,13-dihydroxyaromadendrene and (-)-5,11-epoxycadin-1(10)-en-14-ol. Finally, biotransformation of (+)-ledene yielded three metabolites and were identified as (+)-(10*R*,11*S*)-10,13-dihydroxyaromadendr-1-ene, (+)-(10*R*,11*S*)-10,13-dihydroxy-aromadendr-1-ene and (+)-(10*S*,11*S*)-10,13-dihydroxy-aromadendr-1-ene (Scheme 2.1.9). In all cases, incubations were continued for 10 days before isolation of the products. The differences in oxidation of three aromadendrane type sesquiterpenoids are due to the configuration of the C-1 position.

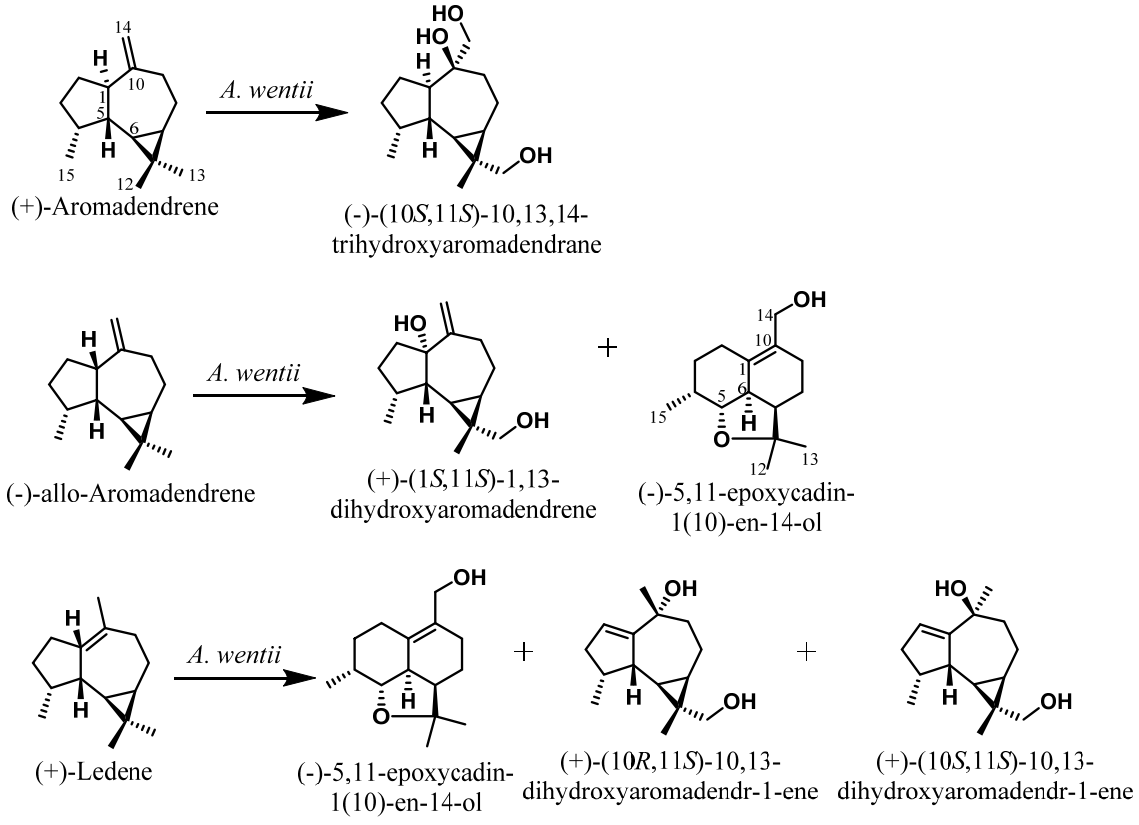

Scheme 2.1.9. Biotransformation of (+)-Aromadendrene, (-)-allo-Aromadendrene and (+)-Ledene by *Aspergillus wentii*.

2.1.4.2.7. Biotransformation of Artemisinin:

Artemisinin, also called 'qinghaosu', is a sesquiterpene lactone endo-peroxide isolated from the Chinese herbal plant *Artemisia annua* L. It is proved to be an effective therapeutic agent against multidrug-resistant *Plasmodium falciparum* strains.[31] Being widely used as a drug to treat malaria, mammalian metabolism of artemisinin forms an integral part of clinical pharmacology and microbial models were set to study its *in vitro* metabolism. Microbial transformation not only overcomes the difficulties associated with the synthetic functionalization of artemisinin, but also produces some of the semi-synthetic precursors for the synthesis of novel analogues possessing increased anti-malarial activities or diverse pharmacological properties. Microbial metabolism of artemisinin has been extensively explored with several modes of biotransformation which produced widely functionalized derivatives (Scheme 2.1.10).[32-38] Zhan *et al*. investigated the metabolism of artemisinin using two different fungal strains to deliver five products.[35] Fermentation of artemisinin with *Mucor polymorphosporus* yielded 9β-hydroxyartemisinin, 3β-hydroxyartemisinin, deoxyartemisinin and 3α-hydroxy-deoxyartemisinin; while that with *Aspergillus niger* generated the later two products along with 1α-hydroxy-deoxyartemisinin. In their continued work, Zhang *et al*. reported the production of 10β-hydroxyartemisinin with *Cunninghamella echinulata*.[34] In another study, Parshikov *et al*. isolated four metabolites from incubation of artemisinin with *Cunninghamella elegans*, which were characterized as 9β-hydroxyartemisinin, 9β-hydroxy-11α-artemisinin, 3α-hydroxydeoxyartemisinin, 10β-hydroxyartemisinin (Scheme 2.1.10).[33] From these products, 9β-hydroxyartemisinin was isolated as the major product which could be converted to 9β-alkyl substituted derivatives, which have been predicted to exhibit higher anti-malarial potential, according to QSAR studies.[33]

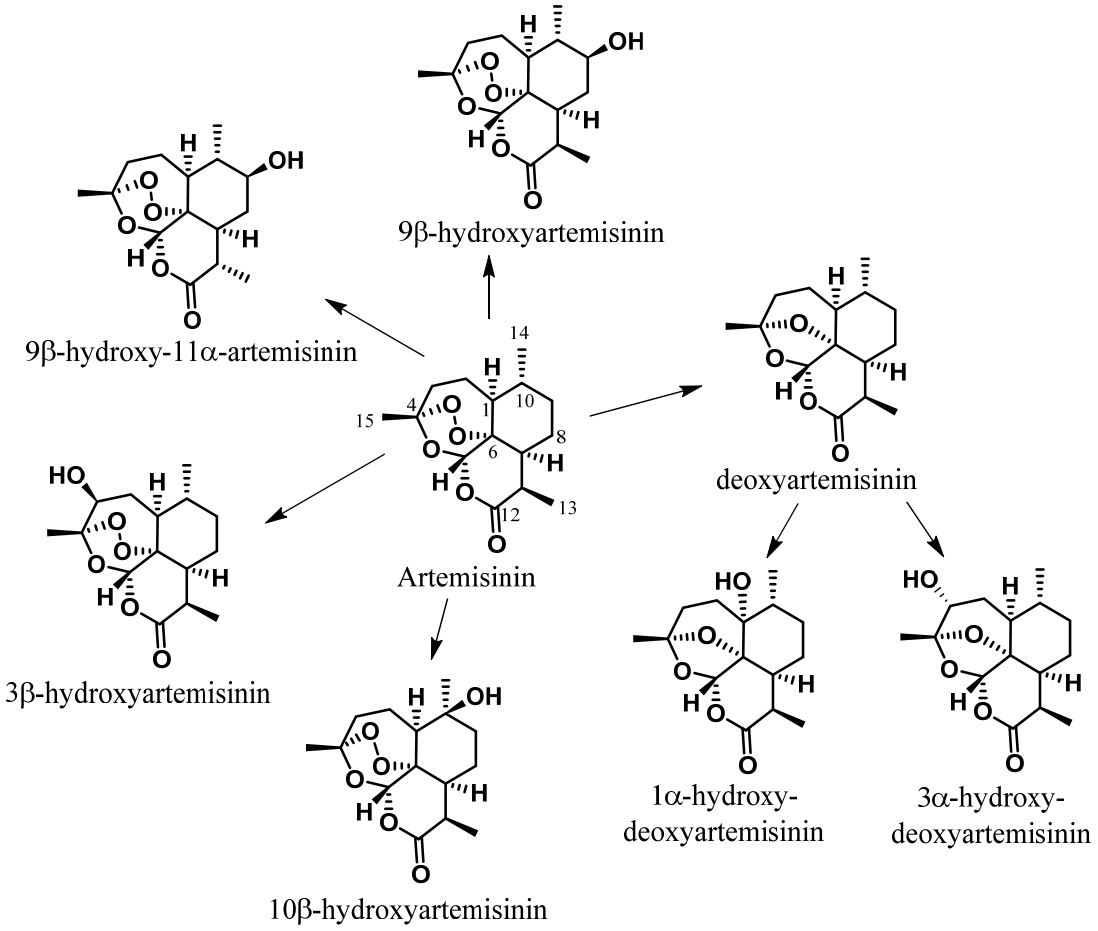

Scheme 2.1.10. Biotransformation of Artemisinin with different microbial cultures.

Section 2.2.

Biotransformation of (*Z*)-α-Santalyl acetate by *M*ucor *piriformis* and Resolution of Epoxy-α-Santalols by Lipases.

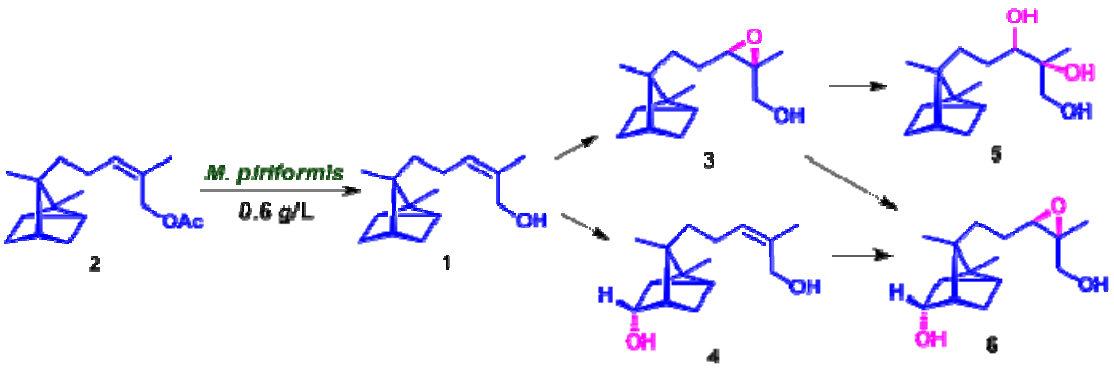

2.2.1. Rationale for Present Work:

Indian Sandalwood, *Santalum album* L., an endangered, medium-sized, evergreen, hemi-root parasitic tree, is widely distributed in South Asia, predominantly in India and is highly valued for its oil content. The major component of Indian Sandalwood oil, (*Z*)-α-santalol (**1**) is biosynthesized at the interface of heartwood and sapwood through cyclization of farnesyl diphosphate by the enzyme *santalene synthase* and further hydroxylation at *cis*-methyl group by cytochrome P450 enzymes.[39,40] Current interest in sesquiterpene[41]**1** stems from its known fragrant and therapeutic potentials as antifungal, antitumor, anti-*Helicobacter pylori*,[42] neuroleptic and chemopreventive effects *in vitro* and *in vivo* bioassay systems.[43-46] In comparison to **1**, its hydroxylated derivative has exhibited more potent activity against the antibiotic resistant strain of *H. pylori* and the activities were comparable to the known drugs, amoxicillin and clarithromycin.[42] The complexity of synthetic chemistry tools to generate diversely modified analogues by functionalization at non-activated carbons prompted us to study the microbial biotransformation of **1** to generate novel and potent analogues which might possess superior biological importance. Although, there are a number of reports on biotransformation of other sesquiterpenoids[47-49] and norbornane type compounds,[50,51] we could not find any precedence on biotransformation of **1**, till date. Herein, we report an efficient regio- and stereo-selective functionalization of **1** by using its acetyl derivative, (*Z*)-α-santalyl acetate (**2**) as substrate with a versatile soil isolated fungal system *Mucor piriformis*[52] as a biocatalyst.

2.2.2. Present work:

In the present investigation, the biotransformation of (*Z*)-α-santalyl acetate (**2**) was studied with a versatile, soil-isolated fungal strain, *Mucor piriformis* which hydrolyzed the substrate to (*Z*)-α-santalol (**1**) and was further able to transform it to four oxygenated derivatives. Incubation of **2** (0.6g/L) with the fungal culture for 6 days and subsequent isolation and purification, resulted in five metabolites, whose structures were determined by extensive analysis of the spectral data from 1D NMR (^{1}H, ^{13}C, DEPT) and 2D-NMR (COSY, NOESY, HSQC, HMBC). These were characterized as (*Z*)-α-santalol (**1**), 10,11-*cis*-β-epoxy-α-santalol (**3**), 5α-hydroxy-(*Z*)-α-santalol (**4**), 10,11-dihydroxy-α-santalol (**5**) and 5α-hydroxy-10,11-*cis*-β-epoxy-α-santalol (**6**).

2.2.2.1. Biotransformation of (*Z*)-α-Santalyl acetate (2):

Various fungal strains were screened for biotransformation of (*Z*)-α-santalol to its metabolites. Incubation of (*Z*)-α-santalol (**1**) did not exhibit noticeable transformation with any of the screened fungal strains due to its potent antifungal activity. In order to mask this activity, its acetyl derivative, (*Z*)-α-santalyl acetate (**2**) was synthesized as mentioned in the experimental section, which was subsequently employed for biotransformation with various fungal strains.

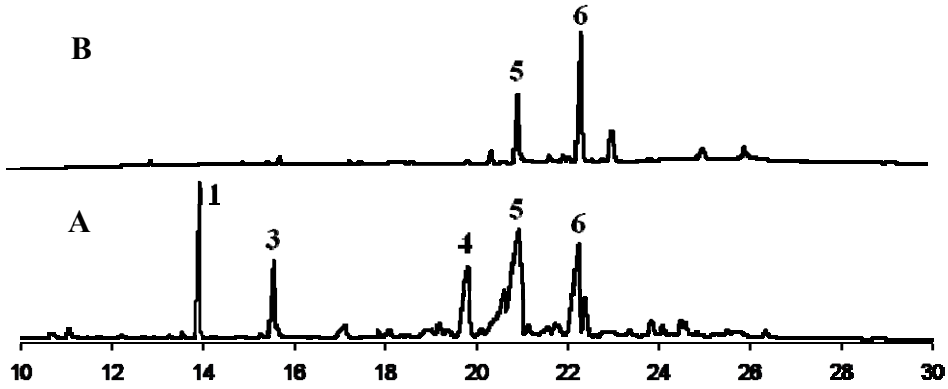

Figure 2.2.1. GC traces for comparison of metabolites from incubations of (**A**) (*Z*)-α-santalyl acetate (**2**) (0.6 g/L) for 6 days and (**B**) 10,11-*cis*-β-epoxy-α-santalol (**3**) (0.4 g/L) for 3 days with *Mucor piriformis*. Incubation of **3** with *M. piriformis* confirmed the biotransformation pathway and formation of metabolites **5** and **6** from **3**. **GC conditions**: HP-5 column; Program 1. The injector and detector temperatures were maintained at 250 °C and operated in split mode.

Among the screened fungal strains that could biotransform **2**, *Mucor piriformis*, a soil isolated fungus was regarded as the most efficient as it could carry out quantitative biotransformation of **2** to its derivatives, within a period of 6 days. *M. piriformis* was subsequently opted for large scale fermentation of **2** and could carry out deacetylation of (*Z*)-α-santalyl acetate and further metabolism of santalols as observed by TLC, GC and GC-EI-MS analyses. GC-EI-MS analysis of the extract also indicated that the metabolites were deacetylated and oxygenated derivatives of **2**.

Substrate concentration of 0.6 g/L with an incubation period of 6 days was optimized from the substrate concentration and time course experiments. Large scale fermentation of (*Z*)-α-santalyl acetate **2** (2.4 g) was carried out with *M. piriformis*, in a batch of 40 Erlenmeyer flasks and the resulting broth was processed as explained in the experimental section. A neutral crude extract of the 6 day old fermentation broth yielded a brownish gum constituting mixture of metabolites (1.1g) which upon TLC and GC-MS analyses indicated the presence of five metabolites including **1** (Figure 2.2.1). This fraction was subjected to column chromatography and the metabolites were eluted with hexane/ ethyl acetate gradient mixtures from (1:0) to (6:4). The purified metabolites were characterized using GC-MS, HRMS, ^{1}H, ^{13}C, DEPT and 2D (COSY, NOESY, HMBC, HSQC) NMR techniques (Scheme 2.2.1).

Elution of the column with 6% ethyl acetate/petroleum ether gradient, afforded a fraction containing the de-acetylated product, (*Z*)-α-santalol (**1**) (R_f 0.95, solvent system **I**; R_t 11.49 min, program **I**), which was proved from GC and GC-EI-MS analyses and co-injection with earlier isolated standard from sandalwood oil. All ^{1}H and ^{13}C NMR spectral data for **1** were unambiguously assigned by 2D NMR spectral analysis (Scheme 2.2.1, Table 2.2.2) and was regarded as a reference in functional group modifications occurred on it after biotransformation process and subsequent structure elucidation of ensuing metabolites. Spectroscopic data for **1** also were in complete agreement with the literature.[53,54]

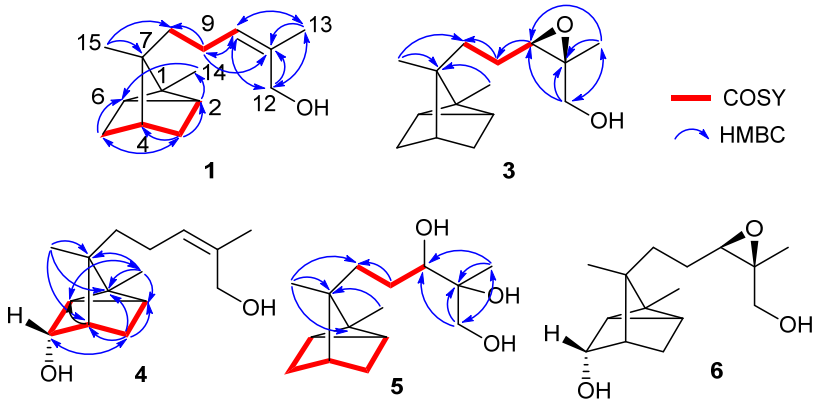

Scheme 2.2.1: Characterization of metabolites by 2D NMR spectral analyses.

Gradual elution with ethyl acetate/petroleum ether (1:9) yielded a fraction containing a metabolite (R_f 0.86, solvent system **I**; R_t 12.74 min, program **I**). Further, purification was carried out by preparative TLC of this fraction using methanol: CH_2Cl_2 (1:49) that yielded **3** as a colorless liquid. The metabolite **3** exhibited an M^+ peak in HR-EI-MS at *m/z* 236.1783 (Calcd. 236.1776, for $C_{15}H_{24}O_2$) 16 amu higher than that of **1** and a molecular formula of $C_{15}H_{24}O_2$ implying an insertion of an oxygen atom to santalol structure. The IR spectrum of **3** showed the peaks at 1036 cm^{-1} (C-O-C), 2944 cm^{-1} (H-C-O), but the peak at 1676 cm^{-1} (C=C) was absent that suggested presence of an ethereal linkage and disappearance of the olefin; whereas, peak at 3400-3450 cm^{-1} corresponding to a hydroxyl group in **1** was relatively unaffected. Signals at δ 5.32 in ^{1}H NMR and at δ 133.6, 129.5 in ^{13}C NMR representing an olefin of **1** were replaced by δ 2.83 in ^{1}H NMR and δ 65.4, 61.0 in ^{13}C NMR of **3** that predicted the possibility of attachment of oxygen with C-10,C-11 to form an epoxide. Other signals in ^{1}H and ^{13}C-NMR spectra for C-1, H-1 to C7, H-7 constituting a tricyclo[2.2.1.0]heptane ring were unaltered. The upfield shift of epoxide proton H-10 appearing at δ 2.83 in comparison to other acyclic oxymethine protons usually resonating at δ 3.5 to 4.5 can be attributed to the ring strain present in epoxides, that supports their presence. In HSQC, key correlations were observed as δ_C 63.9 (C-12)/δ_H 3.68 (H-12), δ_C 65.4 (C-10)/δ_H 2.83 (H-10), δ_C 23.6 (C-9)/δ_H 1.45 (H-9a), δ_H 1.59 (H-9b) and HMBC long range correlations were observed as δ_C 63.9 (C-12)/δ_H 1.39 (H-13); δ_C 61.1 (C-11)/δ_H 1.39 (H-13), δ_H 3.64 (H-12a), δ_H 3.68 (H-12b); δ_C 65.4 (C-10)/δ_H 1.39 (H-13), δ_H 3.64 (H-12a), δ_H 3.68 (H-12b); δ_C 23.6 (C-9)/δ_H 2.83 (H-10); δ_C 30.8 (C-8)/δ_H 0.81 (H-15); δ_C 45.6/δ_H 0.81 (H-15), δ_H 0.85 (H-2 & H-6), δ_H 1.01 (H-14), δ_H 1.05 (H-3a) which established -$C_{(12)}H_2$-$C_{(11)}$(Me-13)-$C_{(10)}H_1$-$C_{(9)}H_2$-$C_{(8)}H_2$-$C_{(7)}$-$C_{(15)}H_3$- side chain unit. The H-10 resonance at

δ 2.83 (t, *J* = 6.4 Hz, H-10) exhibited proton spin coupling correlations with signals assignable to H-9 at δ 1.45 (m, H-9a) and δ 1.59 (m, H-9b) in ^{1}H-^{1}H COSY. These correlations in 2D NMR established the structure of **3** as 10,11-*cis*-epoxy-santalol (Scheme 2.2.1, Table 2.2.3 and 2.2.4). To determine the stereochemistry of epoxide (*cis*-α or *cis*-β) in **3** ($[\alpha]_D$ +12.65, (*c*=2.75, $CHCl_3$)) and its optical purity, mixture of epoxides was synthesized by *m*CPBA from **1**. These two diastereomers were resolved by GC using a HP-Chiral (20% β-cyclodextrin) column (R_t 23.67 min and 23.54 min, Figure 2.2.2) and the metabolite **3** (R_t 23.67 min) was observed to result in almost single peak using the same program, which inferred (de) >96% diastereomeric purity of **3**.

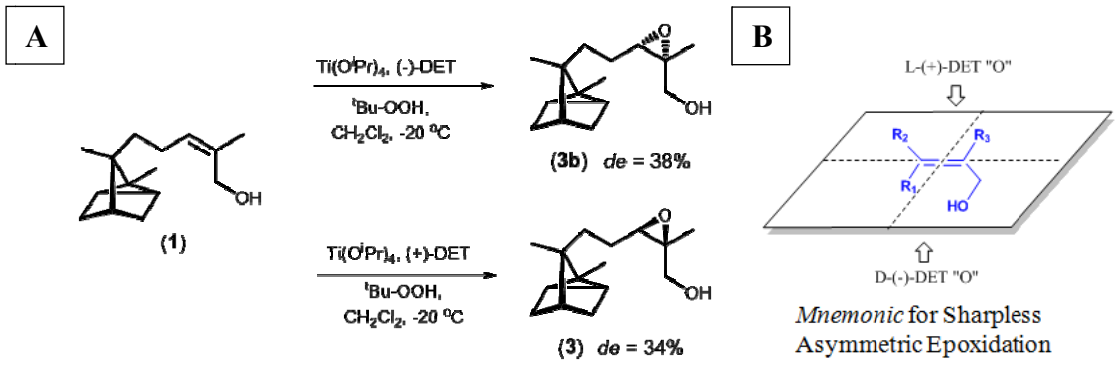

Scheme 2.2.2. (**A**) Synthesis of 10,11-*cis*-α-epoxy-α-santalol (**3b**) with (-)-DET and 10,11-*cis*-β-epoxy-α-santalol (**3**) with (+)-DET as the chiral auxiliary, according to Sharpless asymmetric epoxidation (SAE) methodology; (**B**) *Mnemonic* stating epoxidation from β-face when (+)-DET is used as the chiral auxiliary and from α-face when (-)-DET is used as the chiral auxiliary in Sharpless asymmetric epoxidation.[55]

Further, the stereochemistry of newly introduced epoxy functionality was confirmed by Sharpless asymmetric epoxidation (SAE) of **1** using (+)-diethyl tartarate (DET) or (-)-DET which are known to introduce β-epoxide or α-epoxide, respectively (Scheme 2.2.2).[55] SAE reaction of **1** with (+)-DET yielded epoxide **3** (R_t 23.67 min, 34% de) whereas, with (-)-DET, **3b** (R_t 23.54 min, 38% de) was obtained (Figure 2.2.2). In these experiments, although the diastereomeric ratios were very low, the assignment of individual peaks for a particular diastereomer could be achieved. From the above experiments, the stereochemistry of epoxide in **3** was elucidated as β-epoxide and the metabolite was concluded as 10,11-*cis*-β-epoxy-α-santalol.

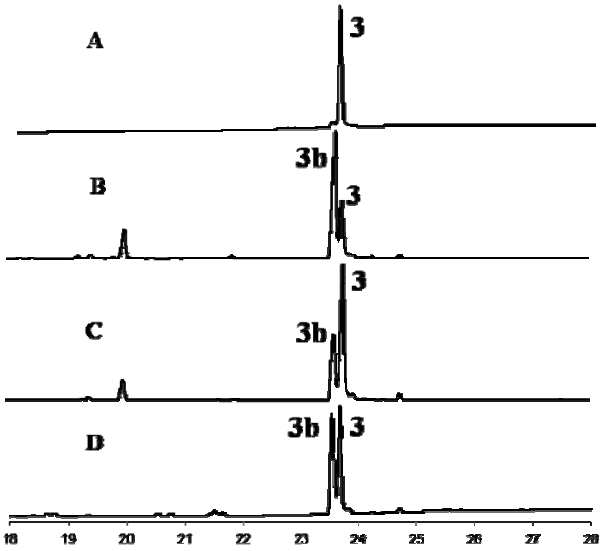

Figure 2.2.2. GC traces of (**A**) 10,11-*cis*-β-epoxy-α-santalol (**3**) obtained from biotransformation of (*Z*)-α-santalyl acetate with *M. piriformis*. Synthesized 10,11-*cis*-epoxy-α-santalols with (**B**) (-)-DET, (**C**) (+)-DET, and (**D**) *m*CPBA.

Continued elution with ethyl acetate/petroleum ether (23:77) obtained metabolite **4** (R_f 0.40, solvent system **I**; R_t 16.00 min, program **I**) that displayed a molecular formula $C_{15}H_{24}O_2$ on the basis of HR-ESI-MS data [*m/z* 259.1746 $(M+Na)^+$, calcd. for $C_{15}H_{24}O_2Na$, 259.1674], and 15 peaks obtained in ^{13}C-NMR analysis. A molecular ion peak $[M]^+$ at *m/z* 236.3 was also obtained from GC-EI-MS analysis, 16 amu higher than **1** and a molecular formula of $C_{15}H_{24}O_2$ implied insertion of an oxygen atom to **1**. When ^{1}H and ^{13}C spectra of **4** were compared with those of **1**, new signals for a hydroxymethine proton and carbon were respectively observed at δ_H 4.22 (m, 1H, H_5) and at δ_C 75.5 in **4** which envisaged the possibility of hydroxylation at either of the four, C-8, C-9, C-3 or C-5 methylene carbons. The ^{1}H NMR spectrum and HSQC correlations in **4** showed signals assignable to a $C_{(12)}H_2$-$C_{(11)}$(Me-13)-$C_{(10)}H_1$-$C_{(9)}H_2$-$C_{(8)}H_2$-$C_{(7)}$-$C_{(15)}H_3$ side chain unit at δ_C 61.5 (C-12)/δ_H 4.14 (s, 2H, H-12), δ_C 129.0 (C-10)/δ_H 5.30 (t, J = 7.53 Hz, 1H, H-10), δ_C 22.7 (C-9)/δ_H 1.88-2.01 (m, 2H, H-9), δ_C 35.6 (C-8)/δ_H 1.14-1.17 (m, 1H, H-8a), δ_H 1.32 (m, 1H, H-8b) and δ_C 17.8 (C-15)/δ_H 0.93 (s, 3H, H-15) (Scheme 2.2.1, Table 2.2.3 and 2.2.4). The spectroscopic features of **4** were essentially analogous to those of (*Z*)-α-santalol (**1**) in respect of signals corresponding to the side chain unit, which informed that oxygen insertion was not in linear part of the compound, but in the cyclic part, thus ruling out hydroxylation at C-8 and C-9. Accordingly, **4** differed from **1** in the signals displayed for tricyclo[2.2.1.0]heptane ring,

due to the probable hydroxylation at C-3 or C-5. In the NOESY spectrum, through space correlations were observed between signals at δ 4.22 (m, 1H) for hydroxymethine proton and the methyl protons at δ 0.93 (s, 3H) which could be assigned for either H-14 or H-15, arising the necessity to spectrally distinguish the signals for C-14/C-15 and H-14/H-15. In HMBC spectrum of **4**, long range correlations for C-7 resonating at δ 45.9 were observed with δ 1.00 (s, 3H, H-14) and δ 0.93 (s, 3H, H-15), which created ambiguity in spectral assignments of H-14 and H-15. But, a signal at δ 1.00 (s, 3H, H-14) showed long range correlations with carbons resonating at δ 45.9 (C-7), δ 32.3 (C-1), δ 26.2 (C-6) and δ 20.7 (C-2), whereas, a signal at δ 0.93 (s, 3H, H-15) showed long range correlations with carbons resonating at δ 45.9 (C-7), δ 44.2 (C-4), δ 35.6 (C-8) and δ 32.3 (C-1). In a similar way, a signal at δ 17.8 (C-15) exhibited weak long range correlations with a proton resonating at δ 1.32 (m, 1H, H-8b) while that at δ 10.7 (C-14) correlated with δ 1.09-1.13 (m, 1H, H-2) and δ 1.03 (m, 1H, H-6) which confirmed the spectral assignments as δ 1.00 (s, 3H, H-14), δ 10.7 (C-14) and δ 0.93 (s, 3H, H-15), δ 17.8 (C-15). NOESY correlations not only confirmed the locus of hydroxyl group at C-5, but also established α-orientation of the hydroxyl group at C-5. The possibility of hydroxylation on C-3 was ruled out as it would have resulted in NOESY correlations between the hydroxymethine proton (H-3) and a methyl at C-14 resonating at δ 1.00 (s, 3H, H-14). HSQC correlations observed in **4** as δ_C 20.7 (C-2)/δ_H 1.09-1.13 (m, 1H, H-2), δ_C 26.9 (C-3) and δ_C 44.2 (C-4)/δ_H 1.59-1.62 (m, 2H, H-3a & H-4) and 1.66 (s, 1H, H-3b), δ_C 75.5 (C-5)/δ_H 4.22 (m, 1H, H-5) and δ_C 26.2 (C-6)/δ_H 1.03 (m, 1H, H-6) confirmed the signals for $C_{(1)}$-$C_{(2)}H_1$-$C_{(3)}H_2$-$C_{(4)}H_1$-$C_{(5)}H(OH)$-$C_{(6)}H_1$-$C_{(7)}$ constituting the tricyclo[2.2.1.0]heptane ring unit. Accordingly, the structure of **4** was determined as 5α-hydroxy-(*Z*)-α-santalol.

Metabolite **5** (R_f 0.32, solvent system **I**; R_t 16.62 min, program **I**) was eluted with ethyl acetate/petroleum ether (1:4). Characteristic absorption for C=C bond stretching vibrations appearing at 1676 cm^{-1} were not observed in IR spectrum of **5**, but a broad, probably intermolecular hydrogen bonded O-H stretch was observed at 3381 cm^{-1}. On comparison of spectral analysis of **5** with that of **1**,different peak was observed at δ_H 3.56 (dd, *J* = 1.93, 9.91 Hz, 1H, H_{10}), with concomitant shift of resonance for H-12 from δ_H 4.15 (s, 2H, H_{12}) to δ_H 3.52 (d, *J* = 11.28 Hz, 1H, H_{12a}), 3.66 (d, *J* = 11.28 Hz, 1H, H_{12b}) and disappearance of signal for olefinic proton in **1** that appeared at δ_H 5.32 (t, *J* = 7.43 Hz, 1H, H_{10}). Concurrently, ^{13}C NMR analysis revealed absence of signals at δ 133.6 (C_{11}), 129.5 (C_{10}) corresponding to an olefin group of **1** with the simultaneous

appearance of resonaces at δ_C 77.2 (C_{10}), 74.0 (C_{11}) for hydroxymethylene and hydroxymethine carbons, respectively (Scheme 2.2.1, Table 2.2.3 and 2.2.4). These observations in spectral analysis of **5** inferred dihydroxylation of C10-C11 olefinic bond present in (Z)-α-santalol (**1**). GC-EI-MS analysis displayed a molecular ion peak at *m*/*z* 254.3 and the compound was shown to have a molecular formula $C_{15}H_{26}O_3$ on the basis of HR-EI-MS data [*m/z* 254.1793 (M^+), calcd. *m/z* 254.1882], indicating addition of 34 amu (2 × -OH) to the mass of **1** which suggested hydroxylations at two carbon centers on the skeleton of **1**. HSQC correlations appearing at δ_C 30.7 (C-8)/δ_H 1.17-1.23 (m, 1H, H_{8a}), δ 1.44-1.46 (m, 1H, H_{8b}), δ_C 26.4 (C-9)/δ_H 1.32-1.41 (m, 2H, H_{9a} and H_{9b}), δ_C 77.2 (C-10)/δ_H 3.56 (dd, *J* = 1.93, 9.91 Hz, 1H, H_{10}), established the signals assignable to the -$C_{(8)}H_2$-$C_{(9)}H_2$-$C_{(10)}H$(OH)- side chain unit. This was confirmed by the long range correlations of δ_H 0.83 (s, Me-15) with δ_C 30.7 (C-8), δ_C 27.4 (C-1), δ_C 45.8 (C_7), δ_C 38.1 (C_4); δ_H 1.10 (s, Me-13) with δ_C 77.2 (C-10), δ_C 74.0 (C-11), δ_C 69.5 (C-12); δ_H 3.52 (d, *J* = 11.28 Hz, 1H, H_{12a}) with δ_C 77.2 (C-10), δ_C 74.0 (C-11), δ_C 19.6 (C-13) and δ_H 3.66 (d, *J* = 11.28 Hz, 1H, H_{12b}) with δ_C 77.2 (C-10), δ_C 19.6 (C-13) in the HMBC spectrum of **5**. The signals assigned for tricyclo[2.2.1.0]heptane ring were nearly unaltered from **1** to **5** implying no functionalization on the cyclic structure. On the basis of above analysis, **5** was identified as 10,11-dihydroxy-α-santalol.

The most polar metabolite **6** (R_f 0.25, solvent system **I**; R_t 18.17 min, program **I**) was obtained with ethyl acetate/petroleum ether (28:72). HR-EI-MS analysis of **6**, revealed a molecular formula $C_{15}H_{24}O_3$ (*m*/*z* 252.1679 [M^+], calcd. *m*/*z* 252.1725) indicating addition of two oxygens to the backbone of **1**. The spectral data for **6** was comparable to that of **3** and **4** in part. Analysis of ^{1}H NMR data except a triplet at δ 4.22 and at δ 75.4 in ^{1}H and ^{13}C NMR, respectively, of **6** represented a hydroxy group and confirmed the structure of **6** as 6-hydroxy-2,4-epoxy-α-santalol (Scheme 2.2.1, Table 2.2.3 and 2.2.4).

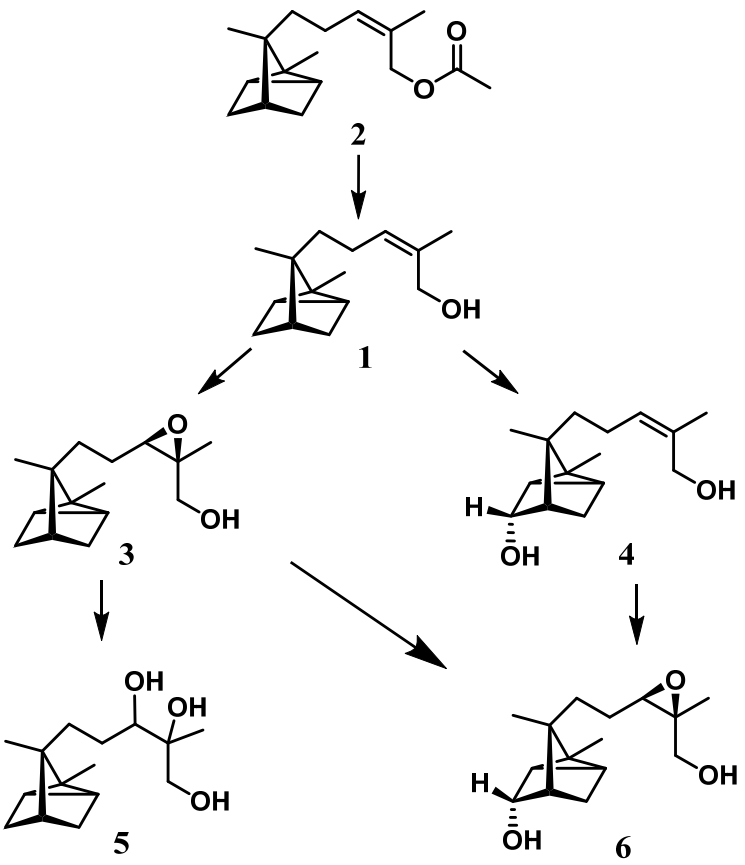

Scheme 2.2.3. Proposed biotransformation pathway of (*Z*)-α-santalyl acetate (**2**) with *M*ucor *piriformis*.

2.2.2.2. Time Course Study:

Time course experiments carried out with **2** revealed complete transformation of the substrate (**2**) into various metabolites (**1**, **3**-**5**) during 5 days of incubation period with *M. piriformis* (Figure 2.2.3) and established the biotransformation pathway (Scheme 2.2.3). From the time course studies, it became clear that biotransformation followed two pathways that mainly concentrated on the side chain of **1**. The first pathway involved epoxidation at C-2/C-4 followed by its opening to yield a vicinal diol, thus leading to **4**, **5** and **6** respectively; the second pathway involved hydroxylation at C-6 leading to **3** and **5**. GC profiles of total metabolites formed at different time intervals indicated that at the end of 6 days, **5** was obtained as the major product (38%) (Figure 2.2.3). Compound **5** was obtained *via* both the pathways as it has an epoxide as well as a hydroxy group in its structure.

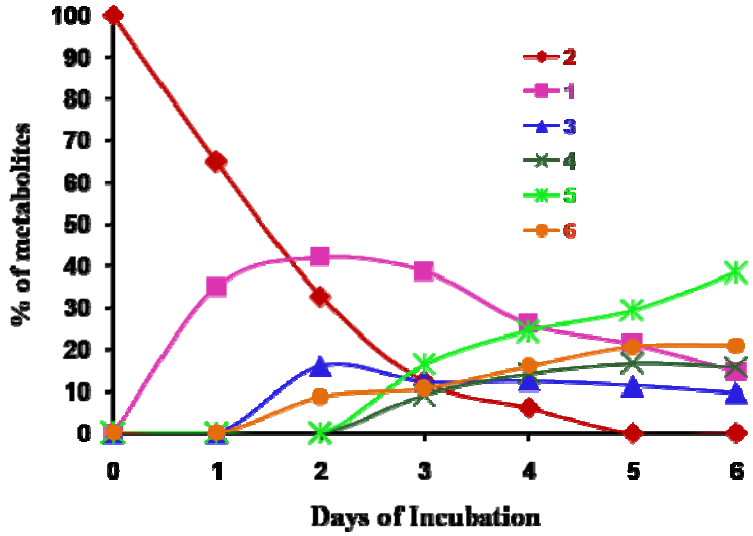

Figure 2.2.3. Time course study of the biotransformation of (*Z*)-α-santalyl acetate (**2**) with *M. piriformis*: (■) (*Z*)-α-santalol (**1**); (♦) (*Z*)-α-santalyl acetate (**2**); (▲) 10,11-*cis*-β-epoxy-α-santalol (**3**); (×) 5α-hydroxy-(*Z*)-α-santalol (**4**); (*) 10,11-dihydroxy-α-santalol (**5**); (●) 5α-hydroxy- 10,11-*cis*-β-epoxy-α-santalol (**6**).

2.2.2.3. Kinetic resolution of 10,11-*cis*-α- / β-epoxy-α-santalol:

For large-scale kinetic resolution of epoxides (*cis*-α or *cis*-β), the prochiral alkene moiety in **1** was subjected to epoxidation with *m*CPBA that delivered diastereomeric mixture of epoxy-α-santalols. A variety of commercially available lipases were screened to achieve kinetic resolution of the two diastereomeric epoxy-α-santalols [R_t 23.54 min and 23.67 min; HP-Chiral (20% β-cyclodextrin) column] by selective acetylation in presence of vinyl acetate, an acyl donor, in hexane (Figure 2.2.7, Table 2.2.1). Promising results were obtained with Amano PS lipase from *B. cepacia* when acetylation of β-epoxide (**3**) was kinetically favored over α-epoxide (**3b**) with oxirane moiety remaining intact (Figure 2.2.5 and 2.2.6). On many instances, resolution of epoxy-alcohols was exercised by epoxide hydrolases which resulted in opening of epoxide in one of the isomer, while the oxirane moiety in another isomer could be retained.[56] But, only a few reports state use of lipases which resolved epoxy-alcohol isomers with retention of both the oxirane moieties,[57-59] as was also observed in the current study.

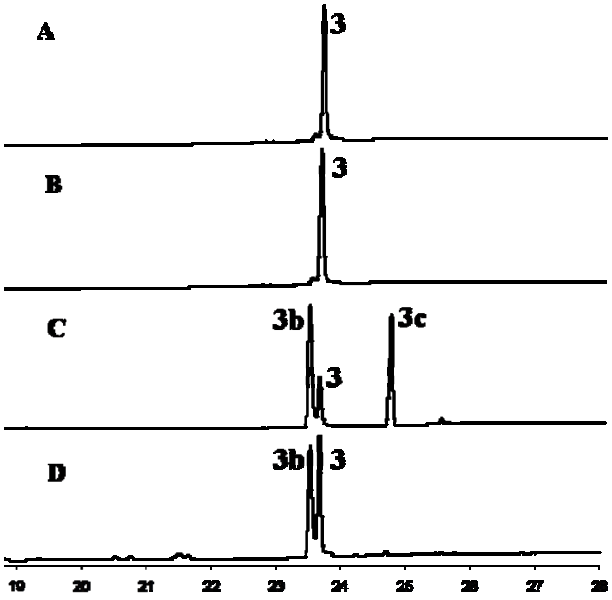

Figure 2.2.4. GC traces for (**A**) 10,11-*cis*-β-epoxy-α-santalol (**3**) obtained from biotransformation of (*Z*)-α-santalyl acetate (**2**) with *M. piriformis*, (**B**) deacetylation product of **3c** obtained after incubation of 10,11-*cis*-epoxy-α-santalol mixture with Amano PS lipase from *B. cepacia* for 2 h, (**C**) incubation of 10,11-*cis*-epoxy-α-santalol mixture with Amano PS lipase from *B. cepacia* for 2 h, to yield β-epoxy-α-santalyl acetate (39%) along with the unspent alcohol. Purification of β-epoxy-α-santalyl acetate followed by deacetylation with LiOH resulted in **3** (96% de). (**D**) 10,11-*cis*-epoxy-α-santalol mixture.

The progress and selectivity of acetylation of epoxy-alcohol diastereomeric mixture (**3** + **3b**) was monitored by analyzing the aliquots drawn at every 1h over a period of 7h (Figure 2.2.6). Incubation of diastereomeric epoxide with lipase for 6h furnished α-epoxide (**3b**) with >99% de (40% yield) (Figure 2.2.4, Scheme 2.2.4). On the other hand, when the reaction was quenched at 2h, β-epoxy-α-santalyl acetate (39%) was obtained which on deacetylation with LiOH furnished **3** with 96% de (Scheme 2.2.5, Figure 2.2.4).

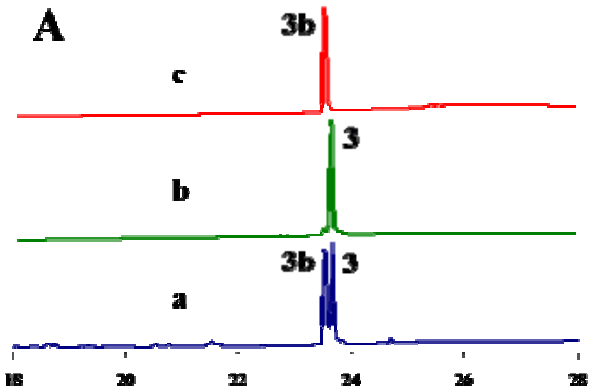

Figure 2.2.5. Kinetic resolution of 10,11-*cis*-epoxy-α-santalol diastereomers by acetylation with vinyl acetate, catalyzed by Amano lipase PS from *B. cepacia*; GC traces for (**a**) racemic-10,11-*cis*-epoxy-α-santalol (**3**+**3b**), (**b**) 10,11-*cis*-β-epoxy-α-santalol (**3**), (c) 10,11-*cis*-α-epoxy-α-santalol (**3b**);

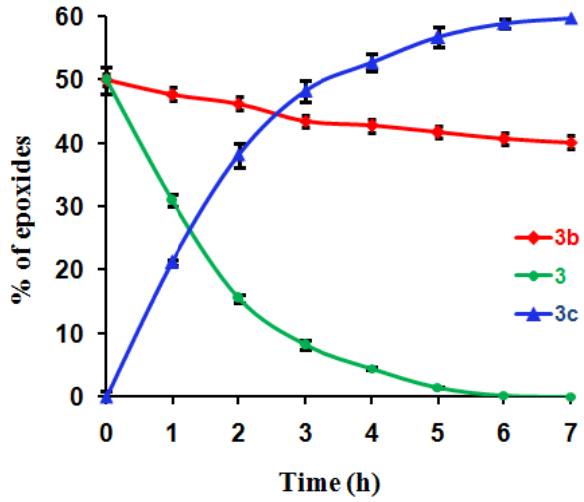

Figure 2.2.6. Time course study plot of kinetic resolution of 10,11-*cis*-epoxy-α-santalol diastereomers in acetylation reaction with vinyl acetate, catalyzed by Amano PS lipase from *B. cepacia* for 7 h; (▲) 10,11-*cis*-epoxy-α-santalyl acetate (**3c**), (●) 10,11-*cis*-β-epoxy-α-santalol (**3**), (♦) 10,11-*cis*-α-epoxy-α-santalol (**3b**).

2.2.3. Summary and Conclusion:

The versatile fungal system, *M. piriformis* efficiently carried out regio- and stereo-selective functionalization of (*Z*)-α-santalyl acetate (**2**) into four novel metabolites through (*Z*)-α-santalol (**1**), which have been characterized for the first time. The metabolites were identified by extensive analysis of 1D and 2D NMR spectra, as 10,11-*cis*-β-epoxy-α-santalol (**3**), 5α-hydroxy-(*Z*)-α-santalol (**4**), 10,11-dihydroxy-α-santalol (**5**) and 5α-hydroxy-10,11-*cis*-β-epoxy-α-santalol (**6**), which might possess potent biological activities. Commercially available lipases were screened for kinetic resolution of diastereomers of 10,11-*cis*-epoxy-α-santalol, among which, Amano PS lipase from *B. Cepacia* exquisitely accomplished the desired resolution.

2.2.4. Experimental:

2.2.4.1. General Experimental Procedure:

Specific optical rotations, $[\alpha]_D$ were recorded on a Jasco P-1020 Polarimeter and are reported in deg dm^{-1} and the concentration (*c*) is in g/100mL, in a specific solvent. Transformations were monitored by thin-layer chromatography (TLC) using silica gel 60-F_{254} pre-coated plates obtained from Merck, Germany and spots were visualized by spraying with a solution of 3.2% anisaldehyde, 2.8% H_2SO_4, 2% acetic acid in methanol followed by heating for 1-2 min. R_f values of (*Z*)-α-santalyl acetate metabolites were calculated by developing TLC with solvent system: ethyl acetate/hexane (1:1). Column chromatography was performed on silica gel (60-120 mesh). ^1H and ^{13}C NMR spectra in $CDCl_3$ were recorded either, on Bruker AC-400 at 400.13 and 100.63 MHz or, on Bruker DRX-500 spectrometer at 500.13 and 125.78 MHz respectively. Chemical shifts are in δ-values relative to TMS (tetramethylsilane) as internal standard. IR spectra in $CHCl_3$ were recorded on Schimadzu 8400 series FT-IR instrument and values are reported in cm^{-1} units. GC analyses were carried out using Agilent 7890 GC system equipped with a hydrogen flame ionization detector (FID) and HP-5 capillary column (30 m × 0.25 mm × 0.25 μm, J & W Scientific). Nitrogen was used as carrier gas at a flow rate of 1 mL/min. The column temperature was increased from 70 °C to 160 °C at the rate of 10 °C min^{-1}, from 160 °C to 170 °C at the rate of 5 °C min^{-1}, from 170 °C to 190 °C at the rate of 2 °C $min^{-1}$and then raised to a final temperature of 230 °C with a 10 °C min^{-1} rise and maintained at 230 °C for 5 min (Program 1). The injector and detector temperatures were maintained at 240 °C and operated in split mode (1:10). Mass spectra were recorded using EI technique on Agilent 5975C mass selective detector interfaced with 7890A gas chromatograph and HP-5 (30m × 0.25 mm × 0.25μm) column with a flow of helium at the rate of 1 mL/min. Exact molecular mass and molecular formula determinations were done by HRGC-EI-MS on a MSI autoconcept UK, with ionization energy 70eV or on Q-Exactive Orbitrap (Thermo Scientific).

2.2.4.2. Microorganism:

The fungal strain used in this study, *Mucor piriformis*, was isolated from garden soil.[52] It was maintained and propagated on Potato Dextrose Agar (PDA) slants and fermentation was carried out in sterilized modified Czapek Dox media (Cz).

2.2.4.3. Procedure for screening of fungal cultures:

The fungal cultures were grown at 30 °C in 500 mL Erlenmeyer flasks containing 100 mL of sterile modified Cz media[60] at 220 rpm. (*Z*)-α-santalyl acetate (**2**) was added aseptically to 36 h well grown cultures at a concentration of 50 mg in 0.2 mL acetone/ 100 mL media and incubation was continued. After 5 days incubation period, the contents of the flasks were filtered through muslin cloth. The broth and mycelia were extracted separately with CH_2Cl_2 (100 mL × 2). The organic layers were separated, dried over anhydrous Na_2SO_4, concentrated and analyzed by TLC, GC and GC-MS.

2.2.4.4. Time course study:

(*Z*)-α-Santalyl acetate (**2**) (0.6 g/L) was added to 36 h well grown cultures in 500 mL Erlenmeyer flasks containing 100 mL media and incubated on a rotary shaker as mentioned above. Aliquots were drawn at every 24 h, extracted with CH_2Cl_2 and analyzed by GC and GC-MS for monitoring the level of formation of each metabolite. At the end of 5 days, complete consumption of the substrate was observed.

2.2.4.5. Large scale biotransformation of (*Z*)-α-santalyl acetate (2):

Large scale fermentation of (*Z*)-α-santalyl acetate (**2**) was carried out using 4L Cz media distributed equally in to 40 Erlenmeyer flasks of 500 mL volume. The flasks were inoculated with 1 mL of *Mucor piriformis* spore suspension in sterile water from a 5-day-old culture grown on Potato Dextrose Agar (PDA) slants and incubated on a rotary shaker. Substrate **2** (2.4 g) was added to 36 h well grown culture at a concentration of 60 mg in 0.2 mL acetone/100 mL media and incubation was continued for six days at 30 °C on a rotary shaker. After this incubation period, the contents of the flasks were pooled and filtered through muslin cloth to separate mycelia and broth. The broth was then saturated with NaCl and extracted with CH_2Cl_2 (4 times, 1:1 v/v). The dried mycelia were also washed with CH_2Cl_2. The two extracts were found to be the same by GC and TLC analyses and therefore were pooled. The crude metabolite mixture was further analyzed by TLC, GC and GC-MS. The crude extract (1.1 g) obtained was subjected to silica gel (60-120 mesh) column chromatography and the metabolites were eluted using a gradient of petroleum ether/ethyl acetate from (1:0) to (6:4).

2.2.4.6. Synthesis of (*Z*)-α-santalyl acetate (2):

To a stirred solution of (*Z*)-α-santalol (**1**) (2g, 9.1 mmol) in CH_2Cl_2 (20 mL) at 0 °C, under inert conditions, was added Et_3N (1.1 g, 10.9 mmol) and the reaction mixture was stirred for 15 min at room temperature. To the above solution again cooled at 0 °C, acetic anhydride (1.2 g, 11.8 mmol) and catalytic amount of DMAP were added. Stirring was continued at room temperature for 3 h. The reaction was quenched by adding ice cooled water (20 mL), organic layer was separated and aqueous layer extracted with CH_2Cl_2 (2 × 25 mL). The combined organic layers were washed with brine, dried over anhydrous Na_2SO_4 and concentrated in *vacuum* to afford a pale yellow liquid (2.4 g). The crude product was purified by silica gel flash chromatography (hexane /ethyl acetate, 99.5:0.5) to furnish **2** as a colourless liquid (2.2 g, 90.4%).

2.2.4.7. Synthesis of 10,11-*cis*-epoxy-α-santalol:

To a stirred solution of **1** (2.0 g, 9.1 mmol) in CH_2Cl_2 (20 mL) at 0 °C, was added *m*CPBA (3.9 g, 13.6 mmol, 60%) and the reaction mixture was stirred for 3 h at room temperature. The reaction was quenched by adding ice cooled saturated $NaHCO_3$ solution (20 mL) and then extracted in CH_2Cl_2 (3 × 25 mL). The combined organic layers were washed with brine, dried over anhydrous Na_2SO_4 and concentrated in *vacuum* to afford pale yellow liquid (2.42 g). This was purified by silica gel flash chromatography (petroleum ether: ethyl acetate, 92:8) to furnish epoxy-α-santalol (1.3 g, 62%) as colourless liquid.

2.2.4.8. Synthesis of chiral α- and β- isomers of 10,11-*cis*-epoxy-α-santalol by Sharpless asymmetric epoxidation:[61]

Crushed 4 Å molecular sieves were heated in vacuum oven at 200 °C and 4 mmHg for at least 3 h. An oven-dried 250 mL three-necked round bottomed flask equipped with a magnetic stirbar, pressure equalizing addition funnel, thermometer, nitrogen inlet, and bubbler was charged with 0.2 g of 4 Å powered activated molecular sieves and anhydrous CH_2Cl_2 (10 mL). The flask was cooled to -20 °C, before D-(-)-Diethyl tartarate (56 mg, 0.27 mmol) and Ti $(O\text{-}^iPr)_4$ (65 mg, 0.23 mmol) were added sequentially *via* a syringe with stirring. The reaction mixture was stirred at -20 °C as *t*-BuOOH (0.27 mL, 5.0 M in decane) was added through the addition funnel over about 10 min. The resulting mixture was stirred at -20 °C for 30 min to which was slowly added a solution of **1** (0.2 g, 0.91 mmol) in anhydrous CH_2Cl_2 (2 mL) over a period of

20 min, being careful to maintain the reaction temperature between -20 to -15 °C. The mixture was stirred for an additional 5 h at -20 to -15 °C and then warmed to 0 °C. The reaction mixture was slowly poured into a beaker containing 200 mL of the pre-cooled (0 °C) solution of $FeSO_4 \cdot 7H_2O$ (0.3 g, 1.1 mmol) and citric acid monohydrate (0.12 g, 0.55 mmol). The two-phase mixture was stirred for 40 min at 0 °C and then transferred to a separatory funnel. The phases were separated and the aqueous phase was extracted with CH_2Cl_2 (2 × 10 mL). The combined organic layers were treated with pre-cooled 30% NaOH (w/v) (1.7 mL). The two-phase mixture was stirred vigorously for 1 h at 0 °C. Following transfer to a separatory funnel the phases were separated. The aqueous layer was extracted with CH_2Cl_2 (2 × 10 mL). The combined organic layers were dried over anhydrous Na_2SO_4, filtered and concentrated. The residue was chromatographed with petroleum ether: ethyl acetate (92:8) to give **3b** (0.18 g, 83% yield, 38% de).

Similar procedure was used for the synthesis of the other diastereomer **3**, where (+)-DET was the chiral auxiliary to yield **3** (0.18 g, 82% yield, 34% de).

2.2.4.9. Screening of lipases for kinetic resolution of epoxy-α-santalol diastereomers:

Commercially available lipases were screened for selective acetylation reactions with vinyl acetate as an acyl donor in hexane. Following lipases were screened:

Table 2.2.1. Lipases screened for resolution of 10,11-*cis*-epoxy-α-santalol diastereomers (**3** and **3b**):

Sr. no.	Lipases	Incubation temperature
1.	Cal-B (Novozyme 435)	40 °C
2.	Lipase from *Rhizopus niveus*	40 °C
3.	Lipase from *Thermomyces lanuginosa*, CLEA	40 °C
4.	Lipase from wheat germ	37 °C
5.	Lipase from *C. rugossa* type VII	37 °C
6.	Amano lipase from *Mucor javanicus*	40 °C
7.	Lipase from *Rhizopus arrhizus*	40 °C
8.	Cal-A immobilized on Immobead 150	40 °C
9.	Amano PS. lipase from *Burkholderia cepacia*	40 °C

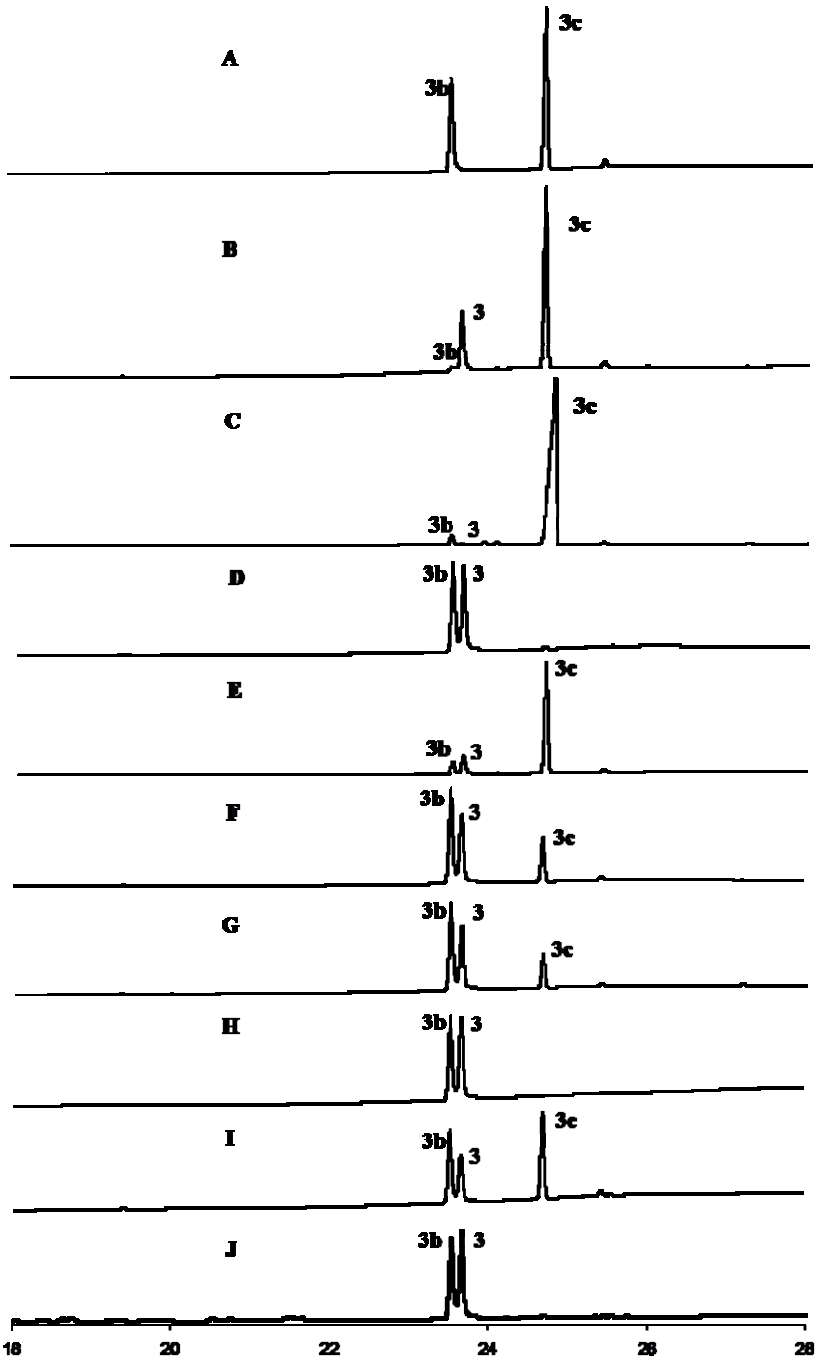

Figure 2.2.7. GC traces for screening of commercial lipases for kinetic resolution of diastereomeric mixture of 10,11-*cis*-epoxy-α-santalols (**A**) Amano lipase PS from *B. Cepacia*, (**B**) lipase from *C. Rugossa*, type-VII, (**C**) Cal-B (Novozyme 435), (**D**) lipase from *R. niveus*, (**E**) Cal A immobilized on Immobead 150, (**F**) lipase from *M. javanicus*, (**G**) lipase from *R. arrrhizus*, (**H**) lipase from wheat germ, (**I**) lipase from *T. lanuginosa*, (**J**) a diastereomeric mixture of 10,11-*cis*-epoxy-α-santalols. All the incubations were performed for 6 h. **GC conditions**: HP-chiral (20% β-cyclodextrin, 30 m × 0.25 mm × 0.25 μm) column, (Program I).

Commercial lipases (4 mg) were added to diastereomeric mixture of epoxy-α-santalol (2 mg) [synthesized from (*Z*)-α-santalol (**1**)] and vinyl acetate (20 µL) in hexane (2 mL). Resulting assay mixture was incubated on a metabolic water bath shaker (200 rpm) at temperatures specified for individual lipases. After 6 h incubation, the reaction mixture was filtered and analyzed by GC equipped with HP-chiral (20% β-cyclodextrin, 30 m × 0.25 mm × 0.25 µm) column (Program I) (Figure 2.2.7).

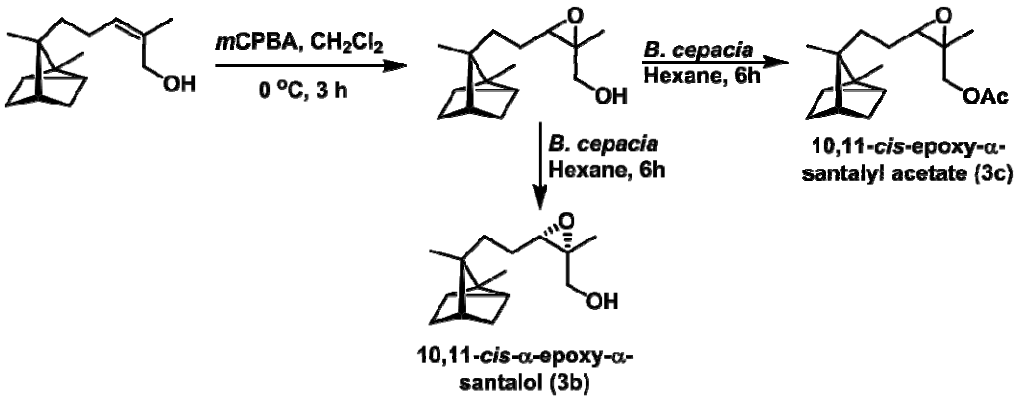

Scheme 2.2.4. Incubation of 10,11-*cis*-epoxy-α-santalol mixture with Amano PS lipase from *B*. *cepacia* for 6 h yielded exclusively α-epoxide (**3b**) (40%, >99% de) along with a mixture of epoxy-α-santalyl acetate (**3c**) (60%) and was purified by column chromatography after the reaction.

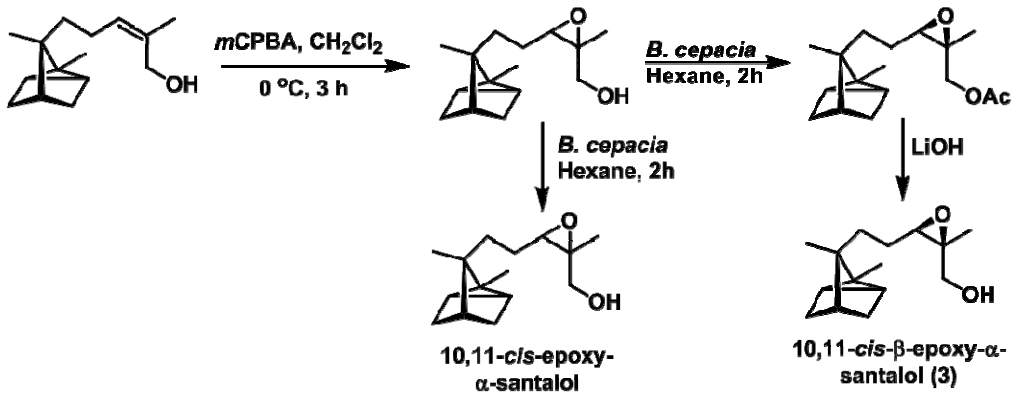

Scheme 2.2.5. Incubation of 10,11-*cis*-epoxy-α-santalol mixture with Amano PS lipase from *B*. *cepacia* was discontinued at 2 h, to yield β-epoxy-α-santalyl acetate (39%) along with the unspent alcohol. Purification of 10,11-*cis*-β-epoxy-α-santalyl acetate followed by deacetylation with LiOH resulted in **3** (96% de).

2.2.4.9. Spectral studies:

(*Z*)-α-Santalol (1):

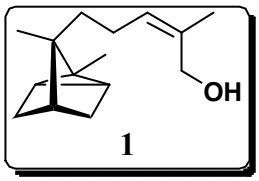

1

Colorless liquid; **[α]$_D$** +17.9 (*c* = 2.65, $CHCl_3$); **IR** ($CHCl_3$): ν_{max} 3399 cm^{-1} (-OH), 1676 cm^{-1} (olefin); **GC-EI-MS:** *m/z* 220.2, 202.2, 187.2, 159.1, 133.1, 121.1, 107.1, 94.1 (100%), 93.1, 91.1, 79.1, 67.1; **HREIMS:** Calcd. for $C_{15}H_{22}$, 202.1721, found 202.1724 $[M-H_2O]^+$.

(*Z*)-α-Santalyl acetate (2):

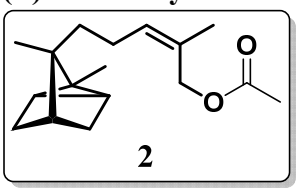

2

[α]$_D$ +13.69 (*c* = 2.40, $CHCl_3$); **IR** ($CHCl_3$, cm^{-1}): ν_{max} 1731 (C=O); **^{1}H NMR** (500 MHz, $CDCl_3$): δ 5.41 (t, *J* = 7.3 Hz, 1H, H_{10}), 4.58 (s, 2H, H_{12}), 2.08 (s, 3H, O=C-$\underline{CH_3}$), 1.92-2.03 (m, 2H, H_9), 1.74 (d, *J* = 1.07 Hz, 3H, H_{13}), 1.54-1.61 (m, 3H, H_{3b}, H_4 & H_{5b}), 1.21-1.27 (m, 1H, H_{8b}), 1.11-1.17 (m, 1H, H_{8a}), 1.03-1.07 (m, 2H, H_{3a} & H_{5a}), 0.99 (s, 3H, H_{14}), 0.83 (bs, 2H, H_2 & H_6), 0.82 (s, 3H, H_{15}); **^{13}C NMR** ($CDCl_3$, 125 MHz): δ 171.2 (C=O), 131.8 (C_{11}), 129.1 (C_{10}), 63.1 (C_{12}), 45.8 (C_7), 38.1 (C_4), 34.6 (C_8), 31.4 (C_5), 30.9 (C_3), 27.3 (C_1), 23.1 (C_9), 21.5 (C_{13}), 20.9 (C), 19.5 (C_6), 19.4 (C_2), 17.5 (C_{15}), 10.6 (C_{14}); **GC-EI-MS:** *m/*z 262.1, 247.1, 220.2, 202.2, 187.2, 159.1, 135.5, 121.2, 107.1, 93.1 (100%), 79.1, 67.1.

10,11-*cis*-β-epoxy-α-Santalol (3):

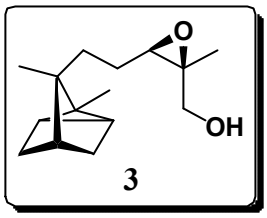

3

Colorless liquid; **[α]$_D$** +12.65 (*c* = 2.75, $CHCl_3$); **IR** ($CHCl_3$, cm^{-1}): ν_{max} 3435 (-OH), 1036 (C-O of epoxide); **GC-EI-MS**: *m/z* 236.2 $[M]^+$, 218.2, 205.2, 187.1, 175.1, 138.1, 121.1, 105.1, 93.1 (100%), 79.1, 67.1; **HR-EI-MS:** Calcd. for $C_{15}H_{24}O_2$, 236.1776, found 236.1783 $[M]^+$.

5α-hydroxy-(*Z*)-α-Santalol (4):

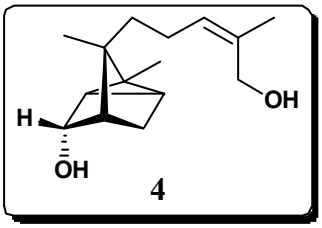

4

Colorless liquid; **[α]$_D$** -8.52 (*c* = 0.3, $CHCl_3$); **IR** ($CHCl_3$, cm^{-1}): ν_{max} 3381 (-OH); **GC-EI-MS:** *m/z* 236.2 $[M]^+$, 218.3, 203.3, 187.2, 137.2, 109.2 (100%), 95.2, 79.1, 67.1, 55.1; **HR-ESI-MS:** Calcd. for $C_{15}H_{24}O_2Na$, 259.1674, found 259.1746 $[M+Na]^+$.

10,11-dihydroxy-α-Santalol (5):

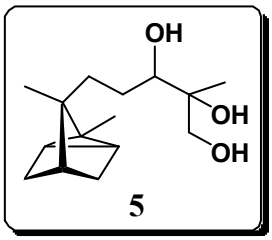

5

Colorless oil; **[α]$_D$** +19.56 (*c* = 0.4, $CHCl_3$); **IR** ($CHCl_3$, cm^{-1}): ν_{max} 3381 (-OH); **GC-EI-MS:** *m/z* 254.3 $[M]^+$, 220.2, 202.2, 187.1, 159.1, 121.1, 107.1, 94.1, 93.1 (100%), 79.1; **HR-EI-MS:** Calcd. for $C_{15}H_{26}O_3$, 254.1881, found 254.1793 $[M]^+$.

5α-hydroxy,*cis*-β-10,11-epoxy-α-Santalol (6):

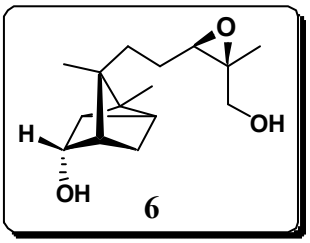

6

Colorless liquid; **IR** ($CHCl_3$, cm^{-1}): ν_{max} 3435 (-OH), 1036 (C-O of epoxide); **GC-EI-MS:** *m/z* 252.1 $[M]^+$, 219.0, 203.1, 159.1, 137.1, 119.1, 107.1 (100%), 91.0, 81.1, 67.1; **HR-EI-MS:** Calcd. for $C_{15}H_{24}O_3$, 252.1725, found 252.1679 $[M]^+$.

Appendix 2

Appendix 2 Index

Table 2.2.2. ^{1}H and ^{13}C assignments of (Z)-α-santalol (**1**) from 2D NMR data analysis.

^{13}C (δ)	**HSQC** (δ)	**HMBC** (δ)	**COSY** (δ)
C1: 27.34 (-C-)	-	H14, H5a, H15	-
C2: 19.45* (-CH)	0.84 (bs, H2)	H3b	-
C3: 30.99 ($-CH_2$)	1.05 (m, H3a), 1.57 (bs, H3b)	H5b	H3a↔H3b
C4: 38.11 (-CH)	1.58 (m, H4)	H3a, H15	-
C5: 31.48 ($-CH_2$)	1.07 (m, H5a), 1.62 (bs, H5b)	H3b	H5a↔H5b
C6: 19.47* (-CH)	0.84 (bs, H6)	H5b, H14	-
C7: 45.83 (-C-)	-	H14, H3a, H15	-
C8: 34.96 ($-CH_2$)	1.15 (m, H8a), 1.23 (m, H8b)	H15, H9	H8b↔H9, H8a
C9: 22.89 ($-CH_2$)	1.91-2.02 (m, H9)	-	H9↔H8b, H10
C10: 129.52 (=CH)	5.32 (t, H10)	H12, H13, H9	H10↔H9, H13
C11: 133.60 (=C)	-	H12, H13, H9	-
C12: 61.55 ($-CH_2$-O)	4.15 (s, H12)	H13, H10	-
C13: 21.23 ($-CH_3$)	1.80 (d, H13)	H12, H10	H13↔H10
C14: 10.62 ($-CH_3$)	1.00 (s, H14)	H2/H6	-
C15: 17.49 ($-CH_3$)	0.83 (s, H15)	H8a (w), H8b (w)	-

All the observed correlations are shown.

* These δ values are interchangeable. (w) implies weak intensity of the signal.

Table 2.2.3. ^{13}C assignments of all the metabolites: (*Z*)-α-santalol (**1**), 10,11-*cis*-β-epoxy-α-santalol (**3**), 5α-hydroxy-(*Z*)-α-santalol (**4**), 10,11-dihydroxy-α-santalol (**5**) and 5α-hydroxy-10,11-*cis*-β-epoxy-α-santalol (**6**).

^{13}C	**(1)** (δ)	**(3)**(δ)	**(4)**(δ)	**(5)**(δ)	**(6)**(δ)
C1:	27.34	27.3	32.3	27.4	32.2
C2:	19.45*	19.4	20.7	19.4	20.7
C3:	30.99	30.9	26.9	31.0	26.9
C4:	38.11	38.1	44.2	38.1	44.2
C5:	31.48	31.4	75.5	31.4	75.4
C6:	19.47*	19.5	26.2	19.5	26.3
C7:	45.83	45.6	45.9	45.8	45.7
C8:	34.96	30.8	35.6	30.7	31.6
C9:	22.89	23.6	22.7	26.4	23.4
C10:	129.52	65.4	129.0	77.2	65.1
C11:	133.60	61.0	133.9	74.0	61.0
C12:	61.55	63.9	61.5	69.5	63.9
C13:	21.23	20.2	21.2	19.6	20.2
C14:	10.62	10.6	10.7	10.7	10.7
C15:	17.49	17.4	17.8	17.5	17.7

* These δ values may interchange.

Table 2.2.4. ^{1}H assignments of all the metabolites: (*Z*)-α-santalol (**1**), 10,11-*cis*-β-epoxy-α-santalol (**3**), 5α-hydroxy-(*Z*)-α-santalol (**4**), 10,11-dihydroxy-α-santalol (**5**) and 5α-hydroxy-10,11-*cis*-β-epoxy-α-santalol (**6**).

^{1}H	**(1)**	**(3)**	**(4)**	**(5)**	**(6)**
1:	-	-	-	-	-
2:	0.84, bs	0.85, bs	1.09-1.13, m	0.86, bs	1.05, dt, *J* = 1.43, 5.27 Hz
3a:	1.05, m	1.05, m	1.59-1.62, m	1.53, m	1.58, m
3b:	1.57, bs	1.52, m	1.66, s	1.04-1.08, m	1.68, bs
4:	1.58, m	1.52, m	1.59-1.62, m	1.56, s	1.55-1.56, m
5a:	1.07, m	1.07, m	4.22, t, *J* = 1.78 Hz	1.63, m	4.22, t, *J* = 1.78 Hz
5b:	1.62, bs	1.59-1.62, m		1.04-1.08, m	
6:	0.84, bs	0.85, bs	1.03, m	0.86, bs	1.13, d, *J* = 5.27 Hz
7:	-	-	-	-	-
8a:	1.15, m	1.31,m	1.14-1.17, m	1.17-1.23, m	1.32-1.38, m
8b:	1.23, m		1.32, m	1.44-1.46, m	
9a:	1.91-2.02, m	1.45, m	1.88-2.01, m	1.32-1.41, m	1.45, m
9b:		1.59-1.62, m			1.55-1.56, m
10:	5.32, t, *J* = 7.43 Hz	2.83, t, *J* = 6.40 Hz	5.30, t, *J* = 7.53 Hz	3.56, dd, *J* = 1.93, 9.91 Hz	2.81, m
11:	-	-	-	-	-
12a:	4.15, s	3.64 - 3.72, m	4.14, s	3.52, d, *J* = 11.28 Hz	3.69, s
12b:				3.66, d, *J* = 11.28 Hz	
13:	1.80, d, *J* = 1.10 Hz	1.39, s	1.80, d, *J* = 1.00 Hz	1.10, s	1.40, s
14:	1.00, s	1.01, s	1.00, s	1.03, s	1.03, s
15:	0.83, s	0.81, s	0.93, s	0.83, s	0.92, s

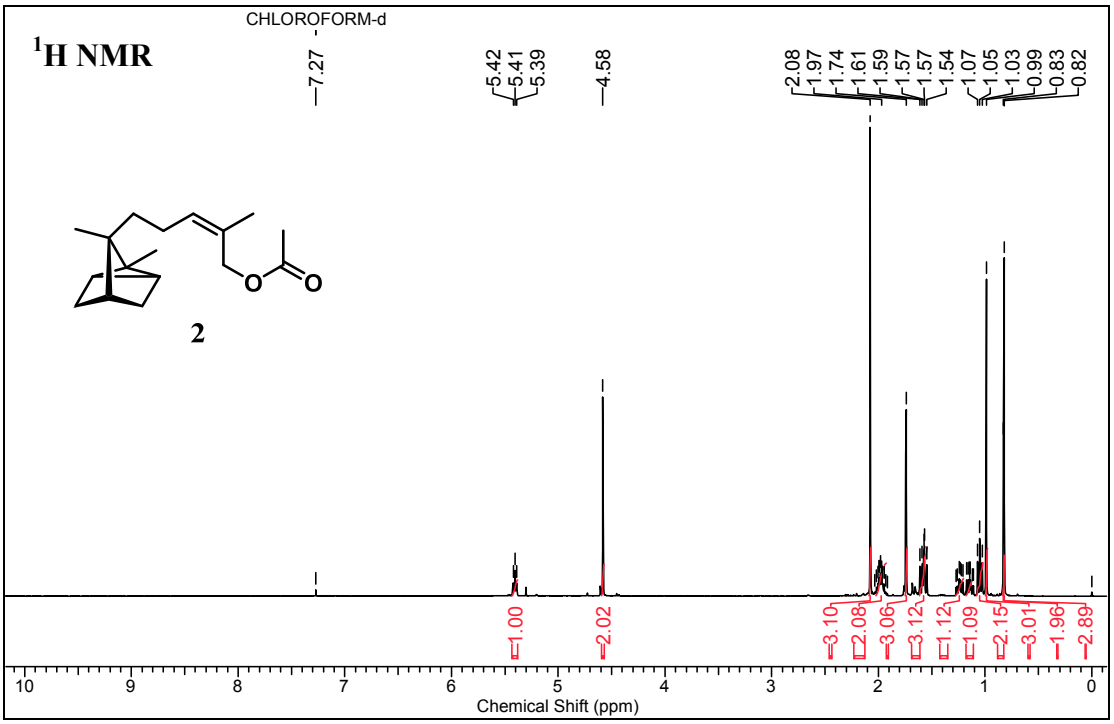
CHLOROFORM-d
^{1}H NMR
7.27
5.42
5.41
5.39
4.58
2.08
1.97
1.74
1.61
1.59
1.57
1.57
1.54
1.07
1.05
1.03
0.99
0.83
0.82
1.00
2.02
3.10
2.08
3.06
3.12
1.12
1.09
2.15
3.01
1.96
2.89
Chemical Shift (ppm)

2

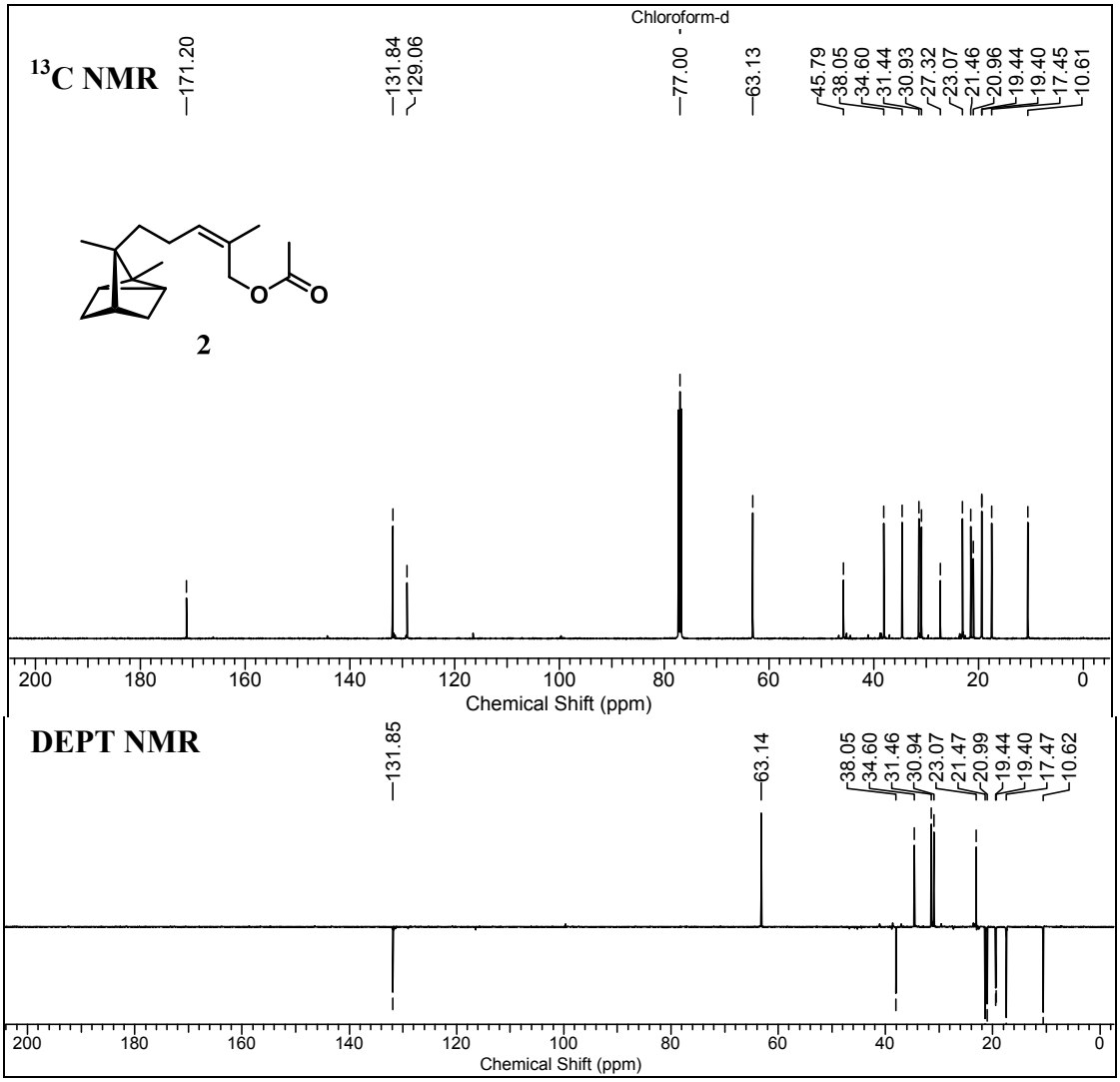
Chloroform-d
^{13}C NMR
171.20
131.84
129.06
77.00
63.13
45.79
38.05
34.60
31.44
30.93
27.32
23.07
21.46
20.96
19.44
19.40
17.45
10.61
Chemical Shift (ppm)

2

DEPT NMR
131.85
63.14
38.05
34.60
31.46
30.94
23.07
21.47
20.99
19.44
19.40
17.47
10.62
Chemical Shift (ppm)

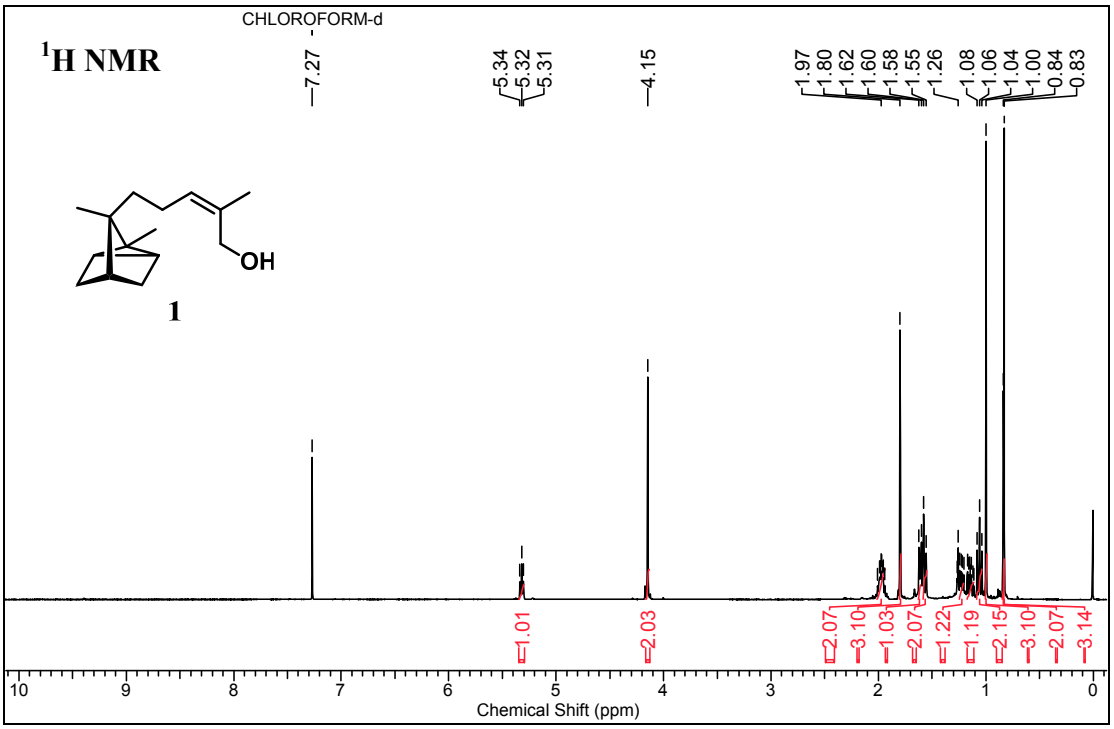
CHLOROFORM-d
^{1}H NMR
7.27
5.34
5.32
5.31
4.15
1.97
1.80
1.62
1.60
1.58
1.55
1.26
1.08
1.06
1.04
1.00
0.84
0.83
OH
1
1.01
2.03
2.07
3.10
1.03
2.07
1.22
1.19
2.15
3.10
2.07
3.14
Chemical Shift (ppm)

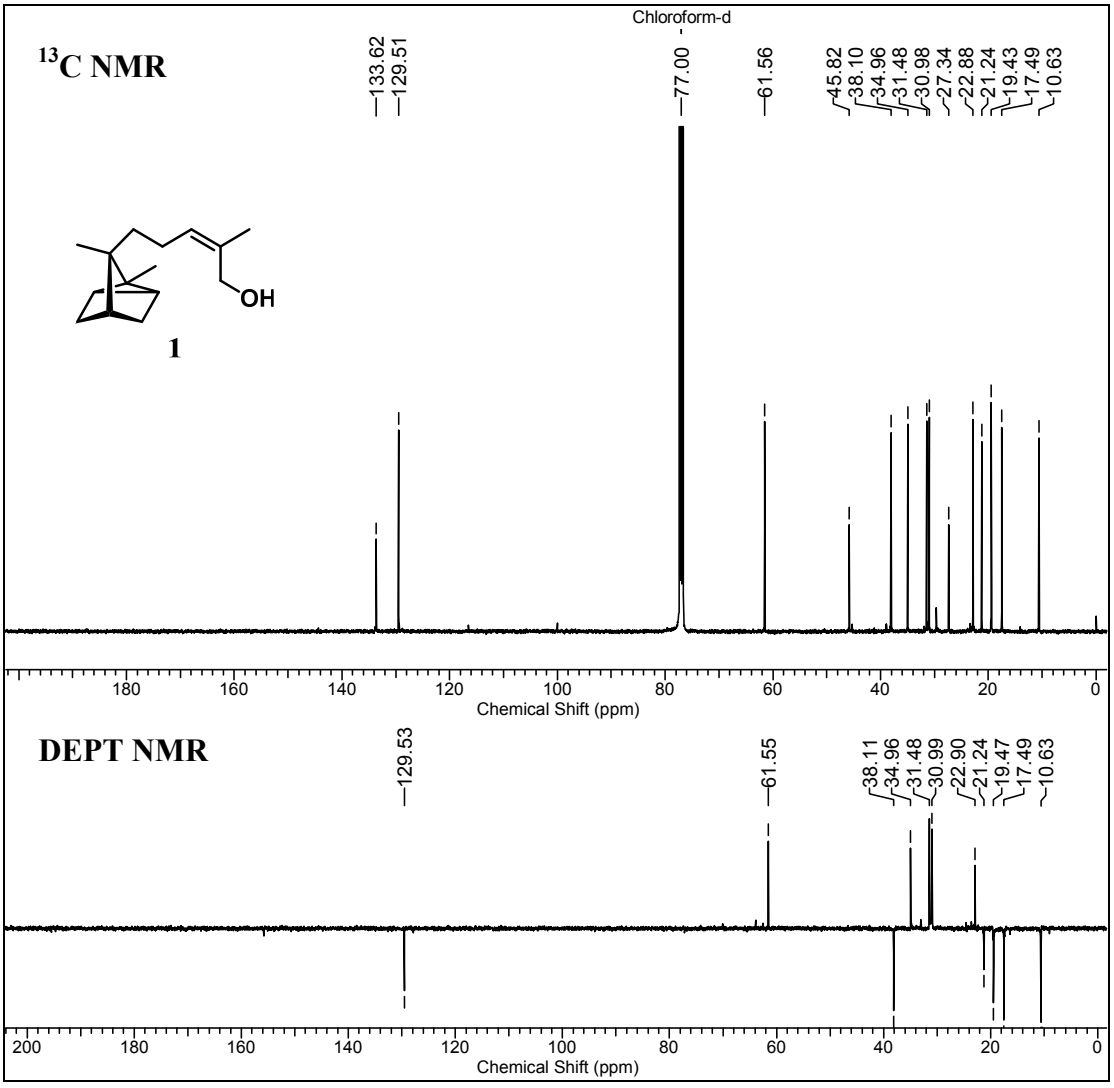
Chloroform-d
^{13}C NMR
133.62
129.51
77.00
61.56
45.82
38.10
34.96
31.48
30.98
27.34
22.88
21.24
19.43
17.49
10.63
OH
1
Chemical Shift (ppm)
DEPT NMR
129.53
61.55
38.11
34.96
31.48
30.99
22.90
21.24
19.47
17.49
10.63
Chemical Shift (ppm)

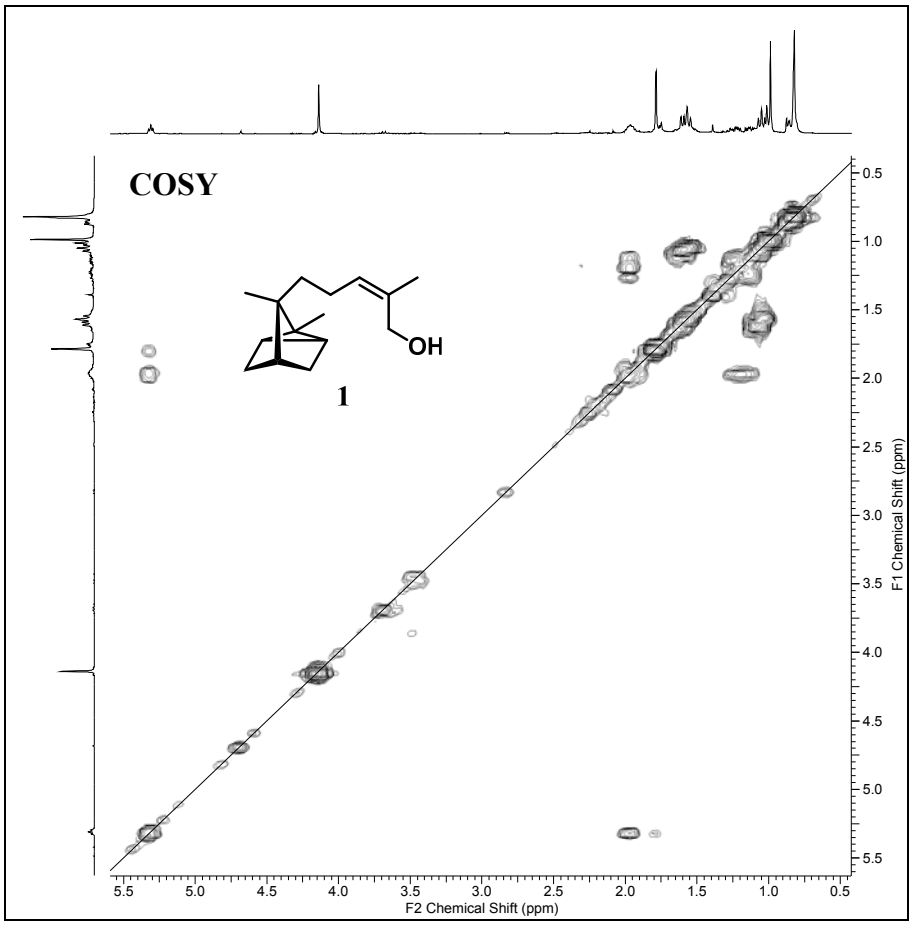
COSY
OH
1
F2 Chemical Shift (ppm)
F1 Chemical Shift (ppm)

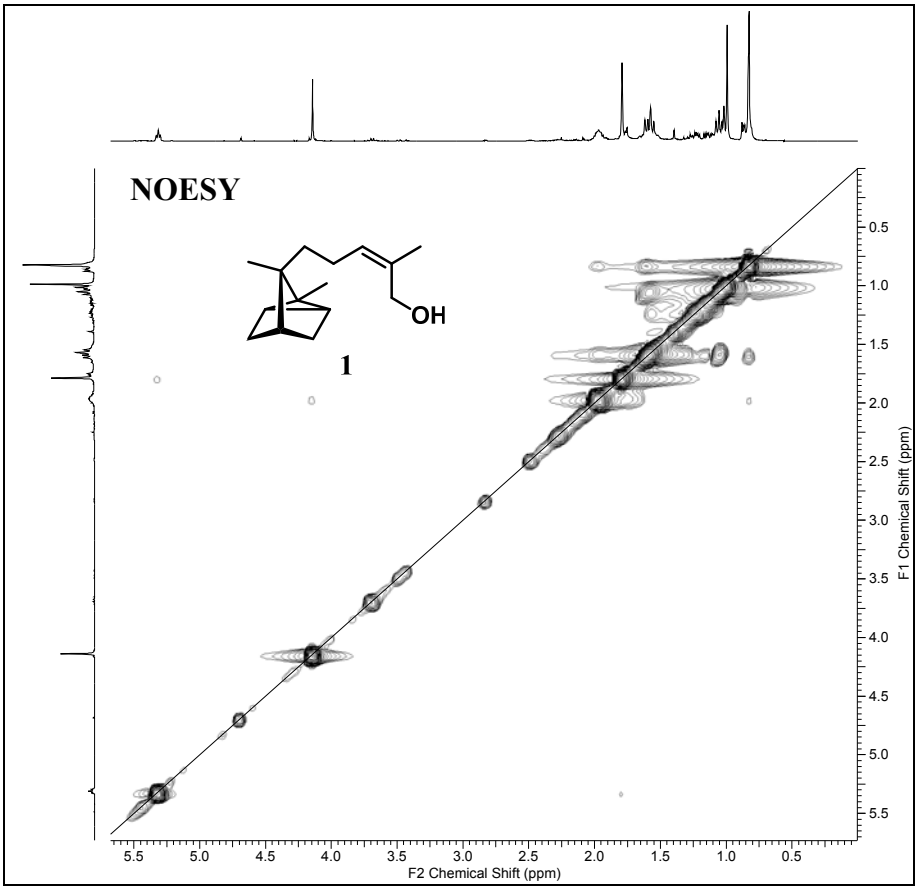
NOESY
OH
1
F2 Chemical Shift (ppm)
F1 Chemical Shift (ppm)

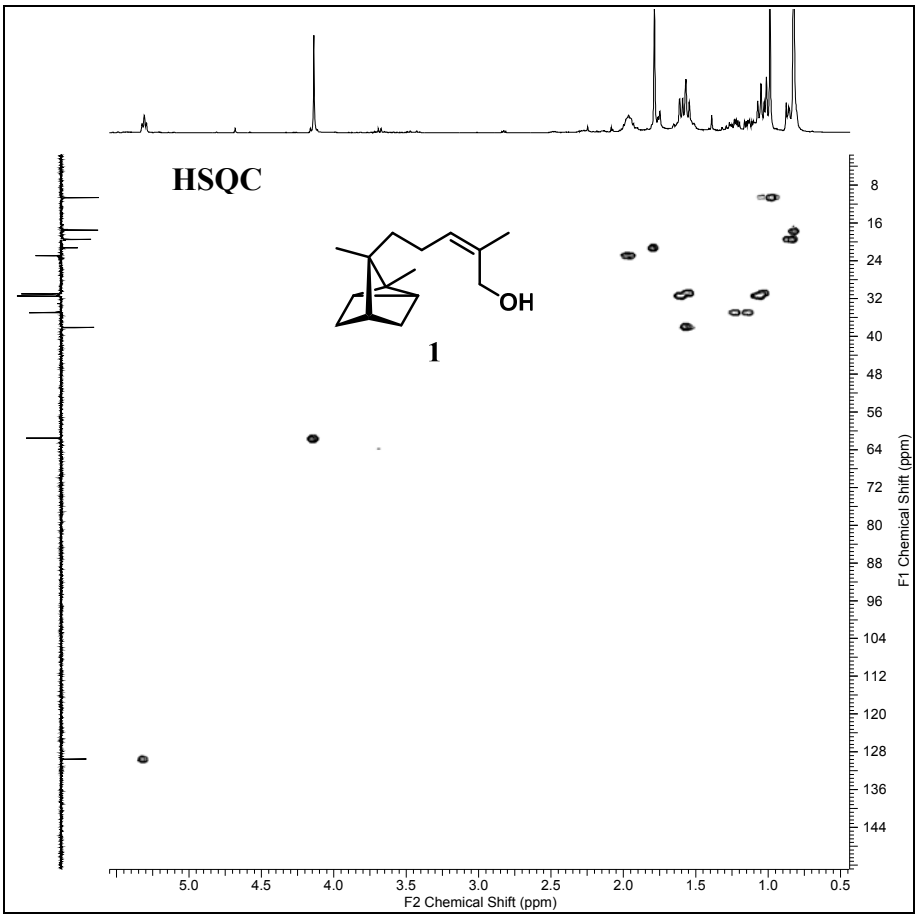
HSQC
OH
1
F2 Chemical Shift (ppm)
F1 Chemical Shift (ppm)

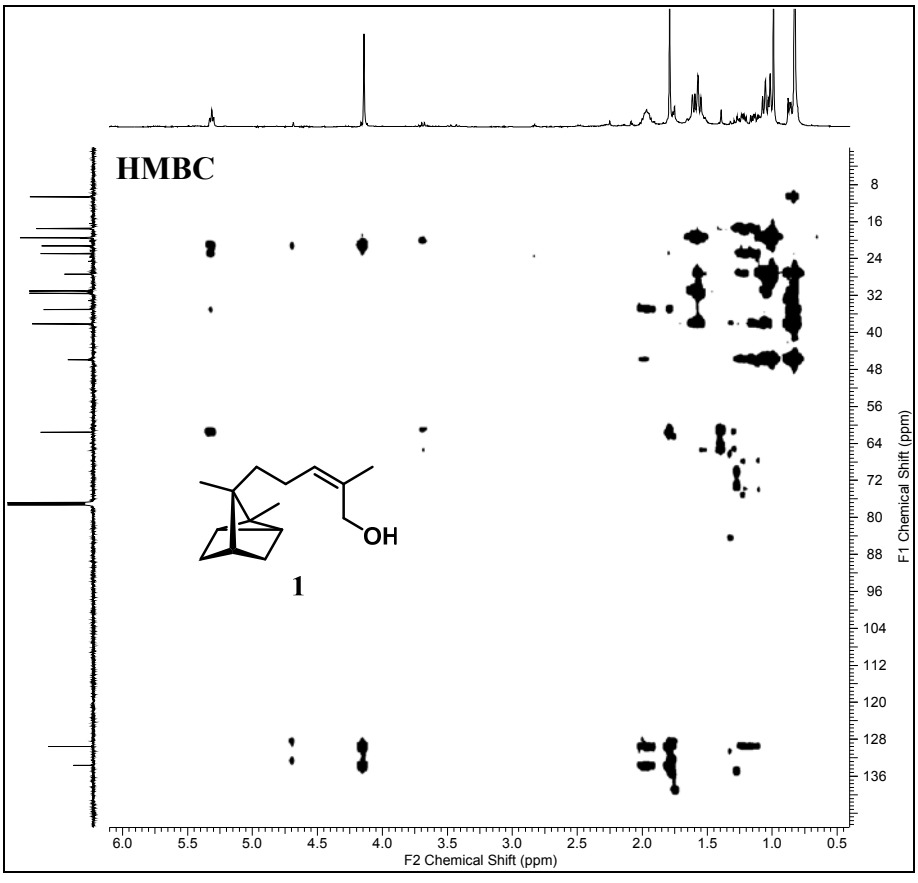
HMBC
OH
1
F2 Chemical Shift (ppm)
F1 Chemical Shift (ppm)

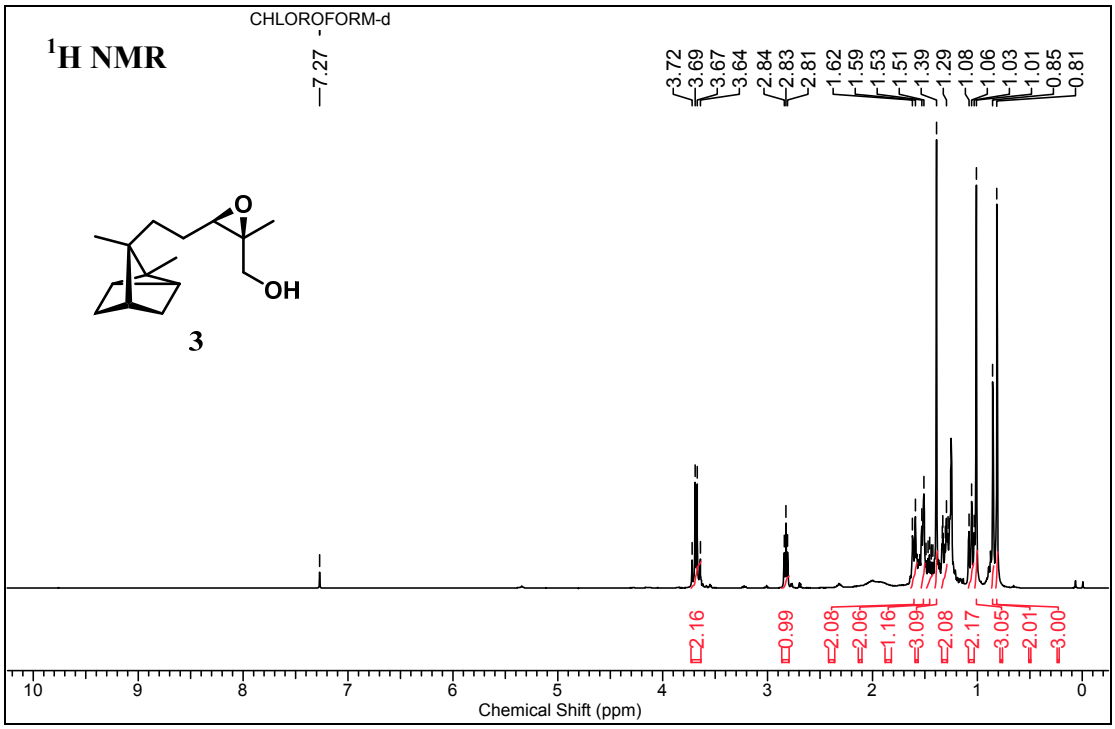
^{1}H NMR
CHLOROFORM-d
7.27
3.72
3.69
3.67
3.64
2.84
2.83
2.81
1.62
1.59
1.53
1.51
1.39
1.29
1.08
1.06
1.03
1.01
0.85
0.81
O
OH
3
2.16
0.99
2.08
2.06
1.16
3.09
2.08
2.17
3.05
2.01
3.00
10
9
8
7
6
5
4
3
2
1
0
Chemical Shift (ppm)

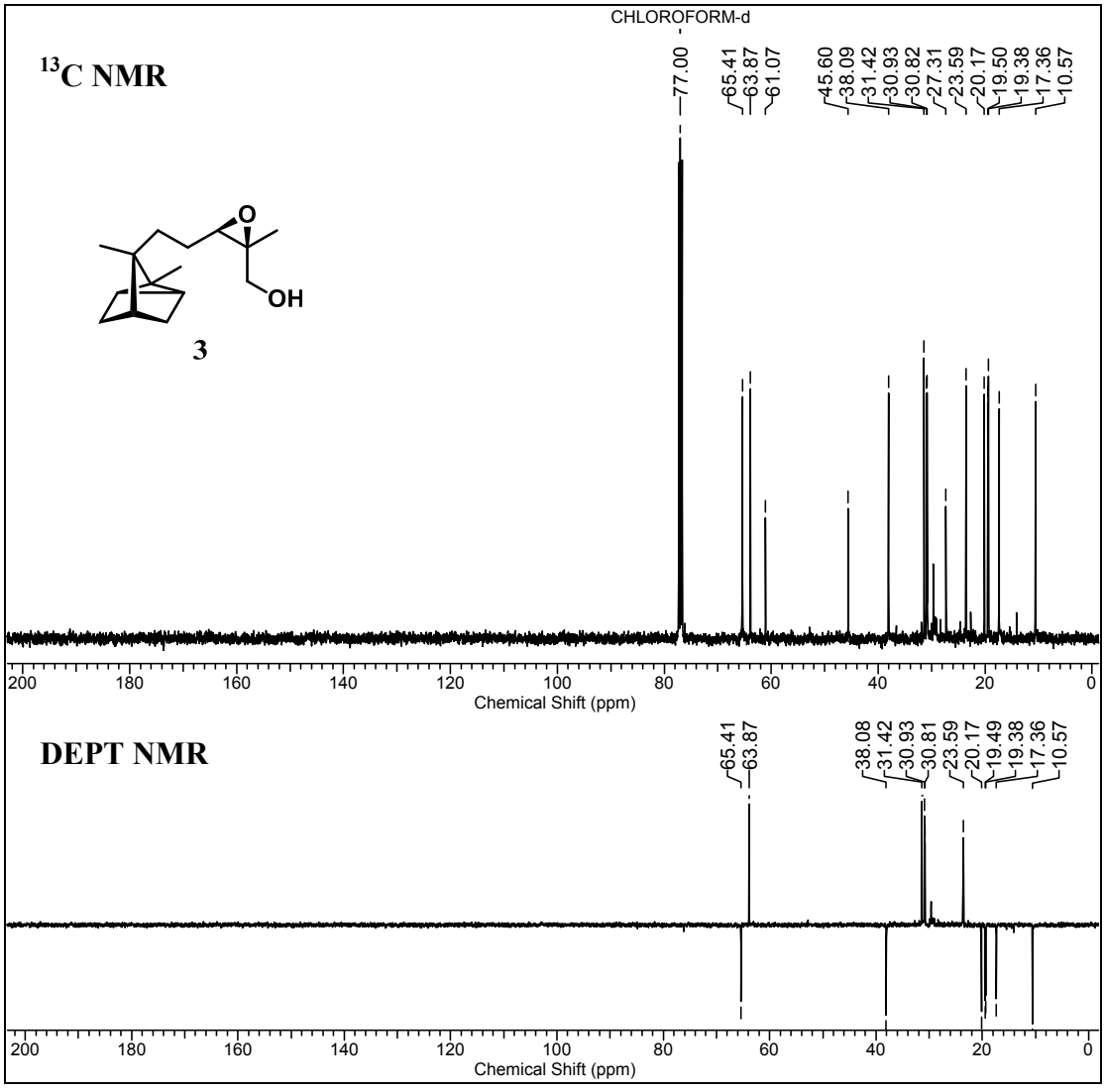
^{13}C NMR
CHLOROFORM-d
77.00
65.41
63.87
61.07
45.60
38.09
31.42
30.93
30.82
27.31
23.59
20.17
19.50
19.38
17.36
10.57
O
OH
3
200
180
160
140
120
100
80
60
40
20
0
Chemical Shift (ppm)
DEPT NMR
65.41
63.87
38.08
31.42
30.93
30.81
23.59
20.17
19.49
19.38
17.36
10.57
200
180
160
140
120
100
80
60
40
20
0
Chemical Shift (ppm)

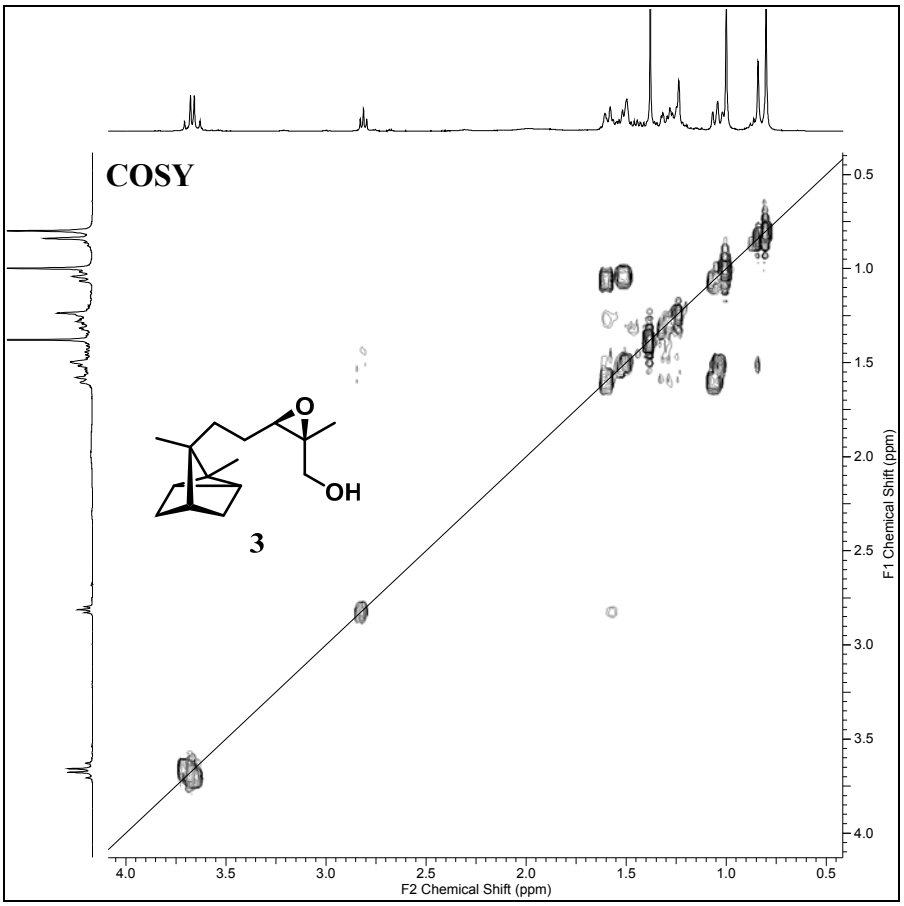
COSY
O
OH
3
F2 Chemical Shift (ppm)
F1 Chemical Shift (ppm)
4.0
3.5
3.0
2.5
2.0
1.5
1.0
0.5

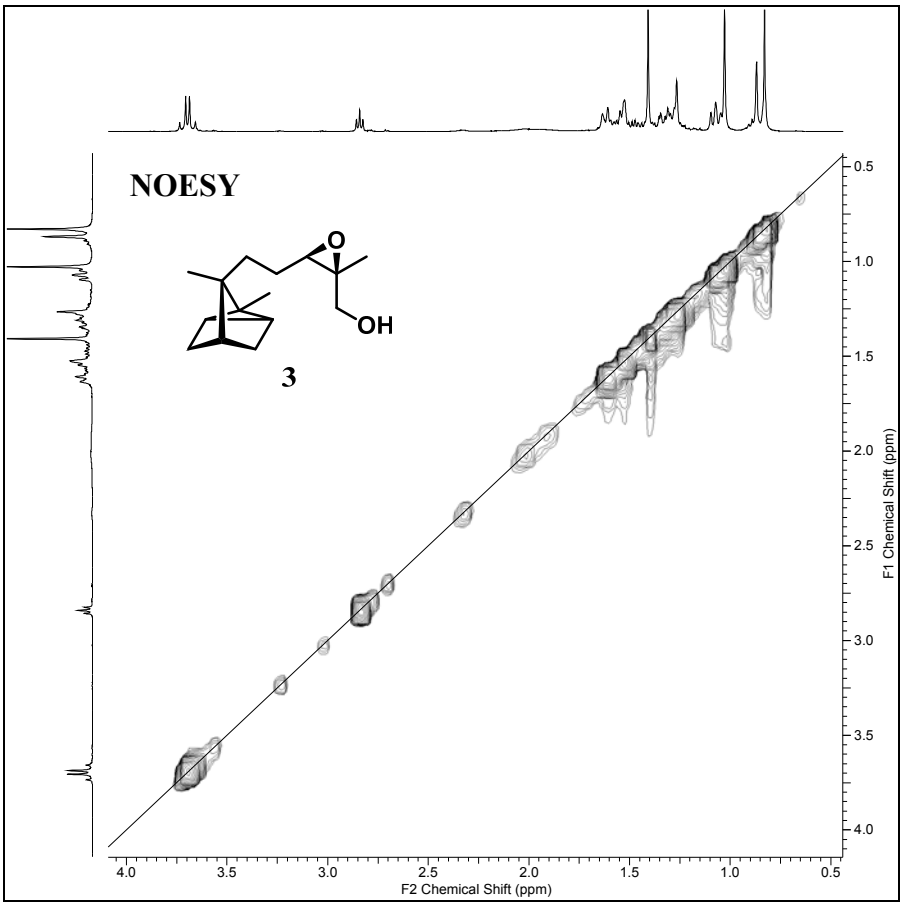
NOESY
O
OH
3
F2 Chemical Shift (ppm)
F1 Chemical Shift (ppm)
4.0
3.5
3.0
2.5
2.0
1.5
1.0
0.5

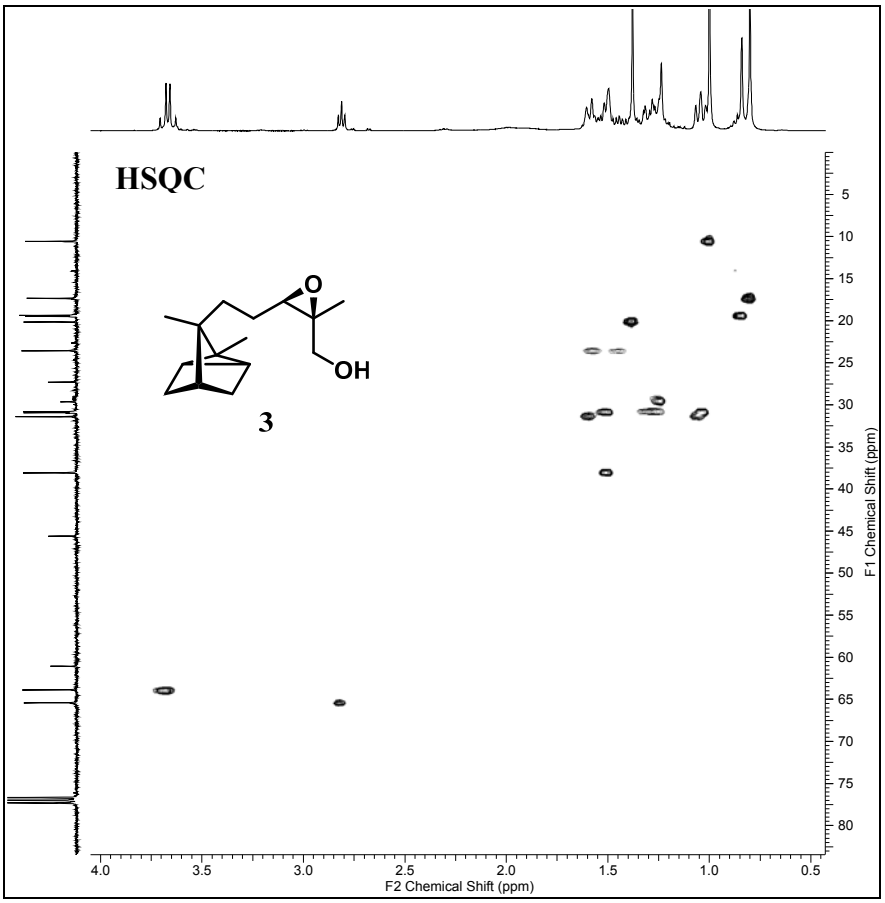
HSQC
O
OH
3
F2 Chemical Shift (ppm)
F1 Chemical Shift (ppm)

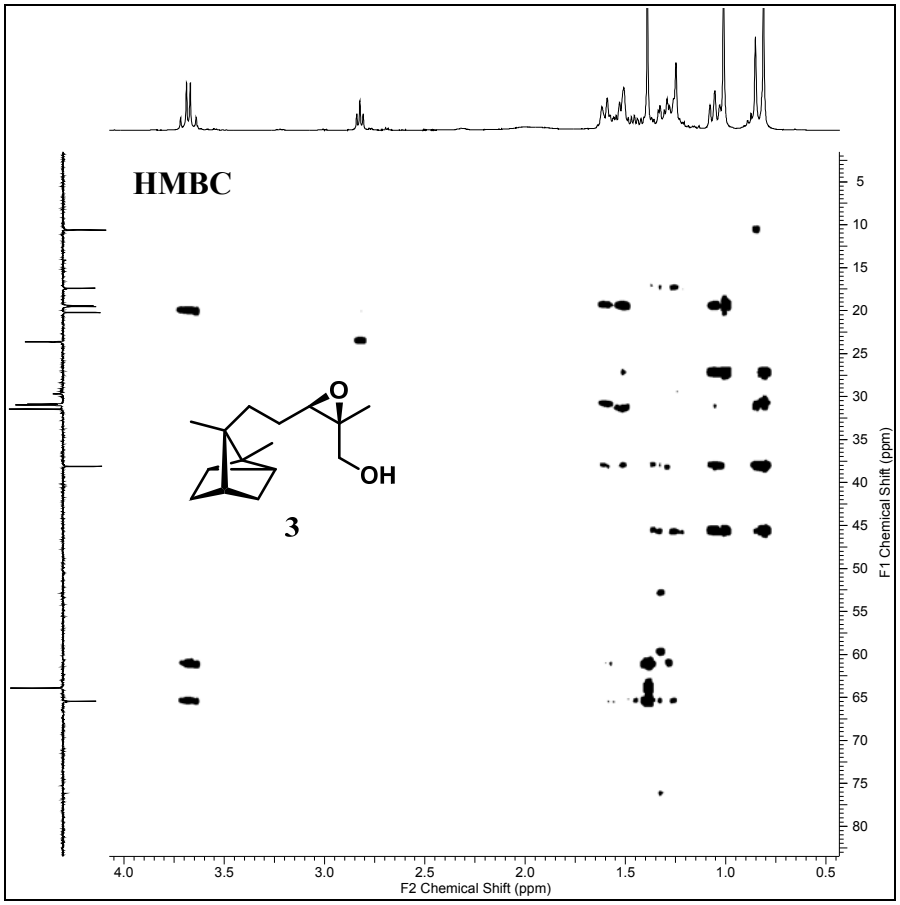
HMBC
O
OH
3
F2 Chemical Shift (ppm)
F1 Chemical Shift (ppm)

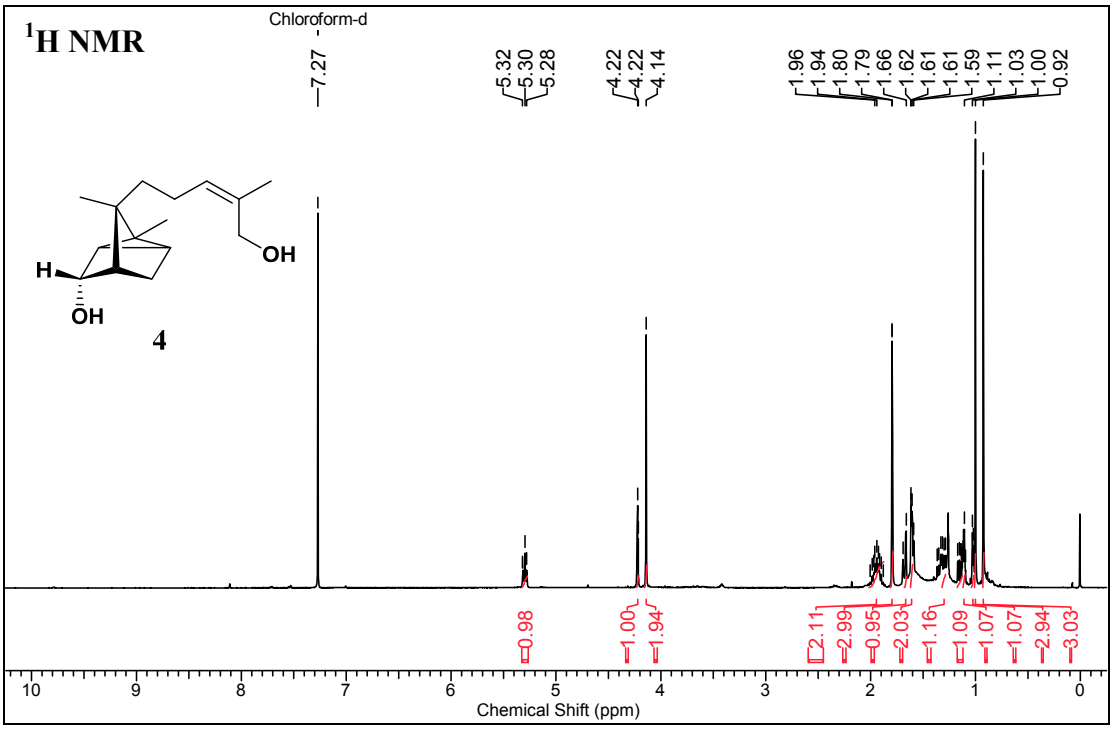
^{1}H NMR
Chloroform-d
7.27
5.32
5.30
5.28
4.22
4.22
4.14
1.96
1.94
1.80
1.79
1.66
1.62
1.61
1.61
1.59
1.11
1.03
1.00
0.92
OH
H
OH
4
0.98
1.00
1.94
2.11
2.99
0.95
2.03
1.16
1.09
1.07
1.07
2.94
3.03
Chemical Shift (ppm)

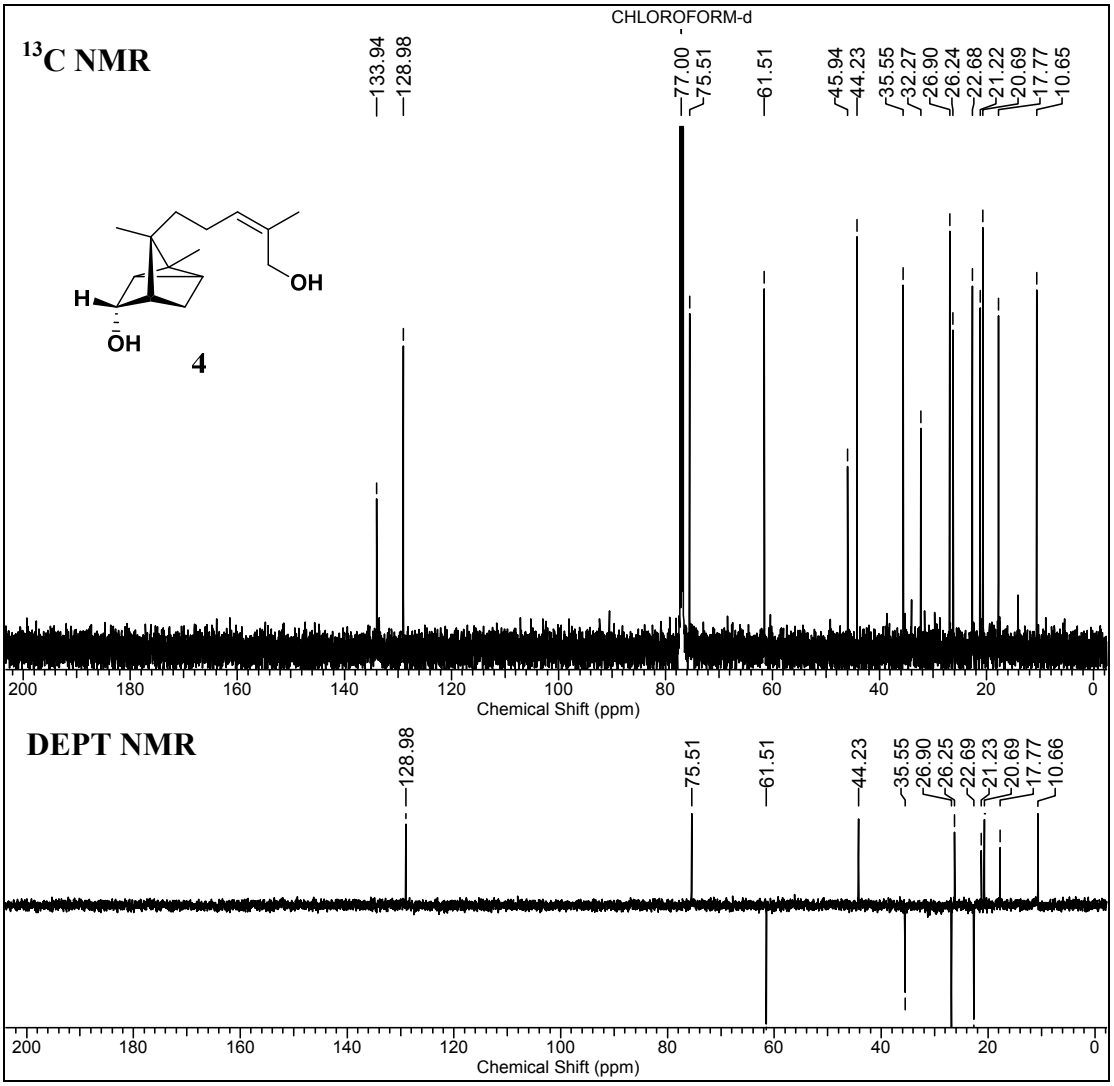
^{13}C NMR
CHLOROFORM-d
133.94
128.98
77.00
75.51
61.51
45.94
44.23
35.55
32.27
26.90
26.24
22.68
21.22
20.69
17.77
10.65
OH
H
OH
4
Chemical Shift (ppm)
DEPT NMR
128.98
75.51
61.51
44.23
35.55
26.90
26.25
22.69
21.23
20.69
17.77
10.66
Chemical Shift (ppm)

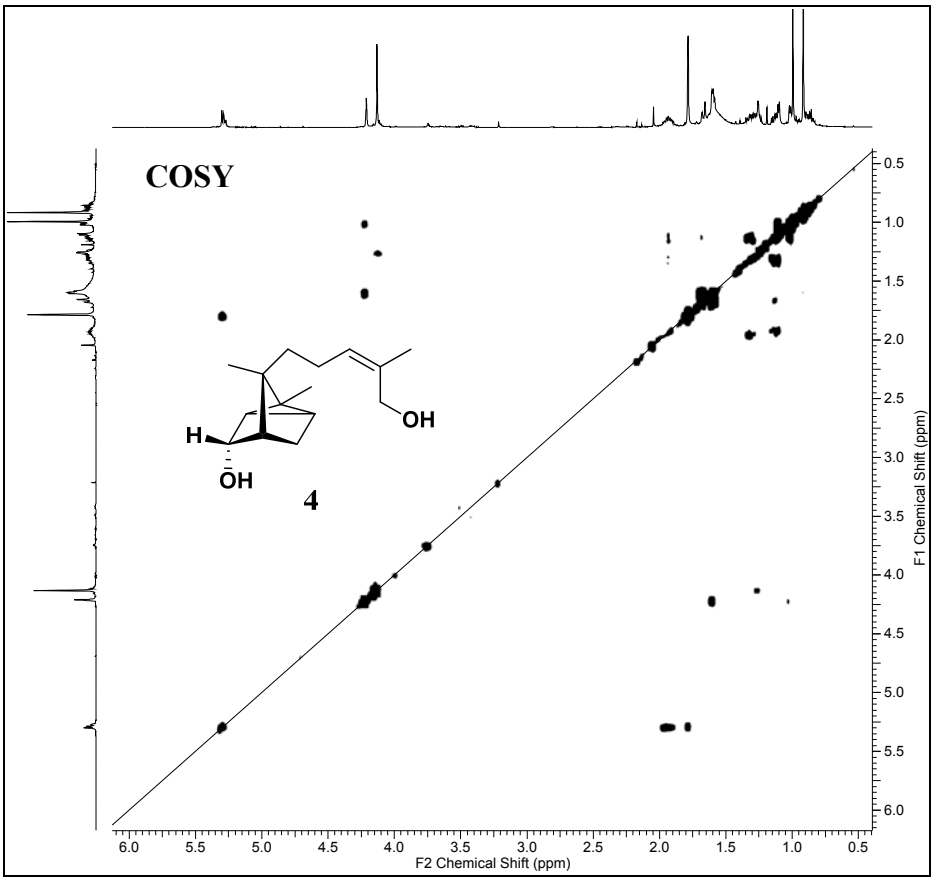
COSY
H
OH
OH
4
F2 Chemical Shift (ppm)
F1 Chemical Shift (ppm)

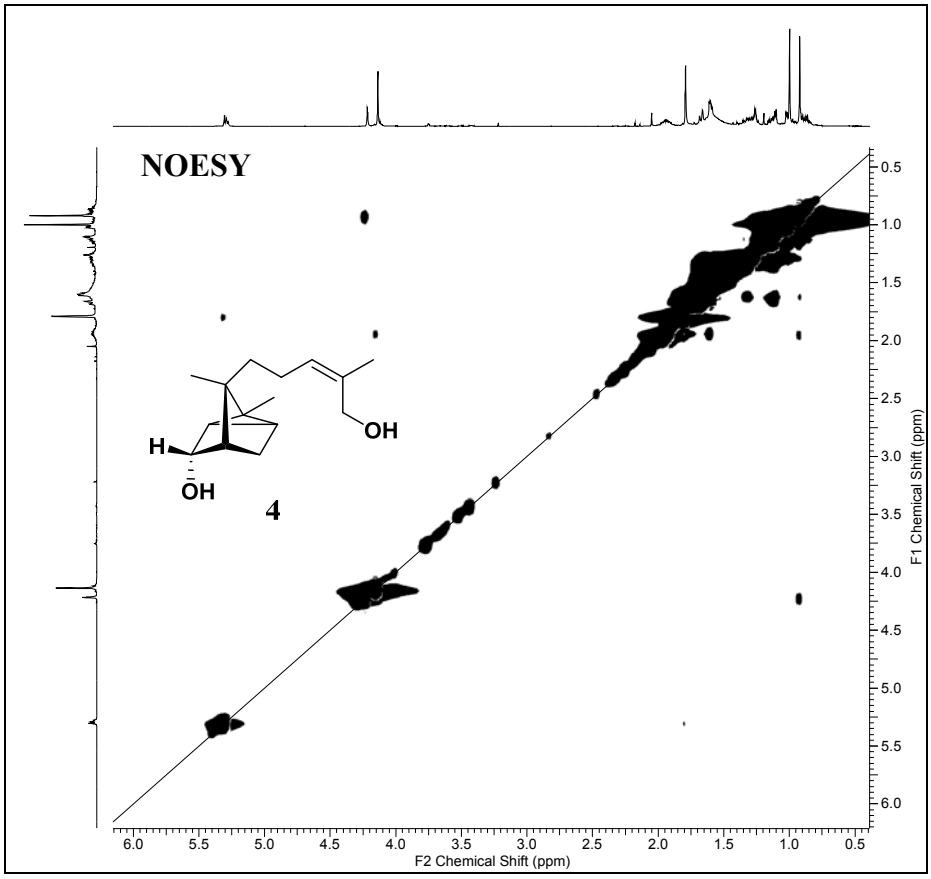
NOESY
H
OH
OH
4
F2 Chemical Shift (ppm)
F1 Chemical Shift (ppm)

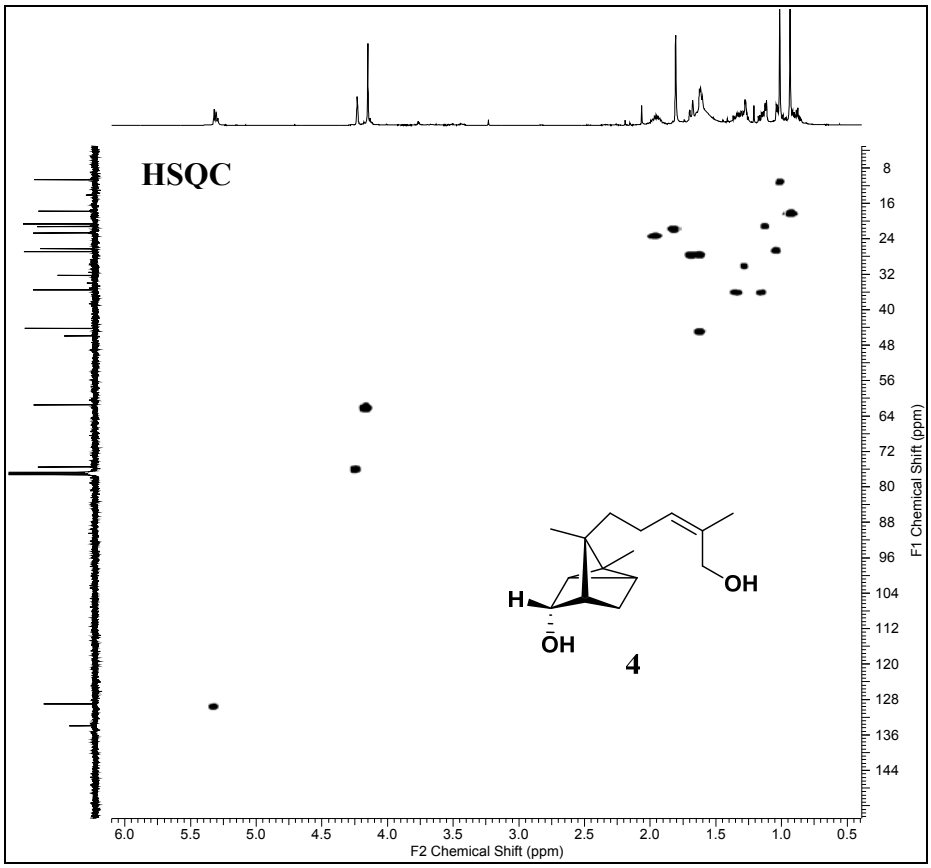
HSQC
H
OH
OH
4
F2 Chemical Shift (ppm)
F1 Chemical Shift (ppm)

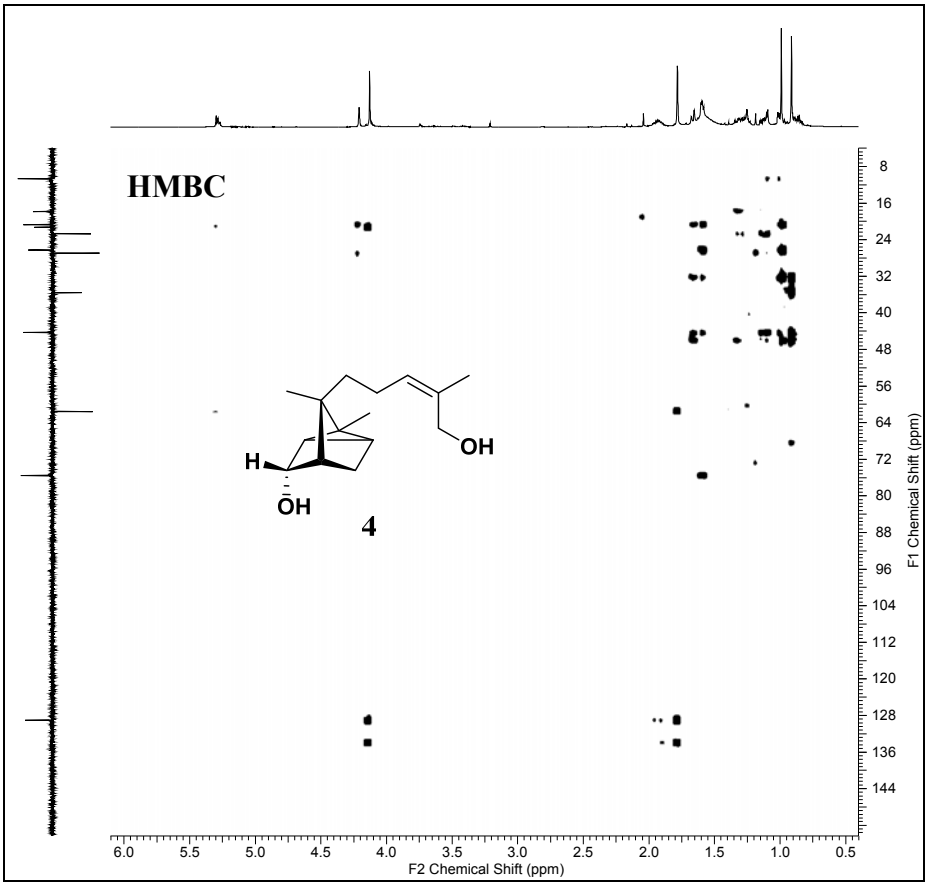
HMBC
H
OH
OH
4
F2 Chemical Shift (ppm)
F1 Chemical Shift (ppm)

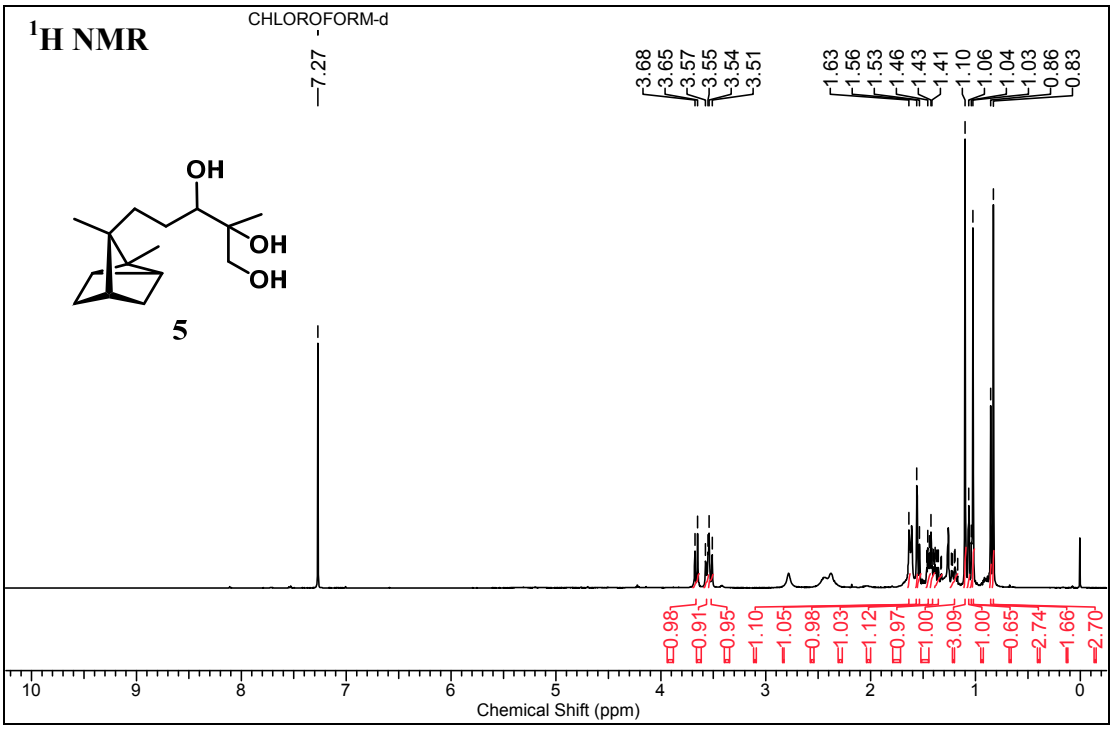
^{1}H NMR
CHLOROFORM-d
7.27
3.68
3.65
3.57
3.55
3.54
3.51
1.63
1.56
1.53
1.46
1.43
1.41
1.10
1.06
1.04
1.03
0.86
0.83
OH
OH
OH
5
0.98
0.91
0.95
1.10
1.05
0.98
1.03
1.12
0.97
1.00
3.09
1.00
0.65
2.74
1.66
2.70
Chemical Shift (ppm)

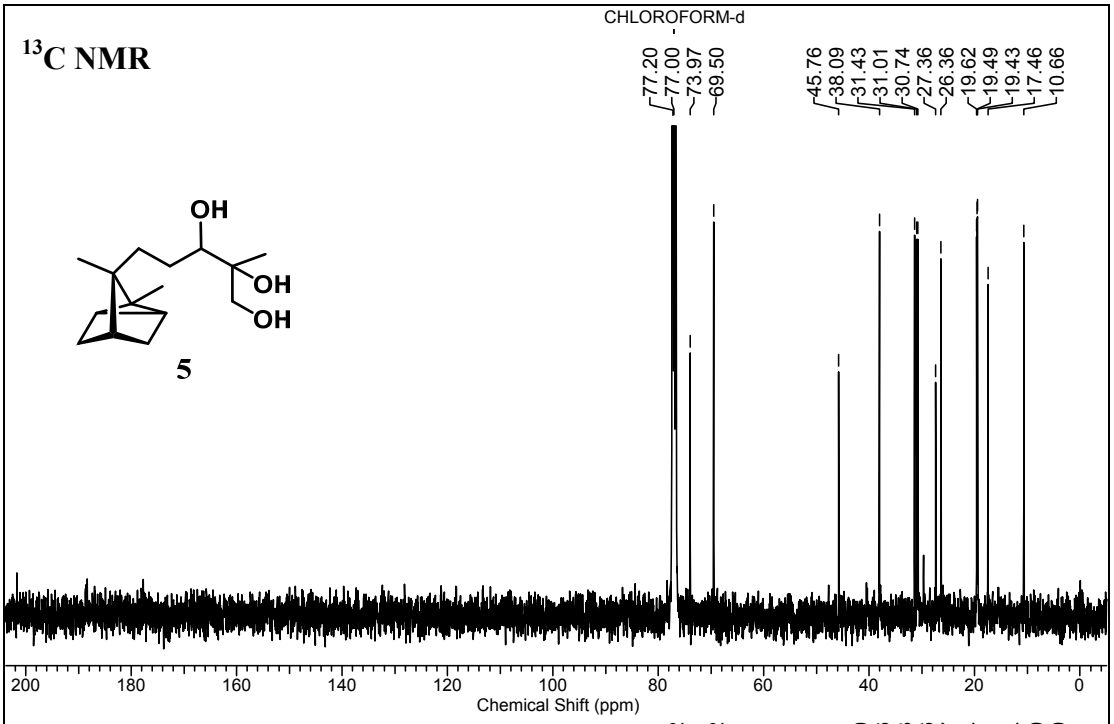
^{13}C NMR
CHLOROFORM-d
77.20
77.00
73.97
69.50
45.76
38.09
31.43
31.01
30.74
27.36
26.36
19.62
19.49
19.43
17.46
10.66
OH
OH
OH
5
Chemical Shift (ppm)

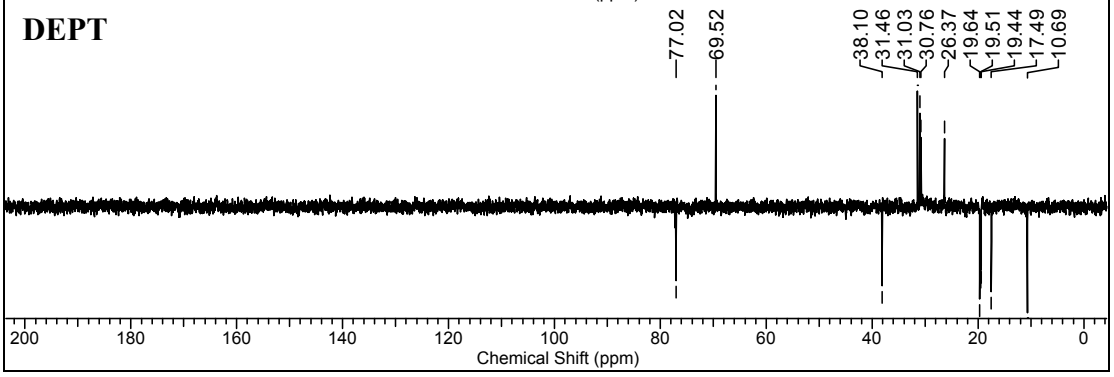
DEPT
77.02
69.52
38.10
31.46
31.03
30.76
26.37
19.64
19.51
19.44
17.49
10.69
Chemical Shift (ppm)

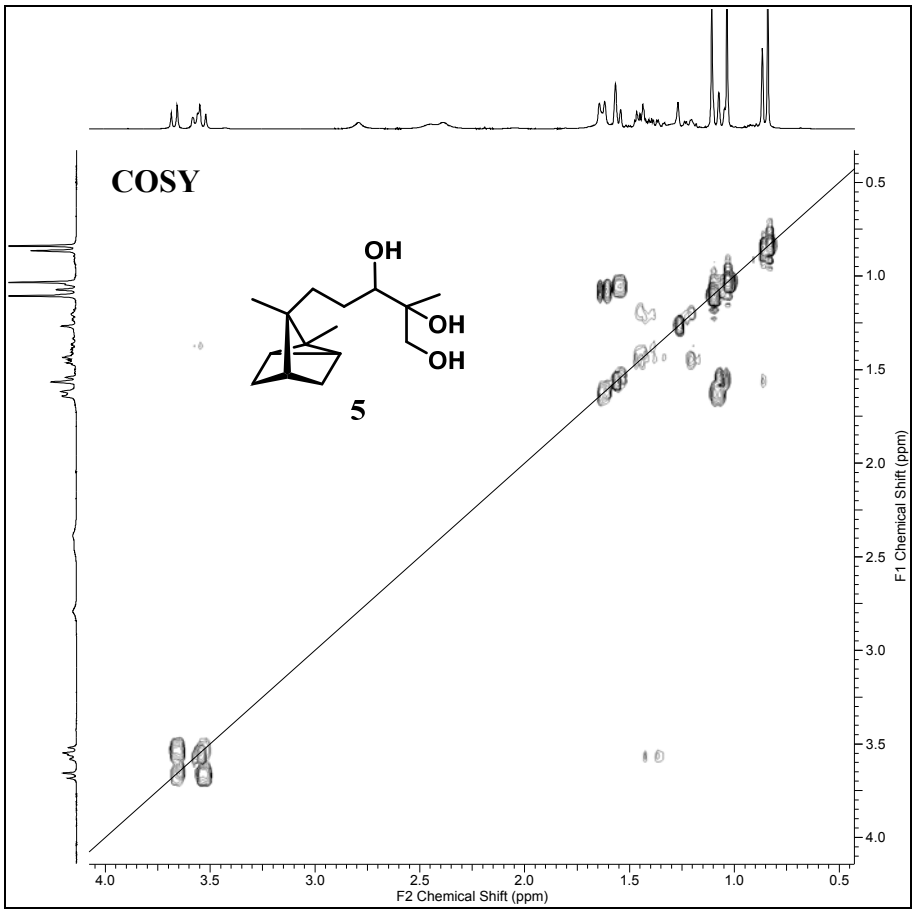
COSY
OH
OH
OH
5
F2 Chemical Shift (ppm)
F1 Chemical Shift (ppm)

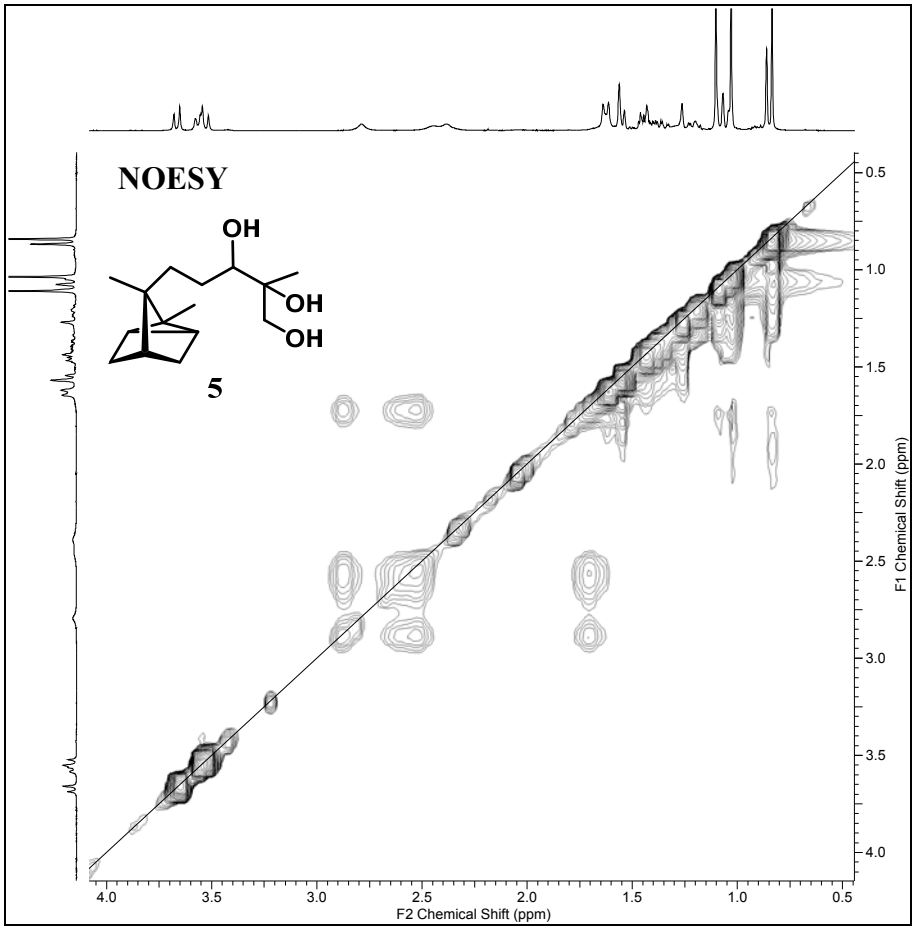
NOESY
OH
OH
OH
5
F2 Chemical Shift (ppm)
F1 Chemical Shift (ppm)

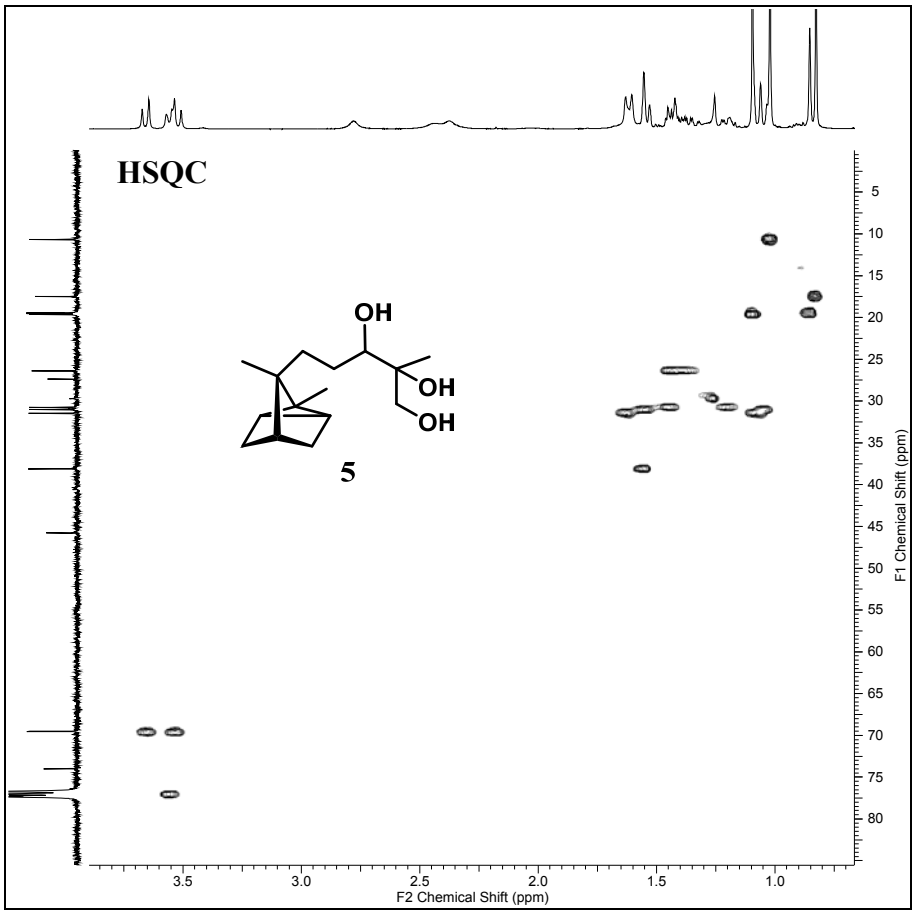
HSQC
OH
OH
OH
5
F2 Chemical Shift (ppm)
F1 Chemical Shift (ppm)

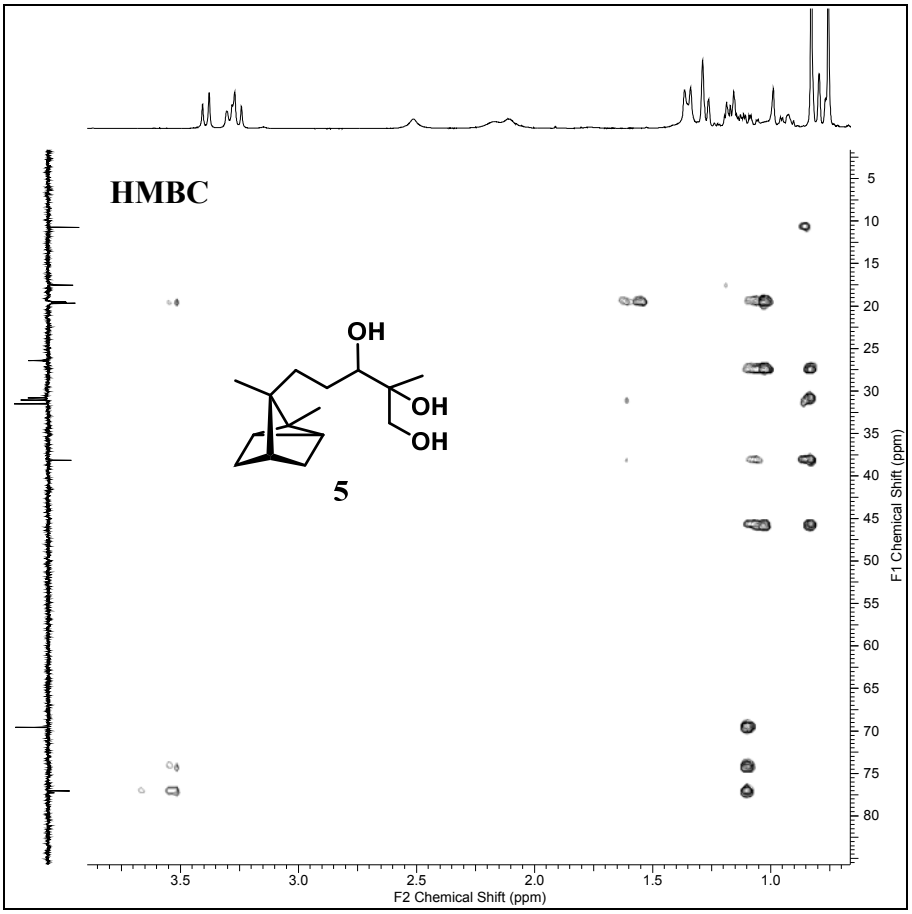
HMBC
OH
OH
OH
5
F2 Chemical Shift (ppm)
F1 Chemical Shift (ppm)

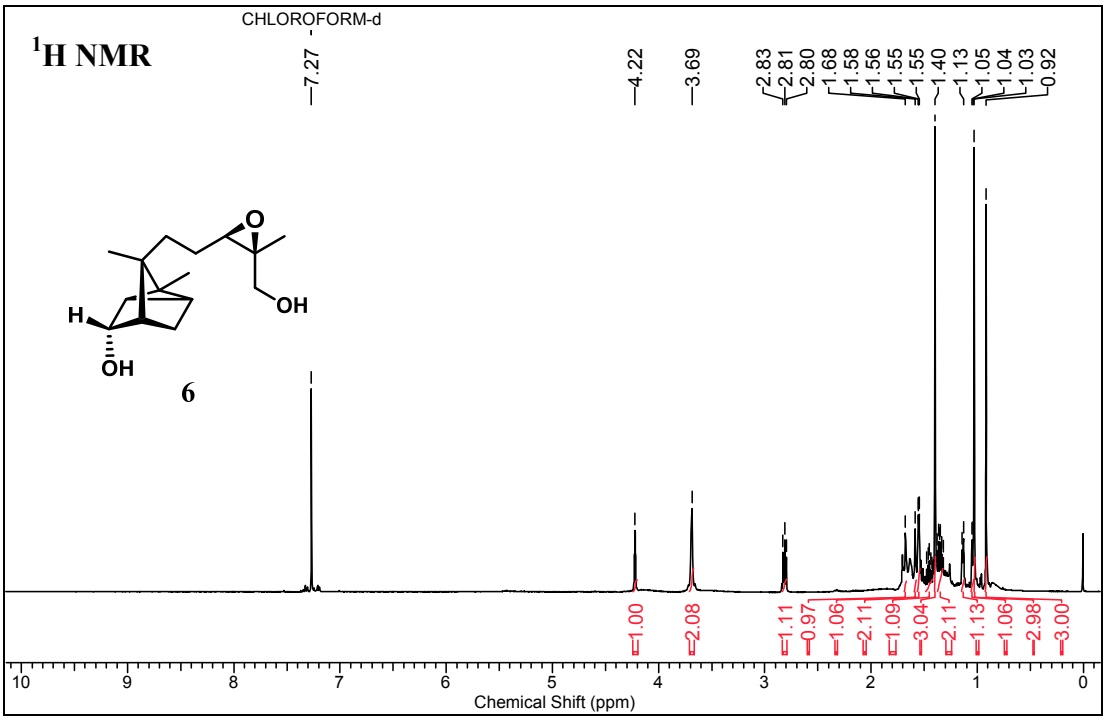
CHLOROFORM-d
^{1}H NMR
7.27
4.22
3.69
2.83
2.81
2.80
1.68
1.58
1.56
1.55
1.55
1.40
1.13
1.05
1.04
1.03
0.92
O
OH
H
OH
6
1.00
2.08
1.11
0.97
1.06
2.11
1.09
3.04
2.11
1.13
1.06
2.98
3.00
10 9 8 7 6 5 4 3 2 1 0
Chemical Shift (ppm)

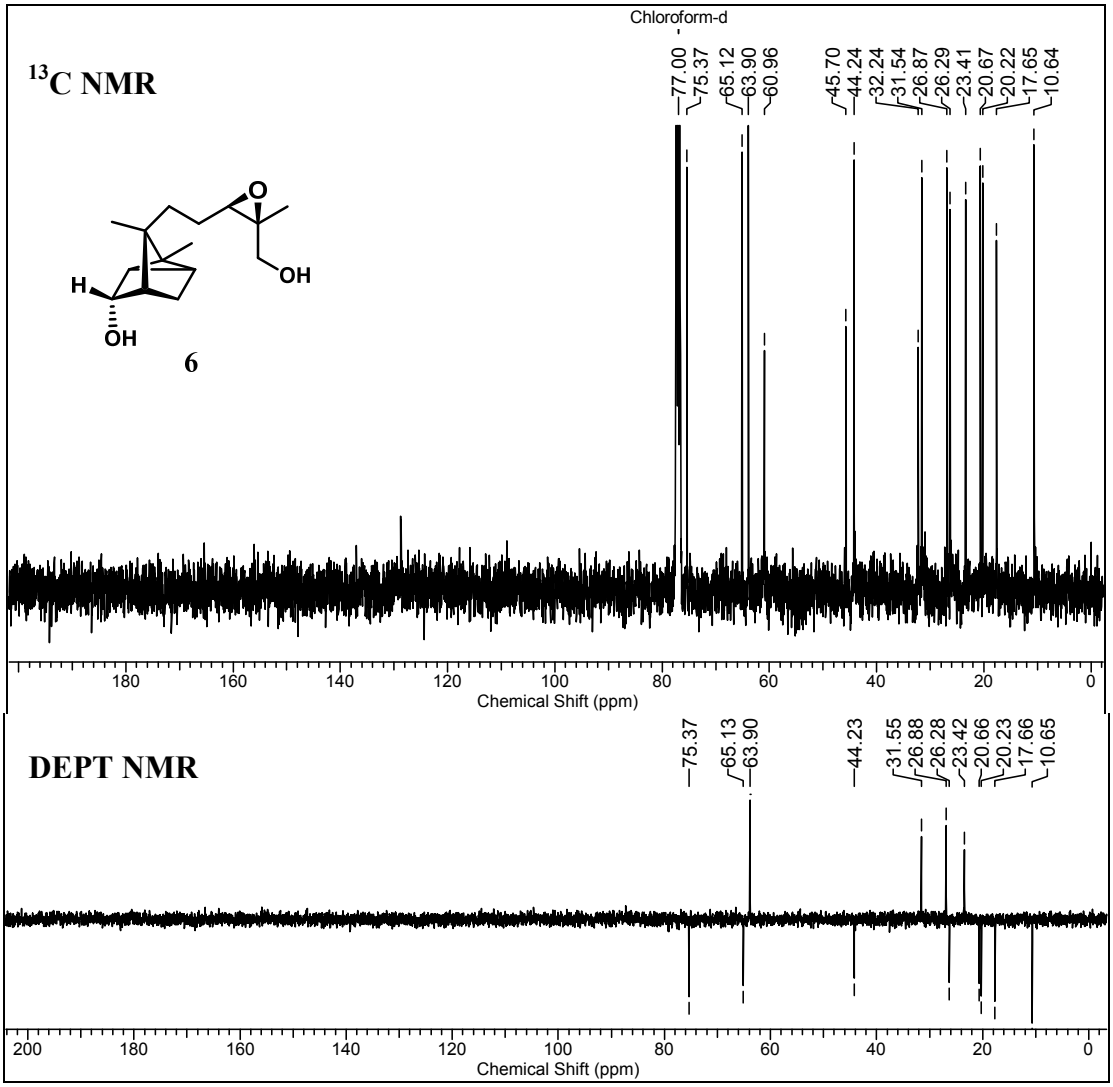
Chloroform-d
^{13}C NMR
77.00
75.37
65.12
63.90
60.96
45.70
44.24
32.24
31.54
26.87
26.29
23.41
20.67
20.22
17.65
10.64
O
OH
H
OH
6
180 160 140 120 100 80 60 40 20 0
Chemical Shift (ppm)
DEPT NMR
75.37
65.13
63.90
44.23
31.55
26.88
26.28
23.42
20.66
20.23
17.66
10.65
200 180 160 140 120 100 80 60 40 20 0
Chemical Shift (ppm)

2.2.5. References:

(1) In *Industrial Biotransformations*; 2nd edition ed.; Andreas Liese, K. S., Christian Wandrey, Ed.; John Wiley & Sons: 2006.
(2) Reetz, M. T. *J. Am. Chem. Soc.* **2013**, *135*, 12480-12496.
(3) van Hylckama Vlieg, J. E. T.; Veiga, P.; Zhang, C.; Derrien, M.; Zhao, L. *Curr. Opin. Biotechnol.* **2011**, *22*, 211-219.
(4) Bicas, J. L.; Dionisio, A. P.; Pastore, G. M. *Chem. Rev.* **2009**, *109*, 4518-4531.
(5) Rathbone, D. A.; Bruce, N. C. *Curr. Opin. Microbiol.* **2002**, *5*, 274-281.
(6) Choudhary, M. I.; Sultan, S.; Khan, M. T. H.; Rahman, A.-u. *Steroids* **2005**, *70*, 798-802.
(7) Lahti, M.; Oikari, A. *Arch. Environ. Con. Tox.* **2011**, *61*, 202-210.
(8) Smith, K. E.; Latif, S.; Kirk, D. N. *J. Steroid Biochem.* **1989**, *32*, 445-451.
(9) Mahato, S. B.; Garai, S. *Steroids* **1997**, *62*, 332-345.
(10) Fernandes, P.; Cruz, A.; Angelova, B.; Pinheiro, H. M.; Cabral, J. M. S. *Enzyme Microb. Tech.* **2003**, *32*, 688-705.
(11) Hogg, J. A. *Steroids* **1992**, *57*, 593-616.
(12) Carballeira, J. D.; Quezada, M. A.; Hoyos, P.; Simeo, Y.; Hernaiz, M. J.; Alcantara, A. R.; Sinisterra, J. V. *Biotechnol. Adv.* **2009**, *27*, 686-714.
(13) Kim, H. J.; Park, H.-S.; Lee, I.-S. *Bioorg. Med. Chem. Lett.* **2006**, *16*, 790-793.
(14) Kouzi, S. A.; McChesney, J. D. *J. Nat. Prod.* **1991**, *54*, 483-490.
(15) Suzuki, Y.; Marumo, S. *Tetrahedron Lett.* **1972**, *13*, 5101-5104.
(16) Madyastha, K. M.; Gururaja, T. L. *Appl. Microbiol. Biot.* **1993**, *38*, 738-741.
(17) Miyazawa, M.; Nankai, H.; Kameoka, H. *Phytochemistry* **1996**, *43*, 105-109.
(18) Miyazawa, M.; Nankai, H.; Kameoka, H. *Phytochemistry* **1995**, *40*, 1133-1137.
(19) Miyazawa, M.; Nankai, H.; Kameoka, H. *J. Agric. Food Chem.* **1996**, *44*, 1543-1547.
(20) Abraham, W. R. *World J. Microb. Biot.* **1993**, *9*, 319-322.
(21) Li, X.; Kim, Y. H.; Jung, J. H.; Kang, J. S.; Kim, D.-K.; Choi, H. D.; Son, B. W. *Enzyme Microb. Tech.* **2007**, *40*, 1188-1192.
(22) Dev, S. *Tetrahedron* **1960**, *8*, 171-180.
(23) Liao, Y.-H.; Houghton, P. J.; Hoult, J. R. S. *J. Nat. Prod.* **1999**, *62*, 1241-1245.
(24) Murakami, A.; Takahashi, M.; Jiwajinda, S.; Koshimizu, K.; Ohigashi, H. *Biosci. Biotech. Biochem.* **1999**, *63*, 1811-1812.
(25) Sakamaki, H.; Itoh, K.-i.; Kitanaka, S.; Sawada, S.; Horiuchi, C. A. *Biotechnol. Lett.* **2008**, *30*, 2025-2029.
(26) Zhou, L.; Xu, W.; Chen, Y.; Zhao, J.; Yu, N.; Fu, B.; You, S. *Catal. Commun.* **2012**, *28*, 191-195.
(27) Rocha, B. A.; Pupo, M. T.; Antonucci, G. A.; Sampaio, S. V.; Paiva, R. d. M. A.; Said, S.; Gobbo-Neto, L.; Costa, F. B. D. *J. Ind. Microbiol. Biot.* **2012**, *39*, 1719-1724.
(28) Choudhary, M. I.; Siddiqui, Z. A.; Nawaz, S. A.; Atta ur, R. *J. Nat. Prod.* **2006**, *69*, 1429-1434.
(29) Heymann, H.; Tezuka, Y.; Kikuchi, T.; Supriyatna, S. *Chem. Pharm. Bull.* **1994**, *42*, 138-146.
(30) Miyazawa, M.; Takahashi, T.; Sakata, K.; Horibe, I. *J. Chem. Technol. Biotechnol.* **2008**, *83*, 1006-1011.
(31) Klayman, D. L. *Science* **1985**, *228*, 1049-1055.
(32) Lee, I.-S.; ElSohly, H. N.; Croom, E. M.; Hufford, C. D. *J. Nat. Prod.* **1989**, *52*, 337-341.

(33) Parshikov, I. A.; Muraleedharan, K. M.; Avery, M. A.; Williamson, J. S. *Appl. Microbiol. Biot.* **2004**, *64*, 782-786.
(34) Zhan, J.; Guo, H.; Dai, J.; Zhang, Y.; Guo, D. *Tetrahedron Lett.* **2002**, *43*, 4519-4521.
(35) Zhan, J.-X.; Zhang, Y.-X.; Guo, H.-Z.; Han, J.; Ning, L.-L.; Guo, D.-A. *J. Nat. Prod.* **2002**, *65*, 1693-1695.
(36) Parshikov, I. A.; Miriyala, B.; Muraleedharan, K. M.; Illendula, A.; Avery, M. A.; Williamson, J. S. *Pharm. Biol.* **2005**, *43*, 579-582.
(37) Patel, S.; Gaur, R.; Verma, P.; Bhakuni, R.; Mathur, A. *Biotechnol. Lett.* **2010**, *32*, 1167-1171.
(38) Lee, I.-S.; Hufford, C. D. *Pharmacol. Ther.* **1990**, *48*, 345-355.
(39) Jones, C. G.; Moniodis, J.; Zulak, K. G.; Scaffidi, A.; Plummer, J. A.; Ghisalberti, E. L.; Barbour, E. L.; Bohlmann, J. *J. Biol. Chem.* **2011**, *286*, 17445-17454.
(40) Daramwar, P. P.; Srivastava, P. L.; Priyadarshini, B.; Thulasiram, H. V. *Analyst* **2012**, *137*, 4564-4570.
(41) Fraga, B. M. *Nat. Prod. Rep.* **2013**, *30*, 1226-1264.
(42) Ochi, T.; Shibata, H.; Higuti, T.; Kodama, K.-h.; Kusumi, T.; Takaishi, Y. *J. Nat. Prod.* **2005**, *68*, 819-824.
(43) Bommareddy, A.; Hora, J.; Cornish, B.; Dwivedi, C. *Anticancer Res.* **2007**, *27*, 2185-2188.
(44) Bommareddy, A.; Rule, B.; VanWert, A. L.; Santha, S.; Dwivedi, C. *Phytomedicine* **2012**, *19*, 804-811.
(45) Dwivedi, C.; Valluri, H. B.; Guan, X.; Agarwal, R. *Carcinogenesis* **2006**, *27*, 1917-1922.
(46) Santha, S.; Dwivedi, C. *Photochem. photobiol.* **2013**, *89*, 919-26.
(47) Hanson, J. R.; Nasir, H. *Phytochemistry* **1993**, *33*, 835-837.
(48) Duran, R.; Corrales, E.; Hernandez-Galan, R.; Collado, I. G. *J. Nat. Prod.* **1998**, *62*, 41-44.
(49) Fraga, B. M. *Nat. Prod. Rep.* **2007**, *24*, 1350-1381.
(50) Levitt, M.; Sandey, H.; Willetts, A. *Biotechnol. Lett.* **1990**, *12*, 197-200.
(51) Nakahashi, H.; Miyazawa, M. *J. Oleo Sci.* **2011**, *60*, 545-548.
(52) Madyastha, K. M.; Thulasiram, H. V. *J. Agric. Food Chem.* **1999**, *47*, 1203-1207.
(53) Sato, K.; Inoue, S.; Takagi, Y.; Morii, S. *B. Chem. Soc. Jpn.* **1976**, *49*, 3351-3352.
(54) Schlosser, M.; Zhong, G.-f. *Tetrahedron Lett.* **1993**, *34*, 5441-5444.
(55) Katsuki, T.; Sharpless, K. B. *J. Am. Chem. Soc.* **1980**, *102*, 5974-5976.
(56) Weijers, C. A. G. M.; de Bont, J. A. M. *J. Mol. Catal. B-Enzymatic* **1999**, *6*, 199-214.
(57) Zagozda, M.; Plenkiewicz, J. *Tetrahedron- Asymmetr.* **2008**, *19*, 1455-1460.
(58) Muto, S.-e.; Mori, K. *Eur. J. Org. Chem.* **2003**, *2003*, 1300-1307.
(59) Ladner, W. E.; Whitesides, G. M. *J. Am. Chem. Soc.* **1984**, *106*, 7250-7251.
(60) Prema, B. R.; Bhattacharyya, P. K. *Appl. Microbiol.* **1962**, *10*, 529-531.
(61) Tian, H.-y.; Sun, B.-g.; Tang, L.-w.; Ye, H.-l. *Flavour Frag. J.* **2010**, *26*, 65-69.

Chapter 3.

Mechanistic Insights in Biosynthesis of Santalenes and Analogous Sesquiterpenes.

Section 3.1.

Introduction:

Terpenes and Terpene Synthases

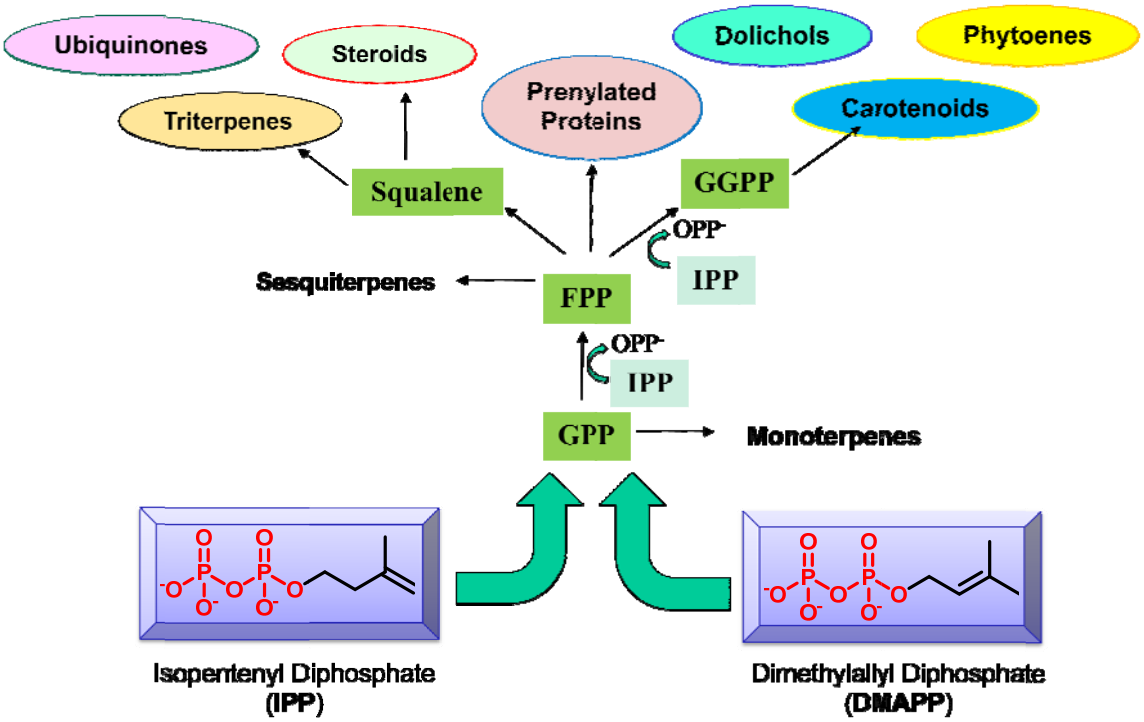

>55,000 members of Terpenoid family are known in nature.

3.1.1. Natural Products:

The chemical compounds synthesized by living organisms in nature are referred to as 'Natural Products'. The simplest definition for a natural product is a small organic molecule that is produced by a biological source. These naturally occurring compounds can be broadly divided into three categories:

(i) Primary Metabolites: Compounds that occur in all cells and play central roles in the metabolism and reproduction of the cells. These include nucleic acids, common amino acids and sugars. Most of these compounds exert their biological effect within the organism and are mandatory for its survival.

(ii) High molecular weight polymeric materials such as cellulose, lignins and proteins, which make the cellular structures.

(iii) Secondary Metabolites: Small molecules (<900 Daltons) those are produced and characteristic of a limited number of species. Although, not essential for the growth and development of the producing organism, they aid in the organism's survival by attracting or repelling other organisms. It has been estimated that well over 300,000 secondary metabolites exist and continue to attract the interest of scientific community due to their biological effect on other organisms. Owing to their immense diversity in structure, function and biosynthesis, it becomes a difficult task to rigidly classify them into a few simple categories. The majority of these compounds belong to one of a number of families, each of which have a particular structural characteristics arising from the way in which they are built up in nature, *i*. *e*. from their biosynthesis. The classes of secondary metabolites are as follows:

- Terpenoids and Steroids,
- Alkaloids,
- Fatty acids and Polyketides,
- Nonribosomal polypeptides,
- Enzyme cofactors.

Among these classes, terpenoids constitute the largest class of compounds which is further subdivided into several categories and is discussed in the preceding sections.

3.1.2. Role of Terpenoids in Nature:

Terpenoids constitute a diverse class of natural products with over 55,000 individual known metabolites, which have now been identified across all life forms and with new advancements in the field the number of defined structures rapidly continues to increase over a period of time.[1,2] Having proved their presence in almost all living systems, terpenoids demonstrate an immense array of structural diversity with an apparently unrelated structures ranging from relatively simple linear hydrocarbon chains to some of the most complex ring structures known. Members of this family, exhibit a bewildering variety in their function, while performing profound and versatile roles in all fields of life.[3] Terpenes and terpenoids, though older terms for these compounds, perhaps convey more descriptive meanings as they recall the old memories of aromatic fragrances like the turpentine oils, predominantly derived from the distillation of conifer resins, from which the first terpenoids were isolated and hence named. In general, the term 'terpenes' refers to the hydrocarbons which are created from 5-carbon 'isoprene' (2-methyl-1,3-butadiene) as the basic structural unit, whereas, 'terpenoids' is used to indicate terpene related compounds that have been ornamentally decorated by oxygen containing functional groups such as alcohols, aldehydes and ketones which impart them the richness of functional diversity. Therefore, these are also referred to as 'isoprenoids'.

In spite of the great structural diversity presented, they originate from very simple hemiterpene (5-carbon) building blocks, isopentenyl diphosphate (IPP, 3-Methyl-3-butenyl diphosphate) and dimethylallyl diphosphate (DMAPP, 3-Methyl-2-butenyl diphosphate) which in turn are produced through mevalonate[4] (MVA) or non-mevalonate pathway[5] (MEP or DXP) depending upon the organisms and cellular organella. Details about MVA and MEP pathway are discussed in the following sections. Terpenoids are classified on the basis of number of 5-carbon isoprene units in their structure[6] as hemiterpenes- C5 (1 isoprene unit), monoterpenes- C10 (2 isoprene units), sesquiterpenes- C15 (3 isoprene units), diterpenes- C20 (4 isoprene units), sesterterpenes- C25 (5 isoprene units), triterpenes- C30 (6 isoprene units), tetraterpenes- C40 (8 isoprene units), and polyterpenes- $(C5)_n$ where 'n' may be 45–30,000. Members of every family execute intense roles in several biological processes, as described below. Monoterpenes act as insect sex pheromones and are used in perfumes due to their characteristic odour; sesquiterpenes act in defence against enemies, steroids as

structure and membrane building units, carotenoids as visual pigments due to their highly conjugated olefinic backbone[7] and prenylated proteins in signaling pathways. Some of the members play vital roles in agriculture sector, for example the tetranortriterpenoid, azadirachtin,[8] exhibits strong anti-feedant activity against most of the insects which popularizes it in pesticide formulations; and they also constitute the medicinal recipes for many of the critical diseases such as taxol as an anti-cancer[9,10] and artemisinin as an anti-malarial drug.[11]

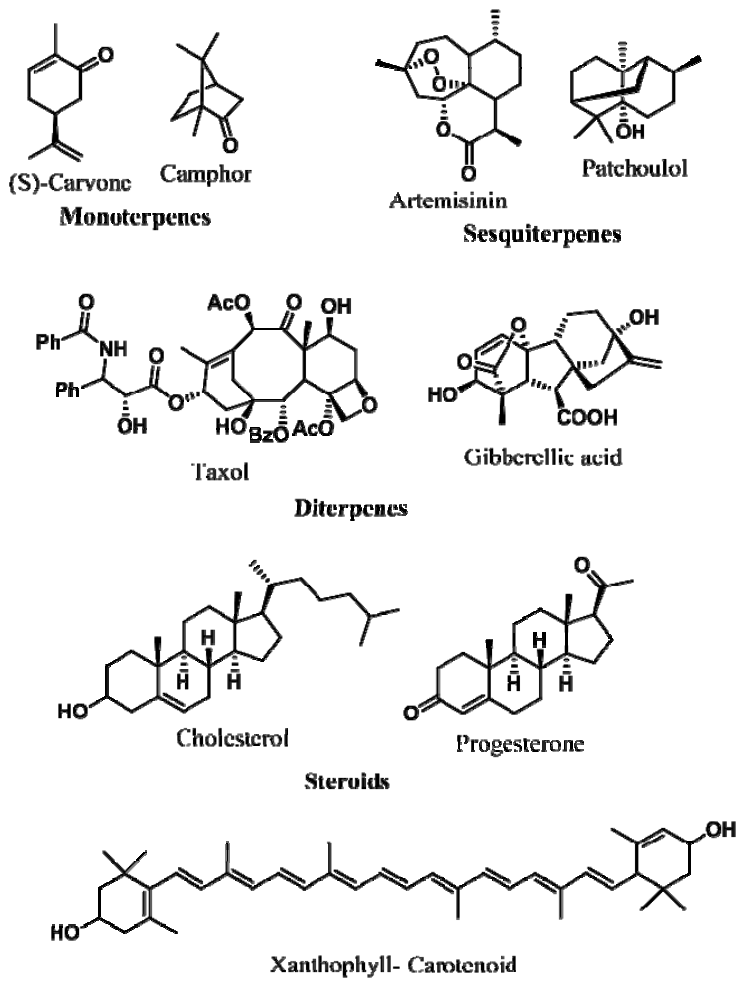

Figure 3.1. Representative examples from different classes of terpenoids.

Terpenoids have also been divided on the basis of the essentiality of their function in sustainance of various life forms as, primary and secondary terpenoids. Types of isoprenoids, such as steroids, retinoids, carotenoids, ubiquinones, gibberellins and prenylated proteins are essential components of the cellular machinery of all organisms due to their roles in a variety of biological processes and are therefore referred to as 'primary terpenoids'. To state some of the examples, retinoids are

involved in morphogenesis and photo-transduction, whereas prenylated proteins, including Ras and Rho GTPases, work as signal transducers; steroids have distinct biological functions, wherein they constitute the components of cell membranes, serve as hormones in sexual development of animals; diterpenes such as gibberellins are plant growth hormones and are ubiquitous in both flowering and non-flowering plants. Other terpenoids such as monoterpenoids, sesquiterpenoids which majorly play roles in defence against attackers, in attracting the opposite sex by acting as pheromones, are referred to as 'secondary terpenoids'.

3.1.3. Terpene Synthases and Biosynthetic Pathways:

Terpene synthases (TPS) are the enzymes which accomplish an ingenious job of construction of the terpenoid scaffolds possessing very simple to magnificent complexity. These are present in all forms of life and numerous TPS genes have been isolated from plant and microbial sources and over 100 TPS enzymes have been functionally characterized.

Terpene synthases catalyze biosynthesis of terpenoids with high regio- and stereo-chemical precision *via* a cascade of complex reactions involving highly reactive carbocationic intermediates that undergo a sequence of reactions like cyclizations, alkylations, rearrangements, deprotonations and hydride shifts.[12-19] The hydrocarbon skeletons thus obtained, further experience addition of functional groups, such as hydroxy group, by the action of upstream enzymes belonging to monooxygenase class.[20] The installed functional groups may subsequently undergo a series of functional group transformations to ultimately result in final terpenoid molecules of higher interest and economic potential.

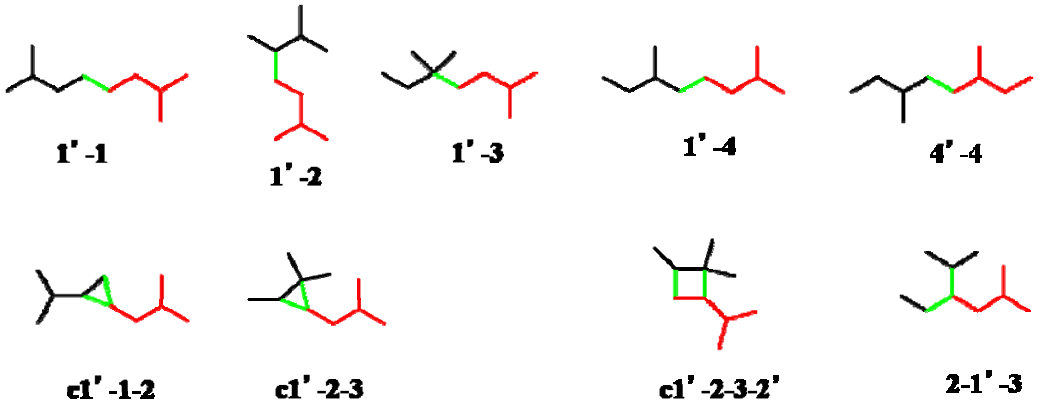

Figure 3.1.1. Fundamental connections in isoprene biosynthesis.

While a total of nine connections are known in isoprenoid biosynthesis (Figure 3.1.1), four of them comprising chain elongation, cyclopropanation, branching and cyclobutanation are most commonly observed. Among these four connections used to couple isoprenoid intermediates to construct highly complex structures (Scheme 3.1.1), chain elongation is the most common reaction which involves head to tail condensation of IPP and allylic linear terpenes[1] which are catalyzed by terpene synthases such as geranyl diphosphate synthase (GDS) and/or farnesyl diphosphate synthase (FDS). Early structural investigations made by Wallach (1914) led him to formulate a principle that, most terpenoids could be hypothetically constructed by a repetitive joining of isoprene units. This formed a major achievement in terpenoid chemistry as it provided the first integrated concept for a common structural relationship among the terpenoid natural products. Subsequently, Ruzicka refined the original concept to establish the 'biogenetic isoprene rule'[21,22] which proposed that all terpenoids arose from an "active" or biogenic isoprene. This hypothesis ignores the specific character of the biological precursor and considers only that their structure is "isoprenoid" in nature. Active isoprene, which was identified as isopentenyl pyrophosphate (IPP), and its allylic ester isomer, dimethylallyl pyrophosphate (DMAPP) are now known to form the basic building block units in all isoprenoid biosynthetic pathways.

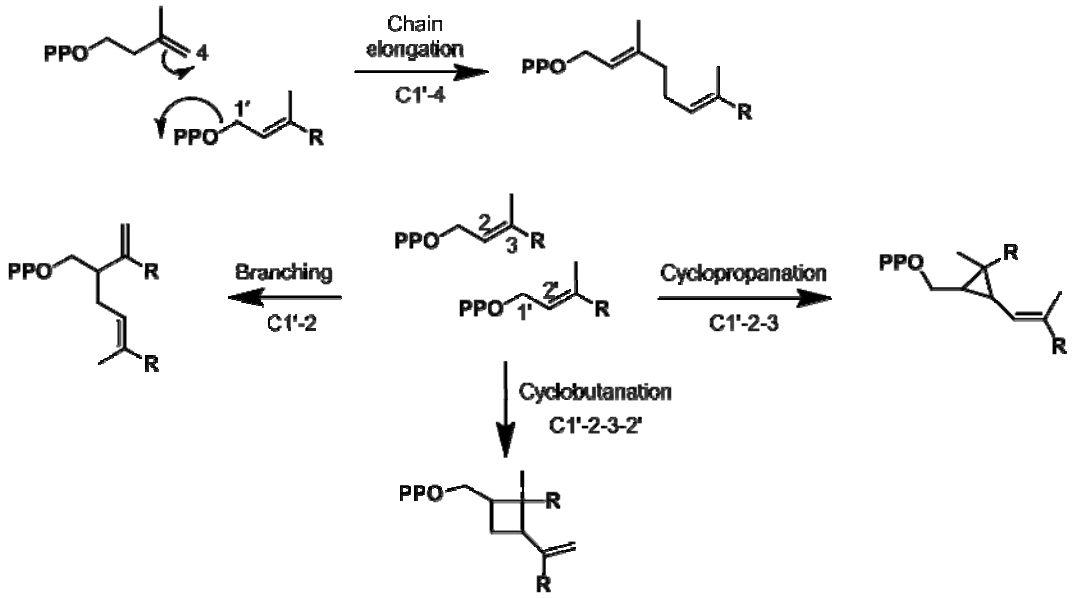

Scheme 3.1.1. Four commonly observed coupling reactions in terpene biosynthesis.[23]

3.1.4. Biosynthesis of IPP and DMAPP:

Two pathways responsible for the synthesis of isoprenoid precursors, IPP and DMAPP exist in nature. The first being classical acetate-mevalonate (MVA) pathway, and the second is more recently discovered mevalonate-independent pathway, also known as MEP or DXP pathway. Experimental evidence obtained since the discovery of the MEP pathway shows that most organisms only use one pathway for IPP biosynthesis, with a few bacterial *Streptomyces* species, most carotenogenic organisms and plants as the exceptions which generate isoprenoid precursors by both the pathways. In plants, both the pathways operate with the localization to different compartments as the MVA pathway is operative in the cytosol while the MEP pathway operates in the plant plastids.[7]

3.1.4.1. MVA Pathway:

MVA pathway, originally described by Block, Lynen, Popjak, and others[24,25] for the production of IPP is predominantly operative in animals, fungi, archea and yeast. Until the late 1990s, MVA pathway was considered to be the sole source of isoprenoid precursors prevailing in all living systems. The schematic representation of MVA pathway leading to the biosynthesis of IPP (in six steps) and DMAPP (in seven steps) is depicted in Scheme 3.1.2. and is also explained below. Following the cellular uptake of acetate (derived from glycolysis pathway) and subsequent conversion to acetyl-CoA by acetyl-CoA synthase, two molecules of acetyl-CoA are initially condensed to acetoacetyl-CoA by acetoacetyl-CoA thiolase (AACT), whereupon an additional acetyl-CoA is added to form (*S*)-3-hydroxy-3-methylglutaryl-CoA (HMG-CoA) *via* the action of HMG-CoA synthase (HMGS). Reduction of HMG-CoA to MVA carried out by HMG-CoA reductase constitutes the rate limiting step in the MVA pathway and is one of the most studied enzymes due to its importance in pharmaceutical industry for development of the drugs.[26] The mevalonic acid undergoes serial phosphorylations by the consecutive actions of mevalonate kinase (MK) and mevalonate-5-phosphate kinase (PMK). The final step to IPP synthesis requires decarboxylative dephosphorylation by one more kinase, mevalonate-5-diphosphate decarboxylase. IPP further experiences intramolecular isomerization to ultimately achieve DMAPP (Scheme 3.1.2).

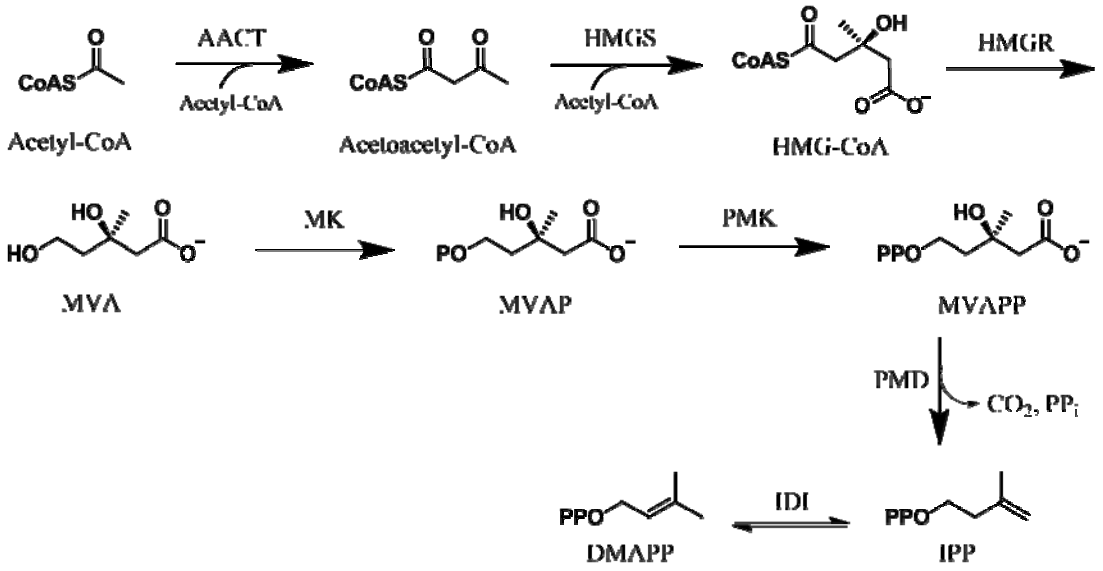

Scheme 3.1.2. The Mevalonate pathway for biosynthesis of IPP and DMAPP.

3.1.4.2. MEP Pathway:

Till early 1990s, MVA pathway was considered to be the universal pathway involved in the biosynthesis of IPP and DMAPP, thereby leading to isoprenoids. However, tracing experiments carried out by different research groups independently using labelled (^{13}C, ^{14}C or ^{2}H) acetate substrates indicated the discrepancy in the position and number of labelled carbons in the resulting isoprenoids. Many of the early attempts to study the biosynthesis of lycopene, hopanoids, taxol, and sterols with the labelled acetates did not result in the expected outcome and revealed differences in distribution of the label within the basic isoprene unit itself, which were not in agreement with a single source of isoprenoid precursors for all terpenoids.[27-29] Due to inconsistency of the results with labeled substrates, several research groups working independently thought of a different pathway other than the MVA, which led to the discovery of a mevalonate-independent pathway in eubacteria,[30] green algae,[31] and higher plants.[29,32] Rohmer *et al*. studied the labeling pattern for incorporation of ^{13}C-labeled glycerol or pyruvate in the biosynthesis of ubiquinone which allowed them to identify the conversion of pyruvate to 1-deoxy-D-xylulose-5-phosphate (DXP) as the first step of the mevalonate-independent pathway.[33] In independent studies, by tracing the fate of [1-^{13}C]- and [2,3,4,5-$^{13}C_4$]-DXP in the labeling pattern of β-carotene, lutein, phytol and sitosterol in cell cultures of *Catharanthus roseus*, Arigoni *et al*. demonstrated the involvement of DXP in the non-mevalonate pathway, also known as the 2C-methyl-D-erythritol-4-phosphate (MEP) pathway and provided further insight in the compartmentalization of isoprenoid

synthesis.[34] Furthermore, Arigoni *et al*. also demonstrated the formation of isoprenoid precursors *via* an intramolecular skeletal rearrangement through the non-mevalonate pathway, as was first proposed by Eisenreich *et al*.[29]

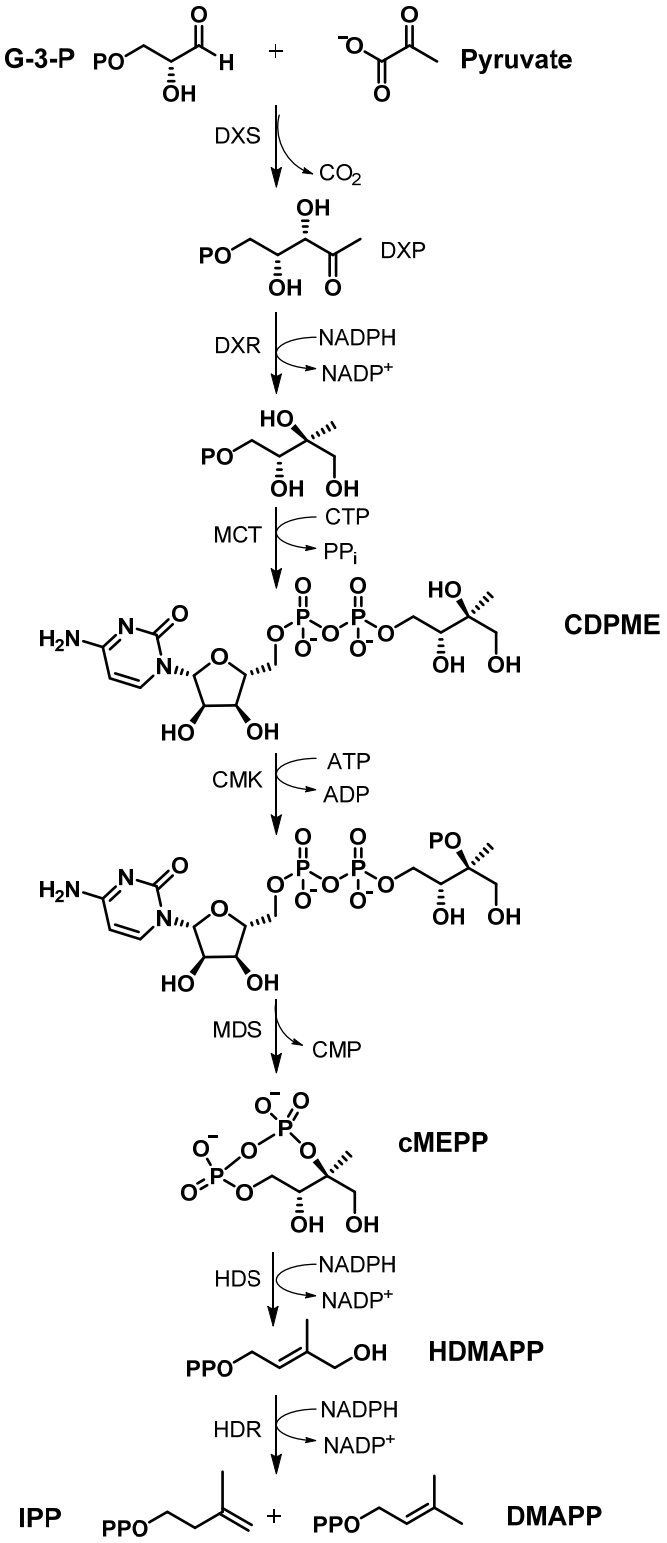

Scheme 3.1.3. MEP Pathway steps leading to the biosynthesis of IPP and DMAPP.

MEP pathway is utilized by a great majority of eubacteria including photosynthetic cyanobacteria, algae, and parasitic pathogens such as *Plasmodium falciparum* and *Toxoplasma gondii*,[35-37] which attributes it as a promising pharmacological target. Terpenoids belonging to a particular class are derived from terpenoid precursors which have specific origins, either cytosolic (MVA derived) or plastidial (MEP derived), such as carotenoids, which are predominantly derived from precursors obtained from plant plastids.[38] A very limited exchange of these precursors between the plant cell compartments has been observed.[39,40]

The biosynthesis of IPP and DMAPP through MEP pathway stems from pyruvate and glyceraldehyde-3-phosphate, as was first proposed by Rohmer *et al*. in bacteria in the mid-1990s.[30,33] The MEP pathway involving seven steps to the formation of final products, is initiated by the condensation of pyruvate and glyceraldehyde-3-phosphate which is catalyzed by 1-deoxy-D-xylulose-5-phosphate synthase (DXS) to form 1-deoxy-D-xylulose-5-phosphate (DXP) as the first product of the pathway and hence imparts its name to the pathway as 'DXP pathway'. A reductive isomerization of DXP by 1-deoxy-D-xylulose-5-phosphate reducto-isomerase (DXR) then yields 2-C-methyl-D-erythritol-4-phosphate (MEP). A cytidyl moiety is then introduced to MEP by 2-C-methyl-D-erythritol-4-phosphate cytidylyl transferase (MCT) to produce 4-(cytidine-5'-diphospho)-2-C-methyl-D-erythritol. This then undergoes phosphorylation by 4-(cytidine-5'-diphospho)-2-C-methyl-D-erythritol kinase (CMK) and cyclisation following the loss of the cytidyl group in a reaction catalyzed by 2-C-methyl-D-erythritol-2,4-cyclodiphosphate synthase (MDS) to form 2-C-methyl-D-erythritol-2,4-cyclodiphosphate. Following the final two steps catalyzed by (*E*)-4-hydroxy-3-methylbut-2-enyl-diphosphate synthase (HDS) and reductase (HDR), IPP and DMAPP are formed (Scheme 3.1.3).

3.1.5. Biosynthesis of Monoterpenes:

'Monoterpenes' belong to a broad class of Terpenoids and are constituted of C-10 units, comprising two isoprene units. Majority of these are produced by plants as 'secondary metabolites' which perform a wide array of biological functions. They perform roles in plant defense against pathogens and feeding-insects. These compounds have been known for several centuries as components of the fragrant oils obtained from leaves, flowers and fruits, attributing to their characteristic pleasant odours.

Monoterpene synthases are the enzymes which carry out chain elongation and cyclization reactions giving rise to a large family of monoterpenoids consisting of over 1000 members. Geranyl diphosphate synthase catalyzes the chain elongation reaction wherein the hydrocarbon cationic moiety generated from DMAPP is added on to IPP to form GPP, the acyclic precursor of monoterpenes (Scheme 3.1.4).

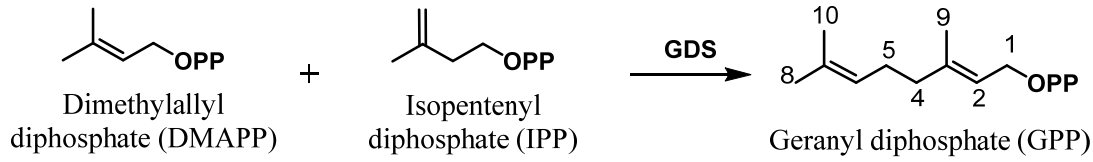

Dimethylallyl diphosphate (DMAPP) + Isopentenyl diphosphate (IPP) → Geranyl diphosphate (GPP)

Scheme 3.1.4. Biosynthesis of GPP by condensation of DMAPP and IPP.

Monoterpene cyclases perform the further task of cyclization of the linear substrate, GPP to a multitude of monocyclic, bicyclic and tricyclic skeletons. It has been established from the exhaustive research over many years that a common carbocationic reaction mechanism for all monoterpene synthases is initiated by the divalent metal ion-dependent ionization of the substrate, GPP. The resulting geranyl cationic intermediate undergoes a series of cyclizations, hydride shifts or other rearrangements producing a diverse reactive carbocationic scaffolds which undergo either proton loss or addition of a nucleophile to terminate the reaction (Scheme 3.1.5). These mechanisms have been deeply investigated by Croteau and co-workers through their comprehensive studies with various substrate analogs, inhibitors, intermediates and native enzymes and their mutants.[14,41-45] Degenhardt *et al*. have summarized the list of monoterpene synthases reported, evidence for their catalysis of the multitude products, features of proteins affecting biosynthesis and correlations between specific amino acid motif and terpene synthase function.[46]

Biosynthetic pathways in monoterpenes leading to the formation of santalene counterparts, camphenes and pinenes have been established by Croteau *et al*.[43] They demonstrated the cyclization of GPP to pinenes and camphenes through a sequence of intermediates such as terpinyl cation, bornyl cation and pinyl or camphyl cation.[47,48] In monoterpene biosynthetic pathways, pinene synthase could carry out the cyclization of geranyl diphosphate (GPP) into bicyclic olefins α-pinene, β-pinene, camphene, and to monocyclic olefins, limonene, terpinolene and to acyclic olefin myrcene, through a series of carbocationic rearrangements. The initial step in the cyclization pathways proceeded by loss of the diphosphate group with a concomitant stereospecific

isomerization of the substrate GPP to the corresponding bound tertiary allylic intermediate, linalyl cation. Rotation of C2-C3 bond to generate a *cisoid*, *anti-endo* conformer facilitated C1-C6 cyclization of the tertiary allylic cation to monocyclic α-terpinyl cation. The linalyl ion pair could also lose a proton resulting in acyclic olefin myrcene. Deprotonation from the α-terpinyl cation could occur in two ways to afford limonene or terpinolene, while second electrophilic cyclization would give rise to bornyl or pinyl cations. Loss of proton from the adjacent methylene or methyl position of pinyl cation would collapse into α-pinene and β-pinene as the final products, respectively; whereas the bornyl cation could undergo Wagner-Meerwein shift to form camphyl cation which on subsequent deprotonation would result in bicyclic product, camphene.

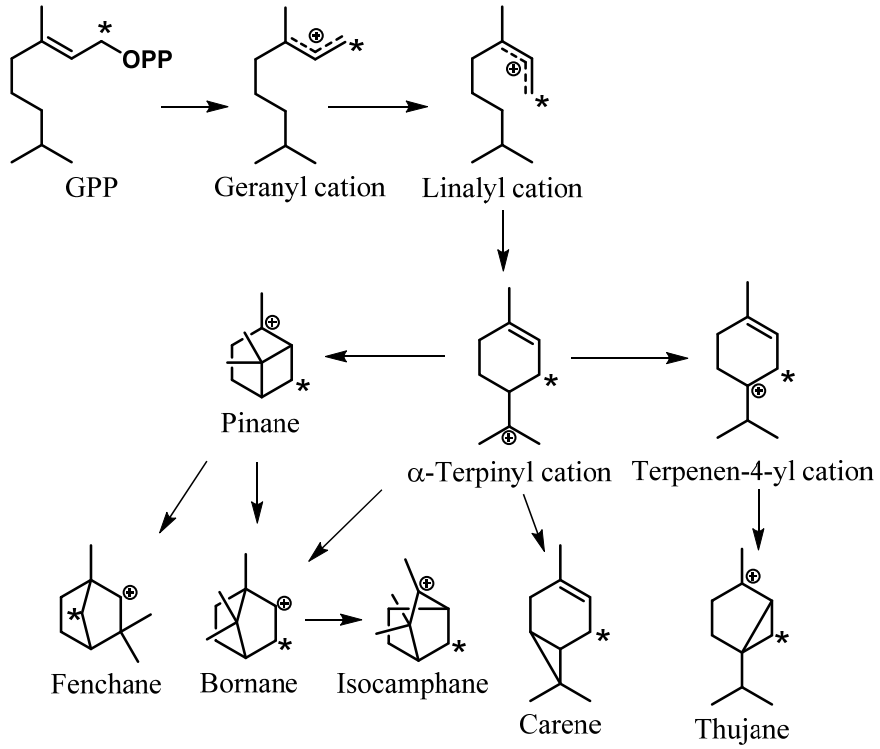

Scheme 3.1.5. Postulated ionic mechanism for cyclization of GPP leading to the formation of monoterpenes via the α-terpinyl cation and the terpinen-4-yl cation. The carbocationic structures are divided into isoprene units and the labeling patterns from C1-labeled acyclic precursor are illustrated (indicated with an asterisk, *).

3.1.6. Biosynthesis of Sesquiterpenes:

Terpenoids constructed from the combination of three isoprene units (one DMAPP and two IPP) and thus containing C15 carbon skeleton are known as 'sesquiterpenoids'. They are one of the structurally rich classes of natural products isolated from a variety of sources such as plants, fungi, bacteria, and marine invertebrates.[13,49] These enzymes synthesize more than 7000 molecules with over 300 stereochemically distinct hydrocarbon skeletons. Although divergence in function has accompanied divergence in sequence within many protein superfamilies, members of a family often share a characteristic functional feature, such as a common binding property or mechanistic strategy in catalysis. Sesquiterpene cyclases possess an aspartate rich conserved amino acid sequence DDXXD at their diphosphate binding site. Sesquiterpene cyclases are ubiquitous in living systems and give rise to a spectrum of products with a dramatic variation in their synthetic yields. Curiously, at discrete instances, they exhibit a high degree of fidelity, being highly specific towards a particular single product as experienced in aristolochene synthase from *Aspergillus terreus*[50] or may be surprisingly promiscuous in nature when they yield more than one products[46,51] in differing ratios as exemplified by γ-humulene synthase that generates 52 distinct products of which γ-humulene itself comprises only 28.6%.[51] In sesquiterpene biosynthesis, both remarkable fidelity and astonishing promiscuity originate from a common linear substrate, (*E*,*E*)-FPP (Scheme 3.1.6).

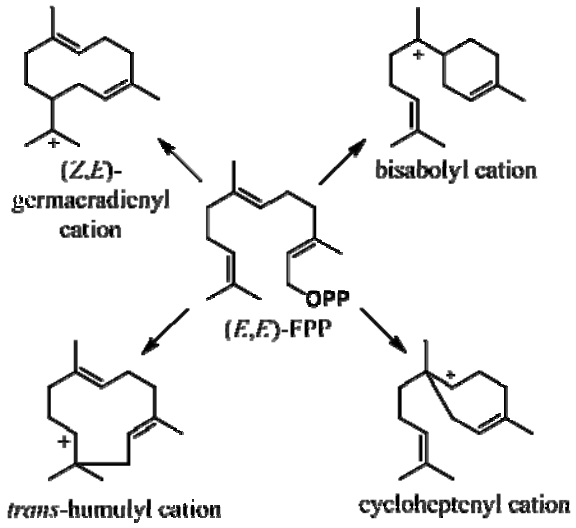

Scheme 3.1.6. Different modes of cyclization adopted by (*E,E*)-FPP.

Labeled substrates have constantly played invaluable roles in biochemical and bioorganic research to investigate and track the biosynthetic pathways. Deuterated prenyl diphosphates, in perticular, have been previously utilized to study the mechanism of cyclization by several sesquiterpene synthases including, *epi*-aristolochene synthase and premnaspirodiene synthase[52], amorphadiene synthase[53], geosmin synthase[54], patchoulol synthase[55] and Cadinene synthase[56]. To demonstrate the importance of isotope labelling of the substrates, some of the sesquiterpenoid biosynthetic pathways which have been elucidated using labelled substrates in the literature are discussed in the following sections.

3.1.6.1. Biosynthesis of (*E*,*E*)-Farnesyl diphosphate [(*E*,*E*)-FPP]:

The fundamental reaction in terpenoids biosynthesis, 'Chain elongation' reaction brings about the formation of linear diphosphates such as geranyl diphosphate (GPP, C10), farnesyl diphosphate (FPP, C15), geranylgeranyl diphosphate (GGPP, C20), geranylfarnesyl diphosphate (GFPP, C25), and so on, which are the linear precursors of all cyclic terpenoids. Polyprenyl diphosphate synthases belonging to a class of prenyltransferases, catalyze the sequential addition of the growing hydrocarbon chain in the allylic isoprenoid diphosphates to the isoprene unit in IPP to result in the higher homologues of the allylic isoprenoid diphosphate, which have well defined chain lengths and contain isoprene units ranging from 2 to >30,000. Each member of this enzyme family is classified according to the length of its final product and the geometry of the newly formed double bonds (*E* or *Z*). Despite the identical condensation mechanisms, these enzymes are very much specific towards the chain lengths of the substrate and the products and never exceed the limit greater than a pre-determined length specific to each prenyltransferase. The ultimate length of the polyisoprenoid chain is governed by the size of a hydrophobic pocket in the interior of the enzyme that binds the growing hydrocarbon chain. Interestingly, by random[57] or site directed mutagenesis, the active sites of these polyprenyl diphosphate synthases have been altered to accommodate the substrates of varying lengths which regulated the generation of the products of shorter[58] or longer[59] chain lengths.[60]

(*E*,*E*)-Farnesyl diphosphate synthase (FDS), a ubiquitous enzyme in all the life forms, is a representative example of the class of polyprenyl diphosphate synthases and particularly of the (*E*)-isomer family. FDS catalyzes the sequential chain elongations of

(i) DMAPP with two units of IPP or (ii) GPP with one unit of IPP to ultimately form FPP. Chain elongation takes place by dissociative electrophilic alkylation of the double bond in IPP with the allylic cation obtained from dissociation of the diphosphate moiety from the allylic substrate, DMAPP or GPP. Apart from engaging itself as the sesquiterpenoid precursor in the cyclization reactions, FPP, the product of FDS, is also involved in several other essential biological processes. FPP is required for the first committed steps (head to head condensation of FPPs to form squalene) in the biosynthesis of cholesterol,[61] farnesylated and geranylgeranylated proteins,[62] ubiquinones,[63] dolichols,[64] and heme *a*[65] and in chain elongation reactions leading to GGPP[66] and consequently to diterpenoids. Experiencing the versatility of FPP in the living systems, the activity of FDS appears to be ubiquitous which forms the central core in terpenoid metabolism and is therefore one of the widely studied enzymes. In 1994, Tarshis *et al*. reported the crystal structure of avian FPP synthase determined to 2.6 Å resolution, the first structure of a prenyltransferase.[67] The enzyme is a homodimer and possesses a novel fold composed of 13 α-helices, ten of which form a large central cavity. The active site is located in this cavity, as are the two conserved aspartate-rich motifs that face each other on opposite walls of the cavity. Tarshis and colleagues also reported the structure of the enzyme with its substrate and showed that these aspartate-rich motifs interact with the substrates *via* Mg^{2+}.

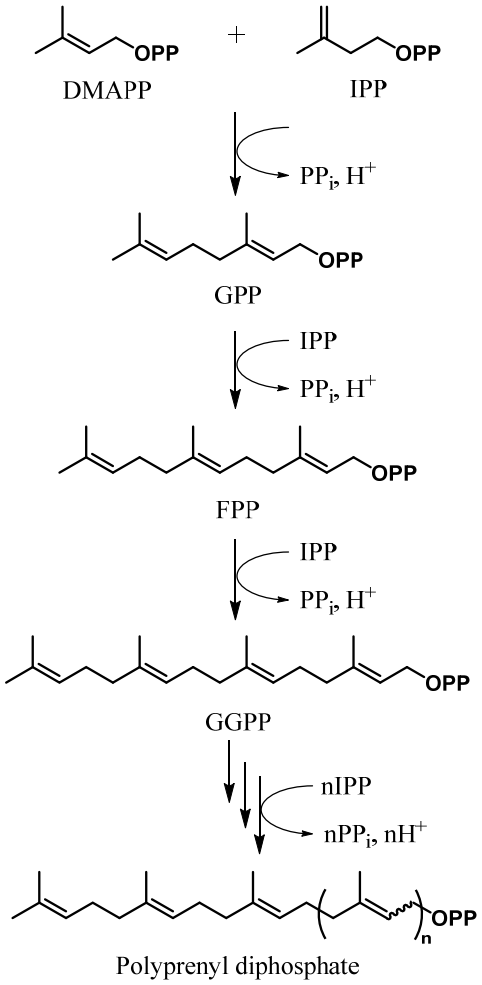

Scheme 3.1.7. Polyprenyl diphosphate synthases catalyzed the chain elongation reactions leading to the biosynthesis of homologous linear isoprenoid diphosphates.

Chemically, the chain elongation reaction proceeds through an electrophilic alkylation reaction mechanism. The reaction proceeds in three discrete steps- (i) cleavage of the carbon-oxygen bond of the allylic diphosphate to form a tight ion pair between the pyrophosphate (PP_i) leaving group and the allylic carbocation; (ii) alkylation of the C3-C4 double bond of IPP by the carbocation to generate a second carbocationic intermediate with positive charge at C3 of the isopentenyl unit; and (iii) stereospecific elimination of a proton from C2 of the isopentenyl unit to generate a new allylic diphosphate extended by an isoprenoid unit. Although, (*E*,*E*)-FPP does not possess any asymmetric center, surprisingly, the steps involved in its biosynthesis were performed in a stereospecific manner. Stereochemical aspects in the biosynthesis of (*E*,*E*)-FPP, catalyzed by FPP synthase were investigated by Cornforth and Popjak in their classical work on squalene biosynthesis.[68] Among a total of 14 questions raised

and answered in different events during biosynthesis of squalene from mevalonate through MVA pathway, we discuss here the determination of the stereochemistry of four distinct events during chain elongation reaction (Scheme 3.1.8). Labeled mevalonates were utilized in determining the stereochemistry of the reactions as below:

(a) A new *E*-double bond is formed between C2 and C3 in the product: Observations with the incorporation of 2-^{14}C-mevalonate into soyasapogenol A and into mycelianamide agreed in indicating that in DMAPP biosynthesized, the new methyl group (from C-2 of mevalonate) is *trans* to the -CH_2-O- group (C-3).

Farnesyl diphosphate synthase from many sources has been shown to synthesize the *E*-isomer in preference to the *Z*-isomer, by Thulasiram and Poulter.[19] The stereochemistry of the newly formed double bonds in the alcohol products, produced following de-phosphorylation of the corresponding diphosphates from chain elongation reactions was monitored by GC and GC-MS analysis with authentic samples. The degree of stereocontrol exerted by FPP synthase in chain elongation reactions was not very high, and the alkylation reactions of IPP with the hydrocarbon cations generated from allylic diphosphate units produced minor amounts of *Z*-congeners as well (3-15%).

(b) New bond between C1 of the allylic substrate and C4 of IPP is formed with inversion at C1 of the allylic substrate: [5R,5-D]-mevalonate (equivalent to 1D-DMAPP or 1D-IPP) was converted to deuterated squalene after incubation with the enzyme preparation from rat liver. The hexa-deuterated squalene was then degraded by ozonolysis to one equivalent of succinic acid formed from the central atoms and to four equivalents of laevulic acid which on separation and subsequent treatment with hypoiodite yielded second set of succinic acids. On comparing the stereochemistry of later set of succinic acids with the standards revealed it as [2*S*, 2-D]-succinic acid. Comparison of the stereochemistry of centres in deuterated squalene with that of the parent mevalonate indicated inversion of configuration at C-1 with formation of each C-C bond.

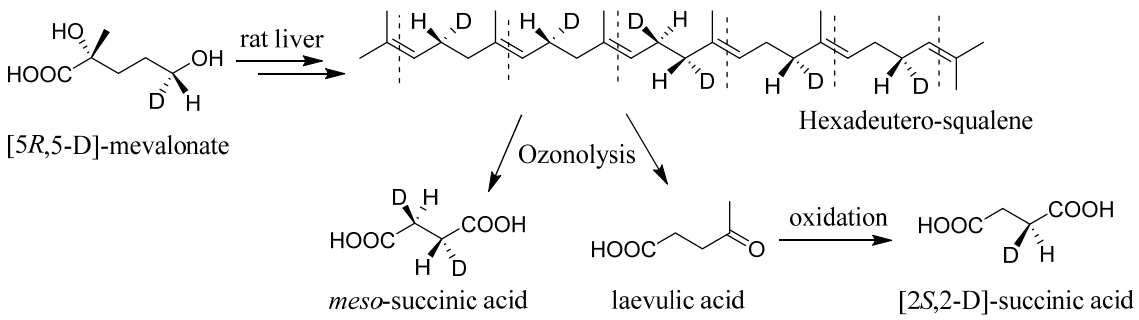

Scheme 3.1.8. Demonstration of inversion of stereochemistry at C1 in chain elongation reaction.

(c) <u>The *pro-R* proton is removed from C2 of IPP:</u> Fundamental studies by Cornforth and Popjack included synthesis of stereochemically pure [4*R*,4-D]- and [4*S*,4-D]-mevalonate analogues. [4*R*,4-D]- and [4*S*,4-D]- mevalonates corresponded to [2*S*,2-D]- and [2*R*,2-D]-IPP, respectively. Both the deuterated mevalonate substrates were converted, by the enzyme preparation from rat liver, into (*E*,*E*)-FPP, which after partial purification were subjected to diphosphate cleavage with alkaline phosphatase to give farnesol. As analyzed from the GC-MS spectra, [4*S*,4-D]-mevalonate gave non-isotopic farnesol, whereas, the tri-deuterated species predominated in the farnesol from [4*R*,4-D]-mevalonate. Thus, it was concluded that, in chain elongation reactions, the hydrogen atoms eliminated from IPP were all 2*R* (corresponding to 4*S* in parent mevalonate). The same stereochemical outcome was also demonstrated later by Poulter C. D. *et al*. while working with pig liver, yeast and avian FPP synthase enzymes.[69]

The stereochemistry for proton elimination from C2 of IPP during the formation of both *E* and *Z* double bonds in the biosynthesis of GPP and FPP was determined by Thulasiram and Poulter for the catalytic activity of chain elongating enzymes from various sources.[19] Incubation of (*R*)-[2-$^{2}H_{1}$]IPP and (*S*)-[2-$^{2}H_{1}$]IPP were carried out with the allylic substrates, DMAPP and GPP to produce the corresponding chain elongated linear diphosphate products, which were successively subjected to hydrolysis of the diphosphate esters by alkaline phosphatase treatment. The insertion or elimination of deuterons in the resulting alcohols were analyzed by GC-MS. For each of the enzymes, GPP, neryl diphosphate (NPP), as well as farnesyl diphosphate isomers (FPP), obtained from incubation of (*R*)-[2-$^{2}H_{1}$]IPP with the allylic diphosphates revealed the molecular ions (*m*/*z*) same as those obtained from incubations with

unlabeled substrates, indicating absence of any deuterium atoms in the products. But, incubation of (*S*)-[2-$^{2}H_{1}$]IPP with DMAPP incorporated the deuteriums when it produced mono-deuterated GPP and di-deuterated FPP. These results concluded that the *pro-R* hydrogen at C2 of IPP is lost when both, *E*- and *Z*-double bond isomers of chain elongated diphosphate products are formed.

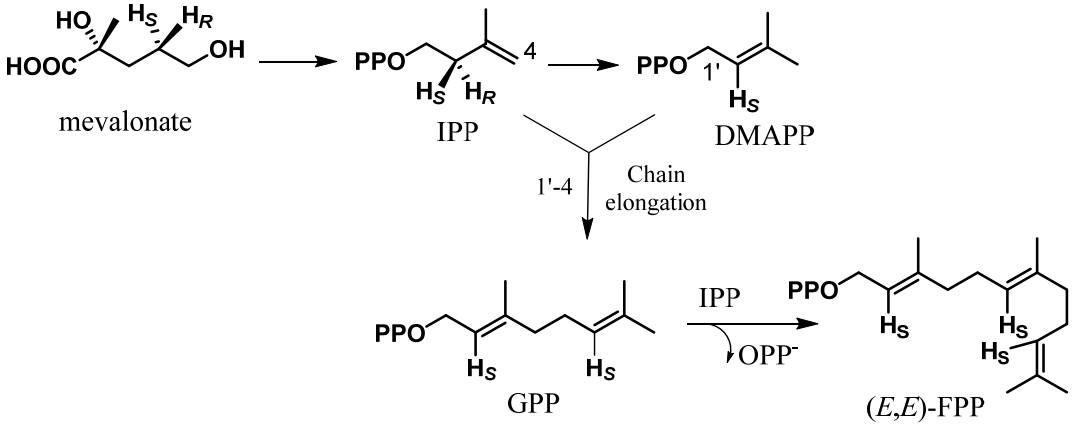

Scheme 3.1.9. Stereochemical aspects of the chain elongation reaction.

(d) C1 of the allylic substrate adds to the *si*-face of the double bond in IPP: From [2R-2-D]-mevalonate, incubation with rat liver preparation formed [*cis*-4-D]-IPP, which on prolonged incubation formed deuterated (*E*,*E*)-FPP possessing two stereocenters, which was subsequently dephosphorylated to trideutero-farnesol. Ozonolysis of the product yielded laevulic acid, which on further treatment with hypoiodite gave *R*-monodeutero-succinic acid. The succinic acid thus obtained was optically pure, which indicated the consistency in addition of DMAPP to the same side of the double bond on both the instances to form (*E*,*E*)-FPP. The stereochemistry of monodeutero-succinic acid which would be similar to that in trideutero-farnesyl diphosphate confirmed *si*-face addition of C1 of allylic substrate to the double bond in IPP.

Further, X-ray structure of the *E. coli* FPP synthase enzyme complexed with IPP and an unreactive thio analogue of DMAPP[70] was analyzed to study the stereochemistry of addition of hydrocarbon units of allylic diphosphates to the double bond of IPP. The observations indicated that the hydrocarbon unit of DMAPP was located on the *si* face of the C3-C4 double bond in IPP with C1 positioned for an inversion of configuration on alkylation.[19] The X-ray crystal structure analysis of the

above complex also confirmed the stereochemical course of all the steps involved in FPP biosynthesis.

The above results thus confirmed the stereochemical stages in the 1′-4 coupling reactions leading to the biosynthesis of (*E*,*E*)-FPP.

3.1.6.2. Biosynthesis of Aristolochene:

Aristolochene is an eremophilane-type, bicyclic sesquiterpene hydrocarbon (Figure 3.1.2), whose (-) enantiomer was first isolated in 1970 from the roots of the plant *Aristolochia indica* (*Aristolociaceae*) by Govindachari *et al*.,[71] while later, it was also reported to occur in *Bixa orellana* leaf oil[64] and in the defensive secretions of *Syntermes* soldier termites.[72,73] The (+) enantiomer was first isolated from the mycelial extracts of the fungus, *Aspergillus terreus* by Cane *et al*. in 1989[74] and from cheese mold *Penicillium roqueforti*. It is evident that the stereochemical configuration of Aristolochene depends on its biological source. The formation of (+)-aristolochene is believed to be the first step in the biosynthesis of a number of fungal toxins.[75] PR-toxin of *Penicillium roqueforti* and sporogen-AO1 of *Aspergillus oryzae* constitute some of the most significant examples of the toxins.[76,77]

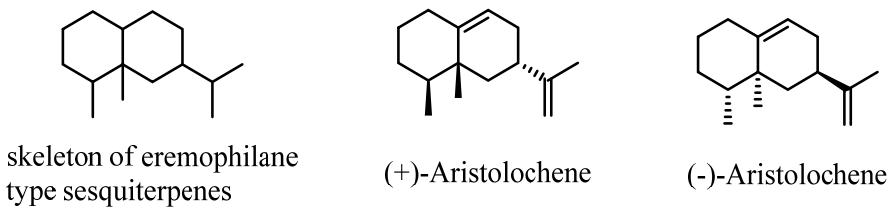

Figure 3.1.2. Structures of (+)- and (-)-Aristolochene.

The biosynthesis of (+)-aristolochene takes place by the cyclization of (*E*,*E*)-farnesyldiphosphate (FPP) to germacrene A and the crucial enzyme involved in the biosynthesis of this compound is a sesquiterpene cyclase, aristolochene synthase. Two distinct aristolochene synthases, acting by identical mechanisms have been isolated. The first aristolochene synthase was isolated from *Penicillium roqueforti*,[78] while the second aristolochene synthase was isolated from *Aspergillus terreus*.[79] X-ray crystal structures of recombinant aristolochene synthase from *A. terreus*[80] and *P. roqueforti*[81] were studied by Christianson *et al*. They also carried out comparison of both the crystal structures to reveal the conservation of a unique active site contour complementary in

shape to their common product despite the substantial divergent evolution of these two enzymes.

The biosynthesis of (+)-aristolochene from (*E*,*E*)-FPP catalysed by aristolochene synthase (AS), isolated from *A. terreus*, was proposed (scheme 3.1.10) and studied by Cane *et al*.[79] According to the proposed mechanism, Mg^{2+} assisted ionization of the farnesyl pyrophosphate and electrophilic attack of the resulting cation at C-10 of the distal double bond, followed by loss of a proton from one of the two adjacent methyl groups, will generate the stable monocyclic intermediate, 'Germacrene A'. Protonation of germacrene A at C-1 is thought to initiate further cyclization by intramolecular electrophilic attack on the 4,5-double bond to form the bicyclic eudesmane cation. The latter intermediate can in turn rearrange to aristolochene by sequential 1,2- hydride and methyl migrations followed by loss of a proton from C-9.

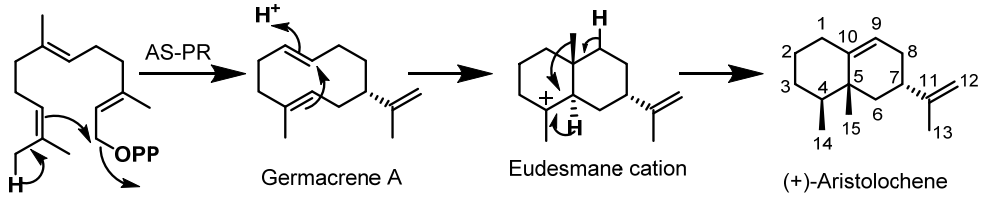

Scheme 3.1.10. Biosynthesis of (+)-Aristolochene from (*E*,*E*)-FPP catalyzed by aristolochene synthase from *A. terreus* (AT-AS).

The product, aristolochene was confirmed by incubating 1-^{3}H-(*E*,*E*)-FPP with the crude cell-free extract of *A. terreus*, which delivered the radio-labelled product that co-eluted with the synthetic standard (±)-aristolochene, when monitored by TLC and radio-GC. Further confirmation was done by using various ^{13}C and ^{14}C labelled substrates, followed by derivatization and characterization of the analogues. In addition to the product authentication, labelled substrate analogues were also utilized to study the stereochemical course and mechanistic principles in the above cyclization reaction. Both (1*R*)- and (1*S*)-[1-^{2}H]-FPP were separately incubated with crude aristolochene synthase from *A. terreus***,** and the purified product from each incubation was analyzed by 61.42-MHz ^{2}H NMR spectroscopy. Incubation of (1*R*)-[1-^{2}H]-FPP with the crude enzyme exhibited a single peak at δ 1.76 corresponding to $H6_{eq}$, while with (1*S*)-[1-^{2}H]-FPP showed a single peak at δ 1.17 corresponding to $H6_{ax}$ of aristolochene. These results implied the inversion of configuration at C1 during the cyclization of FPP to aristolochene (Scheme 3.1.11).

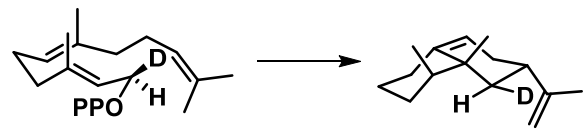

(1*R*)-[1-^{2}H]-FPP

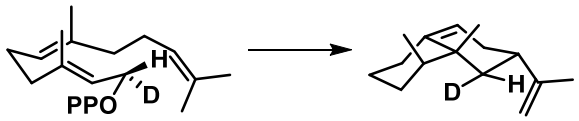

(1*S*)-[1-^{2}H]-FPP

Scheme 3.1.11. Inversion of configuration at C1 demonstrated by using (1*R*)- and (1*S*)-[1-^{2}H]-FPP in the biosynthesis of (+)-aristolochene.

To gain insights in the deprotonation steps from methyl group in the biosynthesis of aristolochene, Cane *et al*. studied incubations of [12,12,12-$^2H_3$]-FPP and [13,13,13-$^2H_3$]-FPP with crude aristolochene synthase isolated from *A*. terreus.[82] The deuterated product was analyzed by ^{2}H NMR spectroscopy at 61.42 MHz to monitor the loci of deuterium atoms. The deuterated analogue of aristolochene obtained from the incubation of [12,12,12-$^2H_3$]-FPP (*Z* isomer) exhibited a single olefinic peak at δ 4.71, corresponding to deuterium at C-12, whereas that obtained from [13,13,13-$^2H_3$]-FPP (*E* isomer) gave rise to a resonance at δ 1.69. Thus, it was concluded that, it is the C-12 (*Z*) methyl group of FPP that undergoes deprotonation to from the intermediate, germacrene A (Scheme 3.1.12).

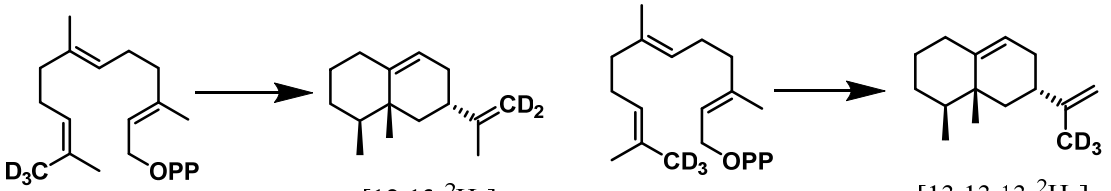

[12,12,12-$^2H_3$]-(*E*,*E*)-FPP

[12,12-$^2H_2$]-aristolochene

[13,13,13-$^2H_3$]-(*E*,*E*)-FPP

[13,13,13-$^2H_3$]-aristolochene

Scheme 3.1.12. Deprotonation steps in the biosynthesis of (+)-aristolochene.

The proton that is lost from C-9 of 4 originates at C-8 of FPP. To establish the stereochemical course of the deprotonation step (4*R*,8*R*)- and (4*S*,8*S*)-[4,8-$^2H_2$]-FPP were individually incubated with aristolochene synthase and the resulting deuterated products were analyzed by ^{2}H-NMR spectroscopy. The deuterated aristolochene

samples from (4*R*,8*R*)-[4,8-$^2H_2$]-FPP retained both the deuterium atoms, whereas that from (4S,8S)-[4,8-$^2H_2$]-FPP, loss of a deuterium from C-8 was observed. These results demonstrated that it is H-8_{si} that is lost in the formation of the 9, 10-double bond of aristolochene[82] (scheme 3.1.12).

Allemann *et al*. have shed light on the molecular details of catalysis and stereochemical control by aristolochene synthase isolated from and operational in the biosynthesis of (+)-aristolochene by cyclization of (*E*,*E*)-FPP.[83] In the biosynthetic reaction of aristolochene and 5-*epi*-aristolochene, intermediacy of germacrene A was proved by the inability to demonstrate its release from any of the sesquiterpene synthases for which it was postulated as an intermediate. Analysis of the X-ray structure of 5-*epi*-aristolochene synthase (EAS) and of the catalytic properties of a mutant EAS showed that Tyr 520 is the active-site acid which protonates germacrene A.[84] Mutation of Tyr 520 to phenylalanine led to the accumulation of germacrene A as the sole reaction product.[85] On the basis of X-ray crystal structure and homology modelling, it was suggested that the hydroxyl group of Tyr 92 acted as a proton donor to C-6 of germacrene A in AS. The identification of a substantial amount of germacrene A during AS catalysis and the formation of large amounts of it by a site-specific mutant, ASY92F confirmed that germacrene A was indeed formed during AS catalysis.[83]

To study the mechanistic principles in the formation of aristolochene and to establish the intermediacy of germacrene A, some of the analogues of substrate, (*E*,*E*)-FPP were utilized. The turnover of the 6,7-dihydro analogue of FPP by AS generated dihydro-germacrene A.[86] Allemann *et al*. visualized the applicability of fluorinated analogue of FPP, 2-fluorofarnesyl diphosphate to determine the pathway intermediates in generation of aristolochene.[87] Incubation of 2-fluorofarnesyl diphosphate during catalysis by AS, produced single product, 2-fluorogermacrene A (Scheme 3.1.11), but did not yield aristolochene, which provided a strong support for a reaction mechanism in which an initial cyclization of FPP to germacryl cation is followed by proton loss from C12 to generate germacrene A (Scheme 3.1.13).

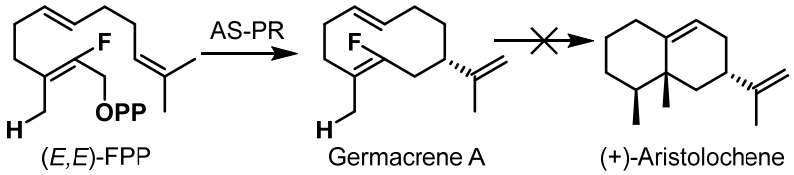

Scheme 3.1.13. Catalysis of 2-fluoro-FPP to 2-fluorogermacrene A by AS.

3.1.6.3. Biosynthesis of Santalenes:

Santalene synthase, isolated from the interface of heartwood and sapwood of *Santalum album*, is a moderately promiscuous sesquiterpene cyclase that catalyzes the metal dependent cyclization of FPP to a mixture of six sesquiterpene hydrocarbon products, the precursors of santalols which are majorly responsible for the woody, pleasant odour and medicinal properties of sandalwood oil.[88-93]

The major sesquiterpenoid alcohols present in the oil that contribute to ~ 6% dry weight[94] of the heartwood of a matured sandalwood tree (>10 years old) are (*Z*)-α-santalol, (*Z*)-α-*exo*-bergamotol, (*Z*)-*epi*-β-santalol, (*Z*)-β-santalol and (*Z*)-lanceol, which contribute to >90% of the total oil content[95] and are proposed to be biosynthesized by hydroxylation at the allylic methyl groups of the sesquiterpene hydrocarbons by cytochrome-P450 systems. The biosynthesis of tricyclic skeleton of α-santalene, bicyclic skeletons of β- and *epi*-β-santalenes, bergamotenes and monocyclic skeleton of curcumenes and zingiberene involves cyclization of the linear sesquiterpene substrate (*E*,*E*)-FPP through a cascade of 'Wagner-Meerwein' rearrangements of unisolable carbocationic intermediates. Although, biosynthetic schemes were proposed in literature involving the formation of some of the common carbocations from terpene pathways and their rearrangements leading to these cyclic terpenoids, efforts have not been made to study the intermediates involved and the mechanism of biosynthesis of these sesquiterpenes is still unexplored. Unavailability of the x-ray crystal structure data hinders knowledge about binding and interaction of diphosphate substrates with the amino acid residues present at the catalytic pocket. In the present investigation, we have proposed a biosynthetic pathway for the formation of sesquiterpenes in sandalwood oil and have provided sufficient proof for the intermediates by deuterium labeling of the substrate (*E*,*E*)-FPP at all the possible positions those are involved in the carbocationic reactions. This proposed biosynthetic pathway for sesquiterpenes from sandalwood has been tailored from the model pathways proposed for sesquiterpenes.[94,96]

Section 3.2.

Synthesis of Deuterated Diphosphate Substrates.

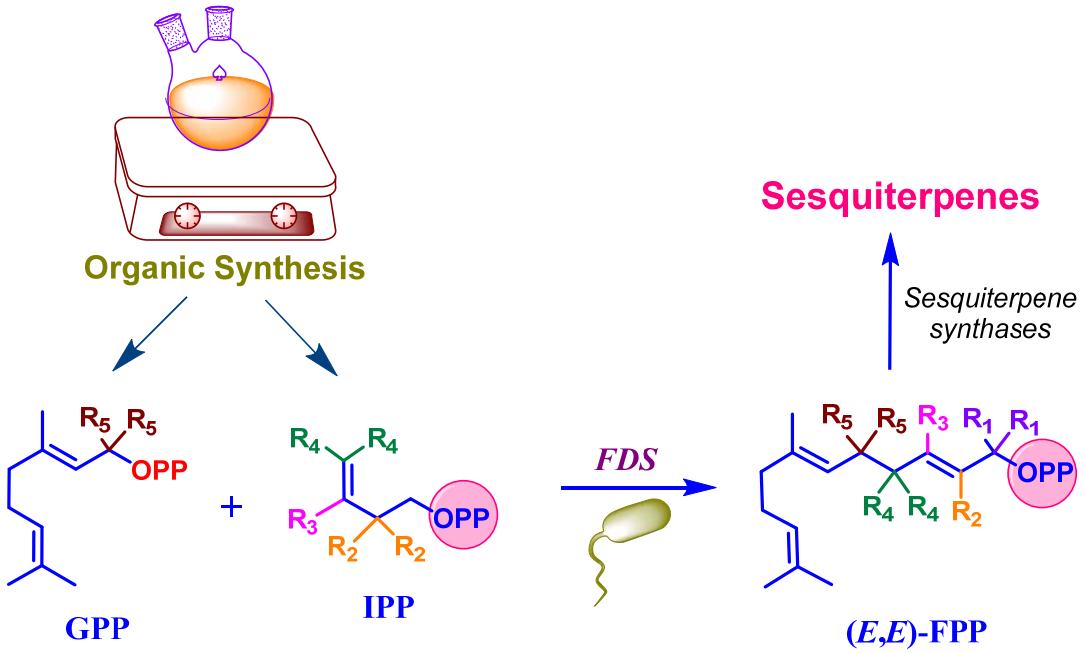

Synthesis of deuterium labeled analogues of (*E*,*E*)-FPP.

3.2.1. Rationale for Present Work:

Sesquiterpenes are one of the structurally most diverse classes of natural products, with more than 300 basic hydrocarbon skeletons. They play some of the vital roles in nature when they act in plants' defence mechanisms, as pheromones to attract insects for pollination and as agents in signal transduction on attaching with proteins (prenylated proteins). Inspite of their enormous diversity, they evolve from a simple acyclic precursor, (*E*,*E*)-farnesyl diphosphate which undergoes a number of carbocationic rearrangements, deprotonations and varied functionalizations with high fidelity. It is interesting and of importance to know the intricate mechanisms that the intermediates follow to yield a particular product with highest degree of precision. Labeled substrates have constantly played invaluable roles in biochemical and bioorganic research to investigate and track the biosynthetic pathways. Deuterated prenyl diphosphates, in perticular, have been previously utilized to study the mechanism of cyclization by several sesquiterpene synthases including, *epi*-aristolochene synthase and premnaspirodiene synthase[52], amorphadiene synthase[53], geosmin synthase[54], patchoulol synthase[55] and Cadinene synthase[56]. In the present investigation, we have implanted deuterium at all the possible centres involved in the cyclization of (*E*,*E*)-FPP, *viz*. C1, C2, C4, C5, C6 and C13. A chemo-enzymatic strategy was adopted for deuterium labeling of (*E*,*E*)-FPP wherein, condensation of deuterated analogues of IPP with DMAPP or GPP was achieved in presence of the chain elongation terpene synthase, (E,E)-farnesyl diphosphate synthase isolated from the interface of S. album. In this section we describe the synthetic methodologies designed for the synthesis of deuterated analogues of IPP (**11**) and GPP (**13**).

3.2.2. Present Work:

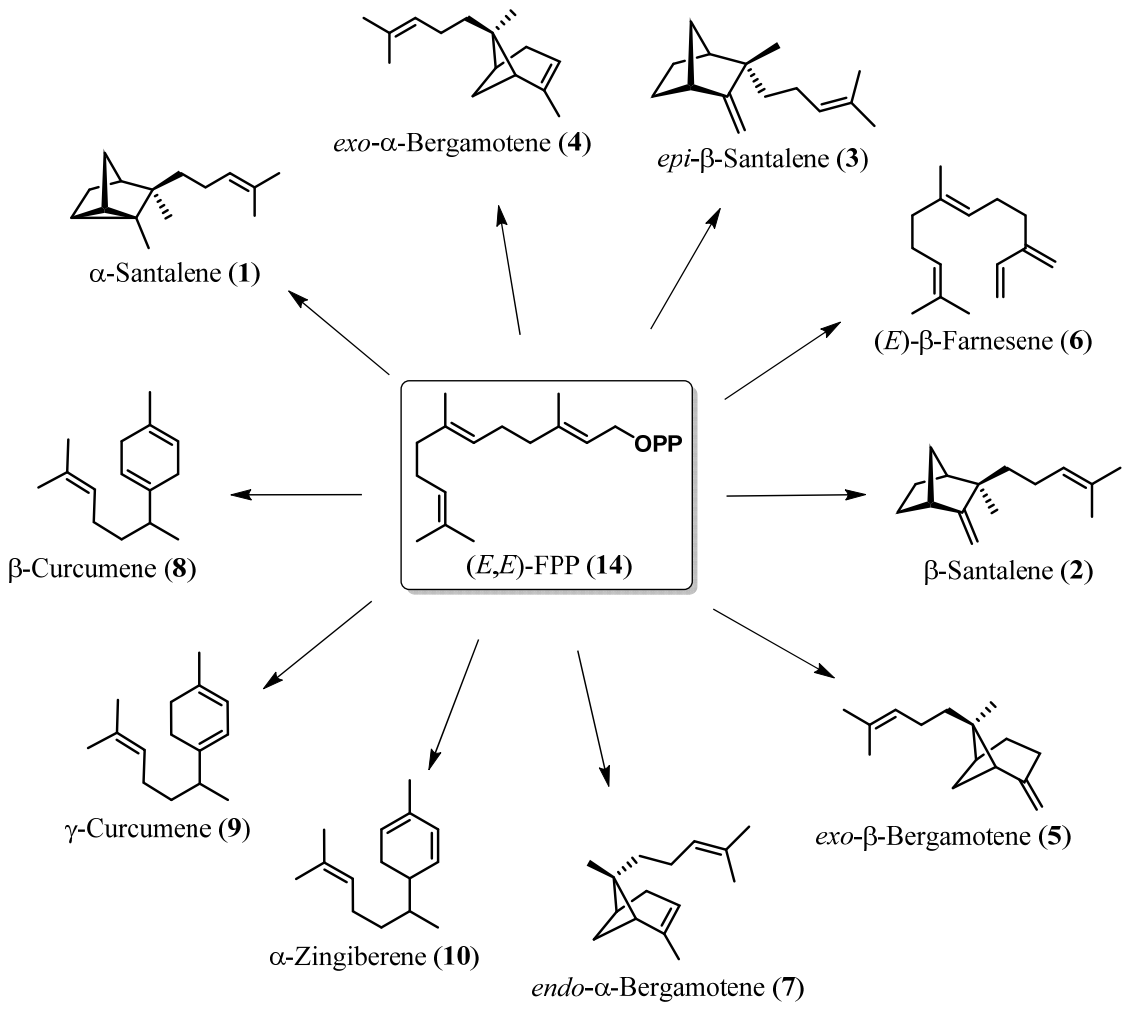

Scheme 3.2.1. Sesquiterpenes generated from cyclization of (*E*,*E*)-FPP (**14**) with santalene synthase (*SaSS*) and its mutants.

Santalene synthase (*SaSS*) was cloned and characterized from the interface of heartwood and sapwood of sandalwood during the ongoing research work in our laboratory.[97] It was found to be a moderately promiscuous enzyme that gave rise to six sesquiterpene products from the common linear sesquiterpene precursor (*E*,*E*)-FPP (**14**). The ability of terpene synthases to convert a prenyl diphosphate substrate to diverse products during different reaction cycles is one of the most unique traits of this enzyme class which is corroborated by the activities of δ-selinene synthase and γ-humulene synthase from Grand Fir (*Abies grandis*).[51] Likewise, 5-*epi*-aristolochene synthase also exhibited highly promiscuous nature by generating 25 different products.[98] The product

promiscuity leading to the production of multiple products may be due to more flexibility of the active site pocket which might accommodate more than one conformations of the substrate and form larger products.[46]

The products formed from *SaSS* were compared with the isolated and purified standards from sandalwood oil, large scale sesquiterpene synthase enzyme assays and from synthesis. These were identified by co-injecting with the standards in GC and were confirmed as α-santalene (**1**), β-santalene (**2**), *epi*-β-santalene (**3**), *exo*-α-bergamotene (**4**), *exo*-β-bergamotene (**5**) and (*E*)-β-farnesene (**6**) (Scheme 3.2.1). The mutants generated by site-directed mutagenesis produced different products which were subsequently characterized as *endo*-α-bergamotene (**7**), β-curcumene (**8**), γ-curcumene (**9**) and α-zingiberene (**10**).[97]

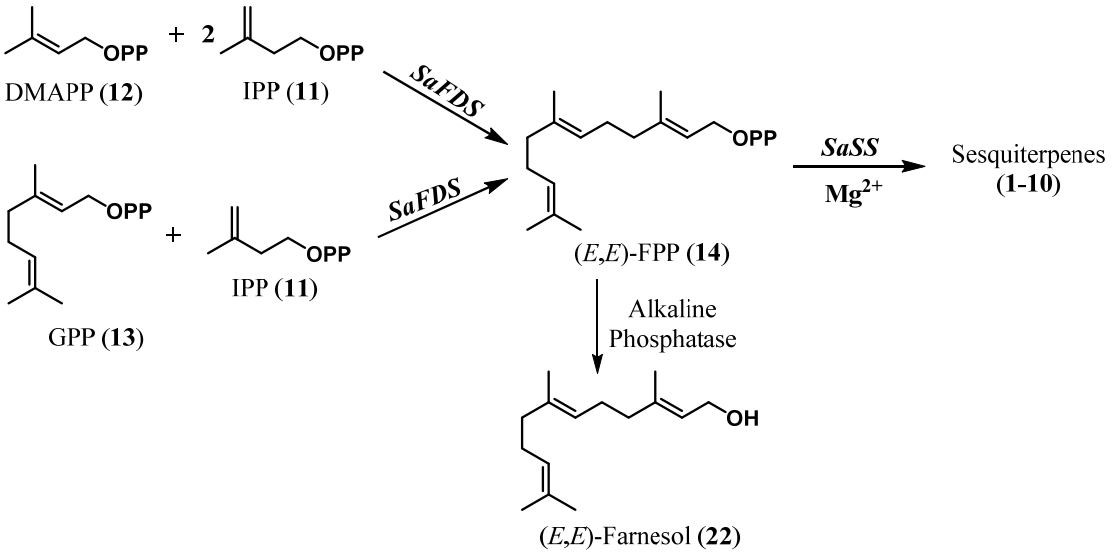

Scheme 3.2.2. Biosynthesis of (*E*,*E*)-FPP (**14**) by dissociative electrophilic alkylation of IPP (**11**) by allylic carbocations generated from DMAPP (**12**) or GPP (**13**). Alkaline phosphatase treatment of **14** hydrolyzed it to (*E*,*E*)-farnesol (**22**) and the product was confirmed by GC and GC-MS analysis. Incubation of **14** with *SaSS* and its mutants resulted in the production of sesquiterpenes.

S. album farnesyl diphosphate synthase (*SaFDS*) was also isolated from the same tissue and was functionally characterized by enzyme assays.[97] *SaFDS* catalyzed the chain elongation reaction wherein, dissociative electrophilic alkylation of the double bond in IPP (**11**) by allylic cations generated from the allylic diphosphate substrates, DMAPP (**12**) or GPP (**13**) afforded (*E*,*E*)-FPP (**14**). Alkaline phosphatase treatment of

14 resulted in hydrolysis of the diphosphate ester to produce (*E*,*E*)-farnesol (**22**) that was further confirmed by co-injecting with the standard in GC, GC-MS and GC-QToF (Scheme 3.2.2). Different sets of assays of *SaSS* with the synthesized all trans substrate (*E*,*E*)-FPP (**14**) or the enzymatically generated substrate **14** from chain elongation reaction of IPP with DMAPP or GPP in presence of *SaFDS* generated the same products (**1**-**6**). Moreover, the ratio of all the products obtained in all the three cases was found to be similar from GC analysis (Figure 3.2.2). This formed the rationale for synthesis of deuterated IPP, GPP and DMAPP analogues which could be combined in presence of *SaFDS* to achieve the labels appropriately at desired centers in **14**. The biosynthesized deuterium labeled analogues of **14** were utilized to investigate the intricate mechanisms involved in cyclization of **14** to a spectrum of polycyclic sesquiterpene products (**1**-**10**).

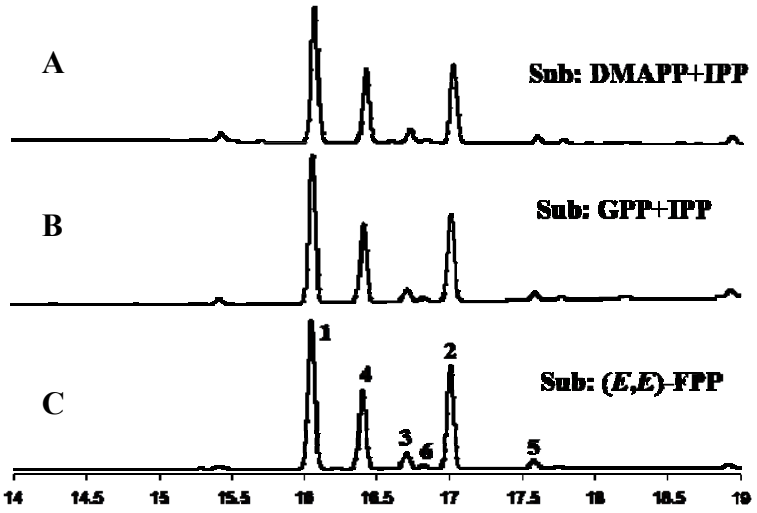

Figure 3.2.1. GC traces of the products from *in vitro* assays of santalene synthase (*SaSS*) with (*E*,*E*)-FPP generated from (**A**) IPP and 2 × DMAPP, (**B**) IPP and GPP, in presence of *SaFDS*, and (C) synthesis. The products were identified as: α-santalene (**1**), β-santalene (**2**), *epi*-β-santalene (**3**), *exo*-α-bergamotene (**4**), *exo*-β-bergamotene (**5**), and (*E*)-β-farnesene (**6**). The ratio of products formed in all the three cases was similar.

According to the procedures designed by Davisson *et al*., isoprenoid diphosphates are synthesized from the corresponding alcohols in two steps. The first step involves activation of the hydroxy bearing carbon, and the second is a direct displacement of the activated group by a phosphorylating agent. The choice of activated derivative to be used in the displacement reaction was important and depended on the nature of alcohol. Allylic alcohols were converted to corresponding halides (bromides

or chlorides), whereas the homoallylic alcohols such as isopentenyl alcohol, which were susceptible to elimination on halogenation, were converted to tosylates. The suggested phosphorylating reagent was *tris*-tetra-*n*-butylammonium hydrogen diphosphate salt (**15**). This was easily obtained by passing a solution of sodium dihydrogen pyrophosphate through a cation-exchange resin (H^+ form) and titrating the eluate to pH 7.3 with tetra-*n*-butylammonium hydroxide followed by lyophilization of the aqueous solution to result in a white, hygroscopic solid that could be stored for several months in a desiccator over anhydrous $CaSO_4$, at -20 °C.

3.2.2.1. Synthesis of isopentenyl diphosphate, IPP (11):

Isopentenyl alcohol (**16**), a homoallylic alcohol was activated as its *p*-toluenesulfonate ester (**17**) followed by the S_N2 displacement of tosylate group with **15**. Replacement of tetra-*n*-butylammonium counter-ion from isopentenyl diphosphate with ammonium ion was achieved by passing the reaction mixture through cation-exchange resin (NH_4^+ form), followed by purification over cellulose to yield **11** as a white, hygroscopic, fluffy solid (Scheme 3.2.3).

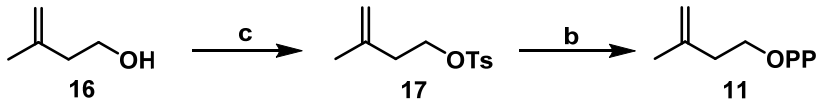

Scheme 3.2.3. *Reagents and conditions*: a) CaH_2, DMAP, TsCl, CH_2Cl_2, 0 °C to rt, 3 h, 82%; b) $[N(n\text{-}Bu)_4]_3P_2O_7H$, CH_3CN, rt, 2 h, 65%.

3.2.2.2. Synthesis of dimethylallyl diphosphate, DMAPP (12):

Dimethylallyl alcohol (**18**) was readily converted to its bromide in presence of phosphorus tribromide at reduced temperatures. To avoid the loss of halogenated intermediates in case of volatile alcohols (especially C_5 systems), bromination was chosen over chlorination as the bromides obtained would be less volatile in comparison to the corresponding chlorides. Dimethylallyl bromide (**19**) was subjected to displacement reaction with **15**, without any purification as it was prone to degradation over silica. Purification of the diphosphate product followed similar steps as for **11** to ultimately result in **12** as a white solid (Scheme 3.2.4).

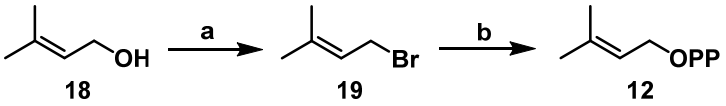

Scheme 3.2.4. *Reagents and conditions*: a) PBr_3, pentane, -20 °C, 15 min, 82%; b) $[N(n\text{-}Bu)_4]_3P_2O_7H$, CH_3CN, rt, 2 h, 67%.

3.2.2.3. Synthesis of geranyl diphosphate, GPP (13):

Geraniol (**20**) was converted to its chloride using Corey-Kim halogenation reaction procedure designed for allylic alcohols.[99] For bulkier alcohols, where volatility was not a serious issue, chlorination was preferred as the chlorides were less prone to degradation during preparation and purification procedures. The halide functionality in geranyl chloride (**21**) was displaced by **15** and the resultant geranyl diphosphate (**13**) was purified using the above mentioned protocol (Scheme 3.2.5).

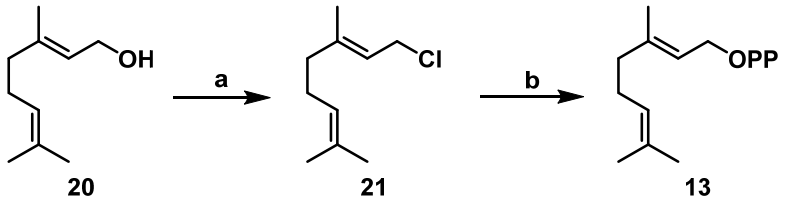

Scheme 3.2.5. *Reagents and conditions*: a) NCS, $(CH_3)_2S$, CH_2Cl_2, -30 °C to rt, 3 h, 82%; b) $[N(n\text{-}Bu)_4]_3P_2O_7H$, CH_3CN, rt, 2 h, 71%.

3.2.2.4. Synthesis of (*E*,*E*)-farnesyl diphosphate, (*E*,*E*)-FPP (14):

Synthesis of (*E*,*E*)-FPP (**14**) was carried out on the similar lines as followed for **13**. Commercially available (*E*,*E*)-farnesol (**22**) was subjected to chlorination to produce **23**, followed by displacement reaction with **15** and purification of the diphosphate product to yield **14** as a white solid (Scheme 3.2.6).

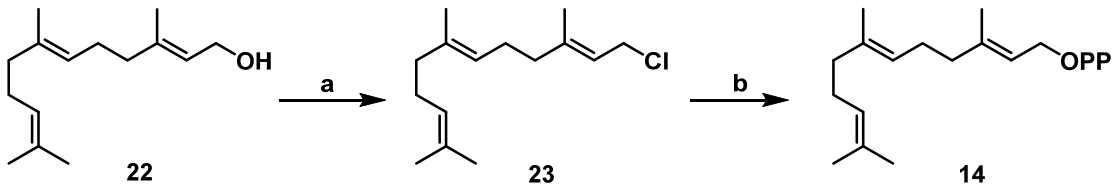

Scheme 3.2.6. *Reagents and conditions*: a) NCS, $(CH_3)_2S$, CH_2Cl_2, -30 °C to rt, 3 h, 82%; b) $[N(n\text{-}Bu)_4]_3P_2O_7H$, CH_3CN, rt, 2 h, 68%.

3.2.2.5. Synthesis of [4,4-$^2H_2$]-Isopentenyl diphosphate ([4,4-$^2H_2$]-11):

Synthesis of **[4,4-$^2H_2$]-11** was initiated from commercially available 4-hydroxybutanone (**24**). Compound **24** was protected as its *tert*-butyldimethylsilyl ether (**25**) and the carbonyl moiety was subjected to Wittig olefination in presence of *n*-BuLi with tri-deuteriomethyl-triphenylphosphonium iodide which itself was synthesized from tri-deuteriomethyl iodide (CD_3I) and triphenylphosphine (PPh_3). The resultant dideuterated olefin **[4,4-$^2H_2$]-26** was deprotected from its silyl group in presence of TBAF to yield free alcohol **[4,4-$^2H_2$]-16**. The volatile alcohol, without any purifications was subjected to tosylation in presence of Ts-Cl and anhydrous CH_2Cl_2 as the solvent to provide **[4,4-$^2H_2$]-17**. The tosylate group was substituted by diphosphate on reacting **[4,4-$^2H_2$]-17** with **15** in CH_3CN under inert conditions. Further purifications of the diphosphate compound according to well documented procedure by Davisson *et al*. delivered **[4,4-$^2H_2$]-11** as trisammonium salt (Scheme 3.2.7). Characterization of the dideuterated diphosphate product was performed by comparing its spectral data with that of **11**. Absence of olefinic protons and terminal olefinic carbon in ^1H and ^{13}C spectra of **[4,4-$^2H_2$]-11** respectively, confirmed the structure. Analysis of the HRMS (ESI) data of **[4,4-$^2H_2$]-11** displayed an increase of 2 amu in the $[M-1]^-$ peak when compared with that of **11** and further supported the dideuteration.

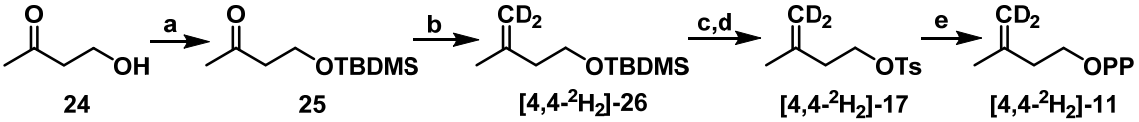

Scheme 3.2.7. *Reagents and conditions*: a) TBDMS-Cl, Et_3N, CH_2Cl_2, 0 °C to rt, 3 h, 91%; b) PPh_3CD_3I, *n*-BuLi, THF, 0 ^oC to rt, 2 h, 78%; c) TBAF, 0 ^oC to rt, THF, 1 h; d) CaH_2, DMAP, Ts-Cl, CH_2Cl_2, 0 °C to rt, 2 h, 74%; e) $[N(n\text{-}Bu)_4]_3P_2O_7H$, CH_3CN, rt, 2h, 49%.

3.2.2.6. Synthesis of [2,2-$^2H_2$]-Isopentenyl diphosphate ([2,2-$^2H_2$]-11):

Synthesis of **[2,2-$^2H_2$]-11** started from easily available ethylacetoacetate (**27**). Dideuteration at α-position was achieved by stirring **27** with D_2O for 24 h to replace the acidic protons with deuterons resulting in **[2,2-$^2H_2$]-27**. Both the carbonyl groups in the labeled compound **[2,2-$^2H_2$]-27** were reduced with DIBAH to diol, **[2,2-$^2H_2$]-28** in 76% yield. Primary hydroxy group of **[2,2-$^2H_2$]-28** was protected as silyl ether, **[2,2-$^2H_2$]-29**

with TBDMS-Cl in presence of Et_3N followed by oxidation of the secondary hydroxy group by Dess-Martin periodinane reagent to ketone, **[2,2-$^2H_2$]-25** with 91% yield. Methylenation of [**2,2-$^2H_2$]-25** was obtained when it was subjected to one carbon Wittig olefination with methyltriphenylphosphonium iodide in presence of *n*-BuLi to result in **[2,2-$^2H_2$]-26**. The resultant 2,2-dideuterated terminal olefin, **[2,2-$^2H_2$]-26** was deprotected from its silyl group in presence of TBAF to yield free alcohol, **[2,2-$^2H_2$]-16**. The resulting volatile alcohol without any purification was subjected to tosylation in presence of Ts-Cl to provide **[2,2-$^2H_2$]-17**. The tosylate group was substituted by diphosphate on reacting with **15** in anhydrous CH_3CN according to procedure standardized and reported by Davisson *et al*. to yield [2,2-$^2H_2$]-isopentenyl diphosphate as a trisammonium salt (**[2,2-$^2H_2$]-11**) (Scheme 3.2.8). The product was confirmed by comparing ^1H, ^{13}C NMR data with that of **11** which showed disappearance of methylene protons at C2 in **[2,2-$^2H_2$]-11** which appeared at δ 2.37 (t, J = 6.65 Hz, 2H). Analysis of the HRMS (ESI) data displayed increment of 2 amu in the $[M-1]^-$ peak when compared with that of **11**.

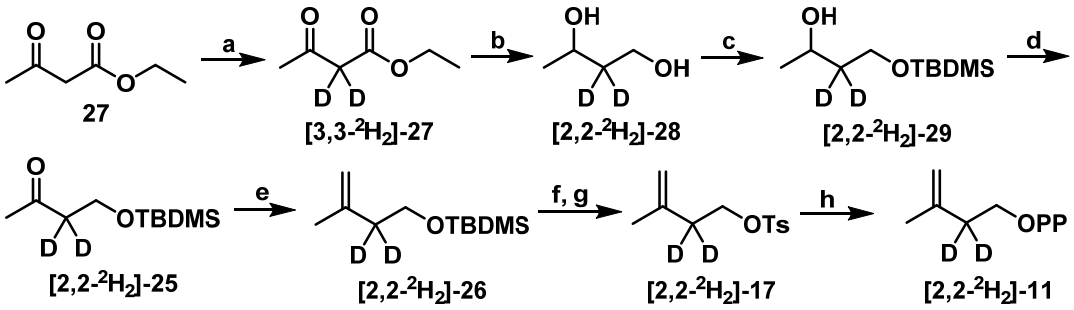

Scheme 3.2.8. *Reagents and conditions*: a) D_2O, rt, 24 h, 2 times, 92%; b) DIBAH, CH_2Cl_2, 0 °C to rt, 5 h, 76%; c) TBDMS-Cl, Et_3N, CH_2Cl_2, 0 °C to rt, 2 h, 88%; d) Dess-Martin periodinane, CH_2Cl_2, 3 h, 91%; e) PPh_3CH_3I, *n*-BuLi, THF, 0 °C to rt, 2 h, 72%; f) TBAF, THF, 0 °C to rt, 1 h; g) CaH_2, DMAP, Ts-Cl, CH_2Cl_2, 0 °C to rt, 3 h, 89%; h) $[N(n\text{-}Bu)_4]_3P_2O_7H$, CH_3CN, rt, 2 h, 31%.

3.2.2.7. Synthesis of [5,5,5-$^2H_3$]-Isopentenyl diphosphate ([5,5,5-$^2H_3$]-11):

Routinely used compound, propylene glycol (**30**) was used as the starting material for the synthesis of **[5,5,5-$^2H_3$]-11**. Selective mono-protection of **30** to its silyl ether **31** was achieved with TBDMS-Cl in presence of Et_3N followed by oxidation of the other

hydroxy group to an aldehyde **32** by refluxing it with IBX in ethyl acetate. The aldehyde **32** was methylated with Grignard reagent, trideuteriomethylmagnesium bromide (CD_3MgBr) in anhydrous THF to get the labeled secondary alcohol **[1,1,1-$^2H_3$]-29**, which was oxidized in presence of IBX under reflux condition in ethyl acetate to yield **[1,1,1-$^2H_3$]-25**. The ketone **[1,1,1-$^2H_3$]-25**, similar to **[2,2-$^2H_2$]-25**, was subsequently subjected to a sequence of reactions, Wittig olefination, silyl deprotection, tosylation and phosphorylation to finally result in the labeled product [5,5,5-$^2H_3$]-isopentenyl diphosphate (**[5,5,5-$^2H_3$]-11**) (Scheme 3.2.9). Structural verification of the trideuterio-methyl product **[5,5,5-$^2H_3$]-11**, was performed by comparing its spectral data with that of **11**, which demonstrated the absence of the allylic methyl signal in ^1H and ^{13}C NMR spectra of the prior, which appeared at δ 1.65 (s, 3H) and δ 21.6 ($-CH_3$), respectively in the later. Further, trideuteration was confirmed by analysis of the HRMS (ESI) data that displayed a molecular formula $C_5H_8{}^2H_3P_2O_7$ and an increment of 3 amu in the $[M-1]^-$ peak when compared to that of **11**.

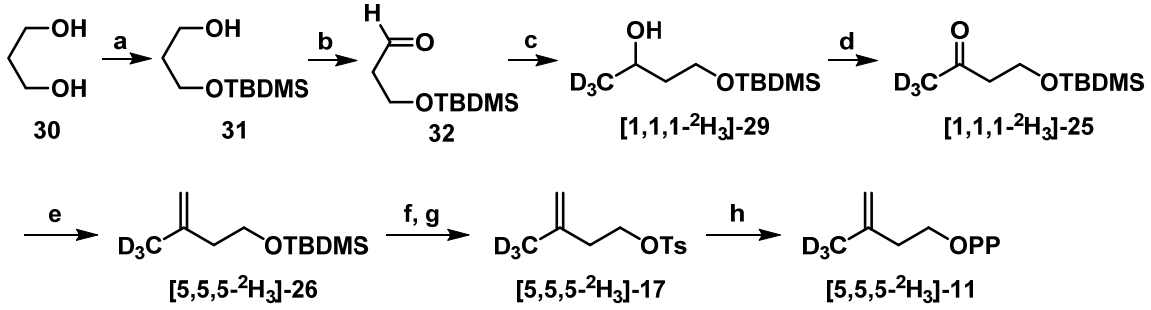

Scheme 3.2.9. *Reagents and conditions*: a) TBDMS-Cl, Et_3N, CH_2Cl_2, 0 °C to rt, 3 h, 91%; b) IBX, ethyl acetate, reflux, 4 h, 91%; c) CD_3MgBr, THF, 0 °C to rt, 2 h, 67%; d) IBX, ethyl acetate, reflux, 4 h, 92%; e) PPh_3CH_3I, *n*-BuLi, THF, 0 °C to rt, 2 h, 70%; f) TBAF, THF, 0 °C to rt, 1 h; g) CaH_2, DMAP, Ts-Cl, CH_2Cl_2, 0 °C to rt, 3 h, 77% over two steps; h) $[N(n\text{-}Bu)_4]_3P_2O_7H$, CH_3CN, rt, 2 h, 39%.

3.2.2.8. Synthesis of [4,4,5,5,5-$^2H_5$]-Isopentenyl diphosphate ([4,4,5,5,5-$^2H_5$]-11):

Intermediate, **[1,1,1-$^2H_3$]-25** (scheme 7) was utilized in the synthesis of **[4,4,5,5,5-$^2H_5$]-11**. Trideuteriomethyl ketone **[1,1,1-$^2H_3$]-25** was subjected to a series of reactions as for **25** in scheme 3.2.7. The reaction sequence followed, one carbon Wittig olefination with trideuteriomethyl-triphenylphosphonium iodide to deliver **[4,4,5,5,5-$^2H_5$]-26**, silyl deprotection to result in **[4,4,5,5,5-$^2H_5$]-16**, immediate tosylation to get **[5,5,5,4,4-$^2H_5$]-**

17 and diphosphorylation to ultimately achieve the labeled product [4,4,5,5,5-$^2H_5$]-isopentenyl diphosphate (**[4,4,5,5,5-$^2H_5$]-11**) (Scheme 3.2.10). Comparison of the spectral data of **[4,4,5,5,5-$^2H_5$]-11** with that of **11** revealed disappearance of signals corresponding to terminal olefin and allylic methyl group. Penta-deuteration in the product **[4,4,5,5,5-$^2H_5$]-11**, was further confirmed by analysis of the HRMS (ESI) data that displayed an increment of 5 amu in the $[M-1]^-$ peak when compared to that of **11** and also matched the molecular formula $C_5H_6{}^2H_5P_2O_7$.

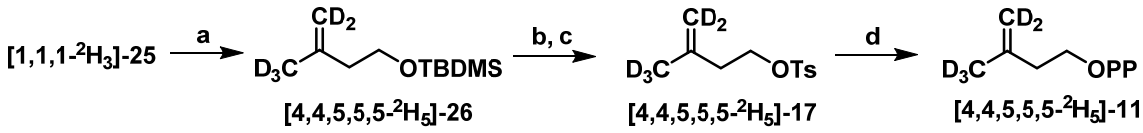

Scheme 3.2.10: *Reagents and conditions*: a) PPh_3CD_3I, *n*-BuLi, THF, 0 °C to rt, 2 h, 78%; b) TBAF, THF, 0 °C to rt, 2 h; c) CaH_2, DMAP, TsCl, CH_2Cl_2, 0 °C to rt, 3 h, 82%; d) $[N(n\text{-}Bu)_4]_3P_2O_7H$, CH_3CN, rt, 2 h, 34%.

3.2.2.9. Synthesis of [1,1-$^2H_2$]-Geranyl diphosphate ([1,1-$^2H_2$]-13):

Dideuteration on the oxymethylene carbon (C1) of **20** was achieved by a series of oxidation-reduction procedures with geraniol (**20**). Oxidation of **20** to geranial (**21**) was carried out in presence of IBX under reflux condition in ethyl acetate, followed by reduction with $LiAlD_4$ at reduced temperatures to yield only 1,2-reduced, mono-deuterated product, **[1-$^2H_1$]-20**. One more cycle of oxidation-reduction with PDC and $LiAlD_4$, respectively was carried out with **[1-$^2H_1$]-20** to yield the dideuterated geraniol (**[1,1-$^2H_2$]-20**). Chlorination of **[1,1-$^2H_2$]-20** to **[1,1-$^2H_2$]-21** was achieved by 'Corey-Kim' reaction procedures standardized for allylic alcohols, as demonstrated in the synthesis of **21**. The halide **[1,1-$^2H_2$]-21** was subjected to diphosphorylation in presence of **15** in anhydrous CH_3CN to yield [1,1-$^2H_2$]-geranyl diphosphate (**[1,1-$^2H_2$]-13**) (Scheme 3.2.11).

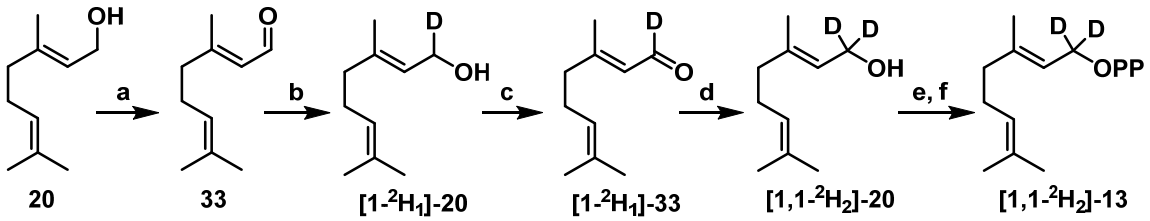

Scheme 3.2.11. *Reagents and conditions*: a) IBX, ethyl acetate, 75 ^{o}C, 3 h, 96%; (b) $LiAlD_4$, THF, -40 ^{o}C, 2 h, 92%; (c) PDC, CH_2Cl_2, rt, 2 h, 81%; (d) $LiAlD_4$, THF, -40 ^{o}C, 2 h, 87%; e) NCS, $(CH_3)_2S$, CH_2Cl_2, -30 °C to rt, 3 h, 90.4%; f) $[N(n\text{-}Bu)_4]_3P_2O_7H$, CH_3CN, rt, 2 h, 64%.

3.2.2.10. Synthesis of [1,1-$^2H_2$]-Farnesyl diphosphate ([1,1-$^2H_2$]-14):

Following an identical sequence of reactions as applied in the synthesis of **[1,1-$^2H_2$]-13**, synthesis of dideuterated product, [1,1-$^2H_2$]-farnesyl diphosphate (**[1,1-$^2H_2$]-14**) was carried out from (*E*,*E*)-farnesol (**22**) (Scheme 3.2.12).

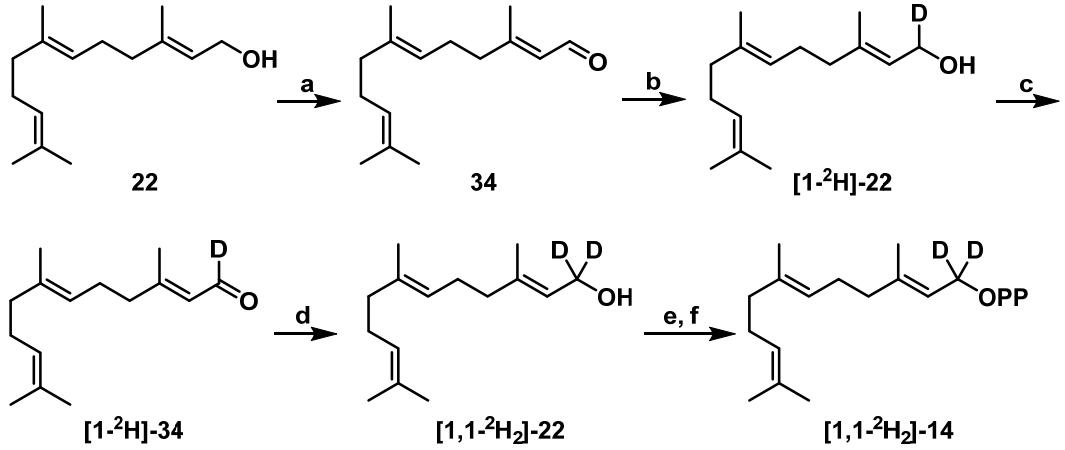

Scheme 3.2.12. *Reagents and conditions*: a) IBX, ethyl acetate, 75 ^{o}C, 3 h, 95%; b) $LiAlD_4$, THF, -40 ^{o}C, 2 h, 82%; c) PDC, CH_2Cl_2, rt, 2 h, 77%; d) $LiAlD_4$, THF, -40 ^{o}C, 2 h, 80%; e) NCS, $(CH_3)_2S$, CH_2Cl_2, -30 °C to rt, 3 h, 83%; f) $[N(n\text{-}Bu)_4]_3P_2O_7H$, CH_3CN, rt, 2 h, 66%.

3.2.2.11. Biosynthesis of deuterated analogues of (*E*,*E*)-FPP (14):

Biosynthesis of deuterated analogues of **14** were obtained by *SaFDS* catalyzed dissociative electrophilic alkylation reactions of synthesized deuterated analogues of **11** with un/deuterated **12** or **13**. (Scheme 3.2.13).

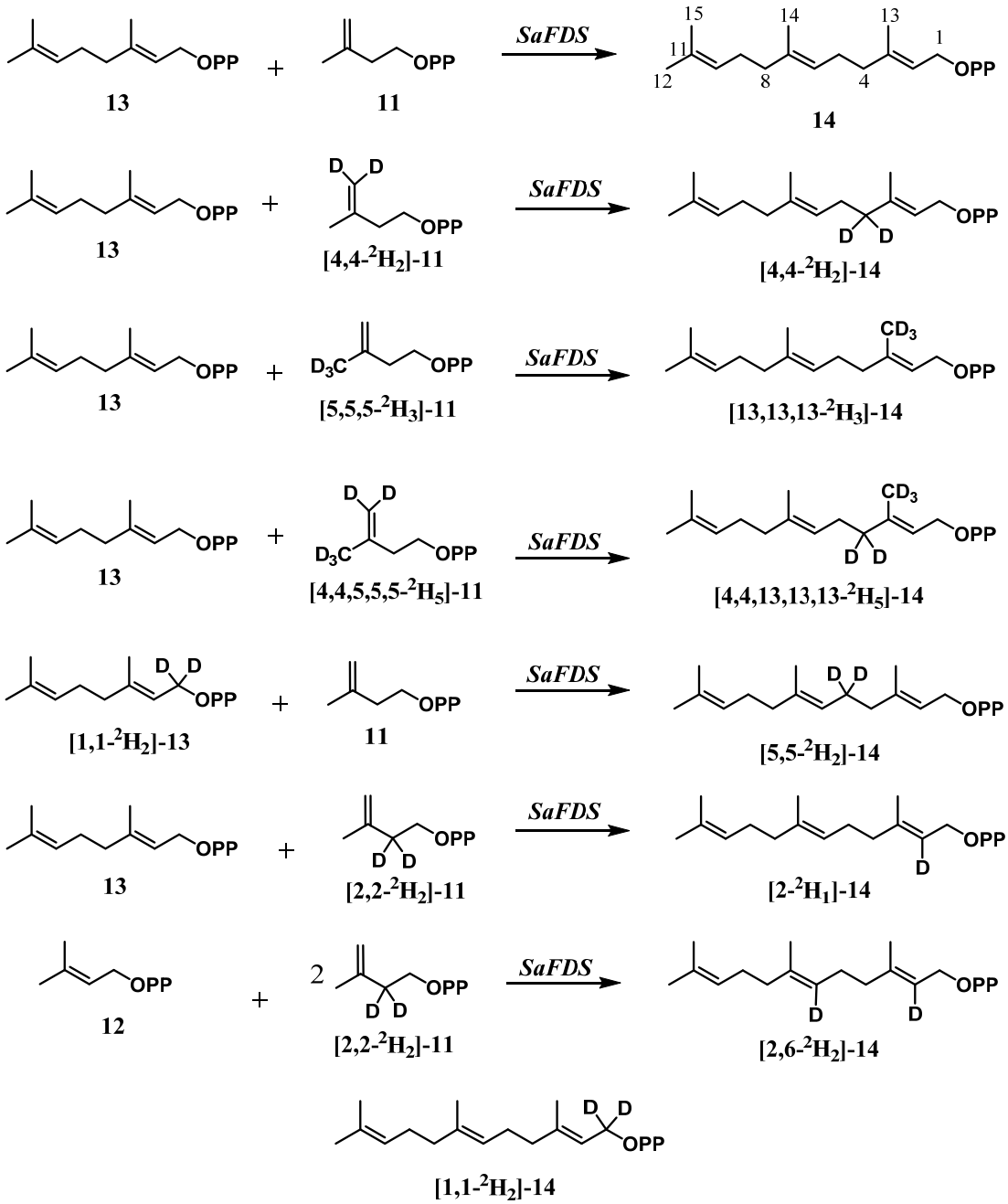

Scheme 3.2.13. Biosynthesis of deuterium labeled analogues of (*E*,*E*)-FPP (**14**) by chain elongation reactions of IPP (**11**) with DMAPP (**12**) or GPP (**13**), catalyzed by *SaFDS*.

3.2.3. Summary and Conclusion:

Diphosphate substrates (IPP, DMAPP, GPP, and FPP) were synthesized from the corresponding alcohols. According to the reported procedures, the alcohols were first activated to corresponding tosylates or halides followed by displacement of the leaving group by the diphosphate salt (**15**). Synthetic methodologies were developed for the synthesis of deuterated analogues of diphosphate substrates, **[4,4-$^2H_2$]-11**, **[2,2-$^2H_2$]-11**, **[5,5,5-$^2H_3$]-11**, **[4,4,5,5,5-$^2H_5$]-11**, **[1,1-$^2H_2$]-13**, **[1,1-$^2H_2$]-14**. Deuteration at the desired centres of (*E*,*E*)-FPP (**14**) was achieved by utilization of biosynthesitic strategies wherein, condensation reactions of deuterated derivatives of **11** with **12**, or **13** were catalyzed by farnesyl diphosphate synthase from *S. album* (*SaFDS*).

3.2.4. Experimental:

Tris-tetra-*n*-butylammonium hydrogen diphosphate (15):

A 2 × 30 cm column was packed with Dowex 50W-8X cation exchange resin (H^+ form) in deionized (DI) water and was washed with 2 column volumes of DI water. In case of reused resin, which was stored in dilute HCl, it was washed until the eluate did not change colour of pH paper. Disodium dihydrogen pyrophosphate (3.13 g, 14 mmol) dissolved in 10 mL DI water was applied on the resin bed and was eluted with DI water, when fractions of 15 mL were collected. The pH of the fractions was monitored, and those exhibiting acidic pH due to presence of free pyrophosphoric acid, were collected in a 1 L round-bottom flask. Collection of the fractions (approximately 100 mL) was stopped when the pH returned to that of DI water. The solution of pyrophosphoric acid was then immediately titrated to pH 7.3 with tetra-*n*-butylammonium hydroxide. The resultant salt was dried by lyophilization to yield **15** (12.53 g, 98%) as a hygroscopic, white solid. This preparation was either immediately employed in the displacement reactions for the synthesis of organic diphosphates or could be stored in a desiccator over anhydrous $CaSO_4$ at -20 °C for future use. **^{1}H NMR** (400 MHz, D_2O): δ 0.90-0.94 (m, 36 H, -CH_3), 1.28-1.38 (m, 24 H, -CH_2), 1.58-1.66 (m, 24 H, -CH_2), 3.15-3.19 (m, 24 H, -CH_2), 4.81 (s, -OH); **^{31}P NMR** (162 MHz, D_2O): δ -7.85 (s).

General procedure for preparation of diphosphates:

Diphosphorylation reactions involving displacement of the halide or tosylate by diphosphate were carried out under an inert atmosphere in a flame-dried round-bottomed flask equipped for magnetic stirring. Typically 1-2 mmol of halide or tosylate were employed in these reactions. To a well stirred solution of 2 equivalents of inorganic diphosphate (**15**) in CH_3CN (0.5-1.0 M) was slowly added *via* syringe a solution of 1 equivalent of tosylate or halide dissolved in minimum quantity of CH_3CN (0.25-0.50 M) and the resulting mixture was stirred at room temperature for 2 h. For homoallylic tosylates, 3 equivalents of **15** was used. After completion of the reaction, solvent was removed by rotary evaporation, and the resulting opaque residue was dissolved in 1:49 (v/v) isopropanol and 25 mM NH_4HCO_3 (ion-exchanger buffer). The clear colorless solution was slowly passed through a column containing 30 equivalents of DOWEX AG 50W-X8 (100-200 mesh) cation-exchange resin (NH_4^+ form) that had been equilibrated with two column volumes of ion-exchange buffer. The column was

eluted with two column volumes of the same buffer and the resultant clear, colorless eluate was lyophilized to dryness to yield a fluffy, white solid. The residue was then dissolved in 0.1 M NH_4HCO_3 (4 mL) and the clear solution was transferred to a centrifuge tube. A mixture of 1:1 (v/v) CH_3CN: isopropanol (solvent-I) (10 mL) was added, and the contents were mixed thoroughly on a vortex mixer, during which time a white precipitate formed. The suspension was cleared by centrifugation for 5 min at 2000 rpm. The supernatant was removed with a pipette and the precipitate was redissolved in 3 mL 0.1 M NH_4HCO_3 and extracted with 7 mL of solvent-I. The final extraction was performed with 2 mL of 0.1 M NH_4HCO_3 and 5 mL of solvent-I. The combined supernatants were concentrated by rotary evaporation at 40 °C and then lyophilized. The resulting solid was dissolved in a minimum amount of chromatography buffer and loaded onto a cellulose flash column. Fractions were analyzed on cellulose TLC plates, developed with iodine or sulfosalicylic acid-ferric chloride spray,[100] pooled, and concentrated by rotary evaporation at 40 °C. The material was transferred to a freeze-drying flask and lyophilized. The resulting white solid was collected and stored at -78 °C for future applications.

3-Methylbut-3-en-1-yl diphosphate ammonium salt, (Isopentenyl diphosphate, IPP) (11):

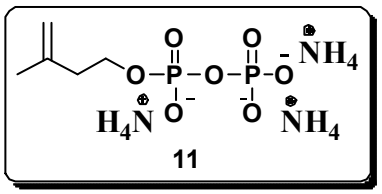

11

In a flame dried flask under inert atmosphere were added isopentenol (**16**) (1.0 g, 11.6 mmol) and anhydrous CH_2Cl_2 (25 mL). The mixture was stirred and cooled at 0 °C followed by addition of Et_3N (1.3 g, 12.8 mmol) and DMAP (0.15 g, 1.2 mmol). To the well stirred mixture was added freshly recrystallized TsCl (2.4 g, 12.8 mmol) and the reaction was stirred for 3 h at room temperature and monitored by TLC. After completion, the reaction was quenched by addition of cold brine (20 mL). The organic layer was separated and the aqueous layer was extracted with CH_2Cl_2 (2 × 25 mL). The combined organic layer was washed with brine (20 mL), dried over anhydrous Na_2SO_4 and concentrated under reduced pressure to furnish yellow oil. Purification by silica gel column chromatography in CH_2Cl_2 yielded **17** (1.79 g, 72%). The product was confirmed by ^{1}H NMR and GC-EI-MS and the data matched with literature. **^{1}H NMR** (200 MHz, $CDCl_3$): δ 1.67 (bs, 3H), 2.35 (t, J = 6.89 Hz, 2H),

2.45 (s, 3H), 4.13 (t, J = 6.82 Hz, 2H), 4.68 (m, 1H), 4.79 (m, 1H), 7.33 (m, 1H), 7.37 (m, 1H), 7.76-7.83 (d, J = 8.34 Hz, 2H).[101]

To a solution of **15** (3.25 g, 3.60 mmol) in anhydrous CH_3CN (3.5 mL) was added a solution of **17** (288 mg, 1.20 mmol) in CH_3CN (0.5 mL) under inert atmosphere and the mixture was allowed to stir at room temperature for 2 h when completion of the reaction was monitored by TLC for disappearance of **17**. The reaction mixture was concentrated by rotary evaporation in vacuum at 40 °C resulting in thick oil that was converted to ammonium (NH_4^+) form by eluting it through 108 mequiv of resin (NH_4^+ form) with ion-exchange buffer followed by lyophilization to result in a white solid. The resulting powder was dissolved in 4 mL of 0.1 M NH_4HCO_3 and extracted with 10 mL of 1:1 (v/v) of isopropanol: CH_3CN (solvent-I). The precipitate formed was separated and redissolved in 3 mL 0.1 M NH_4HCO_3 and extracted with 7 mL of solvent-I. The final extraction was performed with 2 mL of 0.1 M NH_4HCO_3 and 5 mL of solvent-I. Combined extracts were concentrated in vacuum to furnish thick oil that was purified by flash chromatography over cellulose column (3.5 cm × 15 cm) with 4.5:2.5:3 (v/v/v) isopropanol: CH_3CN: 0.1 M NH_4HCO_3 to yield a white solid **11** (195 mg, 65%). **^{1}H NMR** (400 MHz, D_2O): δ 1.65 (s, 3H), 2.37 (t, J = 6.65 Hz, 2H), 3.94 (q, J = 6.68 Hz, 2H); **^{13}C NMR** (100 MHz, D_2O): δ 21.6 (-CH_3), 37.7 (d, $J_{C,P}$ = 7.33 Hz, -CH_2), 64.2 (d, $J_{C,P}$ = 5.87 Hz, O-CH_2), 111.5 (=CH_2), 143.7 (=C); **^{31}P NMR** (162 MHz, D_2O): δ -10.5 (d, J = 21.02 Hz, 1P), -8.2 (d, J = 22.19 Hz, 1P); **HRMS (ESI):** Calcd. for $C_5H_{11}P_2O_7$, $[M-1]^-$ 244.9985, found 244.9989.

3-Methylbut-2-en-1-yl diphosphate ammonium salt, (Dimethylallyl diphosphate, DMAPP) (12):

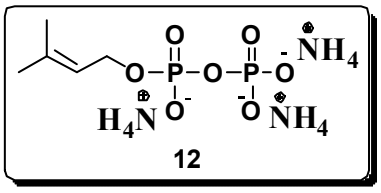

12

To a solution of dimethylallyl alcohol (**18**) (1.72 g, 20 mmol) in dry pentane (25 mL) cooled at -30 °C, was added phosphorus tribromide (PBr_3) (2.16 g, 0.76 mL, 8 mmol) and stirred for 10 min. The product was partitioned between pentane and methanol and pentane layer was concentrated under reduced pressure (taking care of the volatility of the product) to yield **19** (1.96 g, 84%), which was used without further purification for recording spectral data and for the next step (Note: Attempt of purification over silica layers degrades the product). **^{1}H NMR** (200 MHz, $CDCl_3$): δ 1.77 (s, 3H), 1.80 (s, 3H), 4.00 (d, J = 18.46 Hz, 2H), 5.33 (t, J =

8.4 Hz, 1H); **GC-EI-MS**: (*m*/*z*) 150.0 & 148.0 $[M]^+$, 135.0, 132.9, 118.9, 120.9, 92.9, 94.9, 82.0, 79.9, 69.0 (100%), 53.1.

A solution of **15** (2.27 g, 2.52 mmol) in anhydrous CH_3CN (3.5 mL) was treated with a solution of bromide **19** (179 mg, 1.20 mmol) in CH_3CN (0.5 mL) for 2 h. The product was isolated and purified with the same procedure as applied in case of **11** to deliver **12** (204 mg, 67%) as white solid. **^{1}H NMR** (400 MHz, D_2O): δ 1.66 (s, 3H), 1.70 (s, 3H), 4.38 (t, *J* = 6.82 Hz, 2H), 5.39 (tquin, *J* = 1.26, 7.26 Hz, 1H); **^{13}C NMR** (100 MHz, D_2O): δ 17.2 (-CH_3), 24.8 (-CH_3), 62.4 (d, $J_{C,P}$ = 5.39 Hz, O-CH_2), 119.6 (d, *J* = 7.71 Hz, =CH), 139.8 (=C); **^{31}P NMR** (162 MHz, D_2O): δ -10.4 (d, *J* = 22.54 Hz, 1P), -6.7 (d, *J* = 20.81 Hz, 1P); **HRMS (ESI):** Calcd. for $C_5H_{11}P_2O_7$, $[M-1]^-$ 244.9985, found 244.9988.

(*E*)-3,7-Dimethylocta-2,6-dien-1-yl diphosphate ammonium salt, (Geranyl diphosphate, GPP) (13):

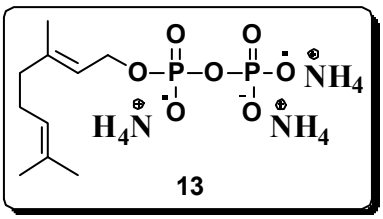

13

The procedure employed for synthesis of **21** was based on a general procedure for the synthesis of allylic chlorides and bromides from corresponding alcohols.[99] A flame-dried, two-neck, 100 mL round bottom flask equipped with a rubber septum, three-way stopcock and a magnetic stirrer was flushed with nitrogen and the inert atmosphere was maintained thought the course of the reaction. N-Chlorosuccinimide (NCS) (2.94 g, 22 mmol) was added to the flask, dissolved in 45 mL of anhydrous CH_2Cl_2 and cooled to -30 °C in an acetonitrile/dry ice bath. Freshly distilled dimethyl sulphide ($(CH_3)_2S$) (1.76 mL, 1.48 g, 24 mmol) was added dropwise by syringe to the cold, well-stirred heterogeneous reaction mixture. The contents of the flask were momentarily allowed to warm to 0 °C and lowered back to -40 °C. A solution of geraniol (**20**) (3.50 mL, 3.08 g, 20 mmol) in anhydrous CH_2Cl_2 (10 mL) was slowly added by syringe to the milky white suspension. The reaction was allowed to warm to 0 °C over 1 h and maintained at that temperature for 1 h. During this period, the mixture became clear and colourless. The ice bath was then removed and the reaction was stirred at room temperature for 15 min before it was quenched with cold brine (25 mL). The aqueous layer was extracted with pentane (2 × 50 mL) and the combined organic layers were washed with cold brine (2 × 20 mL). The organic layer was then dried over anhydrous Na_2SO_4, filtered and concentrated by rotary evaporation

in vacuum to yield **21** as colorless oil (3.11 g, 90.4%). Spectral data was recorded with the isolated product without any purification. **^{1}H NMR** (200 MHz, $CDCl_3$): δ 1.61 (s, 3H), 1.69 (s, 3H), 1.74 (d, *J* = 1.26 Hz, 3H), 2.01-2.16 (m, 4H), 4.11 (d, *J* = 7.93 Hz, 2H), 5.08 (m, 1H), 5.45 (tq, *J* = 1.14, 8.08 Hz, 1H). **GC-EI-MS:** (*m*/*z*) 174.1, 172.1 $[M]^+$, 157.1, 136.1, 128.9, 123.1, 93.0, 69.1 (100%), 53.0.

A solution of **21** (206 mg, 1.20 mmol) in anhydrous CH_3CN (0.5 mL) was added to a well stirred solution of **15** (2.27 g, 2.52 mmol) in anhydrous CH_3CN (3.5 mL) and stirred for 2 h. The product was isolated with the same procedure as applied in case of **11**. Purification over cellulose column (3.5 cm × 11 cm) with 5:2.5:2.5 (v/v/v) isopropanol: CH_3CN: 0.1 M NH_4HCO_3 followed by lyophilisation delivered **13** (273 mg, 71%) as white solid. **^{1}H NMR** (400 MHz, D_2O) δ 1.51 (s, 3H), 1.58 (s, 3H), 1.60 (s, 3H), 1.97-2.07 (m, 4H), 4.36 (t, *J* = 6.52 Hz, 2H), 5.10 (m, 1H), 5.35 (t, *J* = 7.02 Hz, 1H); **^{13}C NMR** (100 MHz, D_2O) δ 142.6 (=C), 133.7 (=C), 124.1 (=CH), 119.9 (d, $J_{C,P}$ = 9.24 Hz, =CH), 62.5 (d, $J_{C,P}$ = 5.39 Hz, O-CH_2), 38.7 (-CH_2), 25.5 (-CH_2), 24.8 (-CH_3), 16.9 (-CH_3), 15.5 (-CH_3); **^{31}P NMR** (162 MHz, D_2O): δ -10.4 (d, *J* = 21.98 Hz, 1P), -6.7 (d, *J* = 21.98 Hz, 1P); **HRMS (ESI)**: Calcd. for $C_{10}H_{19}P_2O_7$ $[M-1]^-$ 313.0611, found 313.0621.

(2*E*,6*E*)-3,7,11-Trimethyldodeca-2,6,10-trien-1-yl diphosphate ammonium salt, ((*E*,*E*)-Farnesyl diphosphate, (*E*,*E*)-FPP) (14):

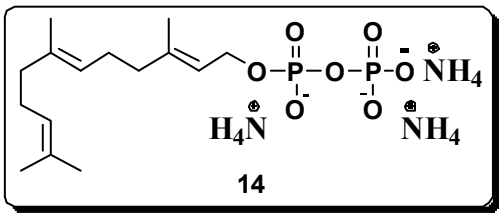

14

Synthesis of (*E*,*E*)-farnesyl chloride (**23**) was accomplished from (*E*,*E*)-farnesol (**22**) in a similar manner as applied in case of **21**. Chlorination of **22** (1.11 g, 5 mmol) furnished **23** (1.16 g, 96%) as colorless oil. **^{1}H NMR** (200 MHz, $CDCl_3$): δ 1.60 (s, 6H), 1.68 (d, *J* = 0.63 Hz, 3H), 1.73 (d, *J* = 1.14 Hz, 3H), 1.98-2.13 (m, 8H), 4.10 (d, *J* = 8.08 Hz, 2H), 5.06-5.12 (m, 2H), 5.41-5.49 (tq, *J* = 1.14, 7.96 Hz, 1H); **GC-EI-MS** (*m*/*z*) 242.1, 240.2 $[M]^+$, 204.2, 189.1, 161.1, 136.1, 119.1, 107.1, 93.0, 69.0 (100%), 55.1.

Diphosphorylation of **23** (640 mg, 2.7 mmol) with **15** (4.8 g, 5.4 mmol) in anhydrous CH_3CN (6 mL) followed by isolation of the product (similar as in case of **11**) and purification by flash chromatography over cellulose column (6 cm × 15 cm) with 5.5:2:1:1.5 (v/v/v/v) isopropanol: $CHCl_3$: CH_3CN: 0.1 M NH_4HCO_3 and lyophilization yielded **14** (698 mg, 68%) as white solid. **^{1}H NMR** (400 MHz, D_2O): δ 5.36 (t, *J* = 6.8

Hz, 1H), 5.06-5.12 (m, 2H), 4.37 (t, *J* = 6.6 Hz, 2H), 1.97-2.08 (m, 6H), 1.92 (m, 2H), 1.62 (s, 3H), 1.58 (s, 3H), 1.51 (s, 6H); **^{13}C NMR** (100 MHz, $CDCl_3$): δ 142.7 (=C), 136.6 (=C), 133.5 (=C), 124.4 (=CH), 124.2 (=CH), 119.8 (d, *J* = 5.40 Hz, =CH), 62.4 (O-CH_2), 38.8 (-CH_2), 38.7 (-CH_2), 25.7 (-CH_2), 25.6 (-CH_2), 24.8 (-CH_3), 16.9 (-CH_3), 15.6 (-CH_3), 15.2 (-CH_3); **^{31}P NMR** (162 MHz, D_2O): δ -10.6 (d, *J* = 22.02 Hz, 1P), -8.2 (d, *J* = 21.02 Hz); **HRMS (ESI):** Calcd. for $C_{15}H_{27}P_2O_7$ $[M-1]^-$ 381.1237, found 381.1249.

4-((Tert-butyldimethylsilyl)oxy)butan-2-one (25):

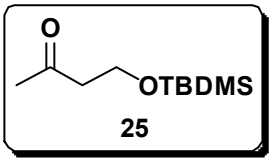

25

To a stirred solution of 4-hydroxy-2-butanone (**24**) (3.52 g, 40 mmol) in anhydrous CH_2Cl_2 (50 mL), Et_3N (5.66 g, 56 mmol) and TBDMSCl (6.63 g, 44 mmol) were added under N_2 atmosphere at 0 °C. After stirring the mixture at room temperature for 3h, it was quenched with brine, extracted with CH_2Cl_2 and dried over anhydrous Na_2SO_4. Silica gel column chromatography (ethyl acetate: pet ether, 15:85) of crude product gave **25** as colorless oil (7.33 g, 91%). **IR** ($CHCl_3$, cm^{-1}): ν_{max} 3020, 1711, 1472, 1215, 1102; **^{1}H NMR** (400 MHz, $CDCl_3$): δ 0.04 (s, 6H), 0.87 (s, 9H), 2.17 (s, 3H), 2.61 (t, *J* = 6.41 Hz, 2H), 3.88 (t, *J* = 6.41 Hz, 2H); **^{13}C NMR** (100 MHz, $CDCl_3$): δ -5.5 (Si-CH_3), 18.2 (-C), 25.8 (-CH_3), 30.8 (-CH_3), 46.5 (-CH_2), 58.8 (O-CH_2), 208.1 (O=C); **GC-EI-MS:** (*m*/*z*) 202.0, 187.1, 145.1 (100%), 131.0, 115.1, 101.1, 75.1; **HRMS (ESI):** Calcd. for $C_{10}H_{22}O_2SiNa$ $[M+Na]^+$ 225.1281, found 225.1286.

4,4-($^2H_2$)-Tert-butyldimethyl((3-methylbut-3-en-1-yl-)oxy)silane ([4,4-$^2H_2$]-26):

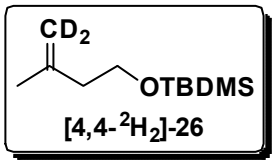

[4,4-$^2H_2$]-26

A flame-dried, 100 mL, three-neck, round-bottomed flask was charged with ($^2H_3$)-methyltriphenylphosphonium iodide (4.92 g, 12.18 mmol) and anhydrous THF (40 mL) under argon atmosphere. The flask contents were cooled to 0 °C and stirred followed by a slow addition of *n*-BuLi (12.18 mmol). The ice bath was removed and the orange suspension containing excess phosphonium salt was stirred at room temperature for 30 min. The reaction mixture was stirred and cooled to 0 °C and a solution of **25** (1.8 g, 8.7 mmol) in anhydrous THF (5 mL) was slowly added by syringe. The reaction mixture was stirred at room temperature for 2 h. The light-orange mixture was hydrolyzed by addition of methanol (0.5 mL) and was concentrated in vacuum to result in slurry. It was diluted

with 200 mL of petroleum ether and the supernatant solution was decanted and filtered through a bed of celite on a Büchner funnel. The solids remaining in the flask were washed with hot petroleum ether (40 °C) (2 × 100 mL) and the supernatant solutions were also filtered through celite. Concentration of the eluate in vacuum provided a clear liquid (1.7 g), which on purification by column chromatography over silica layers (CH_2Cl_2) yielded **[4,4-$^2H_2$]-26** (1.42 g, 78%). **IR** ($CHCl_3$, cm^{-1}): ν_{max} 3019, 2930, 1522, 1438, 1216, 1097; **^{1}H NMR** (400 MHz, $CDCl_3$): δ 0.07 (s, 6H), 0.91 (s, 9H), 1.75 (s, 3H), 2.25 (t, *J* = 7.15 Hz, 2H), 3.72 (t, *J* = 7.02 Hz, 2H); **^{13}C NMR** (100 MHz, $CDCl_3$): δ -5.3 (Si-CH_3), 18.3 (-C), 22.8 (-CH_3), 25.9 (-CH_3), 41.1 (-CH_2), 62.1 (O-CH_2), 142.9 (=C); **GC-EI-MS:** (*m*/*z*) 202.1 $[M]^+$, 187.2, 145.1, 115.1, 101.1 (100%), 89.0, 73.1.

4,4-($^2H_2$)-3-Methylbut-3-en-1-yl-4-methylbenzenesulfonate ([4,4-$^2H_2$]-17):

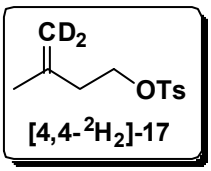

To the solution of **[4,4-$^2H_2$]-26** (0.505 g, 2.5 mmol) in THF (15 mL) was added TBAF (3.0 mmol) at room temperature under argon. The reaction was stirred for 1 h. The solution was concentrated under reduced pressure (not lower than 150 mmHg) and the residue was dissolved in CH_2Cl_2 (10 mL) and treated with CaH_2 (0.67g, 16 mmol) under argon. After stirring for 15 min, DMAP (32.5 mg, 0.27 mmol) and TsCl (0.49 g, 2.6 mmol) were added to the reaction mixture. The resulting solution was stirred for 3 h and thereafter, quenched with brine (5 mL). The organic layer was separated and the aqueous layer was extracted with CH_2Cl_2 (2 × 25 mL). The combined organic layer was washed with brine (20 mL), dried over anhydrous Na_2SO_4 and concentrated under reduced pressure to give yellow oil. This crude product was purified by silica gel column chromatography in CH_2Cl_2 to yield **[4,4-$^2H_2$]-17** (0.45 g, 74%). **IR** ($CHCl_3$, cm^{-1}): ν_{max} 3020, 2974, 1599, 1441, 1216, 1097; **^{1}H NMR** (400 MHz, $CDCl_3$): δ 1.66 (s, 3H), 2.35 (t, *J* = 6.77 Hz, 2H), 2.45 (s, 3H), 4.13 (t, *J* = 6.9 Hz, 2H), 7.35 (d, *J* = 8.03 Hz, 2H), 7.80 (d, *J* = 8.28 Hz, 2H); **^{13}C NMR** (100 MHz, $CDCl_3$): δ 21.6 (-CH_3), 22.3 (-CH_3), 36.7 (-CH_2), 68.5 (O-CH_2), 127.9 (=CH), 129.8 (=CH), 133.1 (=C), 140.0 (=C), 144.7 (=C); **GC-EI-MS:** (*m*/*z*) 242.0 (M^+), 185.0, 207.1, 173.1, 155.0, 91.1 (100%), 69.1; **HRMS (ESI):** Calcd. for $C_{12}H_{14}{}^2H_2O_3SNa$ $[M+Na]^+$ 265.0836, found 265.0827.

4,4-($^2H_2$)-3-Methylbut-3-enyl diphosphate trisammonium salt ([4,4-$^2H_2$]-11):

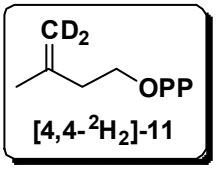

[4,4-$^2H_2$]-11

To a solution of **[4,4-$^2H_2$]-17** (0.18 g, 0.72 mmol) in dry CH_3CN (5 mL), was added **15** (1.92 g, 2.13 mmol) at room temperature. The resulting solution was allowed to stir for 2h. The reaction was worked up as per Davisson *et al*. as demonstrated in the preparation of **11**. Purification by flash chromatography on a cellulose column (2.5 cm × 23 cm) with 5:2.5:2.5 (v/v/v), isoproanol: CH_3CN: 0.l M NH_4HCO_3 yielded **[4,4-$^2H_2$]-11** (0.11 g, 49%) as white powder. **^{1}H NMR** (400 MHz, D_2O): ^2H > 95%, δ 1.65 (s, 3H), 2.27 (t, *J* = 6.65 Hz, 2H), 3.94 (m, 2H); **^{13}C NMR** (100 MHz, D_2O): δ 21.5 (-CH_3), 37.8 (-CH_2), 64.0 (O-CH_2), 143.7 (=C); **^{31}P NMR** (162 MHz, D_2O): δ -10.59 (d, *J* = 21.02 Hz), -7.18 (d, *J* = 22.19 Hz); **HRMS (ESI)**: Calcd. for $C_5H_9{}^2H_2P_2O_7$ $[M-1]^-$ 247.0111, found 247.0111.

2,2-($^2H_2$)-Ethyl-3-oxobutanoate ([2,2-$^2H_2$]-27):

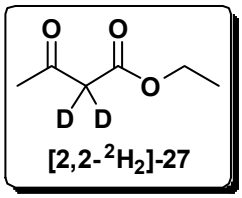

[2,2-$^2H_2$]-27

Ethyl acetoacetate (**27**) (4.0 g, 4.1 mL, 30.77 mmol) was stirred with D_2O (12 mL) for 24 h. The sample was extracted with diethyl ether and concentrated under reduced pressure. The above procedure was repeated with the concentrate to give **[2,2-$^2H_2$]-27** (3.74 g, 92%) as colorless oil. NMR analysis indicated 95% exchange of ^1H for ^2H at the activated methylene position. **^{1}H NMR** (500 MHz, $CDCl_3$): δ 1.29 (t, *J* = 7.02 Hz, 3H), 2.28 (s, 3H), 4.18-4.23 (q, *J* = 7.02 Hz, 2H); **^{13}C NMR** (125 MHz, $CDCl_3$): δ 14.0 (-CH_3), 30.0 (-CH_3), 61.3 (O-CH_2), 167.0 (O=C), 200.6 (O=C); **GC-EI-MS:** (*m*/*z*) 132.0 $[M]^+$, 115.1, 102.1, 88.1, 85.1, 69.0, 60.1, 43.1 (100%).

2,2-($^2H_2$)-Butane-1,3-diol ([2,2-$^2H_2$]-28):

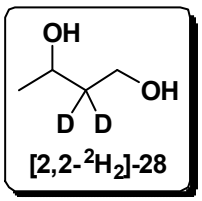

[2,2-$^2H_2$]-28

DIBAH (80 mmol) was added to a stirred solution of **[2,2-$^2H_2$]-27** (2.64 g, 20 mmol) in anhydrous CH_2Cl_2 (50 mL) at 0 ^oC under inert atmosphere. The resulting solution was stirred for 5 h before quenching with saturated aqueous potassium sodium tartrate (10 mL). The resultant compound was washed with CH_2Cl_2 and the combined washings were dried over anhydrous Na_2SO_4 and concentrated. Silica gel column chromatography (ethyl acetate: pet ether, 1:1) of crude product gave **[2,2-$^2H_2$]-28** as colorless oil (1.40 g, 76%). **^{1}H NMR** (200 MHz, $CDCl_3$): δ 1.23 (d, *J* = 6.19 Hz, 3H), 3.76-3.90 (m, 2H), 4.01-4.10

(q, *J* = 5.9 Hz, 1H); **GC-EI-MS**: (*m*/*z*) 92.1 $[M]^+$, 77.1, 74.0, 59.0, 47.0, 45.0, 43.1 (100%).

3,3-($^2H_2$)-4-((Tert-butyldimethylsilyl)oxy)butan-2-ol ([2,2-$^2H_2$]-29):

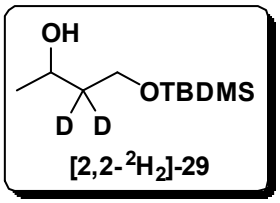

To a stirred and cooled solution of **[2,2-$^2H_2$]-28** (0.46 g, 5 mmol) in anhydrous CH_2Cl_2 (5 mL) was added Et_3N (1.4 mL, 10 mmol) and TBDMS-Cl (0.75 g, 5 mmol) under inert atmosphere. After stirring for 2 h, the reaction was quenched with cold brine, extracted with CH_2Cl_2, dried over anhydrous Na_2SO_4 and concentrated to yield the crude product. Purification by silica gel column chromatography (ethyl acetate: pet ether, 15:85) yielded **[2,2-$^2H_2$]-29** (0.90 g, 88%) as colorless oil. **^{1}H NMR** (400 MHz, $CDCl_3$): δ 0.08 (s, 6H), 0.90 (s, 9H), 1.20 (d, *J* = 6.28 Hz, 3H), 3.80 (d, *J* = 10.2 Hz, 1H), 3.89 (d, *J* = 10.1 Hz, 1H), 4.02 (q, *J* = 6.02 Hz, 1H); **^{13}C NMR** (100 MHz, $CDCl_3$): δ -5.63 (Si-CH_3), -5.58 (Si-CH_3), 18.1 (-C), 23.3 (-CH_3), 25.8 (-CH_3), 62.7 (O-CH_2), 68.2 (O-CH); **GC-EI-MS:** (*m*/*z*) 206.2 $[M]^+$, 191.2, 149.1, 131.1, 117.1, 105.1, 75.0 (100%), 57.0, 45.0.

3,3-($^2H_2$)-4-((Tert-butyldimethylsilyl)oxy)butan-2-one ([2,2-$^2H_2$]-25):

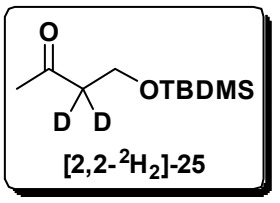

Dess-Martin Periodinane reagent (1.27 g, 3 mmol) was added to a solution of **[2,2-$^2H_2$]-29** (0.21 g, 1 mmol) in anhydrous CH_2Cl_2 (10 mL) and was stirred for 3 h at room temperature. The reaction mixture was then directly filtered through celite bed to give the crude product which was further purified by silica gel column chromatography (ethyl acetate: pet ether, 1:19) to get **[2,2-$^2H_2$]-25** (0.185g, 91%). **^{1}H NMR** (400 MHz, $CDCl_3$): δ 0.05 (s, 6H), 0.88 (s, 9H), 2.19 (s, 3H), 3.88 (s, 2H); **^{13}C NMR** (100 MHz, $CDCl_3$): δ -5.5 (Si-CH_3), 18.2 (-C), 25.8 (-CH_3), 30.9 (-CH_3), 58.8 (O-CH_2).

2,2-($^2H_2$)-Tert-butyldimethyl((3-methylbut-3-en-1-yl)oxy)silane ([2,2-$^2H_2$]-26):

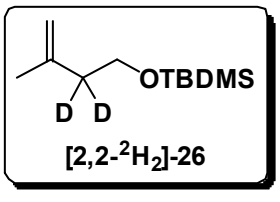

Methyltriphenylphosphonium iodide (502 mg, 1.25 mmol) was dissolved in anhydrous THF (5 mL) and cooled to 0 °C under inert atmosphere prior to the slow addition of *n*-BuLi (0.82 mmol). The resulting orange suspension was stirred at room temperature for 30 min and again cooled to 0 °C before slow addition of ketone (**[2,2-**

$^{2}H_2$]-25) (153 mg, 0.75 mmol) dissolved in anhydrous THF (2 mL). The mixture was stirred at room temperature for 2 h and the progress of the reaction was monitored by TLC. On completion, the reaction was quenched by addition of methanol (0.2 mL). Most of the solvent was removed on rotary evaporator until slurry was obtained. This was diluted with petroleum ether (50 mL); supernatant solution was decanted and filtered through celite. The solids remaining in the flask were washed with hot petroleum ether (~40 °C) (3 × 100 mL) and the supernatant solutions were also filtered through celite. Evaporation of the combined filtrate provided clear liquid, which on purification by column chromatography (CH_2Cl_2) yielded the Wittig product **[2,2-$^{2}H_2$]-26** (0.11 g, 72%). **^{1}H NMR** (400 MHz, $CDCl_3$): δ 0.05 (s, 6H), 0.89 (s, 9H), 1.74 (s, 3H), 3.70 (s, 2H), 4.70 (m, 1H), 4.76 (m, 1H); **^{13}C NMR** (100 MHz, $CDCl_3$): δ -5.3 (Si-CH_3), 18.3 (-C), 22.8 (-CH_3), 25.9 (-CH_3), 62.1 (O-CH_2), 111.5 (=CH_2), 143.1 (=CH).

2,2-($^{2}H_2$)-3-methylbut-3-en-1-yl- 4-methylbenzenesulfonate ([2,2-$^{2}H_2$]-17):

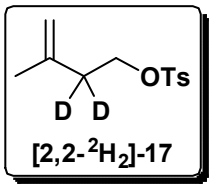

[2,2-$^{2}H_2$]-17

A solution of **[2,2-$^{2}H_2$]-26** (105 mg, 0.52 mmol) in THF (5 mL) was treated with TBAF (0.63 mmol) for 1 h at room temperature. The solution was concentrated under reduced pressure (not lower than 150 mbar) to deliver **[2,2-$^{2}H_2$]-16** that was confirmed by GC-EI-MS. The concentrate, **[2,2-$^{2}H_2$]-16** was dissolved in anhydrous CH_2Cl_2 (10 mL) and treated with CaH_2 (130 mg, 3.1 mmol) at 0 °C under inert atmosphere. After stirring for 15 min, DMAP (6 mg, 0.05 mmol) and Ts-Cl (0.12 g, 0.62 mmol) were added to the reaction mixture at 0 °C. The resulting solution was stirred at room temperature for 3 h and quenched with cold brine (20 mL). The aqueous layer was extracted with CH_2Cl_2 (2 × 25 mL) and the combined organic layer was washed with brine (20 mL), dried over anhydrous Na_2SO_4 and concentrated in vacuum to give yellow oil. This crude product was purified by silica gel column chromatography (CH_2Cl_2) to yield **[2,2-$^{2}H_2$]-17** (0.110g, 89%). **^{1}H NMR** (400 MHz, $CDCl_3$): δ 1.66 (s, 3H), 2.45 (s, 3H), 4.12 (s, 2H), 4.68 (m, 1H), 4.79 (m, 1H), 7.35 (d, *J* = 8.28 Hz, 2H), 7.80 (d, *J* = 8.28 Hz, 2H); **^{13}C NMR** (100 MHz, $CDCl_3$): δ 21.6 (-CH_3), 22.3 (-CH_3), 68.4 (O-CH_2), 113.2 (=CH_2), 127.9 (=CH), 129.8 (=CH), 144.7 (=C).

2,2-($^2H_2$)-3-methylbut-3-en-1-yl diphosphate trisammonium salt ([2,2-$^2H_2$]-11):

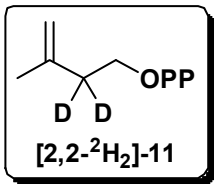

[2,2-$^2H_2$]-11

To a solution of **15** (1.65 g, 1.83 mmol) in anhydrous CH_3CN (3 mL) was added a solution of **[2,2-$^2H_2$]-17** (150 mg, 0.61 mmol) in CH_3CN (0.5 mL) under inert conditions. The resulting solution was allowed to stir for 2 h. The diphosphate product was obtained according to Davisson *et al*. protocol as demonstrated in the synthesis of **11**. Purification by flash chromatography on cellulose column (2.5 cm × 23 cm) with 5:2.5:2.5 (v/v/v) isopropanol: CH_3CN: 0.1 M NH_4HCO_3 yielded **[2,2-$^2H_2$]-11** (0.10 g, 54%) as white solid. **^{1}H NMR** (400 MHz, D_2O): δ 1.62 (s, 3H), 3.90 (d, *J* = 6.02 Hz, 2H); **^{13}C NMR** (100 MHz, D_2O): δ 21.5 (-CH_3), 63.9 (O-CH_2), 111.5 (=CH_2), 143.7 (=C); **^{31}P NMR** (162 MHz, D_2O): δ -10.40 (d, *J* = 22.39 Hz), -6.48 (d, *J* = 21.15 Hz); **HRMS (ESI)**: Calcd. for $C_5H_9{}^2H_2P_2O_7$ $[M-1]^-$ 247.0111, found 247.0116.

3-((Tert-butyldimethylsilyl)oxy)propan-1-ol (31):

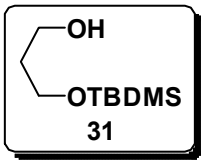

31

To a stirred solution of 1,3-propane diol (**30**) (3.04 g, 40 mmol) in anhydrous CH_2Cl_2 (90 mL) cooled at 0 °C under inert atmosphere was added Et_3N (8.08 g, 80 mmol) followed by TBDMS-Cl (6.04 g, 40 mmol). The reaction was stirred at room temperature for 3 h and the progress was monitored by TLC. On completion, the reaction was quenched with cold brine (30 mL), organic layer separated and aqueous part extracted with CH_2Cl_2 (2 × 40 mL). Combined organic extracts were dried over anhydrous Na_2SO_4 and concentrated in vacuum. Silica gel column chromatography (ethyl acetate: hexane, 3:17) of crude product gave **31** as colorless oil (6.89 g, 91%). **IR** ($CHCl_3$, cm^{-1}): ν_{max} 3489, 3019, 1423, 1215, 1062; **^{1}H NMR** (400 MHz, $CDCl_3$): δ 0.06 (s, 6H), 0.88 (s, 9H), 1.73-1.79 (m, 2H), 2.81 (bs, 1H), 3.78 (bs, 2H), 3.81 (t, *J* = 5.66 Hz, 2H); **^{13}C NMR** (100 MHz, $CDCl_3$): δ -5.6 (-CH_3), 18.1(-C), 25.8(-CH_3), 34.2(-CH_2), 62.1(-CH_2), 62.7(-CH_2); **HRMS (ESI)**: Calcd. for $C_9H_{23}O_2Si$ $[M+H]^+$ 191.1462, found 191.1463.

3-((Tert-butyldimethylsilyl)oxy)propanal (32):

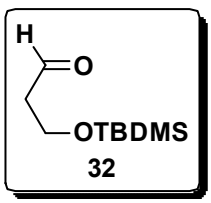

32

A mixture of **31** (2.85 g, 15 mmol) and IBX (12.51 g, 45 mmol) was refluxed in ethyl acetate (50 mL) for 3 h. After completion of the reaction (monitored by TLC), contents were directly filtered through celite and the crude product obtained was further purified by silica gel

column chromatography (ethyl acetate: pet ether, 1:19) to fetch **32** (2.61 g, 91.2%). **IR** ($CHCl_3$, cm^{-1}): ν_{max} 3020, 1721, 1472, 1215, 1103; **^{1}H NMR** (500 MHz, $CDCl_3$): δ 0.07 (s, 6H), 0.89 (s, 9H), 2.60 (td, J = 2.14, 6.10 Hz, 2H), 3.99 (t, J = 6.10 Hz, 2H), 9.81 (t, J = 1.99 Hz, 1H); **^{13}C NMR** (125 MHz, $CDCl_3$): δ -5.5 (-CH_3), 18.2 (-C), 25.8 (-CH_3), 46.6 (-CH_2), 57.4 (-CH_2), 202.0 (-C=O); **HRMS (ESI):** Calcd. for $C_9H_{20}O_2SiK$ $[M+K]^+$ 227.0864, found 227.1077.

1,1,1-($^2H_3$)-4-((Tert-butyldimethylsilyl)oxy)butan-2-ol ([1,1,1-$^2H_3$]-29):

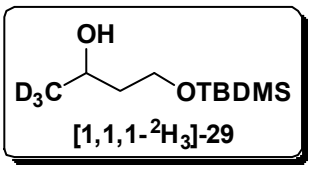

In a flame dried, three necked round bottomed flask equipped for magnetic stirring, was added anhydrous THF (40 mL) and CD_3MgI (2.1 mmol) under inert atmosphere and was stirred well and cooled to 0 °C prior to slow addition of **32** (3.76 g, 2 mmol) dissolved in anhydrous THF (10 mL). The reaction was allowed to stir for 2 h at room temperature and the progress was monitored by TLC. On completion, the reaction was quenched by cold saturated NH_4Cl solution (15 mL), THF was evaporated in vacuum and the product was extracted in ethyl acetate (2 × 25 mL), dried over anhydrous Na_2SO_4 and concentrated to get thick oil that was subsequently subjected to purification by column chromatography over silica layers (ethyl acetate: pet ether, 3:17) to obtain **[1,1,1-$^2H_3$]-29** (2.6 g, 67%). **IR** ($CHCl_3$, cm^{-1}): ν_{max} 3480, 3018, 2956, 1471, 1216, 1080; **^{1}H NMR** (400 MHz, $CDCl_3$): δ 0.08 (s, 6H), 0.90 (s, 9H), 1.58-1.73 (m, 2H), 3.45 (s, 1H), 3.79-3.84 (m, 1H), 3.87-3.92 (m, 1H), 4.01 (d, J = 7.78 Hz, 1H); **^{13}C NMR** (100 MHz, $CDCl_3$): δ -5.63 (Si-CH_3), -5.57 (Si-CH_3), 18.1 (-C), 25.8 (-CH_3), 39.8 (-CH_2), 62.8 (O-CH_2), 68.2 (O-CH_2); **HRMS (ESI):** Calcd. for $C_{10}H_{21}{}^2H_3O_2SiNa$ $[M+Na]^+$ 230.1623, found 230.1624.

1,1,1-($^2H_3$)-4-((Tert-butyldimethylsilyl)oxy)butan-2-one ([1,1,1-$^2H_3$]-25):

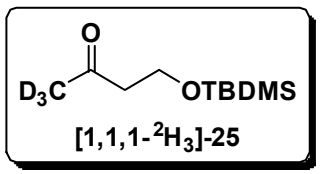

A solution of **[1,1,1-$^2H_3$]-29** (0.62 g, 3.02 mmol) and IBX (0.83 g, 9.06 mmol) in ethyl acetate (15 mL) was refluxed for 3 h under inert conditions. Reaction's completion was monitored by TLC followed by direct filtration of the reaction contents through celite to give the crude product, which was later purified by column chromatography over silica layers (ethyl acetate: pet ether, 1:19) to give **[1,1,1-$^2H_3$]-25** (0.57 g, 92%). **IR** ($CHCl_3$, cm^{-1}): ν_{max} 3019, 2957, 1707, 1473, 1216, 1101; **^{1}H NMR** (400 MHz, $CDCl_3$): δ 0.05 (s,

6H), 0.87 (s, 9H), 2.62 (t, J = 6.41 Hz, 2H), 3.88 (t, J = 6.41 Hz, 2H); **^{13}C NMR** (100 MHz, $CDCl_3$): δ -5.5 (Si-CH_3), 18.2 (-C), 25.8 (-CH_3), 46.5 (-CH_2), 58.8 (O-CH_2), 208.3 (O=C); **HRMS (ESI)**: Calcd. for $C_{10}H_{19}{}^2H_3O_2SiNa$ $[M+Na]^+$ 228.1467, found 228.1475.

Tert-butyldimethyl((3-(^{2}H$_3$-methyl)but-3-en-1-yl)oxy)silane ([5,5,5-^{2}H$_3$]-26):

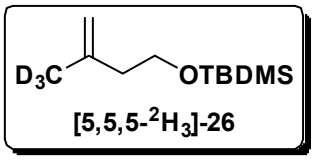

In a flame dried three-necked round-bottomed flask equipped for magnetic stirring, *n*-BuLi (4.55 mmol) was slowly added under inert atmosphere to a well stirred and cooled (0 °C) solution of methyltriphenylphosphonium iodide (3 g, 6.1 mmol) in anhydrous THF (20 mL). The resultant orange suspension was stirred at room temperature for 30 min and again cooled to 0 °C before a solution of ketone, **[1,1,1-^{2}H$_3$]-25** (1.1 g, 4.35 mmol) in anhydrous THF (5 mL) was slowly added *via* syringe. The reaction mixture was stirred at room temperature for 2 h before it was quenched by addition of methanol (0.5 mL). The solvent was removed on a rotary evaporator until slurry resulted. This was diluted with petroleum ether (150 mL) and the supernatant solution was decanted and filtered through celite. The solids remaining in the flask were washed with hot petroleum ether (40 °C) (2 × 50 mL) and the supernatant solutions were also filtered through celite. The combined filtrate was concentrated in vacuum to provide clear liquid, which on subsequent purification by silica gel column chromatography (CH_2Cl_2) yielded the Wittig product **[5,5,5-^{2}H$_3$]-26** (0.77 g, 70%). **IR** ($CHCl_3$, cm^{-1}): ν_{max} 3019, 2927, 1522, 1423, 1215, 1046; **^{1}H NMR** (400 MHz, $CDCl_3$): δ 0.06 (s, 6H), 0.90 (s, 9H), 2.25 (td, J = 0.92, 6.87 Hz, 2H), 3.88 (t, J = 6.41 Hz, 2H); **^{13}C NMR** (100 MHz, $CDCl_3$): δ -5.3 (Si-CH_3), 18.3 (-C), 25.9 (-CH_3), 41.1 (-CH_2), 62.1 (O-CH_2), 111.5 (=CH_2), 143.0 (=C).

3-(^{2}H$_3$-methyl)but-3-en-1-yl,4-methylbenzenesulfonate ([5,5,5-^{2}H$_3$]-17):

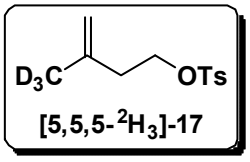

A solution of **[5,5,5-^{2}H$_3$]-26** (0.508 g, 2.5 mmol) in THF (15 mL) was treated with TBAF (5 mmol) at room temperature for 1 h. The solution was concentrated under reduced pressure (not lower than 150 mmHg) and the concentrate was dissolved in anhydrous CH_2Cl_2 (10 mL) followed by treatment with CaH_2 (67.2 mg, 16 mmol) at 0 °C under inert atmosphere. After stirring for 15 min, DMAP (32.5 mg, 0.25 mmol) and Ts-Cl (492 mg, 2.6 mmol) were added to the reaction mixture at 0 °C. The reaction mixture (monitored by TLC) was

stirred at room temperature for 3 h and thereafter, quenched with cold brine (5 mL). The mixture was partitioned between CH_2Cl_2 (2 × 25 mL) and water (20 mL). The organic layer was washed with brine (20 mL), dried over anhydrous Na_2SO_4 and concentrated in vacuum to give yellow oil. This crude product was purified by silica gel column chromatography in CH_2Cl_2 to yield **[5,5,5-$^2H_3$]-17** (0.47 g, 77%). **^{1}H NMR** (400 MHz, $CDCl_3$): δ 2.35 (t, *J* = 6.87 Hz, 2H), 2.45 (s, 3H), 4.13 (t, *J* = 6.87 Hz, 2H), 4.68 (q, *J* = 1.26 Hz, 1H), 4.79 (s, 1H), 7.35 (d, *J* = 7.93 Hz, 2H), 7.80 (d, *J* = 8.24 Hz, 2H); **^{13}C NMR** (100 MHz, $CDCl_3$): δ 21.6 (-CH_3), 36.7 (-CH_2), 68.5 (O-CH_2), 113.1 (=CH_2), 127.9 (=CH), 129.8 (=CH), 133.1 (=C), 140.0 (=C), 144.7 (=C); **GC-EI-MS:** (*m*/*z*) 243.1 $[M]^+$, 226.1, 195.0, 174.1, 155.1, 91.1, 71.2 (100%); **HRMS (ESI)**: calcd. for $C_{12}H_{13}{}^2H_3O_3SNa$ $[M+Na]^+$ 266.0898, found 266.0890.

1-(3-($^2H_3$-methyl)but-3-en-1-yl)diphosphate trisammonium salt ([5,5,5-$^2H_3$]-11):

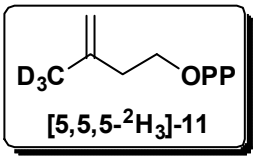

To a solution of **15** (1.8 g, 2.01 mmol) in anhydrous CH_3CN (3 mL) was added a solution of **[5,5,5-$^2H_3$]-17** (165 mg, 0.67 mmol) in anhydrous CH_3CN (0.5 mL) under inert conditions. The resulting solution was allowed to stir for 2 h. The diphosphate product was obtained according to Davisson *et al*. protocol as demonstrated in the synthesis of **11**. Purification by flash chromatography on cellulose column (2.5 cm × 23 cm) with 5:2.5:2.5 (v/v/v) isopropanol: CH_3CN: 0.l M NH_4HCO_3 yielded **[5,5,5-$^2H_3$]-11** (103 mg, 51%) as white powder. **^{1}H NMR** (400 MHz, D_2O): (^{2}H > 95%), δ 2.28 (t, *J* = 6.4 Hz, 2H), 3.94 (m, 2H); **^{13}C NMR** (100 MHz, D_2O): δ 37.8 (-CH_2), 64.1 (O-CH_2), 111.5 (=CH_2), 143.8 (=C); **^{31}P NMR** (162 MHz): δ -10.58 (d, *J* = 21.02 Hz), -7.32 (d, *J* = 19.85 Hz); **HRMS (ESI)**: calcd. for $C_5H_8{}^2H_3P_2O_7$ $[M-1]^-$ 248.0174, found 248.0163.

4,4-($^2H_2$)-Tert-butyldimethyl((3-($^2H_3$-methyl)but-3-en-1-yl-)oxy)silane ([4,4,5,5,5-$^2H_5$]-26):

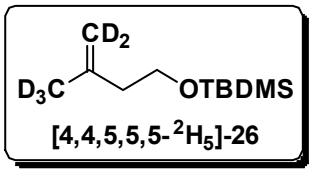

n-BuLi (9.1 mmol) was slowly added under argon atmosphere to a stirred solution of (1,1,1-$^2H_3$-methyl)triphenylphosphonium iodide (5 g, 12.21 mmol) in anhydrous THF (20 mL) at 0 °C. The resulting orange suspension was stirred at room temperature for 30 min and again cooled to 0 °C when a solution of ketone **[1,1,1-$^2H_3$]-25** (1.8 g, 8.7 mmol) in THF (5 mL) was gradually added *via* syringe. The reaction

mixture was stirred at room temperature for 2 h before it was quenched by adding methanol (0.5 mL). Following a similar work up procedure as employed in the synthesis of **[5,5,5-$^2H_3$]-26** delivered the Wittig product **[4,4,5,5,5-$^2H_5$]-26** (1.42 g, 78%). **IR** ($CHCl_3$, cm^{-1}): ν_{max} 2930, 2895, 1607, 1472, 1255, 1102; **^{1}H NMR** (400 MHz, $CDCl_3$): δ 0.06 (s, 6H), 0.90 (s, 9H), 2.24 (t, *J* = 6.41 Hz, 2H), 3.72 (t, *J* = 6.41 Hz, 2H); **^{13}C NMR** (100 MHz, $CDCl_3$): δ -5.3 (Si-CH_3), 18.3 (-C), 25.9 (-CH_3), 41.0 (-CH_2), 62.1 (O-CH_2), 142.8 (=C).

4,4-($^2H_2$)3-($^2H_3$-methyl)but-3-en-1-yl-4-methylbenzenesulfonate ([4,4,5,5,5-$^2H_5$]-17):

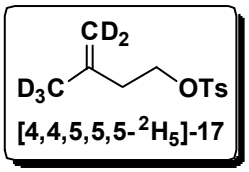

A solution of **[4,4,5,5,5-$^2H_5$]-26** (513 mg, 2.5 mmol) in THF (15 mL) was trerated with TBAF (5 mmol) at room temperature for 1 h. After completion of the desilylation reaction, the solution was concentrated under reduced pressure (not lower than 150 mmHg). The concentrate was dissolved in anhydrous CH_2Cl_2 (10 mL) and treated with CaH_2 (67.2 mg, 16 mmol) at 0 °C under inert atmosphere. After stirring for 15 min, DMAP (32.5 mg, 0.26 mmol) and Ts-Cl (492 mg, 2.6 mmol) were added to the reaction mixture at 0 °C. The reaction was stirred at room temperature for 3 h and monitored by TLC. On completion, it was quenched with cold brine (5 mL) and the mixture was partitioned between CH_2Cl_2 (2 × 25 mL) and water (20 mL). The combined organic layer was washed with brine (20 mL), dried over anhydrous Na_2SO_4 and concentrated in vacuum to give yellow oil. Purification of this crude product by silica gel column chromatography (CH_2Cl_2) yielded **[4,4,5,5,5-$^2H_5$]-17** (43.2 mg, 72%). **^{1}H NMR** (500 MHz, $CDCl_3$): δ 2.35 (t, *J* = 6.87 Hz, 2H), 2.45 (s, 3H), 4.13 (t, *J* = 6.87 Hz, 2H), 7.35 (d, *J* = 7.93 Hz, 2H), 7.80 (d, *J* = 8.24 Hz, 2H); **^{13}C NMR** (125 MHz, $CDCl_3$): δ 21.6 (-CH_3), 36.6 (-CH_2), 68.5 (O-CH_2), 127.9 (=CH), 129.8 (=CH), 133.2 (=C), 139.9 (=C), 144.7 (=C); **GC-EI-MS**: (*m*/*z*) 245.3 $[M]^+$, 207.1, 185.0, 174.1, 155.1, 91.1, 73.2 (100%); **HRMS (ESI)**: Calcd. for $C_{12}H_{11}{}^2H_5O_3SNa$ $[M+Na]^+$ 268.1021, found 268.1018.

4,4-($^2H_2$)-1-((3-$^2H_3$-methyl)but-3-en-1-yl)diphosphate trisammonium salt ([4,4,5,5,5-$^2H_5$]-11):

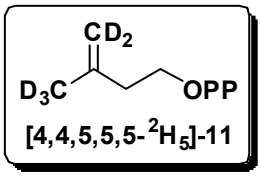

To a solution of **15** (1.92 g, 2.13 mmol) in anhydrous CH_3CN (3 mL) was added a solution of **[4,4,5,5,5-$^2H_5$]-17** (176 mg, 0.71 mmol) in anhydrous CH_3CN (0.5 mL) under inert conditions. The

resulting solution was allowed to stir for 2 h following the work up of the diphosphate product according to Davisson *et al*. protocol as demonstrated in synthesis of **11**. Purification by flash chromatography on cellulose column (2.5 cm × 23 cm) with 5:2.5:2.5 (v/v/v) isopropanol: CH_3CN: 0.1 M NH_4HCO_3 fetched **[4,4,5,5,5-$^2H_5$]-11** (105 mg, 49%) as white powder. **^{1}H NMR** (400 MHz, D_2O): ^2H > 95%, δ 2.27 (t, *J* = 6.65 Hz, 2H), 3.94 (m, 2H); **^{13}C NMR** (100 MHz, D_2O): δ 37.3 (-CH_2), 64.0 (O-CH_2), 143.6 (=C); **^{31}P NMR** (162 MHz, D_2O): δ -10.52 (d, *J* = 22.19 Hz), -6.95 (d, *J* = 21.02 Hz); **HRMS (ESI)**: calcd. for $C_5H_6{}^2H_5P_2O_7$ $[M-1]^-$ 250.0299, found 250.0300.

(*E*)-3,7-dimethylocta-2,6-dienal (33):

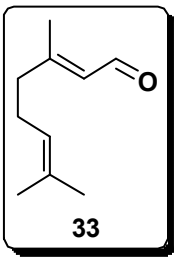

33

In a 100 mL round-bottomed flask fixed with condenser and equipped for magnetic stirring was refluxed a solution of geraniol (**20**) (1.54 g, 10 mmol) and IBX (5.56 g, 20 mmol) in ethyl acetate (50 mL) for 3 h. Progress of the reaction was monitored by TLC and on completion, the mixture was directly filtered through celite bed to give a crude product. Further purification by column chromatography over silica layers (ethyl acetate: pet ether, 1:19) gave the oxidized product, **33** (1.47 g, 96%).

(*E*)-3,7-dimethylocta-2,6-dien-1-^{2}H-1-ol ([1-^{2}H]-20):

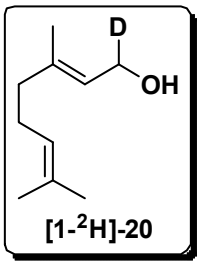

[1-^{2}H]-20

A flame-dried, 50 mL, two-necked, round-bottomed flask was charged with $LiAlD_4$ (0.29 g, 7 mmol) followed by anhydrous THF (8 mL) and the suspension was stirred and cooled to 0 °C. To this was gradually added, a solution of **33** (1.06 g, 7 mmol) in THF (2 mL) and the reaction was stirred at room temperature for 2 h. On completion (monitored by TLC) the reaction was quenched by slow addition of ethyl acetate (6 mmol) at 0 °C until the evolution of hydrogen stopped. 10% aqueous NaOH was added drop by drop to this until the grey colour of the reaction turned to white and stirring was continued for 15 min at room temperature. The mixture was then dried over anhydrous Na_2SO_4 and passed through celite, which was repeatedly washed with ethyl acetate (3 × 20 mL). The combined ethyl acetate fractions were concentrated at reduced pressure and the crude product was chromatographed over silica gel (ethyl acetate: pet ether, 1:9) to give **[1-^{2}H]-20** (0.95 g, 89%). **^{1}H NMR** (200 MHz, $CDCl_3$): δ 1.61 (s, 3H), 1.69 (s, 6H), 2.00-2.09 (m, 4H), 4.11-4.18 (m, 1H), 5.06-5.13 (m, 1H), 5.42 (d, *J* =6.19 Hz, 1H).

1-^{2}H-(*E*)-3,7-dimethylocta-2,6-dienal ([1-^{2}H]-33):

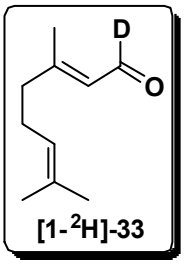

To a solution of **[1-^{2}H]-20** (0.62g, 4 mmol) in anhydrous CH_2Cl_2 cooled to 0 °C was added PDC (1.54 g, 10 mmol). The reaction mixture was allowed to stir for 2 h and progress of the reaction was monitored by TLC. On completion, the mixture was directly filtered through celite bed, dried over anhydrous Na_2SO_4, to give a crude product. Further purification by column chromatography over silica layers (ethyl acetate: pet ether, 1:19) gave the oxidized product, **[1-^{2}H]-33** (0.49 g, 81%). **^{1}H NMR** (200 MHz, $CDCl_3$): δ 1.61 (s, 3H), 1.69 (s, 3H), 2.17 (d, *J* = 1.14 Hz, 3H), 2.23 (m, 4H), 5.03-5.10 (m, 1H), 5.88 (s, 1H).

(*E*)-3,7-dimethylocta-2,6-dien-1,1-^{2}H$_2$-1-ol ([1,1-^{2}H$_2$]-20):

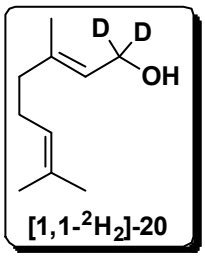

To a flame-dried two neck round-bottomed flask, $LiAlD_4$ (0.14 g, 3.2 mmol) and anhydrous THF (5 mL) were added and the suspension was stirred and cooled to 0 °C. To this was slowly added a solution of **[1-^{2}H]-33** (0.490 g, 3.20 mmol) in anhydrous THF (2 mL). The reaction mixture was allowed to warm to room temperature and stirred for 2 h. The reaction was quenched by adding ethyl acetate (3 mmol) at 0 °C until the evolution of hydrogen stopped followed by dropwise addition of 10% aqueous NaOH and vigorous stirring until the grey coloured reaction mixture became white thick suspension and was continued to stir for 15 min at room temperature. THF was evaporated on rotary evaporator and resultant thick gel was washed with ethyl acetate (3 × 10 mL), dried over anhydrous Na_2SO_4, filtered through celite and concentrated in vacuum to yield the crude product. Chromatographic purification over silica layers (ethyl acetate: pet ether, 1:9) afforded **[1,1-^{2}H$_2$]-20** (0.43 g, 87%). **^{1}H NMR** (200 MHz, $CDCl_3$): δ 1.61 (s, 3H), 1.69 (m, 6H), 2.01-2.16 (m, 4H), 5.07-5.14 (m, 1H), 5.42 (bs, 1H).

1,1-$^2H_2$-(*E*)-3,7-dimethylocta-2,6-dien-1-yl-diphosphate trisammonium salt ([1,1-$^2H_2$]-13):

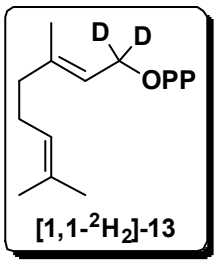

[1,1-$^2H_2$]-13

Chlorination of **[1,1-$^2H_2$]-20** was carried out with the same procedure as employed in the preparation of **21**. **[1,1-$^2H_2$]-20** (0.31 g, 2 mmol) was treated with NCS (0.29 g, 2 mmol) and freshly distilled $(CH_3)_2S$ (0.15 g, 2.4 mmol) to afford **[1,1-$^2H_2$]-21** (0.31 g, 90.4%) as colourless oil.

The chloride **[1,1-$^2H_2$]-21** (170 mg, 0.7 mmol) was immediately converted to **[1,1-$^2H_2$]-13** by treatment with **15** (1.27 g, 1.40 mmol) in anhydrous CH_3CN for 2 h. Isolation of the product was performed in the similar manner as in the synthesis of **13**. Purification over cellulose layers with 5:2.5:2.5 (v/v/v) isopropanol: CH_3CN: 0.1 M NH_4HCO_3 followed by lyophilisation delivered **[1,1-$^2H_2$]-13** (227 mg, 64%) as white solid. **^{1}H NMR** (400 MHz, D_2O): δ 1.60 (s, 3H), 1.66 (s, 3H), 1.69 (m, 3H), 2.05-2.16 (m, 4H), 5.19 (tquin, *J* = 1.25, 6.78 Hz, 1H), 5.43 (bs, 1H); **^{31}P NMR** (162 MHz) -10.47 (d, *J* = 22.39 Hz, 1P), -6.98 (d, *J* = 22.39 Hz, 1P); **HRMS (ESI)** Calcd. for $C_{10}H_{17}D_2O_7P_2$ $[M-1]^-$ 315.0737, found 315.0746.

(2*E*,6*E*)-3,7,11-trimethyldodeca-2,6,10-trienal (34):

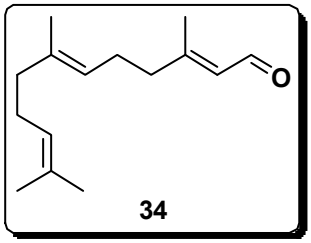

34

In a 100 mL round-bottomed flask fixed with condenser and equipped for magnetic stirring was refluxed a solution of (*E*,*E*)-farnesol (**22**) (4.4 g, 20 mmol) and IBX (11.12 g, 40 mmol) in ethyl acetate (50 mL) for 3 h. Progress of the reaction was monitored by TLC and on completion, the mixture was directly filtered through celite bed to give a crude product. Further purification by column chromatography over silica layers (ethyl acetate: pet ether, 1:19) gave the oxidized product, **34** (4.14 g, 94%). **^{1}H NMR** (200 MHz, $CDCl_3$): δ 1.60 (t-like, 6H), 1.68 (d, *J* = 0.88 Hz, 3H), 1.95-2.08 (m, 4H), 2.18 (d, *J* = 1.26 Hz, 3H), 2.24 (m, 4H), 5.03-5.12 (m, 2H), 5.89 (dq, *J* = 1.14, 8.21, 1H), 10.00 (d, *J* = 8.08, 1H).

1-^{2}H-(2*E*,6*E*)-3,7,11-trimethyldodeca-2,6,10-trien-1-ol ([1-^{2}H]-22):

A flame-dried, 50 mL, two-necked, round-bottomed flask was charged with $LiAlD_4$ (0.40 g, 9.42 mmol) followed by anhydrous THF (8 mL) and the suspension was stirred and cooled to 0 °C. To this was gradually added, a solution of **34** (1.98 g, 9.42 mmol) in

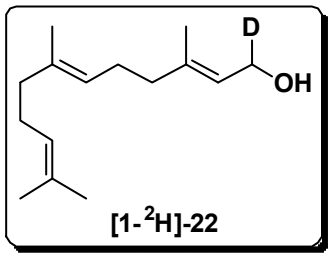

THF (2 mL) and the reaction was stirred at room temperature for 2 h. On completion (monitored by TLC) the reaction was quenched by slow addition of ethyl acetate (6 mmol) at 0 °C until the evolution of hydrogen stopped. 10% aqueous NaOH was added drop by drop to this until the grey colour of the reaction turned to white and stirring was continued for 15 min at room temperature. The mixture was then dried over anhydrous Na_2SO_4 and passed through celite, which was repeatedly washed with ethyl acetate (3 × 20 mL). The combined ethyl acetate fractions were concentrated at reduced pressure and the crude product was chromatographed over silica gel (ethyl acetate: pet ether, 1: 9) to give **[1-^{2}H]-22** (1.65 g, 82%). **^{1}H NMR** (400 MHz, $CDCl_3$): δ 1.61 (s, 6H), 1.69 (s, 6H), 1.97-2.15 (m, 8H), 4.14 (d, *J* = 5.52 Hz, 1H), 5.08-5.13 (m, 2H), 5.42 (d, *J* = 6.78 Hz, 1H).

1-^{2}H-(2*E*,6*E*)-3,7,11-trimethyldodeca-2,6,10-trienal ([1-^{2}H]-34):

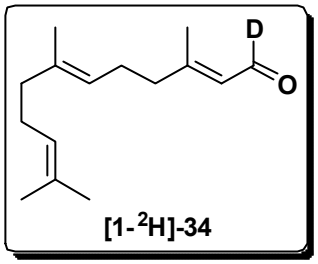

To a solution of **[1-^{2}H]-22** (1.6 g, 7.17 mmol) in anhydrous CH_2Cl_2 (20 mL) at 0 °C was added PDC (4.06 g, 10.76 mmol) followed by stirring for 2 h. After completion of the reaction, the mixture was directly filtered through celite bed, dried over anhydrous Na_2SO_4, to give a crude product. Further purification by column chromatography over silica layers (ethyl acetate: pet ether, 1:19) gave the oxidized product, **[1-^{2}H]-34** (1.21 g, 77%). **^{1}H NMR** (200 MHz, $CDCl_3$): δ 1.60 (s, 6H), 1.68 (d, *J* = 0.76 Hz, 3H), 1.99-2.10 (m, 4H), 2.17 (d, *J* = 1.26 Hz, 3H), 2.24 (m, 4H), 5.04-5.12 (m, 2H), 5.89 (s, 1H).

1,1-^{2}H$_2$-(2*E*,6*E*)-3,7,11-trimethyldodeca-2,6,10-trien-1-ol ([1,1-^{2}H$_2$]-22):

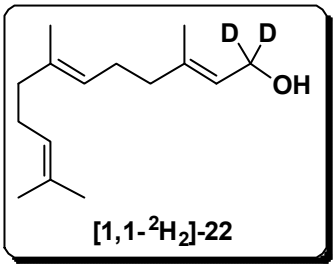

Reduction of **[1-^{2}H]-34** (0.22 g, 1.0 mmol) was carried out with $LiAlD_4$ (0.04 g, 1.0 mmol) in a similar manner as in the synthesis of **[1-^{2}H]-22**, to yield **[1,1-^{2}H$_2$]-22** (0.18 g, 80%). **^{1}H NMR** (500 MHz, $CDCl_3$): δ 1.61 (s, 6H), 1.69 (s, 6H), 1.97-2.00 (m, 2H), 2.03-2.08 (m, 4H), 2.10-2.14 (m, 2H), 5.08-5.13 (m, 1H), 5.42 (bs, 1H); **^{13}C NMR** (125 MHz, $CDCl_3$): δ 16.0 (-CH_3), 16.3 (-CH_3), 17.7 (-CH_3), 25.7 (-CH_3), 26.3 (-CH_2), 26.7 (-CH_2), 39.5 (-CH_2), 39.7 (-CH_2),

123.2 (=CH), 123.8 (=CH), 124.3 (=CH), 131.3 (=C), 135.4 (=C), 140.0 (=C); **GC-EI-MS:** (*m*/*z*) 224.3 $[M]^+$, 206.3, 191.2, 163.2, 135.2, 95.1, 81.1, 69.1 (100%), 55.0.

1,1-$^2H_2$-(2*E*,6*E*)-3,7,11-trimethyldodeca-2,6,10-trien-1-yl-diphosphate trisammonium salt ([1,1-$^2H_2$]-14):

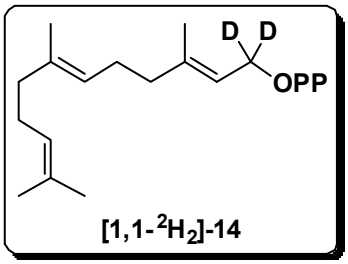

[1,1-$^2H_2$]-14

Synthesis of **[1,1-$^2H_2$]-23** was carried out with a similar procedure as employed in the synthesis of **[1,1-$^2H_2$]-21**. Chlorination of **[1,1-$^2H_2$]-23** (232 mg, 1.03 mmol) in presence of NCS (136 mg, 1.03 mmol) and $(CH_3)_2S$ (74 mg, 1.24 mmol) afforded **[1,1-$^2H_2$]-23** (225 mg, 89%) as thick oil. The chloride was subjected to diphosphorylation reaction without any chromatographic purification.

To a solution of **15** (1.27 g, 1.40 mmol) in anhydrous CH_3CN (3 mL) was added **[1,1-$^2H_2$]-23** (0.17 g, 0.7 mmol) dissolved in CH_3CN (0.5 mL) and the reaction was stirred for 3 h at room temperature. Isolation of the diphosphate product was carried out according to the established procedure by Davisson *et al*. as demonstrated in the synthesis of **[1,1-$^2H_2$]-13**. Purification by flash chromatography over cellulose column (3 cm × 12 cm) with 5.5:2:1:1.5 (v/v/v/v) isopropanol: $CHCl_3$: CH_3CN: 0.1 M NH_4HCO_3 followed by lyophilization yielded **[1,1-$^2H_2$]-14** (217 mg, 61%) as white powder. **^{1}H NMR** (400 MHz, D_2O): δ 1.50 (s, 6H), 1.57 (s, 3H), 1.61 (s, 3H), 1.89-1.93 (m, 2H), 1.98-2.05 (m, 6H), 5.05-5.12 (m, 2H), 5.34 (s, 1H); **^{31}P NMR** (162 MHz, D_2O): δ -10.51 (d, *J* = 22.39 Hz, 1P), -6.82 (d, *J* = 21.06 Hz, 1P); **HRMS (ESI)**: Calcd. for $C_{15}H_{25}D_2O_7P_2$ $[M-1]^-$ 383.1363, found 383.1372.

Appendix 3

Appendix 3 Index

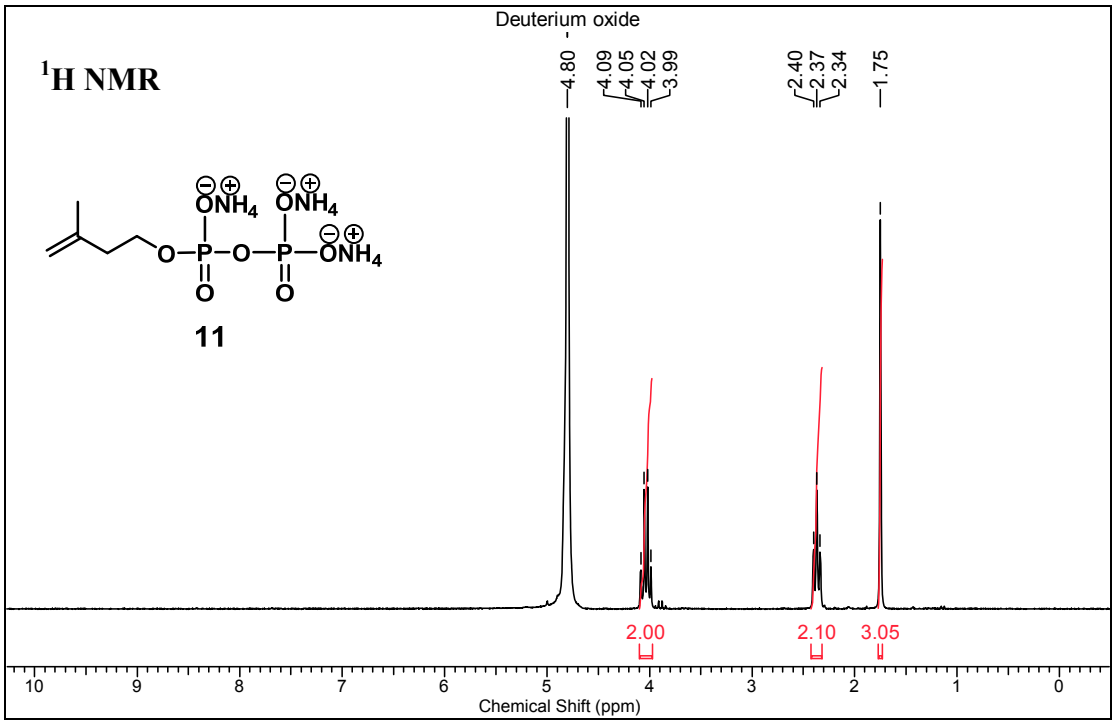
Deuterium oxide
^{1}H NMR
4.80
4.09
4.05
4.02
3.99
2.40
2.37
2.34
1.75
2.00
2.10
3.05
Chemical Shift (ppm)

11

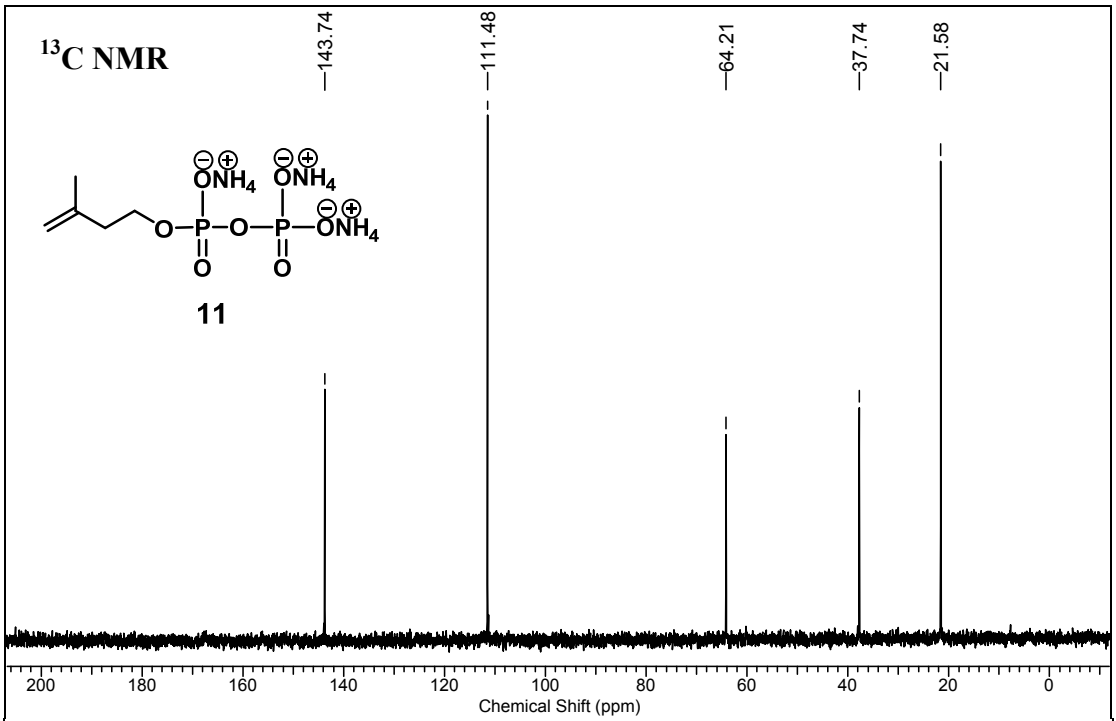
^{13}C NMR
143.74
111.48
64.21
37.74
21.58
Chemical Shift (ppm)

11

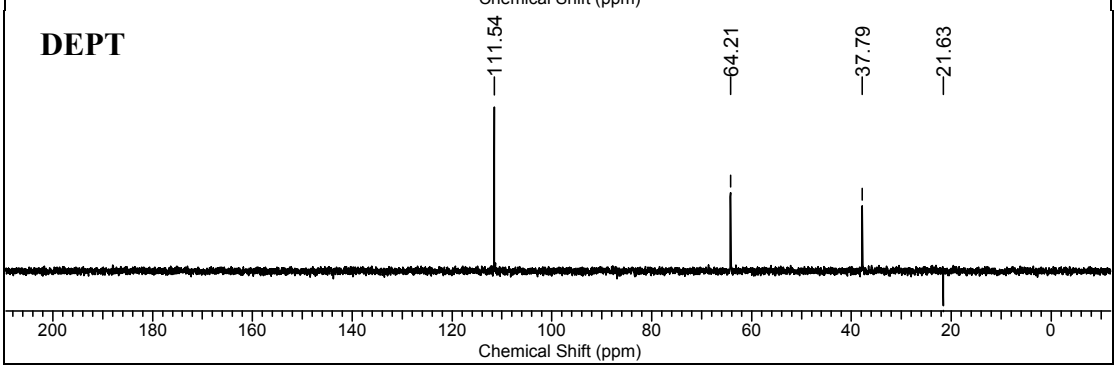
DEPT
111.54
64.21
37.79
21.63
Chemical Shift (ppm)

^{31}P NMR

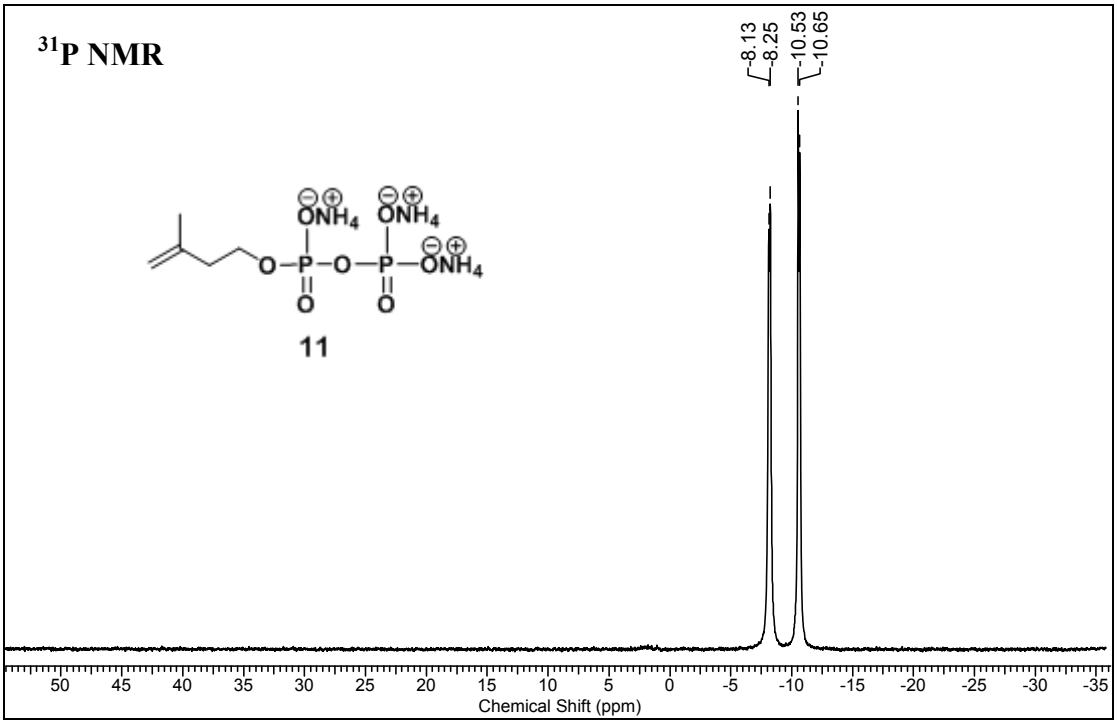

11

HRMS (ESI)

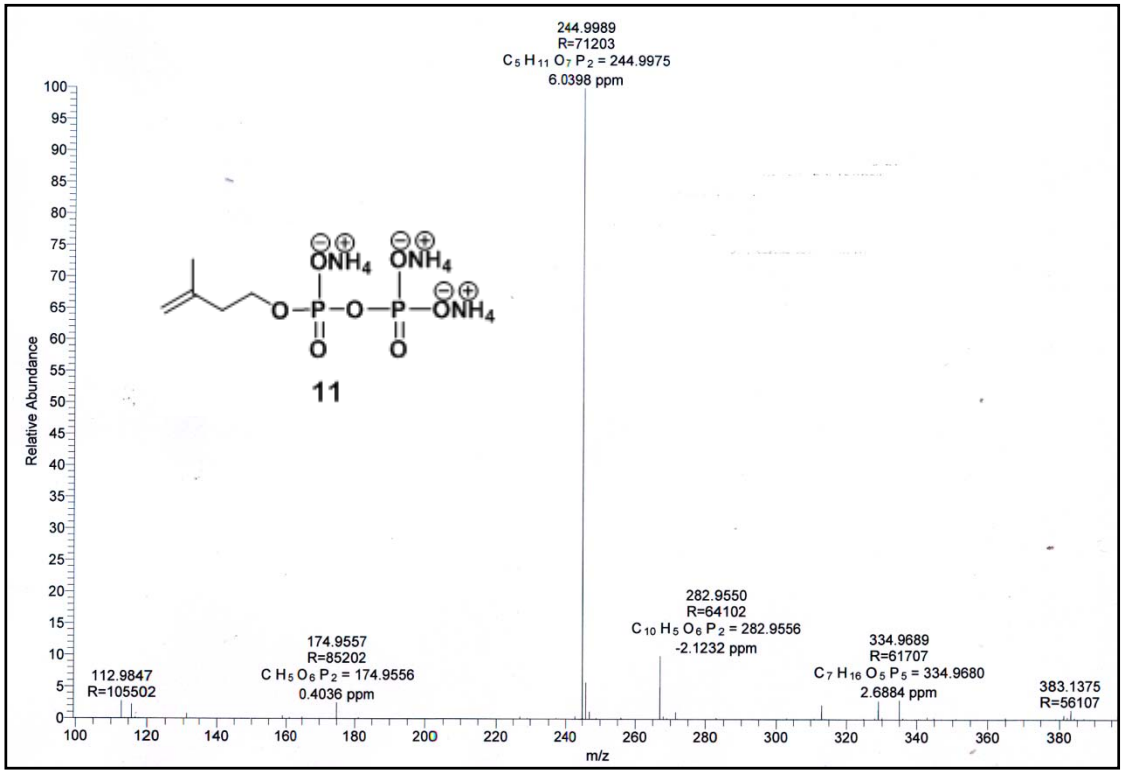

11

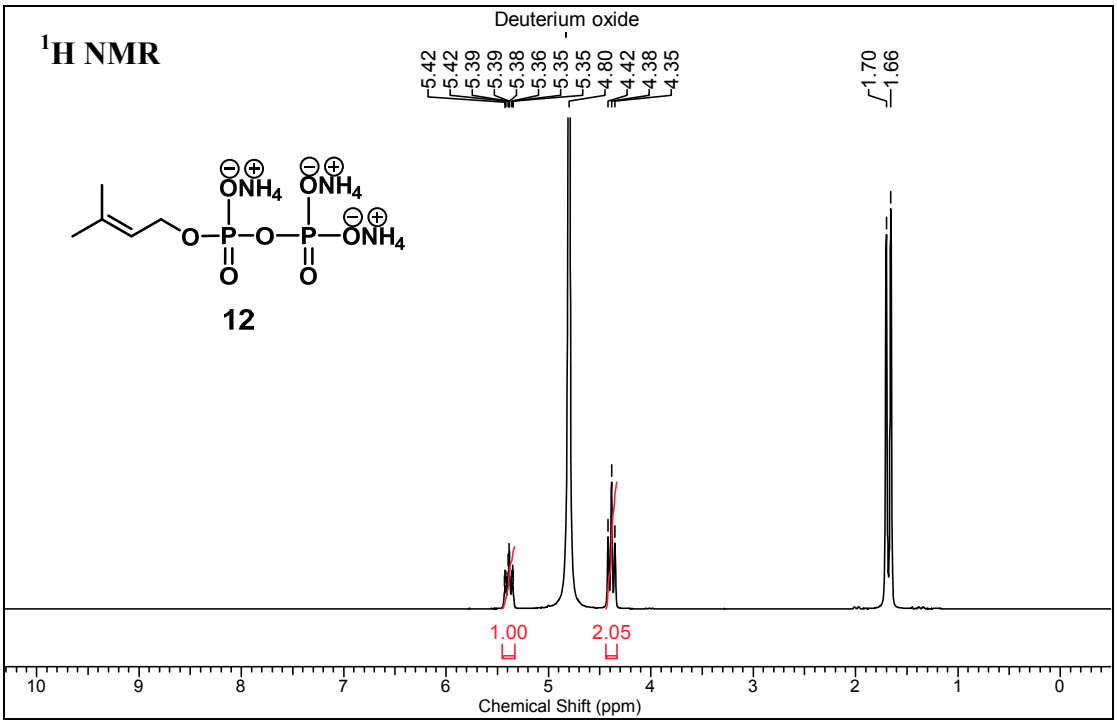
^{1}H NMR
Deuterium oxide
5.42
5.42
5.39
5.39
5.38
5.36
5.35
5.35
4.80
4.42
4.38
4.35
1.70
1.66
ONH4
ONH4
ONH4
O
P
O
P
O
O
O
12
1.00
2.05
10
9
8
7
6
5
4
3
2
1
0
Chemical Shift (ppm)

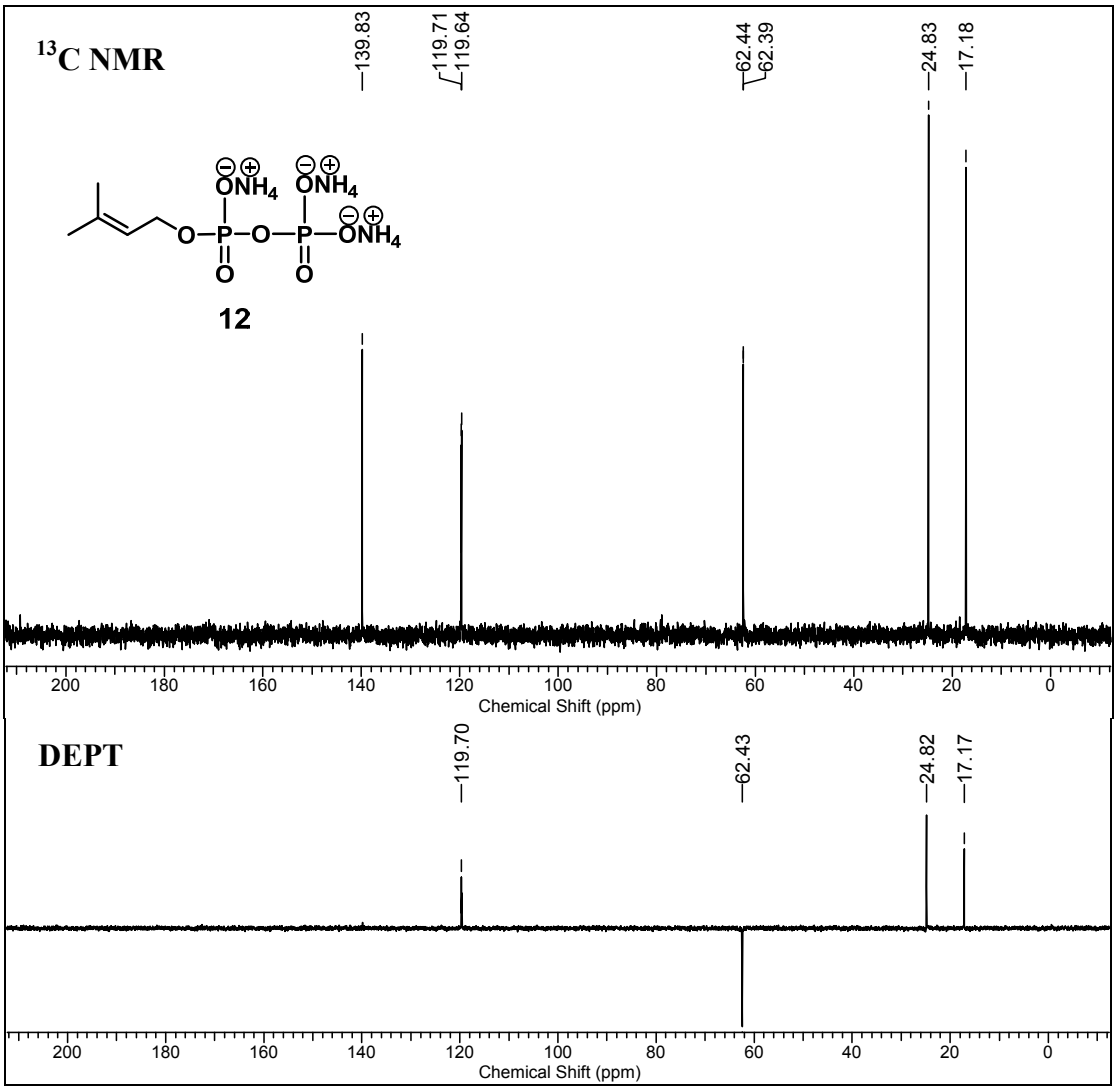
^{13}C NMR
139.83
119.71
119.64
62.44
62.39
24.83
17.18
ONH4
ONH4
ONH4
O
P
O
P
O
O
O
12
200
180
160
140
120
100
80
60
40
20
0
Chemical Shift (ppm)
DEPT
119.70
62.43
24.82
17.17
200
180
160
140
120
100
80
60
40
20
0
Chemical Shift (ppm)

^{31}P NMR

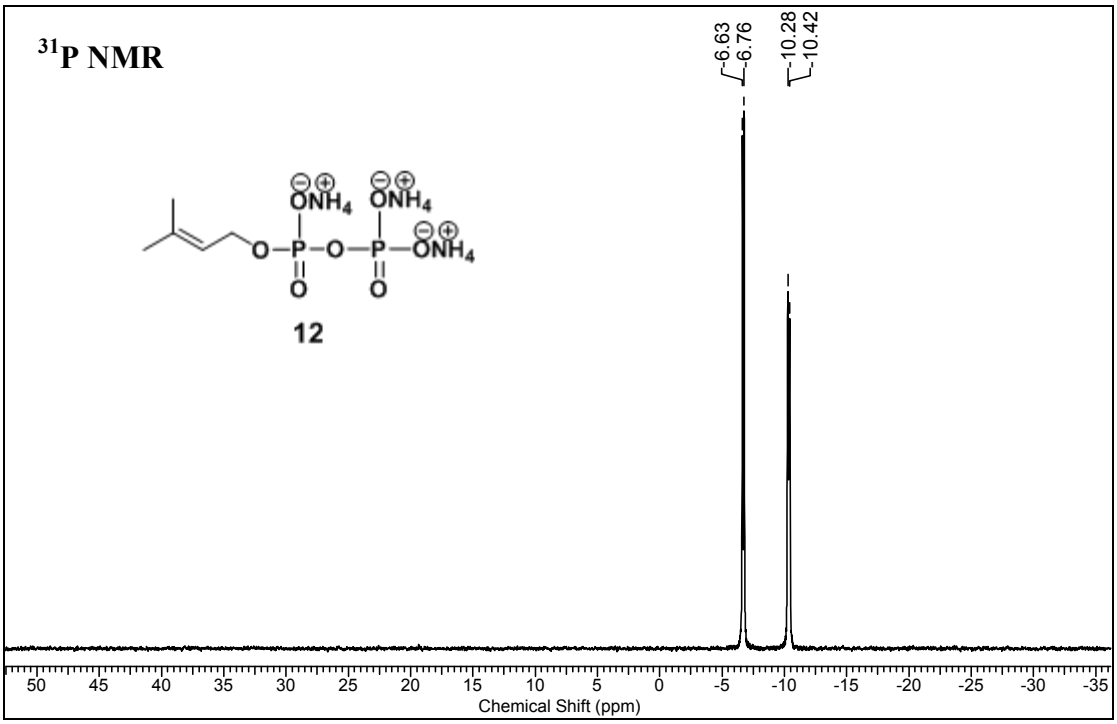

HRMS (ESI)

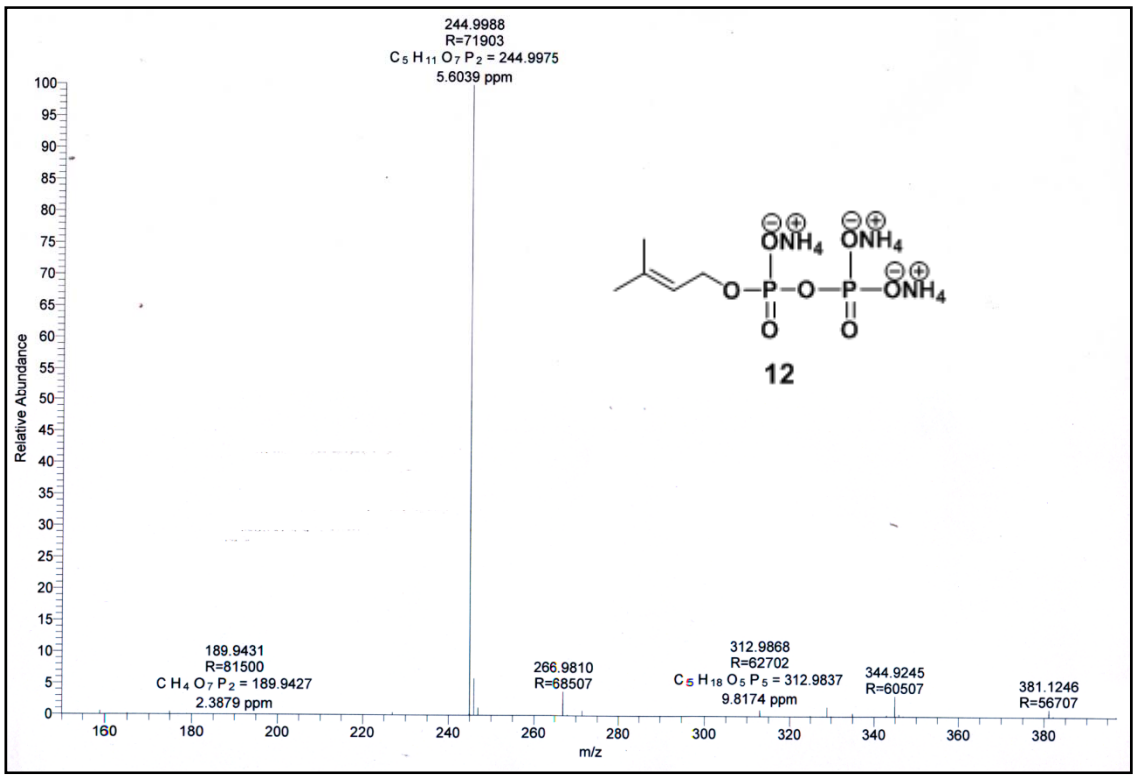

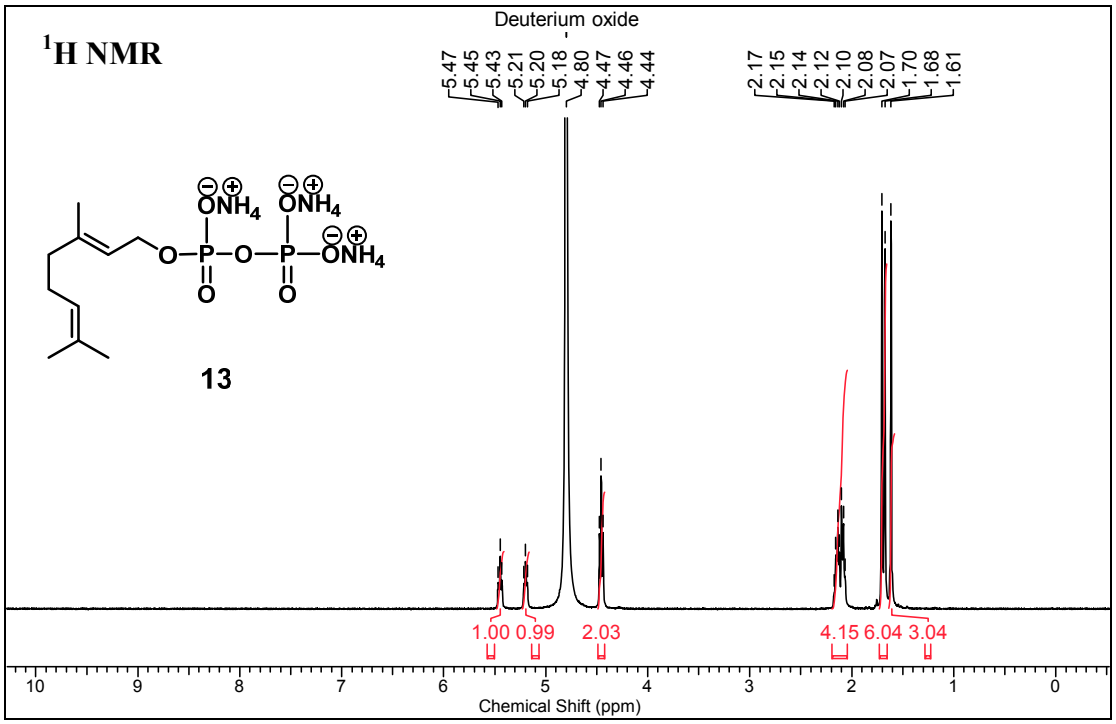
^{1}H NMR
Deuterium oxide
5.47
5.45
5.43
5.21
5.20
5.18
4.80
4.47
4.46
4.44
2.17
2.15
2.14
2.12
2.10
2.08
2.07
1.70
1.68
1.61
ONH4
ONH4
ONH4
O
P
O
P
O
O
O
13
1.00 0.99 2.03
4.15 6.04 3.04
10 9 8 7 6 5 4 3 2 1 0
Chemical Shift (ppm)

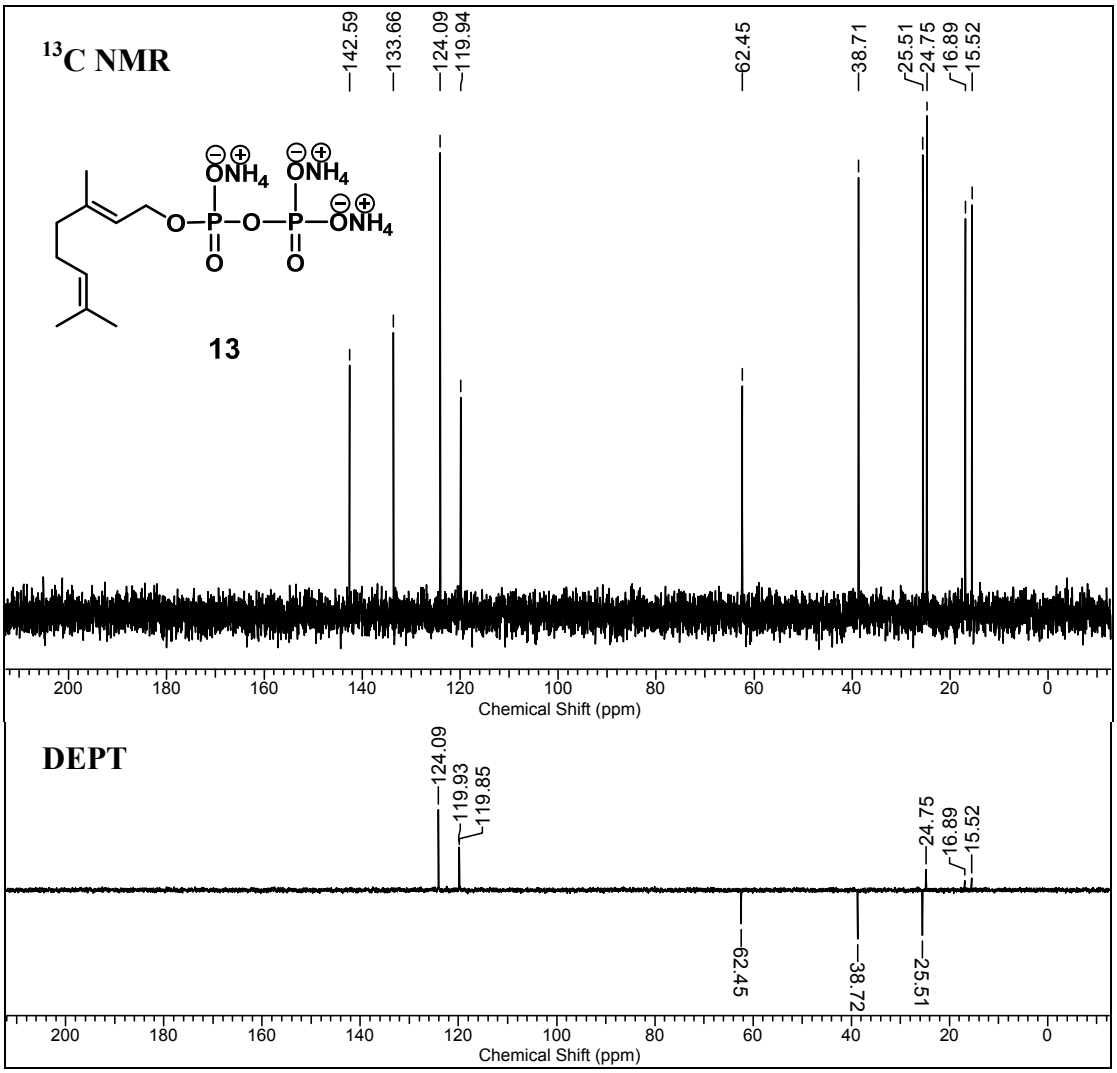
^{13}C NMR
142.59
133.66
124.09
119.94
62.45
38.71
25.51
24.75
16.89
15.52
ONH4
ONH4
ONH4
O
P
O
P
O
O
O
13
200 180 160 140 120 100 80 60 40 20 0
Chemical Shift (ppm)
DEPT
124.09
119.93
119.85
24.75
16.89
15.52
62.45
38.72
25.51
200 180 160 140 120 100 80 60 40 20 0
Chemical Shift (ppm)

^{31}P NMR

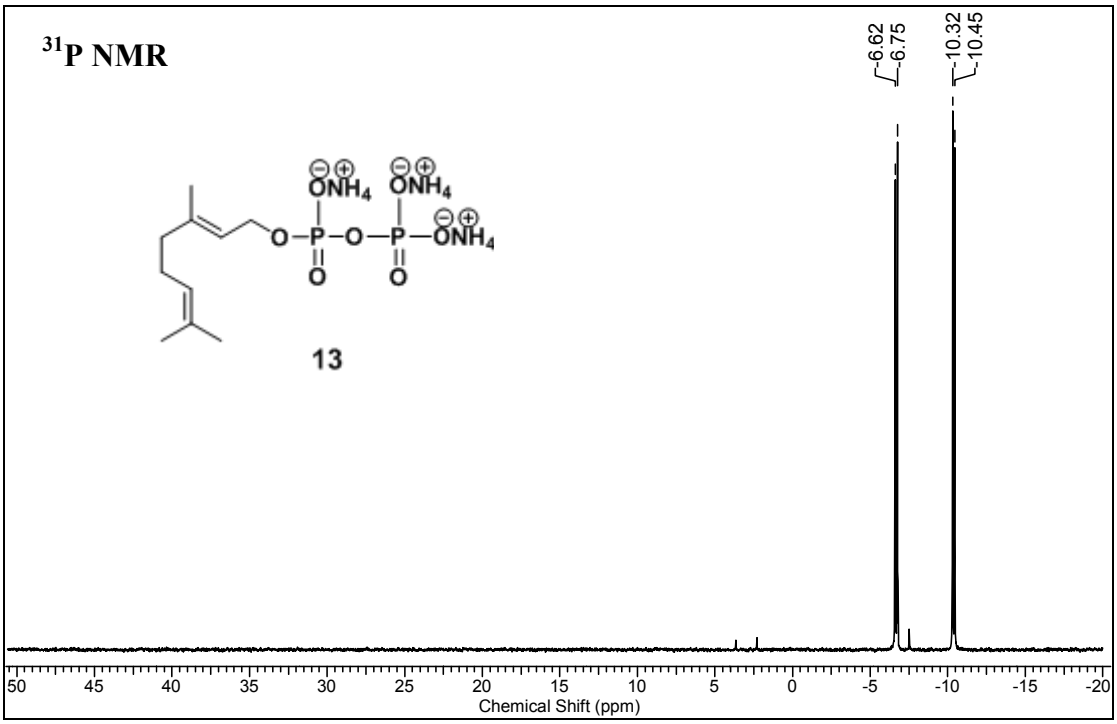

HRMS (ESI)

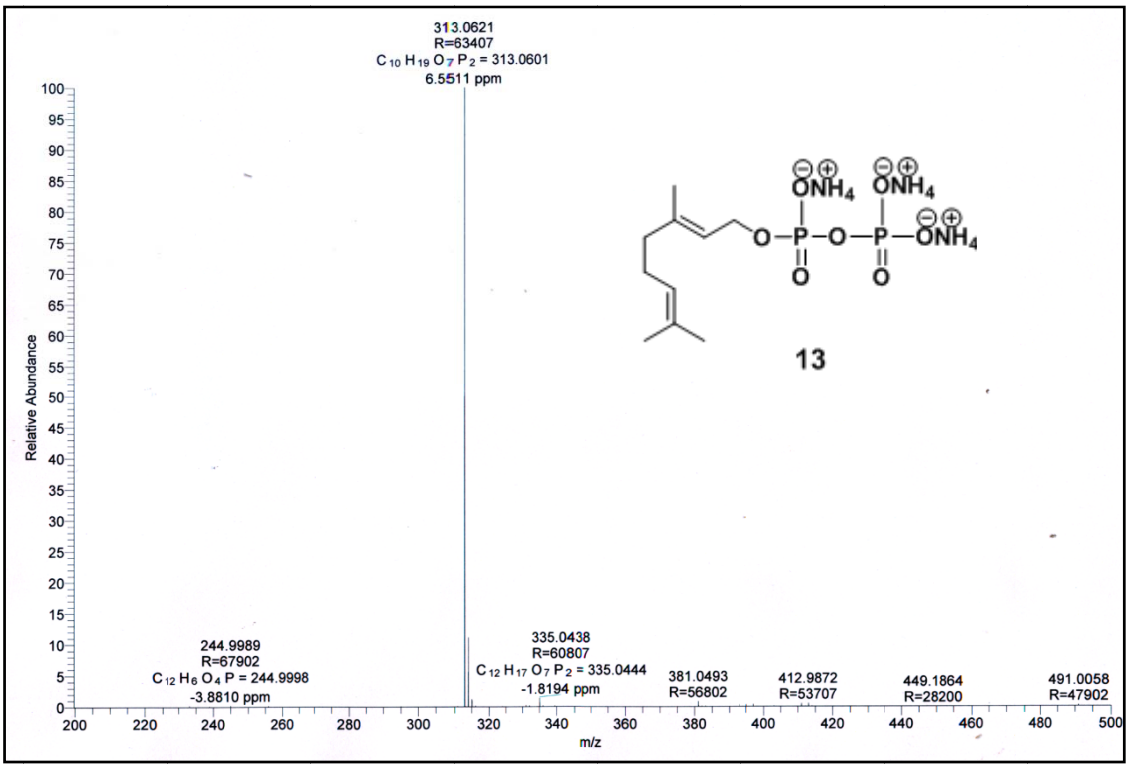

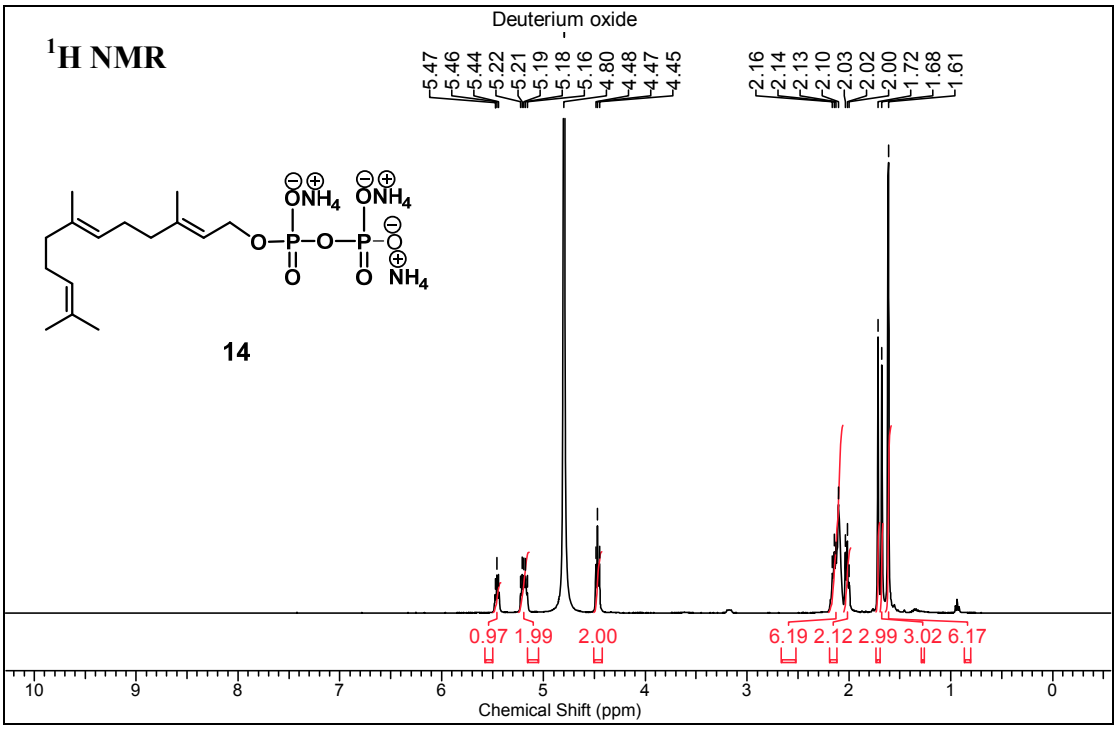
^{1}H NMR
Deuterium oxide
5.47 5.46 5.44 5.22 5.21 5.19 5.18 5.16 4.80 4.48 4.47 4.45
2.16 2.14 2.13 2.10 2.03 2.02 2.00 1.72 1.68 1.61
ONH4 ONH4
O–P–O–P–O
O O NH4
14
0.97 1.99 2.00
6.19 2.12 2.99 3.02 6.17
10 9 8 7 6 5 4 3 2 1 0
Chemical Shift (ppm)

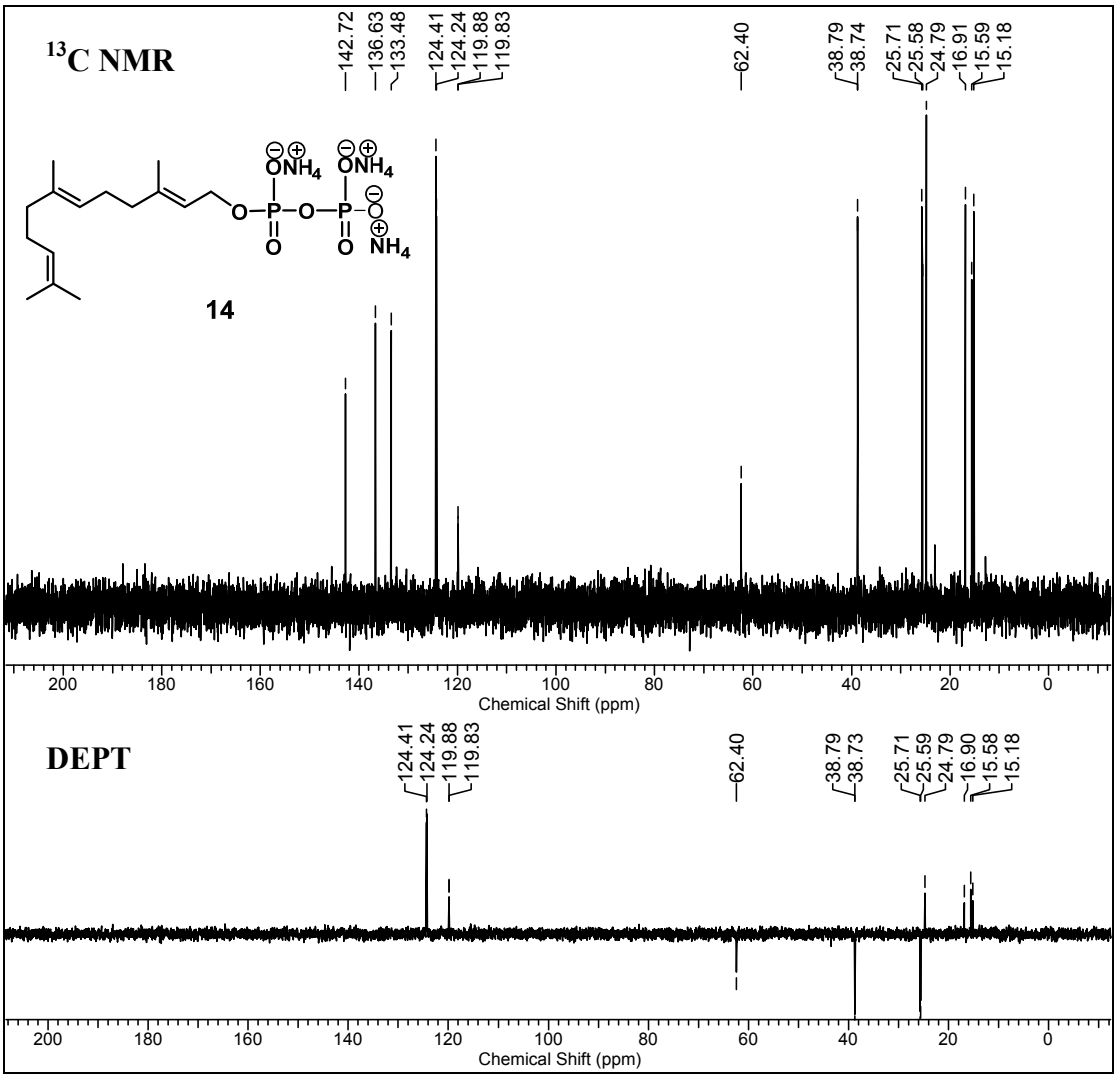
^{13}C NMR
142.72 136.63 133.48 124.41 124.24 119.88 119.83 62.40 38.79 38.74 25.71 25.58 24.79 16.91 15.59 15.18
ONH4 ONH4
O–P–O–P–O
O O NH4
14
200 180 160 140 120 100 80 60 40 20 0
Chemical Shift (ppm)
DEPT
124.41 124.24 119.88 119.83 62.40 38.79 38.73 25.71 25.59 24.79 16.90 15.58 15.18
200 180 160 140 120 100 80 60 40 20 0
Chemical Shift (ppm)

^{31}P NMR

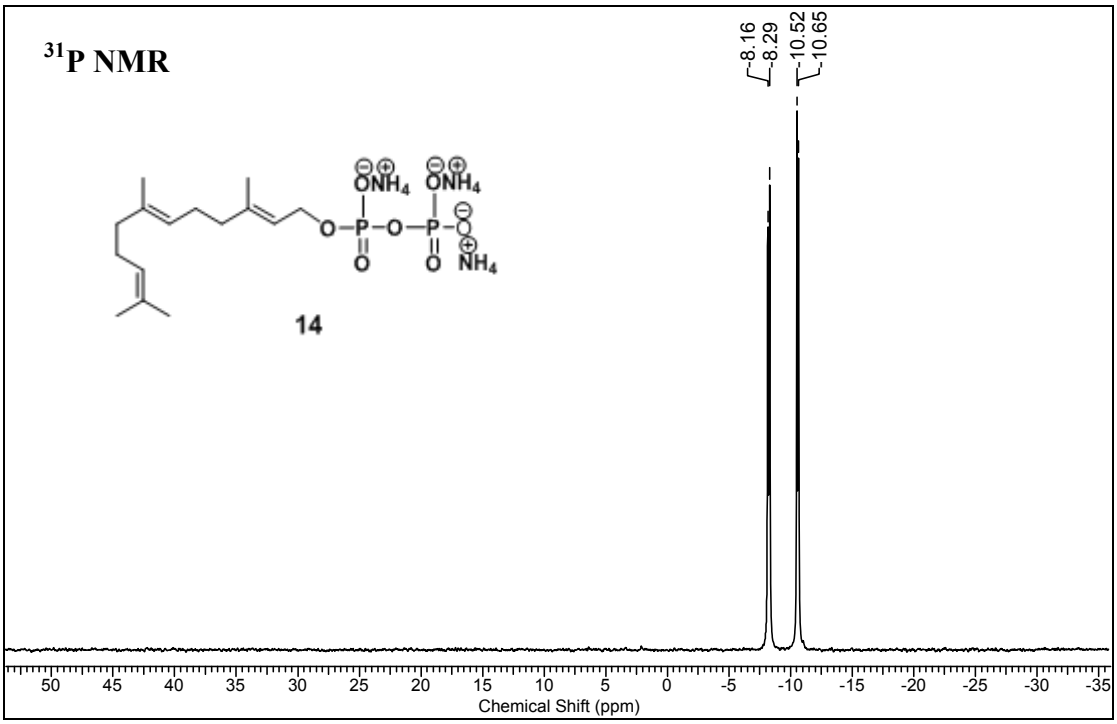

HRMS (ESI)

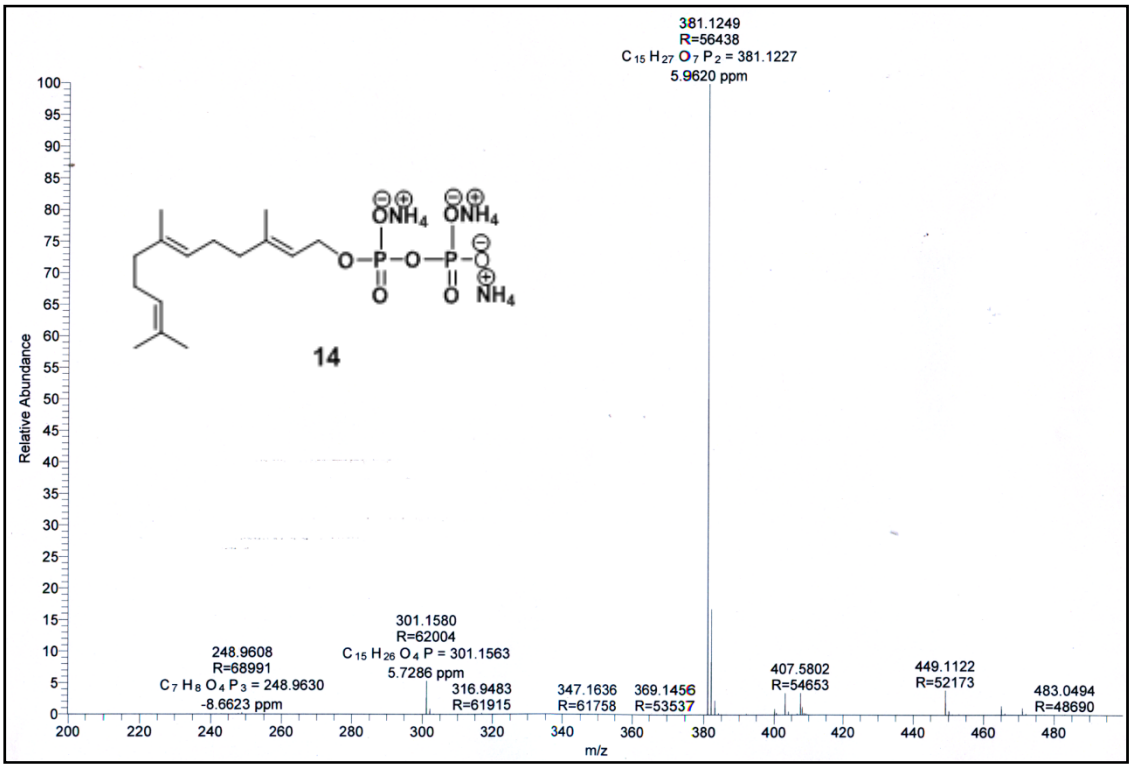

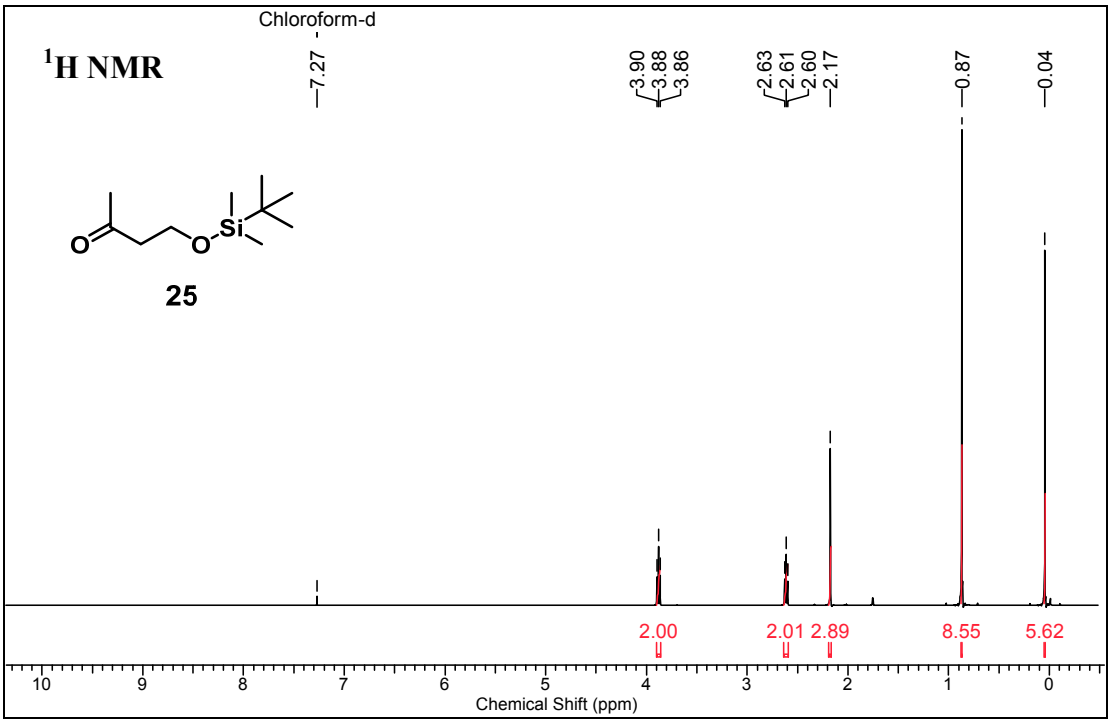
Chloroform-d
^{1}H NMR
7.27
3.90
3.88
3.86
2.63
2.61
2.60
2.17
0.87
0.04
25
2.00
2.01
2.89
8.55
5.62
Chemical Shift (ppm)

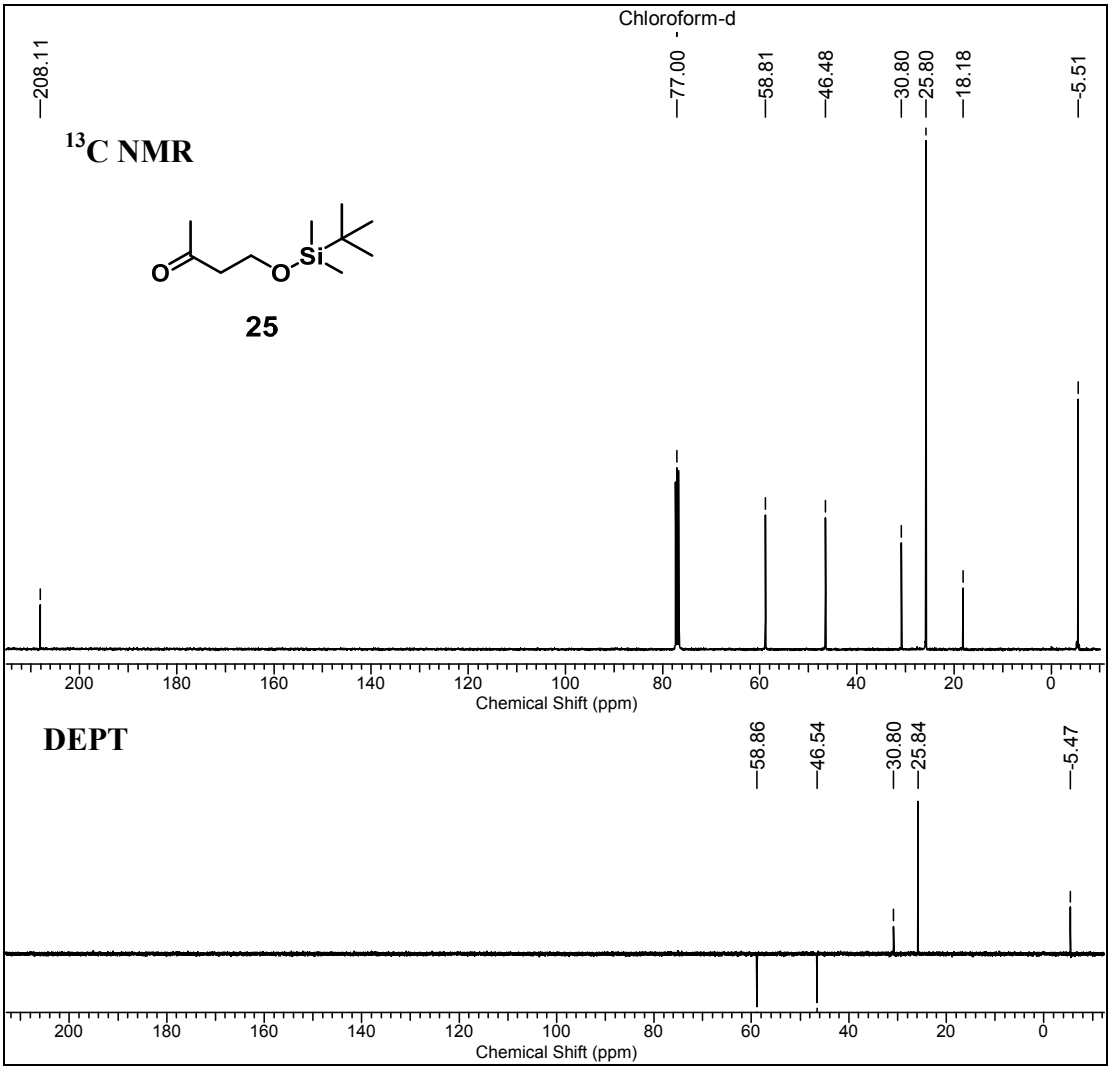
Chloroform-d
208.11
77.00
58.81
46.48
30.80
25.80
18.18
5.51
^{13}C NMR
25
Chemical Shift (ppm)
DEPT
58.86
46.54
30.80
25.84
5.47
Chemical Shift (ppm)

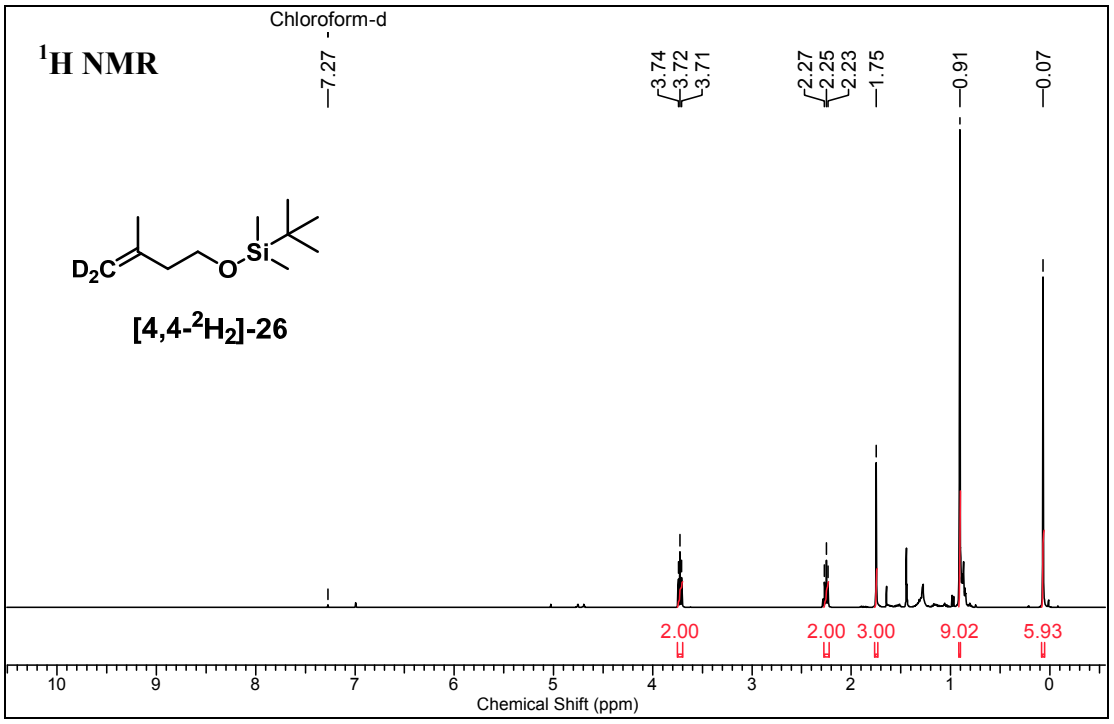
Chloroform-d
^{1}H NMR
7.27
3.74
3.72
3.71
2.27
2.25
2.23
1.75
0.91
0.07
D2C
O
Si
[4,4-2H2]-26
2.00
2.00
3.00
9.02
5.93
Chemical Shift (ppm)

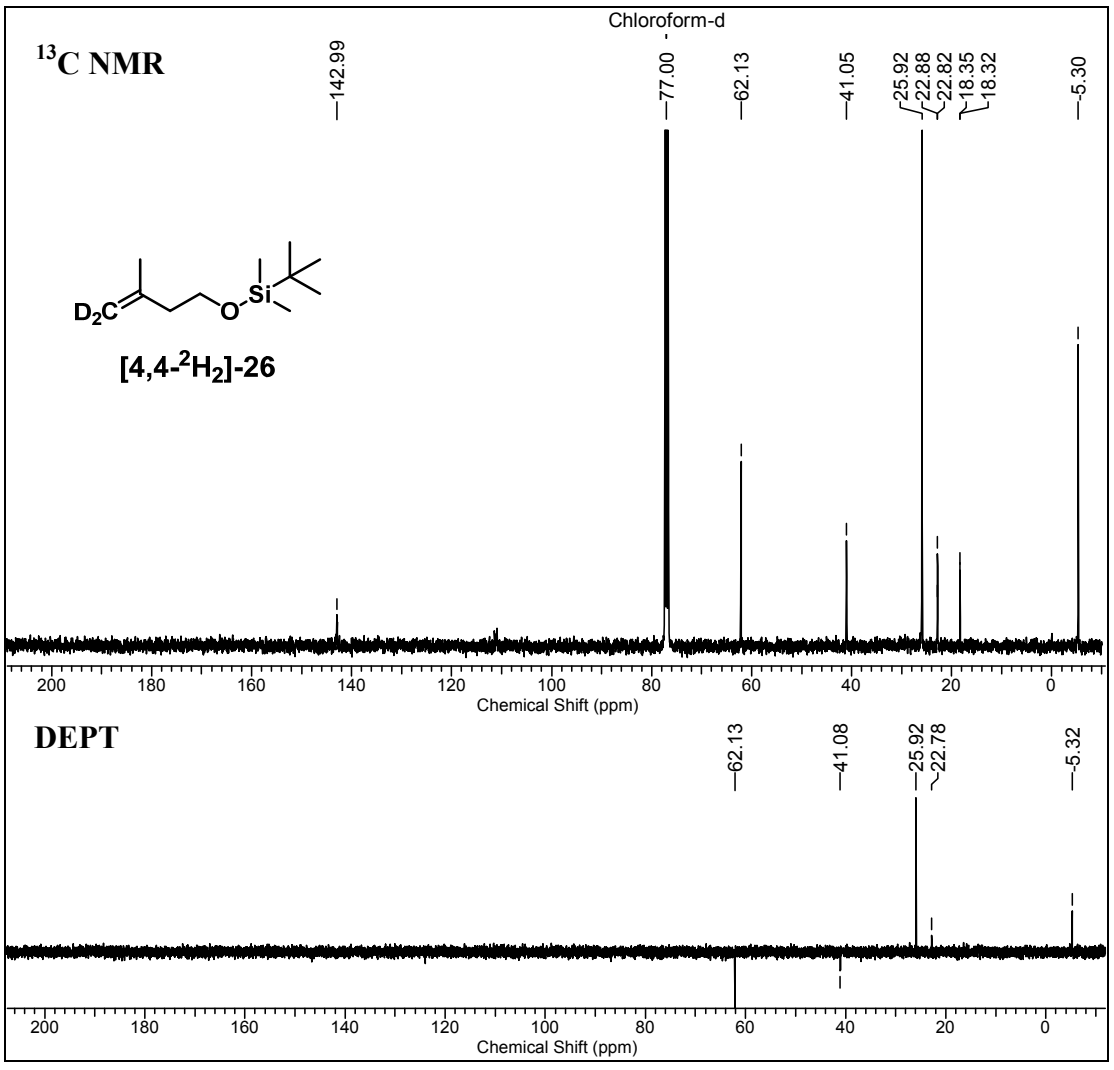
Chloroform-d
^{13}C NMR
142.99
77.00
62.13
41.05
25.92
22.88
22.82
18.35
18.32
5.30
D2C
O
Si
[4,4-2H2]-26
Chemical Shift (ppm)
DEPT
62.13
41.08
25.92
22.78
5.32
Chemical Shift (ppm)

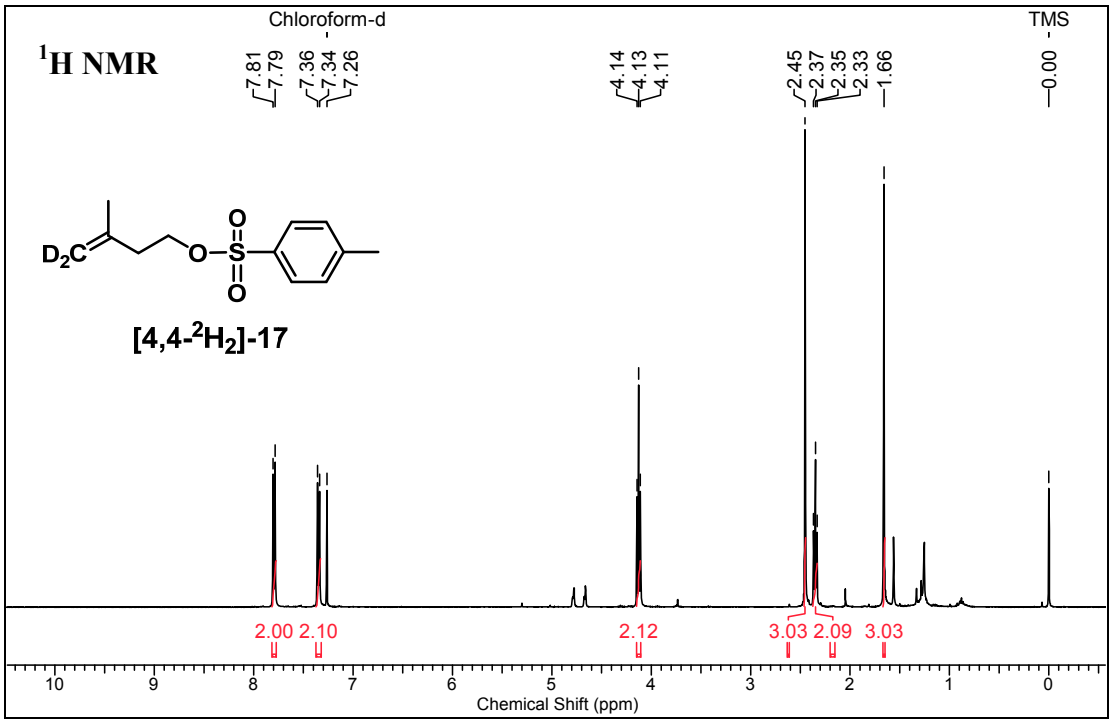
Chloroform-d
TMS
^{1}H NMR
7.81
7.79
7.36
7.34
7.26
4.14
4.13
4.11
2.45
2.37
2.35
2.33
1.66
0.00
D_2C
O
S
O
O
[4,4-$^{2}H_2$]-17
2.00 2.10
2.12
3.03 2.09 3.03
10 9 8 7 6 5 4 3 2 1 0
Chemical Shift (ppm)

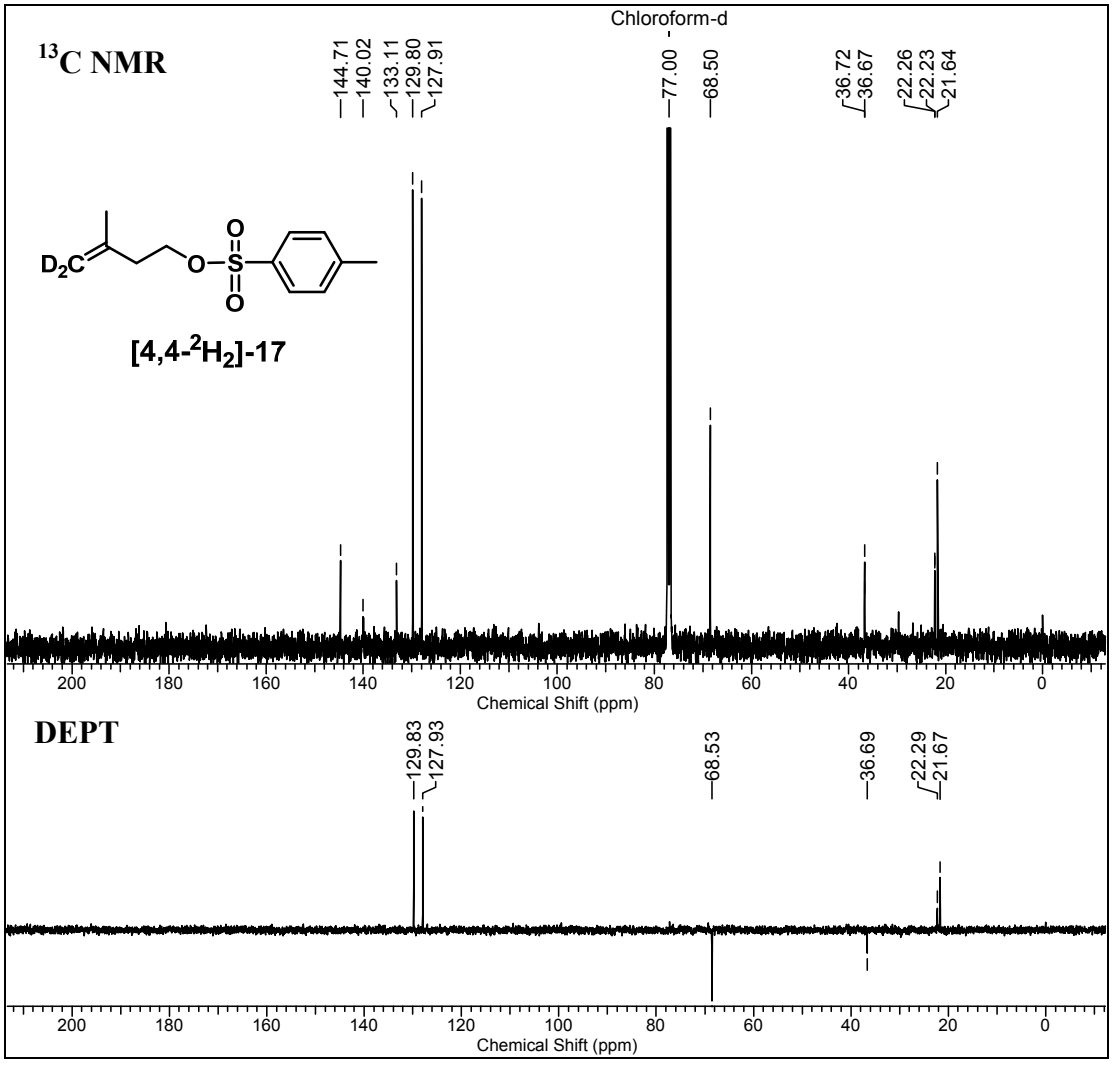
Chloroform-d
^{13}C NMR
144.71
140.02
133.11
129.80
127.91
77.00
68.50
36.72
36.67
22.26
22.23
21.64
D_2C
O
S
O
O
[4,4-$^{2}H_2$]-17
200 180 160 140 120 100 80 60 40 20 0
Chemical Shift (ppm)
DEPT
129.83
127.93
68.53
36.69
22.29
21.67
200 180 160 140 120 100 80 60 40 20 0
Chemical Shift (ppm)

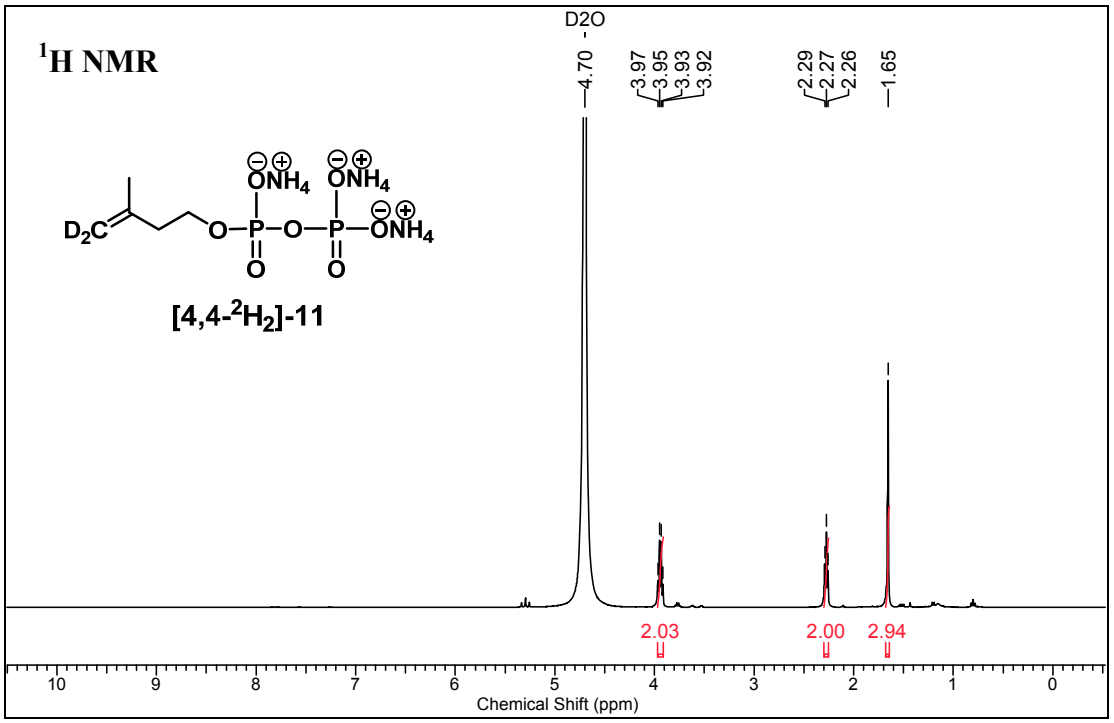
^{1}H NMR
D2O
4.70
3.97
3.95
3.93
3.92
2.29
2.27
2.26
1.65
D_2C
ONH_4
ONH_4
ONH_4
O–P–O–P–
[4,4-$^{2}H_2$]-11
2.03
2.00
2.94
Chemical Shift (ppm)

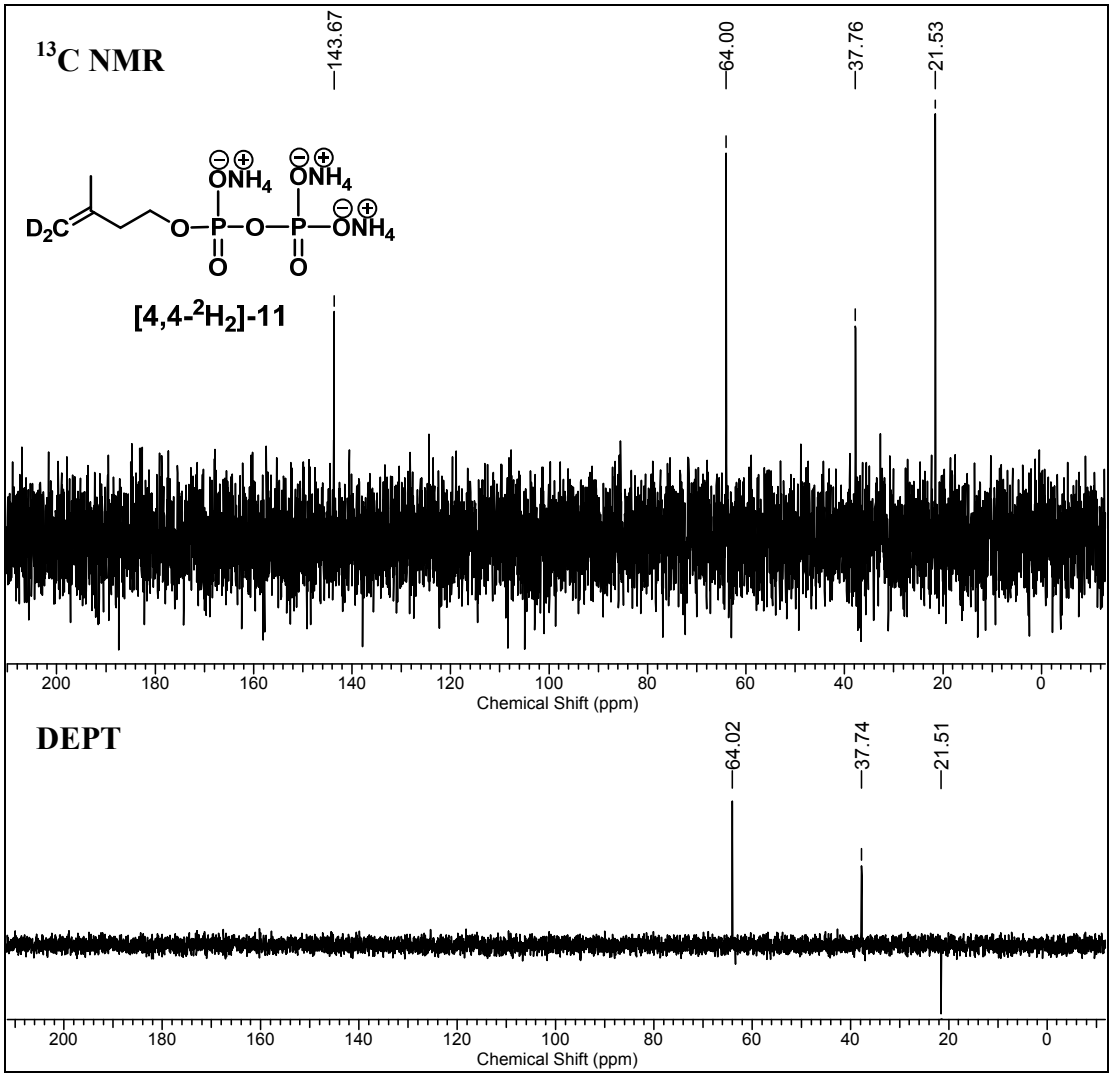
^{13}C NMR
143.67
64.00
37.76
21.53
D_2C
ONH_4
ONH_4
ONH_4
O–P–O–P–
[4,4-$^{2}H_2$]-11
Chemical Shift (ppm)
DEPT
64.02
37.74
21.51
Chemical Shift (ppm)

^{31}P NMR

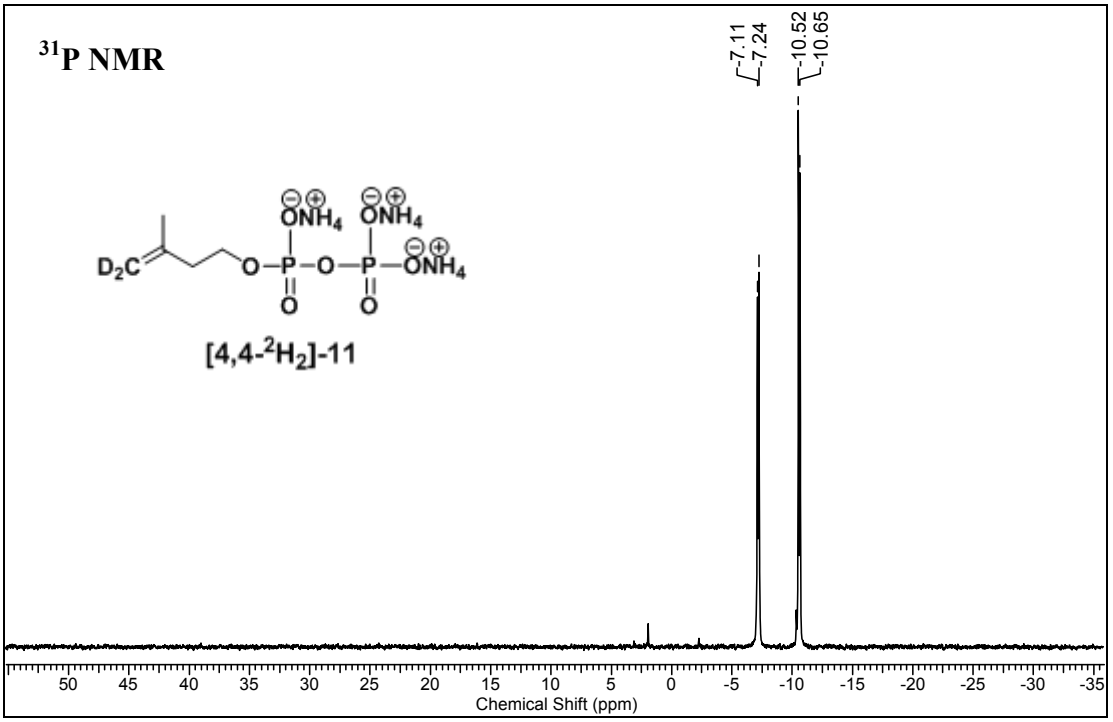

$[4,4\text{-}^{2}H_2]$-11

HRMS (ESI)

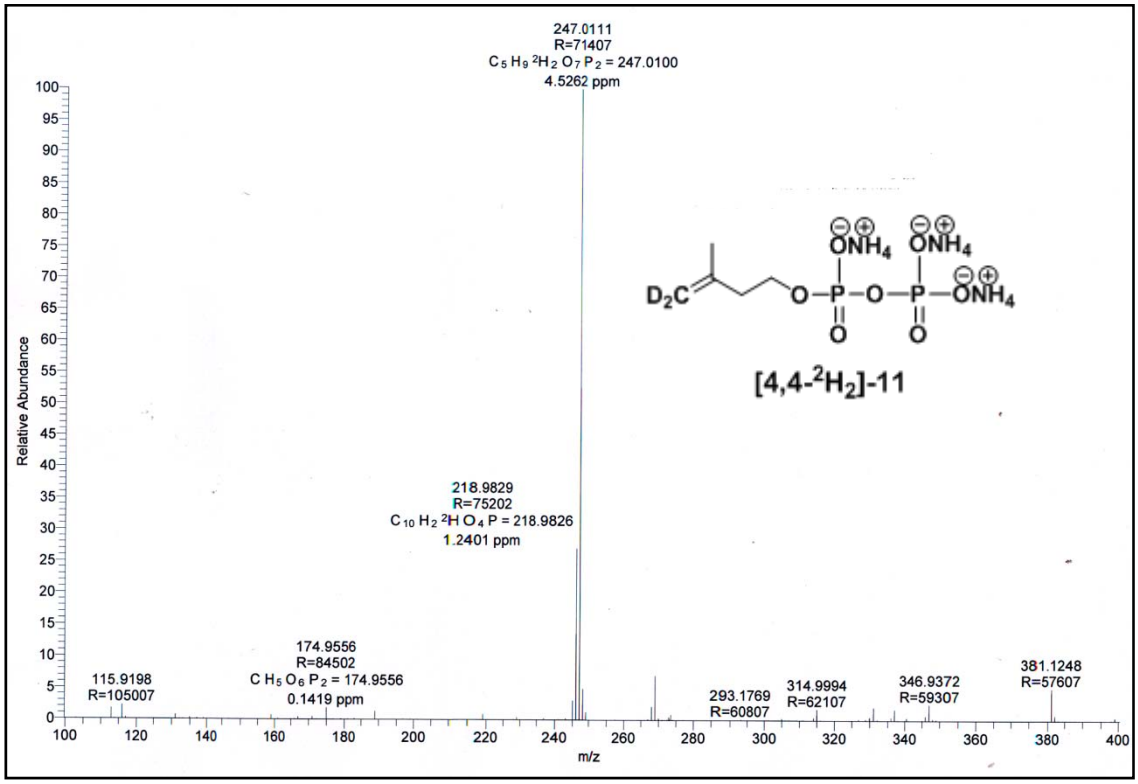

$[4,4\text{-}^{2}H_2]$-11

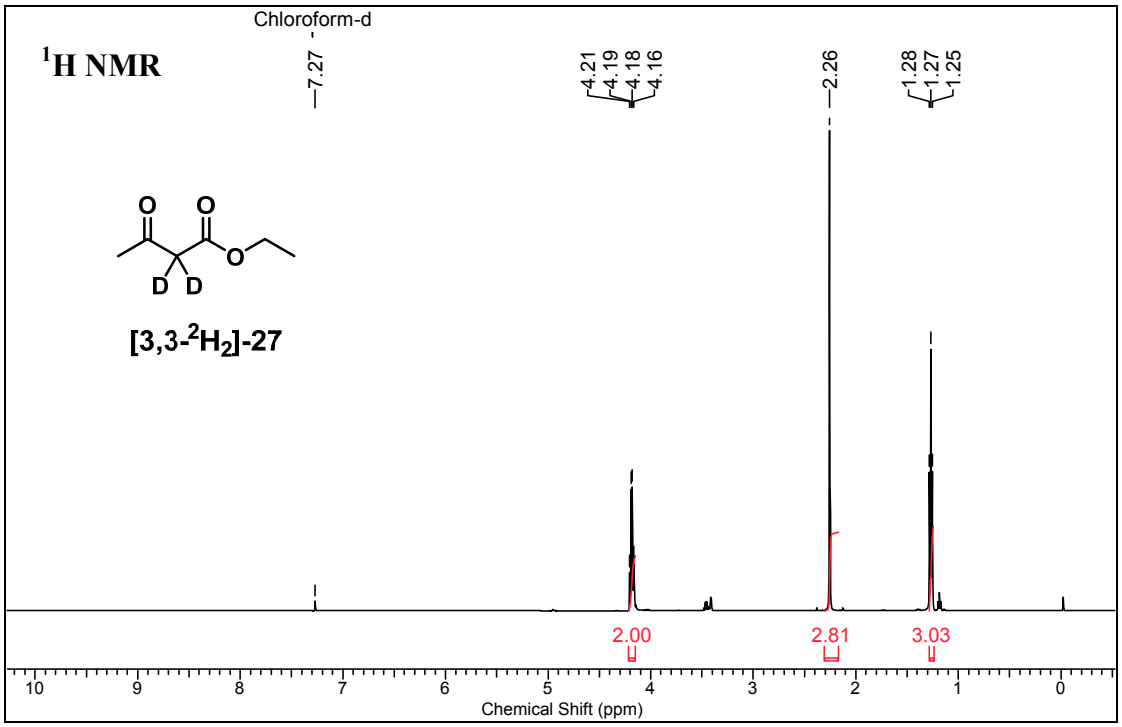
Chloroform-d
^{1}H NMR
7.27
4.21
4.19
4.18
4.16
2.26
1.28
1.27
1.25
O
O
O
D D
[3,3-$^{2}H_2$]-27
2.00
2.81
3.03
10 9 8 7 6 5 4 3 2 1 0
Chemical Shift (ppm)

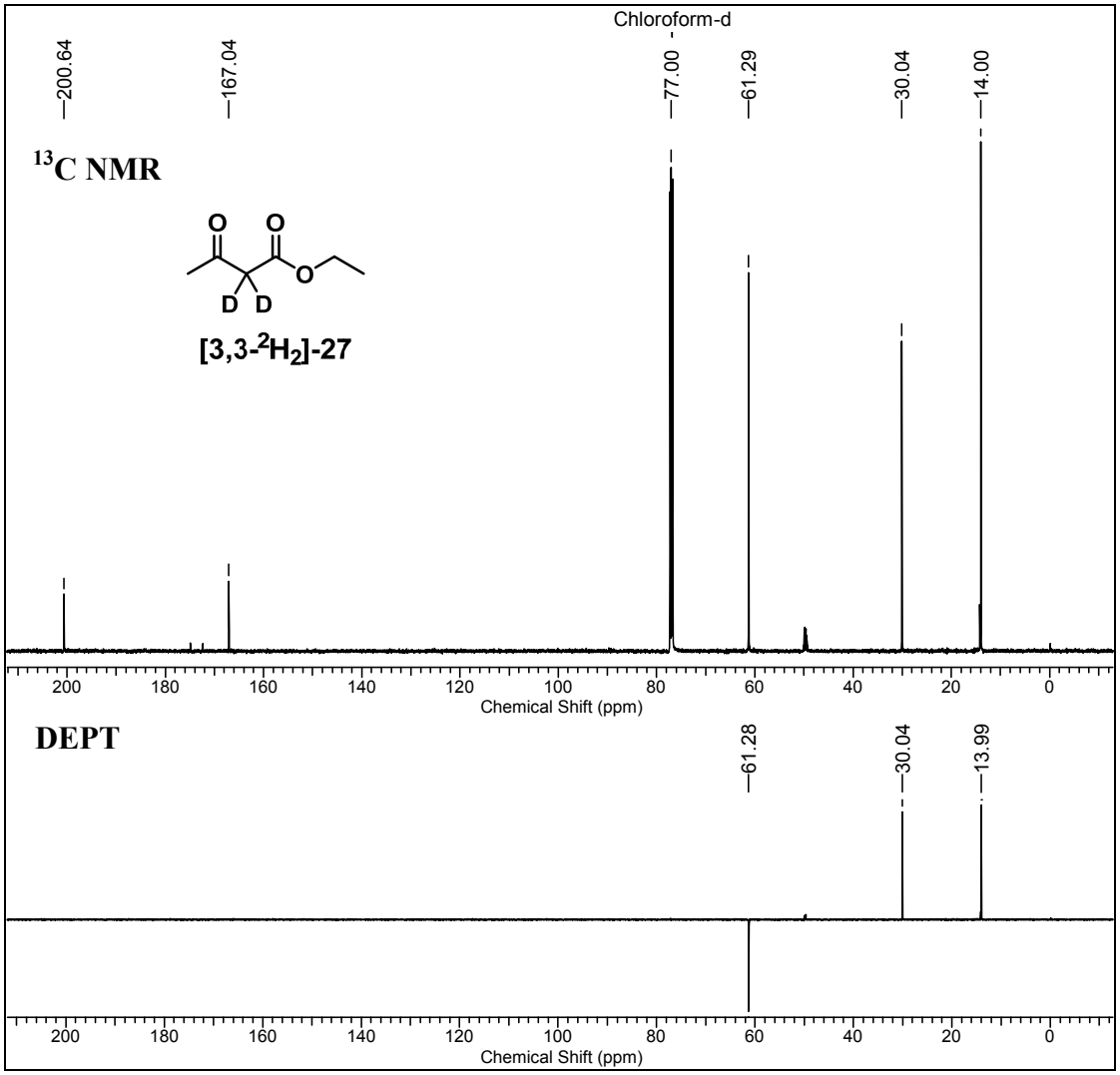
Chloroform-d
200.64
167.04
77.00
61.29
30.04
14.00
^{13}C NMR
O
O
O
D D
[3,3-$^{2}H_2$]-27
200 180 160 140 120 100 80 60 40 20 0
Chemical Shift (ppm)
DEPT
61.28
30.04
13.99
200 180 160 140 120 100 80 60 40 20 0
Chemical Shift (ppm)

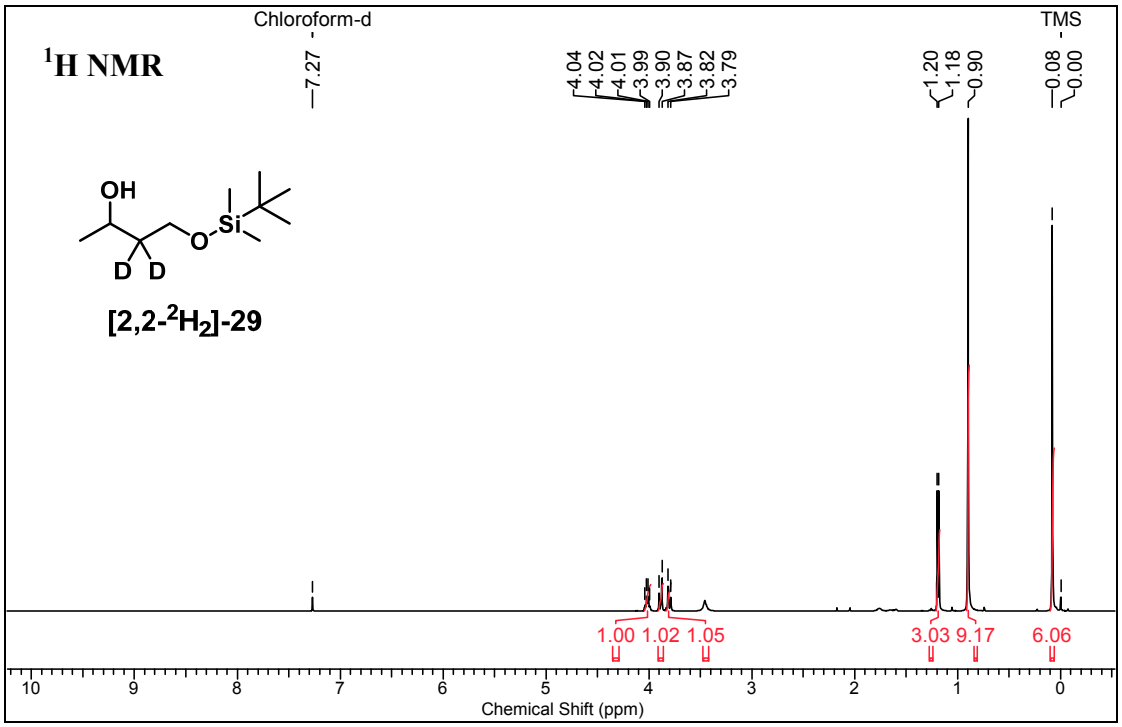
Chloroform-d
TMS
^{1}H NMR
7.27
4.04
4.02
4.01
3.99
3.90
3.87
3.82
3.79
1.20
1.18
0.90
0.08
0.00
OH
Si
O
D D
[2,2-$^2H_2$]-29
1.00 1.02 1.05
3.03 9.17
6.06
Chemical Shift (ppm)

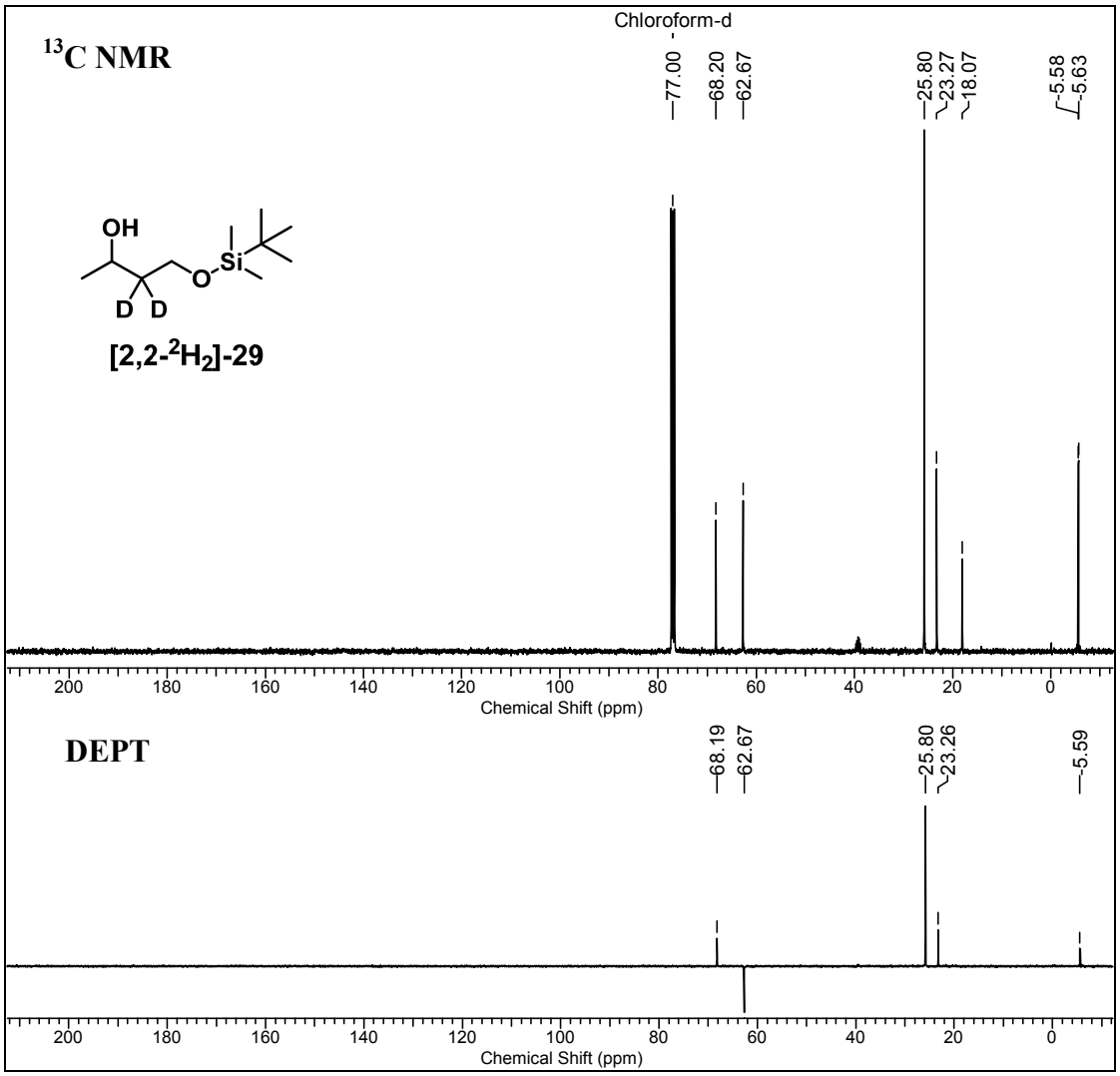
Chloroform-d
^{13}C NMR
77.00
68.20
62.67
25.80
23.27
18.07
-5.58
-5.63
OH
Si
O
D D
[2,2-$^2H_2$]-29
Chemical Shift (ppm)
DEPT
68.19
62.67
25.80
23.26
-5.59
Chemical Shift (ppm)

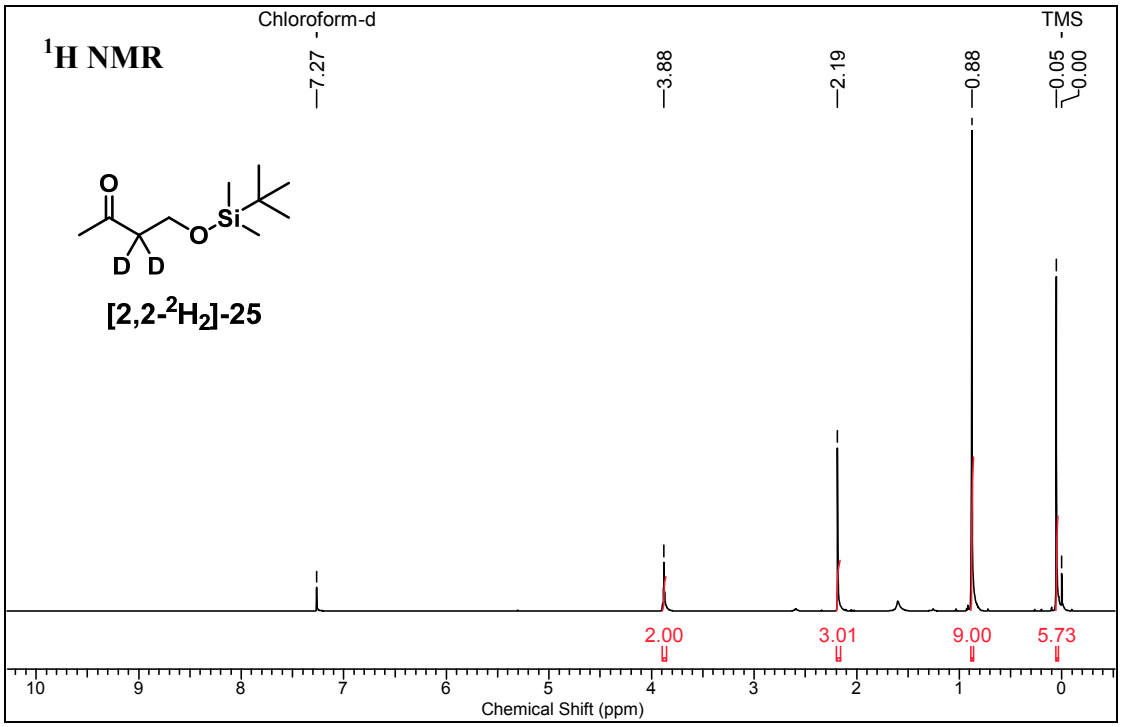
Chloroform-d
TMS
^{1}H NMR
7.27
3.88
2.19
0.88
0.05
0.00
O
Si
O
D D
[2,2-$^{2}H_2$]-25
2.00
3.01
9.00
5.73
10 9 8 7 6 5 4 3 2 1 0
Chemical Shift (ppm)

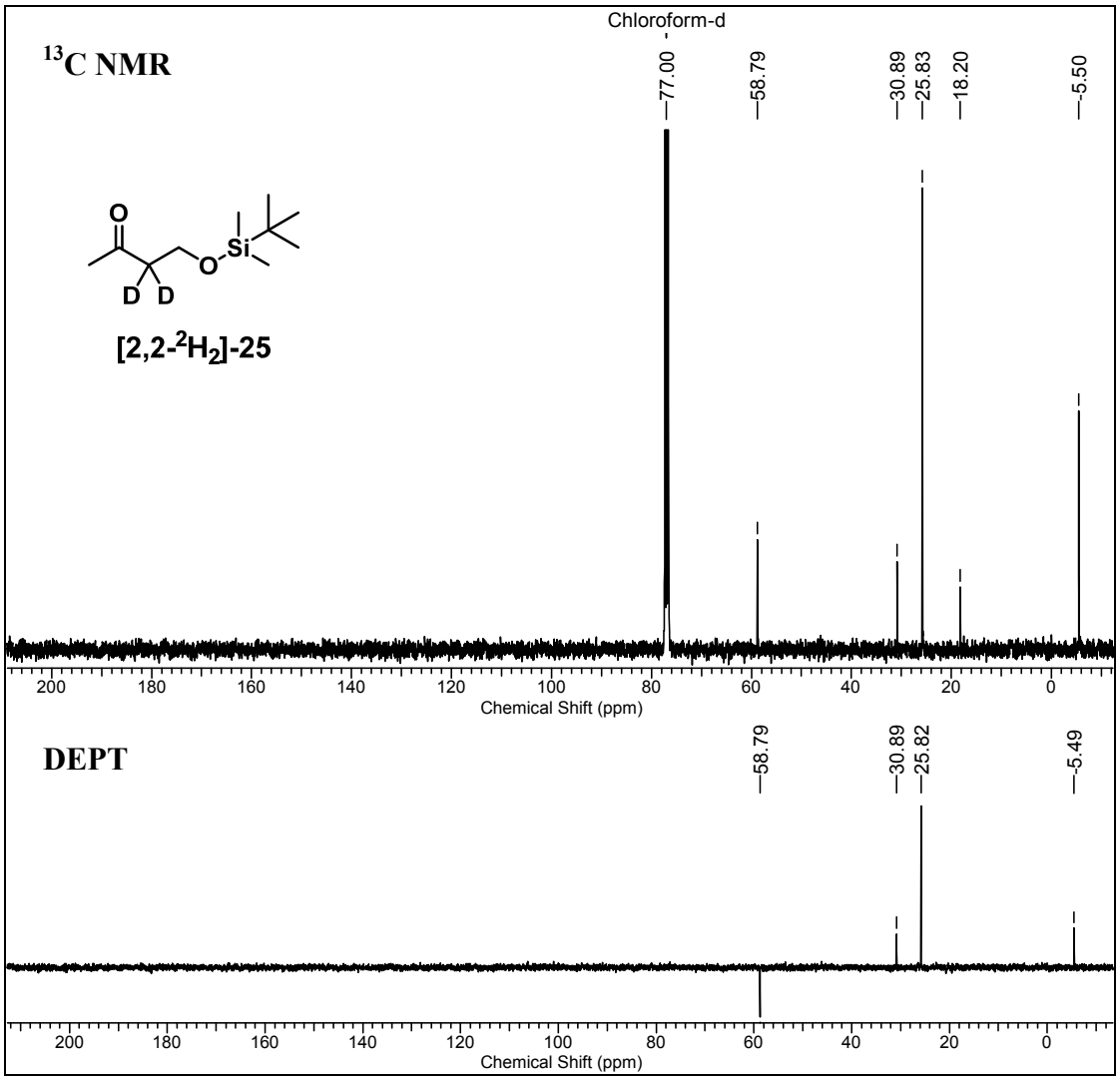
Chloroform-d
^{13}C NMR
77.00
58.79
30.89
25.83
18.20
-5.50
O
Si
O
D D
[2,2-$^{2}H_2$]-25
200 180 160 140 120 100 80 60 40 20 0
Chemical Shift (ppm)
DEPT
58.79
30.89
25.82
-5.49
200 180 160 140 120 100 80 60 40 20 0
Chemical Shift (ppm)

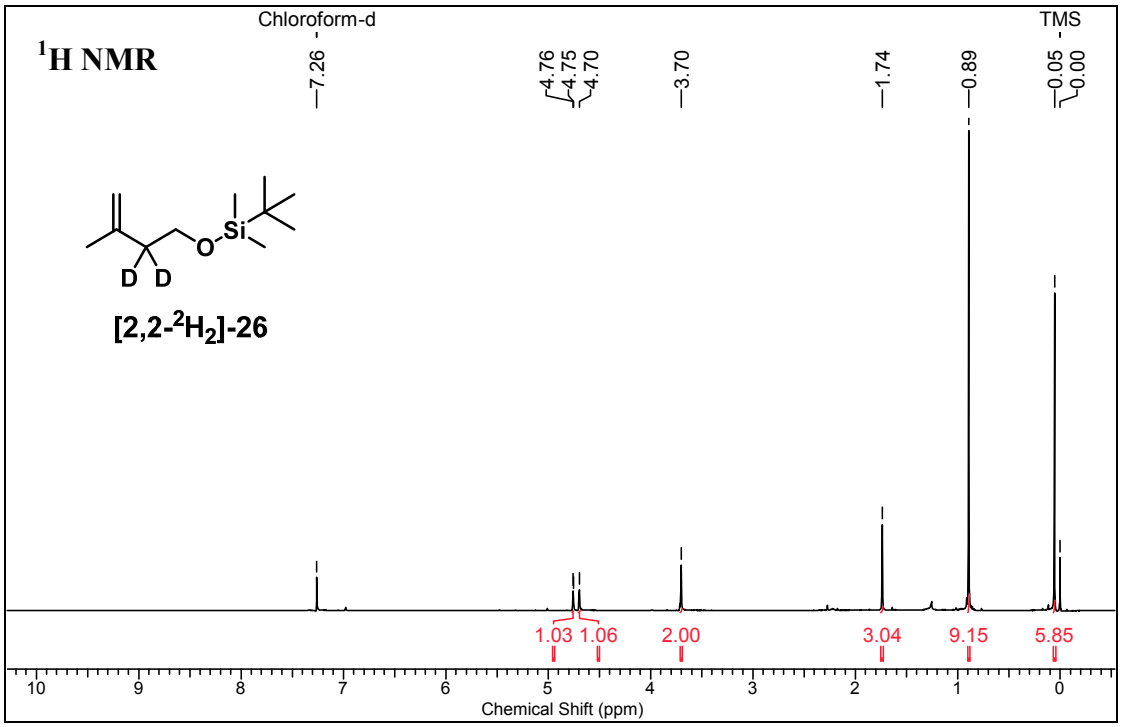
Chloroform-d
TMS
^{1}H NMR
7.26
4.76
4.75
4.70
3.70
1.74
0.89
0.05
0.00
Si
O
D D
[2,2-$^{2}H_2$]-26
1.03 1.06 2.00 3.04 9.15 5.85
Chemical Shift (ppm)

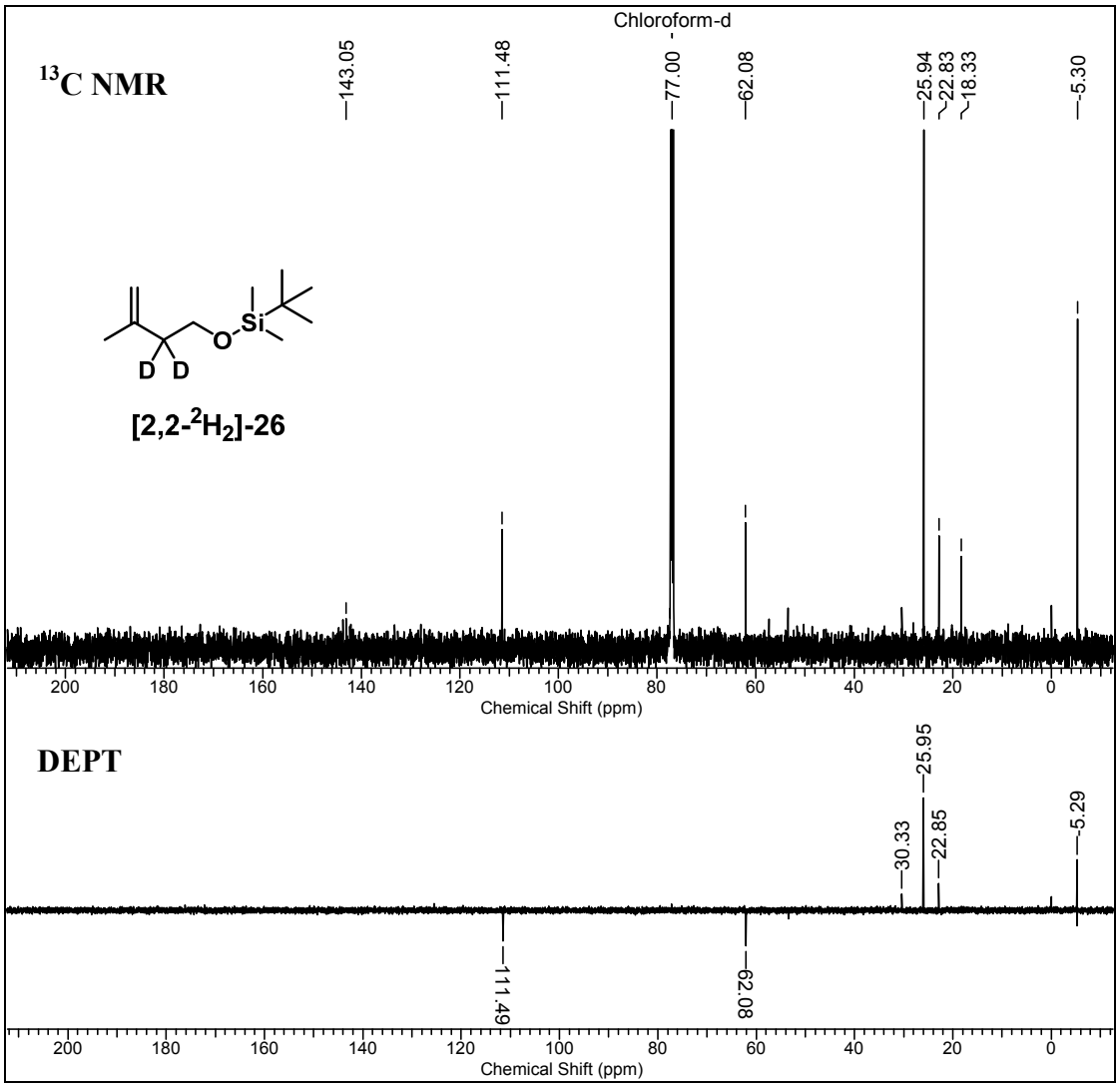
Chloroform-d
^{13}C NMR
143.05
111.48
77.00
62.08
25.94
22.83
18.33
5.30
Si
O
D D
[2,2-$^{2}H_2$]-26
Chemical Shift (ppm)
DEPT
25.95
30.33
22.85
5.29
111.49
62.08
Chemical Shift (ppm)

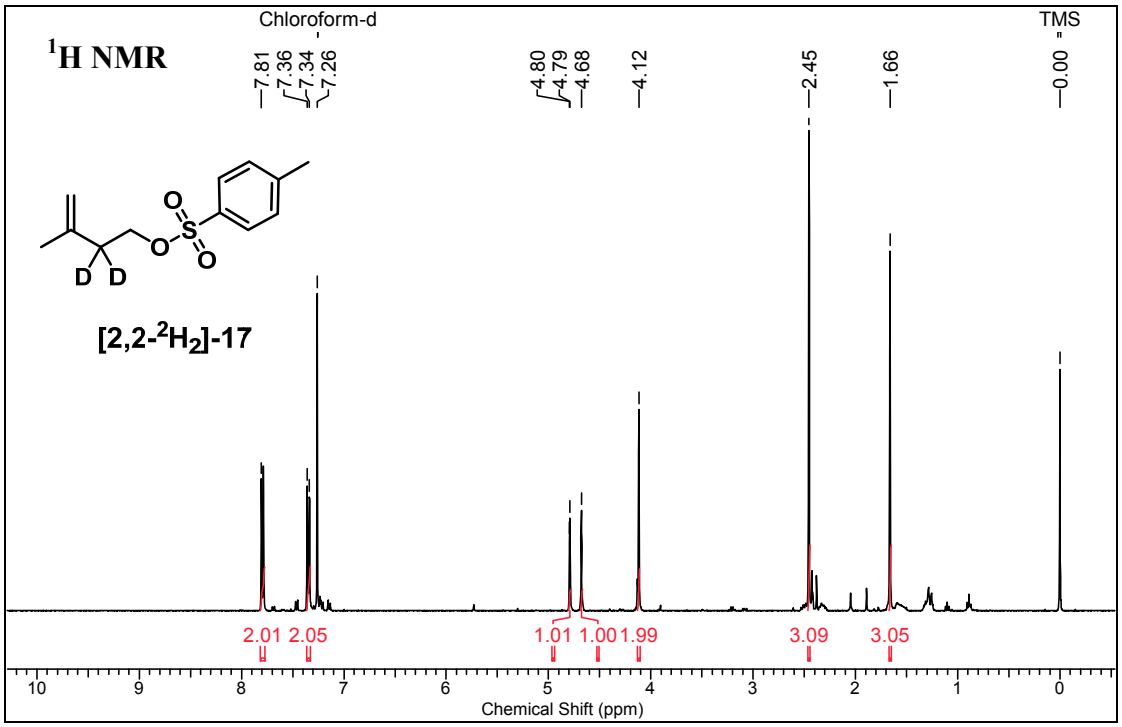
Chloroform-d
TMS
^{1}H NMR
7.81
7.36
7.34
7.26
4.80
4.79
4.68
4.12
2.45
1.66
0.00
[2,2-$^{2}H_2$]-17
2.01 2.05
1.01 1.00 1.99
3.09
3.05
Chemical Shift (ppm)

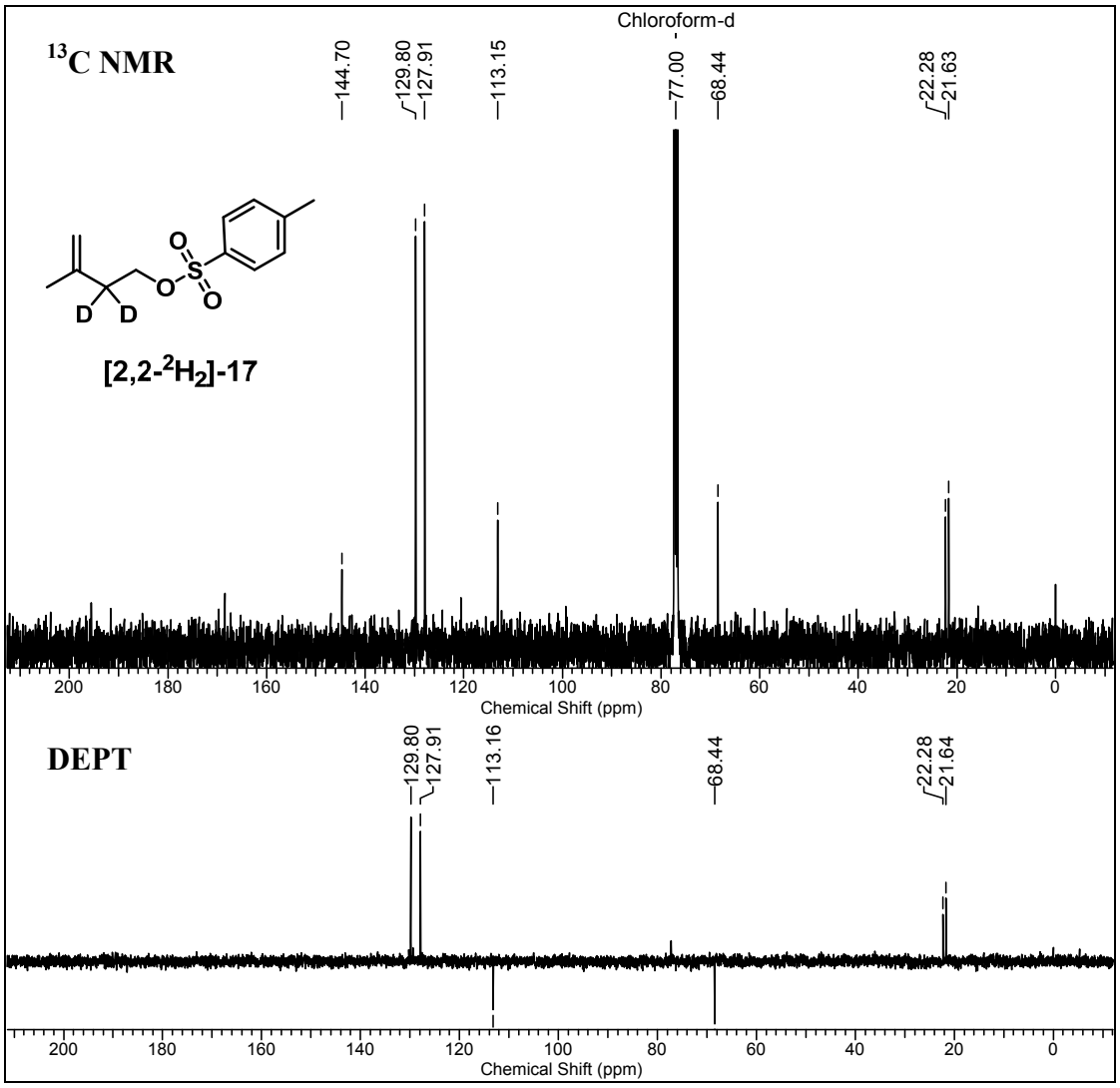
Chloroform-d
^{13}C NMR
144.70
129.80
127.91
113.15
77.00
68.44
22.28
21.63
[2,2-$^{2}H_2$]-17
Chemical Shift (ppm)
DEPT
129.80
127.91
113.16
68.44
22.28
21.64
Chemical Shift (ppm)

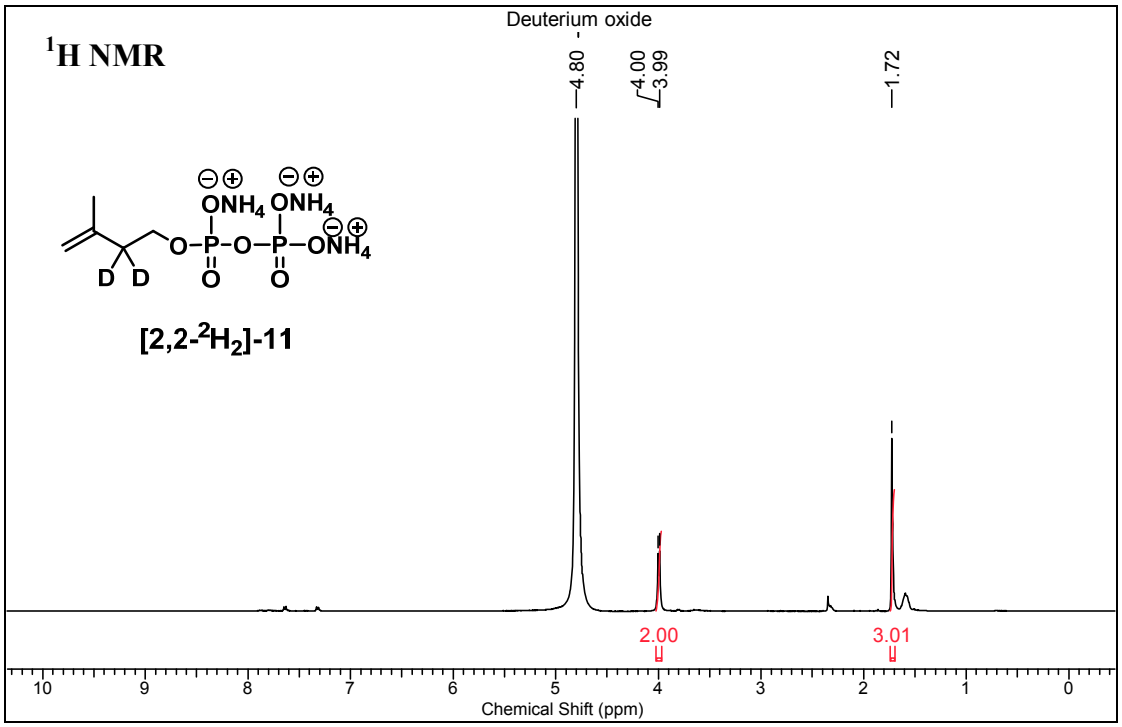
Deuterium oxide
^{1}H NMR
4.80
4.00
3.99
1.72
ONH4 ONH4
O–P–O–P–ONH4
D D
O O
[2,2-^{2}H$_2$]-11
2.00
3.01
10 9 8 7 6 5 4 3 2 1 0
Chemical Shift (ppm)

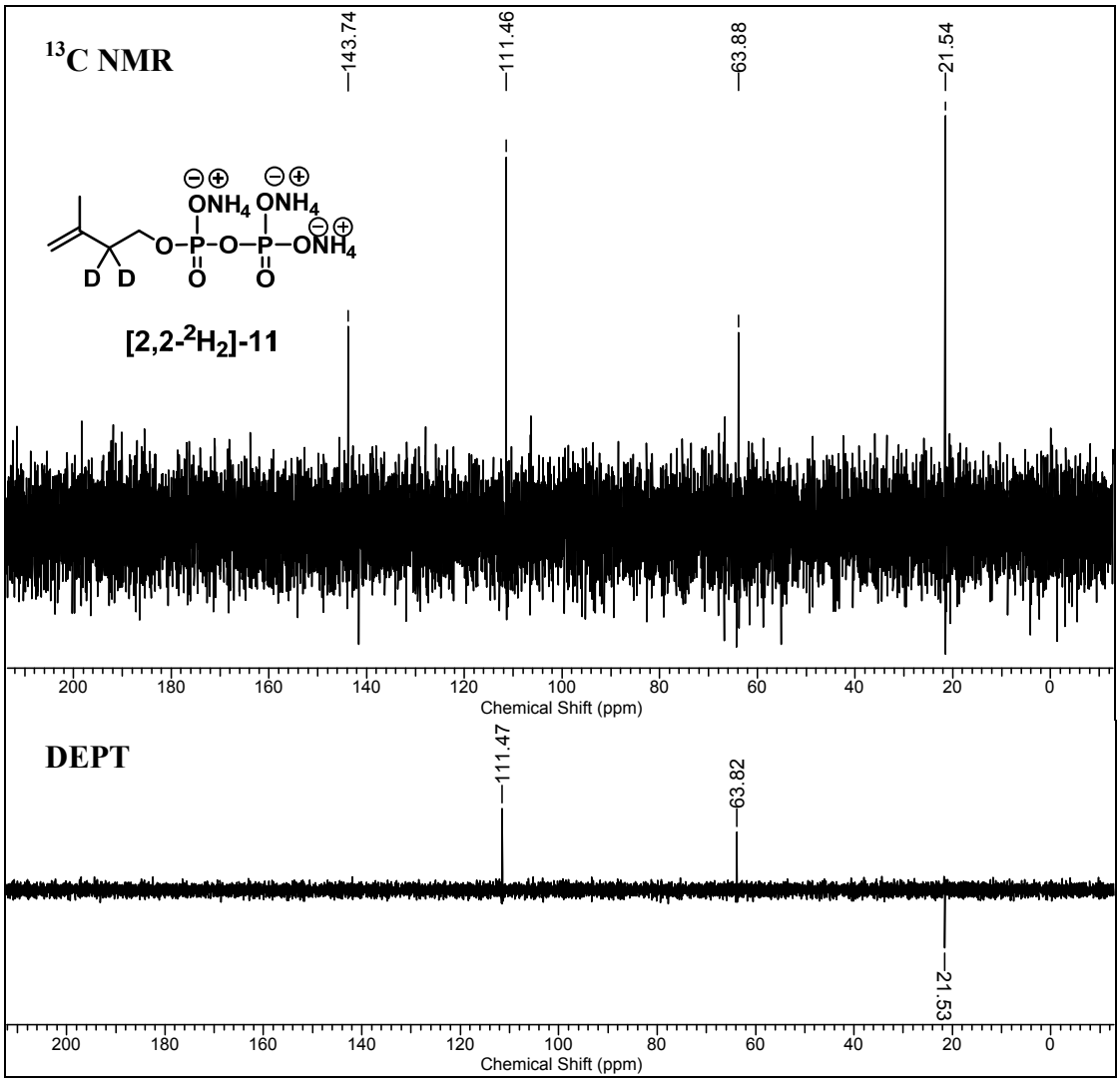
^{13}C NMR
143.74
111.46
63.88
21.54
ONH4 ONH4
O–P–O–P–ONH4
D D
O O
[2,2-^{2}H$_2$]-11
200 180 160 140 120 100 80 60 40 20 0
Chemical Shift (ppm)
DEPT
111.47
63.82
21.53
200 180 160 140 120 100 80 60 40 20 0
Chemical Shift (ppm)

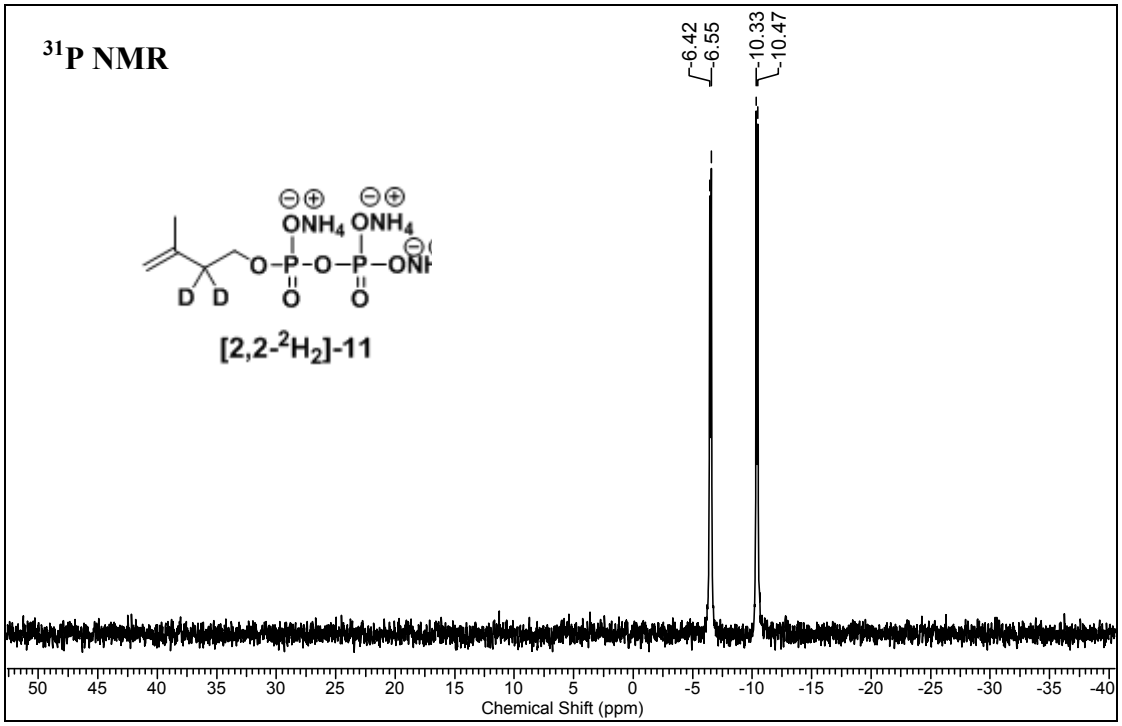
31P NMR
-6.42
-6.55
-10.33
-10.47
ONH4 ONH4
O-P-O-P-ONH
D D
O O
[2,2-2H2]-11
50 45 40 35 30 25 20 15 10 5 0 -5 -10 -15 -20 -25 -30 -35 -40
Chemical Shift (ppm)

HRMS (ESI)

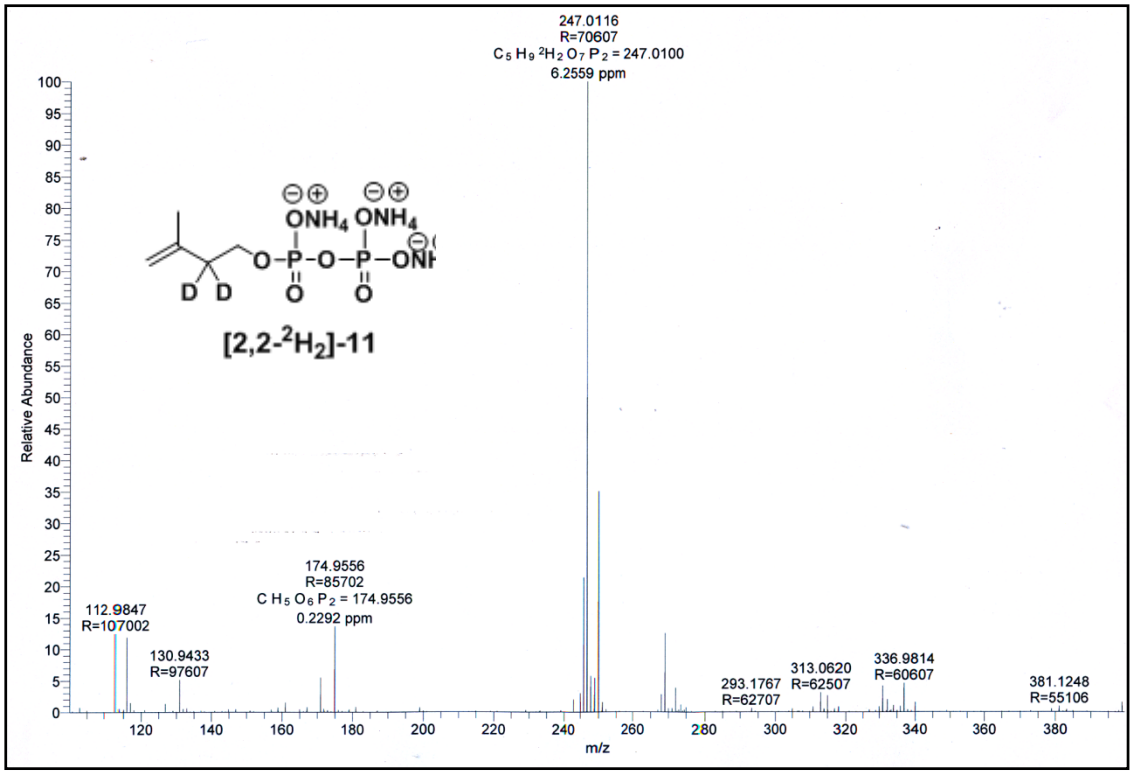
247.0116
R=70607
C5 H9 2H2 O7 P2 = 247.0100
6.2559 ppm
ONH4 ONH4
O-P-O-P-ONH
D D
O O
[2,2-2H2]-11
Relative Abundance
174.9556
R=85702
C H5 O6 P2 = 174.9556
0.2292 ppm
112.9847
R=107002
130.9433
R=97607
293.1767
R=62707
313.0620
R=62507
336.9814
R=60607
381.1248
R=55106
120 140 160 180 200 220 240 260 280 300 320 340 360 380
m/z

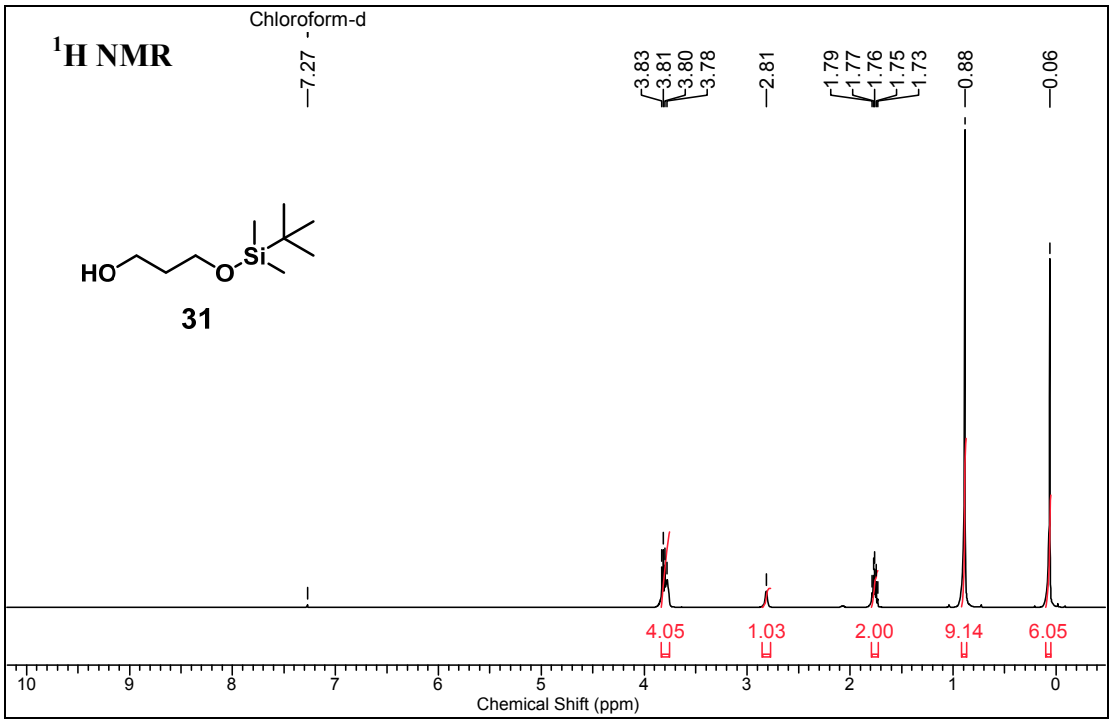
Chloroform-d
^{1}H NMR
7.27
3.83
3.81
3.80
3.78
2.81
1.79
1.77
1.76
1.75
1.73
0.88
0.06
HO
Si
O
31
4.05
1.03
2.00
9.14
6.05
Chemical Shift (ppm)

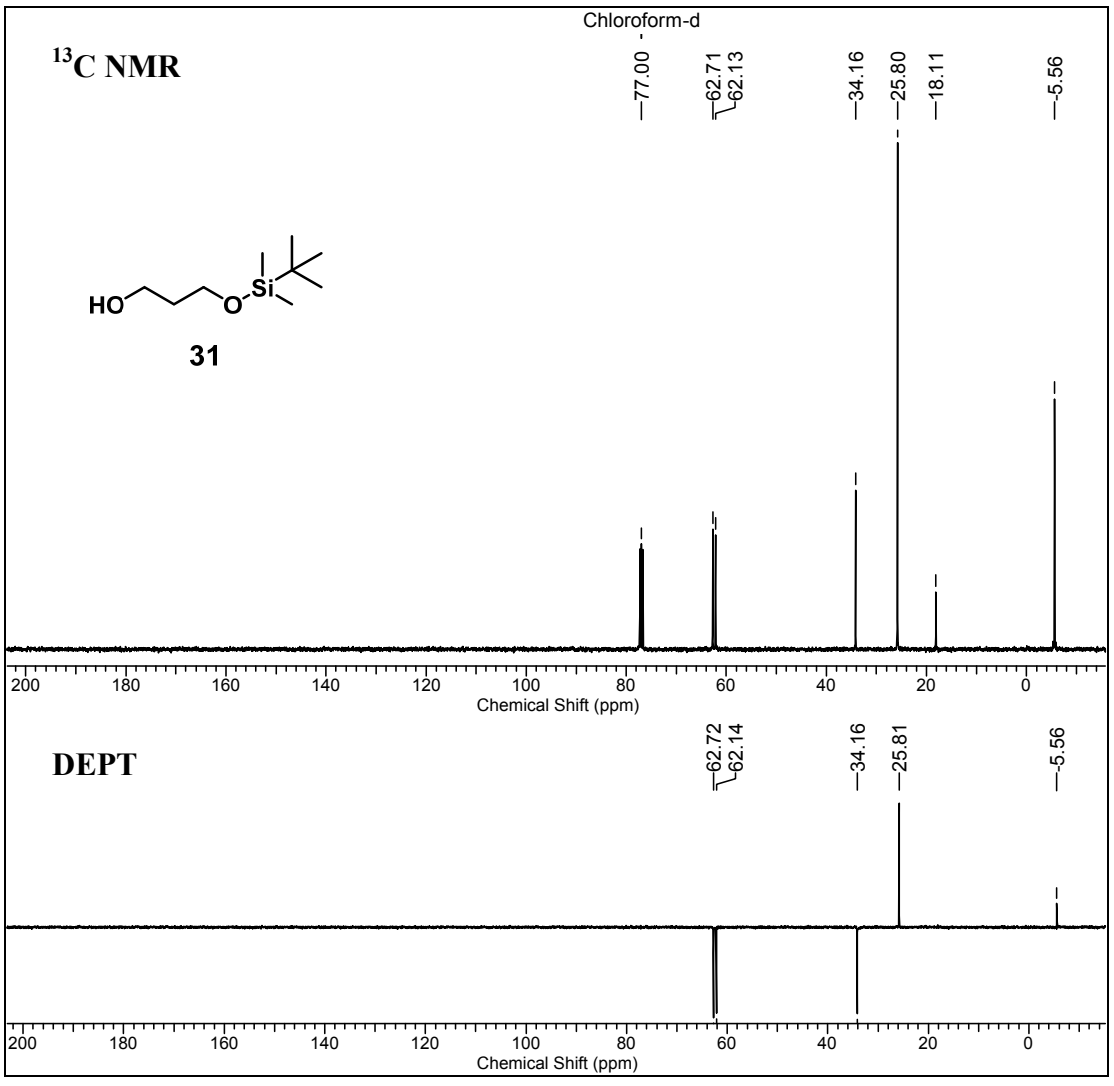
Chloroform-d
^{13}C NMR
77.00
62.71
62.13
34.16
25.80
18.11
5.56
HO
Si
O
31
Chemical Shift (ppm)
DEPT
62.72
62.14
34.16
25.81
5.56
Chemical Shift (ppm)

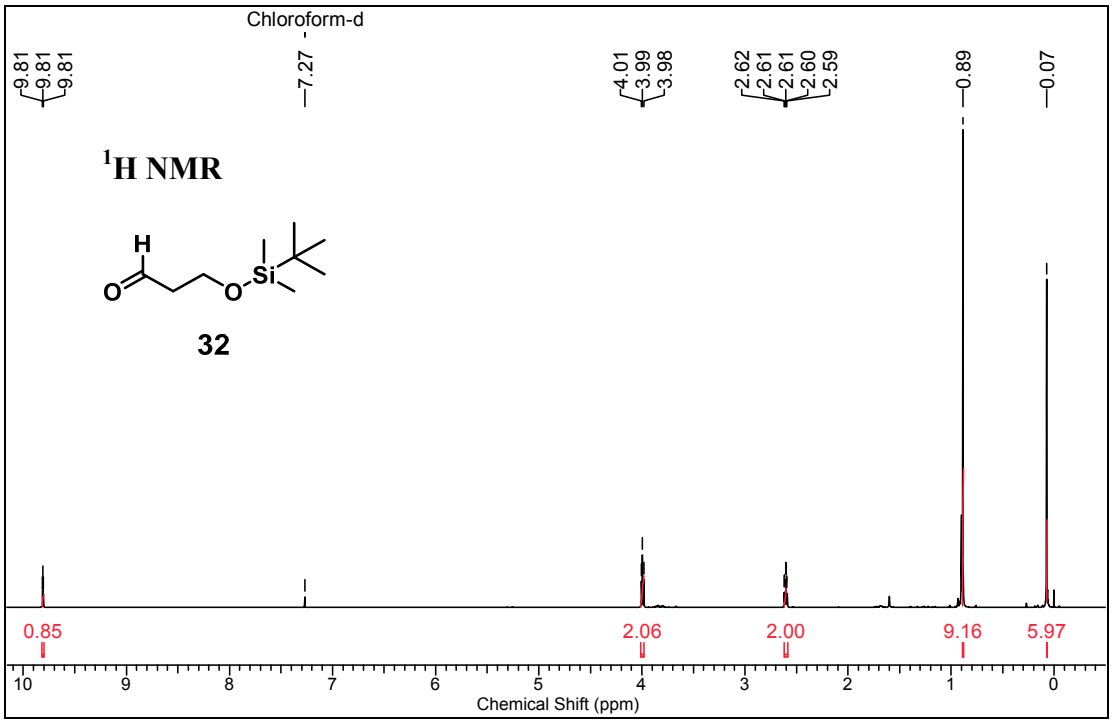
Chloroform-d
9.81
9.81
9.81
7.27
4.01
3.99
3.98
2.62
2.61
2.61
2.60
2.59
0.89
0.07
^{1}H NMR
H
O
O
Si
32
0.85
2.06
2.00
9.16
5.97
10
9
8
7
6
5
4
3
2
1
0
Chemical Shift (ppm)

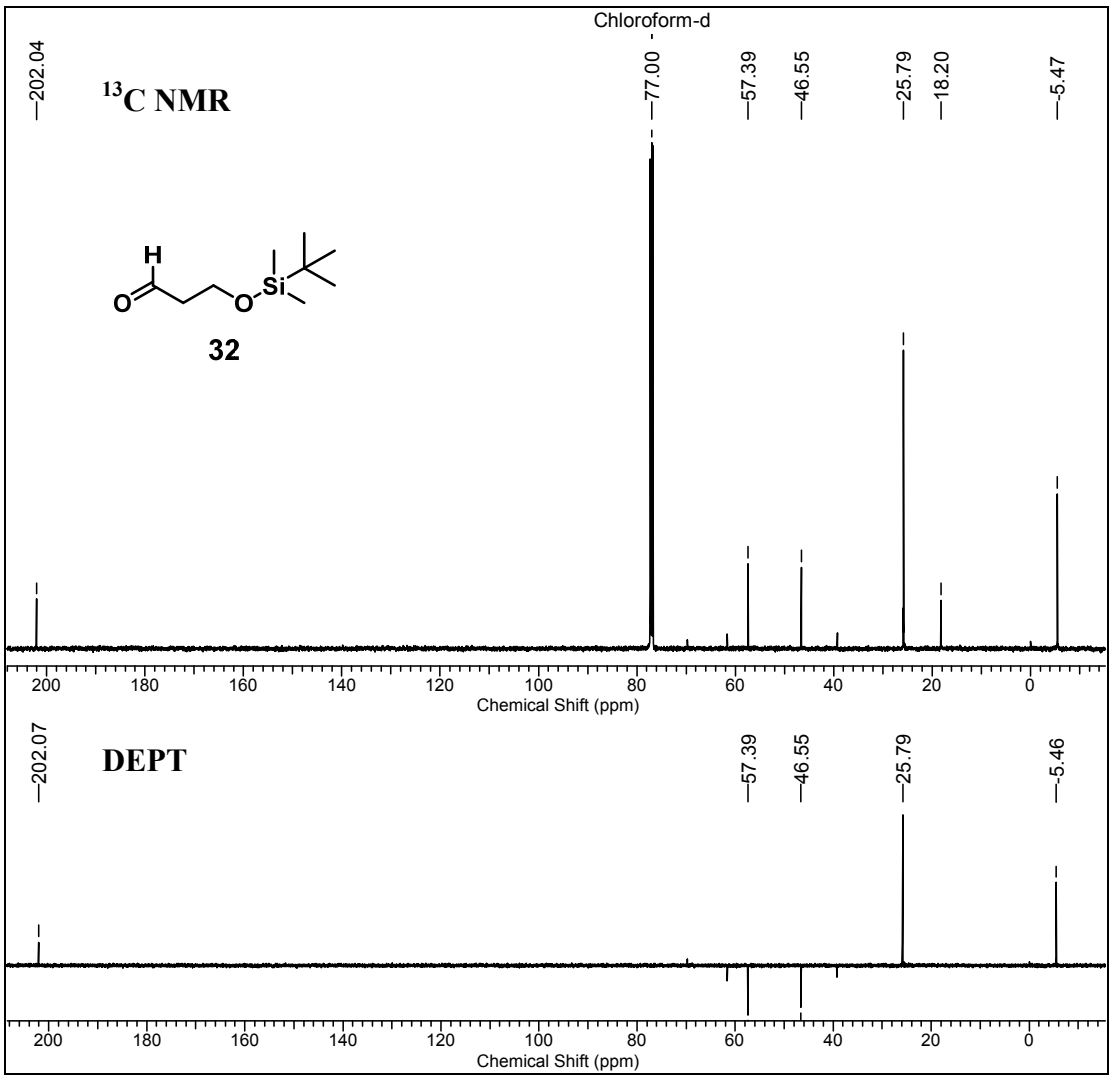
Chloroform-d
202.04
77.00
57.39
46.55
25.79
18.20
5.47
^{13}C NMR
H
O
O
Si
32
200
180
160
140
120
100
80
60
40
20
0
Chemical Shift (ppm)
202.07
57.39
46.55
25.79
5.46
DEPT
200
180
160
140
120
100
80
60
40
20
0
Chemical Shift (ppm)

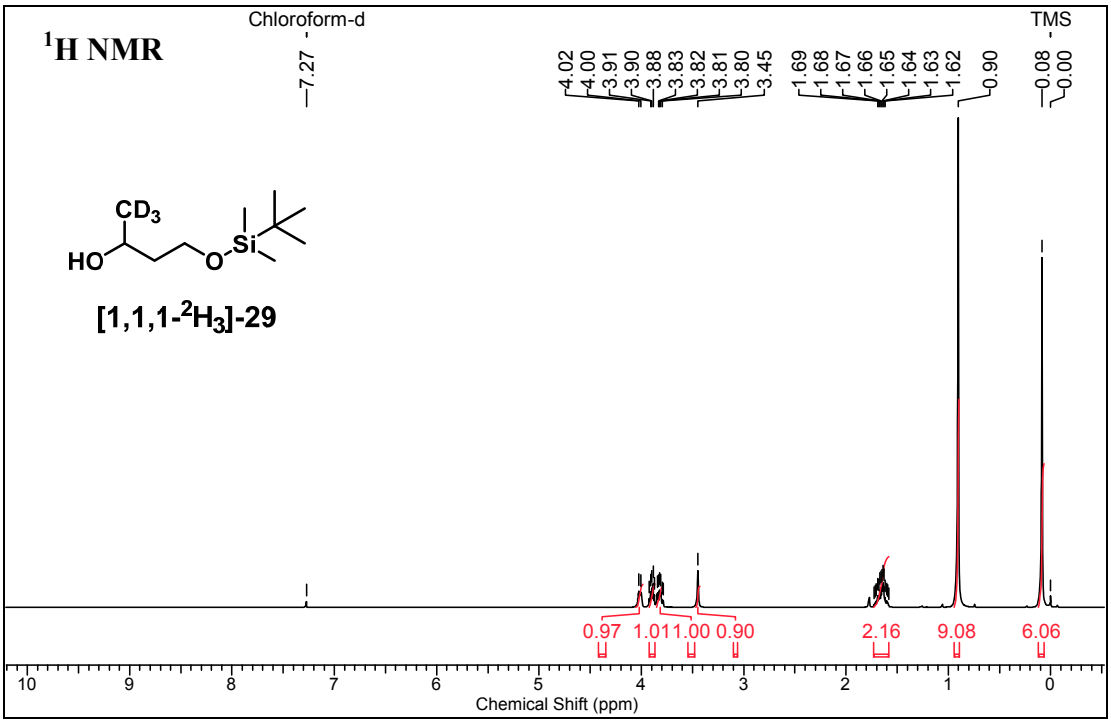
^{1}H NMR
Chloroform-d
TMS
7.27
4.02
4.00
3.91
3.90
3.88
3.83
3.82
3.81
3.80
3.45
1.69
1.68
1.67
1.66
1.65
1.64
1.63
1.62
0.90
0.08
0.00
CD3
HO
O
Si
[1,1,1-2H3]-29
0.97
1.01
1.00
0.90
2.16
9.08
6.06
Chemical Shift (ppm)

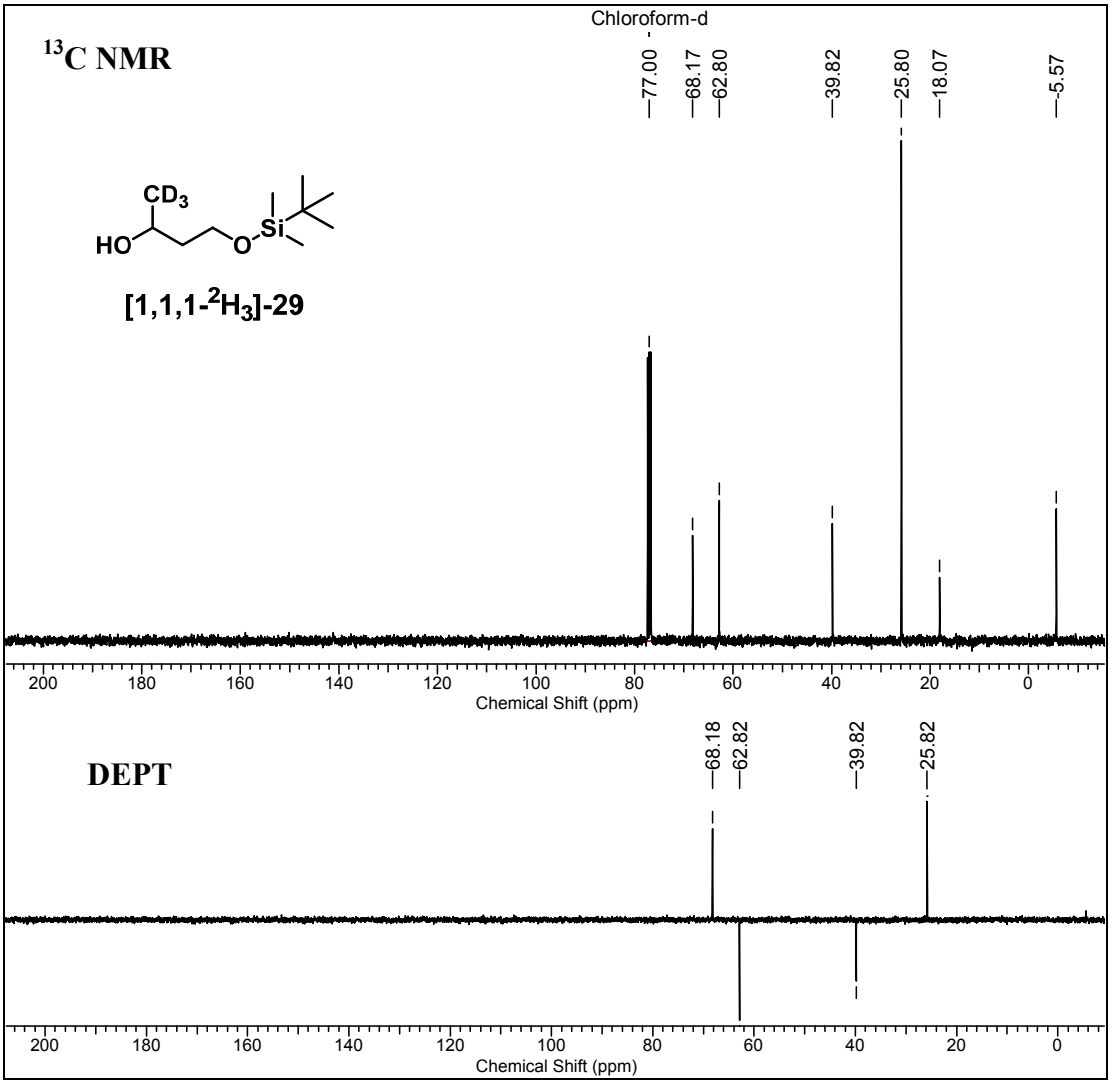
^{13}C NMR
Chloroform-d
77.00
68.17
62.80
39.82
25.80
18.07
5.57
CD3
HO
O
Si
[1,1,1-2H3]-29
Chemical Shift (ppm)
DEPT
68.18
62.82
39.82
25.82
Chemical Shift (ppm)

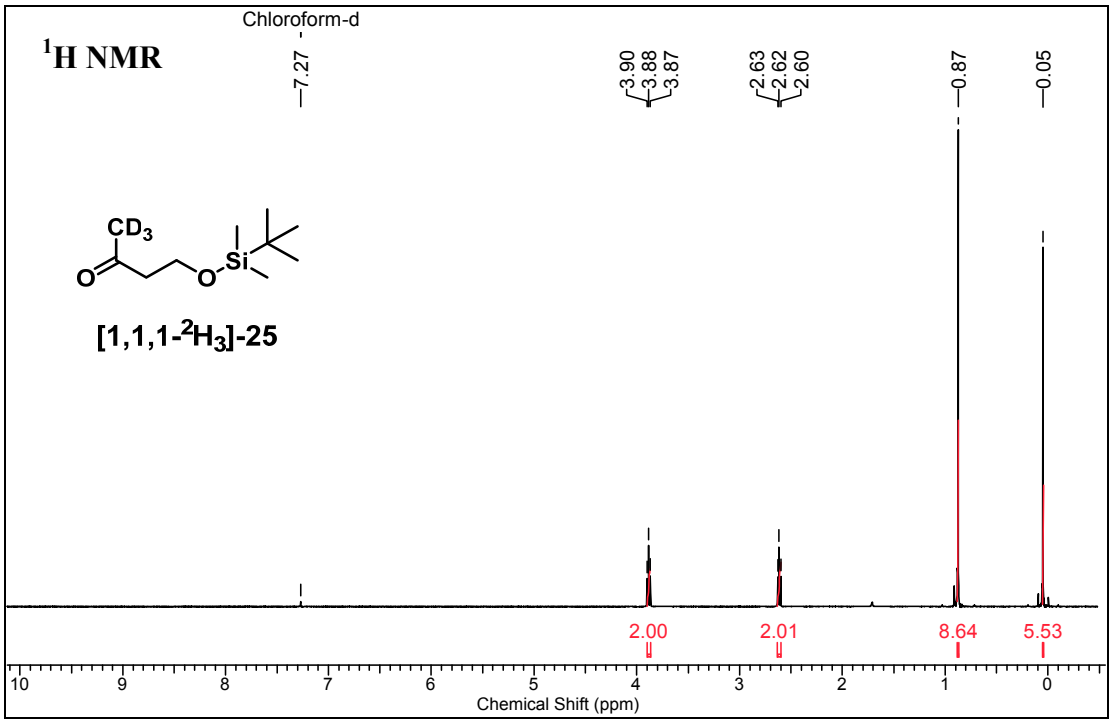
Chloroform-d
^{1}H NMR
7.27
3.90
3.88
3.87
2.63
2.62
2.60
0.87
0.05
CD3
O
O
Si
[1,1,1-^{2}H$_3$]-25
2.00
2.01
8.64
5.53
10
9
8
7
6
5
4
3
2
1
0
Chemical Shift (ppm)

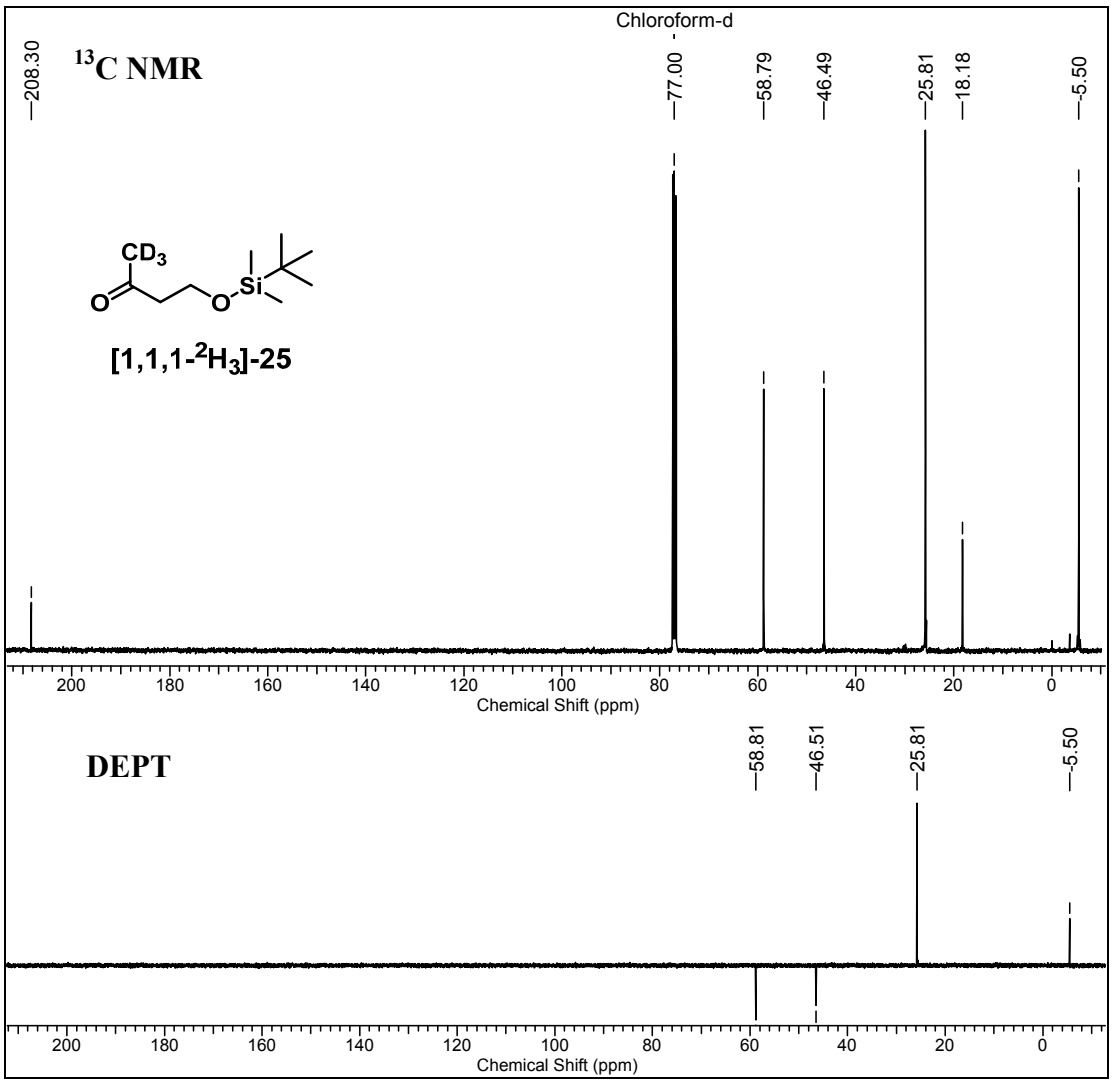
Chloroform-d
208.30
^{13}C NMR
77.00
58.79
46.49
25.81
18.18
5.50
CD3
O
O
Si
[1,1,1-^{2}H$_3$]-25
200
180
160
140
120
100
80
60
40
20
0
Chemical Shift (ppm)
DEPT
58.81
46.51
25.81
5.50
200
180
160
140
120
100
80
60
40
20
0
Chemical Shift (ppm)

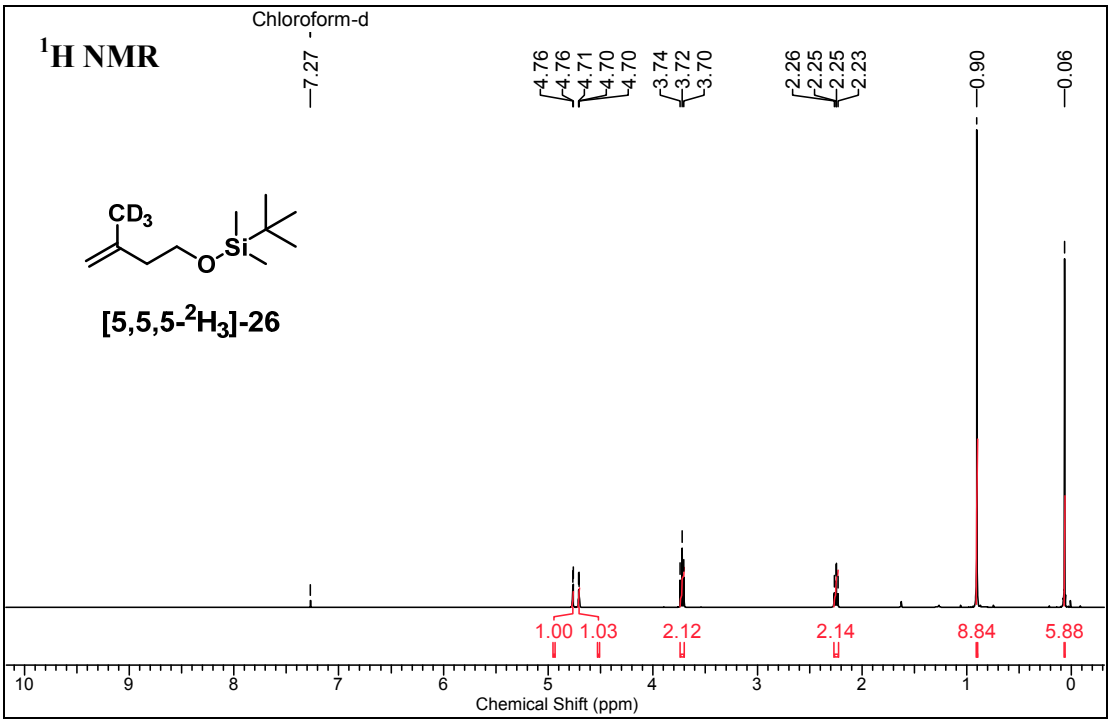
Chloroform-d
^{1}H NMR
7.27
4.76
4.76
4.71
4.70
4.70
3.74
3.72
3.70
2.26
2.25
2.25
2.23
0.90
0.06
CD3
Si
O
[5,5,5-^{2}H$_3$]-26
1.00
1.03
2.12
2.14
8.84
5.88
Chemical Shift (ppm)

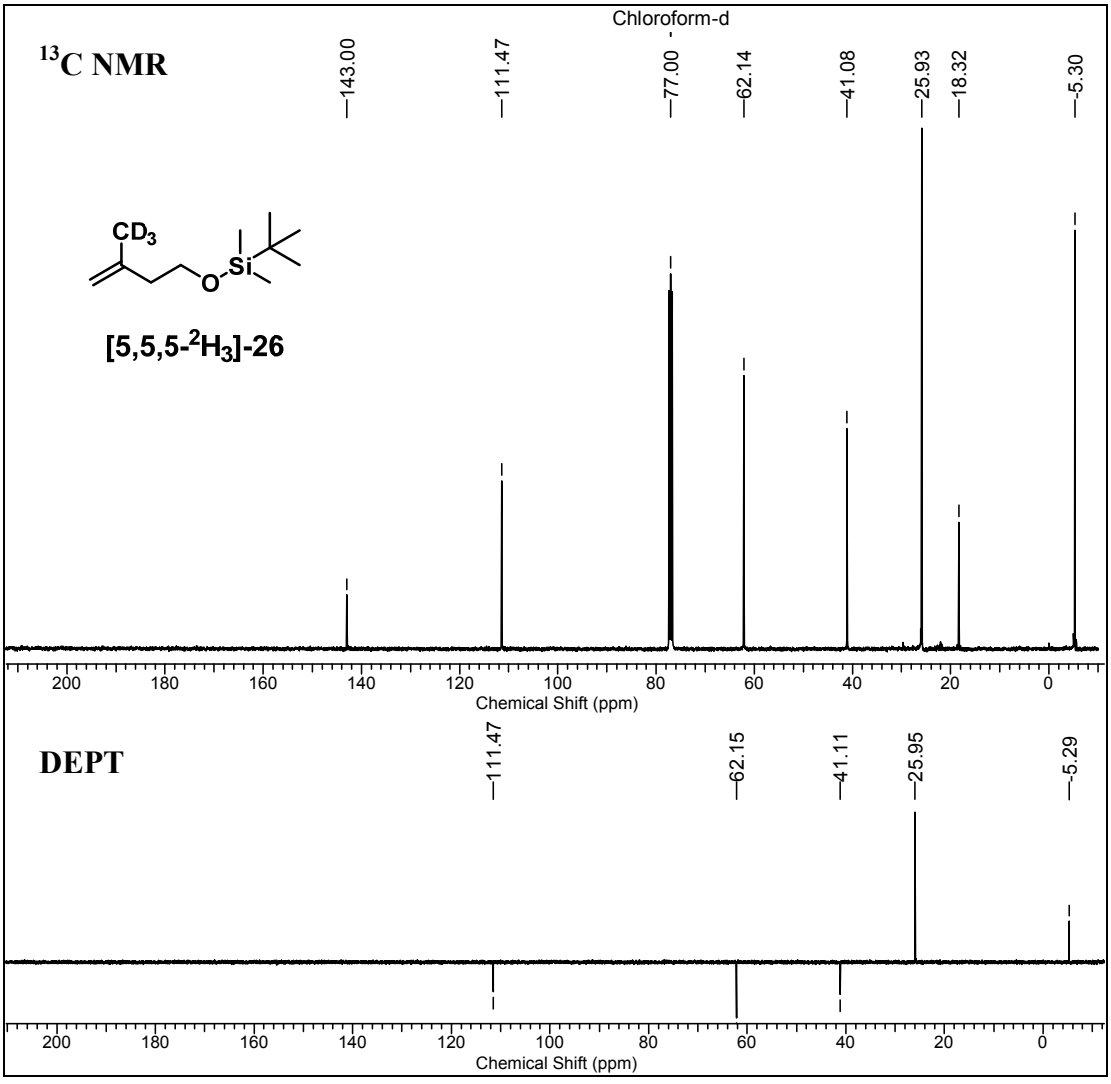
Chloroform-d
^{13}C NMR
143.00
111.47
77.00
62.14
41.08
25.93
18.32
5.30
CD3
Si
O
[5,5,5-^{2}H$_3$]-26
Chemical Shift (ppm)
DEPT
111.47
62.15
41.11
25.95
5.29
Chemical Shift (ppm)

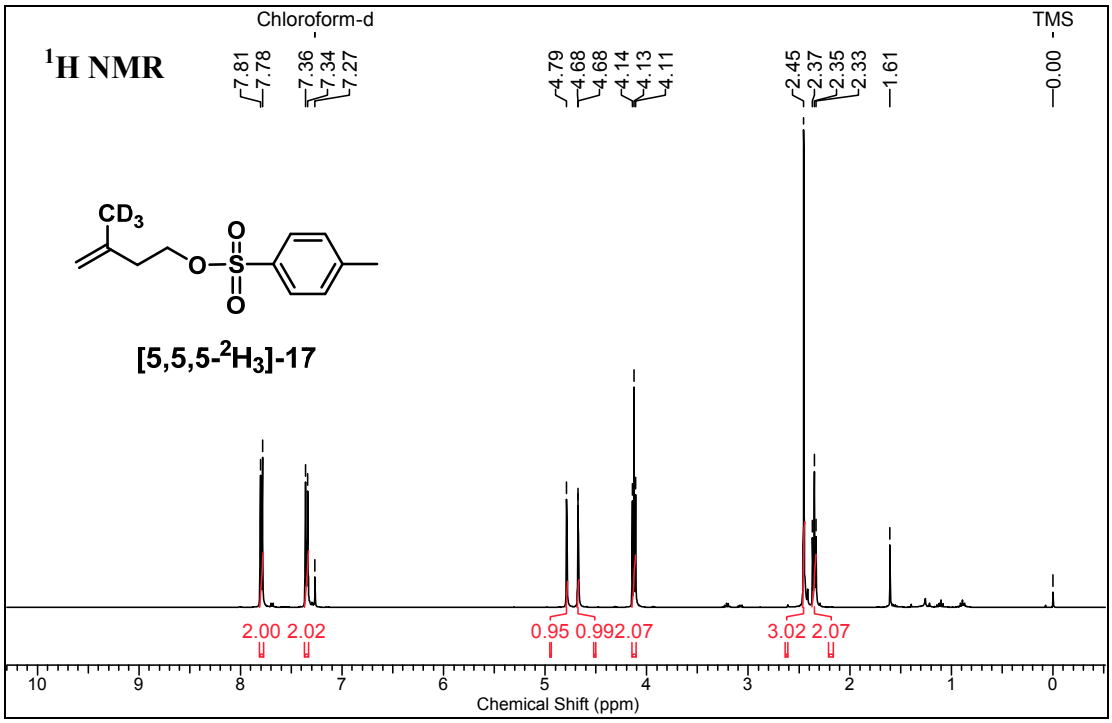
Chloroform-d
TMS
^{1}H NMR
7.81
7.78
7.36
7.34
7.27
4.79
4.68
4.68
4.14
4.13
4.11
2.45
2.37
2.35
2.33
1.61
0.00
CD3
O
S
O
O
[5,5,5-^{2}H$_3$]-17
2.00 2.02
0.95 0.99
2.07
3.02 2.07
10 9 8 7 6 5 4 3 2 1 0
Chemical Shift (ppm)

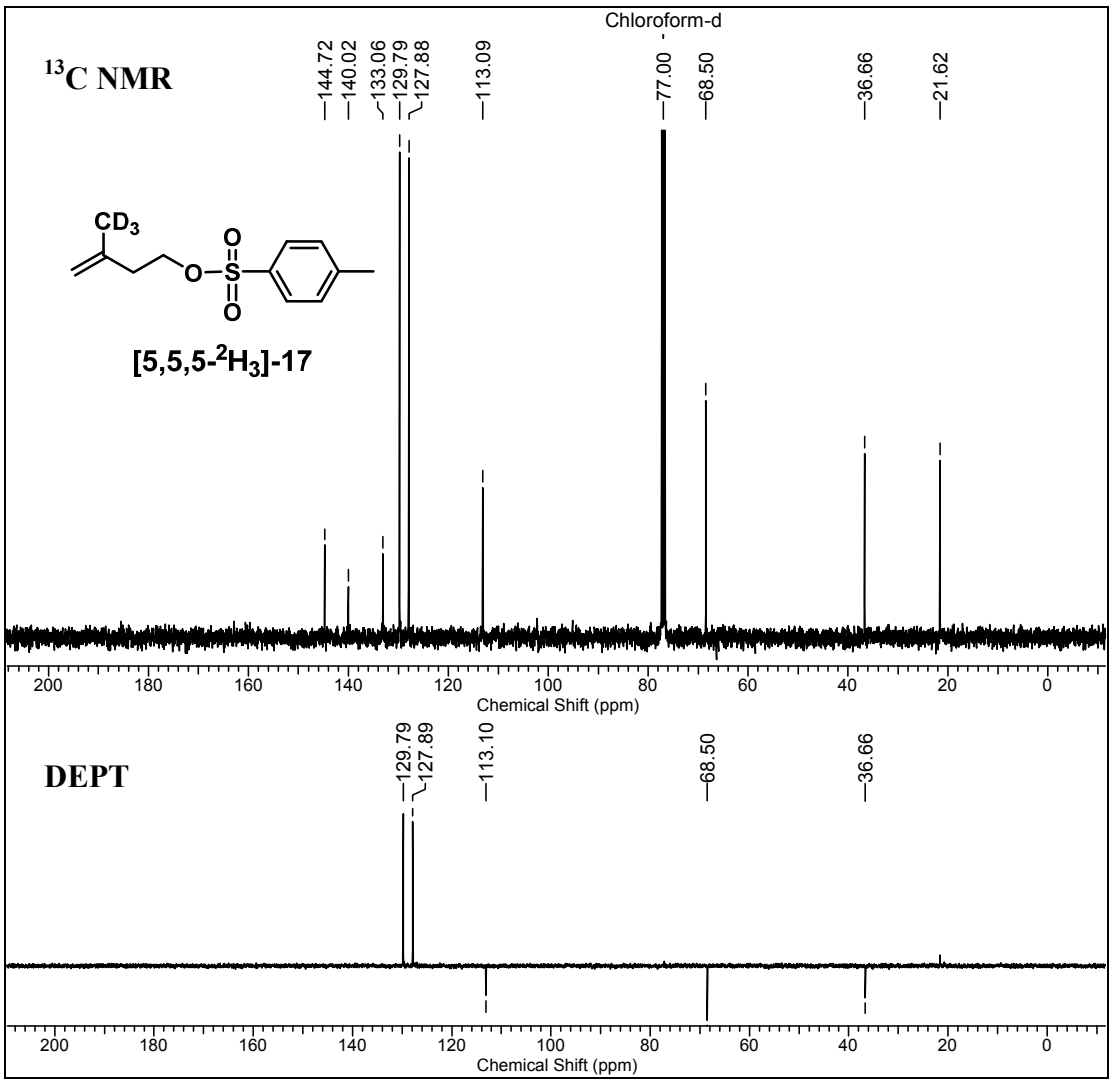
Chloroform-d
^{13}C NMR
144.72
140.02
133.06
129.79
127.88
113.09
77.00
68.50
36.66
21.62
CD3
O
S
O
O
[5,5,5-^{2}H$_3$]-17
200 180 160 140 120 100 80 60 40 20 0
Chemical Shift (ppm)
DEPT
129.79
127.89
113.10
68.50
36.66
200 180 160 140 120 100 80 60 40 20 0
Chemical Shift (ppm)

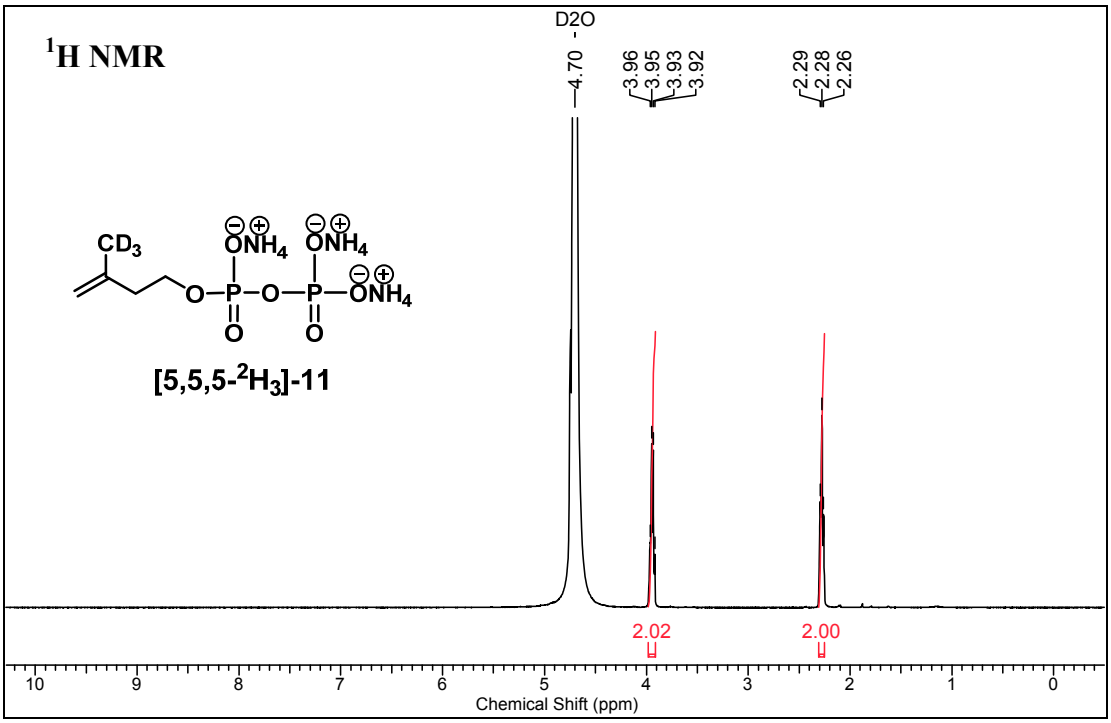
^{1}H NMR
D2O
4.70
3.96
3.95
3.93
3.92
2.29
2.28
2.26
2.02
2.00
Chemical Shift (ppm)
[5,5,5-^{2}H$_3$]-11

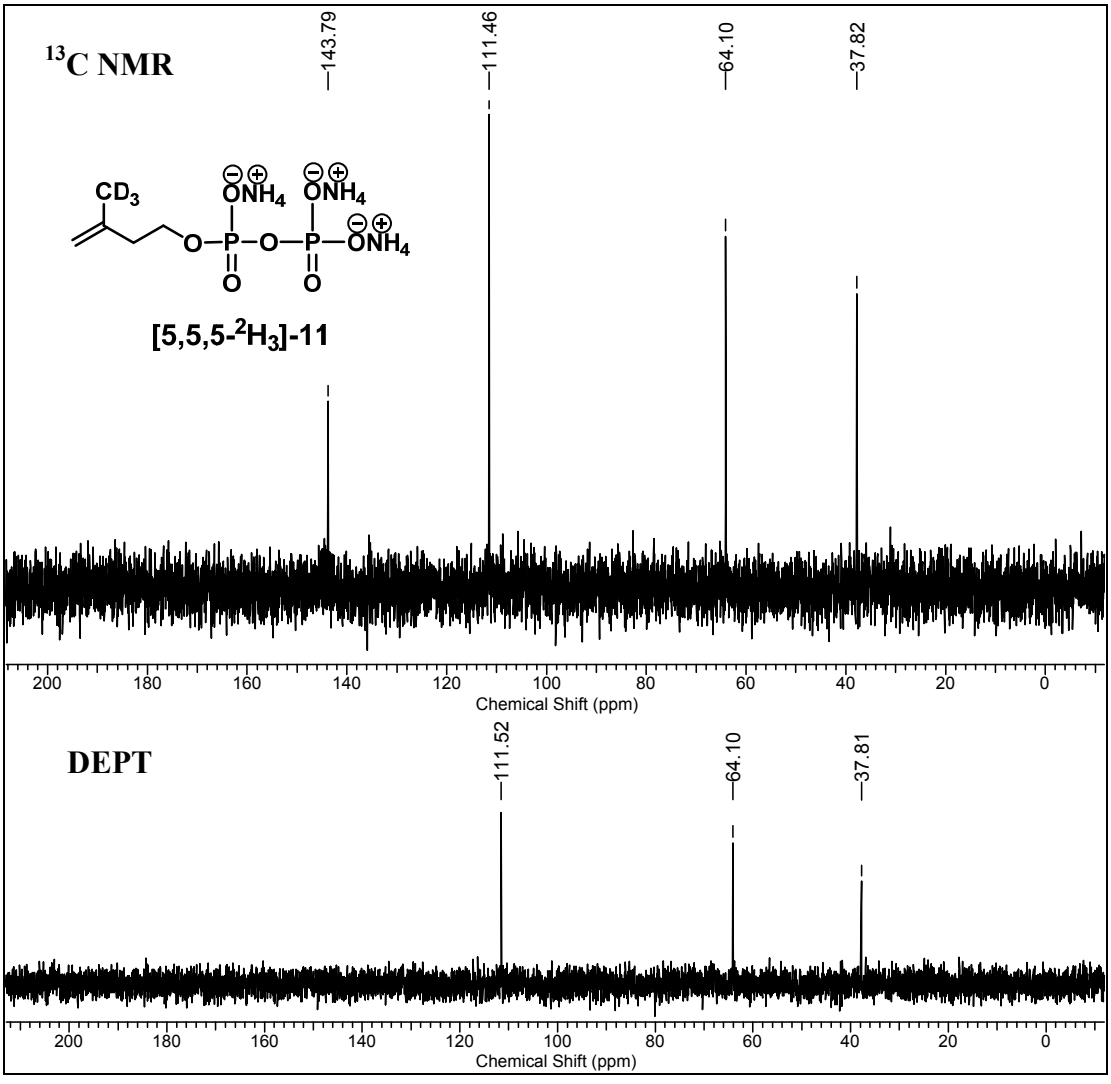
^{13}C NMR
143.79
111.46
64.10
37.82
Chemical Shift (ppm)
[5,5,5-^{2}H$_3$]-11
DEPT
111.52
64.10
37.81
Chemical Shift (ppm)

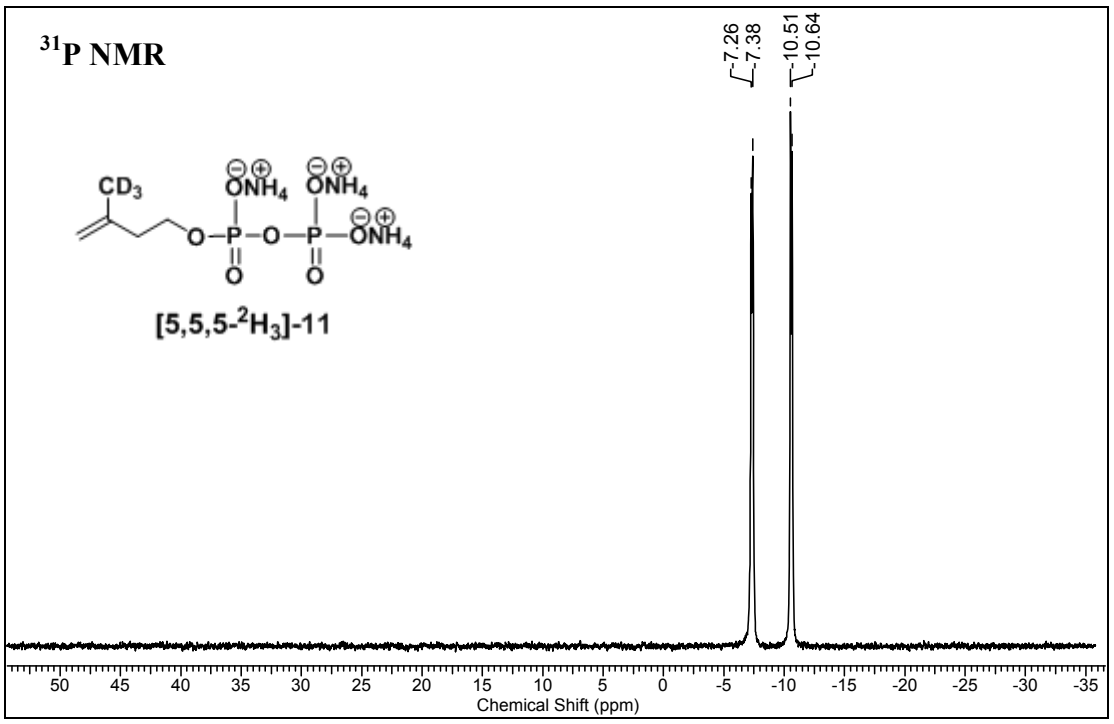
31P NMR
7.26
7.38
10.51
10.64
CD3
ONH4
ONH4
ONH4
O
P
O
P
O
O
O
[5,5,5-2H3]-11
50 45 40 35 30 25 20 15 10 5 0 -5 -10 -15 -20 -25 -30 -35
Chemical Shift (ppm)

HRMS (ESI)

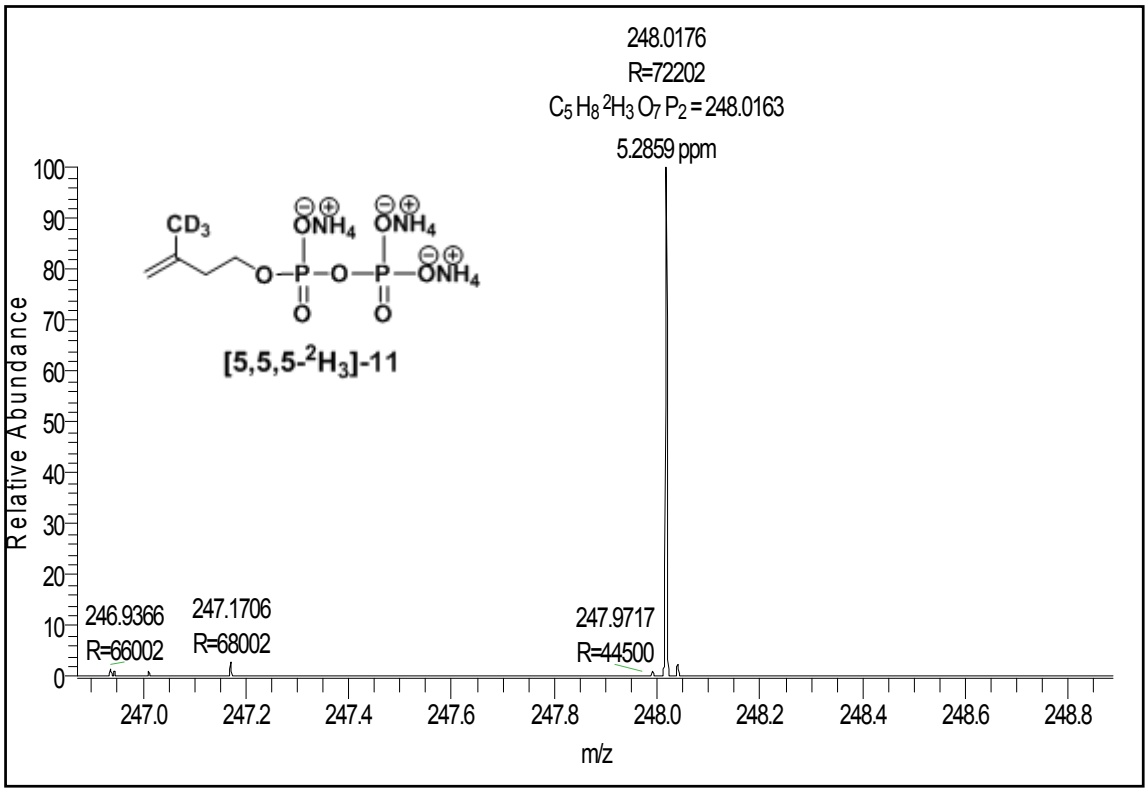
248.0176
R=72202
C5 H8 2H3 O7 P2 = 248.0163
5.2859 ppm
CD3
ONH4
ONH4
ONH4
O
P
O
P
O
O
O
[5,5,5-2H3]-11
Relative Abundance
100
90
80
70
60
50
40
30
20
10
0
246.9366
R=66002
247.1706
R=68002
247.9717
R=44500
247.0 247.2 247.4 247.6 247.8 248.0 248.2 248.4 248.6 248.8
m/z

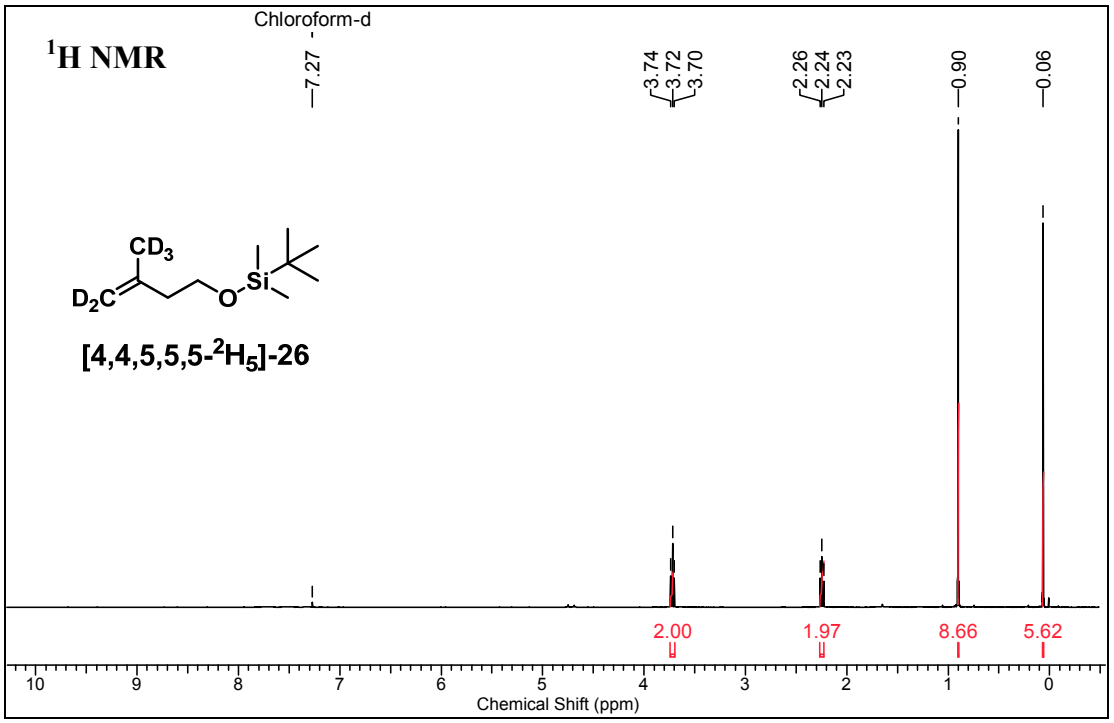
Chloroform-d
^{1}H NMR
7.27
3.74
3.72
3.70
2.26
2.24
2.23
0.90
0.06
CD3
D2C
Si
O
[4,4,5,5,5-2H5]-26
2.00
1.97
8.66
5.62
Chemical Shift (ppm)

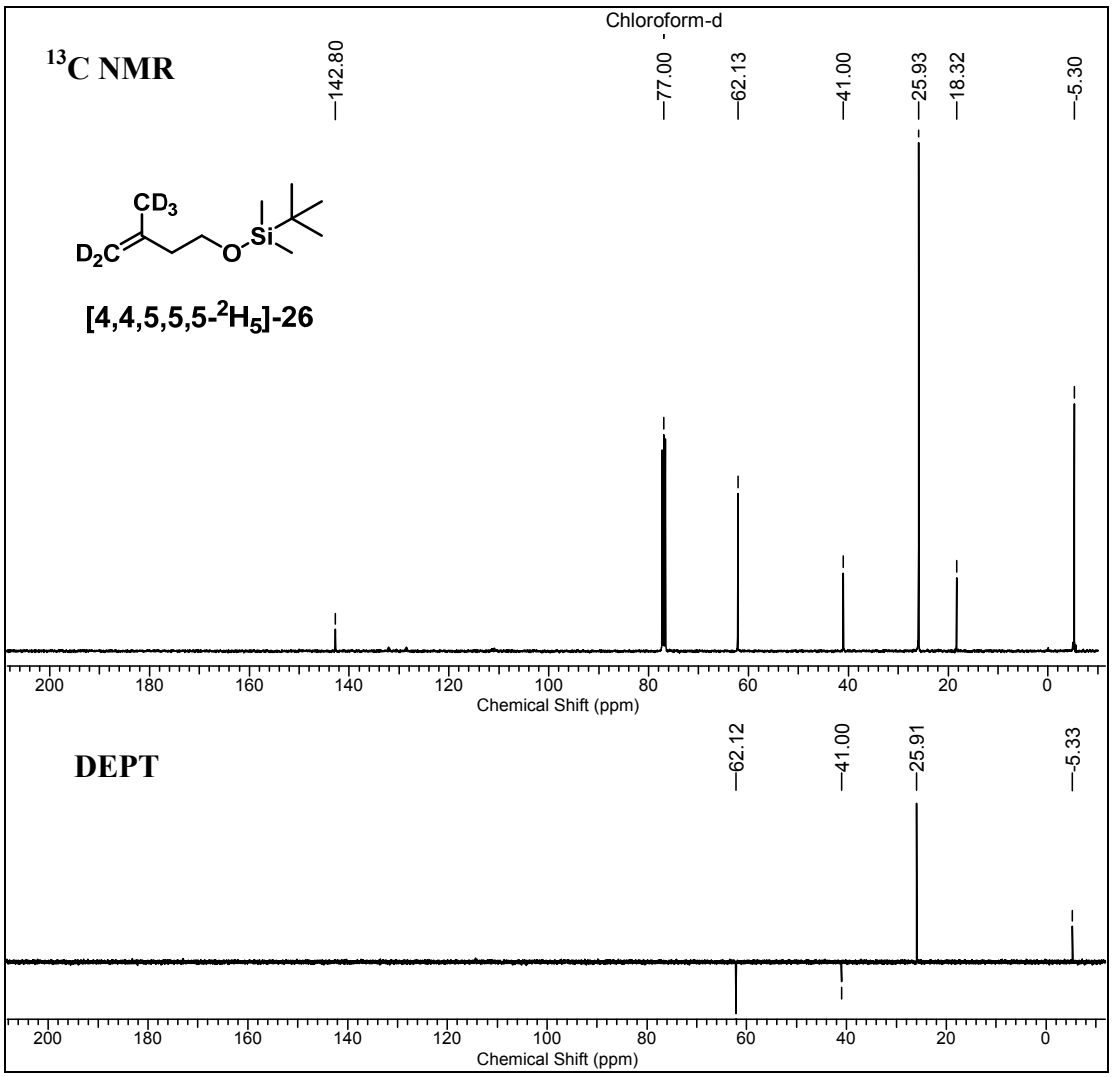
Chloroform-d
^{13}C NMR
142.80
77.00
62.13
41.00
25.93
18.32
5.30
CD3
D2C
Si
O
[4,4,5,5,5-2H5]-26
Chemical Shift (ppm)
DEPT
62.12
41.00
25.91
5.33
Chemical Shift (ppm)

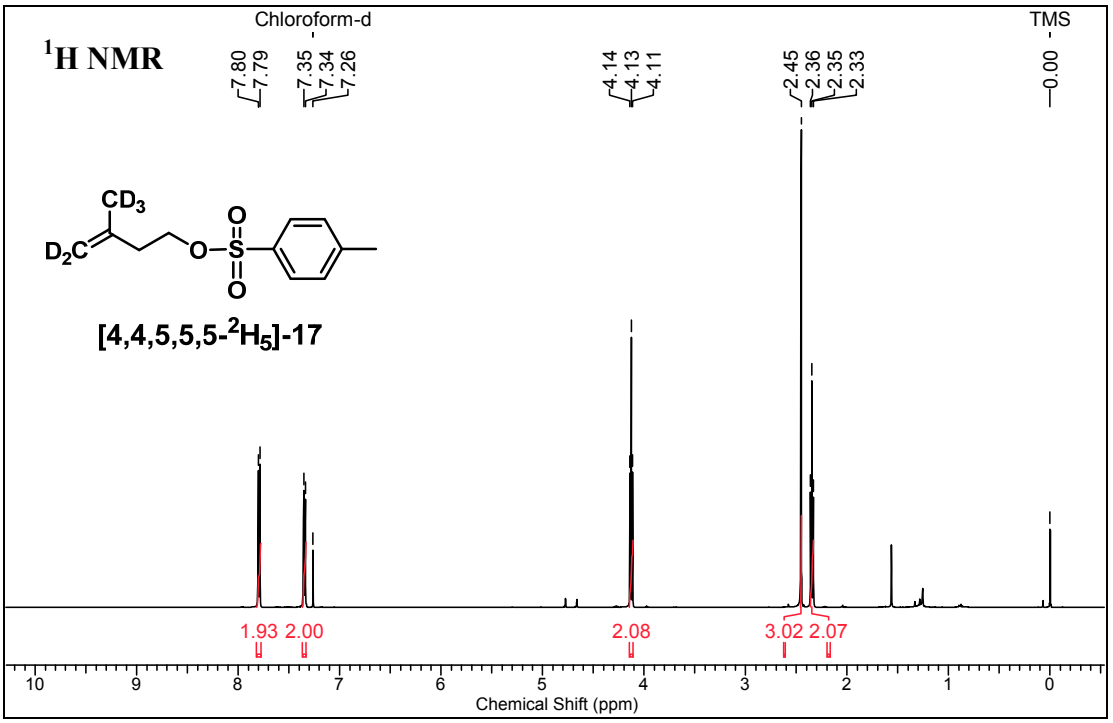
Chloroform-d
TMS
^{1}H NMR
7.80
7.79
7.35
7.34
7.26
4.14
4.13
4.11
2.45
2.36
2.35
2.33
0.00
CD3
D2C
O
S
O
O
[4,4,5,5,5-2H5]-17
1.93
2.00
2.08
3.02
2.07
10
9
8
7
6
5
4
3
2
1
0
Chemical Shift (ppm)

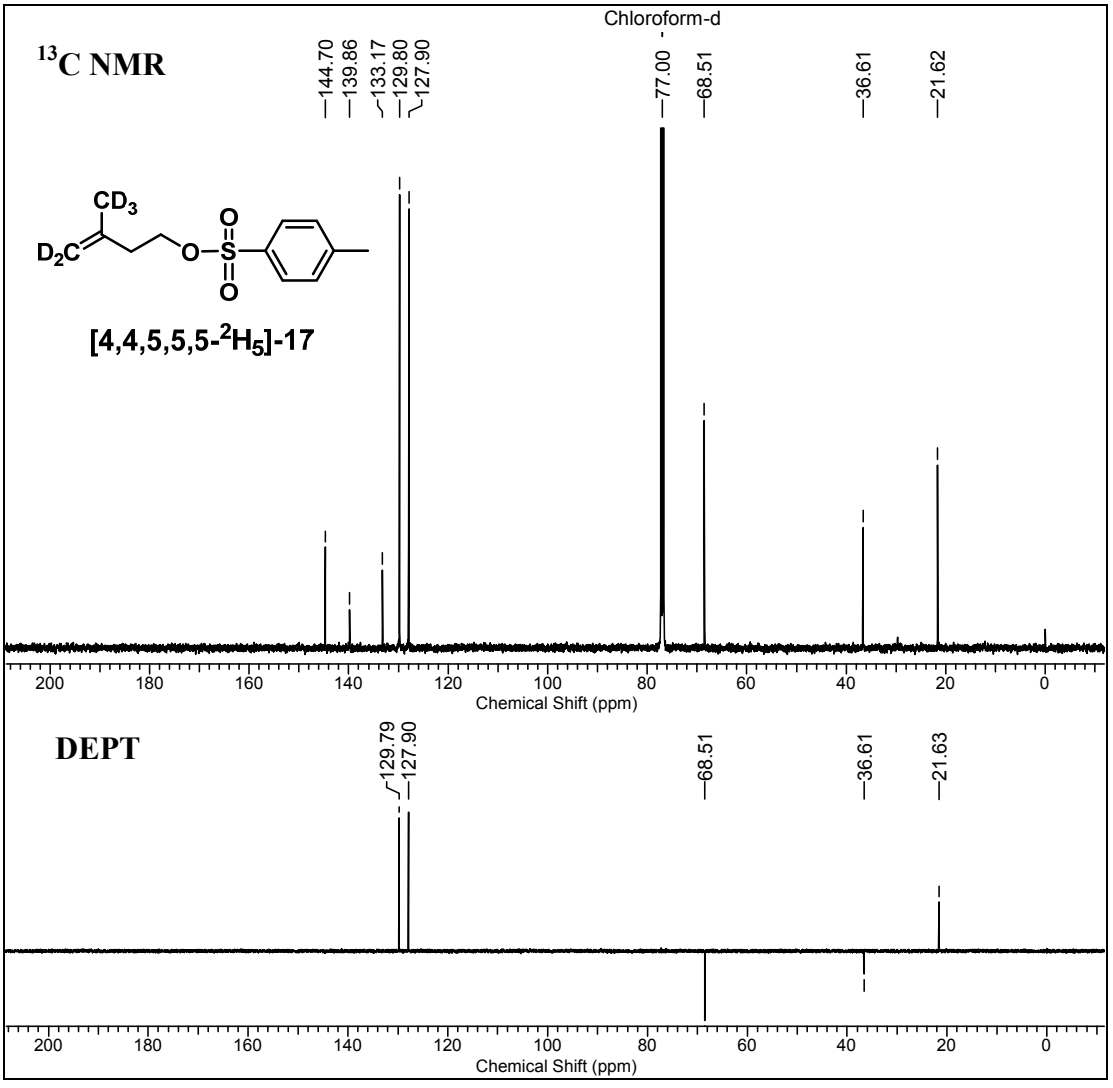
Chloroform-d
^{13}C NMR
144.70
139.86
133.17
129.80
127.90
77.00
68.51
36.61
21.62
CD3
D2C
O
S
O
O
[4,4,5,5,5-2H5]-17
200
180
160
140
120
100
80
60
40
20
0
Chemical Shift (ppm)
DEPT
129.79
127.90
68.51
36.61
21.63
200
180
160
140
120
100
80
60
40
20
0
Chemical Shift (ppm)

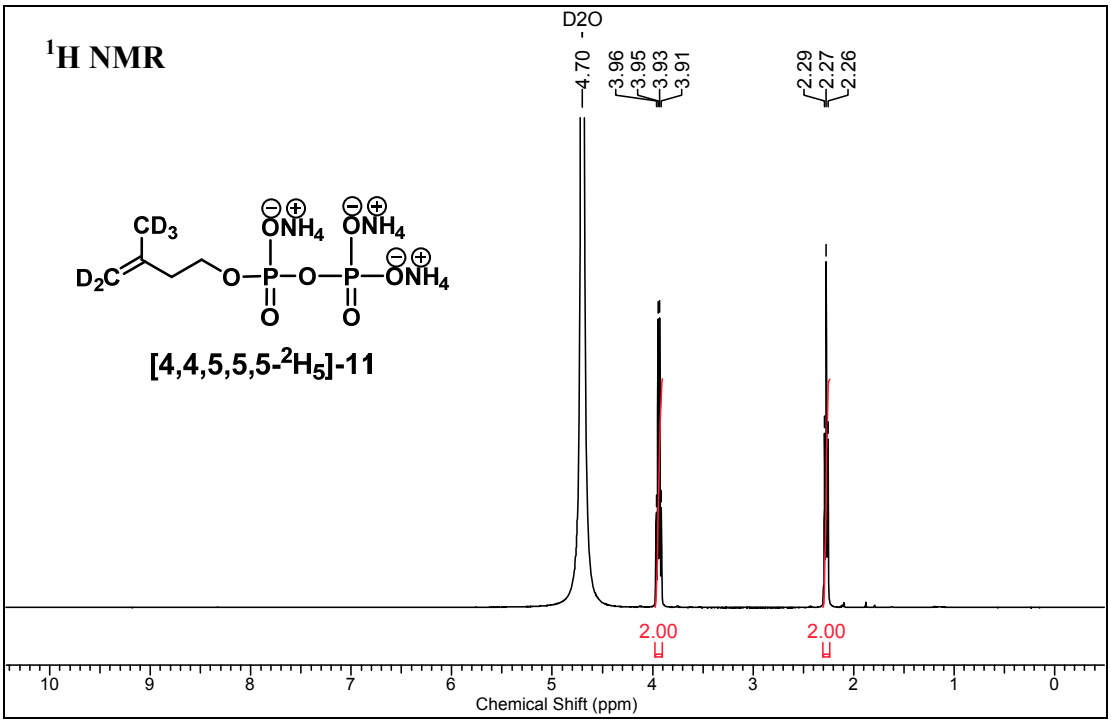

[4,4,5,5,5-$^{2}H_5$]-11

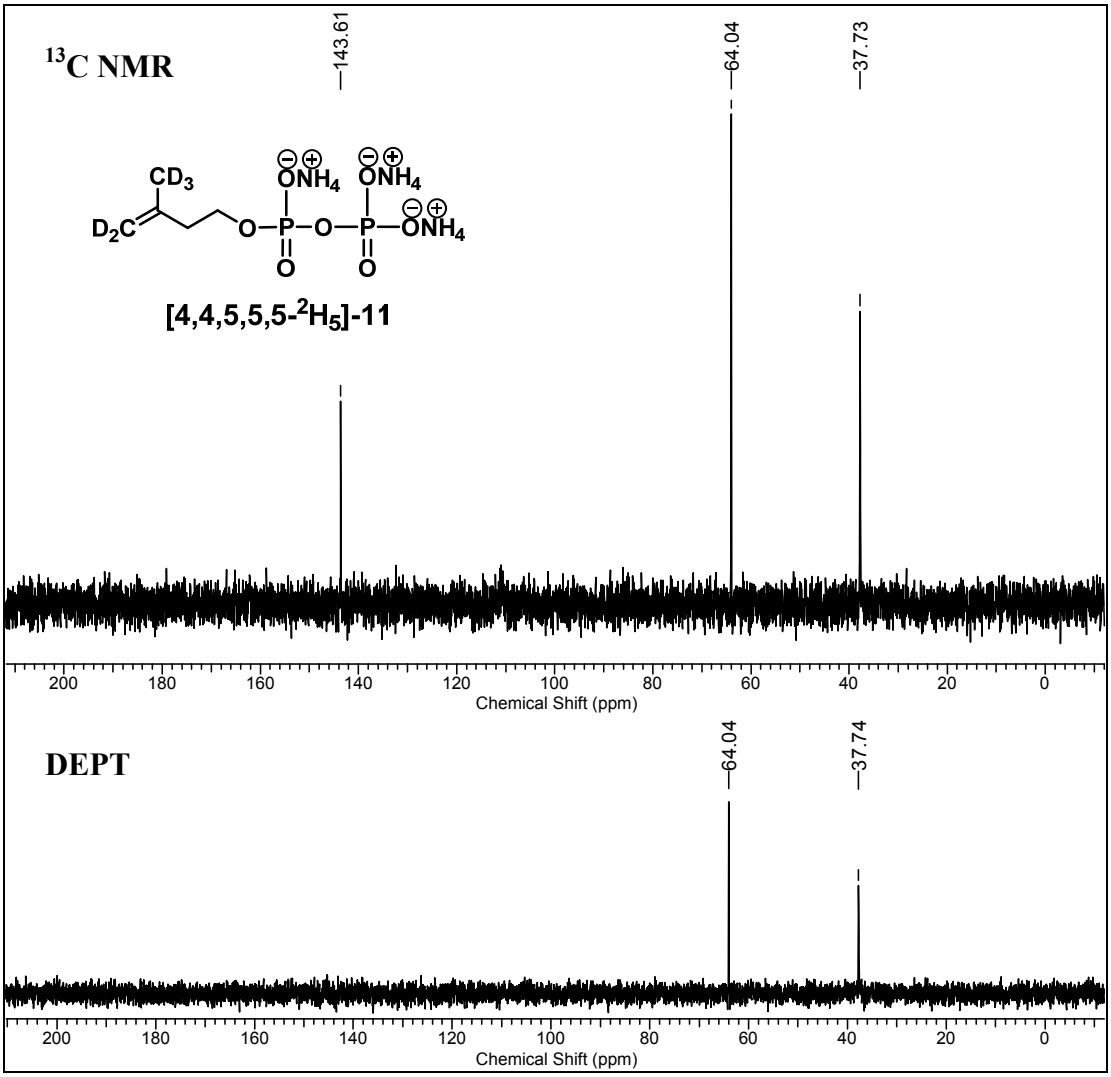

[4,4,5,5,5-$^{2}H_5$]-11

^{31}P NMR

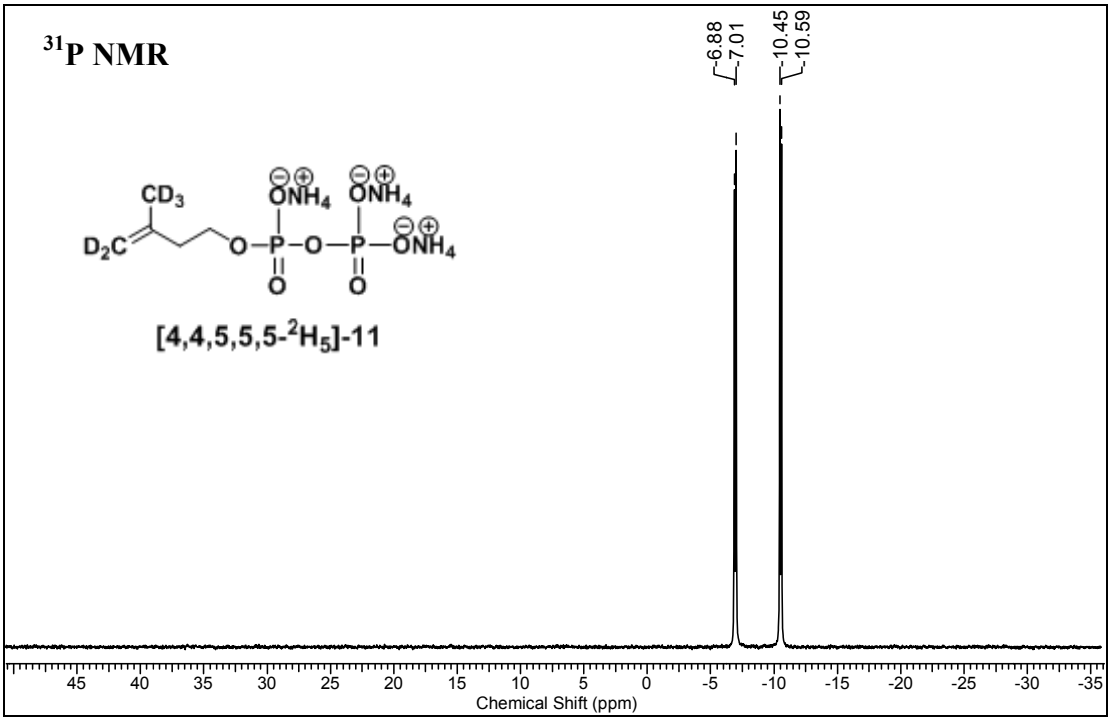

[4,4,5,5,5-$^{2}H_5$]-11

HRMS (ESI)

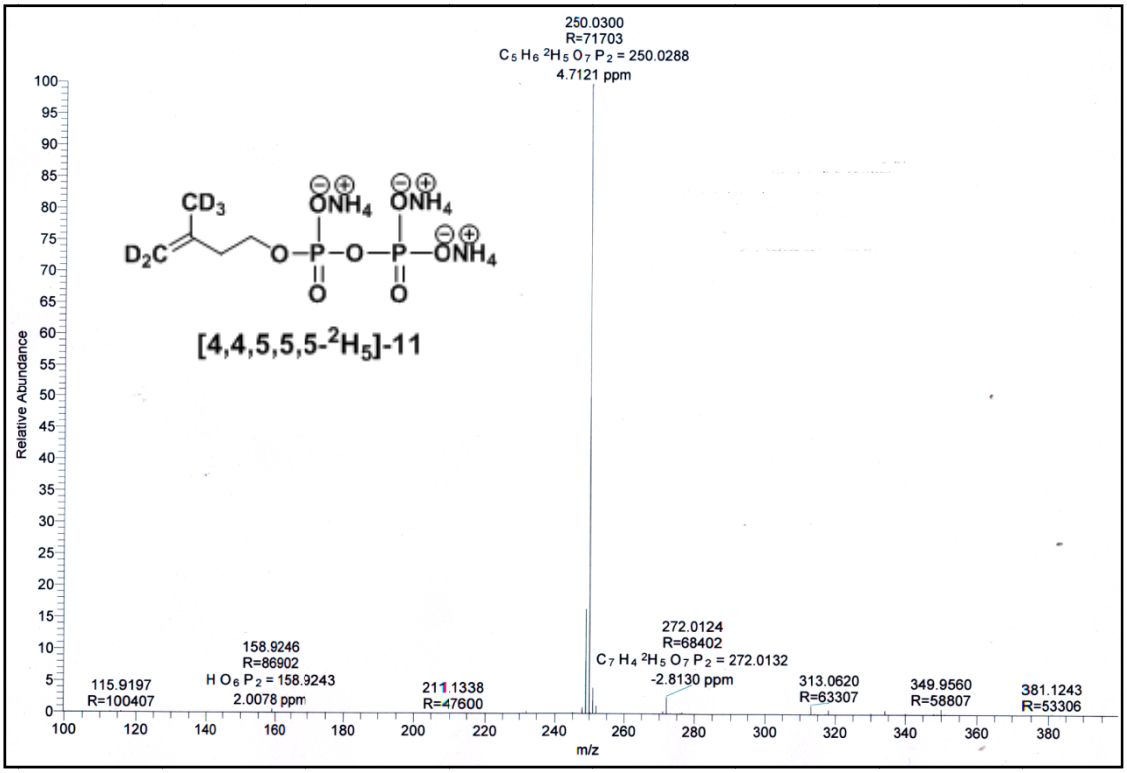

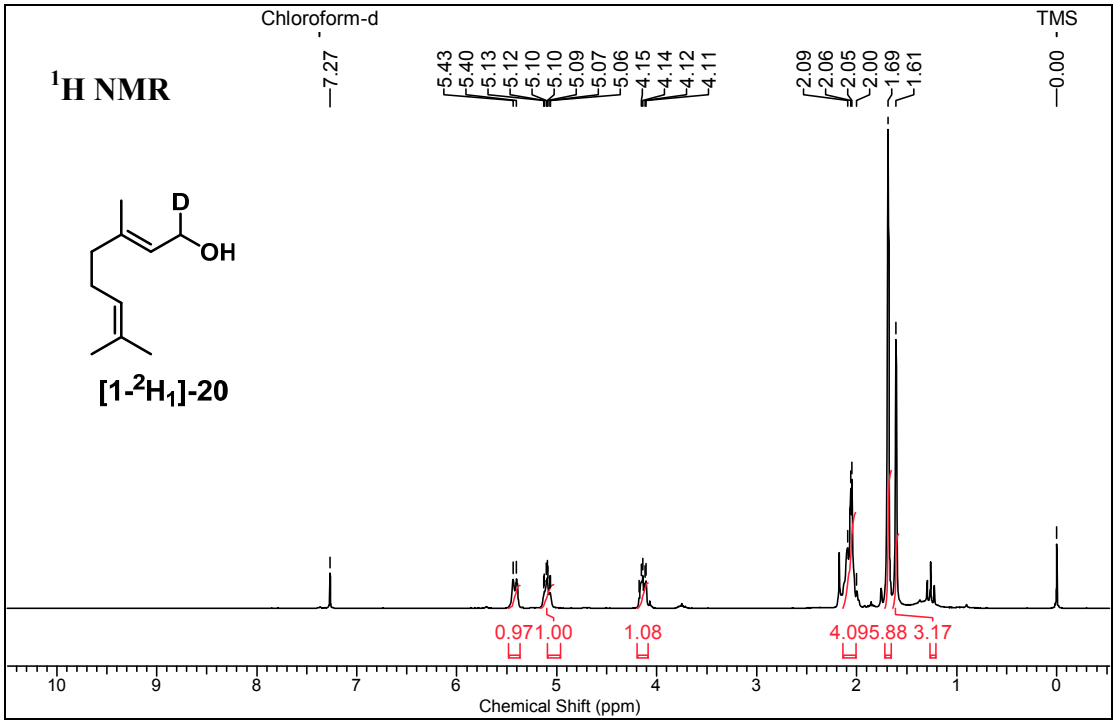
Chloroform-d
TMS
^{1}H NMR
7.27
5.43
5.40
5.13
5.12
5.10
5.10
5.09
5.07
5.06
4.15
4.14
4.12
4.11
2.09
2.06
2.05
2.00
1.69
1.61
0.00
D
OH
[1-^{2}H$_1$]-20
0.97
1.00
1.08
4.09
5.88
3.17
Chemical Shift (ppm)

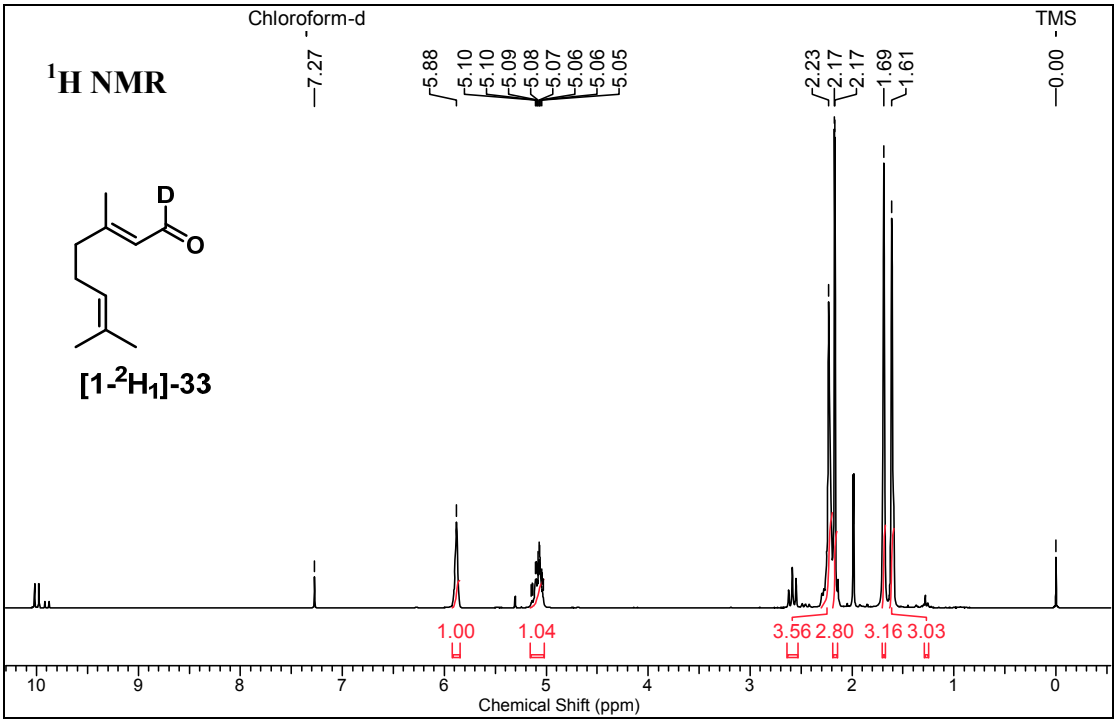
Chloroform-d
TMS
^{1}H NMR
7.27
5.88
5.10
5.10
5.09
5.08
5.07
5.06
5.06
5.05
2.23
2.17
2.17
1.69
1.61
0.00
D
O
[1-^{2}H$_1$]-33
1.00
1.04
3.56
2.80
3.16
3.03
Chemical Shift (ppm)

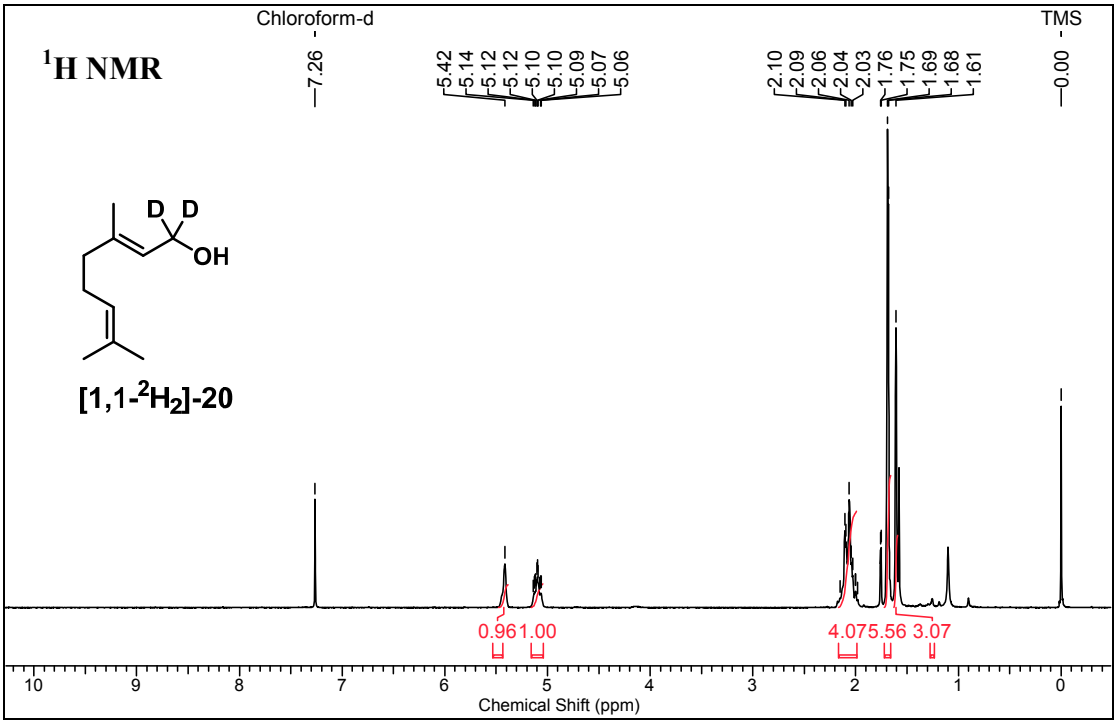
Chloroform-d
TMS
^{1}H NMR
7.26
5.42 5.14 5.12 5.12 5.10 5.10 5.09 5.07 5.06
2.10 2.09 2.06 2.04 2.03 1.76 1.75 1.69 1.68 1.61
0.00
D D
OH
[1,1-$^2H_2$]-20
0.96 1.00
4.07 5.56 3.07
10 9 8 7 6 5 4 3 2 1 0
Chemical Shift (ppm)

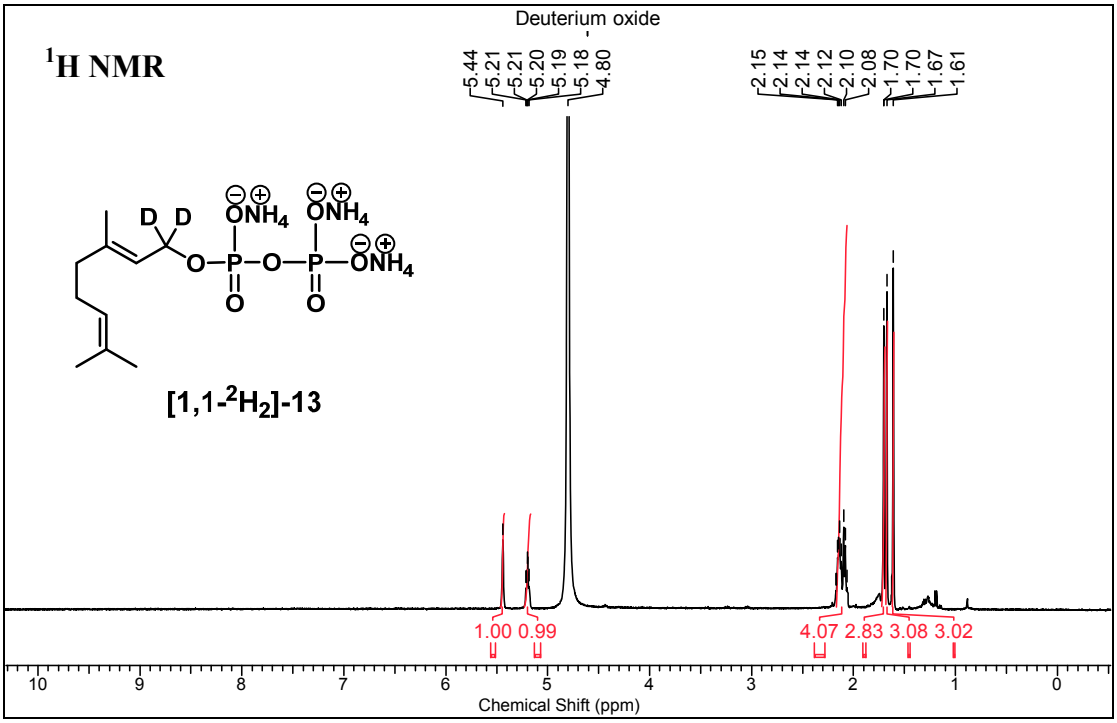
Deuterium oxide
^{1}H NMR
5.44 5.21 5.21 5.20 5.19 5.18 4.80
2.15 2.14 2.14 2.12 2.10 2.08 1.70 1.70 1.67 1.61
D D
ONH4 ONH4 ONH4
O P O P O
O O
[1,1-$^2H_2$]-13
1.00 0.99
4.07 2.83 3.08 3.02
10 9 8 7 6 5 4 3 2 1 0
Chemical Shift (ppm)

^{31}P NMR

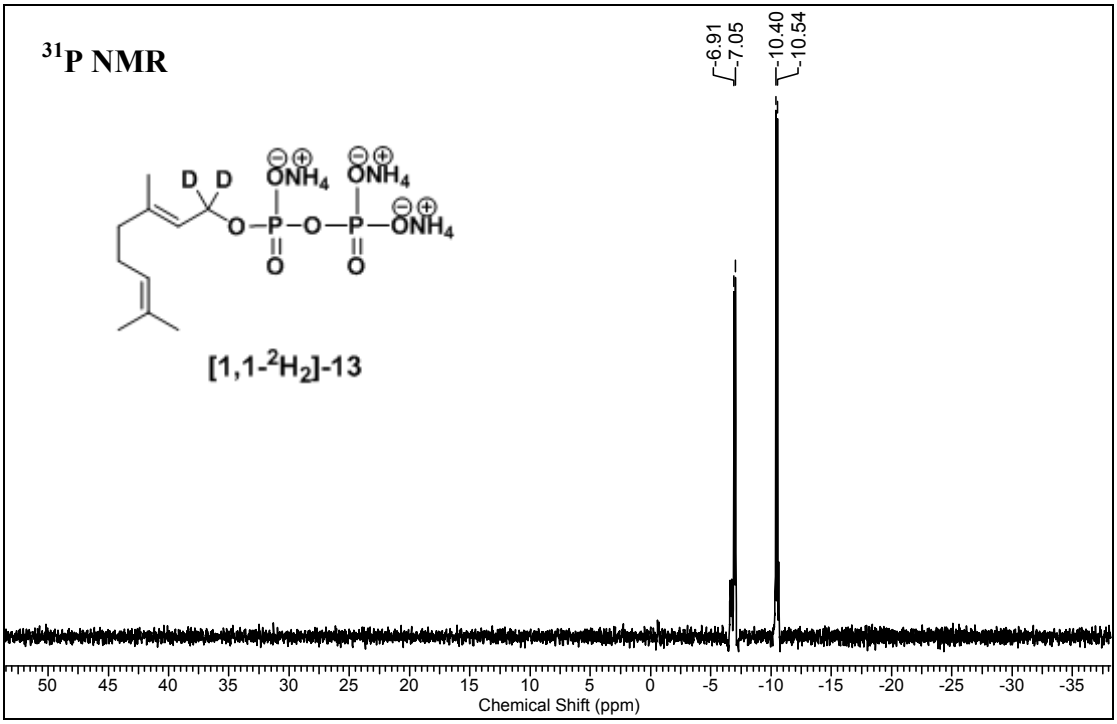

HRMS (ESI)

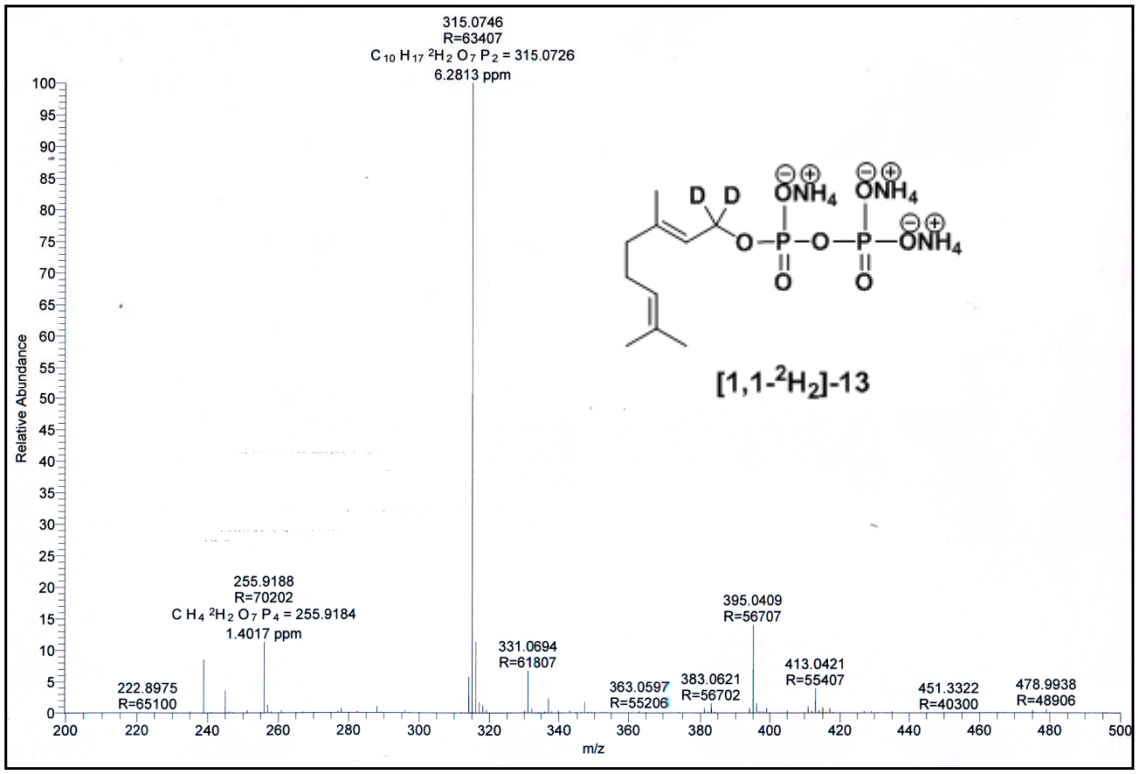

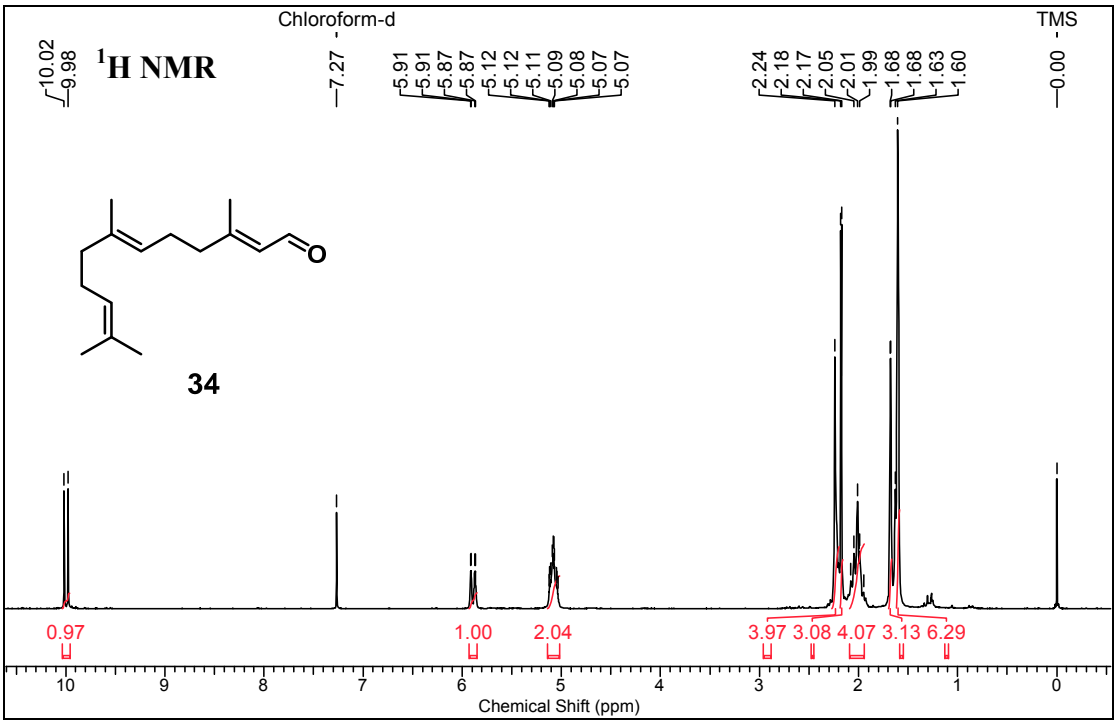
Chloroform-d
TMS
^{1}H NMR
10.02
9.98
7.27
5.91
5.91
5.87
5.87
5.12
5.11
5.09
5.08
5.07
5.07
2.24
2.18
2.17
2.05
2.01
1.99
1.68
1.68
1.63
1.60
0.00
O
34
0.97
1.00
2.04
3.97
3.08
4.07
3.13
6.29
Chemical Shift (ppm)

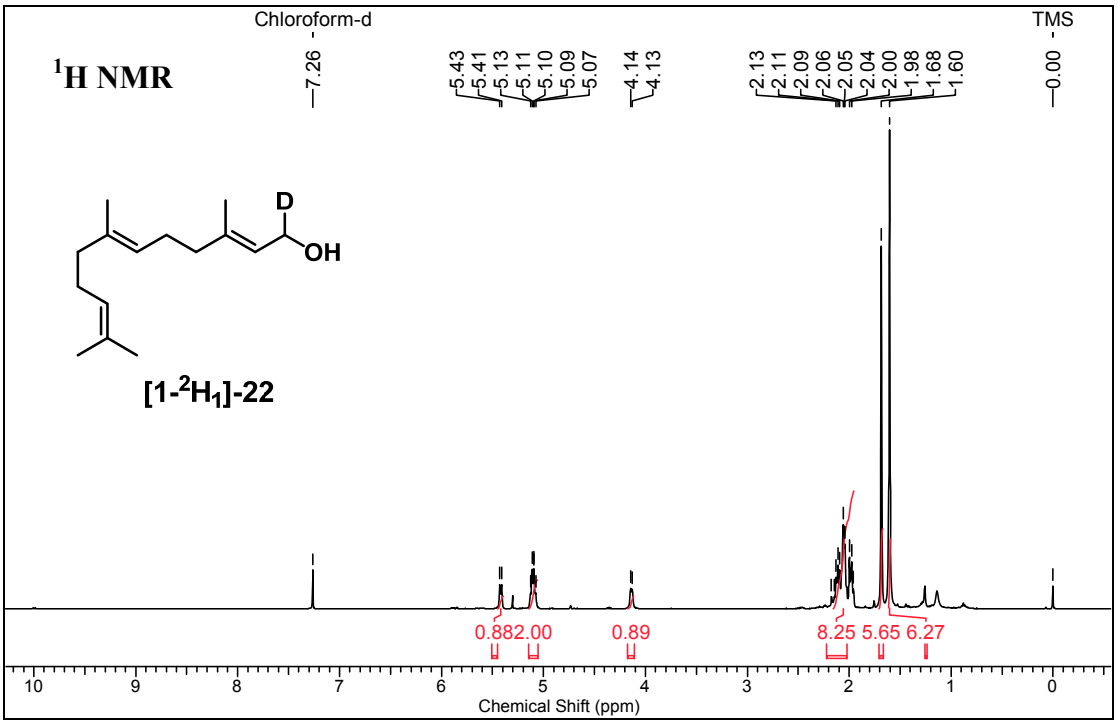
Chloroform-d
TMS
^{1}H NMR
7.26
5.43
5.41
5.13
5.11
5.10
5.09
5.07
4.14
4.13
2.13
2.11
2.09
2.06
2.05
2.04
2.00
1.98
1.68
1.60
0.00
D
OH
[1-^{2}H$_1$]-22
0.88
2.00
0.89
8.25
5.65
6.27
Chemical Shift (ppm)

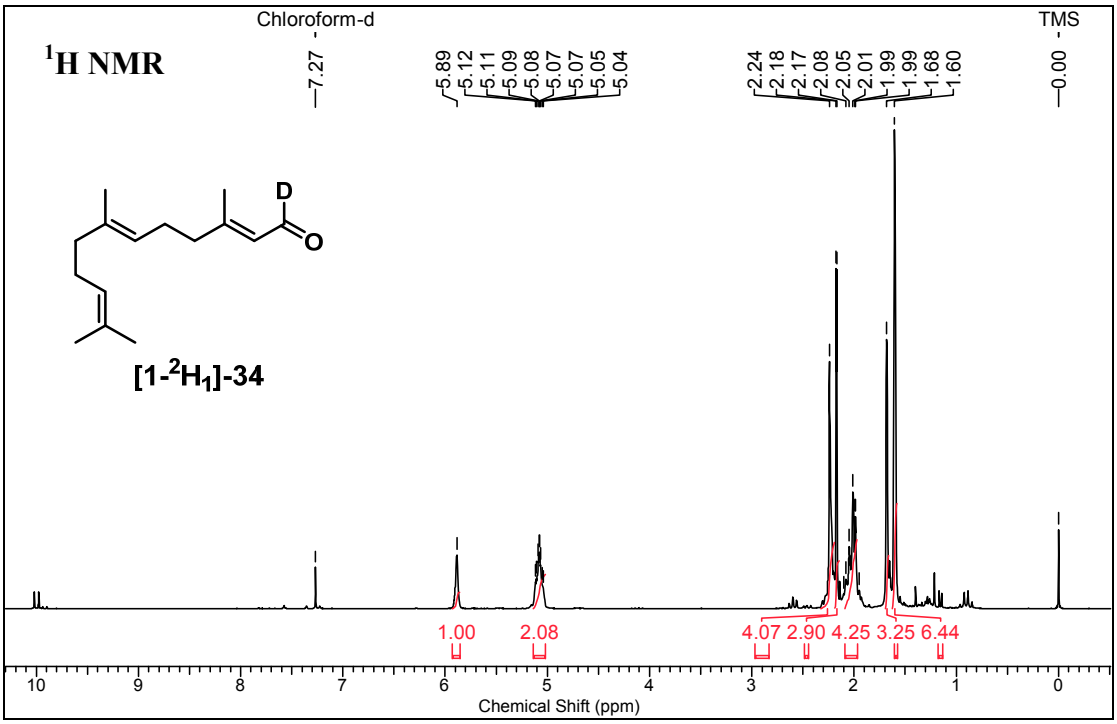
Chloroform-d
TMS
^{1}H NMR
7.27
5.89 5.12 5.11 5.09 5.08 5.07 5.07 5.05 5.04
2.24 2.18 2.17 2.08 2.05 2.01 1.99 1.99 1.68 1.60
0.00
D
O
[1-^{2}H$_1$]-34
1.00 2.08 4.07 2.90 4.25 3.25 6.44
10 9 8 7 6 5 4 3 2 1 0
Chemical Shift (ppm)

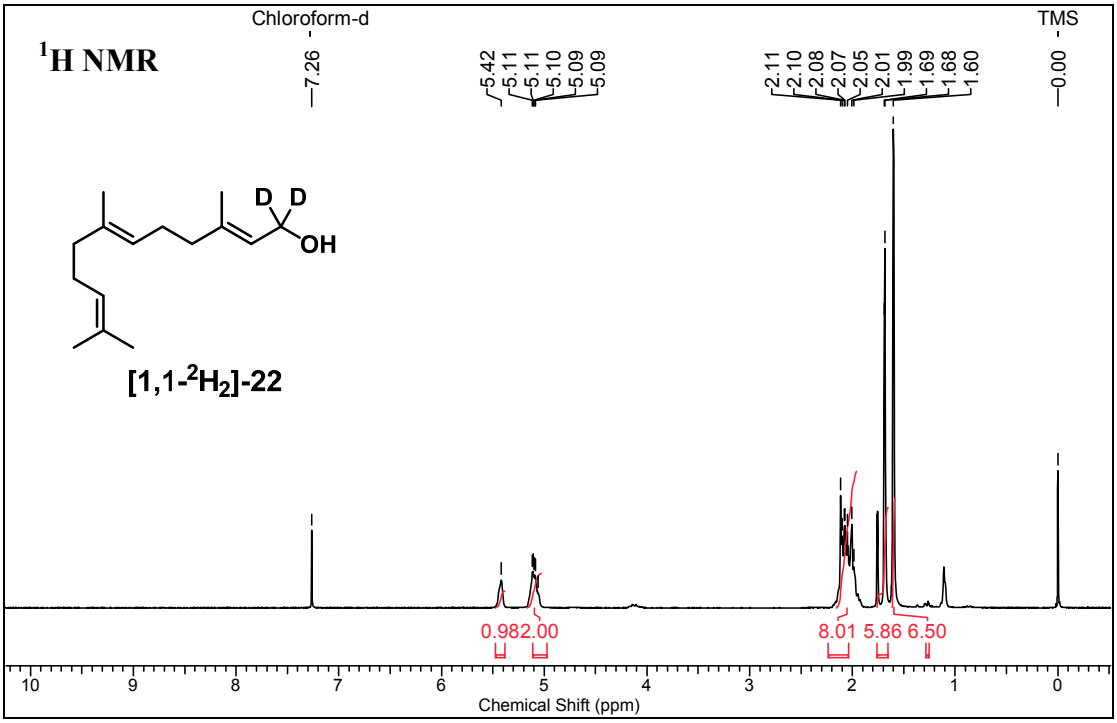
Chloroform-d
TMS
^{1}H NMR
7.26
5.42 5.11 5.11 5.10 5.09 5.09
2.11 2.10 2.08 2.07 2.05 2.01 1.99 1.69 1.68 1.60
0.00
D D
OH
[1,1-^{2}H$_2$]-22
0.98 2.00 8.01 5.86 6.50
10 9 8 7 6 5 4 3 2 1 0
Chemical Shift (ppm)

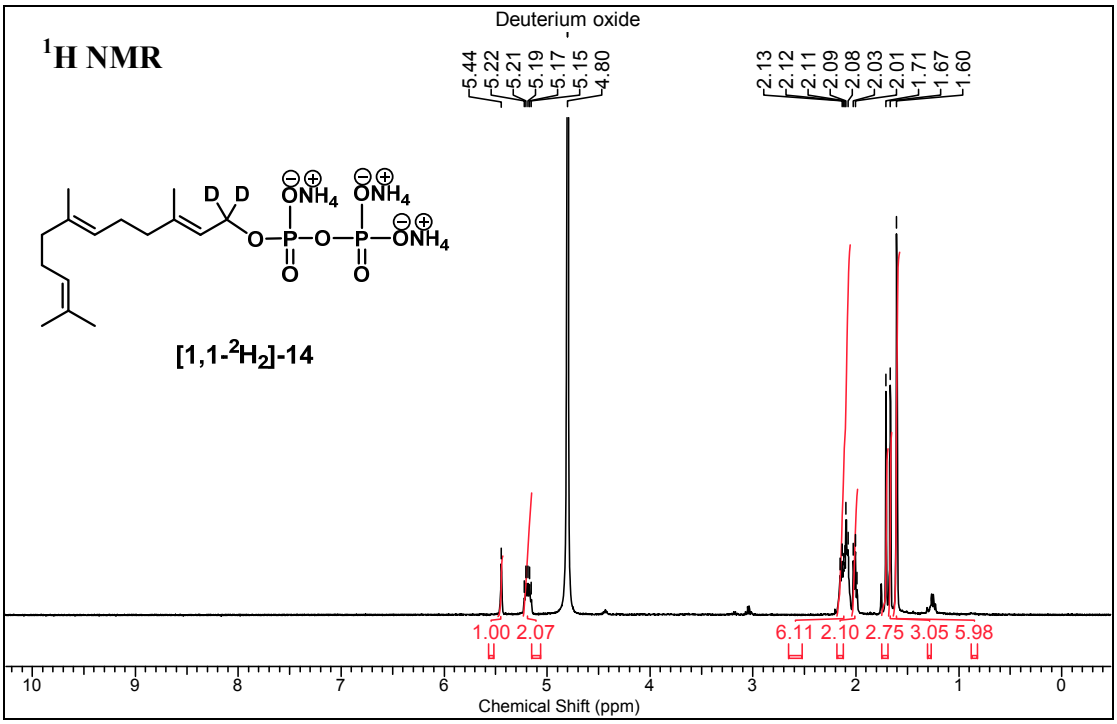
^{1}H NMR
Deuterium oxide
5.44
5.22
5.21
5.19
5.17
5.15
4.80
2.13
2.12
2.11
2.09
2.08
2.03
2.01
1.71
1.67
1.60
D D
ONH4 ONH4
O–P–O–P–ONH4
O O
[1,1-2H2]-14
1.00 2.07
6.11 2.10 2.75 3.05 5.98
10 9 8 7 6 5 4 3 2 1 0
Chemical Shift (ppm)

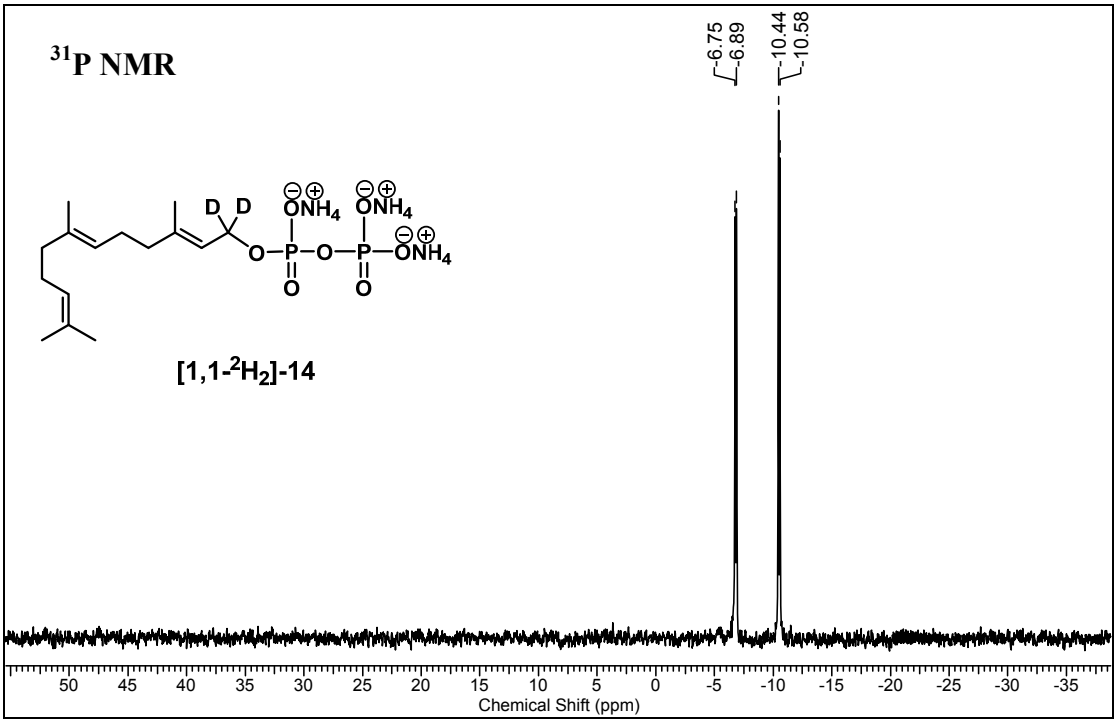
^{31}P NMR
-6.75
-6.89
-10.44
-10.58
D D
ONH4 ONH4
O–P–O–P–ONH4
O O
[1,1-2H2]-14
50 45 40 35 30 25 20 15 10 5 0 -5 -10 -15 -20 -25 -30 -35
Chemical Shift (ppm)

HRMS (ESI)

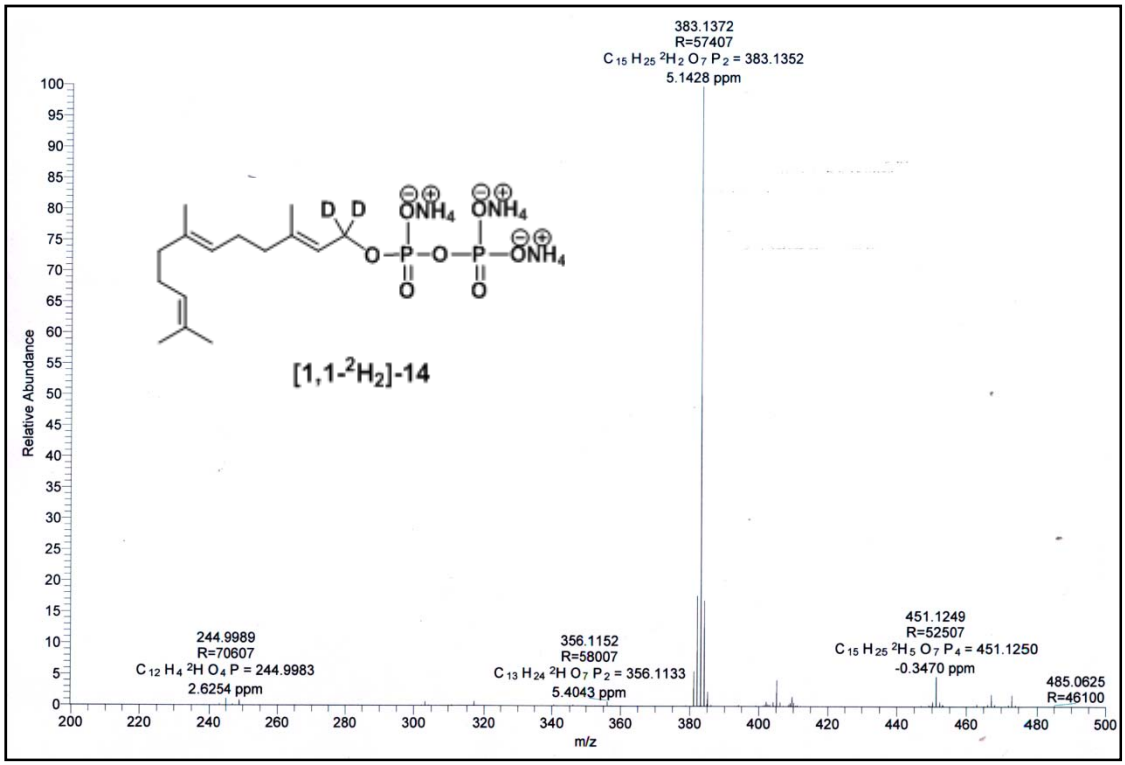
383.1372
R=57407
C 15 H 25 2H 2 O 7 P 2 = 383.1352
5.1428 ppm
[1,1-2H2]-14
244.9989
R=70607
C 12 H 4 2H O 4 P = 244.9983
2.6254 ppm
356.1152
R=58007
C 13 H 24 2H O 7 P 2 = 356.1133
5.4043 ppm
451.1249
R=52507
C 15 H 25 2H 5 O 7 P 4 = 451.1250
-0.3470 ppm
485.0625
R=46100
Relative Abundance
m/z

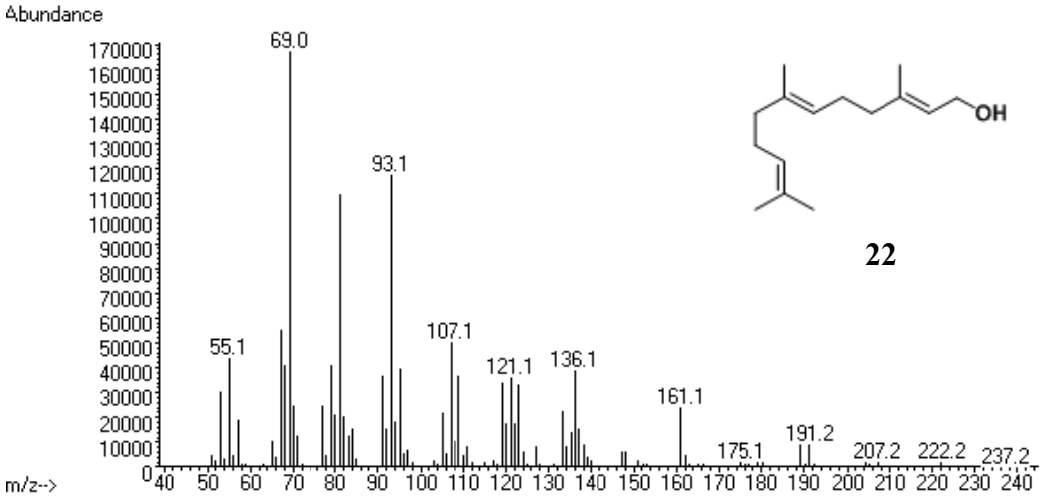

22

Figure A3.1. EI-MS spectrum of (*E*,*E*)-farnesol (**22**).

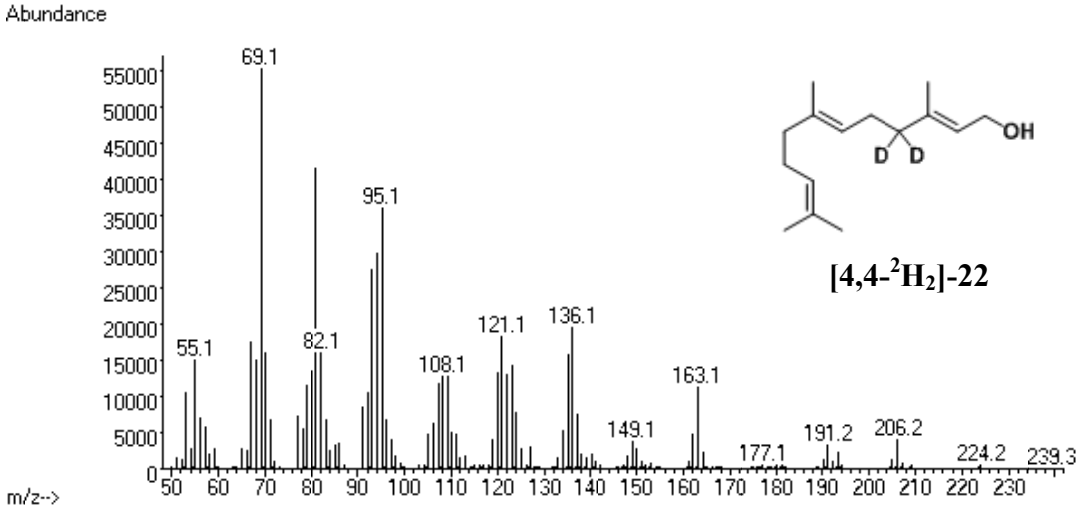

[4,4-^{2}H$_2$]-22

Figure A3.2. EI-MS spectrum of [4,4-^{2}H$_2$]-(*E*,*E*)-farnesol (**[4,4-^{2}H$_2$]-22**).

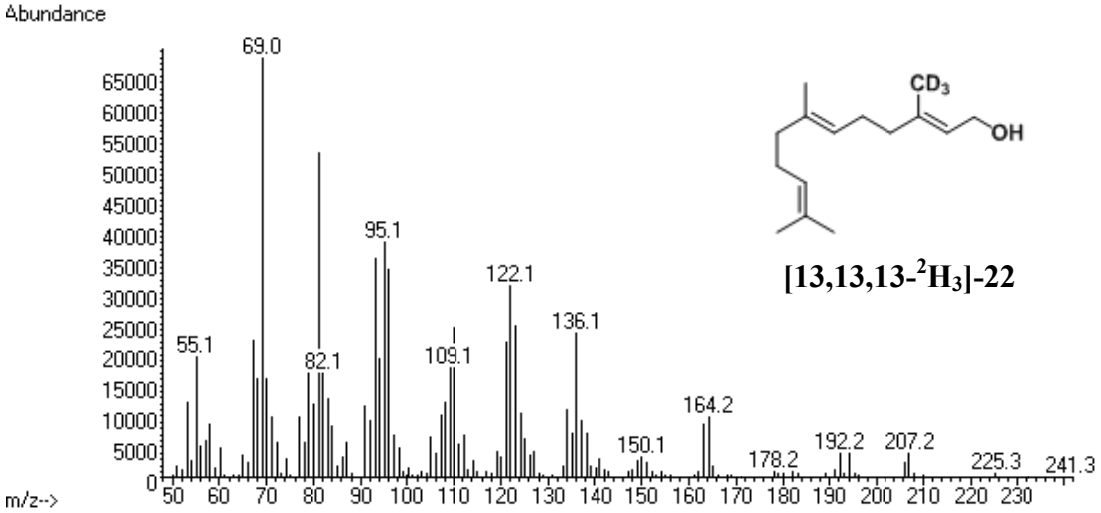

[13,13,13-^{2}H$_3$]-22

Figure A3.3. EI-MS spectrum of [13,13,13-^{2}H$_3$]-(*E*,*E*)-farnesol (**[13,13,13-^{2}H$_3$]-22**).

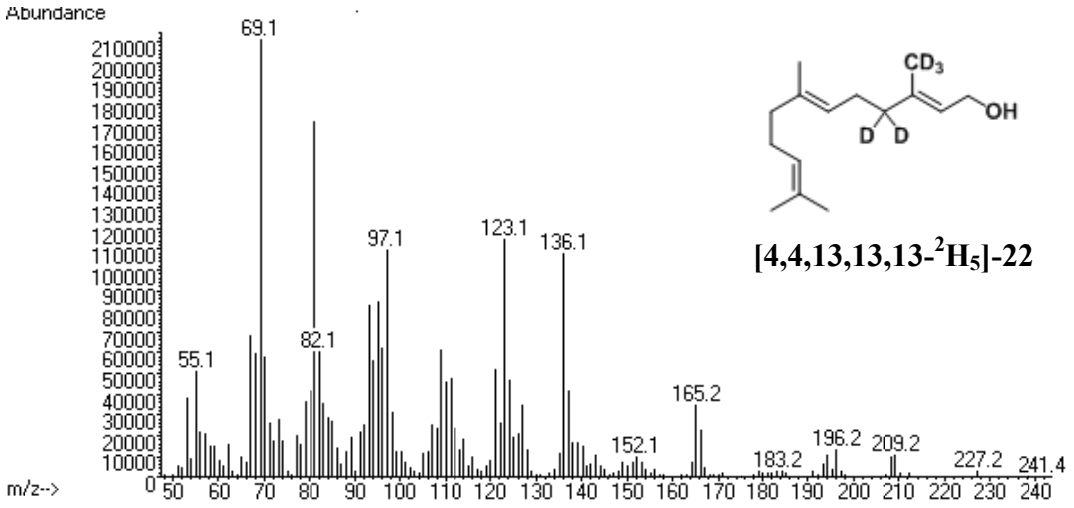

[4,4,13,13,13-$^2H_5$]-22

Figure A3.4. EI-MS spectrum of [13,13,13-$^2H_3$]-(*E*,*E*)-farnesol (**[13,13,13-$^2H_3$]-22**).

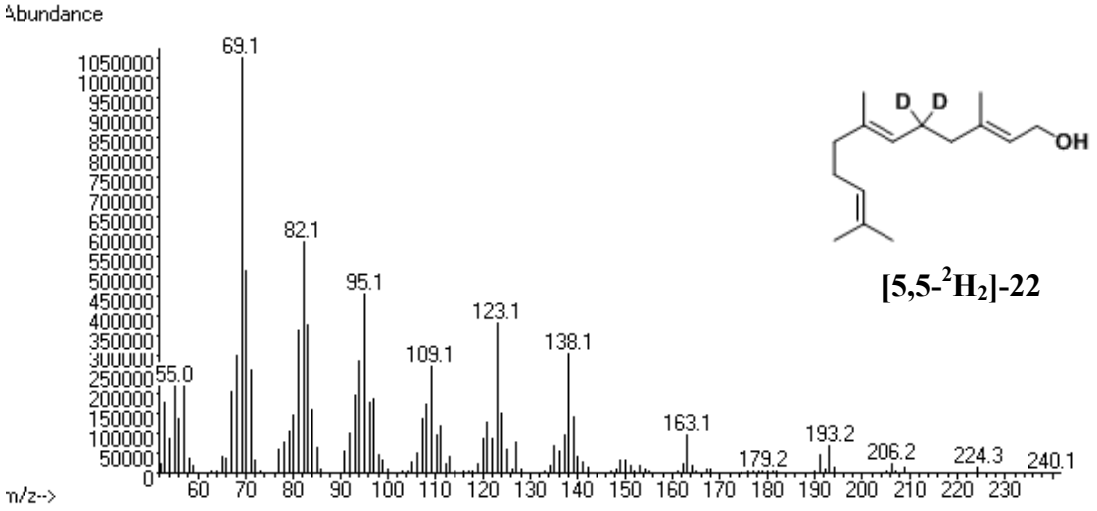

[5,5-$^2H_2$]-22

Figure A3.5. EI-MS spectrum of [4,4,13,13,13-$^2H_5$]-(*E*,*E*)-farnesol (**[4,4,13,13,13-$^2H_5$]-22**).

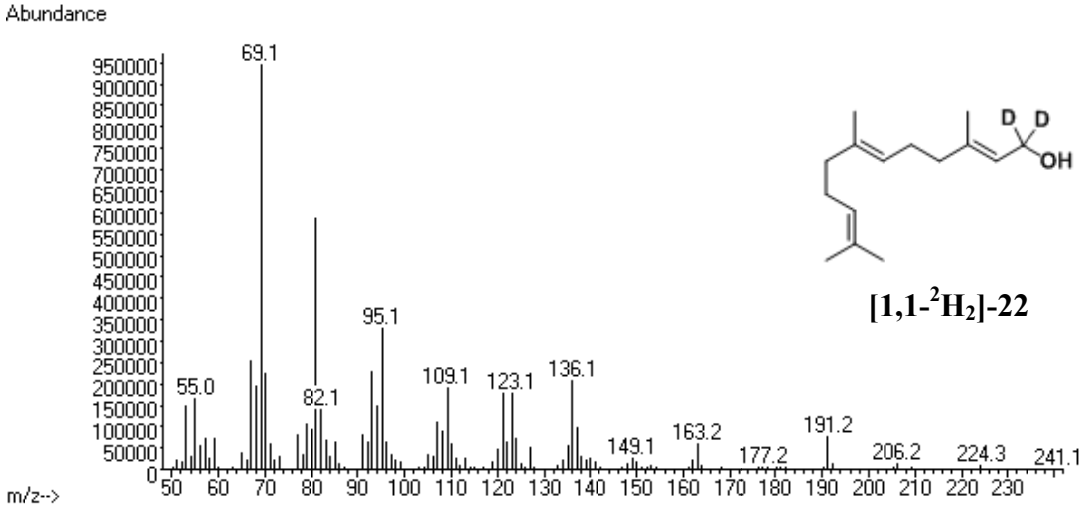

[1,1-$^2H_2$]-22

Figure A3.6. EI-MS spectrum of [1,1-$^2H_2$]-(*E*,*E*)-farnesol (**[1,1-$^2H_2$]-22**).

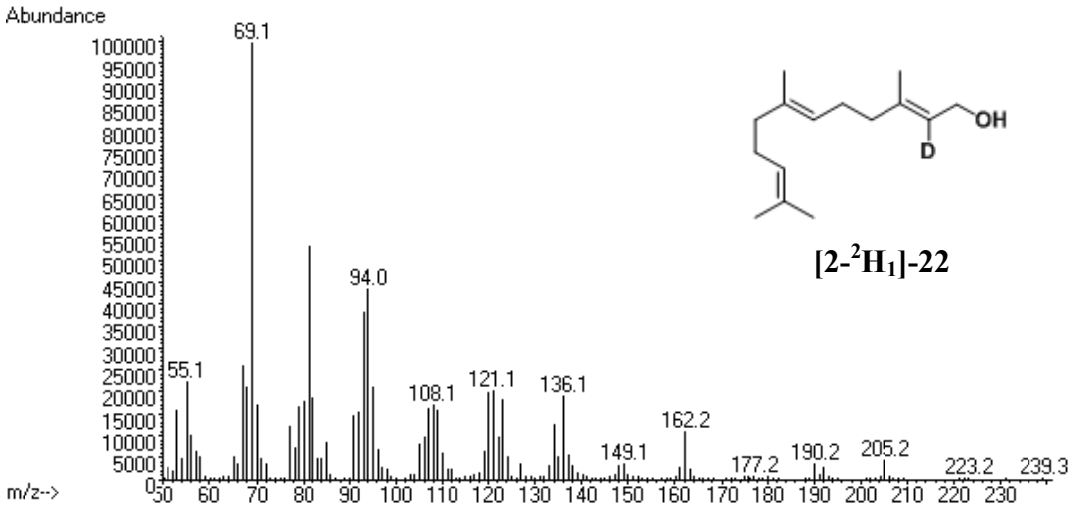

[2-^{2}H$_1$]-22

Figure A3.7. EI-MS spectrum of [2-^{2}H$_1$]-(*E*,*E*)-farnesol (**[2-^{2}H$_1$]-22**).

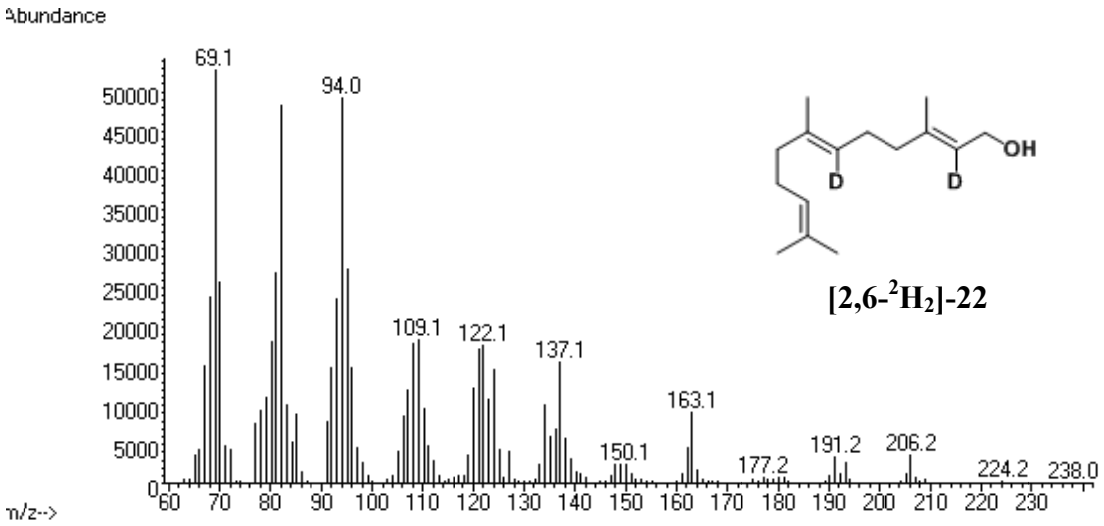

[2,6-^{2}H$_2$]-22

Figure A3.8. EI-MS spectrum of [2,6-^{2}H$_2$]-(*E*,*E*)-farnesol (**[2,6-^{2}H$_2$]-22**).

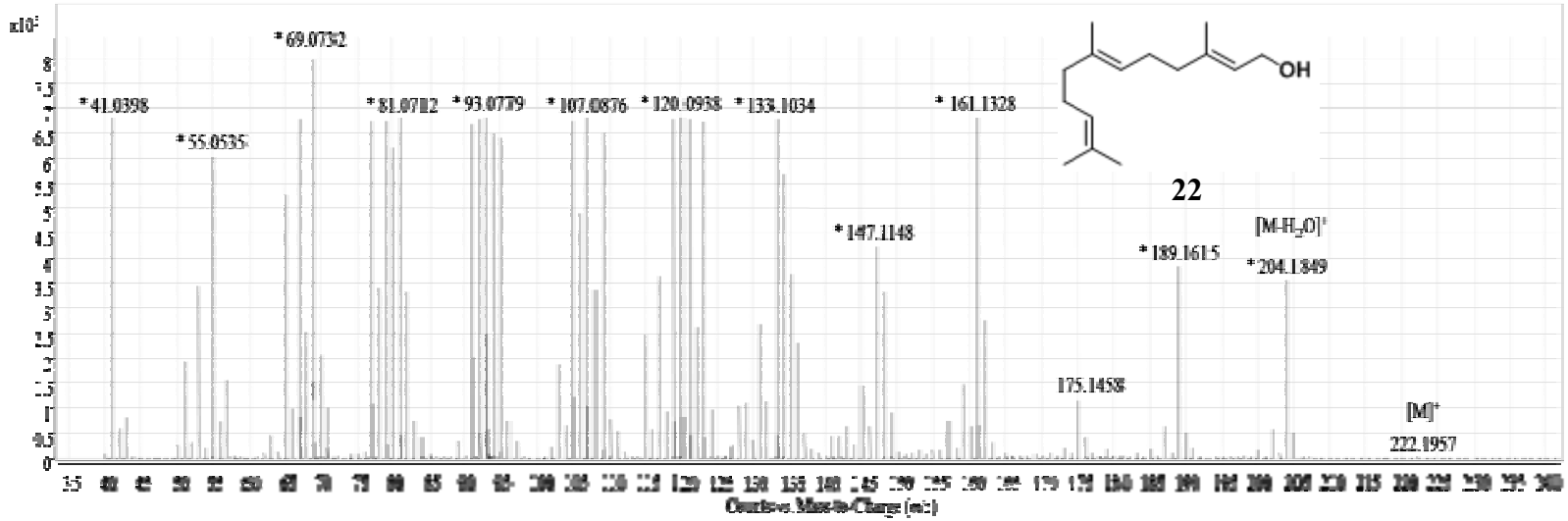

Figure A3.9. GC-EI-QToF-MS spectrum of (*E*,*E*)-farnesol (**22**).

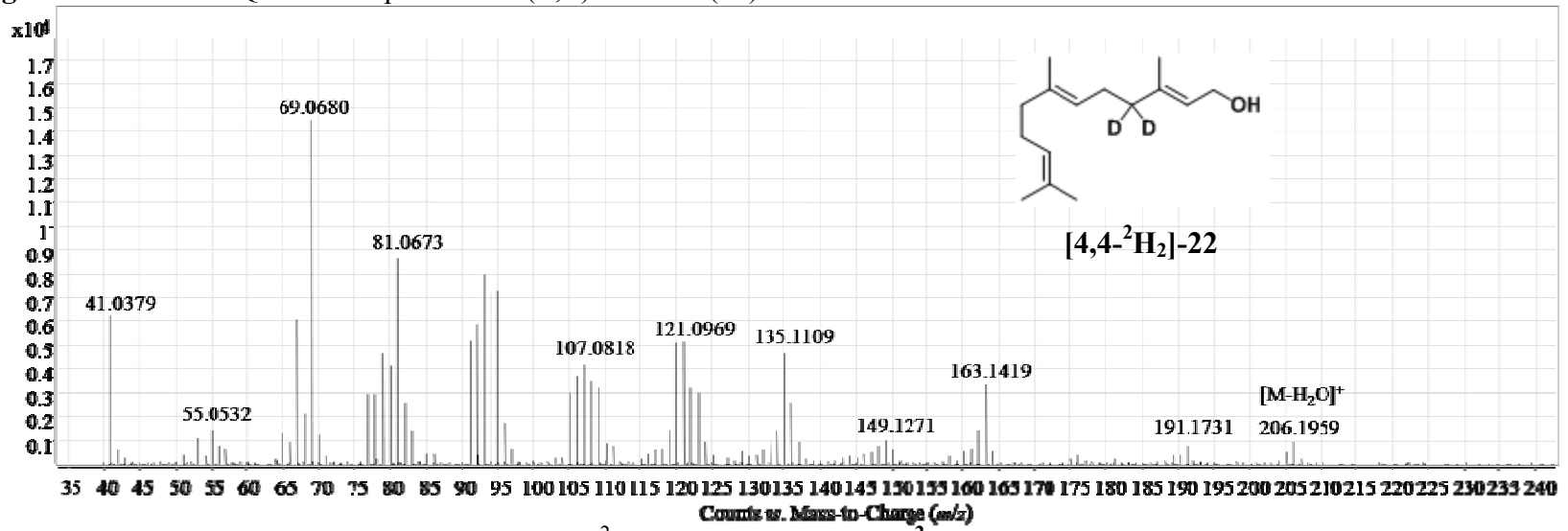

Figure A3.10. GC-EI-QToF-MS spectrum of [4,4-$^2H_2$]-(*E*,*E*)-farnesol (**[4,4-$^2H_2$]-22**).

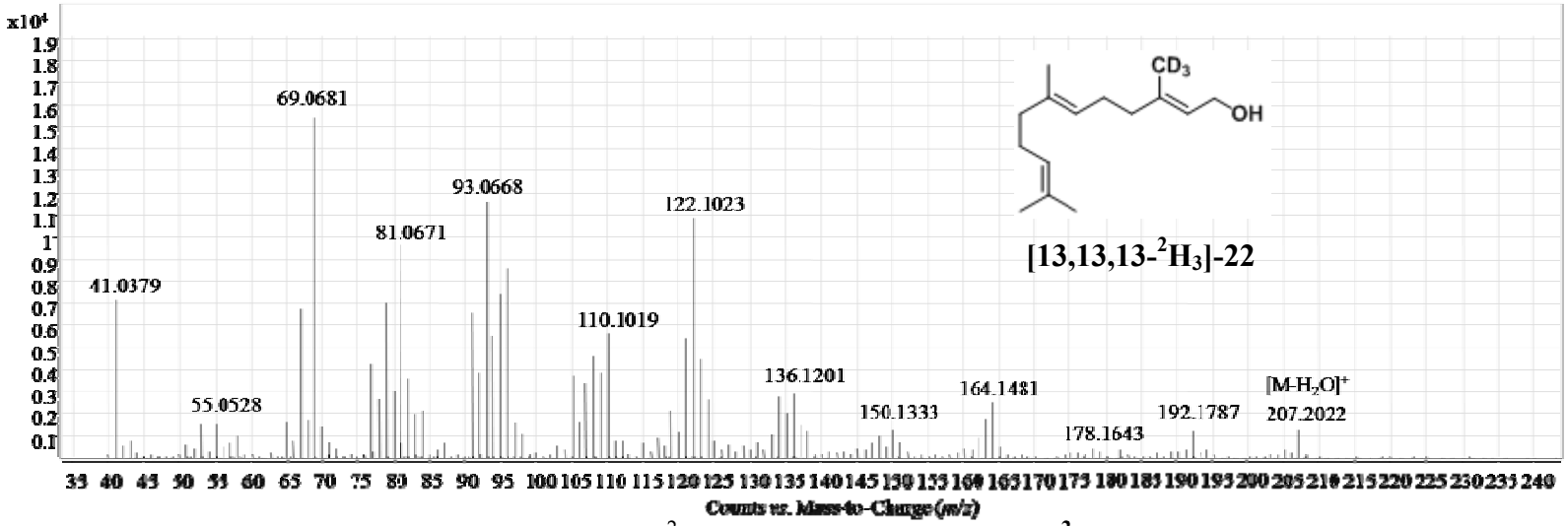

Figure A3.11. GC-EI-QToF-MS spectrum of [13,13,13-$^2H_3$]-(*E*,*E*)-farnesol (**[13,13,13-$^2H_3$]-22**).

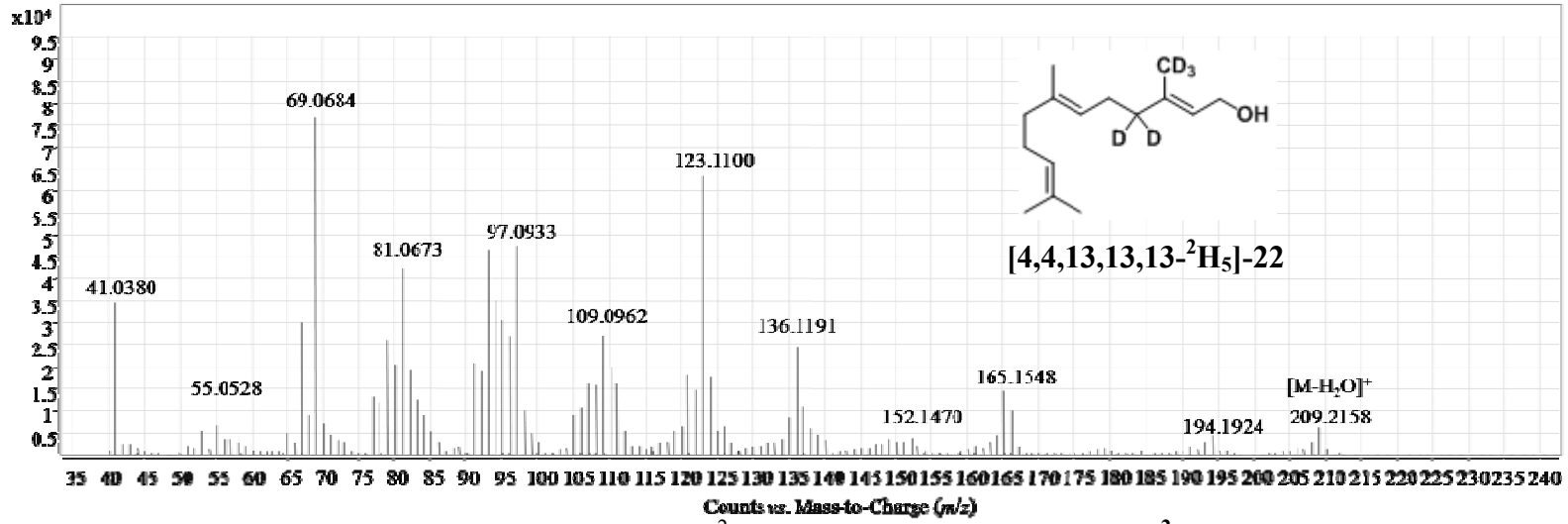

Figure A3.12. GC-EI-QToF-MS spectrum of [4,4,13,13,13-$^2H_5$]-(*E*,*E*)-farnesol (**[4,4,13,13,13-$^2H_5$]-22**).

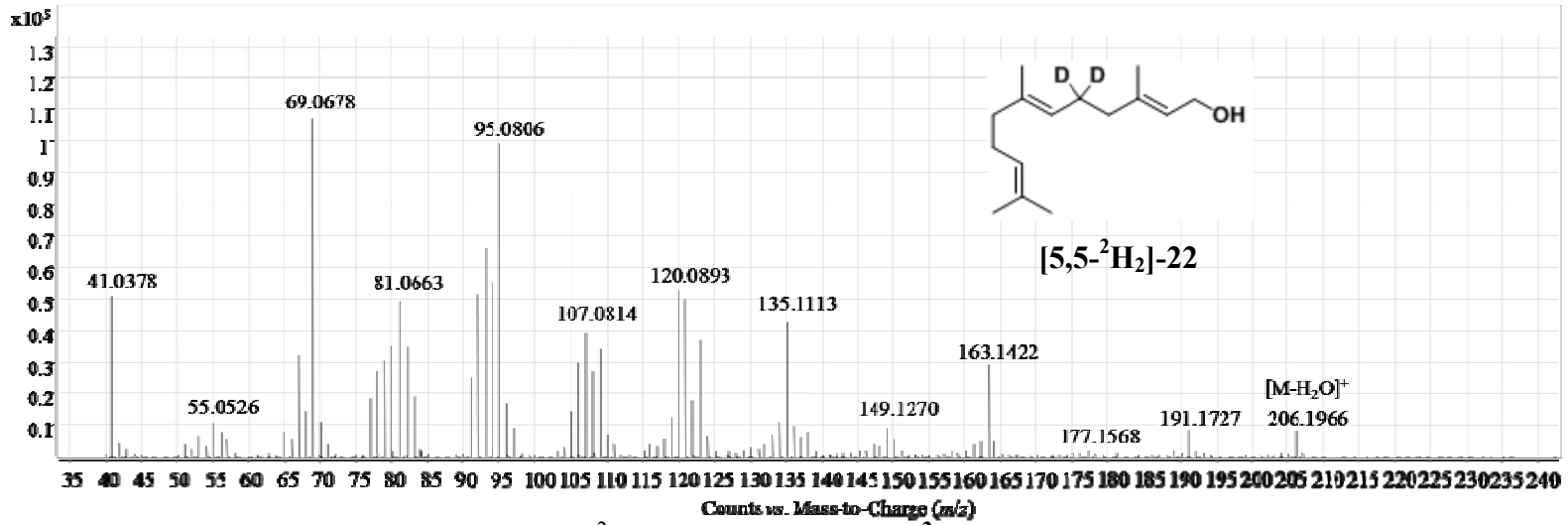

Figure A3.13. GC-EI-QToF-MS spectrum of [5,5-$^2H_2$]-(*E*,*E*)-farnesol (**[5,5-$^2H_2$]-22**).

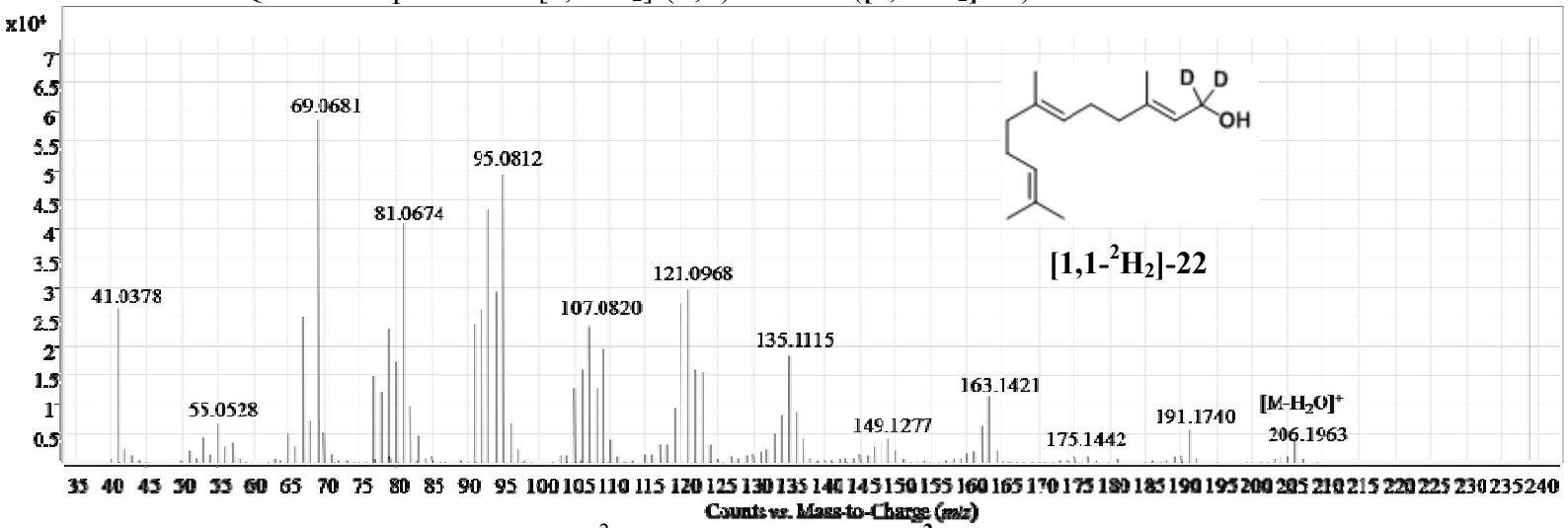

Figure A3.14. GC-EI-QToF-MS spectrum of [1,1-$^2H_2$]-(*E*,*E*)-farnesol (**[1,1-$^2H_2$]-22**).

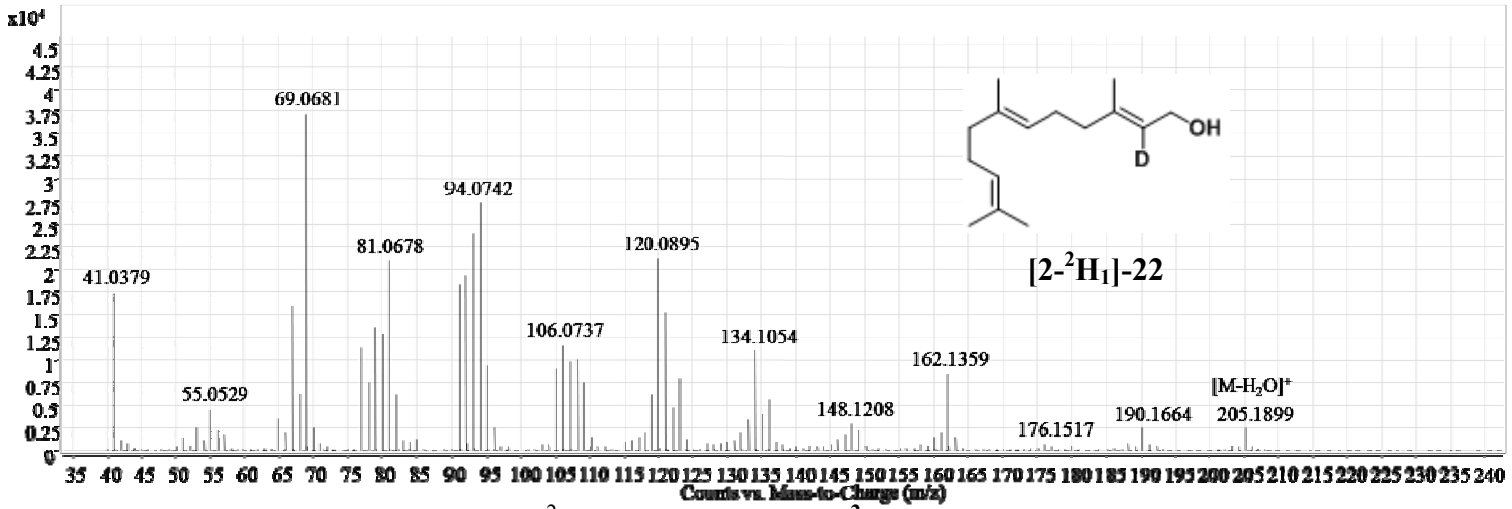

Figure A3.15. GC-EI-QToF-MS spectrum of [2-$^2H_1$]-(*E*,*E*)-farnesol (**[2-$^2H_1$]-22**).

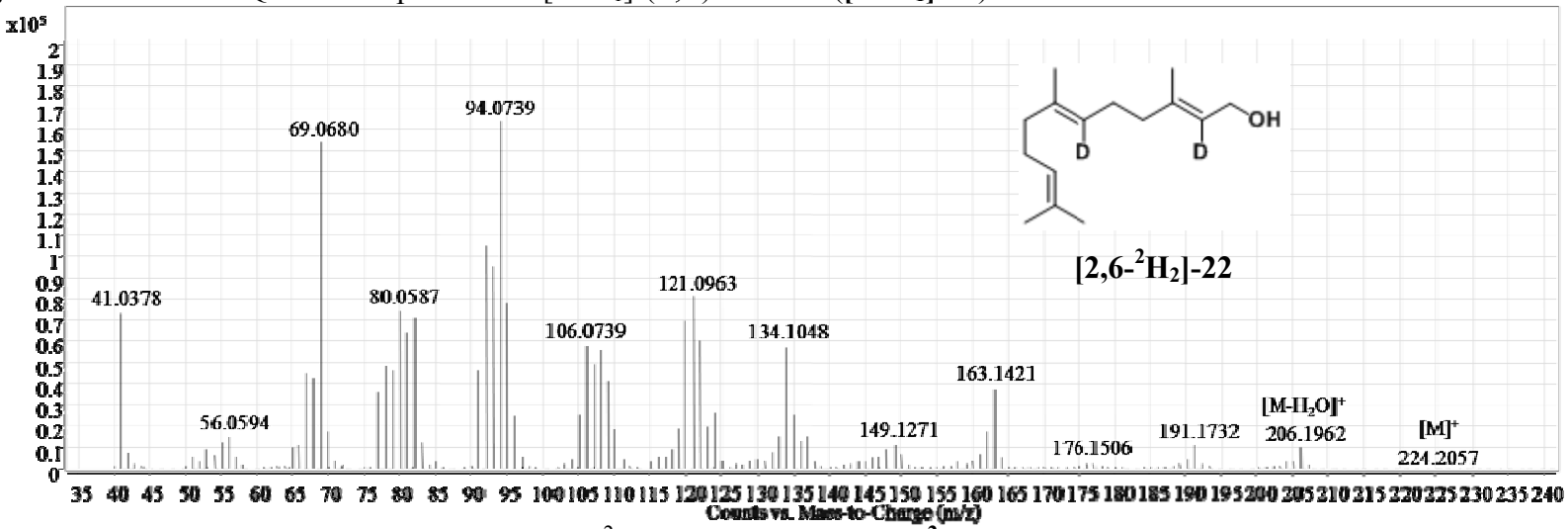

Figure A3.16. GC-EI-QToF-MS spectrum of [2,6-$^2H_2$]-(*E*,*E*)-farnesol (**[2,6-$^2H_2$]-22**).

Section 3.3.

Mechanistic Insights in Biosynthesis of Santalenes and analogous sesquiterpenes

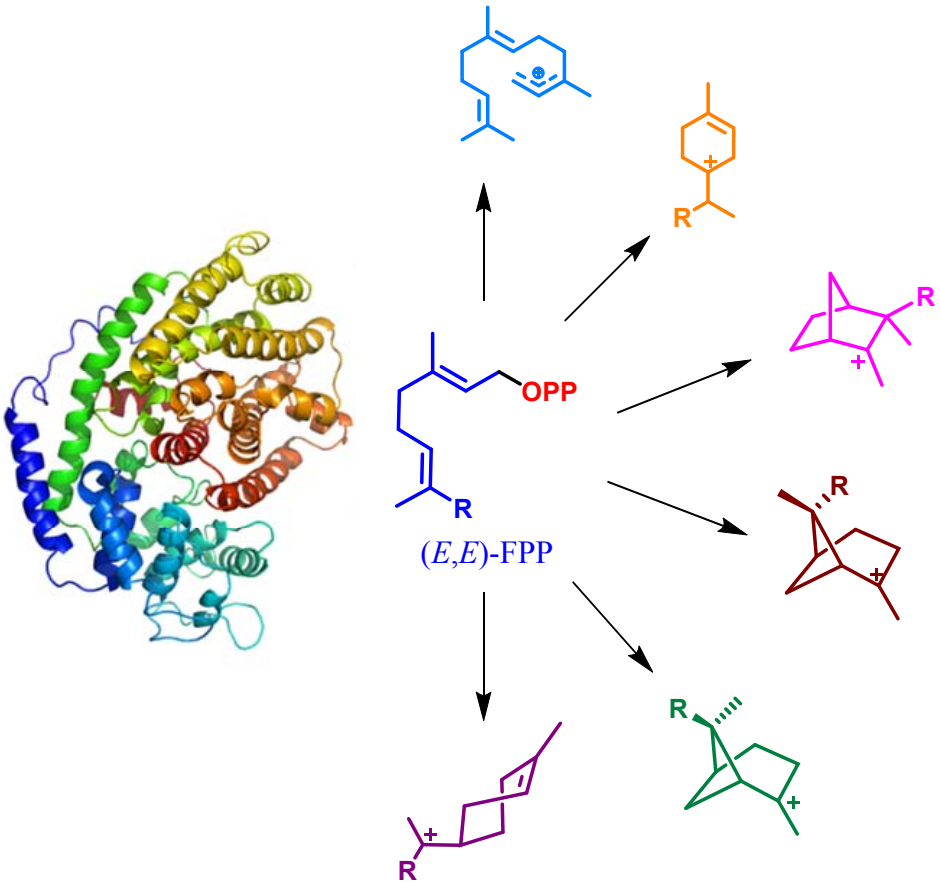

Carbocationic cascades catalyzed by *santalene synthase* in the biosynthesis of sesquiterpenes.

3.3.1. Rationale for Present Work:

Santalene synthase (*SaSS*), a sesquiterpene cyclase from sandalwood, *S. album*, has been cloned and characterized in our group.[97] The *SaSS* was found to be moderately promiscuous in its catalytic action as it displayed the cyclization of the linear substrate, (*E*,*E*)-FPP (**14**) into six sesquiterpenes, α-santalene (**1**), β-santalene (**2**), *epi*-β-santalene (**3**), *exo*-α-bergamotene (**4**), *exo*-β-bergamotene (**5**) and (*E*)-β-farnesene (**6**), which have been characterized and confirmed using GC, GC-MS and GC-QToF.[97] *SaSS* mutants produced by site directed mutagenesis of the amino acid residues around the catalytic site gave rise to other bi- and mono-cyclic sesquiterpenes *viz*., *endo*-α-bergamotene (**7**), β-curcumene (**8**), γ-curcumene (**9**) and α-zingiberene (**10**).[97] A biosynthetic pathway for these sesquiterpenes has been proposed which is tailored from the model pathways proposed for monoterpenes and sesquiterpenes.[94,96] Incubation of the deuterated (*E*,*E*)-FPP analogues with the purified sesquiterpene synthase enzymes yielded labelled sesquiterpene hydrocarbons. The objective of the present work is to investigate the intermediates and their interconversions by monitoring the cascade of deuterium labels in the products. GC-EI-MS fragmentation patterns and GC-FID response of the labelled sesquiterpene products has been studied to establish the reaction cascade and to gain mechanistic insights in the intriguing pathways in biosynthesis of products. The products formed were further confirmed by high resolution mass spectrometry, GC-QToF.

3.3.2. Present Work:

Santalene synthase, isolated from the interface of heartwood and sapwood of *Santalum album*, was observed to be a moderately promiscuous sesquiterpene cyclase that catalyzed the metal dependent cyclization of (*E*,*E*)-FPP to a mixture of six sesquiterpene hydrocarbon products, α-santalene (**1**, 41%), β-santalene (**2**, 29.4%), *epi*-β-santalene (**3**, 4.3%), *exo*-α-bergamotene (**4**, 22.5%), *exo*-β-bergamotene (**5**, 2.2%) and (*E*)-β-farnesene (**6**, 0.7%), when incubated with (*E*,*E*)-Farnesyl pyrophosphate (FPP, **14**).[97] Other variants of this enzyme produced by site directed mutagenesis of the amino acid residues around the catalytic site emanated other bi- and mono-cyclic sesquiterpenes, identified as, *endo*-α-bergamotene (**7**), β-curcumene (**8**), γ-curcumene (**9**) and α-zingiberene (**10**).[97]

While our investigations in the isolation of genes encoding for Santalene synthase from sandalwood were in progress, some of its variants from different biological sources were reported simultaneously by researchers working independently. 'Santalene-bergamotene synthase' was reported from wild tomato *Solanum habrochaites* by Christophe Sallaud *et al*.[102] which produced bergamotenes and santalenes from an atypical substrate (*Z*,*Z*)-FPP and yielded no products with the regular substrate (*E*,*E*)-FPP. Schalk *et al*. disclosed α-santalene synthase[103] from *C*. *lansium* and β-santalene synthase[104] from the roots of *S. album*. Three orthologous terpene synthases were cloned from three divergent sandalwood species by Jones *et al*.[105] that produced α-, β-, *epi*-β-santalene and *exo*-α-bergamotene from (*E*,*E*)-FPP. The santalene synthase isolated from *S. album* of Pune region in our group shared 100% identity with the former.[97] Further, engineering of this santalene synthase by constructing site-directed mutations at specific sites that yielded the mutants wherein they exhibited varied product selectivity. While, some produced *exo*-α-bergamotene as the major product, few produced a varied range of new monocyclic and acyclic sesquiterpene products.[97] The product profiles of some these enzymes have been discussed in proceeding sections.

In sandalwood, the sesquiterpene hydrocarbons (santalenes, bergamotenes, bisabolenes and curcumenes) undergo hydroxylation at the methyl groups of the side chain, reactions catalyzed by enzymes usually belonging to cytochrome P450 family, to produce hydroxylated sesquiterpenoids. These alcohols account for the woody, pleasant odour and medicinal properties of sandalwood oil.[88-93] The major sesquiterpenoid

alcohols present in the oil, (*Z*)-α-santalol and (*Z*)-β-santalol constitute >80% of the total oil content isolated from the heartwood of matured sandalwood tree.[95]

The biosynthesis of polycyclic sesquiterpenes, santalenes, bergamotenes and monocyclic sesquiterpenes, α-zingiberene and curcumenes involves cyclization of the linear sesquiterpene substrate (*E*,*E*)-FPP (**14**) through a cascade of 'Wagner-Meerwein' rearrangements of unisolable carbocationic intermediates. Complexity in terpene skeleton arises from the double bond isomerization, proton elimination, stereo-specific hydride, methyl, and methylene migrations, and premature quenching of carbocations by water to form terpenoid alcohols. Although, biosynthetic schemes involving the formation of some of the common carbocations from terpene pathways and their rearrangements leading to above complex cyclic terpenoids were proposed previously, the mechanism of biosynthesis of these sesquiterpene products passing through specific intermediates is still unexplored. Labelled substrates have constantly played invaluable roles in biochemical and bioorganic research to investigate and track the biosynthetic pathways. They can prove to be a valuable tool and can be put to use to track the pathways traced by the intermediates. Deuterated prenyl diphosphates, in perticular, have been previously utilized to study the mechanism of cyclization by several sesquiterpene synthases including, *epi*-aristolochene synthase and premnaspirodiene synthase,[52] amorphadiene synthase,[53] geosmin synthase,[54] patchoulol synthase,[55] and cadinene synthase.[56]

Analogous biosynthetic pathways in monoterpenes leading to the formation of santalene counterparts, camphenes and pinenes have been established by Croteau *et al*.[43] from *in vitro* assays; while from quantum chemical aspect in gas phase, in the absence of enzymes, *in silico* by Tantillo *et al*.[18] and Weitman *et al*.[48] They demonstrated the cyclization of GPP to pinenes and camphenes through a sequence of intermediates such as terpinyl cation, bornyl cation and pinyl or camphyl cation.[47,48]

Kinetic isotope effects (KIEs) have played a vital role in studying the intriguing mechanisms involved in terpene biosynthetic pathways. A KIE is a mechanistic phenomenon, wherein isotopically labelled molecules react at different rates, as compared to their unlabelled counterparts under the identical reaction conditions. On substitution of an element in a molecule with its higher isotope, although the chemical nature of the bond in both the cases remains the same, their vibration frequencies (ν) differ. Resultantly, their dissociation energies will be slightly different as the atoms of varied mass are involved; the greater the mass, the stronger will be the

bond. This difference in bond strengths is reflected in different rates of breaking of the two bonds (eg. C-H or C-D), under comparable conditions. Thereby, the weaker C-H bond requires lesser energy when compared to the cleavage of C-D bond, during deprotonation steps. Thus, KIE is the ratio of reaction rates for molecules containing light and heavy isotopes, such as k_H/k_D.[106] KIE are primary when they arise from rate differences caused by isotopically labelled bonds that are made or broken in the rate determining step, and are secondary when they do not directly involve the bonds connected to isotopes.[107] With their extensive applications, KIEs have proved as one of the most powerful tools in determining the reaction mechanisms in several fields of science. In the present study, KIE have been determined by comparing the ratio of the products formed from incubation of unlabelled substrates to those from labelled ones with *SaSS* and its mutated enzymes.

Control of these biosynthetic pathways from terpene kingdom and their elucidation should provide new opportunities to study the intriguing chemistry involved and to develop crucial chemotherapeutic agents[108] and isoprenoid-related materials of immense importance. In the present investigation, mechanistic insights for the biosynthesis of sesquiterpenes are explored by utilizing the insightful deuterium labelling of the substrate, **14**. The labels were desired and introduced at centres involved in the carbocationic reactions by chemo-enzymatic strategies (Scheme 3.2.13). Incubation assays of these labeled analogues of **14** with the purified enzymes *SaSS*-WT and its variants were designed. Extraction of the *in vitro* assay reaction mixtures (after specified time period) in hexane delivered the corresponding labelled sesquiterpene products. To examine the loci of deuterium labels in the resultant products, GC-EI-MS fragmentation patterns were studied which explained the hydride shifts and carbocationic rearrangements. Kinetic isotope effects (KIEs) induced by isotope labelling of the substrate were analyzed by comparing the ratio of percentage of products formed from incubations of *SaSS* enzymes with unlabeled **14** to those with its labelled counterparts, which explained the rates of formation of individual products. Based on the integrated results of different incubation experiments with unlabelled and labelled analogues of **14**, a general scheme for the biosynthesis of sesquiterpene hydrocarbons from *S. album* has been elucidated and corroborated with above analyses (Scheme 3.3.1). In the following sections, biosynthesis of individual sesquiterpene hydrocarbon (**1**-**10**) has been discussed in detail.

An initial step in the biosynthesis of santalenes is Mg^{2+} assisted ionization of the allylic diphosphate substrate, (*E*,*E*)-FPP (**14**), at C1 to get the charged diphosphate anion and the farnesyl carbocation (at C1) that subsequently isomerizes to its tertiary counterpart, nerolidyl cation (**I**). Primarily, the *trans*- configuration of C2-C3 double bond in **14** poses an obstacle towards 1,6-electrophilic cyclization. To overcome this state, **I** undergoes a free rotation around energetically accessible C2-C3 σ-bond to adopt a *cisoid* conformation, which can then easily undergo C1-C6 closure generating *endo*-bisabolyl cation (**II**). In many cases, (*E*)-Nerolidol was obtained as a minor product (<0.5%), resulting from premature quenching of **I**, indicating its intermediacy in sesquiterpene biosynthesis. Carbocation **II** serves as an early branching point in sesquiterpene biosynthesis where numerous pathways with low energy barriers are possible, eventually leading to a large spectrum of products.[109] The isomerization-cyclization of **14** is stereospecific and yields chiral products with their stereochemistries depending on the initial, chiral folding of the precursor (**I**), which in turn is induced at the ionization-isomerization step that establishes chirality of the bound tertiary intermediate (**I**) and depends on the binding of appropriate conformer of farnesyl diphosphate with the active site pocket. Ultimately, the absolute configuration at C3 tertiary centre decides the chirality of cyclic products formed, which originally is the result of initial binding of an appropriate conformer of **14**. David Cane has reviewed and supported *endo*-*anti* cyclization for the formation of **II** that further leads to the biosynthesis of bicyclic/ tricyclic products, bergamotenes and santalenes.[12] The *anti* and *syn* notations indicate the manner in which pyrophosphate (OPP^-) group departs from C3. If OPP^- departs from the opposite side of the face of double bond attacked, then it is termed as *anti*. The *endo* and *exo* notations are used to describe the cyclizing conformers. In case of the right handed helix, the *endo* conformer is formed by the *re* face attack of the C6-C7 double bond. Further, cyclization reactions of these carbocationic intermediates leading to individual final products are discussed in following sections.

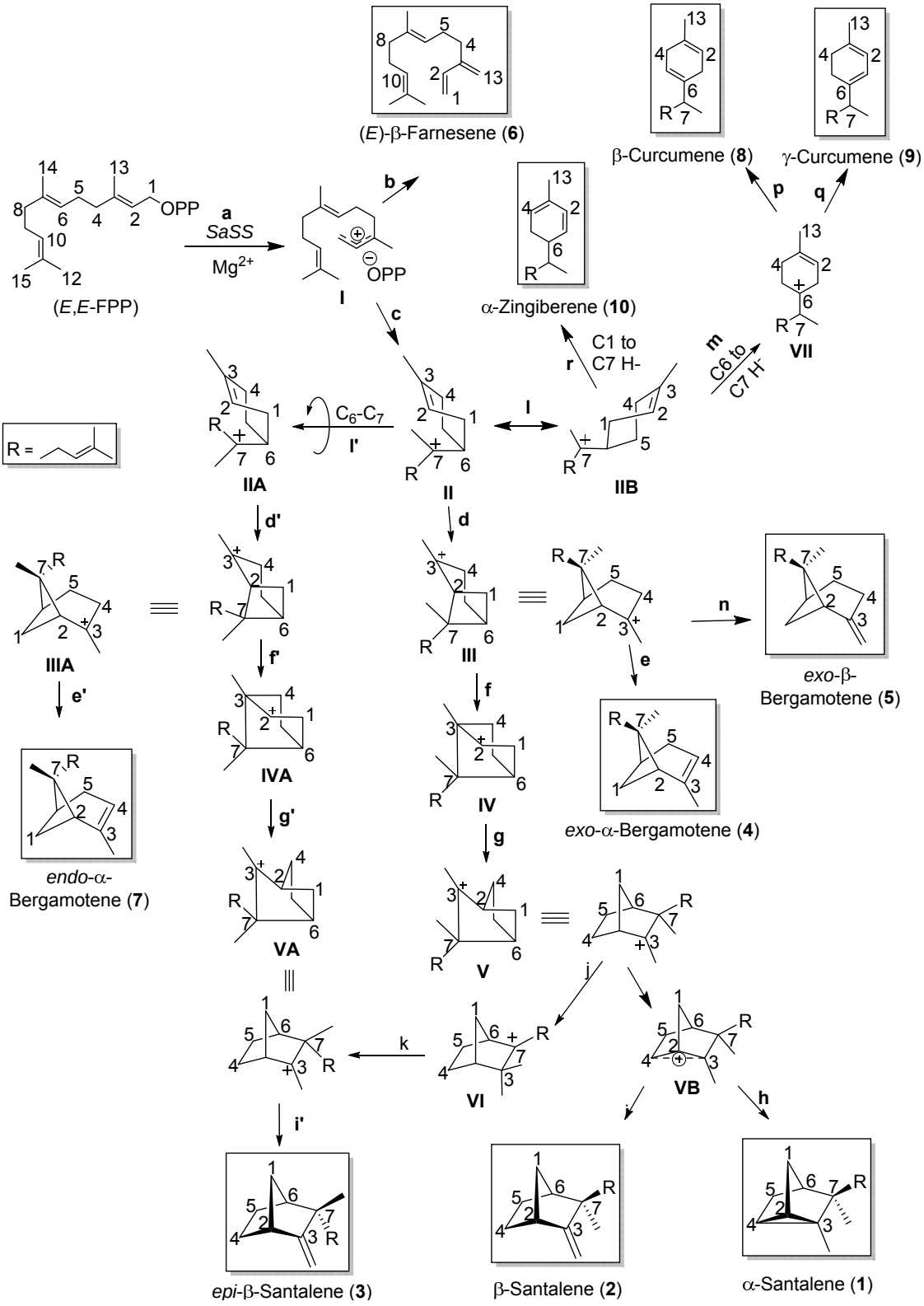

Scheme 3.3.1. Proposed mechanistic pathway for biosynthesis of sesquiterpenes (**1-10**) from (*E*,*E*)-FPP (**14**), catalyzed by *SaSS*-WT and *SaSS* mutants.

3.3.2.1. Biosynthesis of Santalenes (1, 2 and 3) and *exo*-α-Bergamotene (4):

Biosynthesis of santalenes and bergamotenes emanating from **14** and spanning a series of carbocationic intermediates is proposed as shown in scheme 3.3.1. The *endo*-bisabolyl cation (**II**) bearing a C7 carbocation, undergoes cyclization to form a C2-C7 connection constituting a characteristic bicyclo[3,1,1]heptane intermediate (**III**) with a carbocation at C3, which is referred to as 'bergamotyl cation'. The cation **III** acts as a branching point in the biosynthesis of bergamotenes and santalenes. Cation **III** further encounters a shift of a quaternary carbon from C2 to C3 resulting in another non-isolable carbocationic intermediate, **IV**. The intermediate **IV** undergoes 4-3 to 4-2 methylene shift to form the final intermediate, santalyl carbocation (**V**) with a tertiary carbocation at C3. This cation at C3 acts as a branching point in the biosynthesis of santalenes. As observed with chrysanthemyl carbocation,[23] the santalyl carbocation may also involve delocalization of the positive charge to form the cyclopropyl carbocation, **VB**. While, **VB** can subsequently lose a proton from C4 to collapse into α-santalene (**1**) when new C3-C4 sigma bond is formed, or can deprotonate from C13 to form an exocyclic C3-C13 π-bond, to ultimately transform into β-santalene (**2**) (Scheme 3.3.1).

To explore the pathway constituting biosynthesis of santalenes, deuterated analogues of **14** were incubated with *SaSS* and the effects of deuteron shifts/losses on product formation were monitored. Analysis of the GC-MS spectra of all the resulting sesquiterpenes obtained from incubation of unlabelled substrate **14** with *SaSS* enzymes exhibited molecular ion peaks, $[M]^+$ at *m*/*z* 204.1. On incubation of **[4,4-$^2H_2$]-14** with *SaSS*, the molecular ion peak $[M]^+$ for **1** shifted from *m*/*z* 204.1 (unlabeled santalene in control experiments) to *m*/*z* 205.1, thereby indicating an increment of 1 *amu* in the labeled product (Scheme 3.3.2). This also accounted for the loss of a deuterium from C4 due to the newly formed C3-C4 sigma bond, as otherwise a peak at *m/z* 206.1 should have been observed. Similarly, incubation with **[4,4,13,13,13-$^2H_5$]-14** resulted in a parent ion peak at *m/z* 208 with increment of 4 *amu* in $[M]^+$. Expectedly, GC-MS analysis of labeled analogues of **1** obtained from incubation of other analogues of **14** labeled at C1, C2, C5, C6 and C13 with *SaSS* resulted in the retention of all the deuteriums (Fig. A4.8 to A4.13). Locus of deuterium at C4 in **[4-$^2H_1$]-1** obtained from **[4,4-$^2H_2$]-14** incubations was visualized from the GC-MS fragmentation pattern. The ions appearing at *m*/*z* 204.1 $[M]^+$, 189.1, 161.1, 121.1, 107.1, and 94.1 (100%) (Fig. A4.6) from the analysis of TIC for **1** shifted to *m*/*z* 205.1 $[M]^+$, 190.1, 162.1, 122.1, 108.1, and 95.0 (100%) (Fig. A4.7), respectively, indicating the formation of **[4-$^2H_1$]-1**.

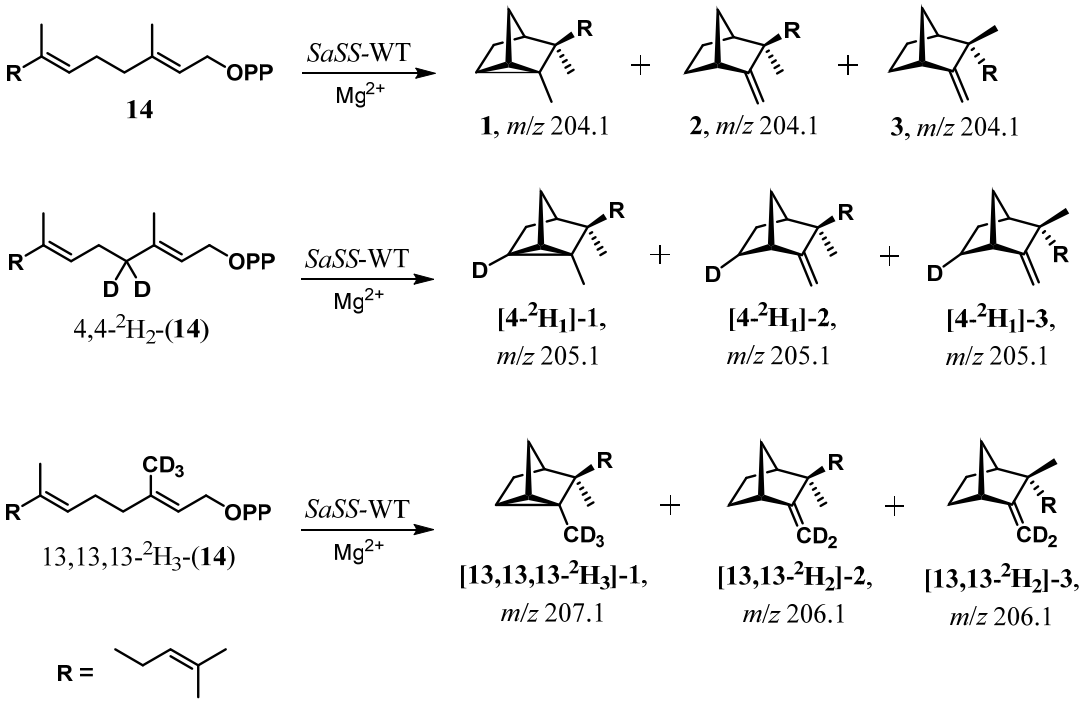

Scheme 3.3.2. Labelled products, α-santalene (**1**), β-santalene (**2**) and *epi*-β-santalene (**3**), obtained from incubation of **14**, **4,4-^{2}H$_2$-14** and **13,13,13-^{2}H$_3$-14** with *SaSS*-WT.

Incubation of the labelled substrate, **[13,13,13-^{2}H$_3$]-14** with *SaSS*, followed by analysis of GC-MS spectrum of the labeled product showed a shift of molecular ion, $[M]^+$ from *m/z* 204.1 to *m/z* 206.1 indicating the formation of **[13,13-^{2}H$_2$]-2**. The presence of two deuteriums on the exocyclic methylene group was evident from the GC-MS fragmentation analysis of **[13,13-^{2}H$_2$]-2** which showed the peaks at *m/z* 206.1 $[M]^+$, 191.1, 163.1, 124.1, and 96.1 (100%) (Fig. A4.16) in comparison to the corresponding peaks for unlabeled **2** at *m/z* 204.1 $[M]^+$, 189.1, 161.1, 122.1, and 94.1 (100%) (Fig. A4.14), respectively. These observations clearly indicate loss of one deuterium from C13 for the formation of an exocyclic C3-C13 π-bond (Scheme 3.3.2). Incubation of **[4,4-^{2}H$_2$]-14** with *SaSS*-WT produced **[4-^{2}H$_1$]-2** with a molecular ion at *m/z* 205.1 and not **[4,4-^{2}H$_2$]-2** (*m/z* 206.1). Further the fragmentation pattern revealed that the product was **[4-^{2}H$_1$]-2** (Fig. A4.15) This result indicated formation of the delocalized cyclopropyl carbocation (**VB**), where the deuteron/proton at C4 position might be exchanged between the carbocation intermediate (**V**/**VB**) and the closely interacting active site amino acid residues. However, this fact will be confirmed only after structure determination of *SaSS*, when the exact specifications on the spatial interactions of amino acids with the intermediate species will be determined. Similarly,

from the incubation of **[4,4,13,13,13-$^2H_5$]-14** with *SaSS* produced **[4,13,13-$^2H_3$]-2** with $[M]^+$ ion at *m*/*z* 207.2 (Fig. A4.17). Incubation of other substrates, deuterium labeled at C1, C2, C5, and C6 showed retention of all the deuterium atoms in the resulting labeled derivatives of **2** (Fig. A4.18 to A4.21).

As discussed above, bergamotyl cation (**III**) is proposed to act as a branching point in the biosynthesis of bergamotenes and santalenes. Differential deprotonations from specific sites of **III** gives rise to the formation of new π-bonds leading to the formation of *exo*-α-bergamotene (**4**) and *exo*-β-bergamotene (**5**). The C3 carbocation **III**, which forms a precursor to **4**, essentially, is quenched by deprotonation from C4, accompanied by the formation of C3-C4 π-bond. To derive mechanistic details of the reaction cascade, deuterium labeled substrates **[4,4-$^2H_2$]-14** and **[4,4,13,13,13-$^2H_5$]-14** were incubated with *SaSS*, followed by GC-MS analysis of the assay extracts that yielded the corresponding deuterium labeled products, **[4-$^2H_1$]-4** and **[4,13,13,13-$^2H_4$]-4**. The molecular ion peak $[M]^+$ for **4** appearing at *m/z* 204.1 shifted to *m/z* 205.1 and *m/z* 208.2 for **[4-$^2H_1$]-4** and **[4,13,13,13-$^2H_4$]-4**, respectively. The results were in agreement with the elimination of a deuterium from C4 and concomitant formation of C3-C4 π-bond. The molecular ions of labelled derivatives of **4** obtained from incubation of other analogues of **14** labeled at C1, C2, C5, C6 and C13 with *SaSS* did not exhibit the loss of deuteriums and retained all the deuteriums as were in the substrate (Fig. A4.32 and A4.34 to A4.37). Presence of a deuterium at C4 was indicated from the analysis of GC-MS fragmentation pattern. The fragment ions appearing at *m*/*z* 204.2 $[M]^+$, 161.1, 119.0 (100%), 93.0 and 69.1 in **4** (Fig. A4.30) shifted to *m*/*z* 205.1 $[M]^+$, 162.1, 120.1 (100%), 94.0 and 69.0 in **[4-$^2H_1$]-4** (Fig. A4.31), and to *m*/*z* 208.3 $[M]^+$, 165.1, 123.1 (100%), 97.1 and 69.1 in **[4,13,13,13-$^2H_4$]-4** (Fig. A4.33).

Area under the individual product peak was calculated from GC-FID analysis of the hexane extracts of enzyme assays to realize the percentage of corresponding products formed and further to monitor the changes in product ratio that occurred due to deuterium isotope effects induced in the partitioning steps. The percentage of the products was dominated by relative rates of deprotonations in the partitioning steps. In the formation of santalenes, product ratio [**1**/**2**], obtained from incubation of **[4,4-$^2H_2$]-14** decreased to 0.76 from 1.56 obtained from incubation with unlabeled **14**. A deuterium kinetic isotope effect (KIE), $[(\mathbf{1}/\mathbf{2})^H/(\mathbf{1}/\mathbf{2})^D]$ of 2.05 was consistent with the cleavage of C-D bond at C4 in the formation of **1** (Table 3.3.1).

Table 3.3.1. Variation of the distribution of major sesquiterpene products obtained from incubations of *SaSS*-WT with labelled analogues of **14**. The ratios of the products were tabulated from the GC-FID response analysis of the hexane extracts of the reaction mixtures[a]. Key: α-santalene (**1**), β-santalene (**2**), *epi*-β-santalene (**3**), *exo*-α-bergamotene (**4**), and *exo*-β-bergamotene (**5**).

	***SaSS*-WT**			
Substrate	**[1/2]**	**[2/1]**	**[4/2]**	**[2/4]**
(*E*,*E*)-FPP	1.56 ± 0.02	0.64 ± 0.01	1.01 ± 0.02	0.99 ± 0.02
4,4-$^2H_2$-(*E*,*E*)-FPP	0.76 ± 0.01	1.32 ± 0.01	0.42 ± 0.00	2.38 ± 0.00
13,13,13-$^2H_3$-(*E*,*E*)-FPP	4.46 ± 0.04	0.22 ± 0.00	3.22 ± 0.02	0.31 ± 0.00
4,4,13,13,13-$^2H_5$-(*E*,*E*)-FPP	2.35 ± 0.00	0.43 ± 0.00	2.20 ± 0.04	0.45 ± 0.01
5,5-$^2H_2$-(*E*,*E*)-FPP	1.59 ± 0.02	0.63 ± 0.01	1.00 ± 0.01	1.00 ± 0.01
1,1-$^2H_2$-(*E*,*E*)-FPP	1.51 ± 0.01	0.66 ± 0.01	0.92 ± 0.04	1.09 ± 0.05
2-$^2H_1$-(*E*,*E*)-FPP	1.62 ± 0.00	0.62 ± 0.00	0.96 ± 0.01	1.04 ± 0.01
2,6-$^2H_2$-(*E*,*E*)-FPP	1.67 ± 0.01	0.60 ± 0.00	1.11 ± 0.01	0.90 ± 0.01

[a] Each value is an average of two independent incubations under identical conditions.

On the other hand, when **14** was replaced with **[13,13,13-$^2H_3$]-14** in bioassays with purified *SaSS*, the product ratio **[2**/**1]**, decreased from 0.65 to 0.23 (Table 3.3.1). A KIE, $[(\mathbf{2}/\mathbf{1})^H/(\mathbf{2}/\mathbf{1})^D]$= 2.89 for the substrate **[13,13,13-$^2H_3$]-14** was in good agreement with the preference of the enzyme to form **1** from carbocation flux of **VB**. However, when **[4,4,13,13,13-$^2H_5$]-14** was used as the substrate with *SaSS*, a KIE of $[(\mathbf{2}/\mathbf{1})^H/(\mathbf{2}/\mathbf{1})^D]$=1.50 was observed indicating that the formation of **1** was preferred over **2**. This fact further supports the delocalization of tertiary carbocation into cyclopropyl carbocation, **VB** as proposed in scheme 3.3.1.

As described above, **III** can either yield **4** and **5**, or can undergo 7-2 to 7-3 shift, generating a secondary carbocation at C2 in **IV** which further moves to the production of santalenes (Scheme 3.3.1). The intermediates **III** and **IV** can be viewed as inter-converting structures which can collapse into one of the products, in this case, *exo*-α-bergamotene (**4**) by formation of C3-C4 π-bond or may proceed to the formation of santalenes, whose fate depends on the extent of deprotonation at C4. The largest decrease in the product ratio [**4**/**2**] was observed from 1.01 to 0.42 when incubations with **14** were replaced by **[4,4-$^2H_2$]-14**, which was in agreement with a KIE,

[(**4/2**)^{H}/(**4/2**)^{D}] = 2.39 observed due to cleavage of C-D bond at C4 (Table 3.3.1). Further, when substrate **14** was replaced with **[13,13,13-^{2}H$_3$]-14**, product ratio [**2**/**4**] decreased from 0.99 to 0.31, along with an observed KIE, [(**2**/**4**)^{H}/(**2**/**4**)^{D}] = 3.20. These results indicate that **III** is the intermediate carbocation for the formation of santalenes as well as bergamotenes, with the carbocations **III**, **IV**, **V** and **VB** being interconvertible. On replacing **14** with **[4,4,13,13,13-^{2}H$_5$]-14**, the product ratio **[2/4]** decreased from 0.99 to 0.45 with an intrinsic KIE, [**2**/**4**]^{H}/[**2**/**4**]^{D}= 2.19 and a preference for the formation of **4** over **2**. Although formation of **[4,13,13,13-^{2}H$_4$]-1**, **[4,13,13,13-^{2}H$_4$]-4** and **[4,13,13-^{2}H$_3$]-2** from **[4,4,13,13,13-^{2}H$_5$]-14** by *SaSS* enzyme involves loss of deuterons, due to observed KIEs, it is evident that **4** is the preferred enzymatic product over **1** and **2** when **[4,4,13,13,13-^{2}H$_5$]-14** is used as a substrate. In conclusion, α-santalene (**1**), β-santalene (**2**), and *exo*-α-bergamotene (**4**) are formed from *cisoid* nerolidyl carbocation (**I**), followed by its cyclization to bisabolyl carbocation (**II**), which further undergoes bicyclization to form bergomotyl carbocation (**III**). *exo*-α-Bergomotene (**4**) is formed by deprotonation at C4 of **III** to form C3-C4 π-bond. Further, **III** undergoes Wagner-Meerwein rearrangements to form **IV**, **V** and **V/B** which are interconvertible in nature. Further, the sesquiterpene hydrocarbons **1** and **2** are formed by deprotonation at C4 and C13 of **VB**, respectively

Biosynthesis of *epi*-β-santalene (**3**) from (*E*,*E*)-FPP (**14**) can be proposed in two ways. First pathway could be traversed through epimerization of **II** to **IIA** following a free, low-energy rotation about C6-C7 and further cyclization to the *epi*-santalyl cation (**VA**), pursuing the intermediates (**IIIA** and **IVA**) formed through a similar reaction cascade as followed in the biosynthesis of **2**. The other way could be through two consecutive methyl shifts from the intermediate **V**. The first methyl (C13) shift from C7-*endo* to C3, resulting in cation at C7 (**VI**), which may undergo another methyl (C14) shift from C3-*exo* to C7 resulting in the formation of *epi*-santalyl cation (**VA**). Ultimately, deprotonation from C13 in **VA** would yield **3** with a C3-C13 exocyclic π-bond (Scheme 3.3.3).

Within the experimental errors, incubations of all deuterated analogues of **14** resulted in the formation of **3** at the same levels, as observed in control experiments with *SaSS* (Table A4.1). These results thereby indicated the absence of competing reactions and intermediates, and unaffected rates of formation of **3** in all the incubation sets. This observation exquisitely revealed the existence of a different carbocation cascade for the formation of **3**. Further, GCMS analysis of the assay extract using

[13,13,13-$^2H_3$]-14 indicated that formation of **[13,13-$^2H_2$]-3** with $[M]^+$ at *m/z* 206.1 indicating that there is no CD_3 shift between C3 to C7 where one should observe $[M]^+$ at *m/z* 207.1. This observation rules out the possibility of the carbocation cascade from **V**/**VB** to **VA** for the formation **3**. GC-MS fragments for **3** from incubation of **14** with *SaSS* detected at *m*/*z* 204.2 $[M]^+$, 189.1, 161.1, 122.1, 94.1 (100%) and 69.0 (Fig. A4.22) shifted to *m*/*z* 206.1 $[M]^+$, 191.1, 163.1, 124.1, 96.0 (100%) and 69.1 (Fig. A4.24) for **[13,13-$^2H_2$]-3** obtained after incubation of **[13,13,13-$^2H_3$]-14** with *SaSS*. If biosynthesis of **3** were to follow pathway-2, -CD_3 group from substrate **[13,13,13-$^2H_3$]-14** would have shifted to C7 from C3 (Scheme 3.3.2) and the molecular ion peak should have been observed at *m/z* 207.1 that would contradict the observed peak at *m/z* 206.1. Further, GC-MS fragmentation pattern at *m*/*z* 205.1 $[M]^+$, 190.2, 162.1, 123.1, 95.0 (100%) and 69.0 (Fig. A4.23) for **[4-$^2H_1$]-3** obtained from incubation of **[4,4-$^2H_2$]-14** with *SaSS* indicated loss of one deuteron from C4, similar to that observed with its epimeric counterpart **[4-$^2H_1$]-2**.

From above results, the probable implications in the biosynthesis of **3** could be drawn, wherein allowed rotation about C6-C7 bond gave rise to the *epi*-isomer and justified the prevalence of pathway-1, while eliminating the possibility of pathway-2 (Scheme 3.3.3). However, this proposed pathway for the biosynthesis of **3** needs complete evaluation by using suitably labeled FPP with an enzyme that will produce **2** and **3** as major products.

Other sesquiterpene products from incubation of **14** with *SaSS* were *exo*-β-bergamotene (**5**, 2.2%) and (*E*)-β-farnesene (**6**, 0.7%), which were obtained as minor constituents of the enzyme assay extracts. Although, incubation of *SaSS* with differentially deuterium labeled analogues of **14** could bring about alterations of the product ratios **[5/4]** and **[6/4]** in comparison to that with unlabeled **14**, these ratios have been discussed in incubations with *SaSS* mutant enzymes where these products could be obtained in higher levels. The mechanistic aspects of biosynthesis of these minor components are discussed in following part of the thesis.

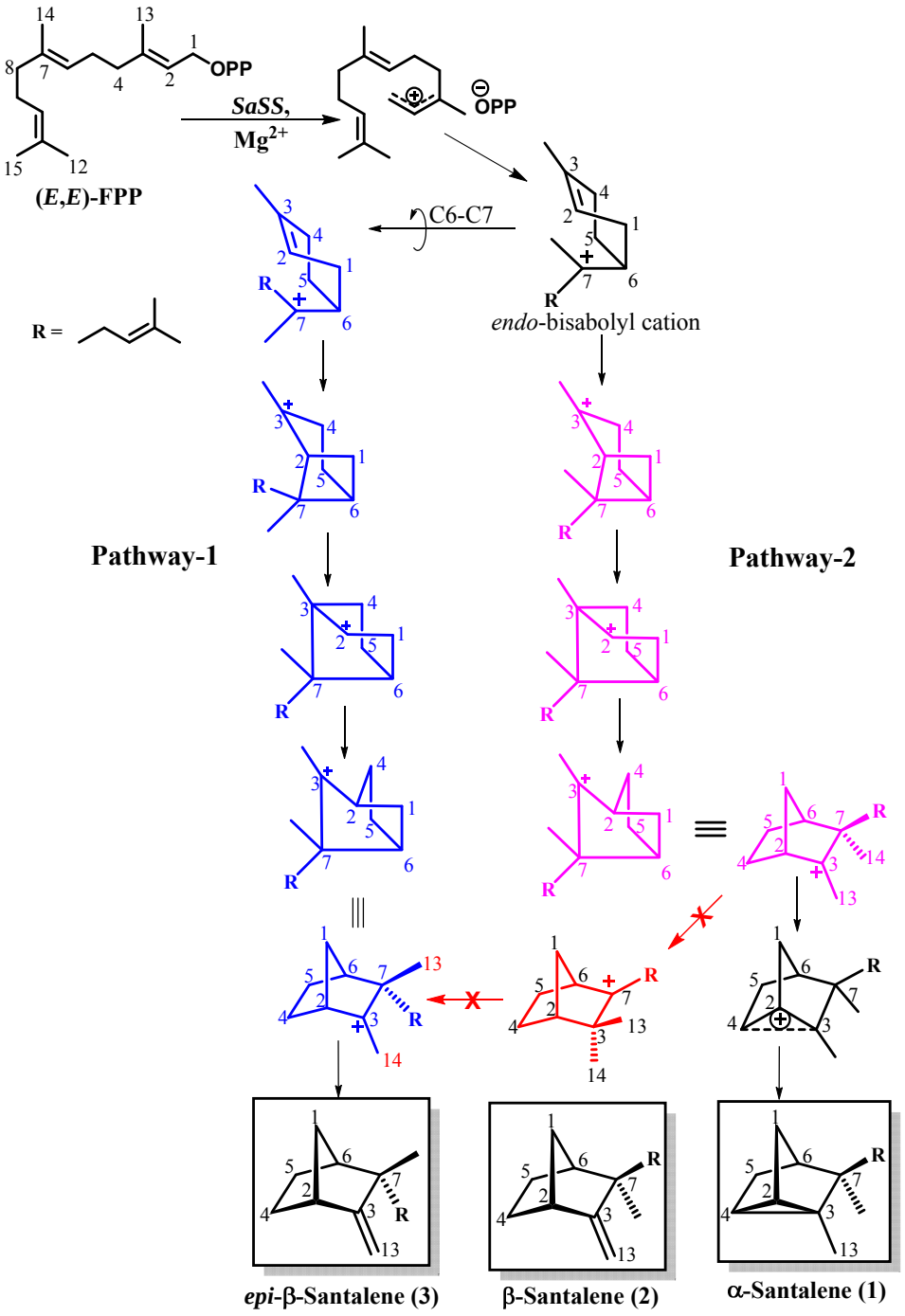

Scheme 3.3.3. Proposed biosynthetic pathway for the formation of α-Santalene (**1**), β-Santalene (**2**), and *epi*-β- Santalene (**3**).

3.3.2.2. Biosynthesis of *exo*-β-Bergamotene (5) and *endo*-α-Bergamotene (7):

The biosynthesis of *exo*-β-Bergamotene (**5**) originates from the bergamotyl cation (**III**) that follows loss of a proton from C13 to quench the carbocation at C3, with a simultaneous formation of exocyclic C3-C13 π-bond. Incubations of **[13,13,13-$^{2}H_3$]-14** with *SaSS* as well as with a mutant enzyme R474L-*SaSS* fetched **[13,13-$^{2}H_2$]-5**

containing two deuterium atoms as seen by shift of the molecular ion $[M]^+$ to *m*/*z* 206.2 from *m*/*z* 204.1 observed for **5**. Similarly, incubation of **[4,4,13,13,13-$^2H_5$]-14** with both *SaSS* enzymes yielded **[4,4,13,13-$^2H_4$]-5** containing four deuterium atoms, that was determined from shift of $[M]^+$ from *m*/*z* 204.1 to *m*/*z* 208.2. These results illustrated deprotonation from C13 during the formation of exocyclic C3-C13 π-bond in **5**. The deuterated analogues of **5** obtained from incubation of **14** labeled at C1, C2, C4, C5 and C6 with *SaSS* enzymes retained all the deuterium atoms as present in the substrate (Fig A4.42 to A4.45). The locus of two deuterium atoms on C13 was verified from the fragmentation pattern of **5**, when the fragments at *m*/*z* 204.1 $[M]^+$, 189.1, 161.1, 93.0 and 69.0 (100%) (Fig. A4.38) for **5** shifted to *m*/*z* 206.2 $[M]^+$, 191.1, 163.1, 95.0 and 69.0 (100%) (Fig. A4.40) and *m*/*z* 208.2 $[M]^+$, 193.2, 165.1, 96.0 and 69.1 (100%) (Fig. A4.41) in **[13,13-$^2H_2$]-5** and **[13,13-$^2H_2$]-5**, respectively (Scheme 3.3.4).

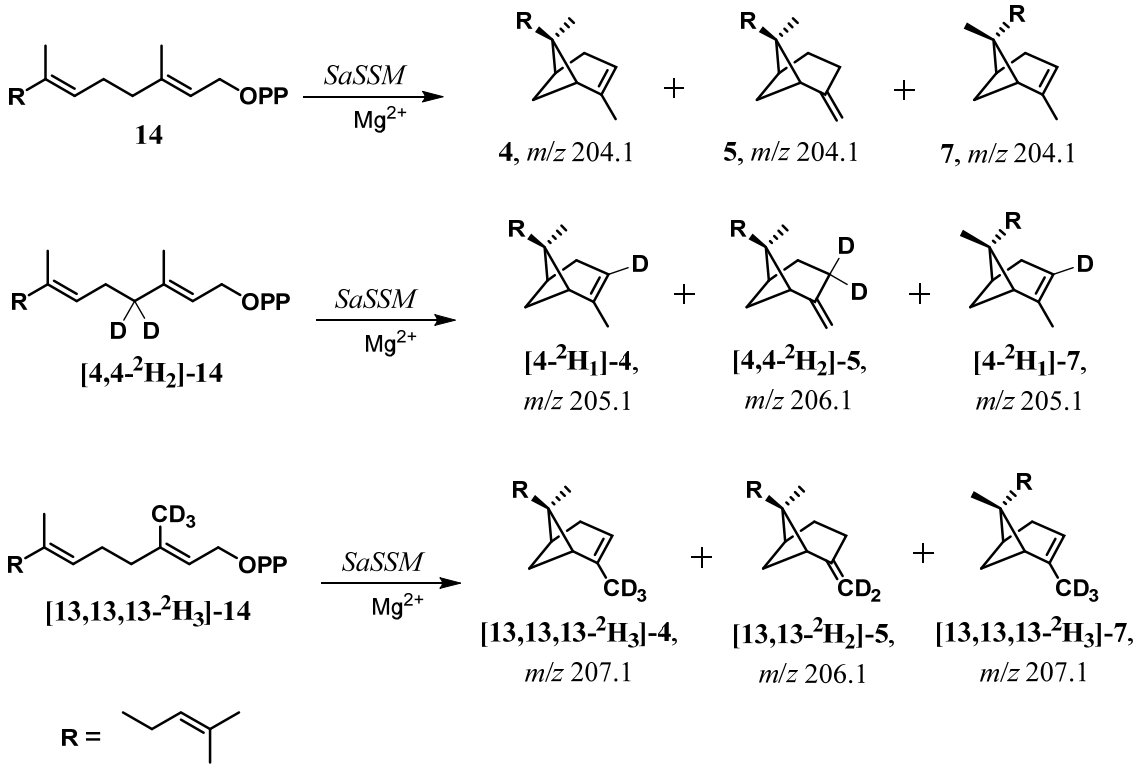

Scheme 3.3.4. Labelled products, *exo*-α-bergamotene (**4**), *exo*-β-bergamotene (**5**) and *endo*-α-bergamotene (**7**), obtained from incubation of **14**, [**4,4-$^2H_2$]-14** and [**13,13,13-$^2H_3$]-14** with *SaSS*-WT and *SaSS* mutants.

Though, *exo*-β-bergamotene (**5**) was as a minor component (2.2%) formed among the sesquiterpenes from incubations of **14** with *SaSS*, the mutant R474L-*SaSS* was able to functionalize cyclization of (*E*,*E*)-FPP (**14**) to only two sesquiterpenes, **4**

(74.7%) and **5** (25.3%). This R474L-*SaSS* mutant enzyme was subsequently used for studying the mechanistic insight for the biosynthesis of **4** and **5**. When **14** was replaced with **[4,4-$^2H_2$]-14**, the ratio of products, **[4/5]** decreased from 2.93 to 1.06, while exhibiting a KIE, [(**4**/**5**)^H/(**5**/**4**)^D] = 2.77, resulting from cleavage of C-D bond at C4 in the formation of **4** (Table 3.3.2). In contrast, when **14** was replaced with **[13,13,13-$^2H_3$]-14**, the ratio **[5/4]** decreased from 0.34 to 0.09 revealing a KIE, [(**5**/**4**)^H/(**5**/**4**)^D] = 3.72 (Table 3.3.2). These results indicate the formation of **5** and **4** through deprotonation of **III** at C13 and C4, respectively (Scheme 3.3.1).

Table 3.3.2. Variation of the distribution of major sesquiterpene products obtained from incubations of *SaSS* enzymes with labeled analogues of **14**. The ratios of the products were tabulated from the GC-FID response analysis of the hexane extracts of the reaction mixtures[a]. *Key*: *exo*-α-bergamotene (**4**), *exo*-β-bergamotene (**5**). *endo*-α-bergamotene (**7**).

	***SaSSM* (R474L)**	***SaSSM* (R474L)**	***SaSSM* (Y539W)**
Substrate	**[5/4]**	**[4/5]**	**[7/5]**
(*E*,*E*)-FPP	0.34 ± 0.00	2.93 ± 0.03	0.91 ± 0.00
4,4-$^2H_2$-(*E*,*E*)-FPP	0.95 ± 0.00	1.06 ± 0.00	0.37 ± 0.00
13,13,13-$^2H_3$-(*E*,*E*)-FPP	0.09 ± 0.00	10.91 ± 0.07	1.80 ± 0.00
4,4,13,13,13-$^2H_5$-(*E*,*E*)-FPP	0.34 ± 0.01	2.90 ± 0.04	0.58 ± 0.00
5,5-$^2H_2$-(*E*,*E*)-FPP	0.37 ± 0.00	2.70 ± 0.01	0.87 ± 0.02
1,1-$^2H_2$-(*E*,*E*)-FPP	0.32 ± 0.00	3.16 ± 0.02	0.93 ± 0.01
2-$^2H_1$-(*E*,*E*)-FPP	0.36 ± 0.01	2.75 ± 0.04	1.00 ± 0.01
2,6-$^2H_2$-(*E*,*E*)-FPP	0.35 ± 0.00	2.83 ± 0.01	0.97 ± 0.00

[a] Each value is an average of two independent incubations under identical conditions.

Further, another mutant enzyme Y539W-*SaSS* produced a total of six sesquiterpene products, α-santalene (**1**, 10.5%), *epi*-β-santalene (**3**, 1.3%), *exo*-α-bergamotene (**4**, 32.2%), *exo*-β-bergamotene (**5**, 24.1%), (*E*)-β-farnesene (**6**, 9.8%), and *endo*-α-bergamotene (**7**, 22.0%), when incubated with **14**. Biosynthesis of **7** is proposed to proceed through *endo*-bisabolyl cation (**IIA**) which initially experiences a free rotation around C6-C7 (path l', Scheme 3.3.1) from **II**, a pathway similar to that

encountered in the biosynthesis of **3**. Cation **IIA** subsequently underwent C2-C7 closure (path d', Scheme 3.3.1) to produce the characteristic bicyclo[3,1,1]heptane intermediate (**IIIA**) with a carbocation at C3, which was referred to as '*endo*-bergamotyl cation'. Further, **IIIA** encountered deprotonation from C4 to quench the C3 carbocation and result in the final product **7** with a C3-C4 π-bond, analogous to that observed in case of **4**. Incubation of **[4,4-$^2H_2$]-14** and **[4,4,13,13,13-$^2H_5$]-14** with Y539W-*SaSS* mutant resulted in **[4-^{2}H]-7** and **[4,13,13,13-$^2H_4$]-7**, which exhibited a shift of molecular ion peak $[M]^+$ from *m*/*z* 204.1 to *m*/*z* 205.1 and *m*/*z* 208.1, respectively, as deduced from GC-MS spectral analysis. Incubations with other analogues of **14** labelled at C1, C2, C5, C6 and C13 resulted in the retention of all the deuterium labels. The fragmentation pattern of **7** (Fig. A4.54 to A4.61) was similar to that observed for **4** demonstrating loss of a proton from C4 in the formation of **7** (Scheme 3.3.4).

The rate of biosynthesis of **5** formed from the intermediate **II** was compared with that of **7**, also formed through the same intermediate, following a similar path as that of **4**, but after an energy-feasible bond rotation around C6-C7 (Scheme 3.3.1). The product ratio, **[7**/**5**] was compared in incubations of **14** and **[4,4-$^2H_2$]-14** with Y539W-*SaSS* mutant. When the substrate **14** was replaced with [**4,4-$^2H_2$]-14**, GC analysis of the assay products revealed a decrease in the ratio **[7**/**5**] from 0.91 to 0.37 demonstrating a KIE, $[(\mathbf{7}/\mathbf{5})^H/(\mathbf{7}/\mathbf{5})^D] = 2.45$ (Table 3.3.3). These results indicate that **III** and **IIIA** are interconvertible through **II** with C6-C7 bond rotations, while the sesquiterpene **7** is formed through deprotonation at C4 of **IIIA** (Scheme 3.3.1).

3.3.2.5. Biosynthesis of Monocyclic sesquiterpenes (8, 9, and 10):

As discussed in previous sections, bridged polycyclic sesquiterpenes (santalenes and bergamotenes) are derived from successive rearrangements and cyclizations of *endo*-conformations of bisabolyl carbocation (**II**). On the other hand, *exo*- conformations (**IIB**) of bisabolyl carbocation are conformationally rigid and are impotent towards bicyclization due to remoteness of C7 cation from C2-C3 π-bond, which does not allow its rearrangement to bergamotyl cation (**III**). Nevertheless, these conformations give rise to a spectrum of rearranged products and thus experience a series of hydride shifts and deprotonations, ultimately resulting in mutually competing monocyclic sesquiterpenes such as curcumenes and zingiberene. The *exo*-bisabolyl cation (chair conformation) can either directly emerge from *exo-anti* cyclization of nerolidyl cation or by flipping of *endo*-conformer (boat conformation) that involves crossing a low

energy barrier passing through homo-bisabolyl cation (half-chair conformation). Incubation of **14** with I422A-*SaSS* mutant yielded monocyclic sesquiterpene products, β-curcumene (**8**, 64.3%), γ-curcumene (**9**, 13.6%), and α-zingiberene (**10**, 1.7%), along with other sesquiterpenes, **1** (1.6%), **2** (2.1%), **4** (11.5%), **6** (3.4%), and **7** (1.7%).

Table 3.3.3. Variation of the distribution of major sesquiterpene products obtained from incubations of *SaSS* mutants with labelled analogues of **14**. The ratios of the products were tabulated from the GC-FID response analysis of the hexane extracts of the reaction mixtures[a]. Key: *exo*-α-bergamotene (**4**), (*E*)-β-farnesene (**6**), β-curcumene (**8**), γ-curcumene (**9**), and α-zingiberene (**10**).

KIE calculated in	***SaSSM* (L427A)**	***SaSSM* (I422A)**	***SaSSM* (I422A)**	***SaSSM* (I422A)**
Substrate	**[6/4]**	**[8/4]**	**[8/9]**	**[9/8]**
(*E*,*E*)-FPP	0.65 ± 0.01	5.03 ± 0.04	4.71 ± 0.02	0.21 ± 0.00
4,4-$^2H_2$-(*E*,*E*)-FPP	0.71 ± 0.01	5.36 ± 0.05	4.58 ± 0.01	0.22 ± 0.00
13,13,13-$^2H_3$-(*E*,*E*)-FPP	0.14 ± 0.01	5.77 ± 0.29	5.38 ± 0.06	0.19 ± 0.00
4,4,13,13,13-$^2H_5$-(*E*,*E*)-FPP	0.19 ± 0.01	4.73 ± 0.11	4.48 ± 0.06	0.22 ± 0.00
5,5-$^2H_2$-(*E*,*E*)-FPP	0.58 ± 0.00	3.93 ± 0.25	2.47 ± 0.01	0.40 ± 0.00
1,1-$^2H_2$-(*E*,*E*)-FPP	0.66 ± 0.01	4.41 ± 0.05	11.92 ± 0.49	0.08 ± 0.00
2-$^2H_1$-(*E*,*E*)-FPP	0.54 ± 0.00	4.54 ± 0.03	4.44 ± 0.03	0.23 ± 0.00
2,6-$^2H_2$-(*E*,*E*)-FPP	0.54 ± 0.00	2.31 ± 0.06	6.09 ± 0.31	0.16 ± 0.01

[a] Each value is an average of two independent incubations under identical conditions.

Biosynthesis of curcumenes (**8** and **9**) initiates from ionization of **14**, followed by C1-C6 cyclization of **I** forming **IIB**. A 1,2-hydride shift in **IIB** from C6 to C7 produced homo-bisabolyl cation (**VII**) with a carbocation at C6 which consequently followed direct deprotonations from C1 or C5, depending on the interactions of carbocation with interacting amino acid residues, yielding β-curcumene (**8**) or γ-curcumene (**9**), respectively. When **14** was incubated with mutant I422A-*SaSS*, **8** (65%) and **9** (13%) were two of the products formed in major and both displayed a molecular ion peak $[M]^+$ at *m*/*z* 204.1. Assays using labeled derivatives of **14** were carried out with mutant I422A-*SaSS* to study the loci of labels in the emanating products. The deuterated product **[1,1-$^2H_2$]-8** resulting from enzymatic assay of **[1,1-$^2H_2$]-14** with mutant I422A-

SaSS showed a molecular ion peak at *m/z* 206.2 containing both the deuterium atoms as were in the substrate, but from **[5,5-$^2H_2$]-14** incubations, the monodeuterated product **[5-$^2H_1$]-8** showed a molecular ion peak at *m/z* 205.2. An increment of one mass unit in **[5-$^2H_1$]-8** when compared with **8** from the unlabeled substrate (*m/z* 204.1) also corresponded to the elimination of a deuterium from C5 due to creation of a C5-C6 π-bond. The presence of deuterium atoms was revealed from GC-MS fragmentation analysis of analogues of **8**, which displayed shift of ions from *m/z* 204.2 $[M]^+$, 189.2, 161.1, 119.1 (100%), 93.1, and 69.0 (Fig. A4.62) to *m/z* 205.2 $[M]^+$, 190.1, 162.1, 120.1 (100%), 94.0, and 69.0 for **[5-$^2H_1$]-8** (Fig. A4.66) and to *m/z* 206.2 $[M]^+$, 191.2, 163.1, 120.1 (100%), 95.1 and 69.0 for **[1,1-$^2H_2$]-8** (Fig. A4.67). Deuterium atoms at C4, C13 and C2 were observed to be unaffected.

On the similar lines, when **[1,1-$^2H_2$]-14** was incubated with *SaSS*-mutant (I422A), the labeled product **[1-$^2H_1$]-9** containing only one deuterium displayed a shift of molecular ion peak to *m/z* 205.2, while with the substrate **[5,5-$^2H_2$]-14**, the molecular ion peak for the resultant product **[5,5-$^2H_2$]-9** shifted to *m/z* 206.2 containing both the deuterium atoms as were in the substrate. Thus, loss of a deuterium from C1 quenched the cation **VII** with concomitant construction of a C1-C6 π-bond. GC-MS analysis informed the shift of ion fragments from *m/z* 204.2 $[M]^+$, 189.2, 161.2, 119.1 (100%), 93.0, and 69.0 (Fig. A4.70) obtained for **9** to *m/z* 205.1 $[M]^+$, 190.1, 162.1, 120.1 (100%), 94.0, and 69.1 for **[1-$^2H_1$]-9** (Fig. A4.75) and to *m/z* 206.2 $[M]^+$, 191.1, 163.1, 123.1 (100%), 95.0 and 69.1 for **[5,5-$^2H_2$]-9** (Fig. A4.74). Deuterium atoms at C4, C13 and C2 were analyzed to be unaffected.

It is however possible that **9** is biosynthesized by hydride shift from C1→C7, a 1,3 hydride shift commonly observed in terpene biosynthesis, followed by deprotonation from C6 to form C1-C6 π-bond. Similarly, biosynthesis of **8** is possible through hydride shift from C5→C7, followed by deprotonation from C6 to form C5-C6 π-bond. A shift of molecular ion, from *m/z* 204.1 displayed for both unlabelled monocyclic sesquiterpene products, **[1-$^2H_1$]-9** and **[5-$^2H_1$]-8**, to *m/z* 205.2 as explained above, abolished the possibility of hydride migration from C1 or C5, else the molecular ions containing both the deuterium atoms should have showed $[M]^+$ at *m/z* 206.2, the dideuterated products. Coherently, shift of the diagnostic fragment at *m/z* 93.1 arising from the cyclohexadienyl unit in the unlabeled products, **8** and **9**, to *m/z* 94.1 in labelled products **[2,7-$^2H_2$]-8** and **[2,7-$^2H_2$]-9**, arising from incubations of **[2,6-$^2H_2$]-14** supported the deuteride shift from C6→C7, subsequently resulting in cation **VII**

(Scheme 3.3.5). Further, the molecular ion at *m/z* 204.1 for unlabelled **8** and **9** shifted to *m/z* 206.1 for both **[2,7-$^2H_2$]-8** (Fig. A4.69) and **[2,7-$^2H_2$]-9** (Fig. A4.77), demonstrating the presence of both the deuterium atoms.

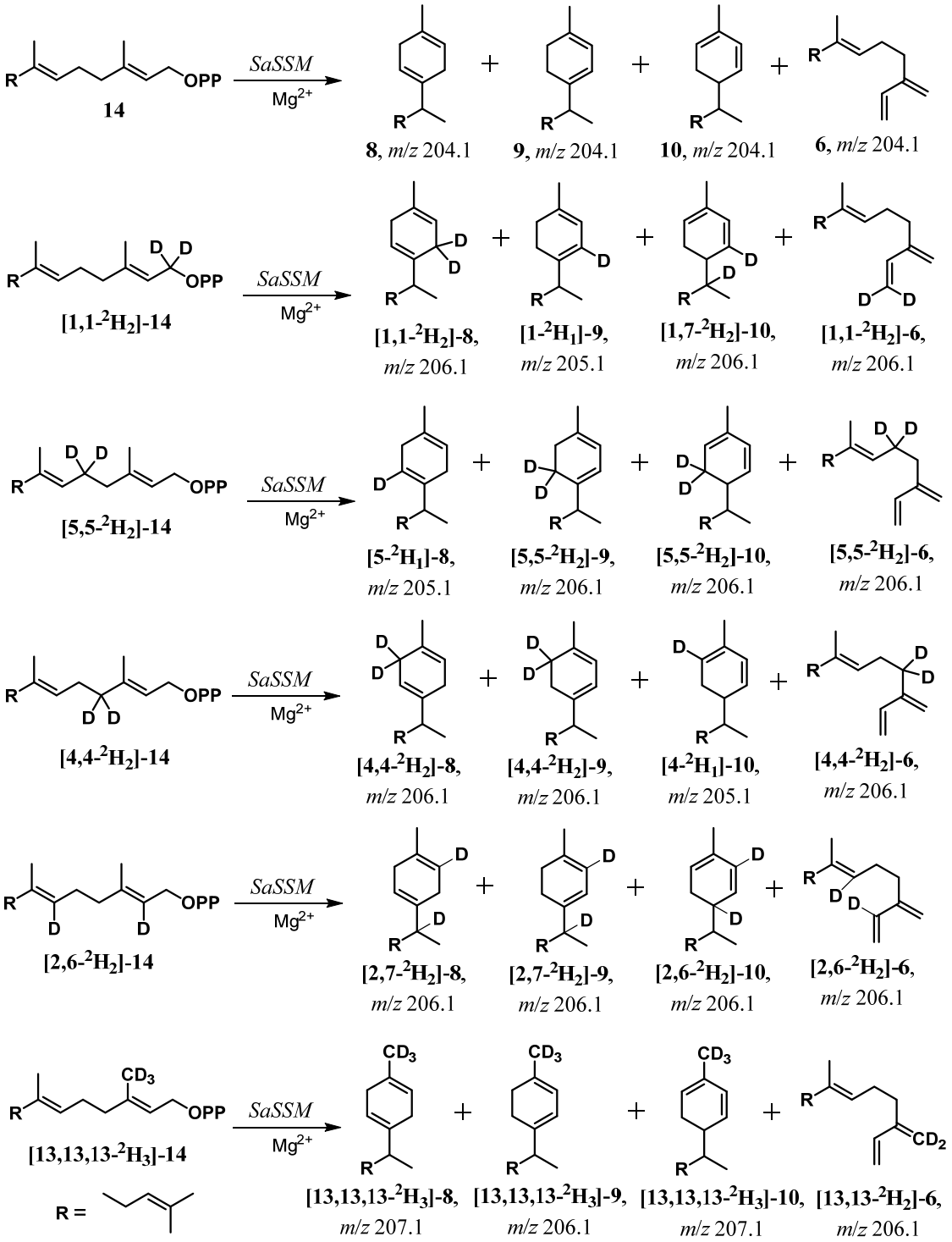

Scheme 3.3.5. Labeled analogues of β-curcumene (**8**), γ-curcumene (**9**), α-zingiberene (**10**), and (*E*)-β-farnesene (**6**) obtained from incubation of **14**, **[1,1-$^2H_2$]-14**, **[5,5-$^2H_2$]-14**, **[4,4-$^2H_2$]-14**, **[2,6-$^2H_2$]-14** and **[13,13,13-$^2H_3$]-14** with *SaSS*-mutants.

The hydride shift, C6→C7 was further corroborated by comparing the product ratio **[8/4]** in the incubations of **14** and **[2,6-^{2}H$_2$]-14** with mutant I422A-*SaSS*. On substituting the substrate **14** with **[2,6-^{2}H$_2$]-14**, the ratio **[8/4]** decreased from 5.03 to 2.31, whereas the product ratio **[8/4]** with substrate **[2-^{2}H$_1$]-14** changed to 4.54, a very minor and negligible change (Table 3.3.3). The large value of KIE, [(**8/4**)^H/(**8/4**)^D]= 2.18, indicated that biosynthesis of **4** (as explained in previous sections) does not involve any hydride migration from C6, but that of **8** and **9** showed C6→C7 hydride migration. These observations visualized the mechanisms in the biosynthesis of **8** and **9** as shown in scheme 3.3.1.

The monocyclic sesquiterpenes **8** and **9** were biosynthesized from the common intermediate **VII** followed by independent deprotonations from different carbon centres. This hypothesis was analyzed by considering the product ratio **[8/9]** and **[9/8]** in incubations of differentially labeled substrates with mutant I422A-*SaSS*. The product ratio [**8**/**9**]^H= 4.71 from incubation with **14** decreased to [**8**/**9**]^D= 2.47 for incubation with **[5,5-^{2}H$_2$]-14**. The 1.91 fold decrease in the ratio [**8**/**9**]^H/[**8**/**9**]^D corresponded for the intrinsic deuterium KIE arising due to cleavage of C-D bond at C5, while formation of **8** (Table 3.3.3).

Similarly, product ratio **[9/8]** was monitored in the carbocationic cascades (**p** and **q**) from incubation of various deuterium labeled substrates with mutant I422A-*SaSS*. The product ratio [**9**/**8**]^H= 0.21 from incubation of unlabeled **14**, decreased to [**9**/**8**]^D=0.08 observed for incubations of **[1,1-^{2}H$_2$]-14**, which indicated a large, [**9**/**8**]^H/[**9**/**8**]^D= 2.52 fold deuterium kinetic isotope effect which is in complete agreement with proton loss from C1 in the biosynthesis of **9** (Table 3.3.3). These product ratios established the divergence of pathways from the common intermediate **VII** leading to **8** and **9** and also informed about the extent of deprotonations from different carbon centres.

In biosynthesis of α-zingiberene (**10**), the *exo*-bisabolyl cation undergoes hydride shift from C1 to C7 along with the shift of π-electron density from C2-C3 to form C1-C2 π-bond generating a carbocation at C3. Ultimate deprotonation from C4 immediately follows in a fast step to form a new C3-C4 π-bond generating **10** (Scheme 3.3.1). Incubations of **[5,5-^{2}H$_2$]-14** with I422A-*SaSS* mutant generated **[5,5-^{2}H$_2$]-10** which contained two deuterium atoms, analyzed from a molecular ion peak at *m*/*z* 206.1, while, that with **[4,4-^{2}H$_2$]-14** resulted in **[4-^{2}H$_1$]-10** with that at *m*/*z* 205.1 containing only one deuterium, which supported the deprotonation from C4. A

prospective hydride shift from C4 to C7 and subsequent deprotonation from C5 to form C4-C5 π-bond with retention of C2-C3 π-bond was postulated by Kollner *et al*.[109] On elucidation of the fragmentation pattern of **10**, it was ascertained that the fragment appearing at *m*/*z* 93.0 corresponded to the cyclohexadienyl part structure which did not comprise of C7. Incubations with **[5,5-$^2H_2$]-14** detected the shift of ion from *m*/*z* 93.0 for **10** to *m*/*z* 95.0 for di-deuterated labelled product, indicating that the labels were not scrambled. Interestingly, in assays with **[1,1-$^2H_2$]-14**, the fragment shifted to *m*/*z* 94.0 that contained only one deuterium due to C1→C7 hydride shift (in this case deuteride shift) and ruled out C4→C7 hydride shift. Above results indicated the biosynthetic pathway of **10**.

The monocyclic sesquiterpenes with skeletons similar to those of **8**, **9** and **10** find applications not only as fragrance and pheromone components, but have also been identified as biosynthetic alternatives to D2 diesel[110] in energy sector.

3.3.2.6. Biosynthesis of acyclic sesquiterpene, (*E*)-β-Farnesene (6):

The *cisoid* conformers of nerolidyl cation (**I**) which were capable of undergoing cyclizations gave rise to structurally and strereochemically diverse sesquiterpene products. Conversely, the *transoid* conformers of **I**, which cannot undergo 1,6-cyclization due to remoteness of the reacting centers, suffer deprotonations yielding acyclic and 1,4-eliminated products such as farnesenes. The semiochemical (*E*)-β-farnesene, an acyclic sesquiterpene produced both by plants and animals[111,112] is obtained through the regiospecific 1,4-conjugated elimination of hydrogen diphosphate (HOPP, i.e., inorganic pyrophosphate and a proton) from diphosphate **14**.[113] Elimination of a proton from C13 to form a new π-bond at C3-C13 accompanied by shift of C2-C3 π-bond to terminal C1-C2 was monitored by incubating the labelled analogues of **14** with mutant L427A-*SaSS*. Enzymatic assay of **14** with a single point mutant L427A-*SaSS*, where leucine at 427 was replaced with alanine in *SaSS*, yielded three sesquiterpene products, which were identified as **1** (9.5%), **4** (57.3%), and **6** (33.2%). Incubation of **14** with the mutant L427A-*SaSS* delivered **6**, that displayed a molecular ion peak $[M]^+$ at *m*/*z* 204.1, while that with **[13,13,13-$^2H_3$]-14** resulted in **[13,13-$^2H_2$]-6** with the shift of molecular ion to *m*/*z* 206.2, indicating the presence of two deuterium atoms, but elimination of a deuterium from C13 when C3-C13 π-bond was formed. The presence of deuterium atoms in the labelled products was assigned from the GC-MS fragmentation pattern of the product. The mass ion fragments showed a shift from 204.1

$[M]^+$, 189.1, 161.1, 133.0, 93.0, 69.0 (100%) for **6** (Fig. A4.46) to 206.1 $[M]^+$, 191.2, 163.1, 134.0, 95.0, 69.0 (100%) for the labelled product **[13,13-$^2H_2$]-6** (Fig. A4.48).

The product ratio **[6/4]** decreased from 0.65 to 0.14 when **14** was replaced with **[13,13,13-$^2H_3$]-14** in the enzymatic assays with L427A-*SaSS* mutant. Mandatory dissociation of a deuteron from C13 resulted in the decreased rates for the formation of **[13,13-$^2H_2$]-6** which supported a large kinetic isotope effect, $[\mathbf{6}/\mathbf{4}]^H/[\mathbf{6}/\mathbf{4}]^D$= 4.58. While in incubations of **[13,13,13-$^2H_3$]-14** the flux was diverted towards the cyclic products, a small increase in the ratio, $[\mathbf{6}/\mathbf{4}]^H/[\mathbf{6}/\mathbf{4}]^D$= 1.09 fold did not favour the reverse reaction when **[4,4-$^2H_2$]-14** was the substrate. This indicated that the formation of cyclic cation **II** from the acyclic precursor cation **I** was not reversible. Within the experimental limits, the product ratio **6**/**4** obtained from incubation with other labeled substrates was found to be the same (Table 3.3.3). Above analyses supported the biosynthetic pathway for **4**, as shown in scheme 3.3.1.

3.3.3. Summary and Conclusion:

This work using the multiproduct enzyme *SaSS* from *S. album* and its site specific mutants demonstrates viable mechanistic pathways for the formation of a structurally diverse group of sesquiterpene hydrocarbons including tricyclic (**1**), bicyclic (**2**, **3**, **4**, **5**, **7**) monocyclic (**8**, **9**, **10**) and acyclic (**6**) skeletons. We validated our proposed biosynthetic pathway using specifically deuterium labeled analogues of the substrate, (*E*,*E*)-FPP (**14**), proceeding *via* initial ionization-isomerization to nerolidyl cation followed by a cascade of Wagner-Meerwein rearrangements of the emanating carbocations. Furthermore, our results emphasize the importance of proton transfer reactions in sesquiterpene biosynthesis and show how these reactions expand the versatility of terpene synthases capable of generating an array of product which play some of the vital roles in nature. Our analysis of the incubation experiments with (*E*,*E*)-FPP and its deuterium labeled analogues at C1, C2, C4, C5, C6, and C13 catalyzed by *SaSS* enzymes, followed by GC-MS analysis of the generated un/labeled products gave us information about the loci of labels, thereby providing insights in the hydride migration and proton losses involved in course of the reaction cascade. Similarly, GC analysis of the ratio of products and the resulting kinetic isotope effects from above experiments explained about the tight control of enzymes in the reaction steps. Mechanistic insights in the biosynthesis of α-Santalene (**1**), β-Santalene (**2**), *epi*-β-Santalene (**3**), *exo*-α-bergamotene (**4**), *exo*-β-bergamotene (**5**), (*E*)-β-farnesene (**6**), *endo*-α-bergamotene (**7**), β-curcumene (**8**), γ-curcumene (**9**), and α-zingiberene (**10**) from *SaSS* enzyme catalyzed reactions of the common linear substrate (*E*,*E*)-FPP (**14**) have been elaborated in scheme 3.3.6.

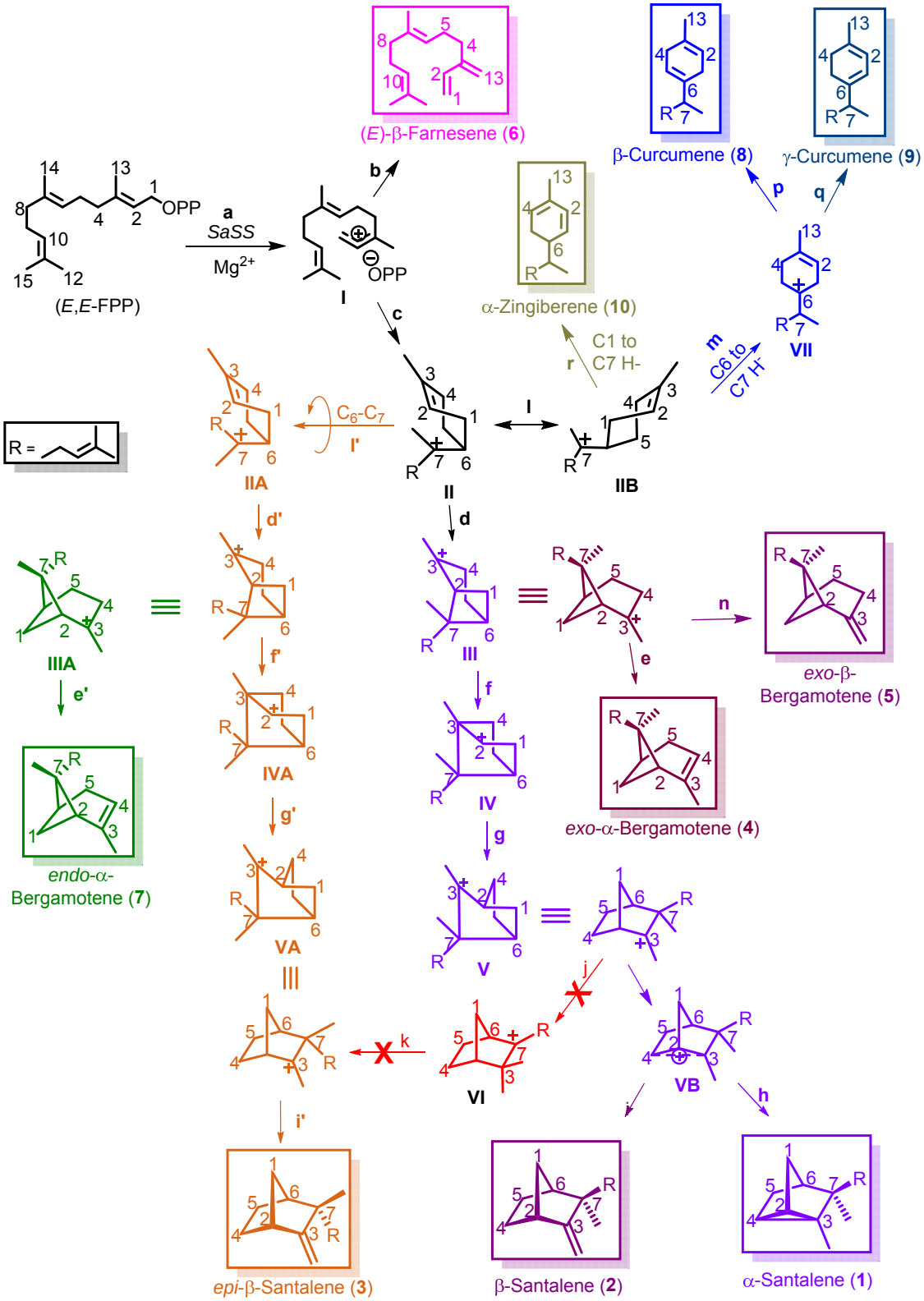

Scheme 3.3.6. Proposed mechanistic pathway for biosynthesis of sesquiterpenes (**1-10**) from (*E*,*E*)-FPP (**14**), catalyzed by *SaSS* enzymes.

3.3.4. Experimental:

3.3.4.1. Reagents and chemicals:

All the chemicals and deuterated reagents required for synthesis of substrates and buffer preparations were purchased from Sigma-Aldrich. Alkaline phosphatase was purchased from Sigma as its lyophilized stock. All the diphosphate salts were synthesized as mentioned in the procedure or as reported in the literature. HPLC grade solvents were used for extraction of the products from enzyme reaction mixtures.

3.3.4.2. Enzyme assays:

All the enzyme assays were performed in HEPES buffer constituting 25 mM HEPES, 5 mM DTT, 10 mM $MgCl_2$, 10% glycerol, pH 7.4. Alkaline phosphatase solution was prepared in 0.5 M glycine buffer, 5 mM $ZnCl_2$, pH 10.5. For the enzymatic reaction, 200 μM substrates were incubated with 20 μg purified and desalted proteins in HEPES buffer to a final volume of 0.5 mL and were incubated at 30 °C. GPP and IPP were incubated with *SaFDS* for 1 h which allowed the biosynthesis of (*E*,*E*-FPP). The cyclization reaction was initiated by addition of *SaSS* proteins to the same reaction mixture and incubation was continued for next 2 h. Positive control experiments were also carried out wherein, unlabeled substrates were incubated under similar conditions to those of labelled substrates. After reaction, the hydrocarbon products from *SaSS* assay were extracted with *n*-hexane (HPLC grade, Spectrochem) (3 × 1 mL). *SaSS* enzymes were not added to the 'substrate control' experiments and the isoprenoid diphosphates were hydrolysed to corresponding alcohols by addition of 80 μL of 0.5 M glycine buffer, pH 10.5, containing 5 mM $ZnCl_2$ and 80 units of alkaline phosphatase from bovine intestinal mucosa (Sigma), followed by incubation at 37 °C for 2h. Alcohols formed after alkaline phosphatase treatments were extracted with *tert*-butyl methyl ether (*t*-BME) (3 × 1 mL). The combined organic extracts (hexane as well as *t*-BME) were washed with equal volumes of DI water and dried by passing through a 1 × 5 cm column of anhydrous Na_2SO_4. The organic phase was concentrated to ~50 μL with a stream of dry N_2. 1 μL of the concentrated extract was injected in GC and GC-MS. All the sets were performed in duplicates and the percentage area values are mean of the two readings along with the deviations about mean.

3.3.4.3. GC and GC-MS analyses:

The product extracts were analysed by GC on an Agilent 7890 instrument equipped with a hydrogen flame ionization detector and HP-5 capillary column (30 m × 0.32 mm × 0.25 μm, J & W Scientific). Nitrogen was used as carrier gas at a flow rate of 1 mL/min. Column temperature was initialized from 70 °C, followed by a temperature gradient from 70 °C to 170 °C at 5 °C min^{-1} and finally to a temperature of 180 °C with a 15 °C min^{-1} rise and maintained for 5 min at 180 °C. The injector and detector temperatures were maintained at 220 °C and operated in splitless mode. Percentages of the products formed were calculated from the area under the peak corresponding to their FID responses. Determination of *m*/*z* values and the fragmentation analysis of all the products were performed on Agilent 5975C mass selective detector interfaced with Agilent 7890A gas chromatograph. GC-MS analyses were performed under similar conditions, but using a HP-5-MS capillary column (30 m × 0.32 mm × 0.25 μm, J & W Scientific) and helium as the carrier gas. The products formed were identified by analyzing their mass fragmentation pattern and comparison with NIST and Wiley mass spectral libraries. These were also confirmed by co-injecting with the standards synthesized chemically or purified from the large scale fermentations of (*E*,*E*)-FPP with the purified protein or from sources like natural oils. Santalenes and *exo*-α-bergamotene were purified from the terpene fraction of sandalwood oil. All the extractions were performed with HPLC grade *n*-hexane. All the purifications were performed on 5% $AgNO_3$ coated silica gel with *n*-hexane. The purified sesquiterpenes were analyzed and confirmed from the spectral data which have been reported in our previous report.

3.3.4.4. Spectral studies:

Infrared (IR) spectra were recorded on a Shimadzu FTIR 8400 spectrophotometer. Mass spectra (MS) were recorded on an MSI 65 auto-concept UK with ionization energy 70eV and on Waters make QTOF (Synapt-HDMS).Samples for nuclear magnetic resonance (NMR) analysis were prepared in appropriate solvents like D_2O for diphosphate salts and $CDCl_3$ for rest of the products. ^{1}H, ^{13}C and ^{31}P NMR spectra were recorded at room temperature on Bruker DRX-500 (500MHz), Bruker AV-400 (400MHz), Bruker AC-200 (200MHz) spectrometers. Chemical shifts are reported in parts per million, with respect to tetramethylsilane as the internal standard.

Appendix 4

Appendix IV Index

Table A4.1. GC distribution of sesquiterpene products from incubation of un/labelled (*E*,*E*)-FPP analogues with *SaSS*[a].

Substrate/ products	α-Santalene (**1**) (%)	β-Santalene (**2**) (%)	*epi*-β-Santalene (**3**) (%)	*exo*-α-Bergamotene (**4**) (%)	*exo*-β-Bergamotene (**5**) (%)	(*E*)-β-Farnesene (**6**) (%)
(*E*,*E*)-FPP	40.46 ± 0.11	25.97 ± 0.34	3.73 ± 0.14	26.12 ± 0.25	2.60 ± 0.14	1.13 ± 0.03
[4,4-$^2H_2$]-(*E*,*E*)-FPP	32.17 ± 0.18	42.45 ± 0.21	3.96 ± 0.13	17.85 ± 0.11	2.87 ± 0.05	0.72 ± 0.06
[13,13,13-$^2H_3$]-(*E*,*E*)-FPP	48.71 ± 0.15	10.91 ± 0.06	3.76 ± 0.10	35.15 ± 0.06	1.16 ± 0.06	0.38 ± 0.04
[4,4,13,13,13-$^2H_5$]-(*E*,*E*)-FPP	40.05 ± 0.48	17.03 ± 0.19	3.67 ± 0.06	37.45 ± 0.27	1.26 ± 0.04	0.16 ± 0.02
[5,5-$^2H_2$]-(*E*,*E*)-FPP	41.08 ± 0.19	25.92 ± 0.23	3.30 ± 0.01	25.93 ± 0.10	2.79 ± 0.02	0.99 ± 0.04
[1,1-$^2H_2$]-(*E*,*E*)-FPP	40.73 ± 0.28	27.00 ± 0.42	3.81 ± 0.02	24.80 ± 0.65	2.51 ± 0.05	1.18 ± 0.02
[2-$^2H_1$]-(*E*,*E*)-FPP	42.31 ± 0.05	26.06 ± 0.01	3.17 ± 0.18	25.04 ± 0.25	2.55 ± 0.12	0.88 ± 0.01
[2,6-$^2H_2$]-(*E*,*E*)-FPP	41.28 ± 0.10	24.78 ± 0.13	2.89 ± 0.01	27.46 ± 0.10	2.73 ± 0.04	0.86 ± 0.01

[a]all the assays were performed in duplicates.

Table A4.2. GC distribution of sesquiterpene products from incubation of un/labelled (*E*,*E*)-FPP analogues with Y539W-*SaSS* mutant.[a]

Substrate/ products	α-Santalene (**1**) (%)	*epi*-β-Santalene (**3**) (%)	*exo*-α-Bergamotene (**4**) (%)	*exo*-β-Bergamotene (**5**) (%)	(*E*)-β-Farnesene (**6**) (%)	*endo*-α-Bergamotene (**7**) (%)
(*E*,*E*)-FPP	9.66 ± 0.07	1.18 ± 0.01	31.27 ± 0.07	25.19 ± 0.05	9.90 ± 0.09	22.81 ± 0.04
[4,4-$^{2}H_2$]-(*E*,*E*)-FPP	19.97 ± 0.01	1.08 ± 0.03	21.05 ± 0.17	34.85 ± 0.07	10.20 ± 0.11	12.87 ± 0.02
[13,13,13-$^{2}H_3$]-(*E*,*E*)-FPP	12.73 ± 0.01	1.23 ± 0.06	45.37 ± 0.05	13.54 ± 0.04	2.76 ± 0.06	24.38 ± 0.05
[4,4,13,13,13-$^{2}H_5$]-(*E*,*E*)-FPP	25.22 ± 0.14	1.42 ± 0.07	32.42 ± 0.10	23.51 ± 0.02	3.82 ± 0.12	13.63 ± 0.01
[5,5-$^{2}H_2$]-(*E*,*E*)-FPP	9.99 ± 0.39	1.16 ± 0.12	29.64 ± 0.01	26.31 ± 0.64	9.92 ± 0.09	23.00 ± 0.05
[1,1-$^{2}H_2$]-(*E*,*E*)-FPP	8.63 ± 0.09	0.75 ± 0.00	35.75 ± 0.33	25.37 ± 0.06	5.99 ± 0.59	23.52 ± 0.23
[2-$^{2}H_1$]-(*E*,*E*)-FPP	8.76 ± 0.11	1.38 ± 0.00	31.57 ± 0.22	23.76 ± 0.01	10.70 ± 0.01	23.80 ± 0.15
[2,6-$^{2}H_2$]-(*E*,*E*)-FPP	7.43 ± 0.27	0.96 ± 0.07	28.94 ± 0.20	26.68 ± 0.11	10.21 ± 0.09	25.78 ± 0.11

[a]all the assays were performed in duplicates

Table A4.3. GC distribution of sesquiterpene products from incubation of un/labelled (*E*,*E*)-FPP analogues with R474L-*SaSS* mutant.[a]

Substrate/ products	*exo*-α-Bergamotene (**4**) (%)	*exo*-β-Bergamotene (**5**) (%)
(*E*,*E*)-FPP	74.55 ± 0.19	25.46 ± 0.20
[4,4-$^2H_2$]-(*E*,*E*)-FPP	51.37 ± 0.09	48.64 ± 0.09
[13,13,13-$^2H_3$]-(*E*,*E*)-FPP	91.60 ± 0.05	8.40 ± 0.05
[4,4,13,13,13-$^2H_5$]-(*E*,*E*)-FPP	74.37 ± 0.26	25.63 ± 0.26
[5,5-$^2H_2$]-(*E*,*E*)-FPP	72.98 ± 0.07	27.03 ± 0.06
[1,1-$^2H_2$]-(*E*,*E*)-FPP	75.99 ± 0.11	24.02 ± 0.11
[2-$^2H_1$]-(*E*,*E*)-FPP	73.35 ± 0.31	26.66 ± 0.32
[2,6-$^2H_2$]-(*E*,*E*)-FPP	73.91 ± 0.08	26.10 ± 0.07

[a]all the assays were performed in duplicates

Table A4.4 GC distribution of sesquiterpene products from incubation of un/labelled (*E*,*E*)-FPP analogues with L427A-*SaSS* mutant.[a]

Substrate/ products	α-Santalene (**1**) (%)	*exo*-α-Bergamotene (**4**) (%)	(*E*)-β-Farnesene (**6**) (%)
(*E*,*E*)-FPP	8.69 ± 0.30	55.43 ± 0.18	35.89 ± 0.48
[4,4-$^2H_2$]-(*E*,*E*)-FPP	9.07 ± 0.18	53.16 ± 0.19	37.78 ± 0.37
[13,13,13-$^2H_3$]-(*E*,*E*)-FPP	13.60 ± 0.08	75.70 ± 0.55	10.71 ± 0.46
[4,4,13,13,13-$^2H_5$]-(*E*,*E*)-FPP	12.40 ± 0.09	73.73 ± 0.47	13.88 ± 0.55
[5,5-$^2H_2$]-(*E*,*E*)-FPP	7.89 ± 0.00	58.73 ± 0.01	33.78 ± 0.01
[1,1-$^2H_2$]-(*E*,*E*)-FPP	9.64 ± 0.12	54.29 ± 0.12	36.08 ± 0.23
[2-$^2H_1$]-(*E*,*E*)-FPP	6.87 ± 0.18	60.54 ± 0.29	32.60 ± 0.11
[2,6-$^2H_2$]-(*E*,*E*)-FPP	6.60 ± 0.09	60.81 ± 0.08	32.60 ± 0.16

[a]all the assays were performed in duplicates

Table A4.5 GC distribution of sesquiterpene products from incubation of un/labelled (*E*,*E*)-FPP analogues with I422A-*SaSS* mutant.[a]

Substrate/ products	α-Santalene (**1**) (%)	β-Santalene (**2**) (%)	*exo*-α-Bergamotene (**4**) (%)	(*E*)-β-Farnesene (**6**) (%)	*endo*-α-Bergamotene (**7**) (%)	β-Curcumene (**8**) %	γ-Curcumene (**9**) (%)	α-Zingiberene (**10**) (%)
(*E*,*E*)-FPP	1.45 ± 0.01	1.81 ± 0.07	12.84 ± 0.07	3.59 ± 0.02	1.69 ± 0.01	64.51 ± 0.20	12.80 ± 0.11	1.34 ± 0.05
[4,4-$^2H_2$]-(*E*,*E*)-FPP	1.42 ± 0.02	2.04 ± 0.01	11.95 ± 0.12	3.48 ± 0.07	1.68 ± 0.03	64.02 ± 0.07	13.98 ± 0.01	1.46 ± 0.04
[13,13,13-$^2H_3$]-(*E*,*E*)-FPP	2.09 ± 0.06	1.51 ± 0.02	11.80 ± 0.47	0.92 ± 0.10	1.84 ± 0.11	67.95 ± 0.74	12.64 ± 0.02	1.27 ± 0.01
[4,4,13,13,13-$^2H_5$]-(*E*,*E*)-FPP	1.73 ± 0.05	1.27 ± 0.05	13.59 ± 0.32	1.13 ± 0.01	2.05 ± 0.02	64.22 ± 0.01	14.35 ± 0.20	1.68 ± 0.03
[5,5-$^2H_2$]-(*E*,*E*)-FPP	1.45 ± 0.03	1.64 ± 0.09	13.65 ± 0.72	3.76 ± 0.06	2.17 ± 0.11	53.53 ± 0.52	21.67 ± 0.28	2.15 ± 0.02
[1,1-$^2H_2$]-(*E*,*E*)-FPP	1.81 ± 0.02	1.86 ± 0.04	15.53 ± 0.17	3.29 ± 0.03	2.42 ± 0.01	68.53 ± 0.02	5.76 ± 0.24	0.84 ± 0.02
[2-$^2H_1$]-(*E*,*E*)-FPP	0.97 ± 0.02	0.89 ± 0.03	13.61 ± 0.09	3.51 ± 0.07	2.20 ± 0.05	61.82 ± 0.04	13.92 ± 0.07	3.11 ± 0.06
[2,6-$^2H_2$]-(*E*,*E*)-FPP	2.15 ± 0.06	2.88 ± 0.07	23.17 ± 0.22	4.28 ± 0.11	3.32 ± 0.14	53.41 ± 0.80	8.79 ± 0.32	2.02 ± 0.14

[a]all the assays were performed in duplicates

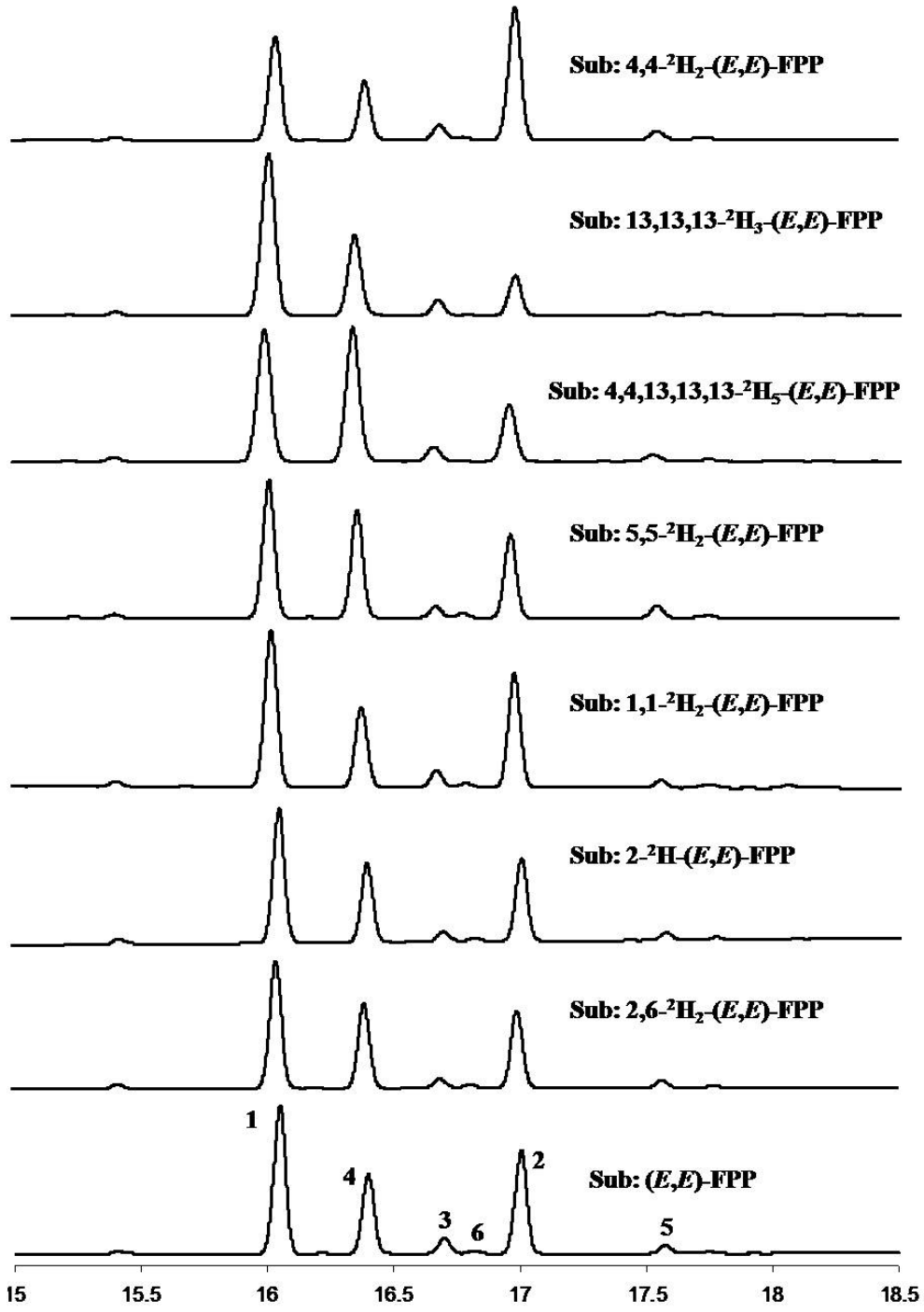

Figure A4.1. GC traces of products of *SaSS* with deuterium un/labeled (*E*,*E*)-FPP analogues; **1**: α-Santalene, **2**: β-Santalene, **3**: *epi*-β-Santalene, **4**: *exo*-α-Bergamotene, **5**: *exo*-β-Bergamotene **6**: (*E*)-β-Farnesene,.

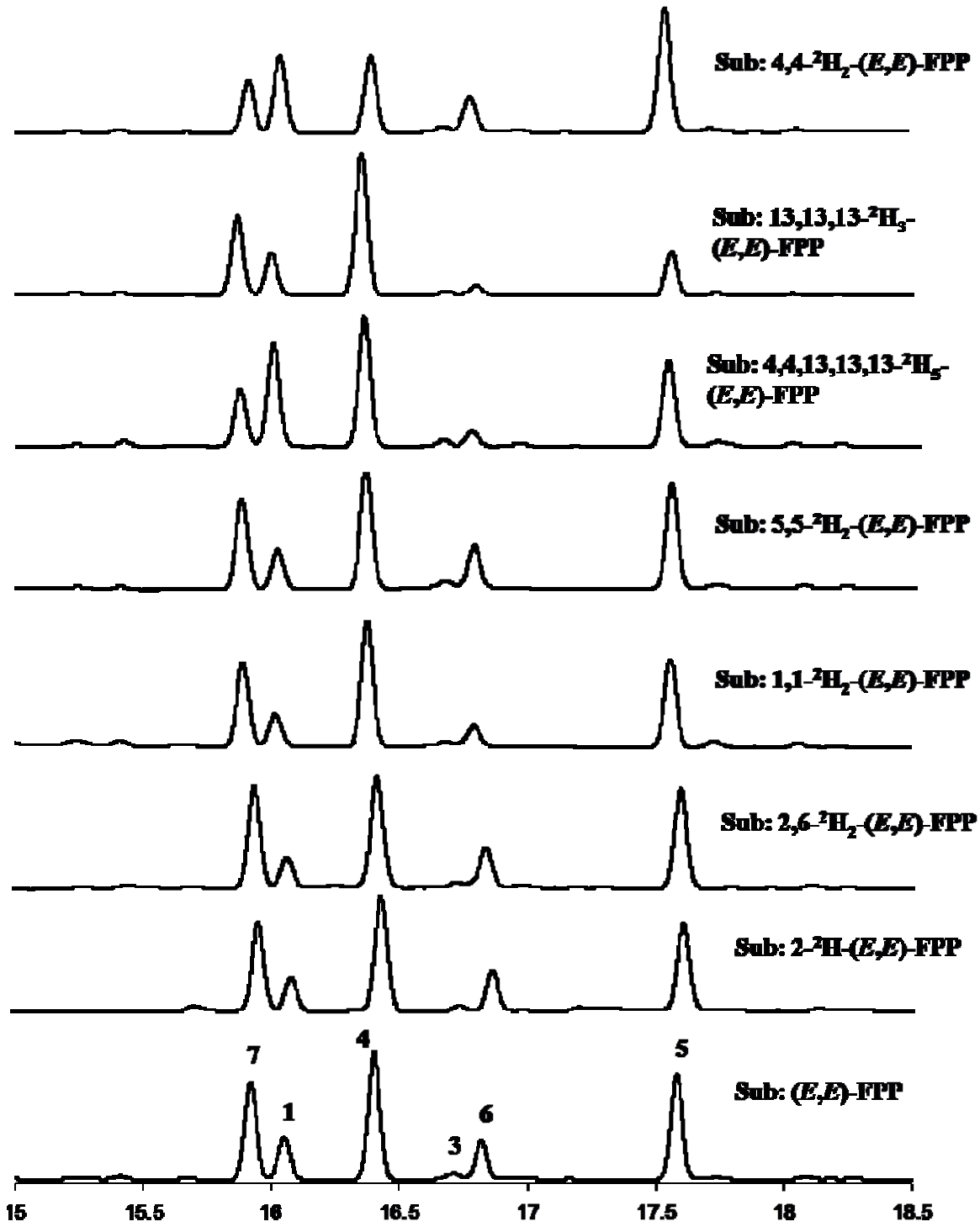

Figure A4.2. GC traces of products of Y539W-*SaSS* mutant with deuterium un/labeled (*E*,*E*)-FPP analogues; **1**: α-Santalene, **3**: *epi*-β-Santalene, **4**: *exo*-α-Bergamotene, **5**: *exo*-β-Bergamotene, **6**: (*E*)-β-Farnesene.

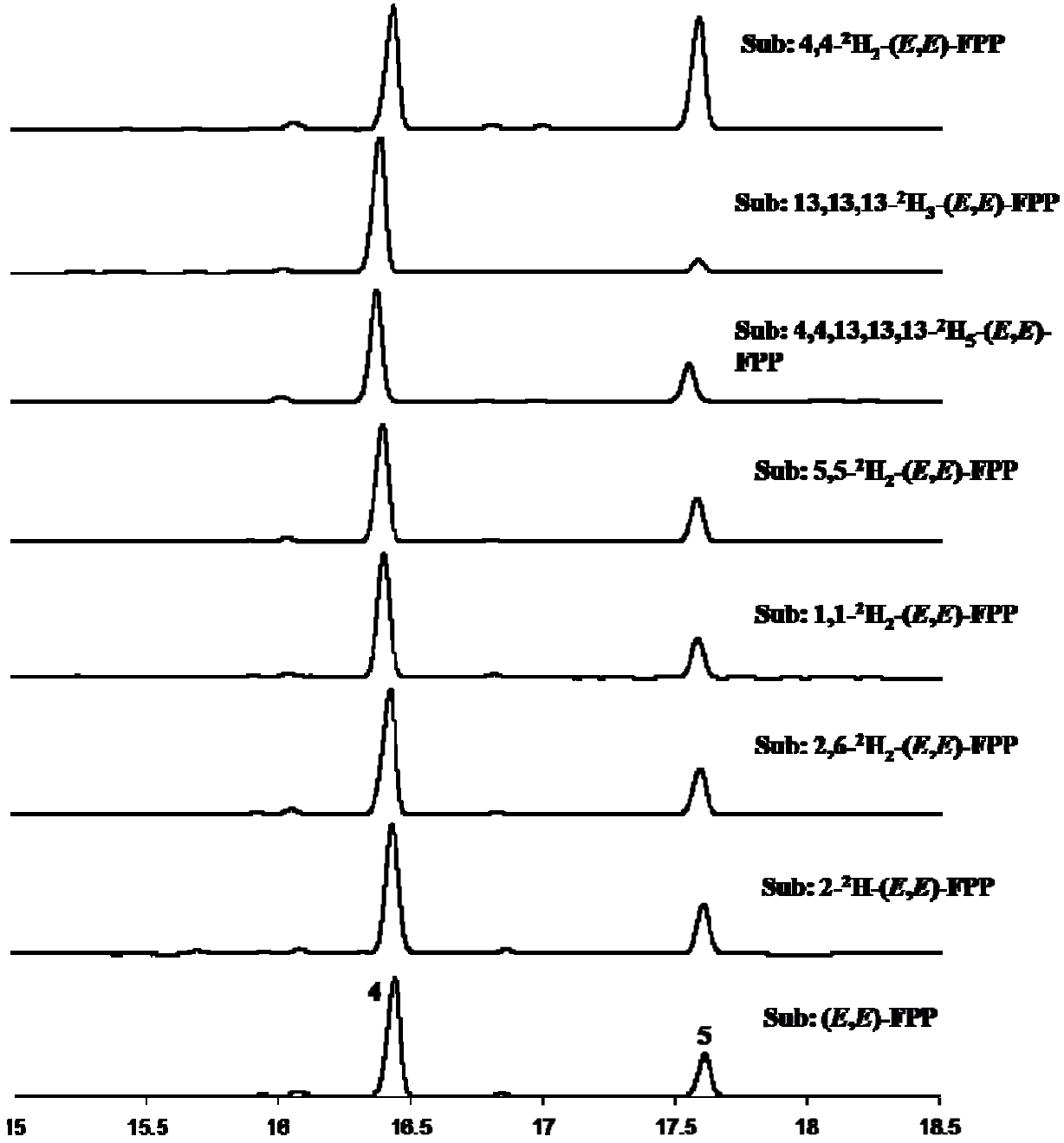

Figure A4.3: GC traces of products of R474L-*SaSS* mutant with deuterium un/labeled (*E*,*E*)-FPP analogues; **4**: *exo*-α-Bergamotene, **5**: *exo*-β-Bergamotene.

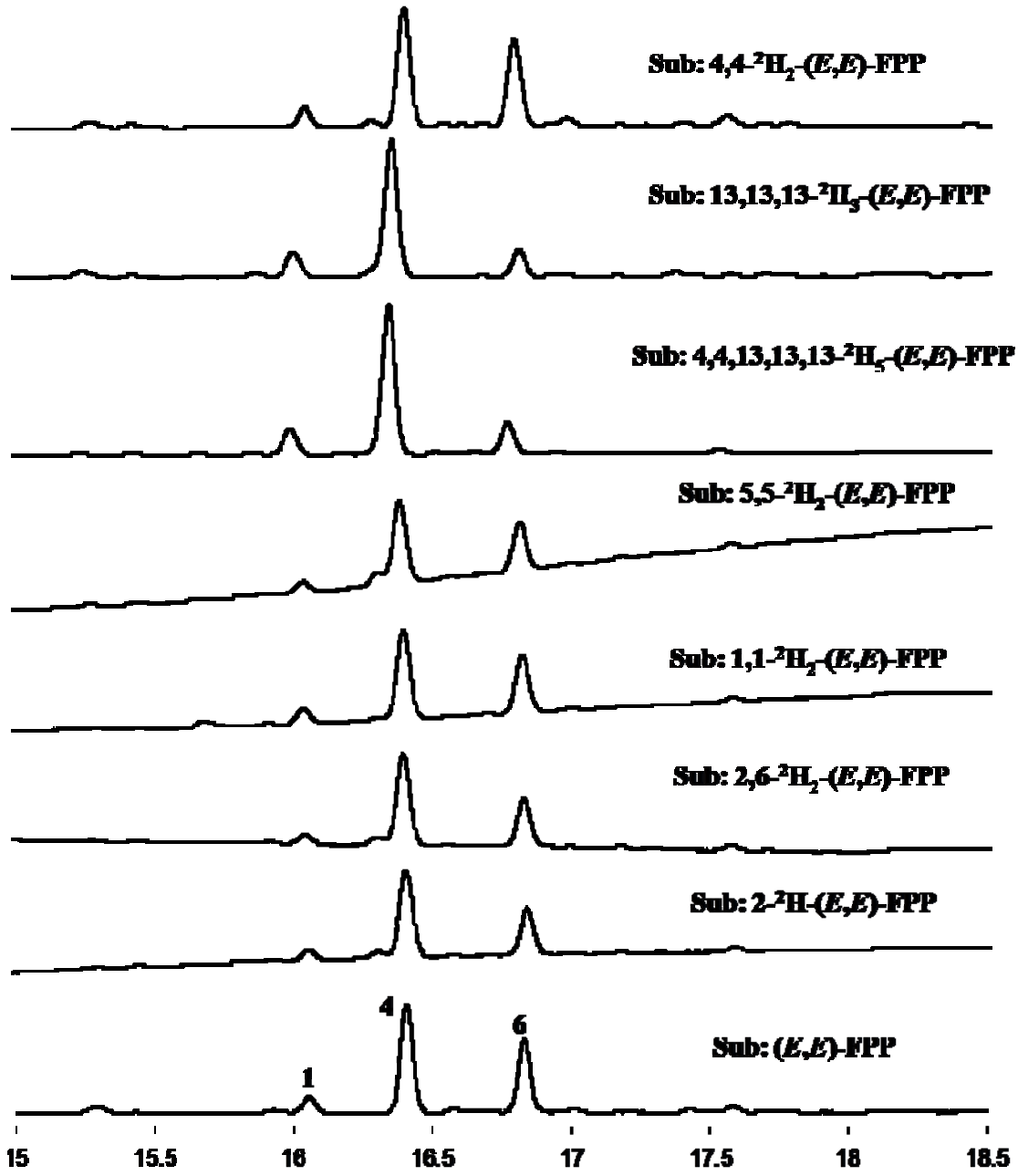

Figure A4.4: GC traces of products of L427A-*SaSS* mutant with deuterium un/labeled (*E*,*E*)-FPP analogues; **1**: α-Santalene, **4**: *exo*-α-Bergamotene, **6**: (*E*)-β-Farnesene.

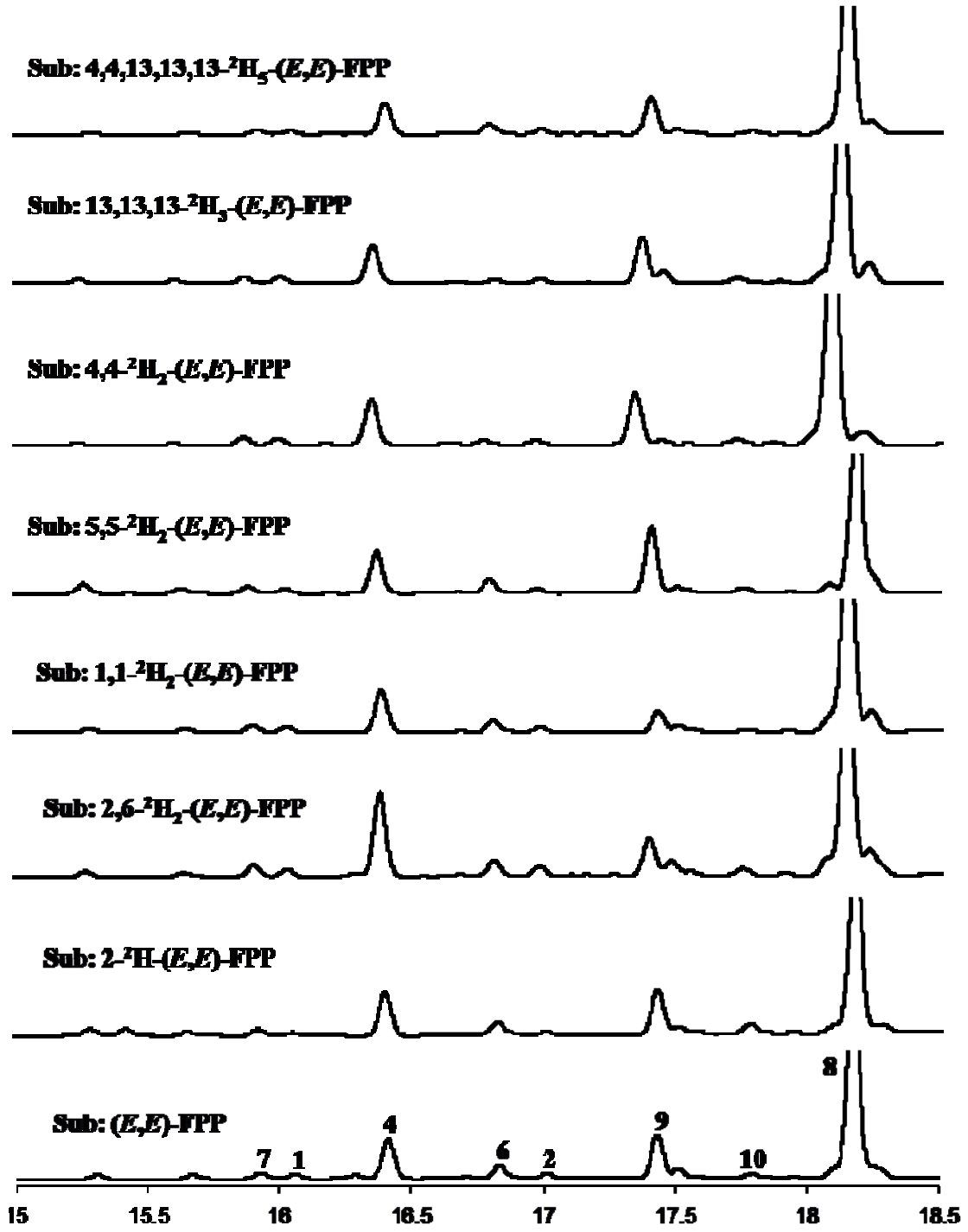

Figure A4.5: GC traces of products of I422A-*SaSS* mutant with deuterium un/labeled (*E*,*E*)-FPP analogues; **1**: α-Santalene, **2**: β-Santalene, **4**: *exo*-α-Bergamotene, **6**: (*E*)-β-Farnesene, **7**: *endo*-α-Bergamotene, **8**: β-Curcumene, **9**: γ-Curcumene, **10**: α-Zingiberene.

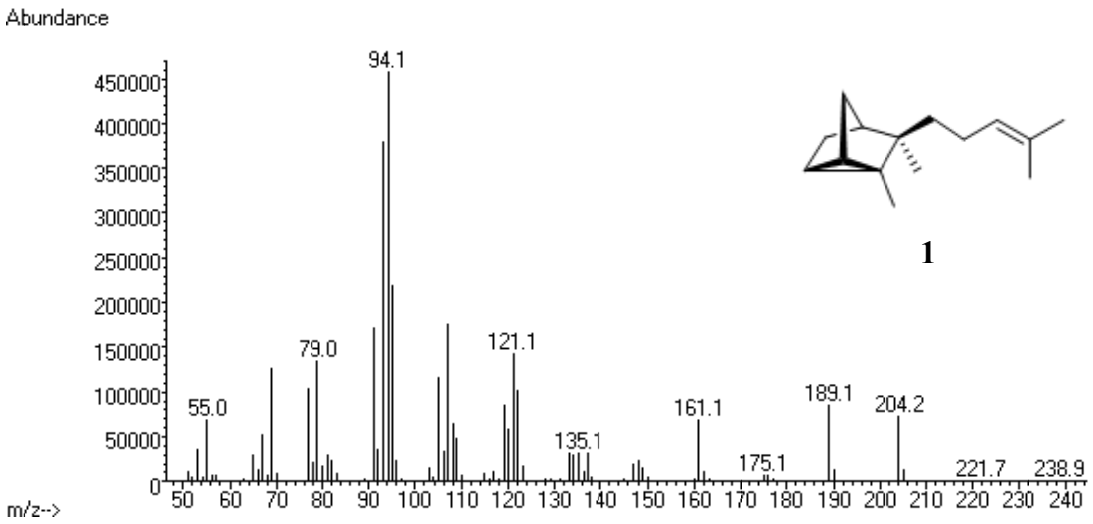

Figure A4.6. EI-MS spectrum of α-santalene (**1**).

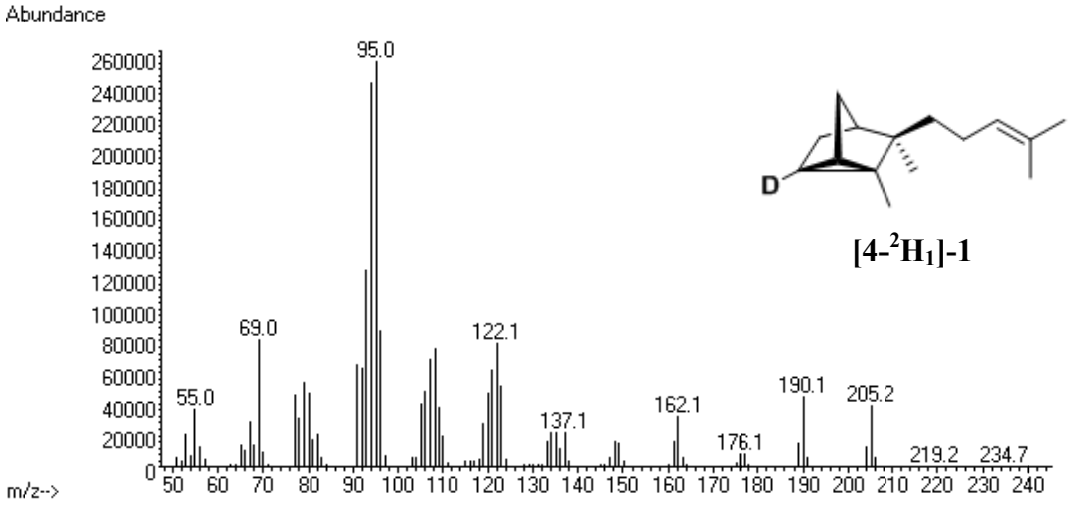

Figure A4.7. EI-MS spectrum of [4-$^2H_1$]-α-santalene (**[4-$^2H_1$]-1**).

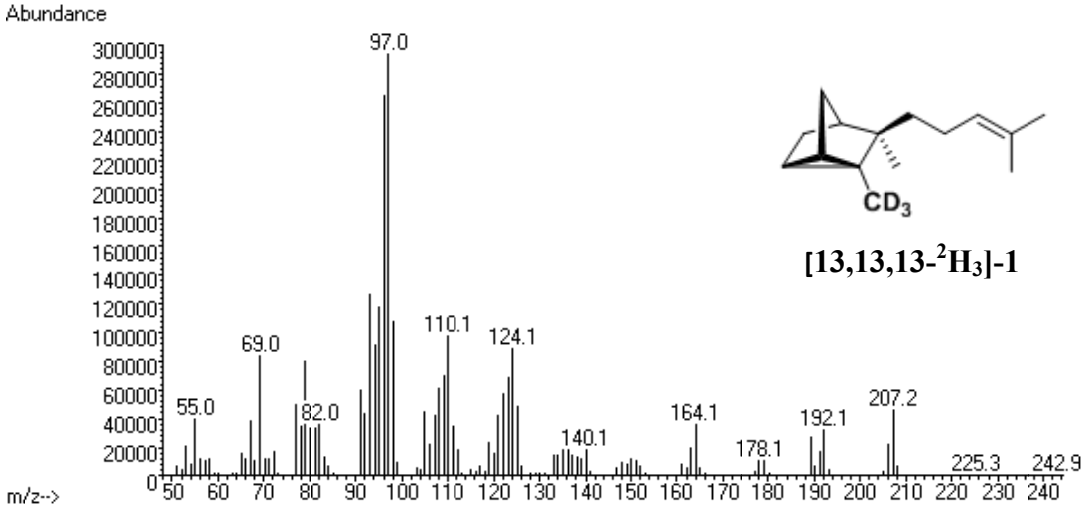

Figure A4.8. EI-MS spectrum of [13,13,13-$^2H_3$]-α-santalene (**[13,13,13-$^2H_3$]-1**).

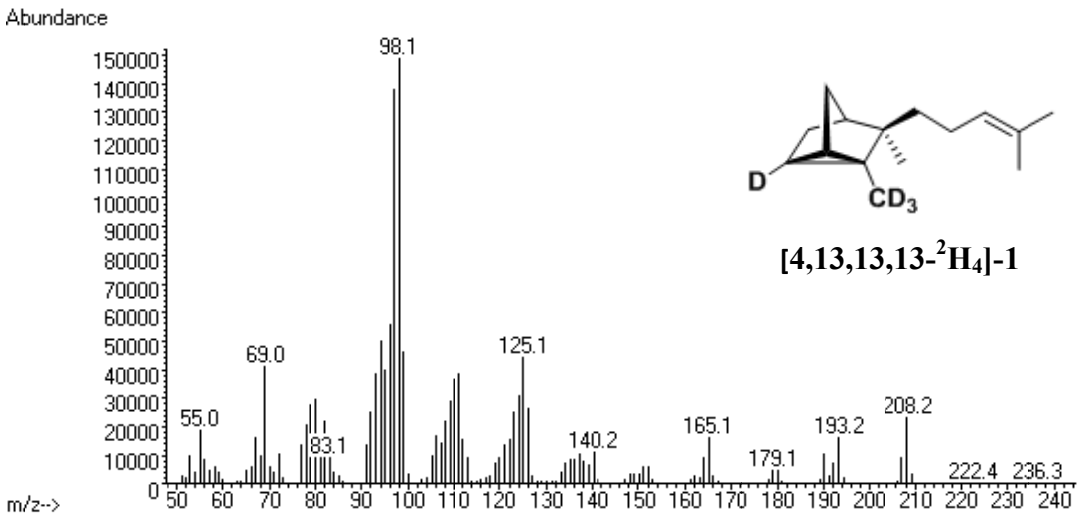

Figure A4.9. EI-MS spectrum of [4,13,13,13-$^2H_4$]-α-santalene (**[4,13,13,13-$^2H_4$]-1**).

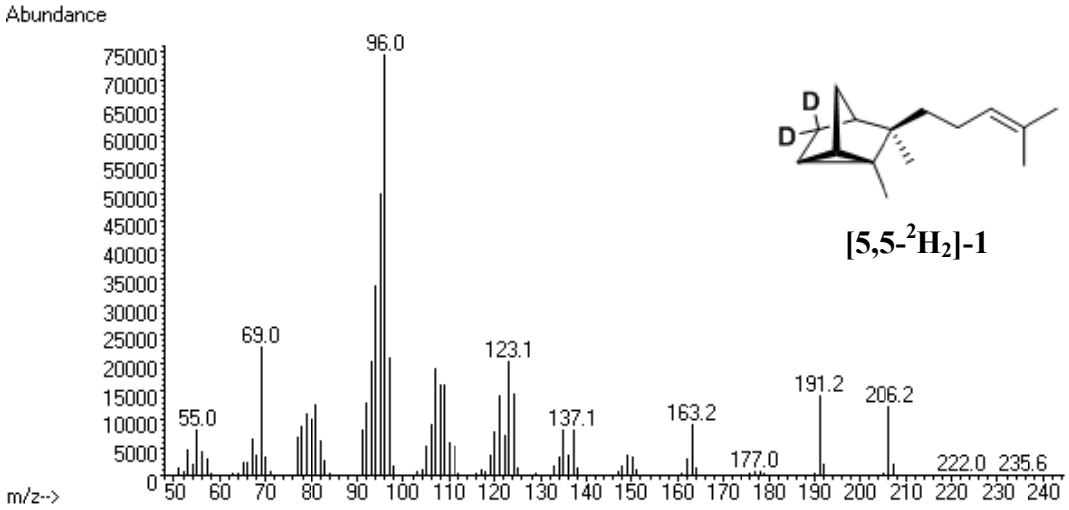

Figure A4.10. EI-MS spectrum of [5,5-$^2H_2$]-α-santalene (**[5,5-$^2H_2$]-1**).

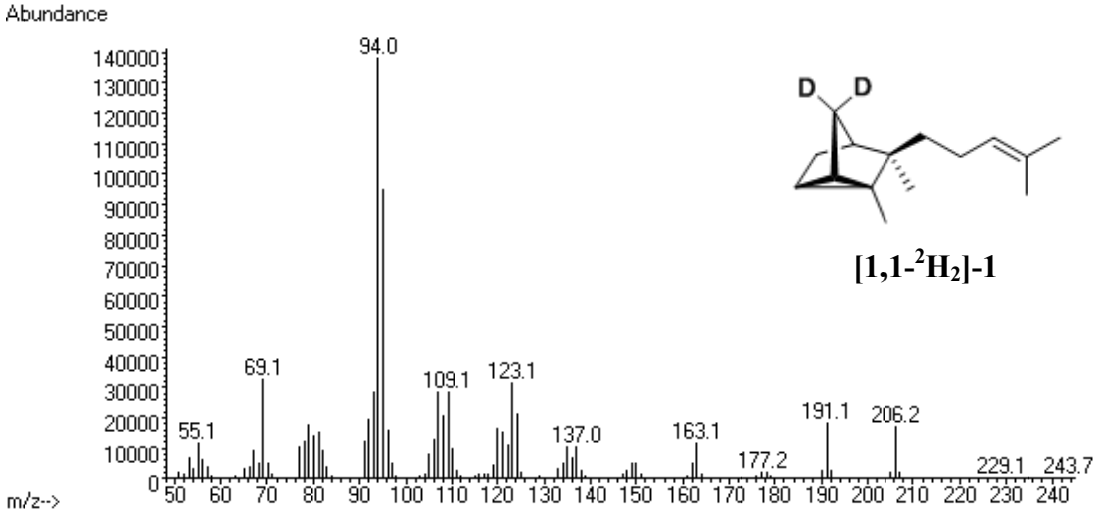

Figure A4.11. EI-MS spectrum of [1,1-$^2H_2$]-α-santalene (**[1,1-$^2H_2$]-1**).

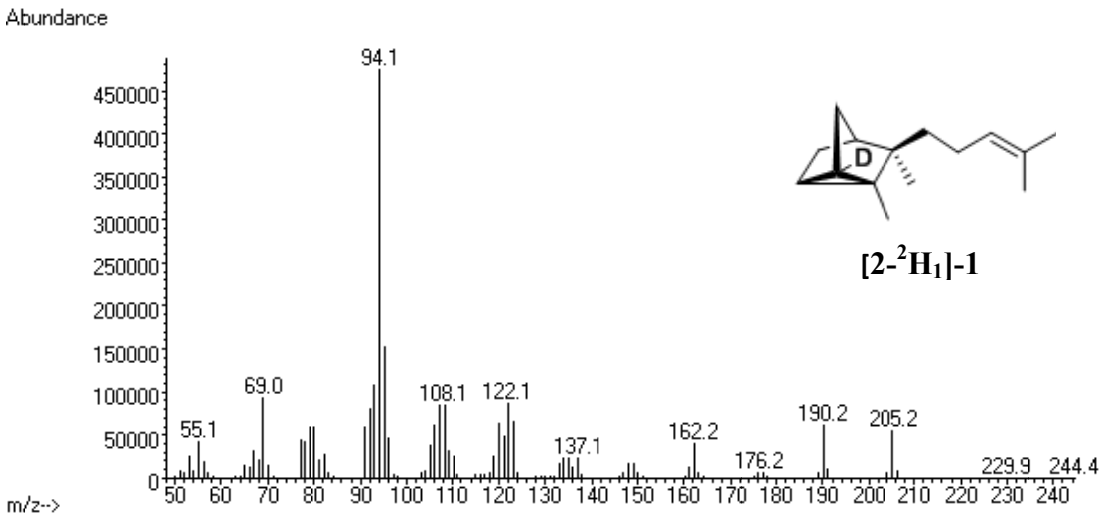

Figure A4.12. EI-MS spectrum of [2-^{2}H$_1$]-α-santalene (**[2-^{2}H$_1$]-1**).

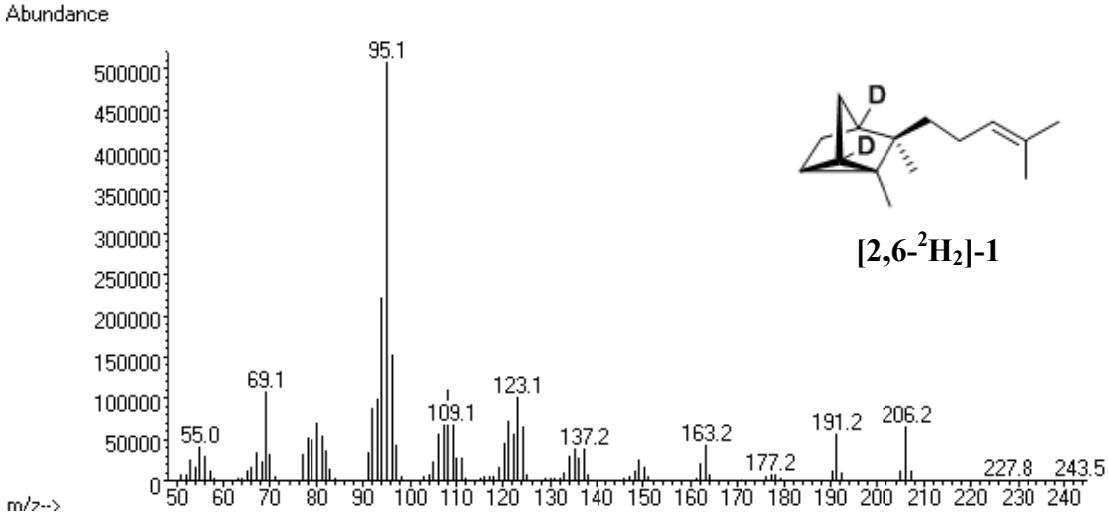

Figure A4.13. EI-MS spectrum of [2,6-^{2}H$_2$]-α-santalene (**[2,6-^{2}H$_2$]-1**).

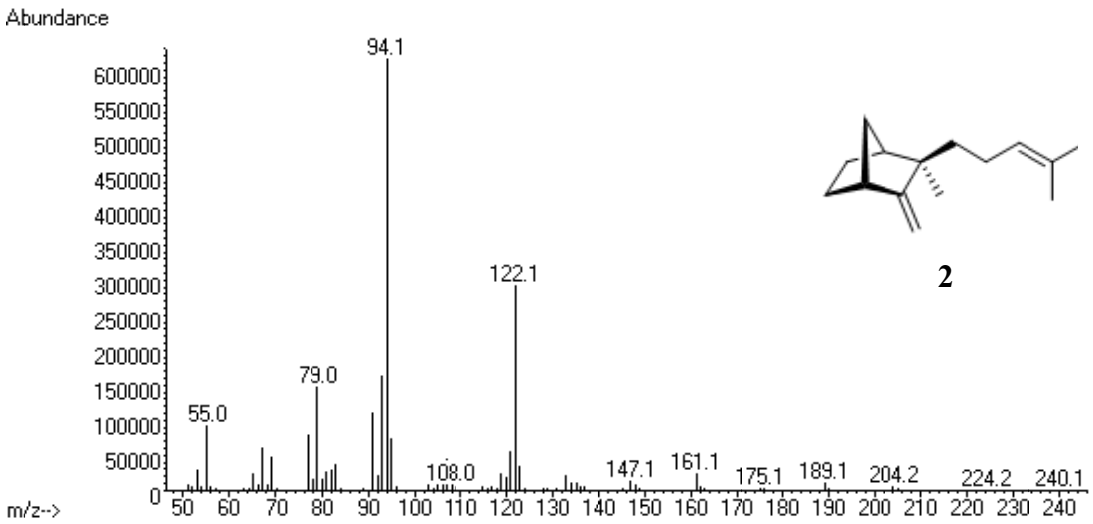

2

Figure A4.14. EI-MS spectrum of β-santalene (**2**).

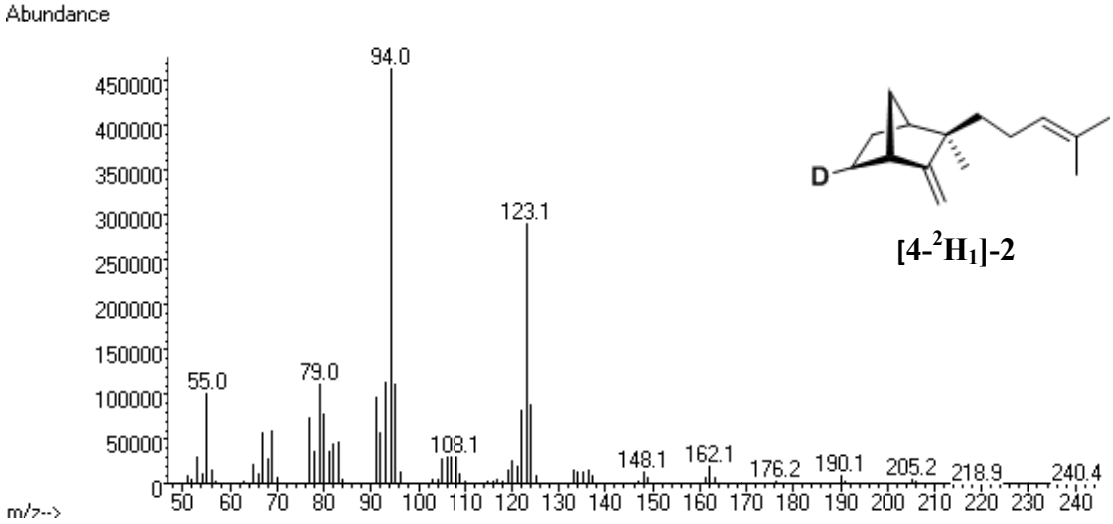

[4-^{2}H$_1$]-2

Figure A4.15. EI-MS spectrum of [4-^{2}H$_1$]-β-santalene (**[4-^{2}H$_1$]-2**).

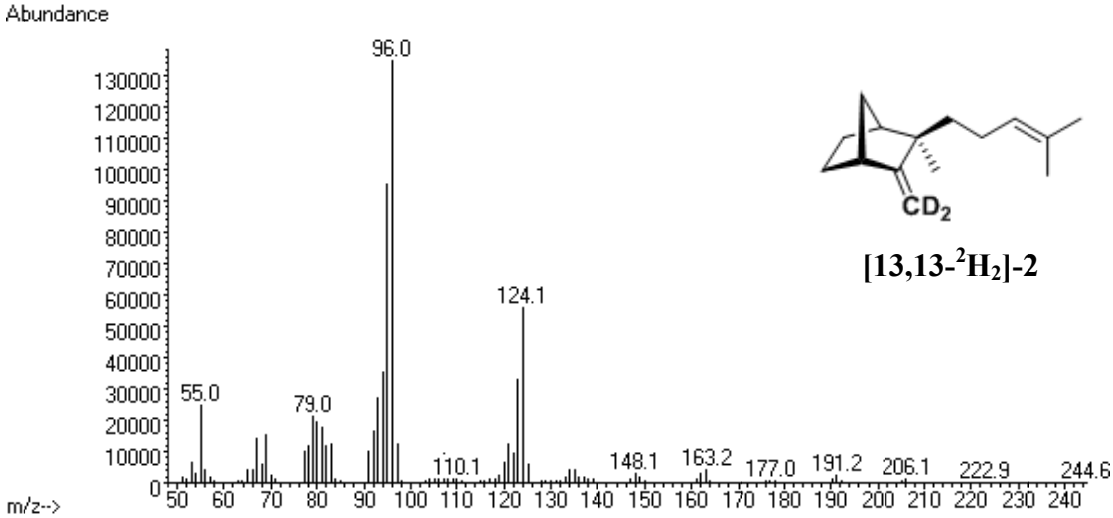

[13,13-^{2}H$_2$]-2

Figure A4.16. EI-MS spectrum of [13,13-^{2}H$_2$]-β-santalene (**[13,13-^{2}H$_2$]-2**).

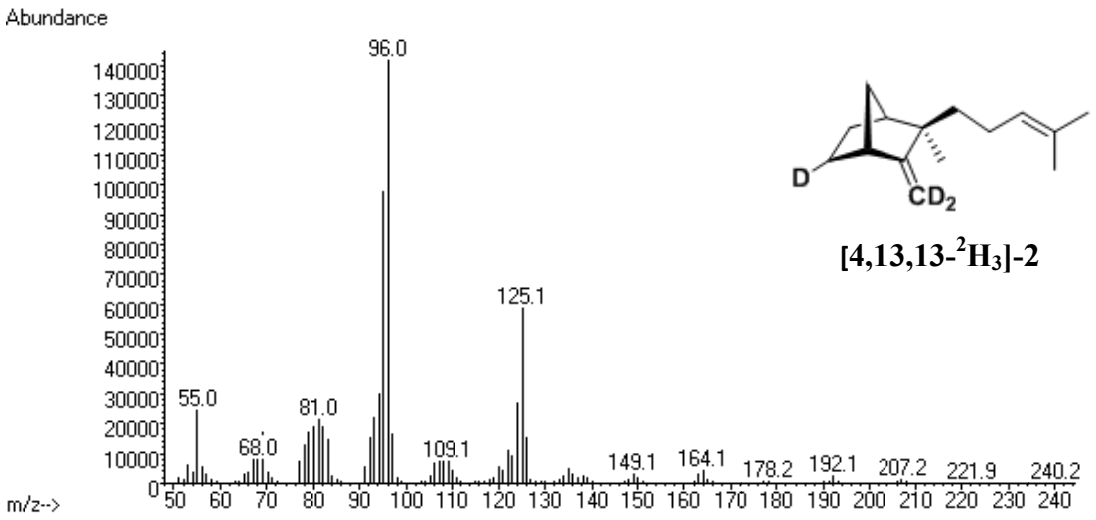

[4,13,13-$^2H_3$]-2

Figure A4.17. EI-MS spectrum of [4,13,13-$^2H_3$]-β-santalene (**[4,13,13-$^2H_3$]-2**).

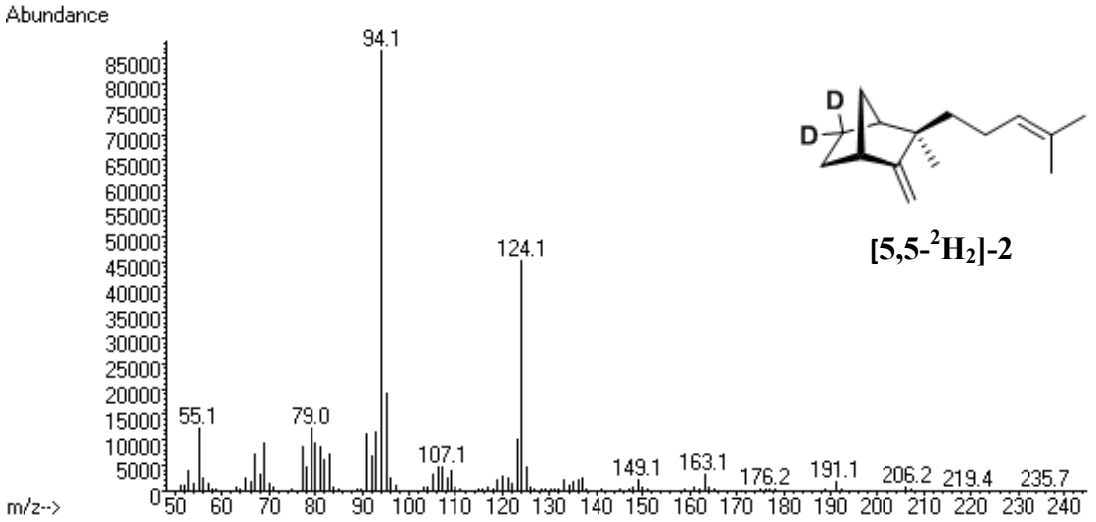

[5,5-$^2H_2$]-2

Figure A4.18. EI-MS spectrum of [5,5-$^2H_2$]-β-santalene (**[5,5-$^2H_2$]-2**).

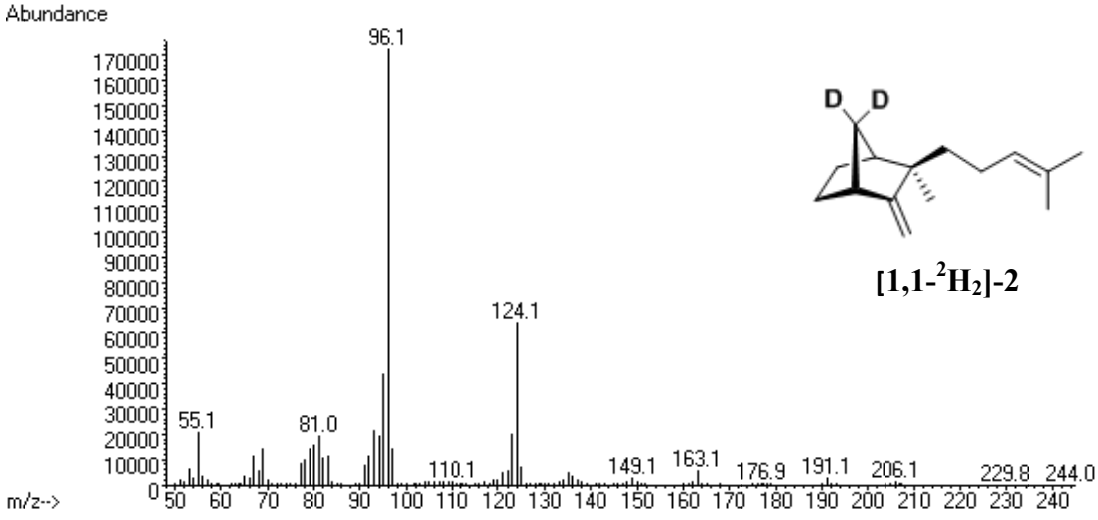

[1,1-$^2H_2$]-2

Figure A4.19. EI-MS spectrum of [1,1-$^2H_2$]-β-santalene (**[1,1-$^2H_2$]-2**).

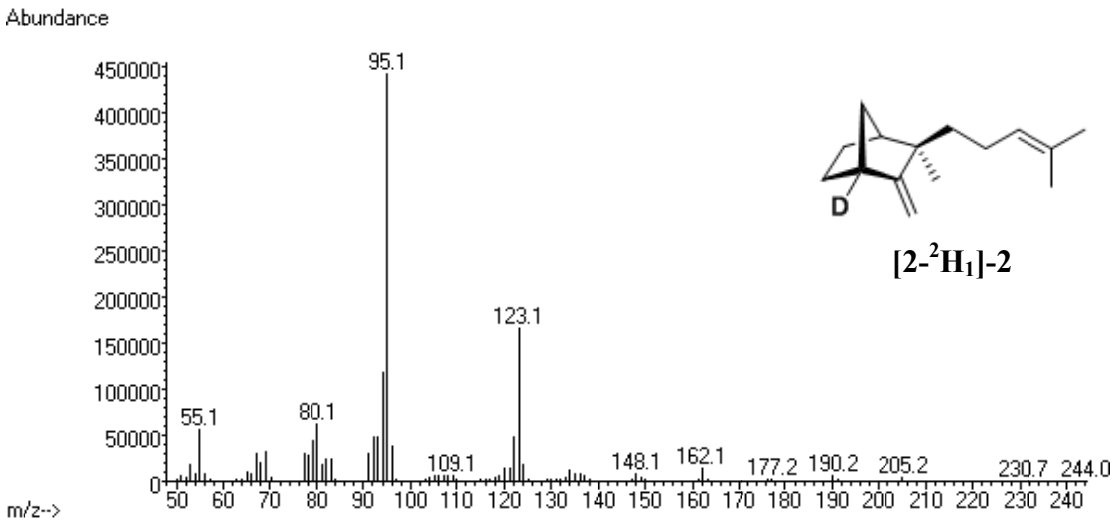

[2-^{2}H$_1$]-2

Figure A4.20. EI-MS spectrum of [2-^{2}H$_1$]-β-santalene (**[2-^{2}H$_1$]-2**).

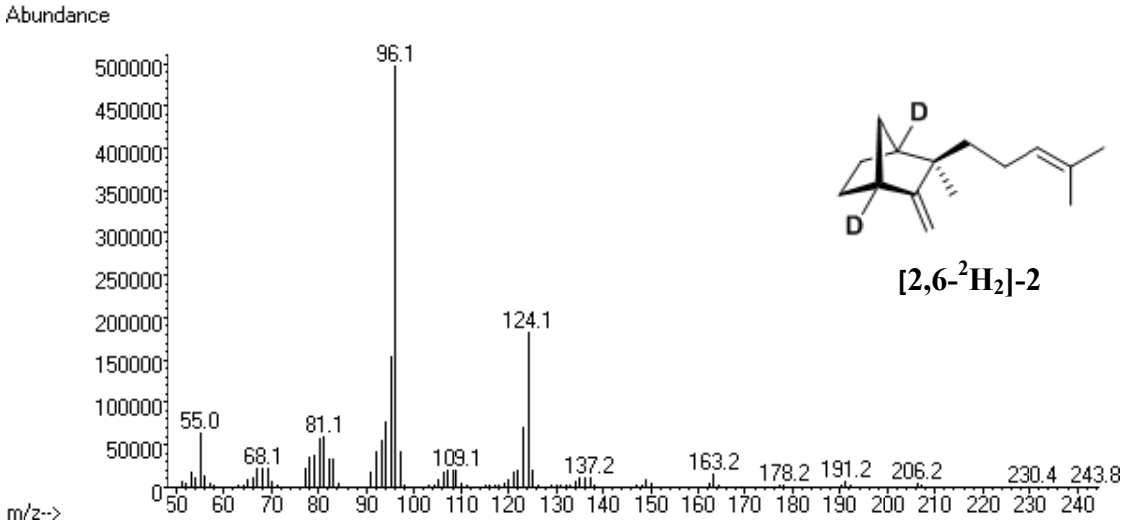

[2,6-^{2}H$_2$]-2

Figure A4.21. EI-MS spectrum of [2,6-^{2}H$_2$]-β-santalene (**[2,6-^{2}H$_2$]-2**).

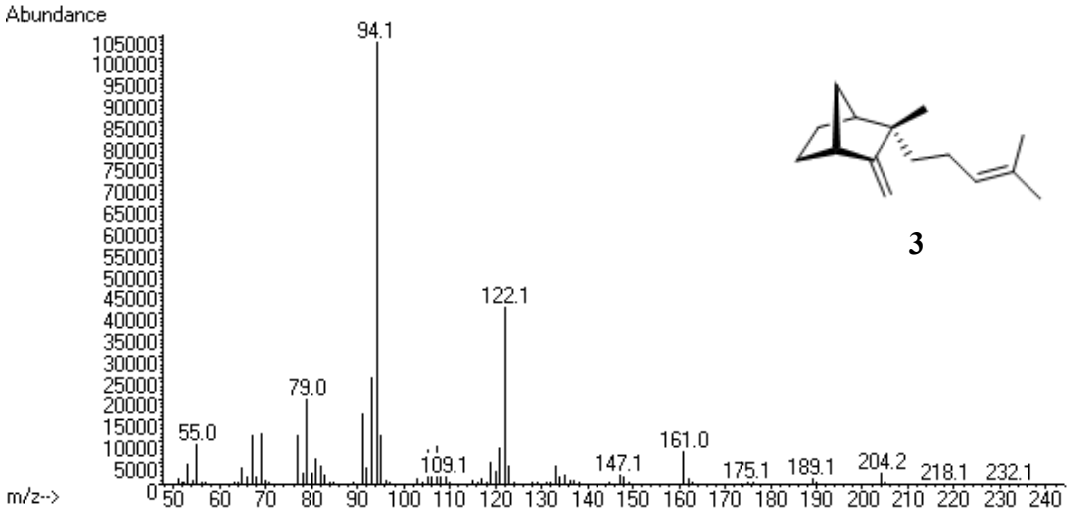

3

Figure A4.22. EI-MS spectrum of *epi*-β-santalene (**3**).

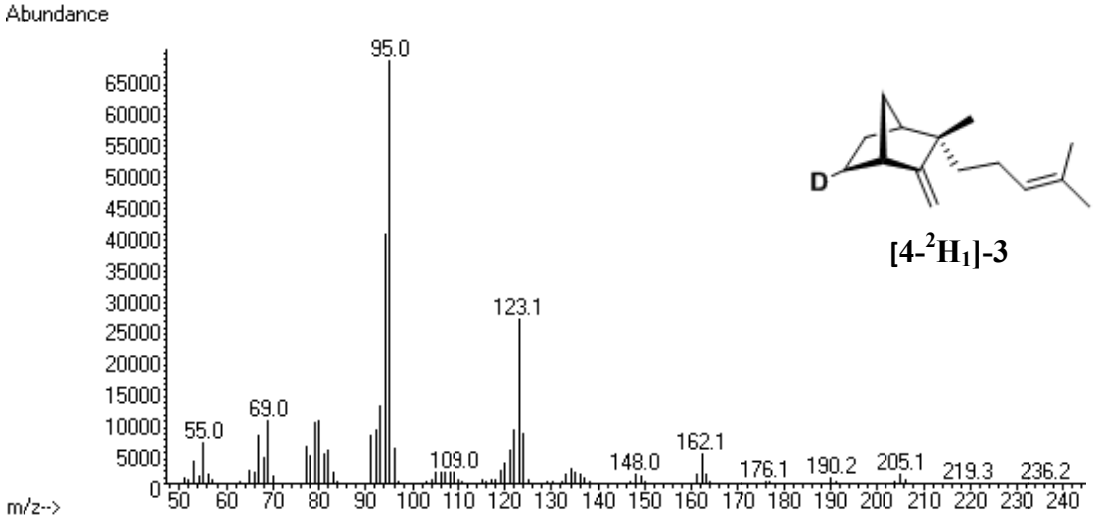

[4-^{2}H$_1$]-3

Figure A4.23. EI-MS spectrum of [4-^{2}H$_1$]-*epi*-β-santalene (**[4-^{2}H$_1$]-3**).

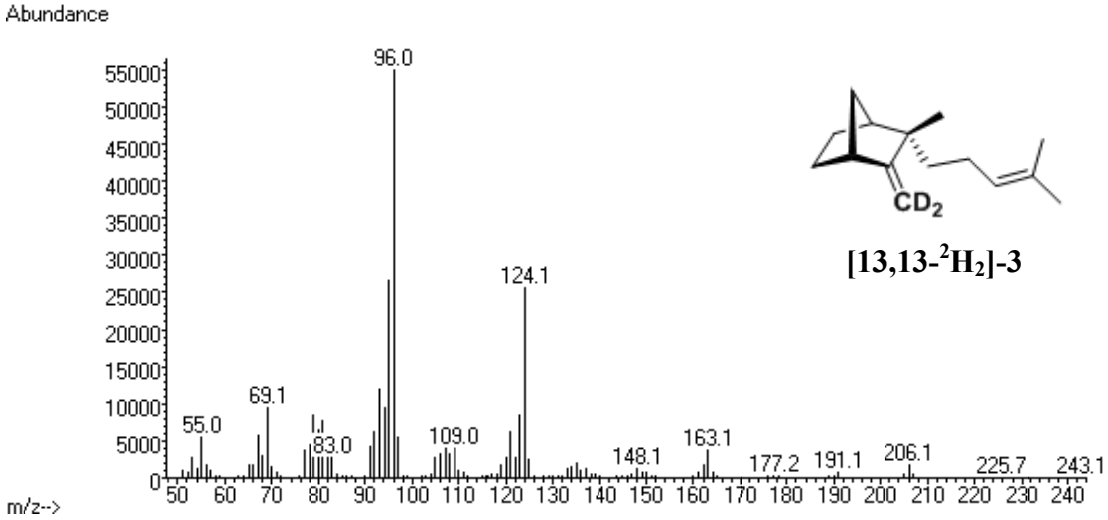

[13,13-^{2}H$_2$]-3

Figure A4.24. EI-MS spectrum of [13,13-^{2}H$_2$]-*epi*-β-santalene (**[13,13-^{2}H$_2$]-3**).

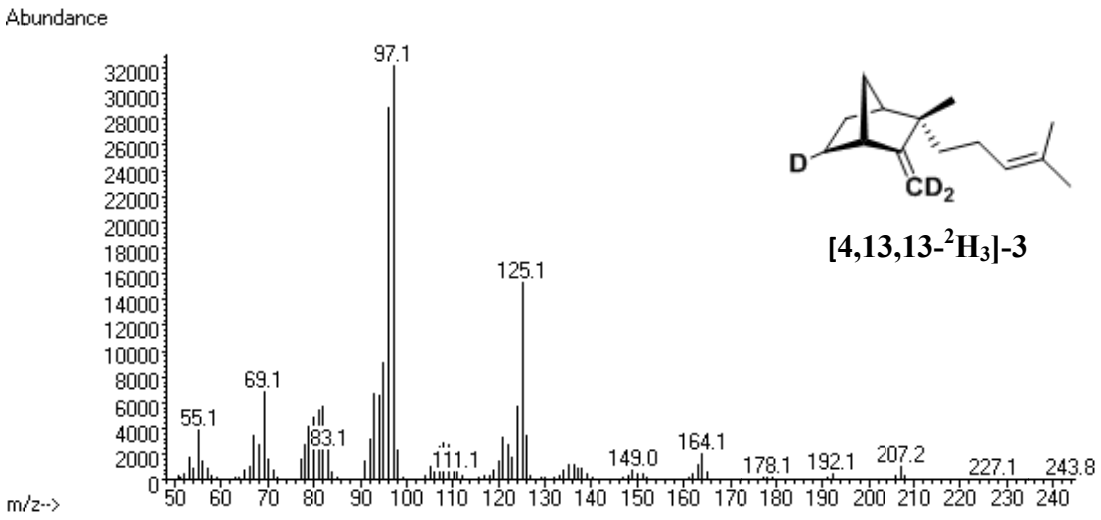

[4,13,13-$^2H_3$]-3

Figure A4.25. EI-MS spectrum of [4,13,13-$^2H_3$]-*epi*-β-santalene (**[4,13,13-$^2H_3$]-3**).

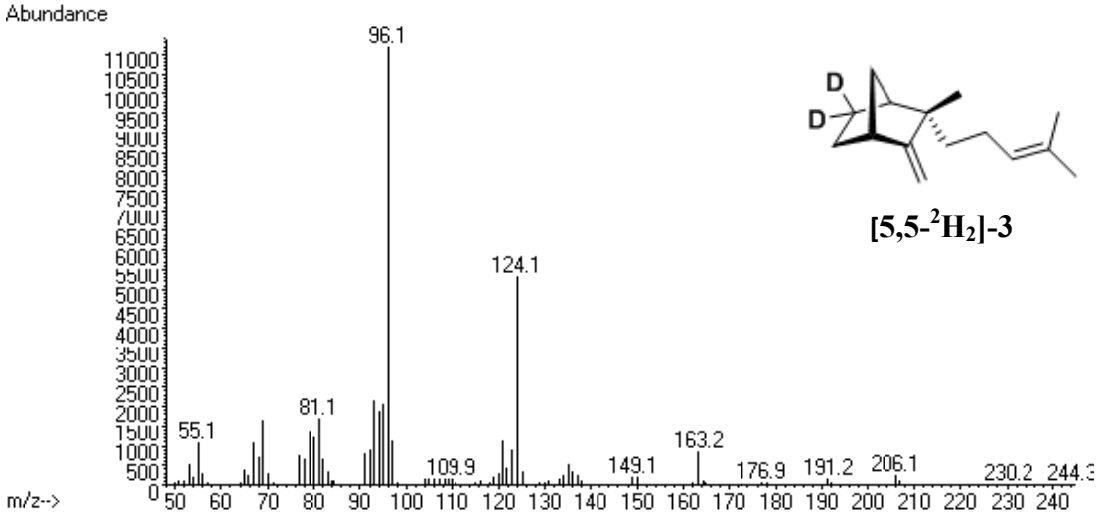

[5,5-$^2H_2$]-3

Figure A4.26. EI-MS spectrum of [5,5-$^2H_2$]-*epi*-β-santalene (**[5,5-$^2H_2$]-3**).

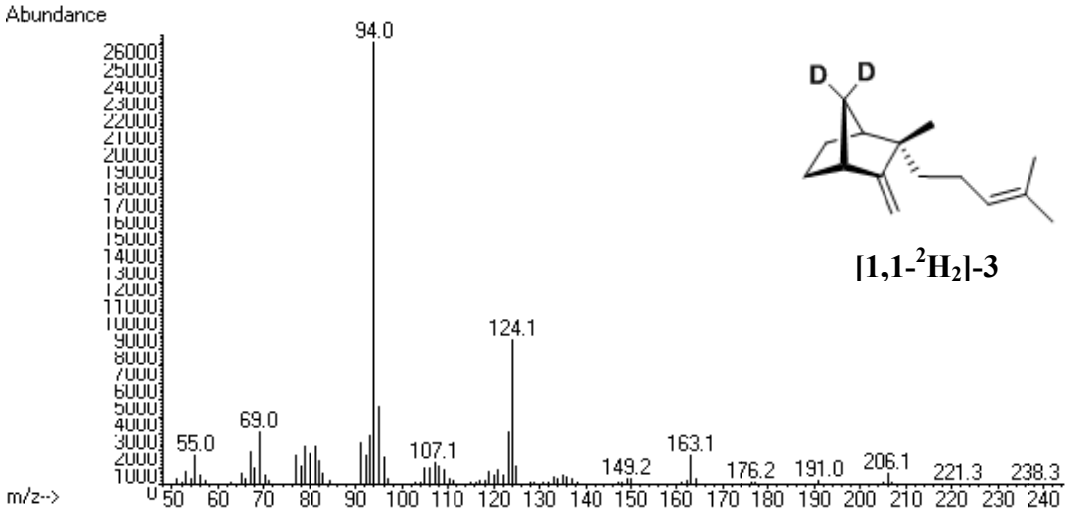

[1,1-$^2H_2$]-3

Figure A4.27. EI-MS spectrum of [1,1-$^2H_2$]-*epi*-β-santalene (**[1,1-$^2H_2$]-3**).

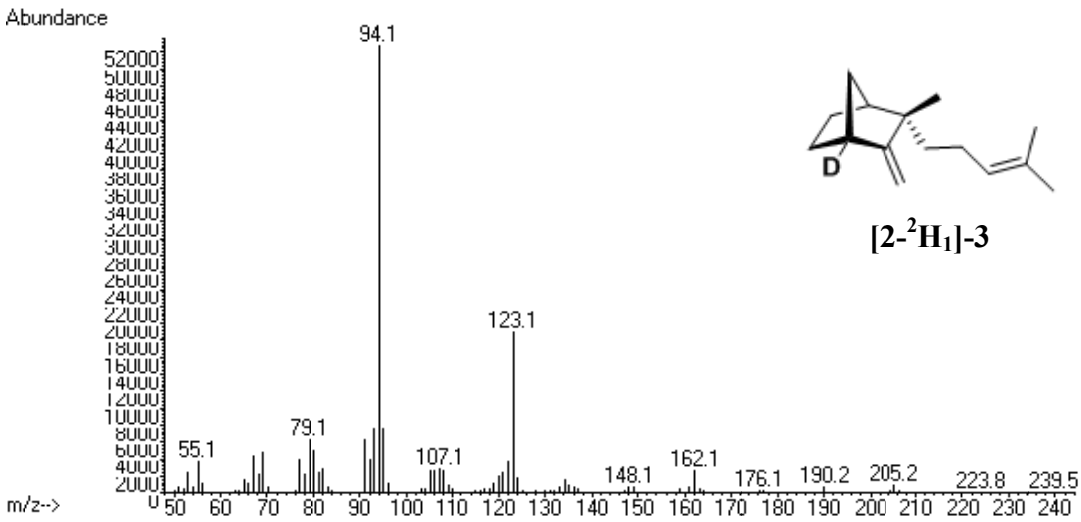

[2-^{2}H$_1$]-3

Figure A4.28. EI-MS spectrum of [2-^{2}H$_1$]-*epi*-β-santalene (**[2-^{2}H$_1$]-3**).

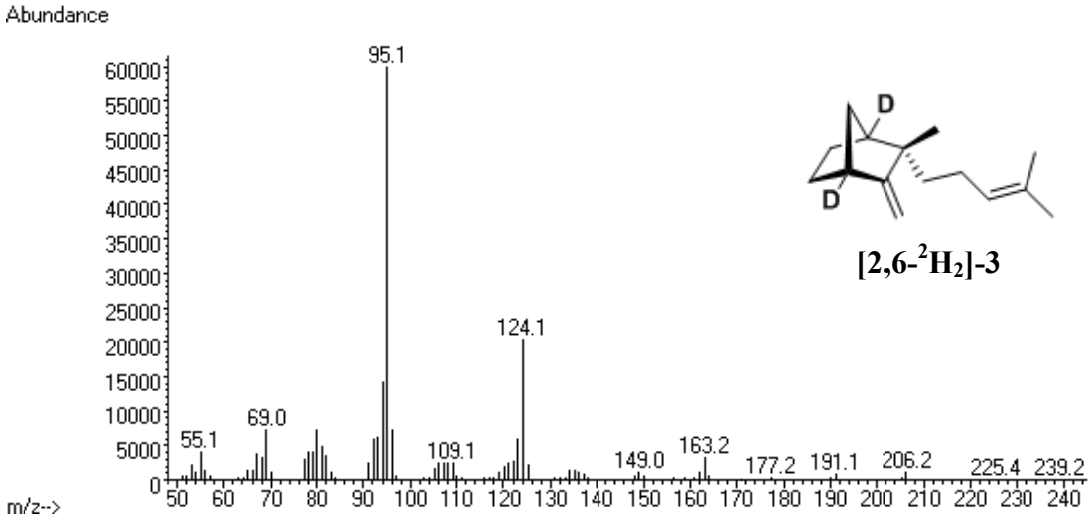

[2,6-^{2}H$_2$]-3

Figure A4.29. EI-MS spectrum of [2,6-^{2}H$_2$]-*epi*-β-santalene (**[2,6-^{2}H$_2$]-3**).

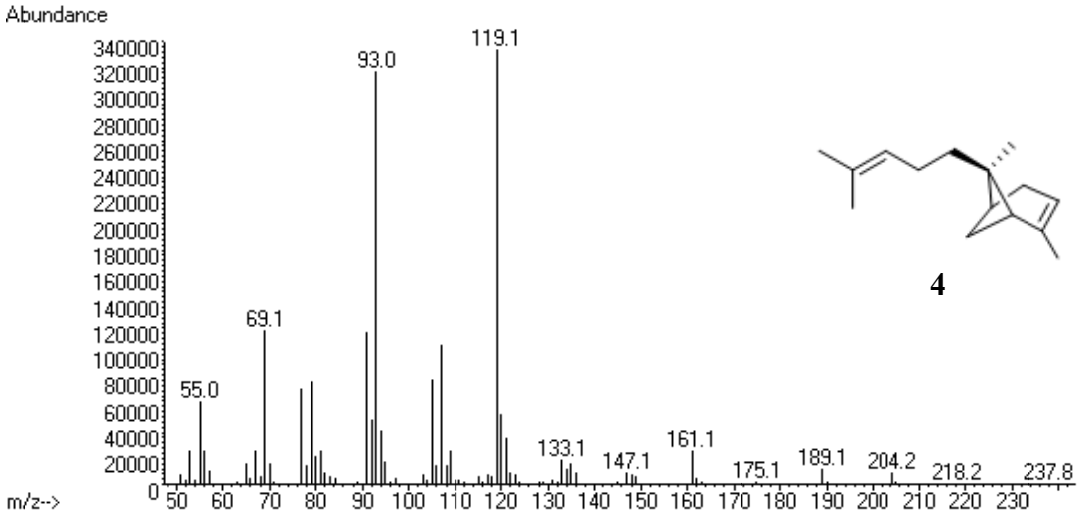

Figure A4.30. EI-MS spectrum of *exo*-α-bergamotene (**4**).

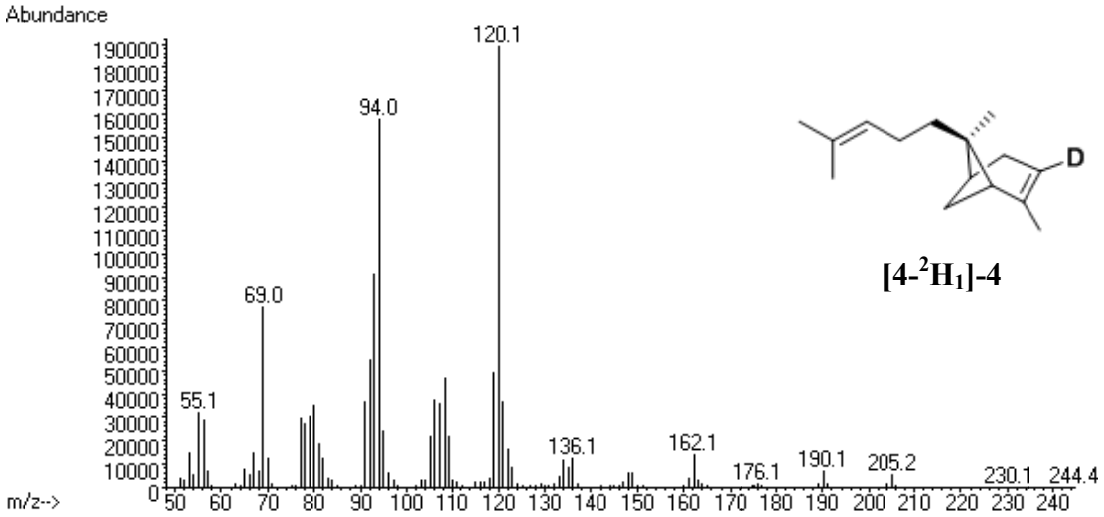

Figure A4.31. EI-MS spectrum of [4-$^2H_1$]-*exo*-α-bergamotene (**[4-$^2H_1$]-4**).

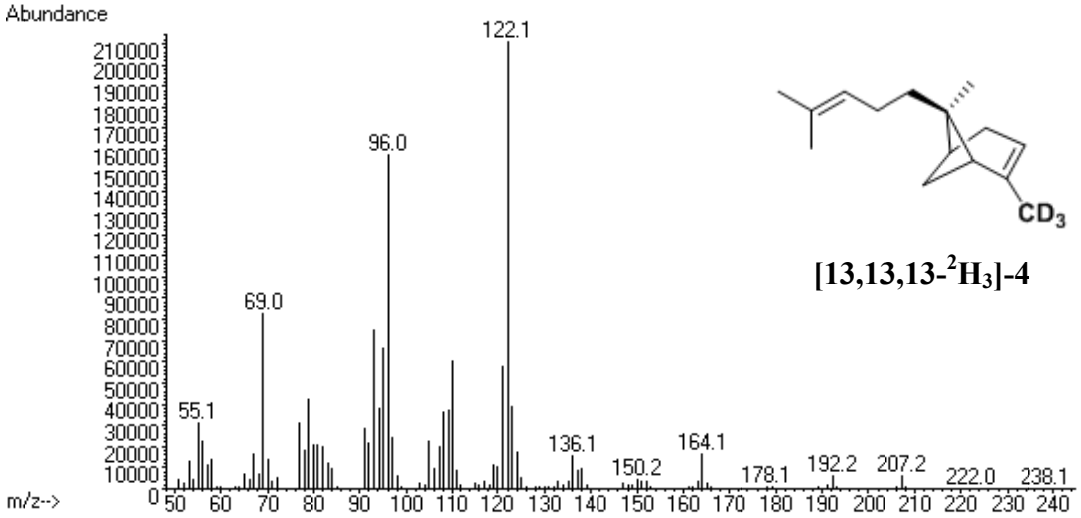

Figure A4.32. EI-MS spectrum of [13,13,13-$^2H_3$]-*exo*-α-bergamotene (**[13,13,13-$^2H_3$]-4**).

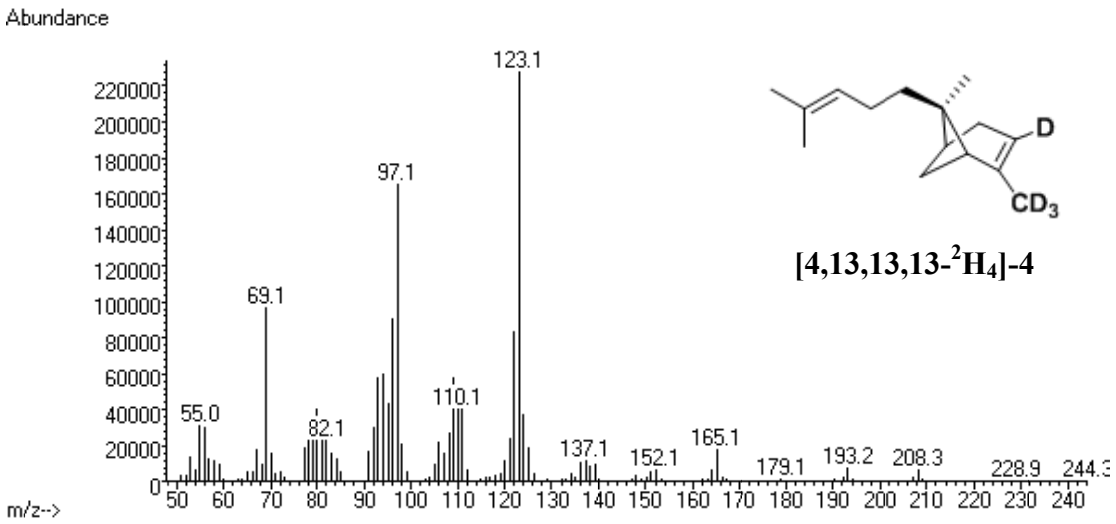

Figure A4.33. EI-MS spectrum of [4,13,13,13-$^2H_4$]-*exo*-α-bergamotene (**[4,13,13,13-$^2H_4$]-4**).

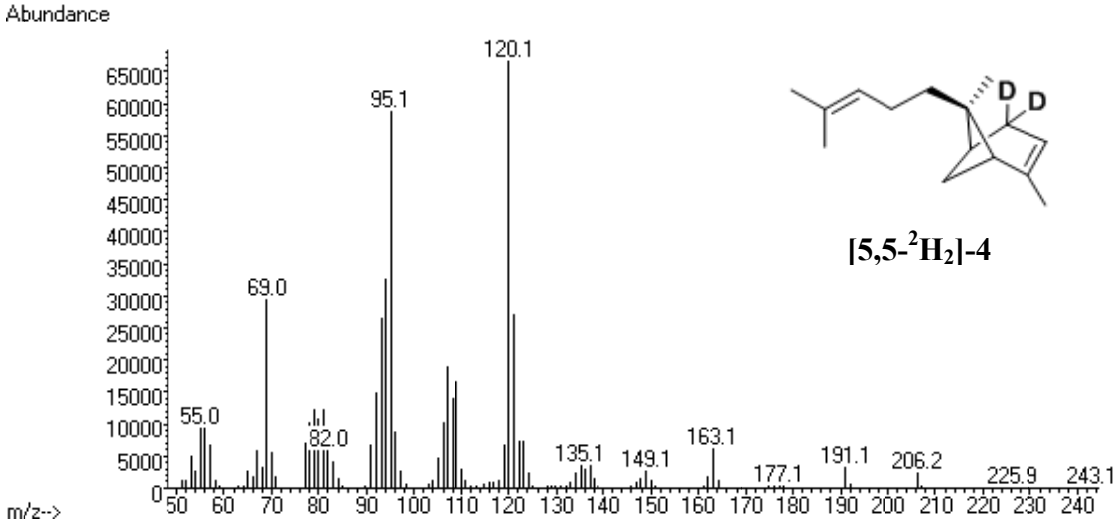

Figure A4.34. EI-MS spectrum of [5,5-$^2H_2$]-*exo*-α-bergamotene (**[5,5-$^2H_2$]-4**).

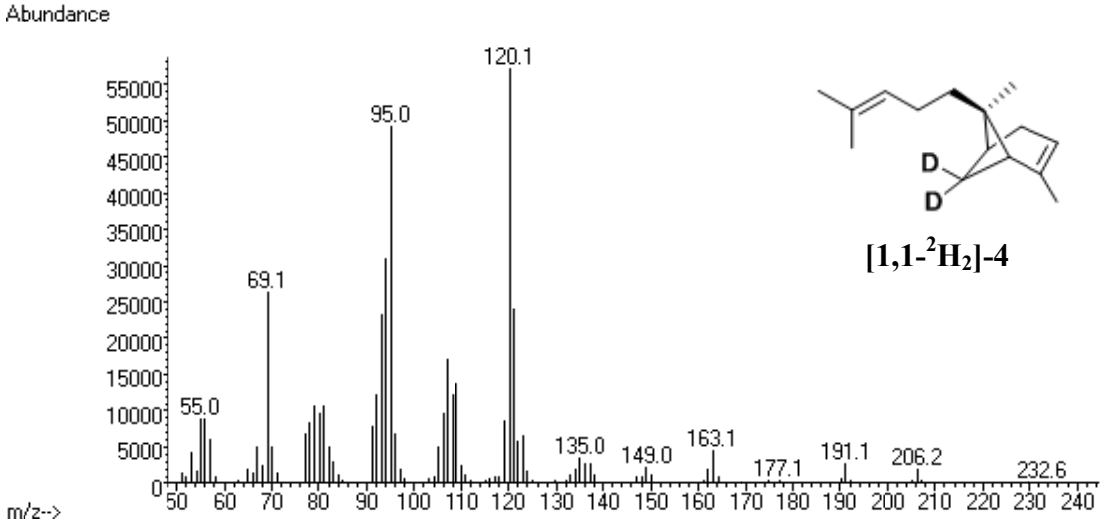

Figure A4.35. EI-MS spectrum of [1,1-$^2H_2$]-*exo*-α-bergamotene (**[1,1-$^2H_2$]-4**).

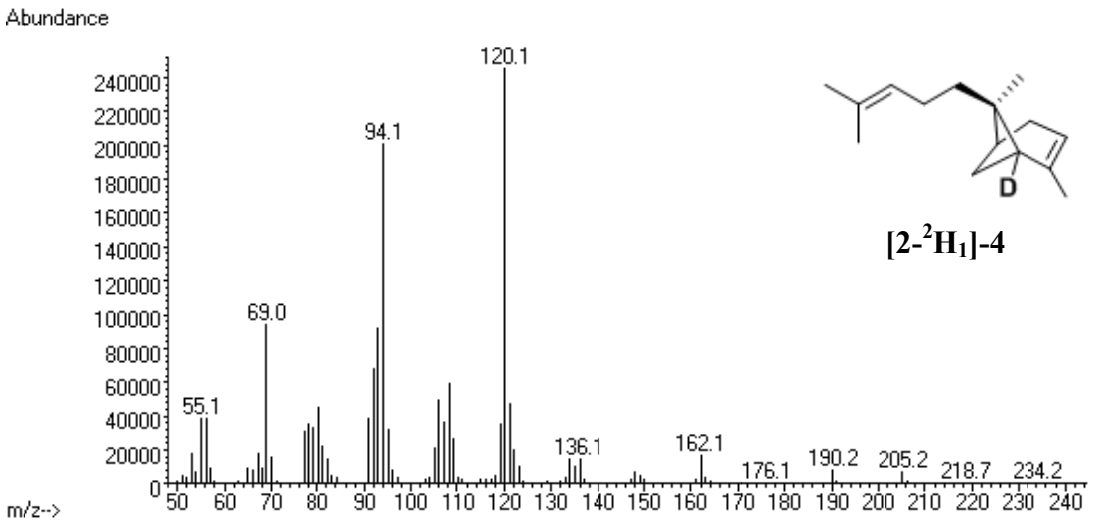

Figure A4.36. EI-MS spectrum of [2-^{2}H$_1$]-*exo*-α-bergamotene (**[2-^{2}H$_1$]-4**).

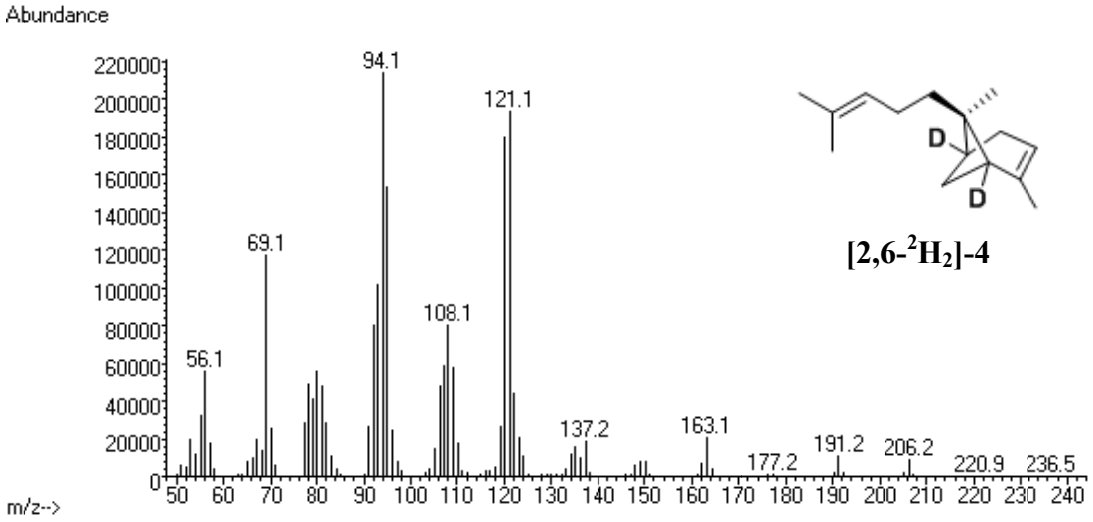

Figure A4.37. EI-MS spectrum of [2,6-^{2}H$_2$]-*exo*-α-bergamotene (**[2,6-^{2}H$_2$]-4**).

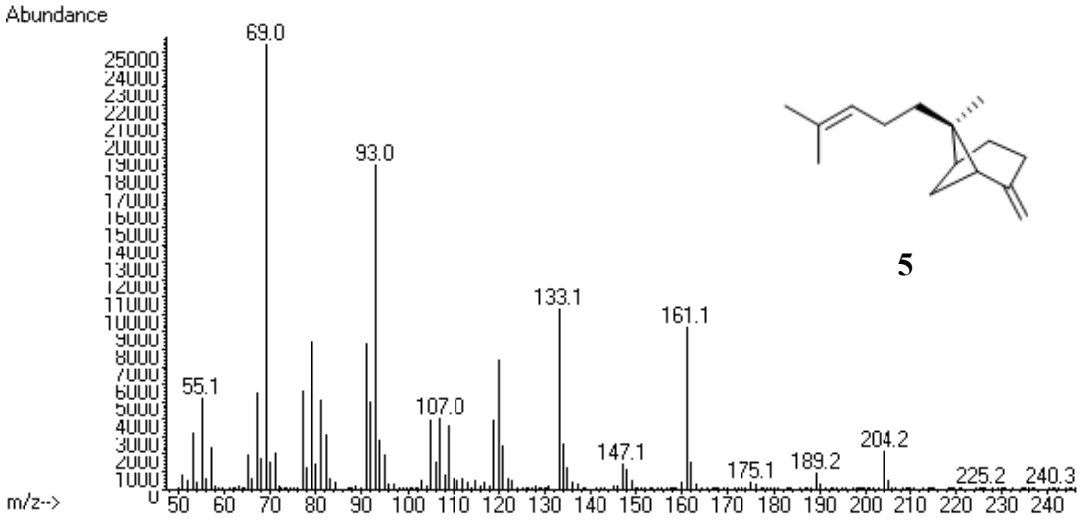

Figure A4.38. EI-MS spectrum of *exo*-β-bergamotene (**5**).

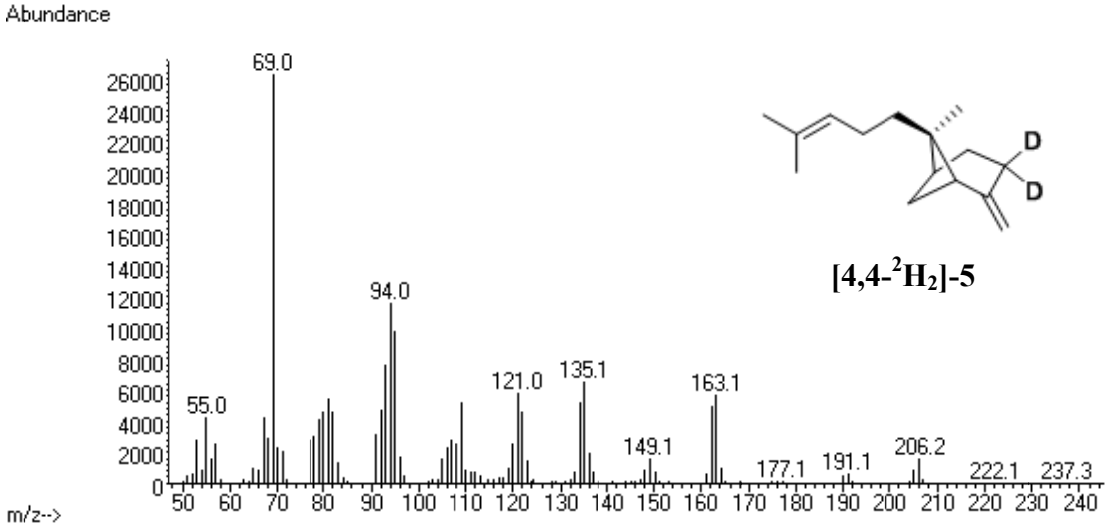

Figure A4.39. EI-MS spectrum of [4,4-$^2H_2$]-*exo*-β-bergamotene (**[4,4-$^2H_2$]-5**).

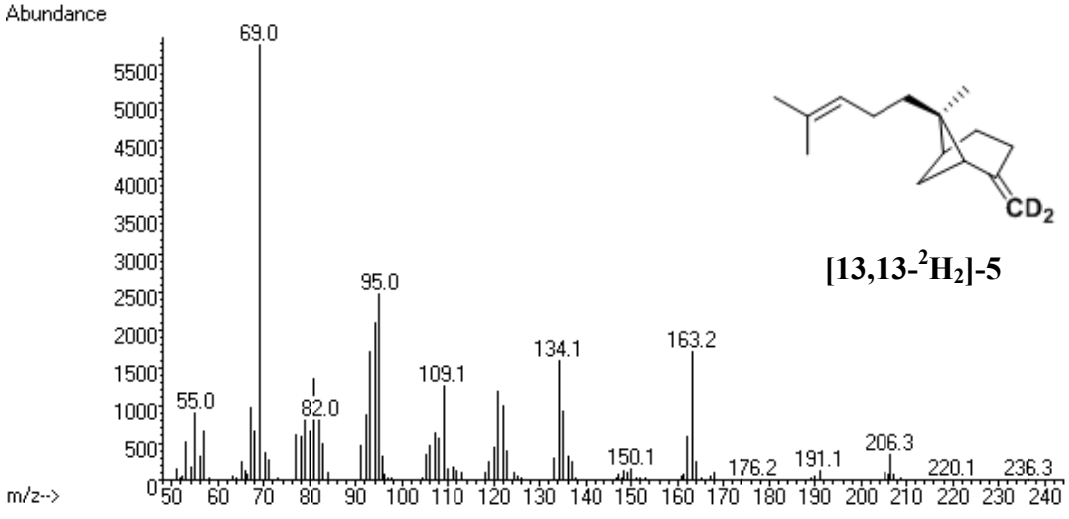

Figure A4.40. EI-MS spectrum of [13,13-$^2H_2$]-*exo*-β-bergamotene (**[13,13-$^2H_2$]-5**).

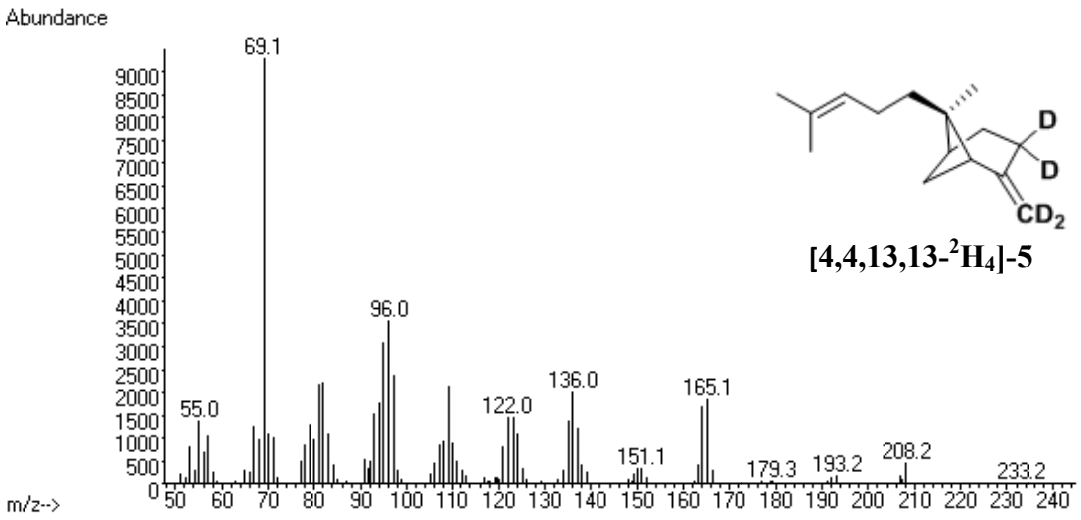

[4,4,13,13-$^2H_4$]-5

Figure A4.41. EI-MS spectrum of [4,4,13,13-$^2H_4$]-*exo*-α-bergamotene (**[4,4,13,13-$^2H_4$]-5**).

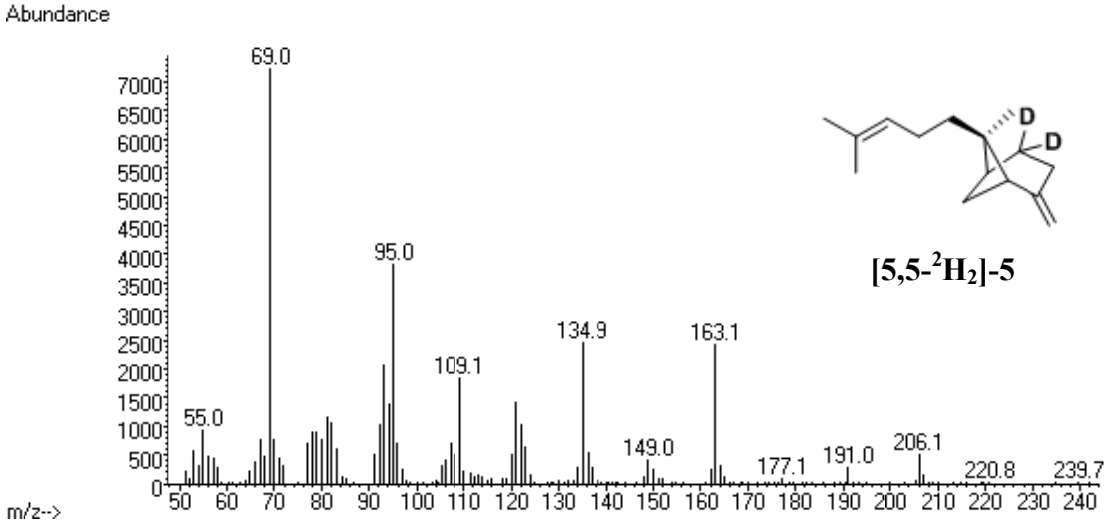

[5,5-$^2H_2$]-5

Figure A4.42. EI-MS spectrum of [5,5-$^2H_2$]-*exo*-β-bergamotene (**[5,5-$^2H_2$]-5**).

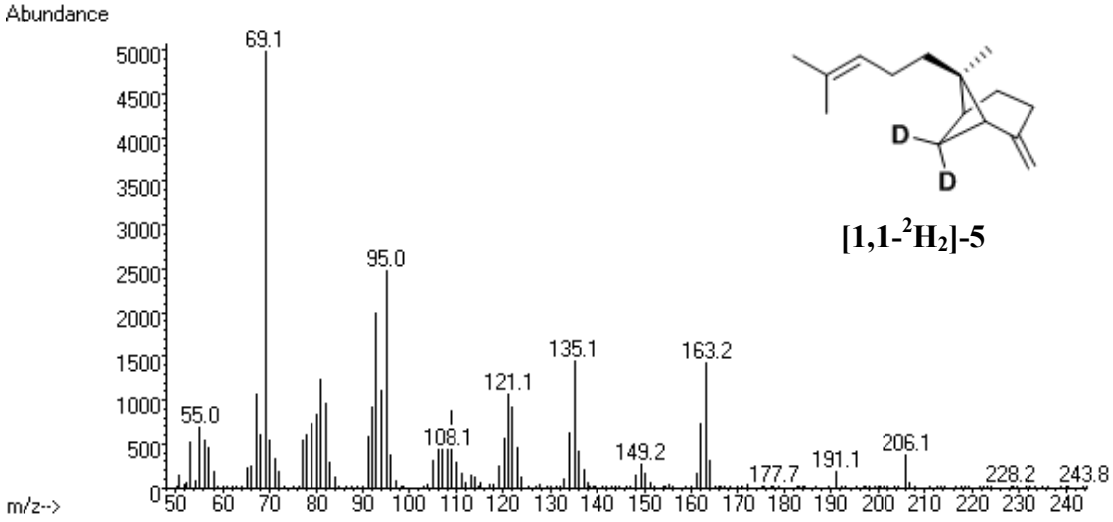

[1,1-$^2H_2$]-5

Figure A4.43. EI-MS spectrum of [1,1-$^2H_2$]-*exo*-β-bergamotene (**[1,1-$^2H_2$]-5**).

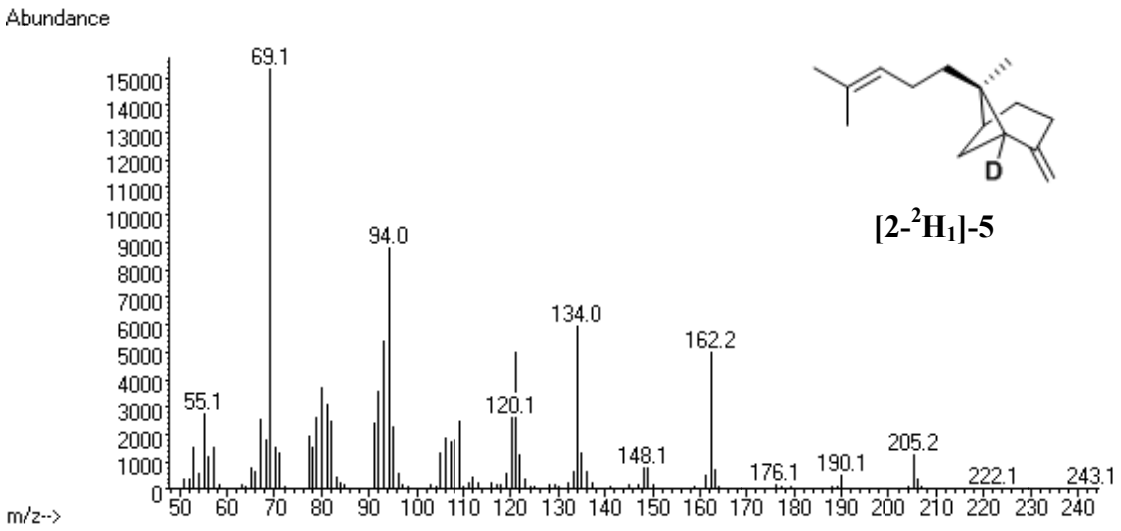

[2-^{2}H$_1$]-5

Figure A4.44. EI-MS spectrum of [2-^{2}H$_1$]-*exo*-β-bergamotene (**[2-^{2}H$_1$]-5**).

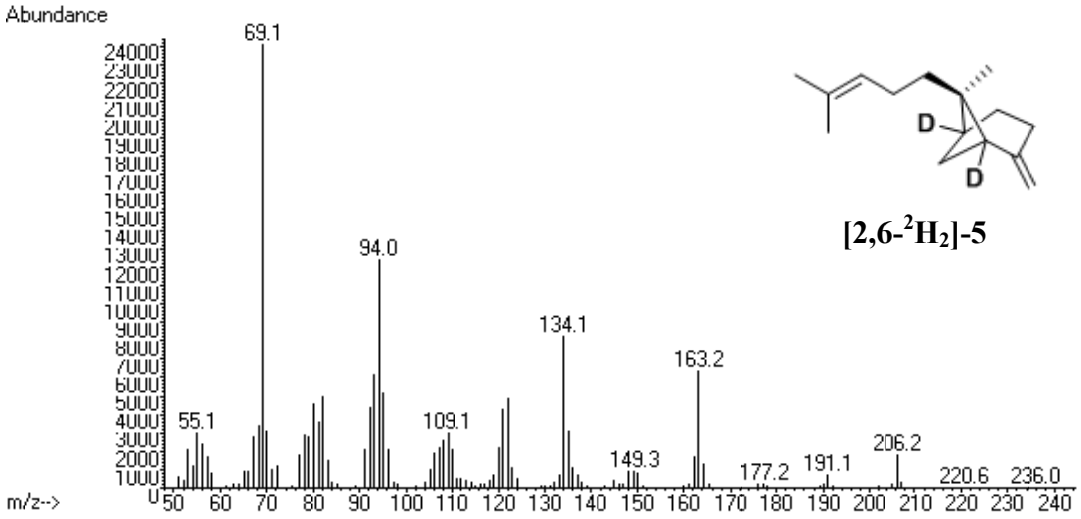

[2,6-^{2}H$_2$]-5

Figure A4.45. EI-MS spectrum of [2,6-^{2}H$_2$]-*exo*-β-bergamotene (**[2,6-^{2}H$_2$]-5**).

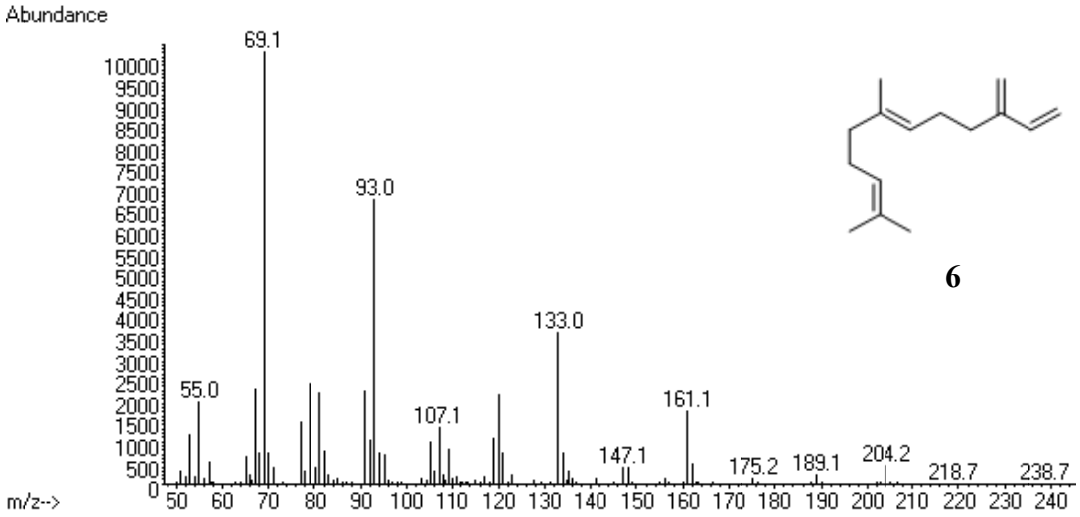

6

Figure A4.46. EI-MS spectrum of (*E*)-β-farnesene (**6**).

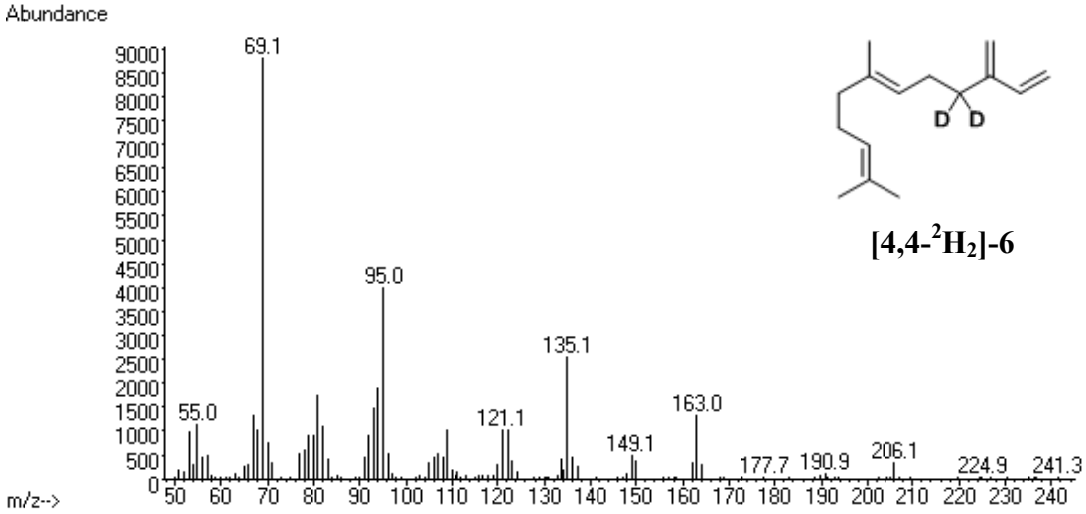

[4,4-$^2H_2$]-6

Figure A4.47. EI-MS spectrum of [4,4-$^2H_2$]-(*E*)-β-farnesene (**[4,4-$^2H_2$]-6**).

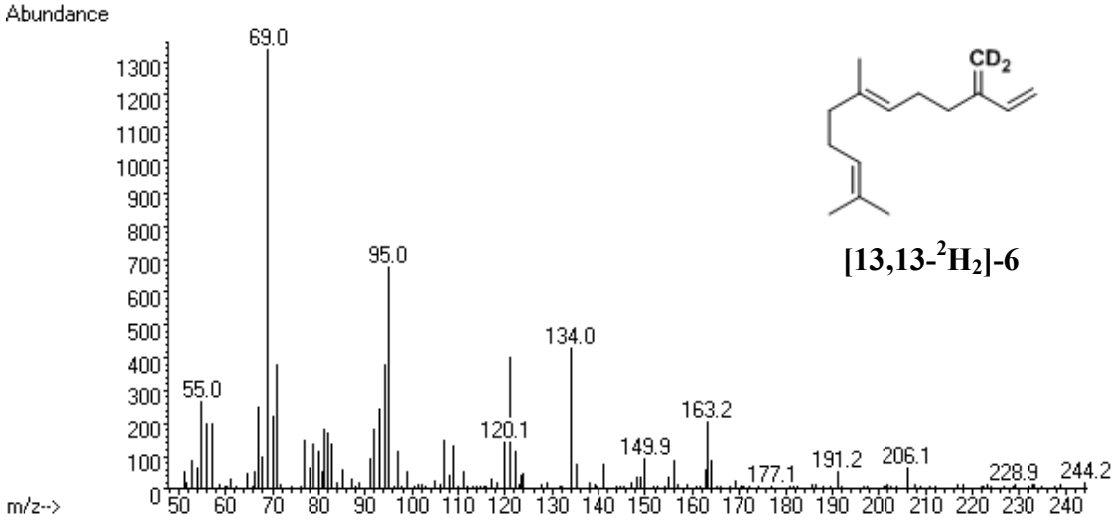

[13,13-$^2H_2$]-6

Figure A4.48. EI-MS spectrum of [13,13-$^2H_2$]-(*E*)-β-farnesene (**[13,13-$^2H_2$]-6**).

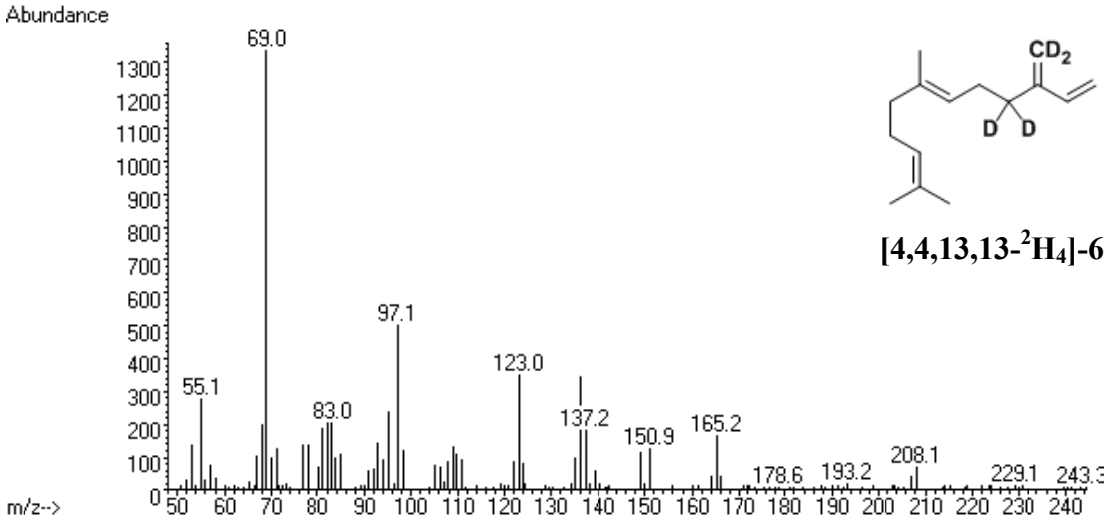

[4,4,13,13-$^2H_4$]-6

Figure A4.49. EI-MS spectrum of [4,4,13,13-$^2H_4$]-(*E*)-β-farnesene (**[4,4,13,13-$^2H_4$]-6**).

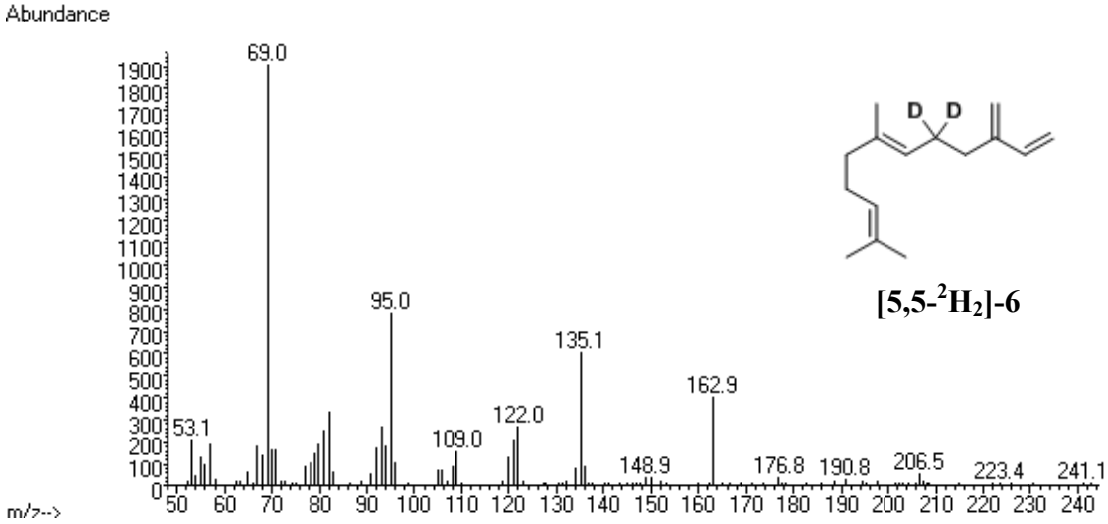

[5,5-$^2H_2$]-6

Figure A4.50. EI-MS spectrum of [5,5-$^2H_2$]-(*E*)-β-farnesene (**[5,5-$^2H_2$]-6**).

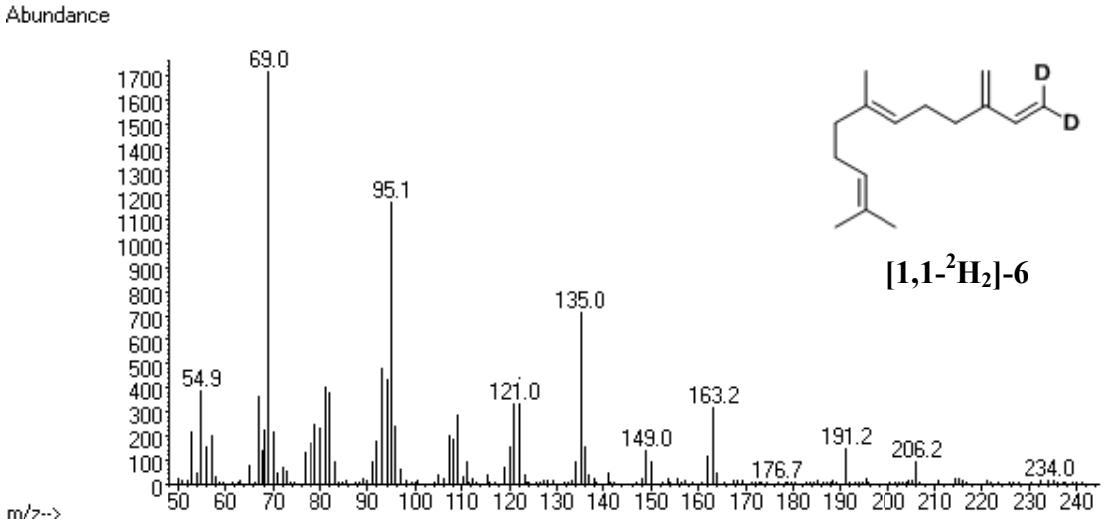

[1,1-$^2H_2$]-6

Figure A4.51. EI-MS spectrum of [1,1-$^2H_2$]-(*E*)-β-farnesene (**[1,1-$^2H_2$]-6**).

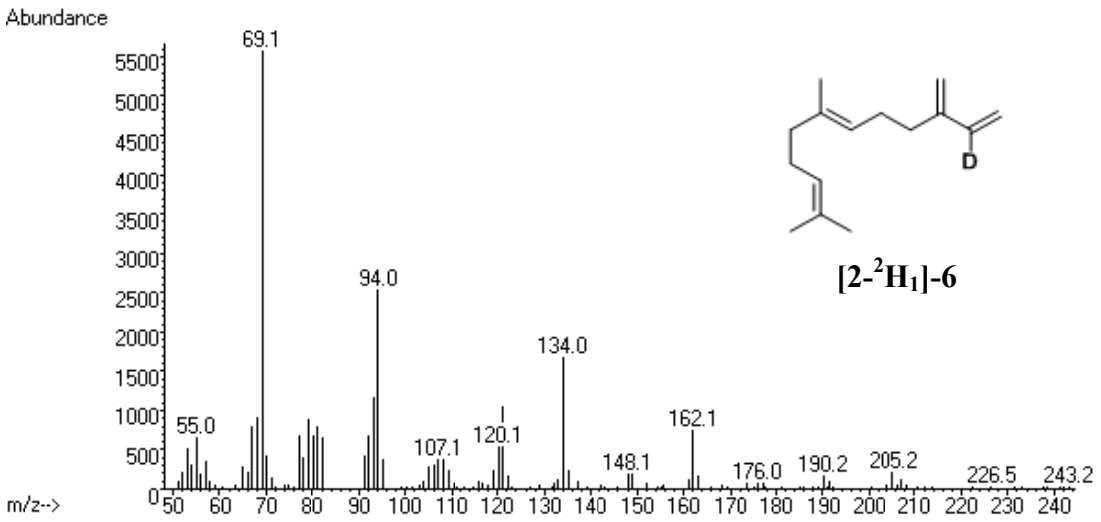

Figure A4.52. EI-MS spectrum of [2-^{2}H$_1$]-(*E*)-β-farnesene (**[2-^{2}H$_1$]-6**).

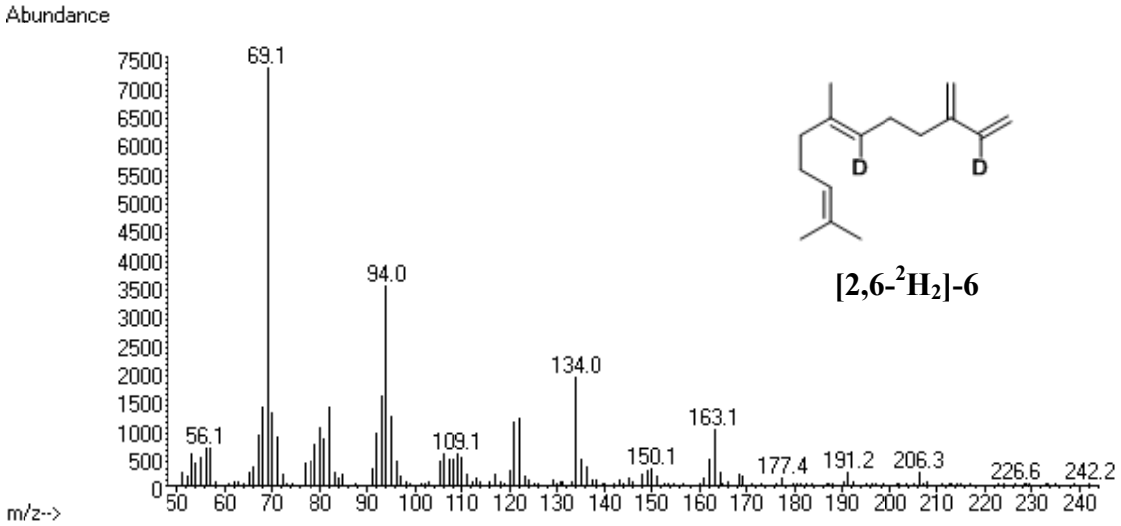

Figure A4.53. EI-MS spectrum of [2,6-^{2}H$_2$]-(*E*)-β-farnesene (**[2,6-^{2}H$_2$]-6**).

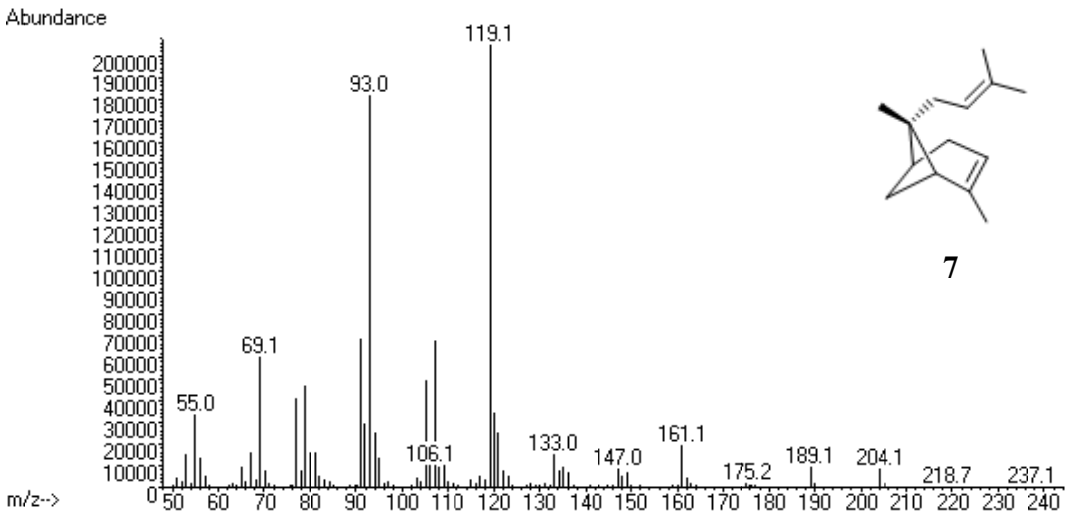

Figure A4.54. EI-MS spectrum of *endo*-α-bergamotene (**7**).

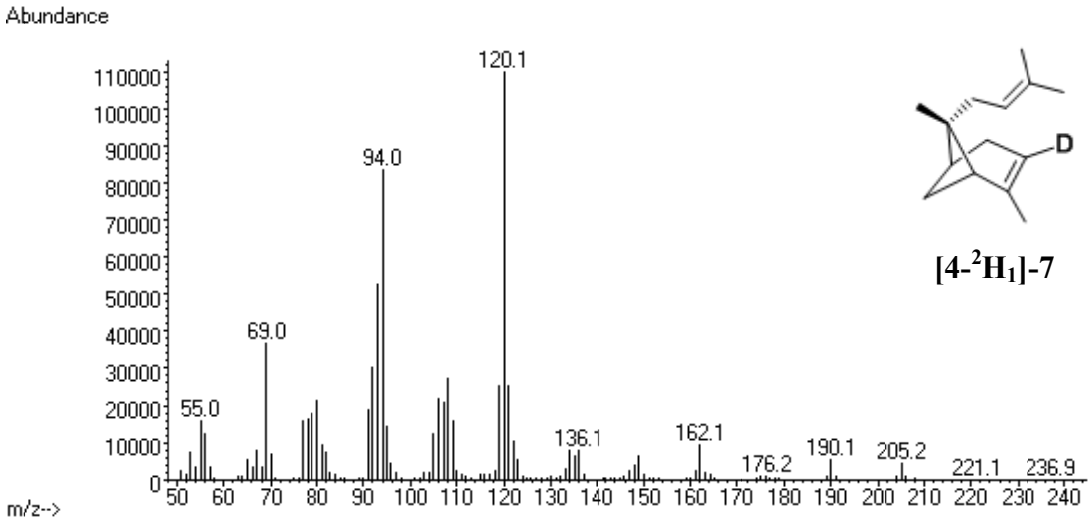

Figure A4.55. EI-MS spectrum of [4-$^2H_1$]-*endo*-α-bergamotene (**[4-$^2H_1$]-7**).

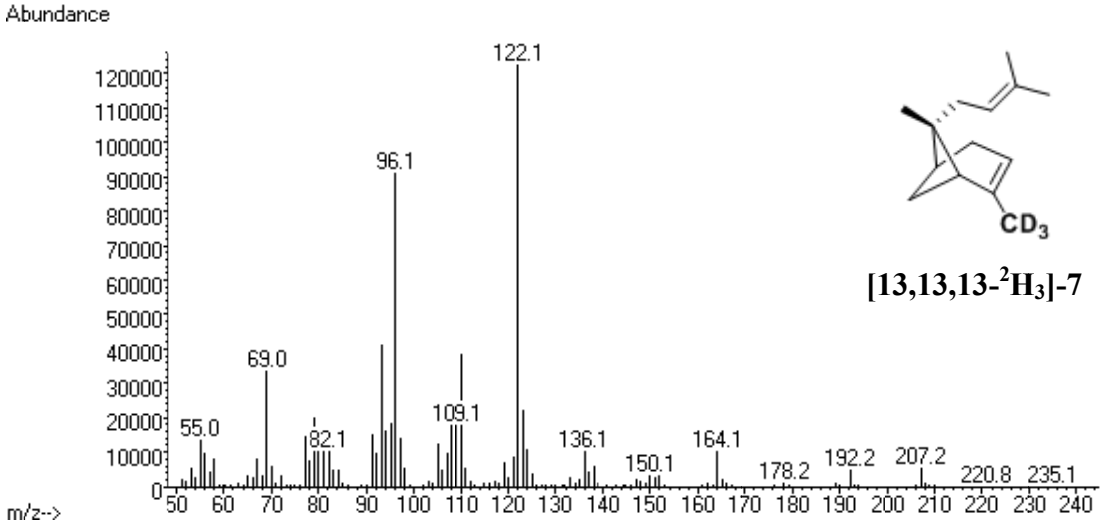

Figure A4.56. EI-MS spectrum of [13,13,13-$^2H_3$]-*endo*-α-bergamotene (**[13,13,13-$^2H_3$]-7**).

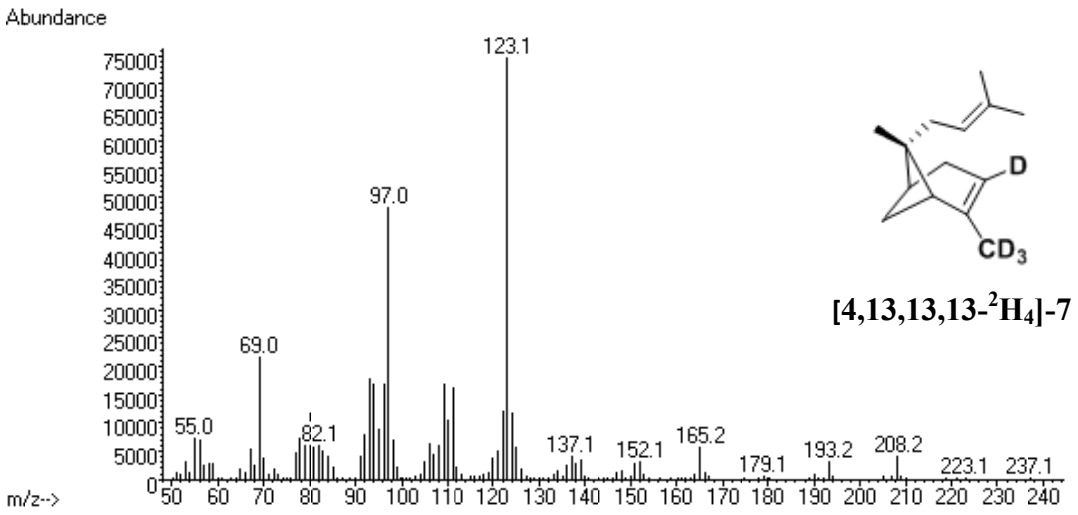

Figure A4.57. EI-MS spectrum of [4,13,13,13-$^2H_4$]-*endo*-α-bergamotene (**[4,13,13,13-$^2H_4$]-7**).

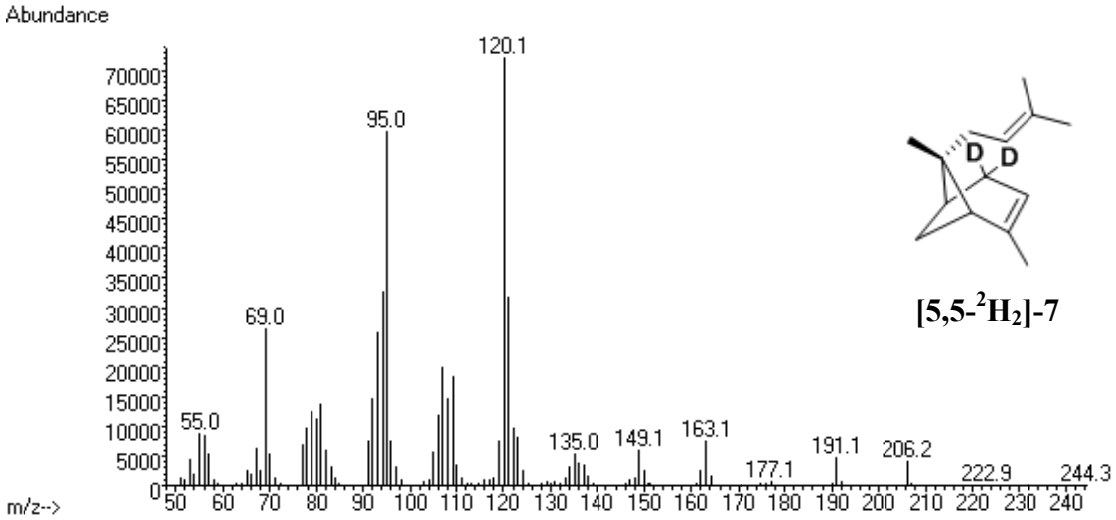

Figure A4.58. EI-MS spectrum of [5,5-$^2H_2$]-*endo*-α-bergamotene (**[5,5-$^2H_2$]-7**).

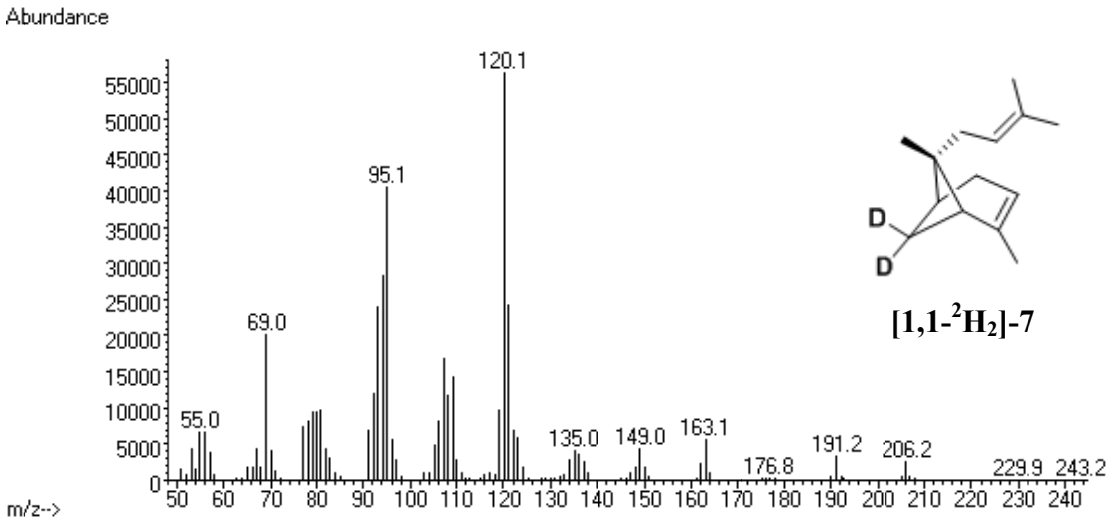

Figure A4.59. EI-MS spectrum of [1,1-$^2H_2$]-*endo*-α-bergamotene (**[1,1-$^2H_2$]-7**).

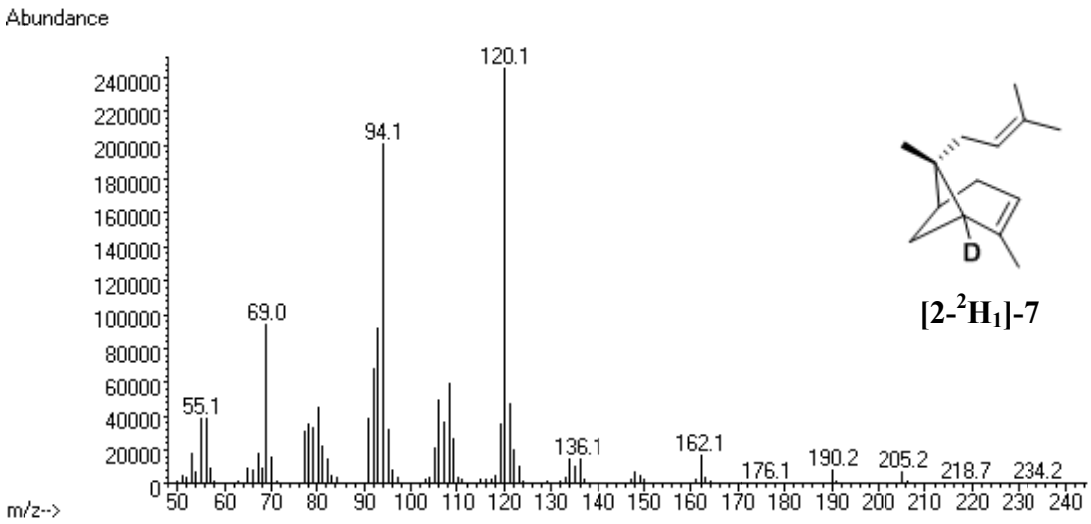

[2-^{2}H$_1$]-7

Figure A4.60. EI-MS spectrum of [2-^{2}H$_1$]-*endo*-α-bergamotene (**[2-^{2}H$_1$]-7**).

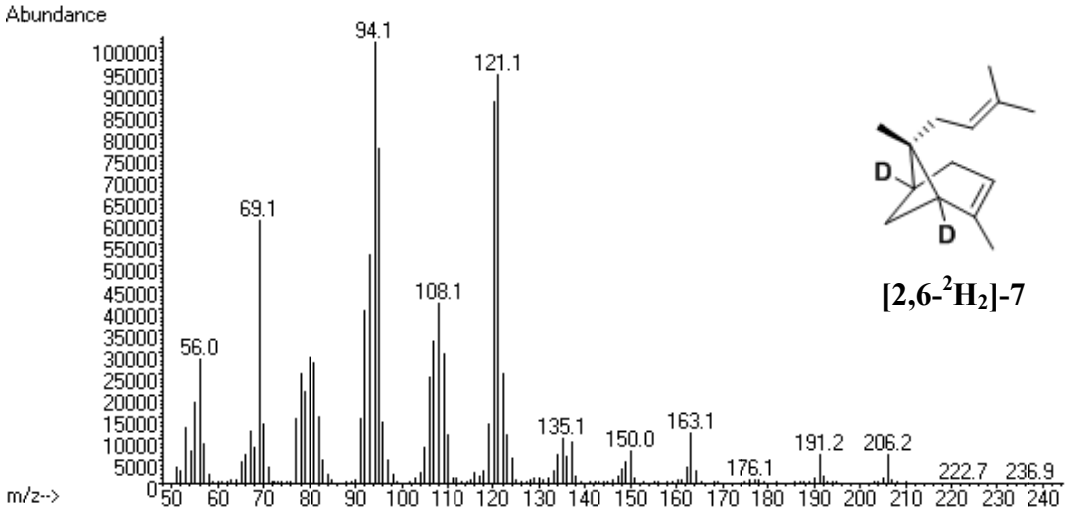

[2,6-^{2}H$_2$]-7

Figure A4.61. EI-MS spectrum of [2,6-^{2}H$_2$]-*endo*-α-bergamotene (**[2,6-^{2}H$_2$]-7**).

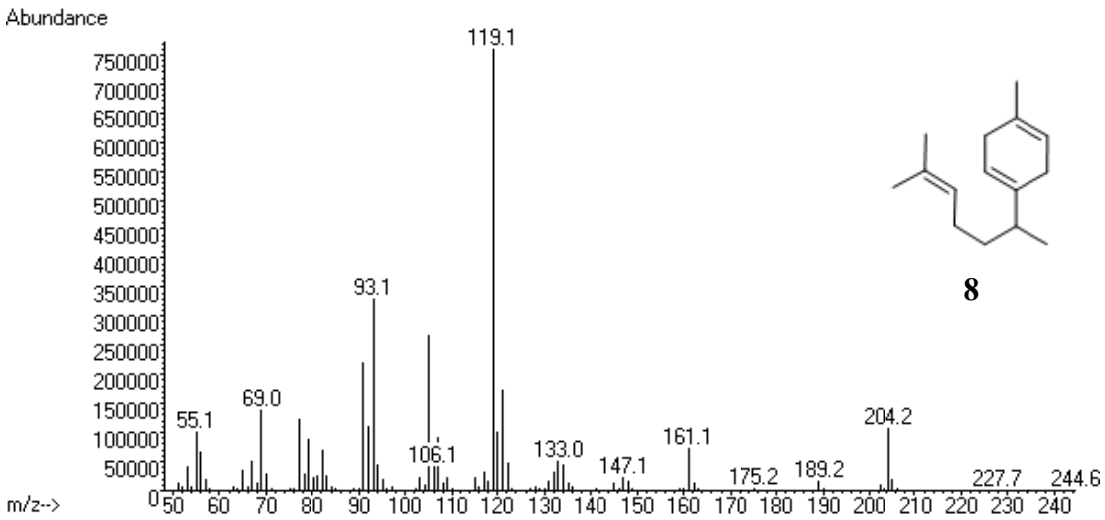

Figure A4.62. EI-MS spectrum of β-curcumene (**8**).

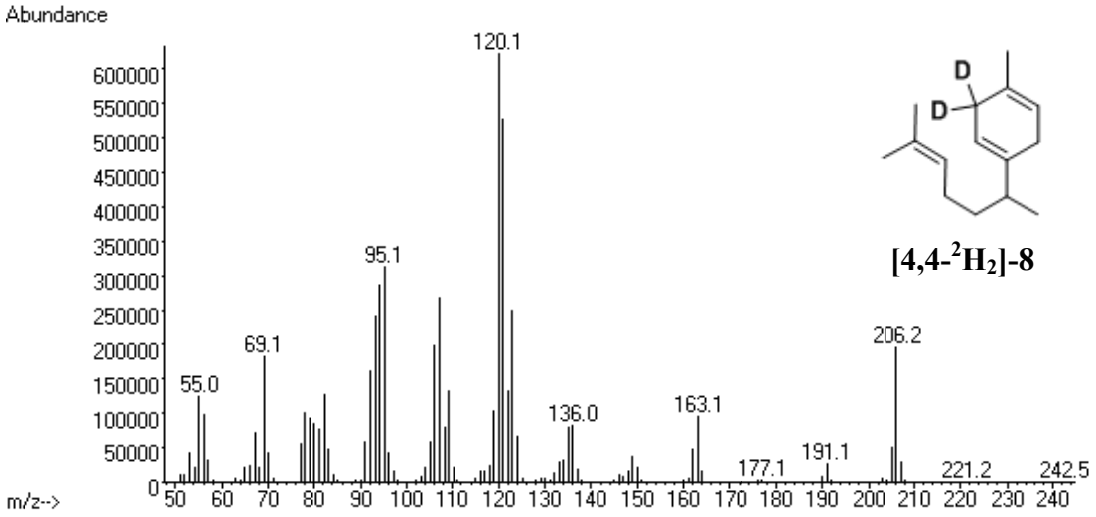

Figure A4.63. EI-MS spectrum of [4,4-$^2H_2$]-β-curcumene (**[4,4-$^2H_2$]-8**).

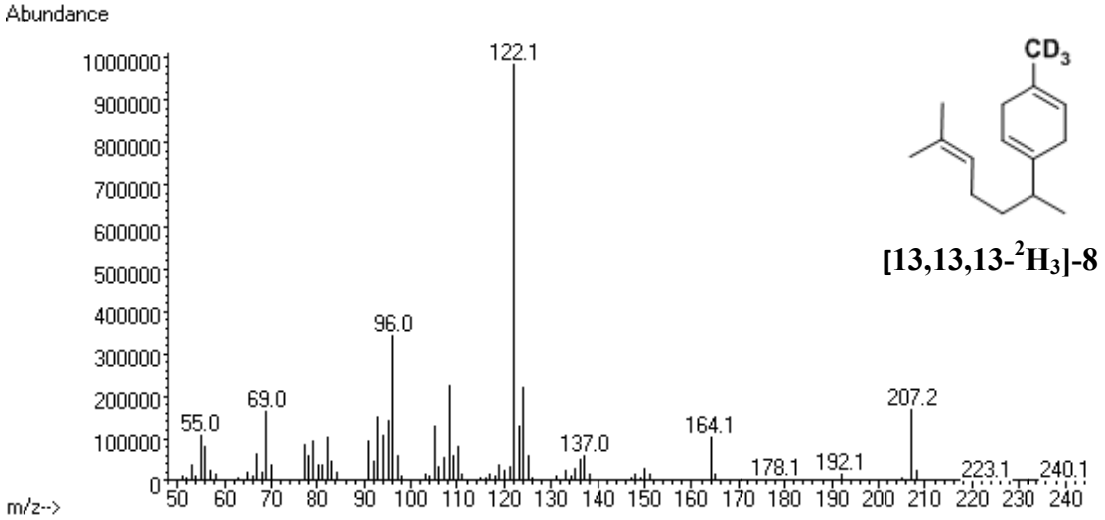

Figure A4.64. EI-MS spectrum of [13,13,13-$^2H_3$]-β-curcumene (**[13,13,13-$^2H_3$]-8**).

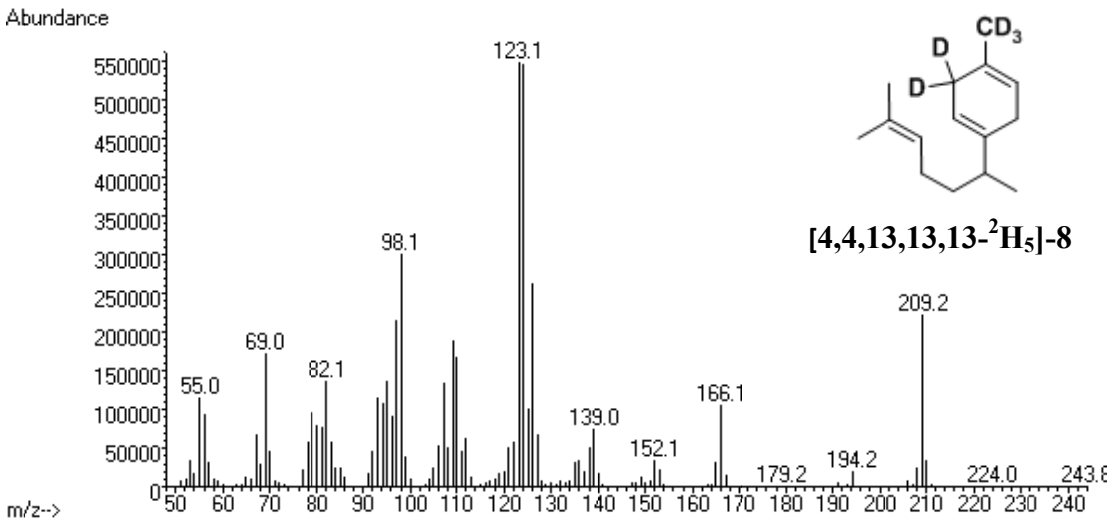

Figure A4.65. EI-MS spectrum of [4,4,13,13,13-$^{2}H_5$]-β-curcumene (**[4,4,13,13,13-$^{2}H_5$]-8**).

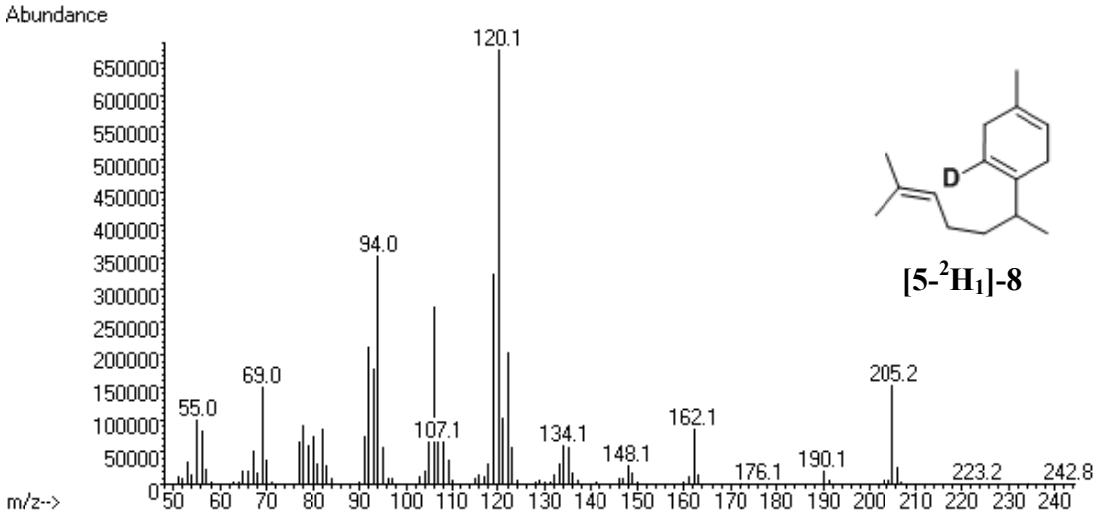

Figure A4.66. EI-MS spectrum of [5-$^{2}H_1$]-β-curcumene (**[5-$^{2}H_1$]-8**).

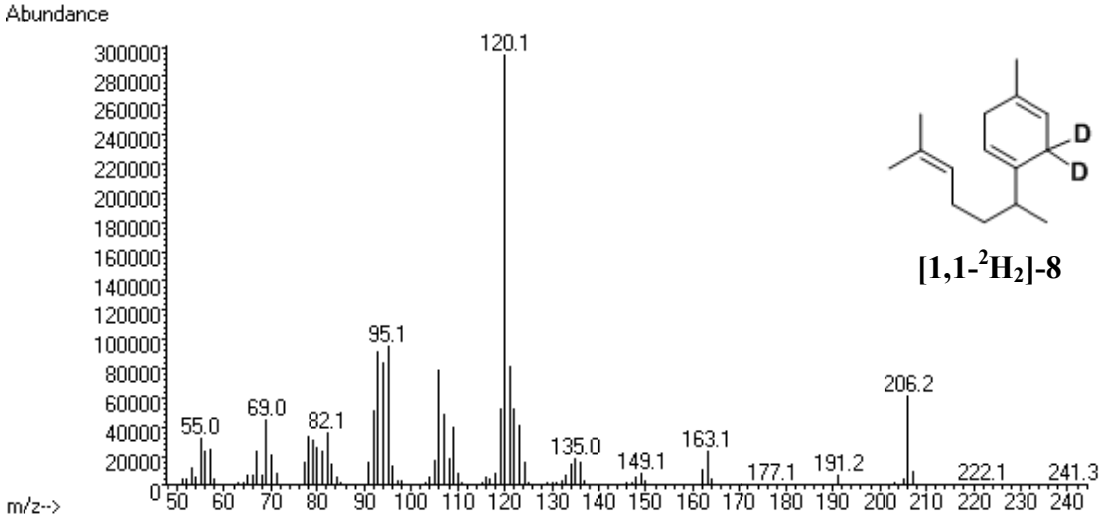

Figure A4.67. EI-MS spectrum of [1,1-$^{2}H_2$]-β-curcumene (**[1,1-$^{2}H_2$]-8**).

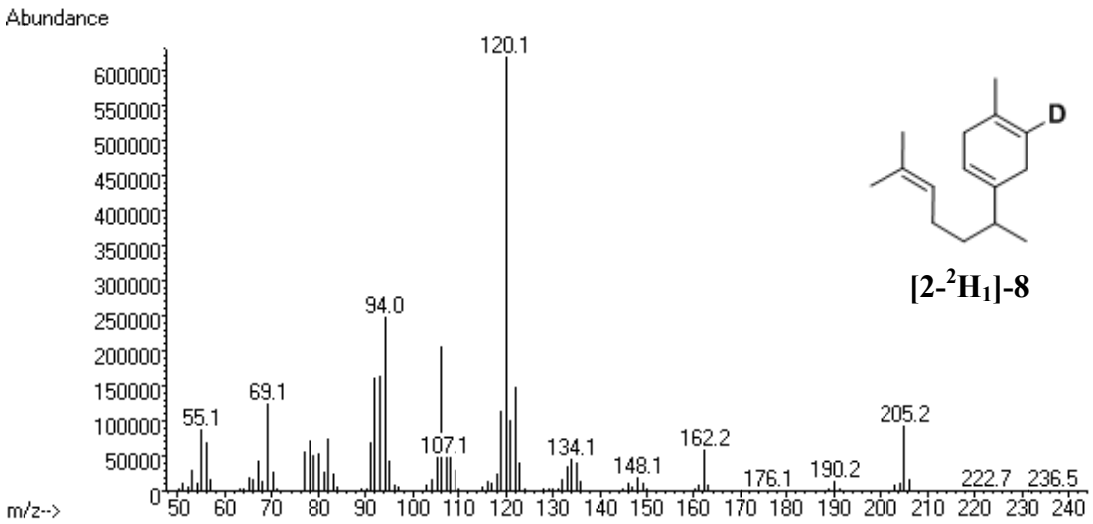

Figure A4.68. EI-MS spectrum of [2-$^{2}H_{1}$]-β-curcumene (**[2-$^{2}H_{1}$]-8**).

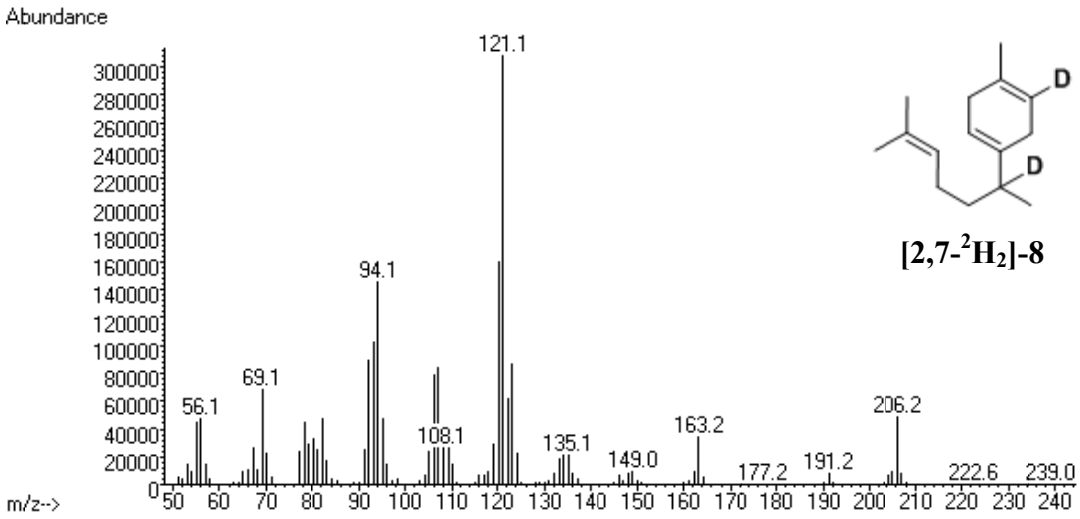

Figure A4.69. EI-MS spectrum of [2,7-$^{2}H_{2}$]-β-curcumene (**[2,7-$^{2}H_{2}$]-8**).

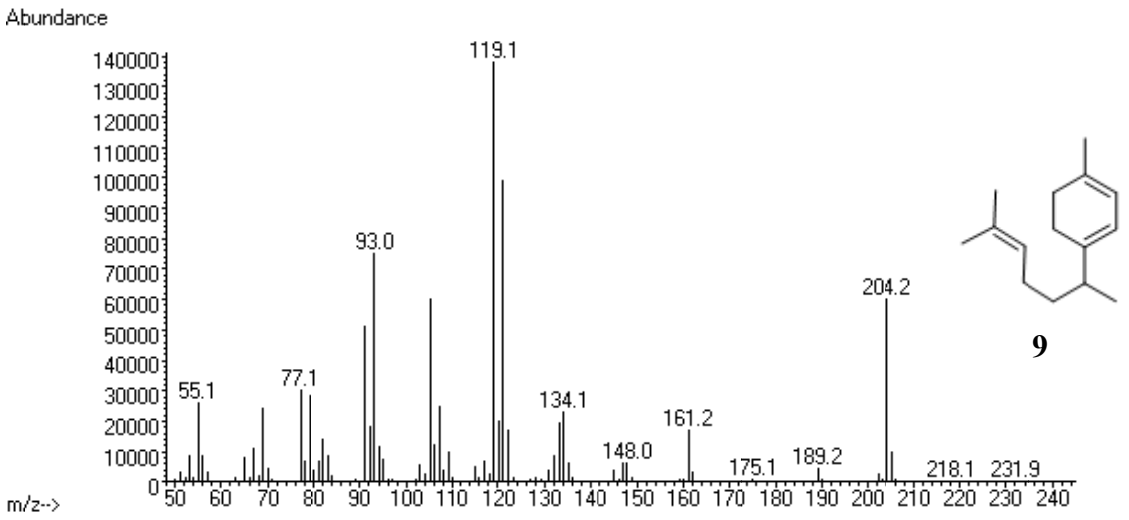

Figure A4.70. EI-MS spectrum of γ-curcumene (**9**).

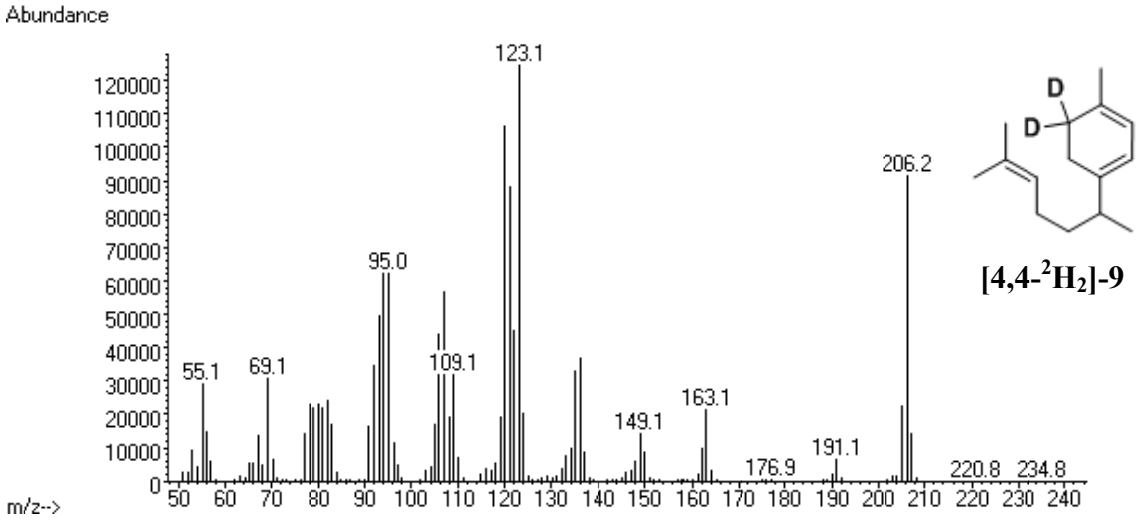

Figure A4.71. EI-MS spectrum of [4,4-$^2H_2$]-γ-curcumene (**[4,4-$^2H_2$]-9**).

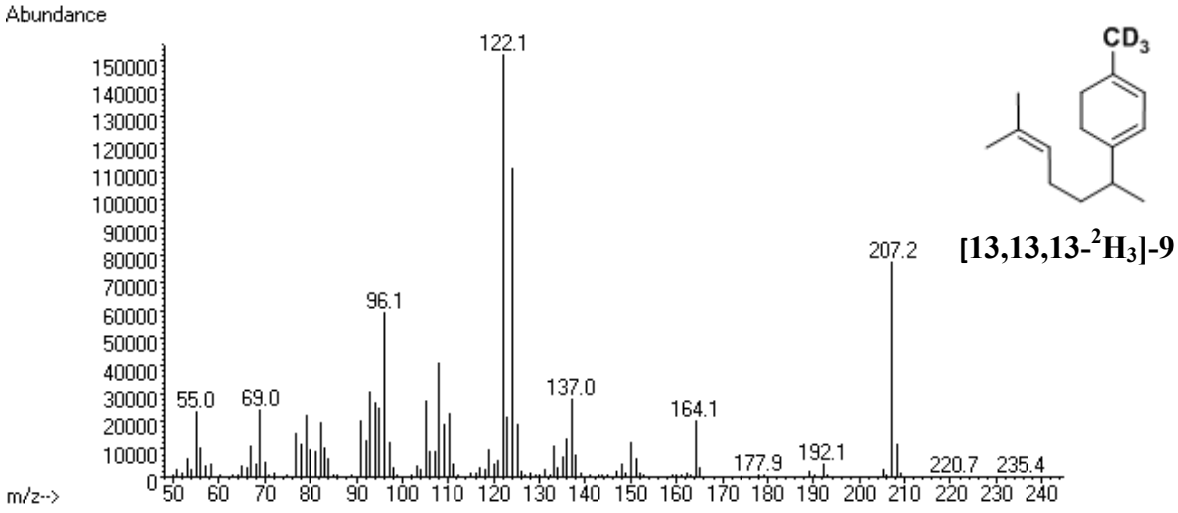

Figure A4.72. EI-MS spectrum of [13,13,13-$^2H_3$]-γ-curcumene (**[13,13,13-$^2H_3$]-9**).

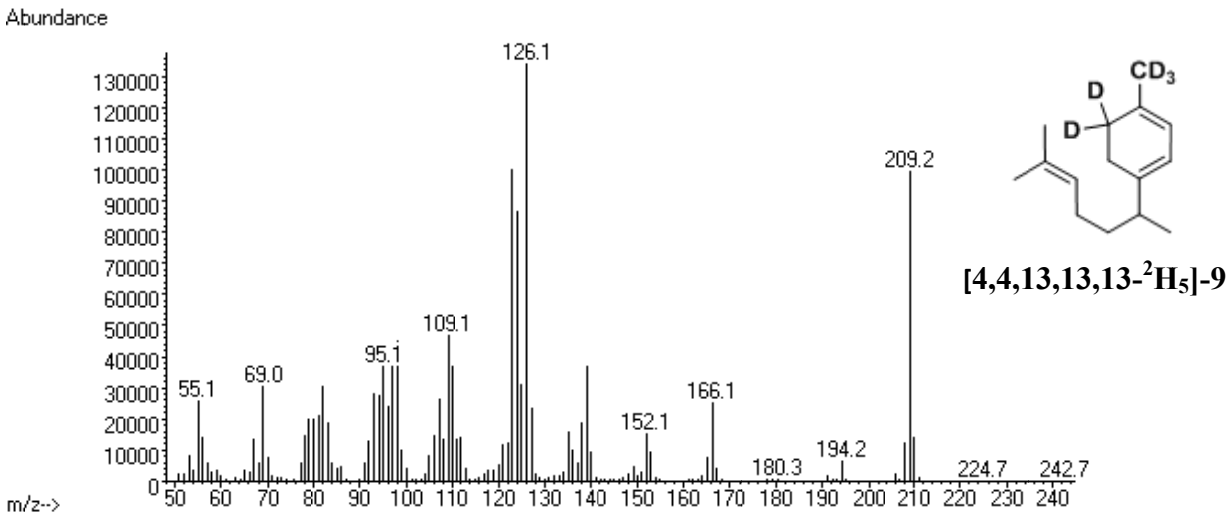

Figure A4.73. EI-MS spectrum of [4,4,13,13,13-$^2H_5$]-γ-curcumene (**[4,4,13,13,13-$^2H_5$]-9**).

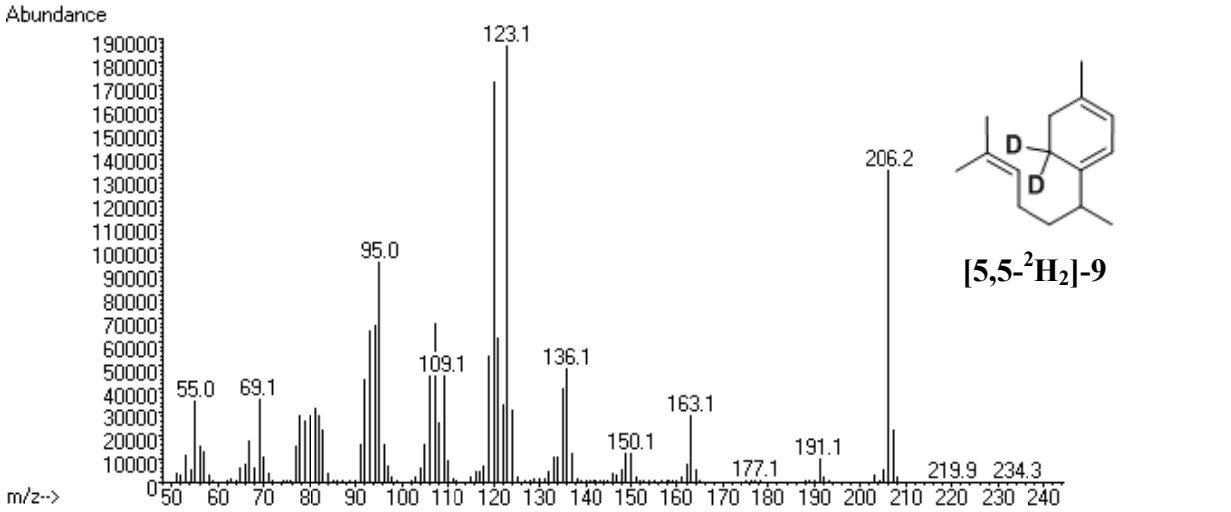

Figure A4.74. EI-MS spectrum of [5,5-$^2H_2$]-γ-curcumene (**[5,5-$^2H_2$]-9**).

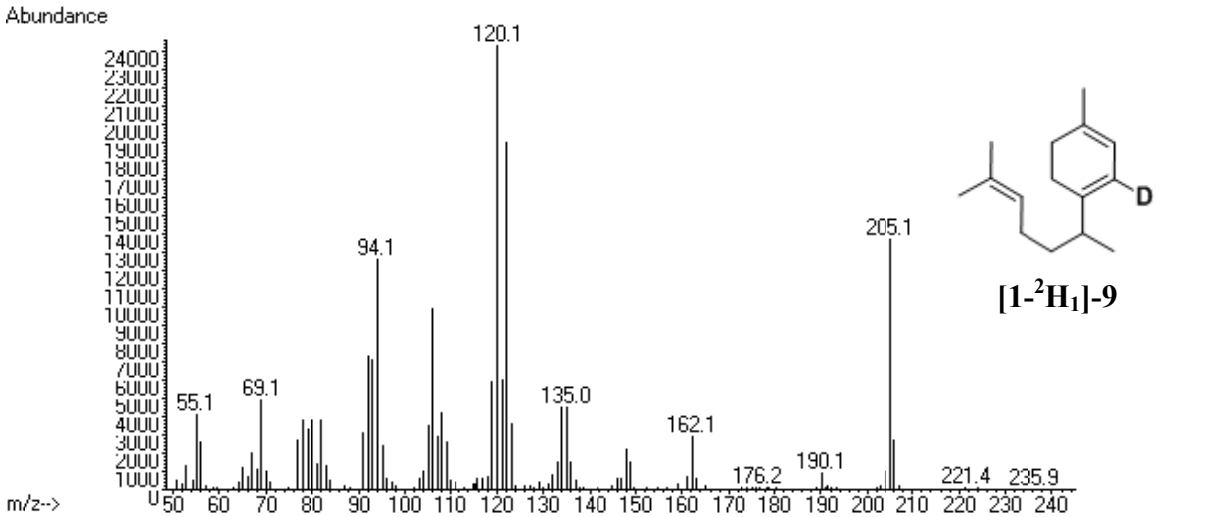

Figure A4.75. EI-MS spectrum of [1-$^2H_1$]-γ-curcumene (**[1-$^2H_1$]-9**).

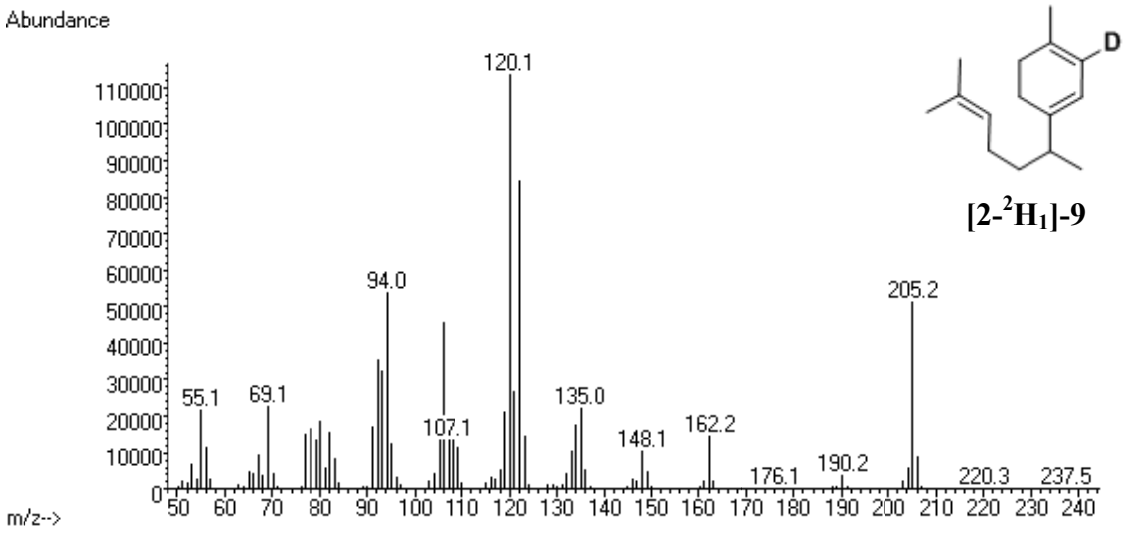

Figure A4.76. EI-MS spectrum of [2-^{2}H$_1$]-γ-curcumene (**[2-^{2}H$_1$]-9**).

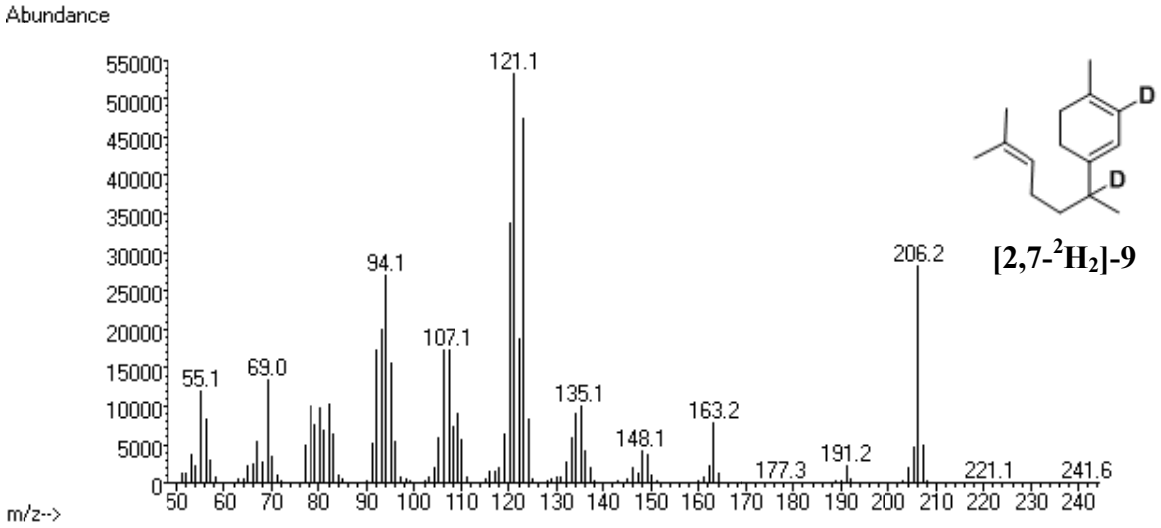

Figure A4.77. EI-MS spectrum of [2,7-^{2}H$_2$]-γ-curcumene (**[2,7-^{2}H$_2$]-9**).

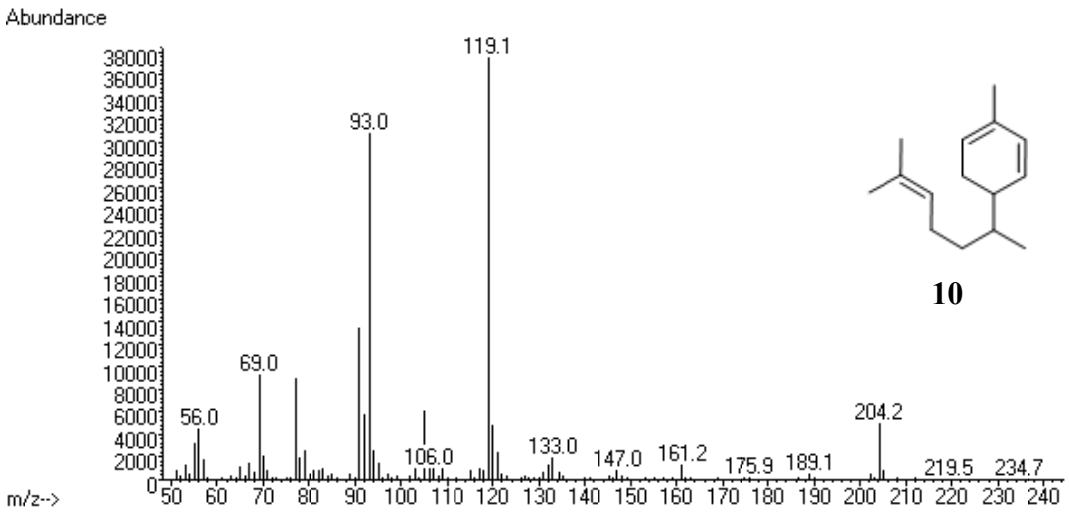

10

Figure A4.78. EI-MS spectrum of α-zingiberene (**10**).

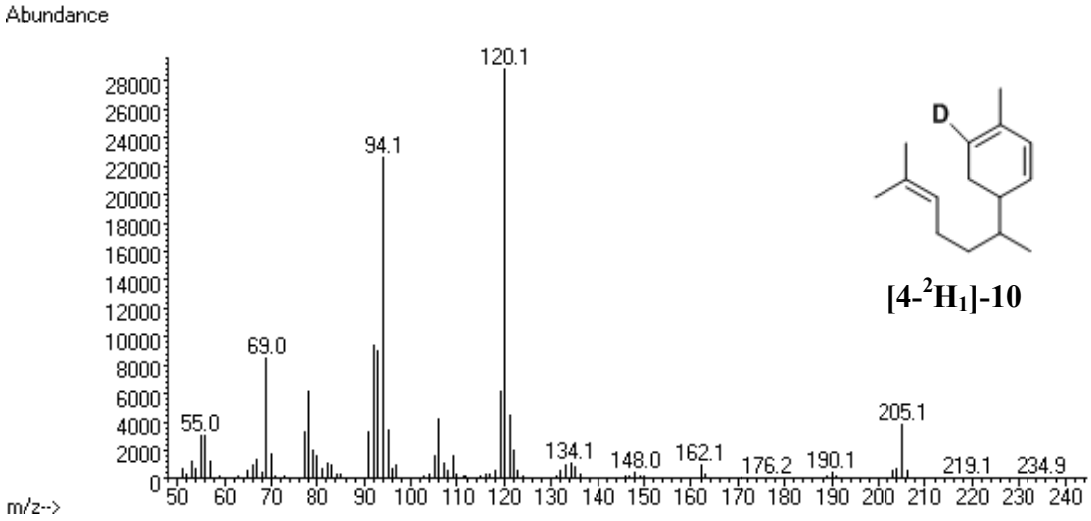

[4-^{2}H$_1$]-10

Figure A4.79. EI-MS spectrum of [4-^{2}H$_1$]-α-zingiberene (**[4-^{2}H$_1$]-10**).

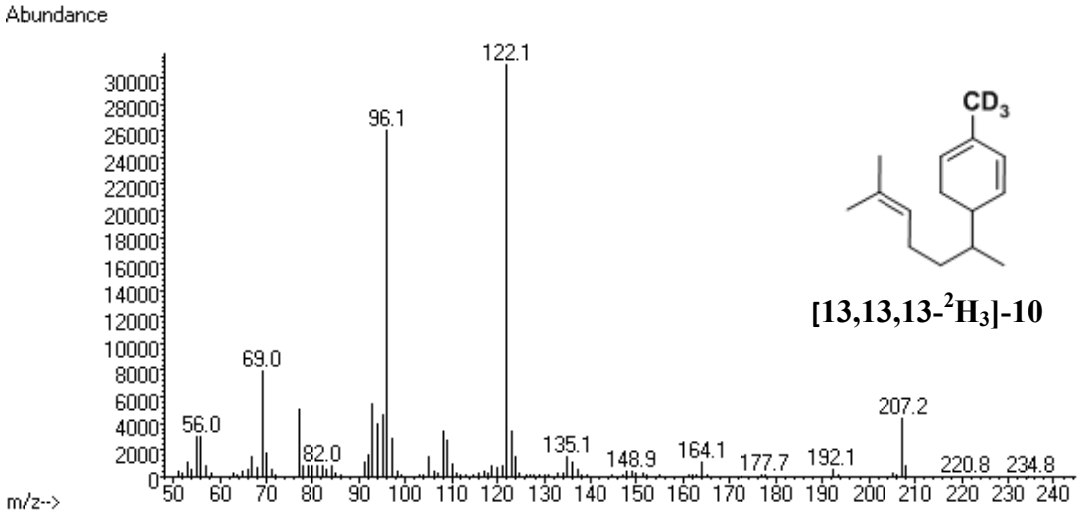

[13,13,13-^{2}H$_3$]-10

Figure A4.80. EI-MS spectrum of [13,13,13-^{2}H$_3$]-α-zingiberene (**[13,13,13-^{2}H$_3$]-10**).

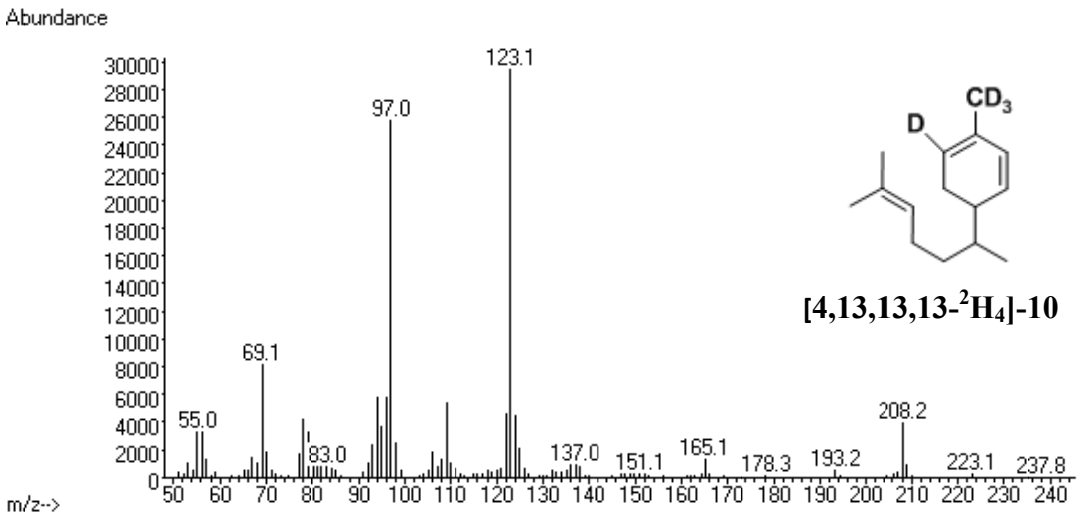

[4,13,13,13-$^2H_4$]-10

Figure A4.81. EI-MS spectrum of [4,13,13,13-$^2H_3$]-α-zingiberene (**[4,13,13,13-$^2H_3$]-10**).

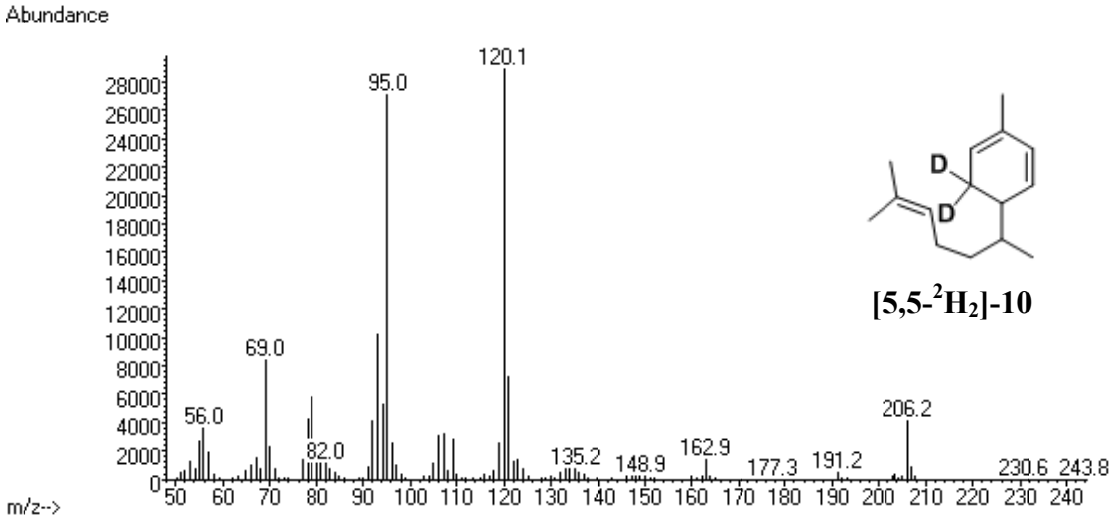

[5,5-$^2H_2$]-10

Figure A4.82. EI-MS spectrum of [5,5-$^2H_2$]-α-zingiberene (**[5,5-$^2H_2$]-10**).

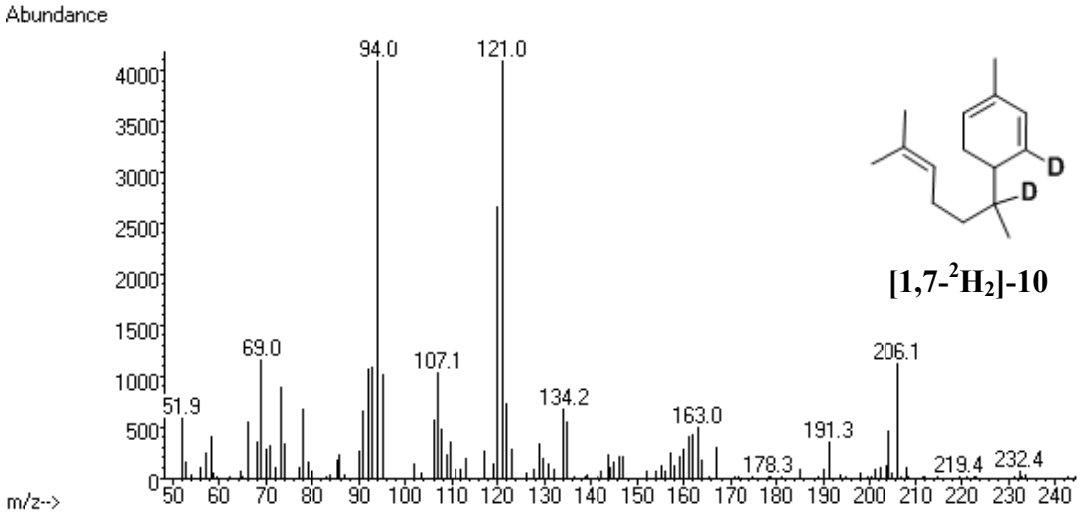

[1,7-$^2H_2$]-10

Figure A4.83. EI-MS spectrum of [1,7-$^2H_2$]-α-zingiberene (**[1,7-$^2H_2$]-10**).

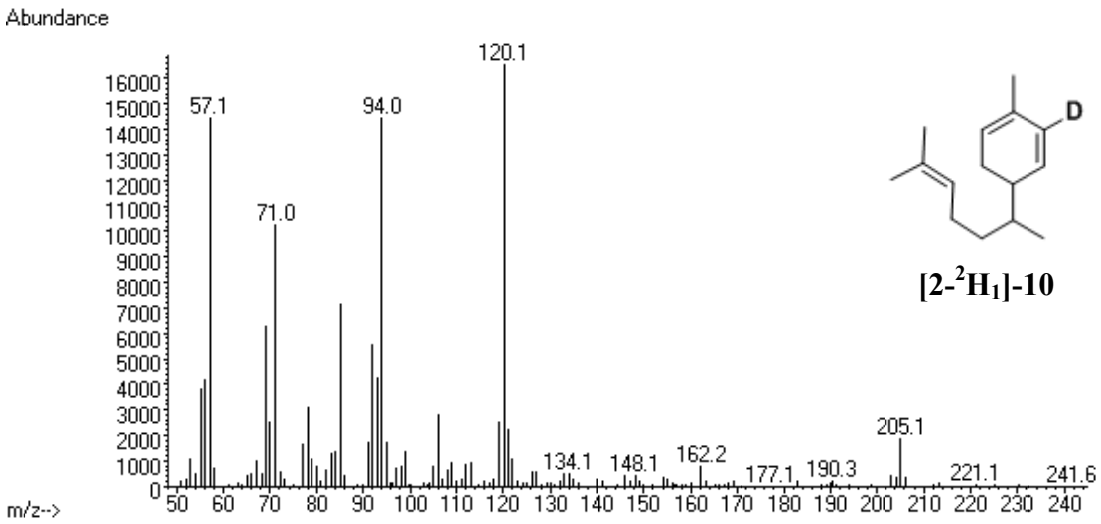

Figure A4.84. EI-MS spectrum of [2-$^2H_1$]-α-zingiberene (**[13,13,13-$^2H_3$]-10**).

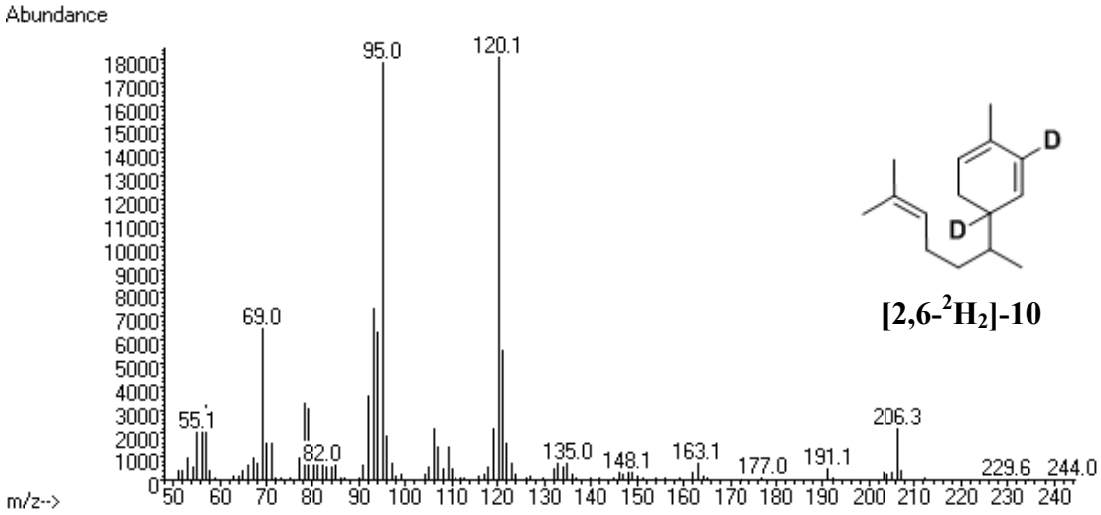

Figure A4.85. EI-MS spectrum of [2,6-$^2H_2$]-α-zingiberene (**[2,6-$^2H_2$]-10**).

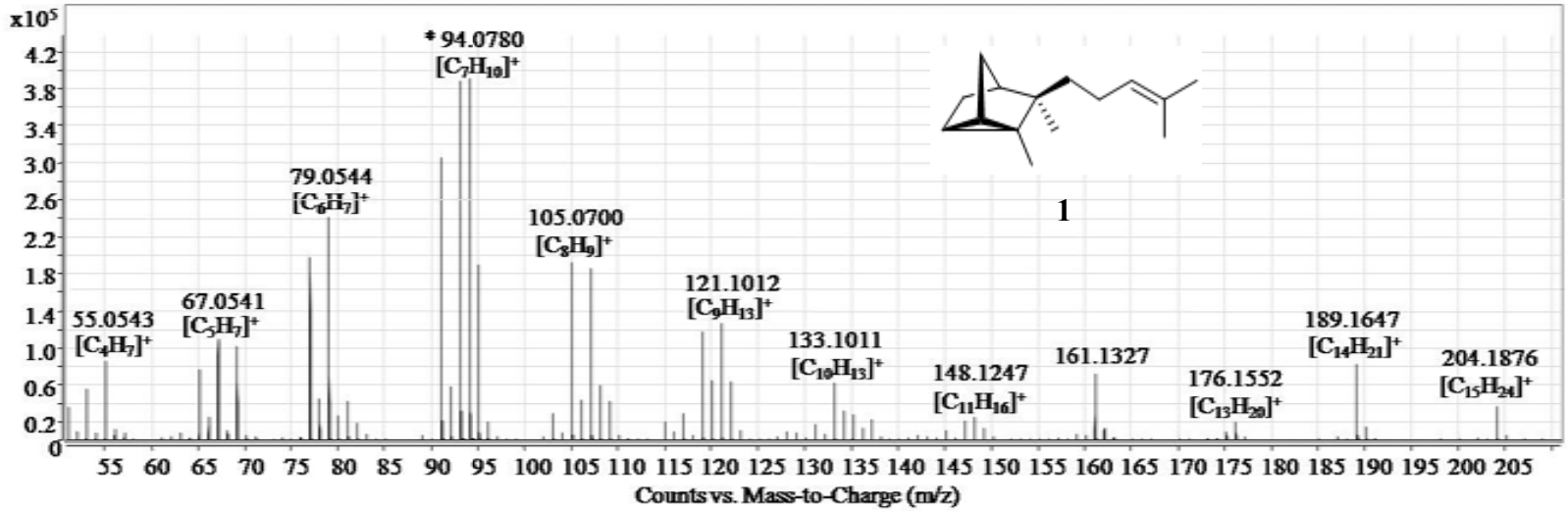

Figure A4.86. GC-EI-QToF-MS spectrum of α-santalene (**1**).

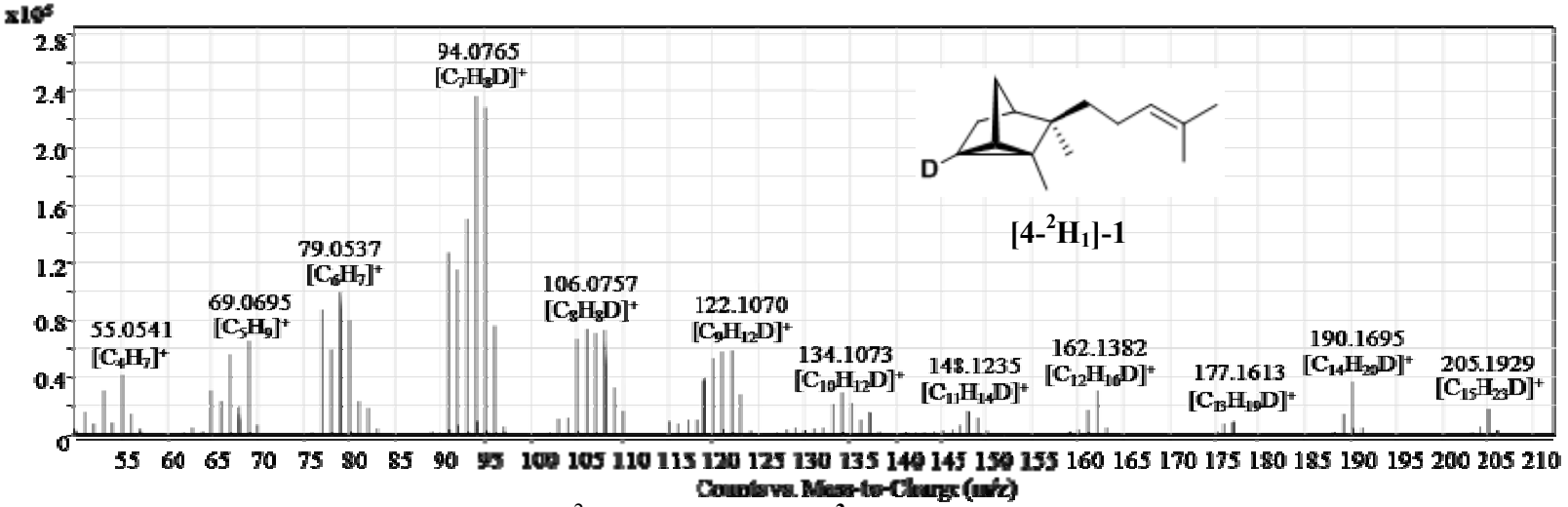

Figure A4.87. GC-EI-QToF-MS spectrum of [4-$^2H_1$]-α-santalene (**[4-$^2H_1$]-1**).

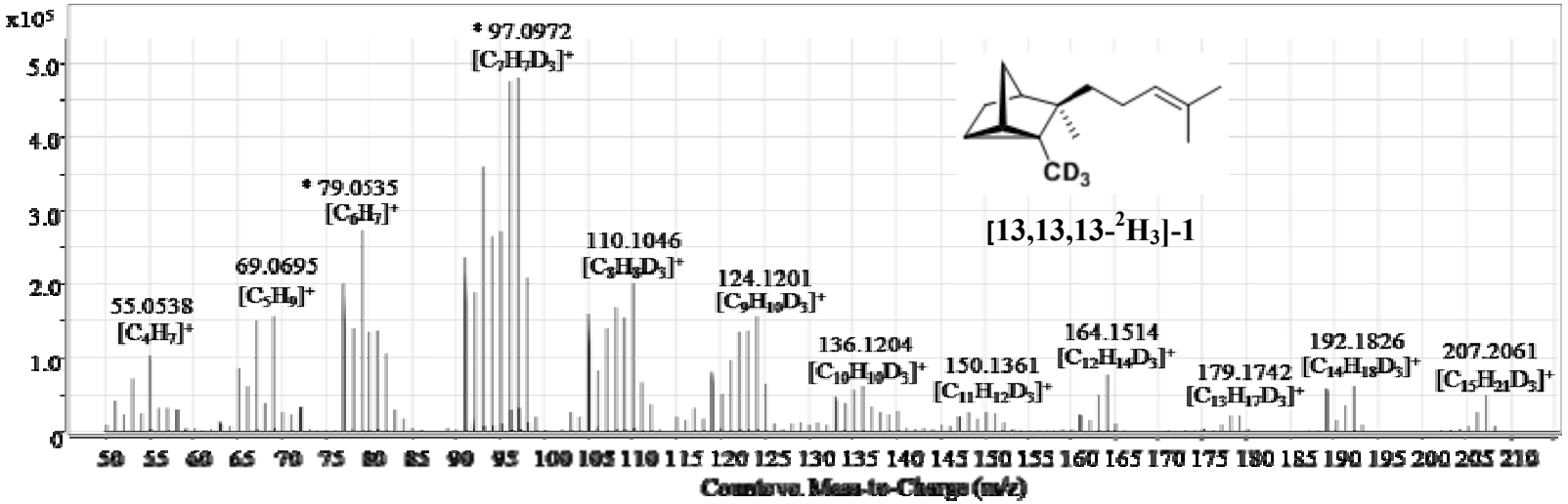

Figure A4.88. GC-EI-QToF-MS spectrum of [13,13,13-$^2H_3$]-α-santalene (**[13,13,13-$^2H_3$]-1**).

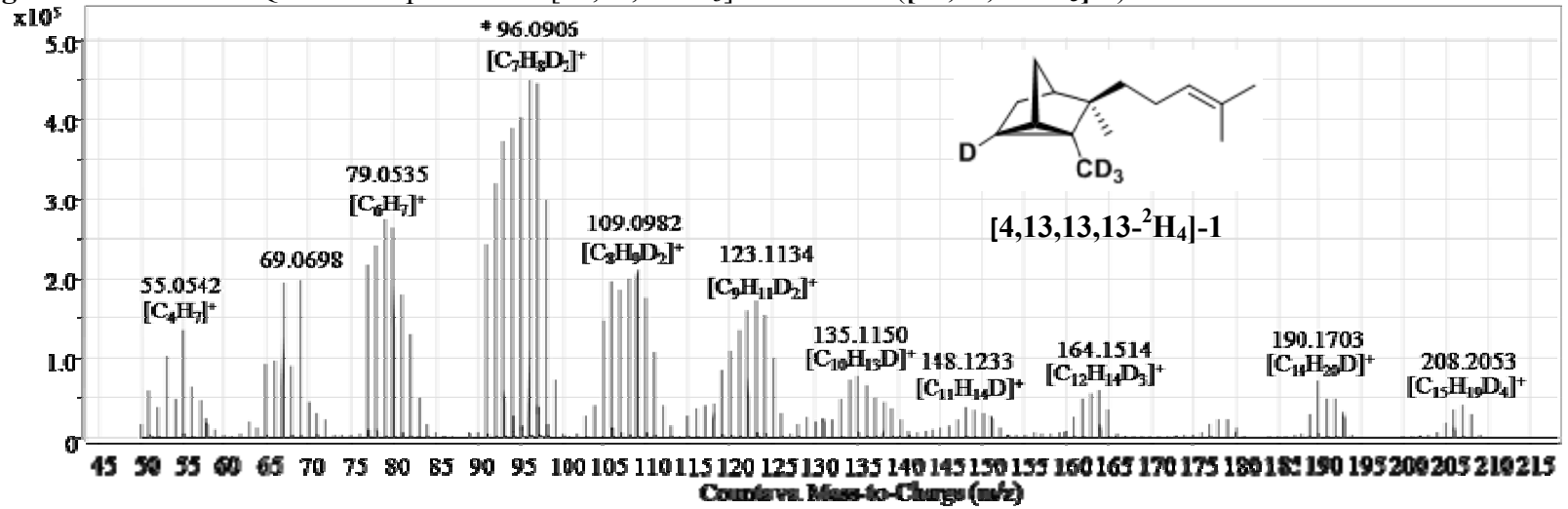

Figure A4.89. GC-EI-QToF-MS spectrum of [4,13,13,13-$^2H_4$]-α-santalene (**[4,13,13,13-$^2H_4$]-1**).

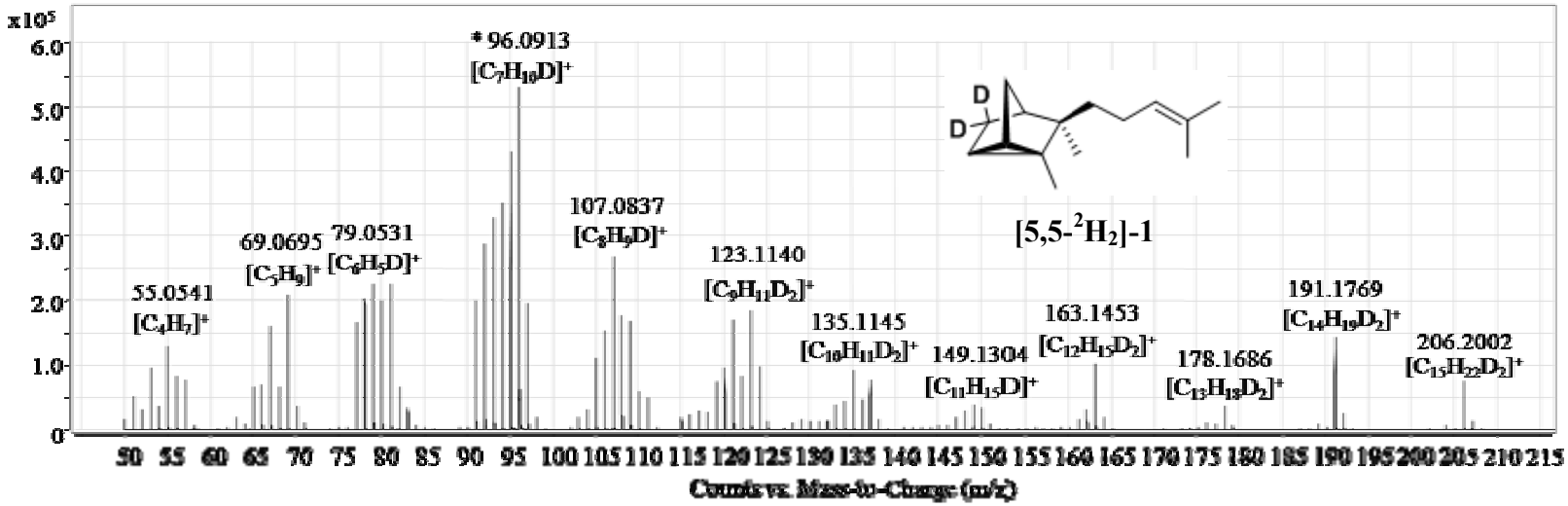

Figure A4.90. GC-EI-QToF-MS spectrum of [5,5-$^2H_2$]-α-santalene (**[5,5-$^2H_2$]-1**).

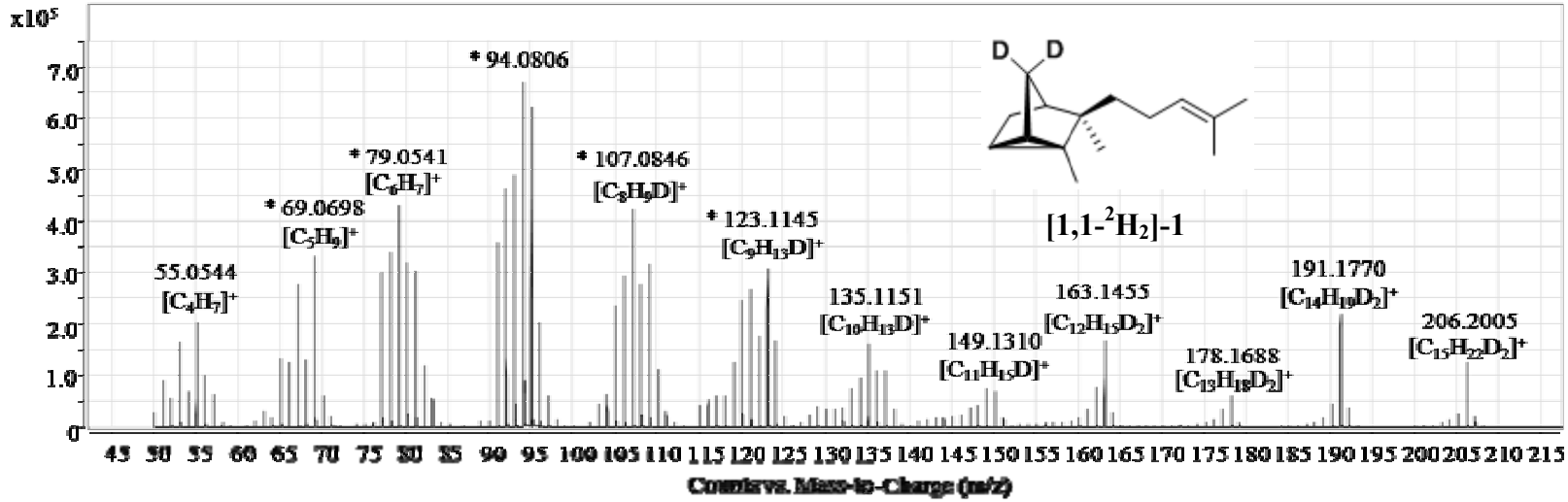

Figure A4.91. GC-EI-QToF-MS spectrum of [1,1-$^2H_2$]-α-santalene (**[1,1-$^2H_2$]-1**).

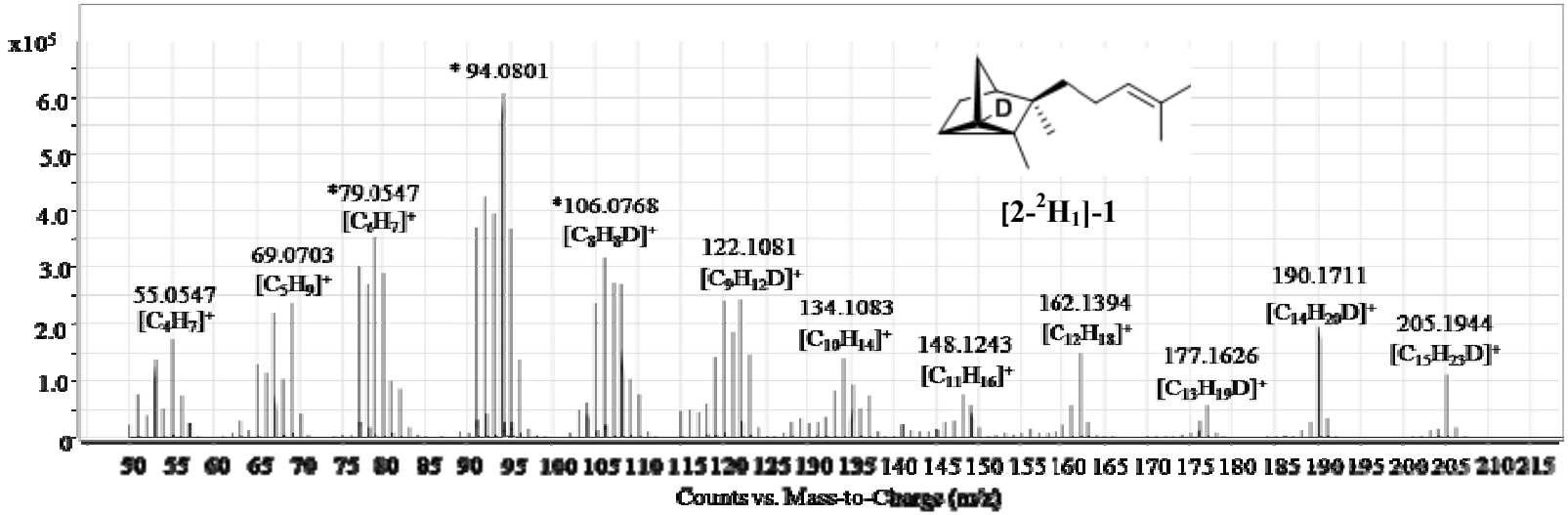

Figure A4.92. GC-EI-QToF-MS spectrum of [2-$^2H_1$]-α-santalene (**[2-$^2H_1$]-1**).

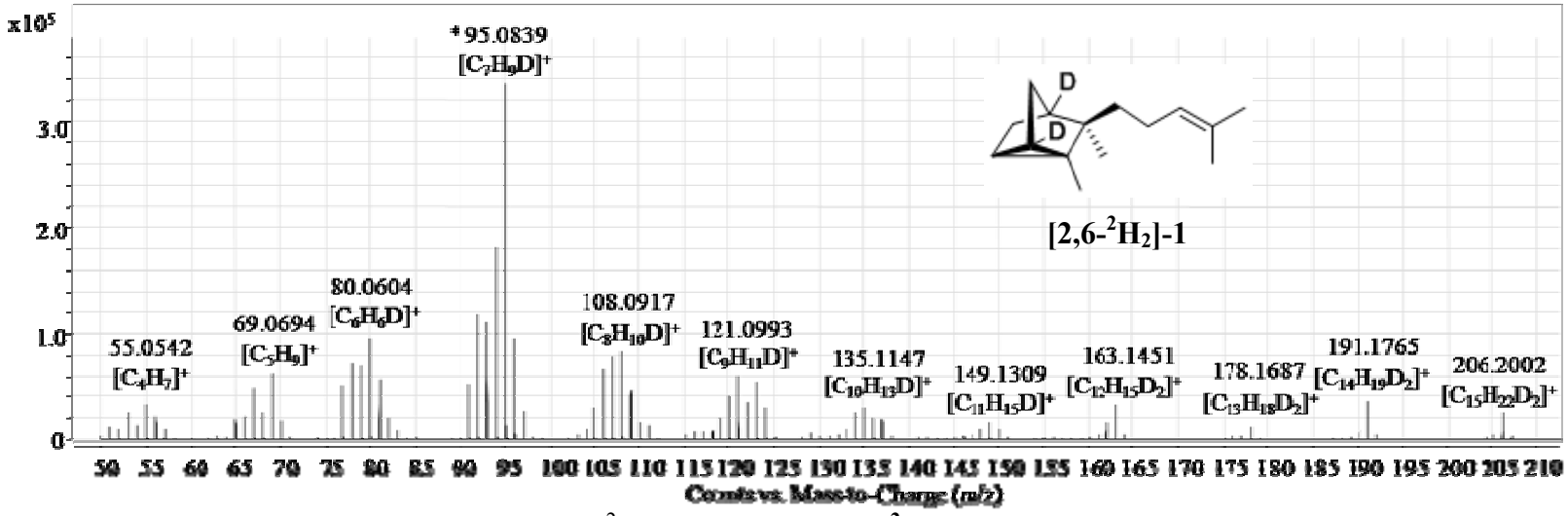

Figure A4.93. GC-EI-QToF-MS spectrum of [2,6-$^2H_2$]-α-santalene (**[2,6-$^2H_2$]-1**).

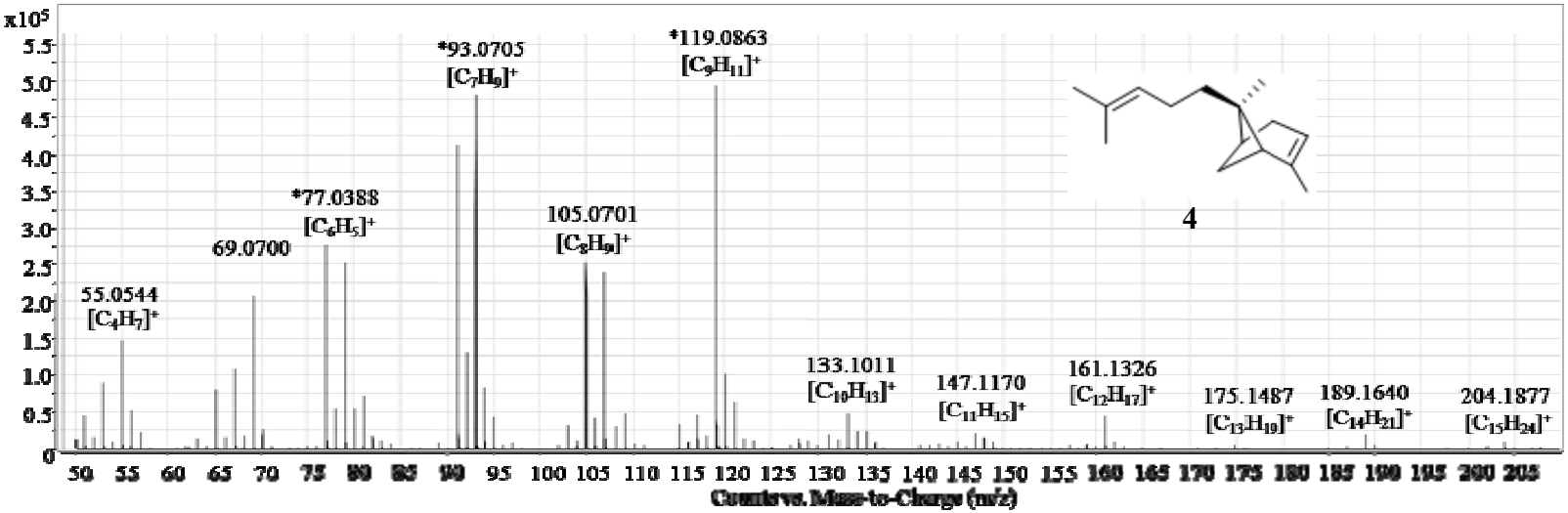

Figure A4.94. GC-EI-QToF-MS spectrum of *exo*-α-bergamotene (**4**).

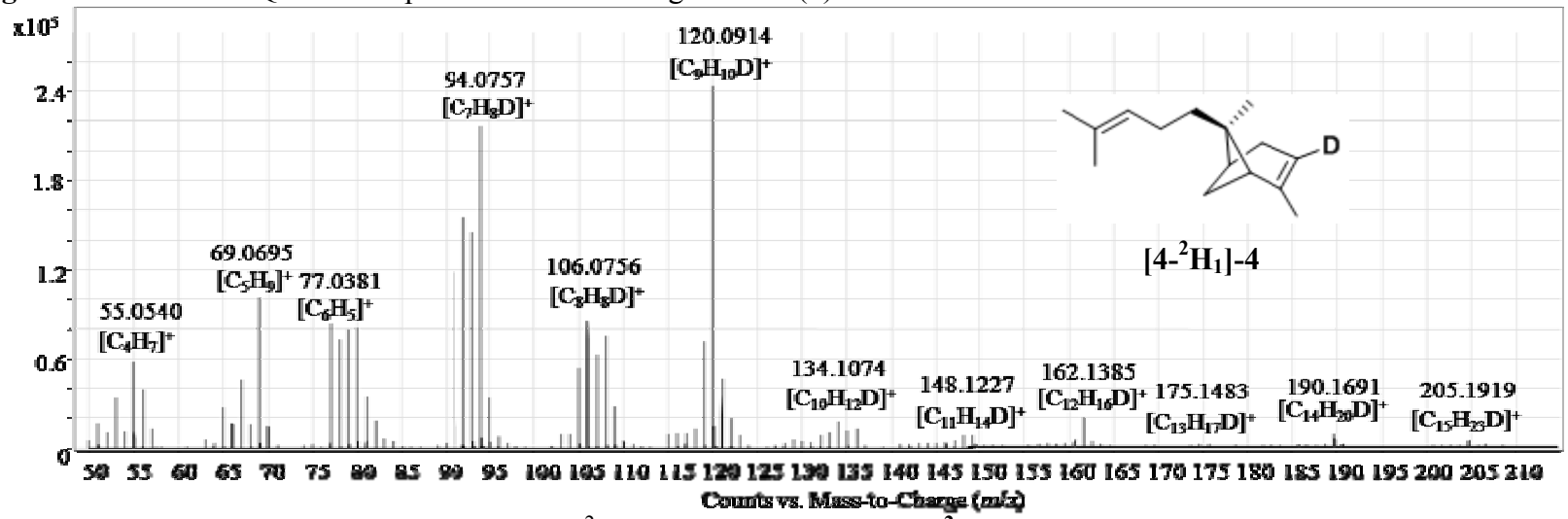

Figure A4.95. GC-EI-QToF-MS spectrum of [4-$^2H_1$]-*exo*-α-bergamotene (**[4-$^2H_1$]-4**).

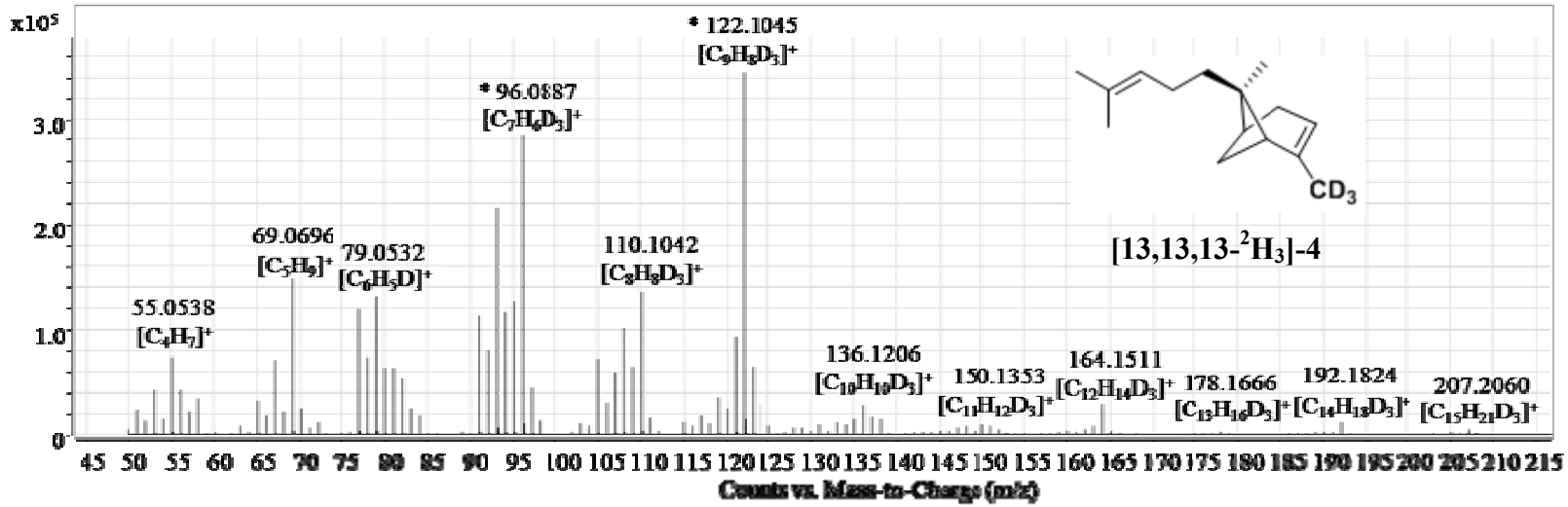

Figure A4.96. GC-EI-QToF-MS spectrum of [13,13,13-$^2H_3$]-*exo*-α-bergamotene (**[13,13,13-$^2H_3$]-4**).

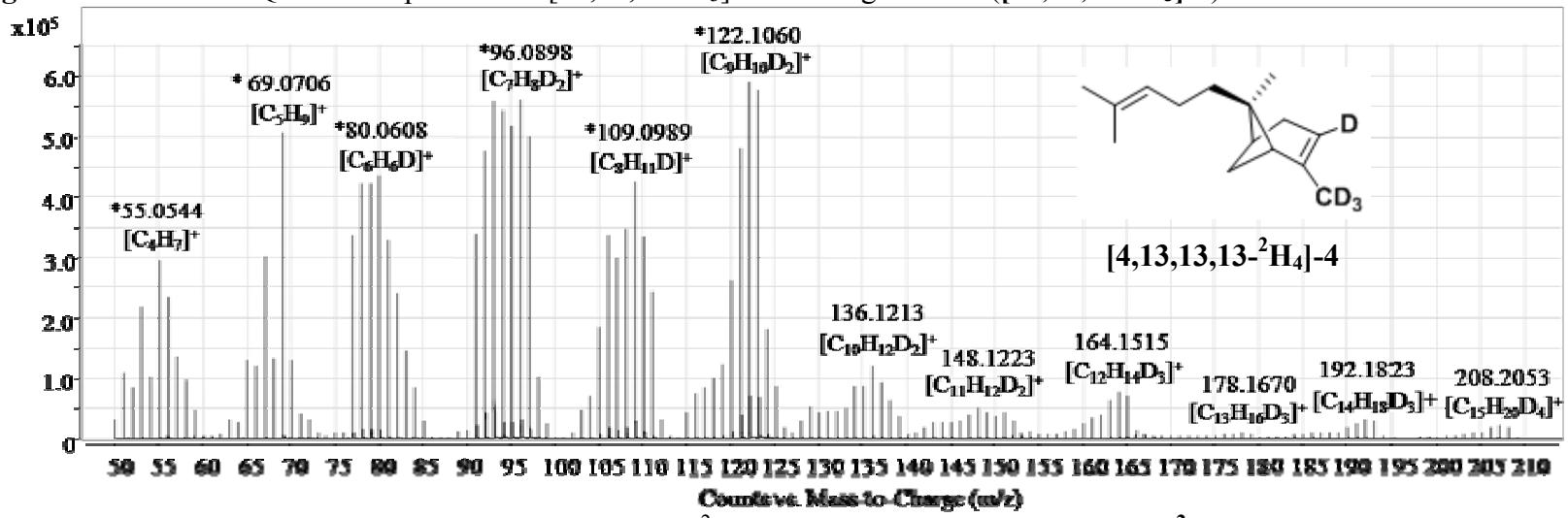

Figure A4.97. GC-EI-QToF-MS spectrum of [4,13,13,13-$^2H_4$]-*exo*-α-bergamotene (**[4,13,13,13-$^2H_4$]-4**).

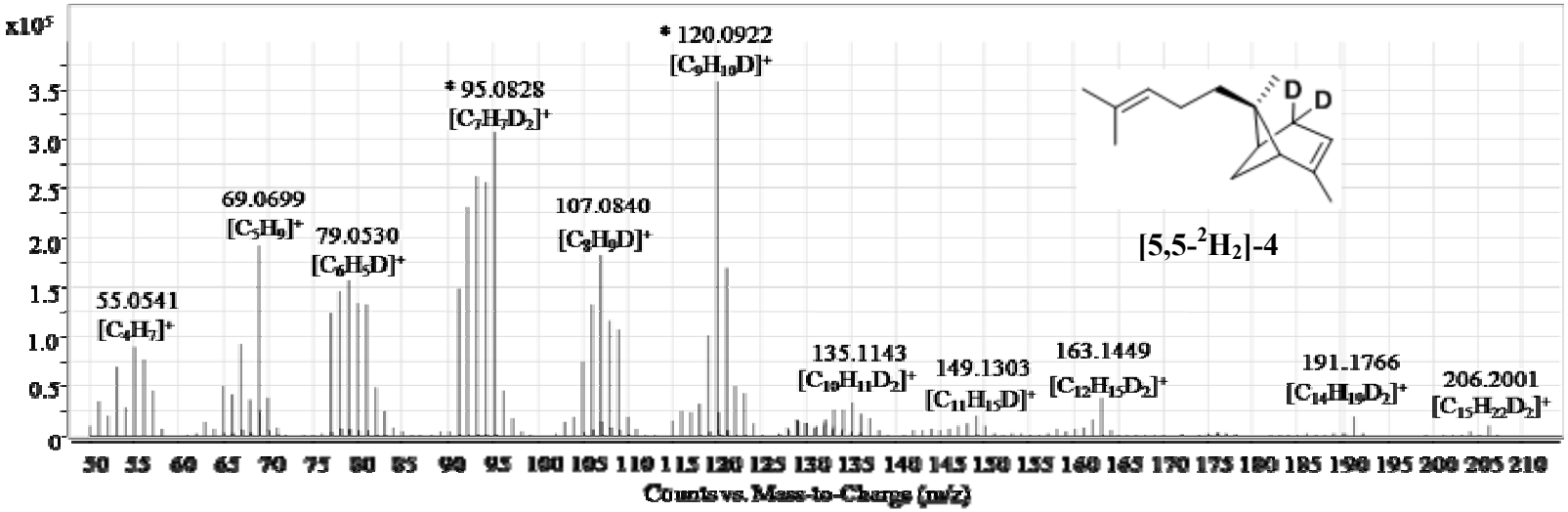

Figure A4.98. GC-EI-QToF-MS spectrum of [5,5-$^2H_2$]-*exo*-α-bergamotene (**[5,5-$^2H_2$]-4**).

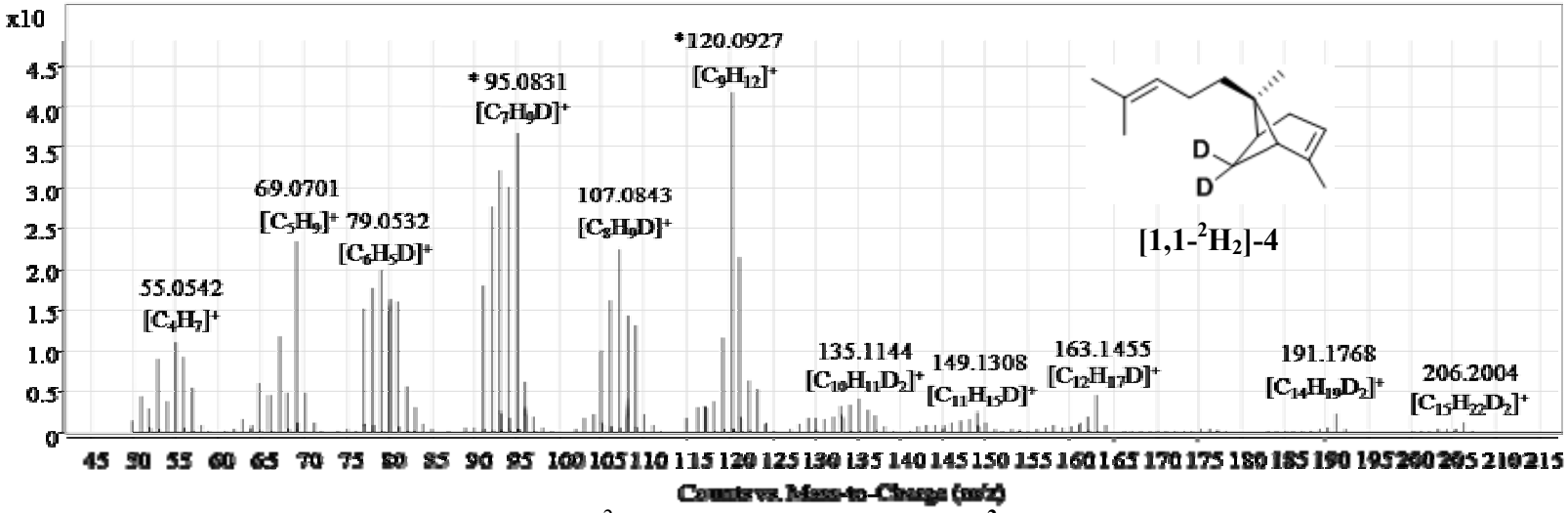

Figure A4.99. GC-EI-QToF-MS spectrum of [1,1-$^2H_2$]-*exo*-α-bergamotene (**[1,1-$^2H_2$]-4**).

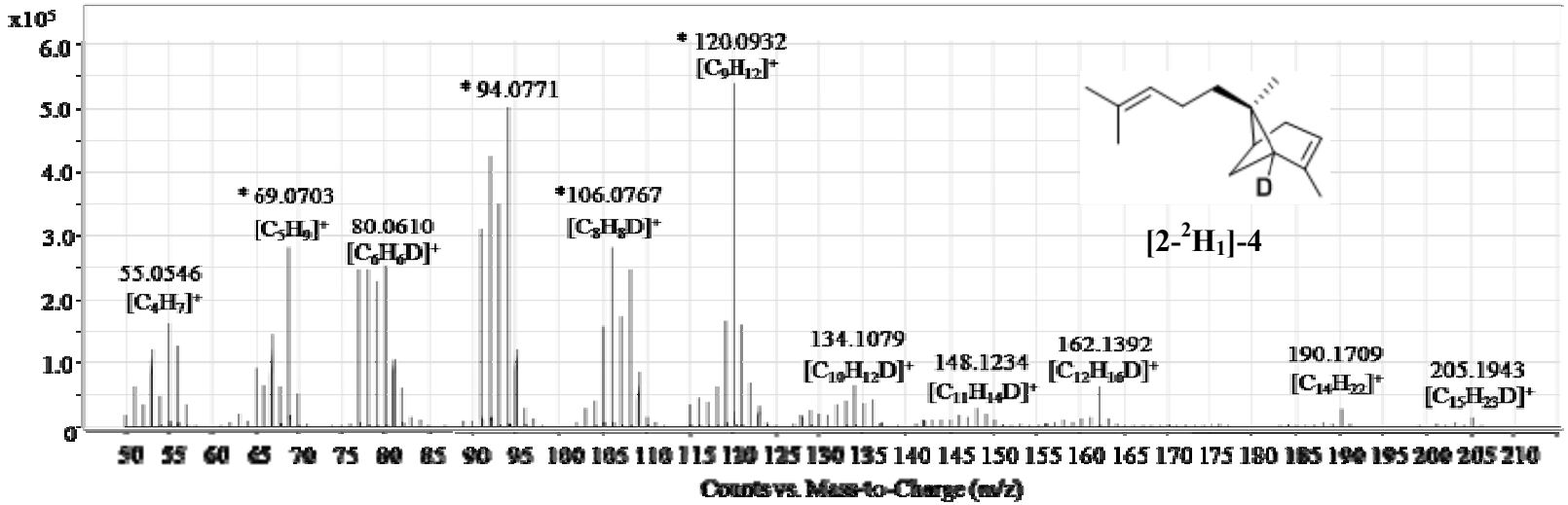

Figure A4.100. GC-EI-QToF-MS spectrum of [2-$^2H_1$]-*exo*-α-bergamotene (**[2-$^2H_1$]-4**).

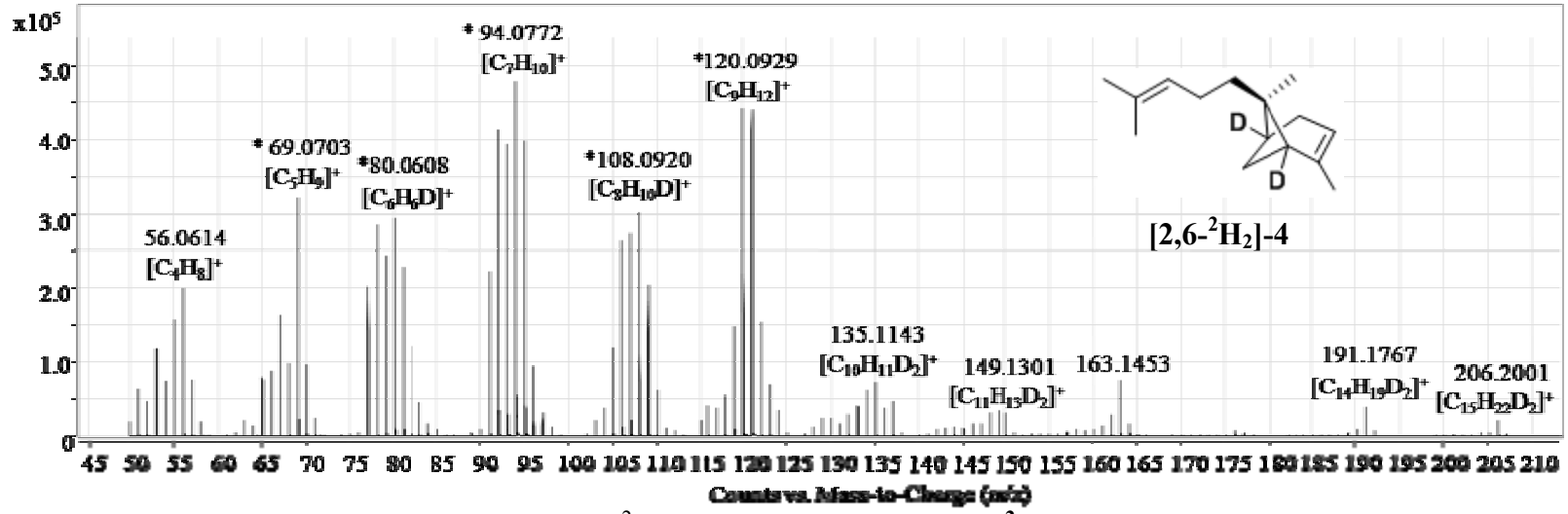

Figure A4.101. GC-EI-QToF-MS spectrum of [2,6-$^2H_2$]-*exo*-α-bergamotene (**[2,6-$^2H_2$]-4**).

3.4. References:

(1) Thulasiram, H. V.; Erickson, H. K.; Poulter, C. D. *Science* **2007**, *316*, 73-76.
(2) Christianson, D. W. *Curr. Opin. Chem. Biol.* **2008**, *12*, 141-150.
(3) Gershenzon, J.; Dudareva, N. *Nat. Chem. Biol.* **2007**, *3*, 408-414.
(4) Bochar, D. A.; Freisen, J.; Stauffacher, C. V.; Rodwell, V. W.; Barton, S. D.; Nakanishi, K.; Meth-Cohn, O. In *Comprehensive Natural Products Chemistry*; Pergamon: Oxford, 1999, p 15-44.
(5) Rohmer, M.; Barton, S. D.; Nakanishi, K.; Meth-Cohn, O. In *Comprehensive Natural Products Chemistry*; Pergamon: Oxford, 1999, p 45-67.
(6) McGarvey, D. J.; Croteau, R. *Plant Cell* **1995**, *7*, 1015-26.
(7) Moise, A. R.; Al-Babili, S.; Wurtzel, E. T. *Chem. Rev.* **2013**.
(8) Morgan, E. D. *Bioorgan. Med. Chem.* **2009**, *17*, 4096-4105.
(9) Wani, M. C.; Taylor, H. L.; Wall, M. E.; Coggon, P.; McPhail, A. T. *J. Am. Chem. Soc.* **1971**, *93*, 2325-&.
(10) Jordan, M. A.; Wilson, L. *Nat. Rev. Cancer* **2004**, *4*, 253-265.
(11) Klayman, D. L. *Science* **1985**, *228*, 1049-1055.
(12) Cane, D. E. *Accounts Chem. Res.* **1985**, *18*, 220-226.
(13) Cane, D. E. *Chem. Rev.* **1990**, *90*, 1089-1103.
(14) Croteau, R. *Chem. Rev.* **1987**, *87*, 929-954.
(15) Davis, E. M., Croteau, R. ; Springer: 2000; Vol. 209, p 53-95.
(16) Lesburg, C. A.; Caruthers, J. M.; Paschall, C. M.; Christianson, D. W. *Curr. Opin. Struc. Biol.* **1998**, *8*, 695-703.
(17) Poulter, C. D. *Phytochem. Rev.* **2006**, *5*, 17-26.
(18) Tantillo, D. J. *Nat. Prod. Rep.* **2011**, *28*, 1035-1053.
(19) Thulasiram, H. V.; Poulter, C. D. *J. Am. Chem. Soc.* **2006**, *128*, 15819-15823.
(20) Ohnishi, T.; Yokota, T.; Mizutani, M. *Phytochemistry* **2009**, *70*, 1918-1929.
(21) Ruzicka, L.; Stoll, M. *Helv. Chim. Acta* **1922**, *5*, 923-936.
(22) Ruzicka, L. *Experientia* **1953**, *9*, 357-67.
(23) Thulasiram, H. V.; Erickson, H. K.; Poulter, C. D. *J. Am. Chem. Soc.* **2008**, *130*, 1966-1971.
(24) Wuersch, J.; Huang, R. L.; Bloch, K. *J. Biol. Chem.* **1952**, *195*, 439-446.
(25) Cornforth, J. W.; Hunter, G. D.; Popjak, G. *Biochem. J.* **1953**, *54*, 597-601.
(26) Haines, B. E.; Wiest, O.; Stauffacher, C. V. *Accounts Chem. Res.* **2013**, *46*, 2416-2426.
(27) Zabin, I. *J. Biol. Chem.* **1957**, *226*, 851-859.
(28) Flesch, G.; Rohmer, M. *Eur. J. Biochem.* **1988**, *175*, 405-411.
(29) Eisenreich, W.; Menhard, B.; Hylands, P. J.; Zenk, M. H.; Bacher, A. *Proc. Natl. Acad. Sci.* **1996**, *93*, 6431-6436.
(30) Rohmer, M.; Knani, M.; Simonin, P.; Sutter, B.; Sahm, H. *Biochem. J.* **1993**, *295*, 517-524.
(31) Schwender, J.; Seemann, M.; Lichtenthaler, H. K.; Rohmer, M. *Biochem. J.* **1996**, *316*, 73-80.
(32) Brechbuh.S; Coscia, C. J.; Loew, P.; Vonszcze.C; Arigoni, D. *Chem. Commun.* **1968**, 136.
(33) Rohmer, M.; Seemann, M.; Horbach, S.; Bringer-Meyer, S.; Sahm, H. *J. Am. Chem. Soc.* **1996**, *118*, 2564-2566.

(34) Arigoni, D.; Sagner, S.; Latzel, C.; Eisenreich, W.; Bacher, A.; Zenk, M. H. *Proc. Natl. Acad. Sci.* **1997**, *94*, 10600-10605.
(35) Schwender, J.; Gemunden, C.; Lichtenthaler, H. K. *Planta* **2001**, *212*, 416-423.
(36) Jomaa, H.; Wiesner, J.; Sanderbrand, S.; Altincicek, B.; Weidemeyer, C.; Hintz, M.; Tarbachova, I.; Eberl, M.; Zeidler, J.; Lichtenthaler, H. K.; Soldati, D.; Beck, E. *Science* **1999**, *285*, 1573-1576.
(37) Nair, S. C.; Brooks, C. F.; Goodman, C. D.; Strurm, A.; McFadden, G. I.; Sundriyal, S.; Anglin, J. L.; Song, Y.; Moreno, S. N. J.; Striepen, B. *J. Exp. Med.* **2011**, *208*, 1547-1559.
(38) Lichtenthaler, H. K.; Schwender, J. r.; Disch, A.; Rohmer, M. *FEBS lett.* **1997**, *400*, 271-274.
(39) Rodriguez-Concepcion, M.; Fores, O. F.; Martinez-Garcia, J. F.; Gonzalez, V.; Phillips, M. A.; Ferrer, A.; Boronat, A. *Plant Cell* **2004**, *16*, 144-156.
(40) Schuhr, C.; Radykewicz, T.; Sagner, S.; Latzel, C.; Zenk, M.; Arigoni, D.; Bacher, A.; Rohdich, F.; Eisenreich, W. *Phytochem. Rev.* **2003**, *2*, 3-16.
(41) Croteau, R.; Alonso, W. R.; Koepp, A. E.; Johnson, M. A. *Arch. Biochem. Biophys.* **1994**, *309*, 184-192.
(42) Croteau, R.; Karp, F. *Arch. Biochem. Biophys.* **1979**, *198*, 523-532.
(43) Croteau, R.; Satterwhite, D. M.; Cane, D. E.; Chang, C. C. *J. Biol. Chem.* **1988**, *263*, 10063-10071.
(44) Croteau, R.; Satterwhite, D. M.; Wheeler, C. J.; Felton, N. M. *J. Biol. Chem.* **1989**, *264*, 2075-80.
(45) Pyun, H. J.; Coates, R. M.; Wagschal, K. C.; McGeady, P.; Croteau, R. B. *J. Org. Chem.* **1993**, *58*, 3998-4009.
(46) Degenhardt, J.; Kollner, T. G.; Gershenzon, J. *Phytochemistry* **2009**, *70*, 1621-1637.
(47) Hong, Y. J.; Tantillo, D. J. *Org. Biomol. Chem.* **2010**, *8*, 4589-4600.
(48) Weitman, M.; Major, D. T. *J. Am. Chem. Soc.* **2009**, *132*, 6349-6360.
(49) Connolly, J. D.; Hill, R. A. *Dictionary of Terpenoids*; Chapman & Hall: New York, 1992.
(50) Felicetti, B.; Cane, D. E. *J. Am. Chem. Soc.* **2004**, *126*, 7212-7221.
(51) Steele, C. L.; Crock, J.; Bohlmann, J. r.; Croteau, R. *J. Biol. Chem.* **1998**, *273*, 2078-2089.
(52) Schenk, D. J.; Starks, C. M.; Manna, K. R.; Chappell, J.; Noel, J. P.; Coates, R. M. *Arch. Biochem. Biophys.* **2006**, *448*, 31-44.
(53) Picaud, S.; Mercke, P.; He, X. F.; Sterner, O.; Brodelius, M.; Cane, D. E.; Brodelius, P. E. *Arch. Biochem. Biophys.* **2006**, *448*, 150-155.
(54) Jiang, J.; Cane, D. E. *J. Am. Chem. Soc.* **2008**, *130*, 428-+.
(55) Faraldos, J. A.; Wu, S.; Chappell, J.; Coates, R. M. *J. Am. Chem. Soc.* **2010**, *132*, 2998-3008.
(56) Benedict, C. R.; Lu, J. L.; Pettigrew, D. W.; Liu, J. G.; Stipanovic, R. D.; Williams, H. J. *Plant Physiol.* **2001**, *125*, 1754-1765.
(57) Ohnuma, S.-i.; Nakazawa, T.; Hemmi, H.; Hallberg, A.-M.; Koyama, T.; Ogura, K.; Nishino, T. *J. Biol. Chem.* **1996**, *271*, 10087-10095.
(58) Stanley Fernandez, S. M.; Kellogg, B. A.; Poulter, C. D. *Biochemistry* **2000**, *39*, 15316-15321.

(59) Tarshis, L. C.; Proteau, P. J.; Kellogg, B. A.; Sacchettini, J. C.; Poulter, C. D. *Proc. Natl. Acad. Sci.* **1996**, *93*, 15018-15023.
(60) Wang, K.; Ohnuma, S.-i. *Trends Biochem. Sci.* **1999**, *24*, 445-451.
(61) Zhang, D. L.; Jennings, S. M.; Robinson, G. W.; Poulter, C. D. *Arch. Biochem. Biophys.* **1993**, *304*, 133-143.
(62) Clarke, S. *Annu. Rev. Biochem.* **1992**, *61*, 355-386.
(63) Ashby, M. N.; Edwards, P. A. *J. Biol. Chem.* **1990**, *265*, 13157-64.
(64) Matsuoka, S.; Sagami, H.; Kurisaki, A.; Ogura, K. *J. Biol. Chem.* **1991**, *266*, 3464-8.
(65) Weinstein, J. D.; Branchaud, R.; Beale, S. I.; Bement, W. J.; Sinclair, P. R. *Arch. Biochem. Biophys.* **1986**, *245*, 44-50.
(66) Barbar, A.; Couture, M.; Sen, S. E.; Beliveau, C.; Nisole, A.; Bipfubusa, M.; Cusson, M. *Insect Biochem. Molec.* **2013**, *43*, 947-958.
(67) Tarshis, L. C.; Yan, M.; Poulter, C. D.; Sacchettini, J. C. *Biochemistry* **1994**, *33*, 10871-10877.
(68) Popjak, G.; Cornforth, J. W. *Biochem. J.* **1966**, *101*, 553-&.
(69) Leyes, A. E.; Baker, J. A.; Poulter, C. D. *Org. Lett.* **1999**, *1*, 1071-1073.
(70) Hosfield, D. J.; Zhang, Y.; Dougan, D. R.; Broun, A.; Tari, L. W.; Swanson, R. V.; Finn, J. *J. Biol. Chem.* **2004**, *279*, 8526-8529.
(71) Govindachari, T. R.; Mohamed, P. A.; Parthasarathy, P. C. *Tetrahedron* **1970**, *26*, 615-619.
(72) Lawrence, B. M.; Hogg, J. W. *Phytochemistry* **1973**, *12*, 2995.
(73) Baker, R.; Coles, H.; Edwards, M.; Evans, D.; Howse, P.; Walmsley, S. *J. Chem. Ecol.* **1981**, *7*, 135-145.
(74) Cane, D. E.; Rawlings, B. J.; Yang, C. C. *J. Antibiotics* **1987**, *40*, 1331-1334.
(75) Jelen, H. H. *J. Agr. Food Chem.* **2002**, *50*, 6569-6574.
(76) Demyttenaere, J. C. R.; Adams, A.; Van Belleghem, K.; De Kimpe, N.; KÃ¶nig, W. A.; Tkachev, A. V. *Phytochemistry* **2002**, *59*, 597-602.
(77) Proctor, R. H.; Hohn, T. M. *J. Biol. Chem.* **1993**, *268*, 4543-8.
(78) Hohn, T. M.; Plattner, R. D. *Arch. Biochem. Biophys.* **1989**, *272*, 137-143.
(79) Cane, D. E.; Prabhakaran, P. C.; Salaski, E. J.; Harrison, P. H. M.; Noguchi, H.; Rawlings, B. J. *J. Am. Chem. Soc.* **1989**, *111*, 8914-8916.
(80) Shishova, E. Y.; Di Costanzo, L.; Cane, D. E.; Christianson, D. W. *Biochemistry* **2007**, *46*, 1941-1951.
(81) Caruthers, J. M.; Kang, I.; Rynkiewicz, M. J.; Cane, D. E.; Christianson, D. W. *J. Biol. Chem.* **2000**, *275*, 25533-25539.
(82) Cane, D. E.; Prabhakaran, P. C.; Oliver, J. S.; McIlwaine, D. B. *J. Am. Chem. Soc.* **1990**, *112*, 3209-3210.
(83) Calvert, M. J.; Ashton, P. R.; Allemann, R. K. *J. Am. Chem. Soc.* **2002**, *124*, 11636-11641.
(84) Starks, C. M.; Back, K. W.; Chappell, J.; Noel, J. P. *Science* **1997**, *277*, 1815-1820.
(85) Rising, K. A.; Starks, C. M.; Noel, J. P.; Chappell, J. *J. Am. Chem. Soc.* **2000**, *122*, 1861-1866.
(86) Cane, D. E.; Tsantrizos, Y. S. *J. Am. Chem. Soc.* **1996**, *118*, 10037-10040.
(87) Miller, D. J.; Yu, F.; Allemann, R. K. *ChemBioChem* **2007**, *8*, 1819-1825.
(88) Banerjee, S.; Ecavade, A.; Rao, A. R. *Cancer Lett.* **1993**, *68*, 105-109.

(89) Burdock, G. A.; Carabin, L. G. *Food Chem. Toxicol.* **2008**, *46*, 421-432.
(90) Dwivedi, C.; Maydew, E. R.; Hora, J. J.; Ramaeker, D. M.; Guan, X. M. *Eur. J. Cancer Prev.* **2005**, *14*, 473-476.
(91) Hongratanaworakit, T. *Nat. Prod. Commun.* **2010**, *5*, 157-162.
(92) Jirovetz, L.; Buchbauer, G.; Denkova, Z.; Stoyanova, A.; Murgov, I.; Gearon, V.; Birkbeck, S.; Schmidt, E.; Geissler, M. *Flavour Frag. J.* **2006**, *21*, 465-468.
(93) So, P.-L.; Tang, J. Y.; Epstein, E. H. *Expert Opin. Inv. Drug.* **2010**, *19*, 1099-1112.
(94) Jones, C. G.; Ghisalberti, E. L.; Plummer, J. A.; Barbour, E. L. *Phytochemistry* **2006**, *67*, 2463-2468.
(95) Daramwar, P. P.; Srivastava, P. L.; Priyadarshini, B.; Thulasiram, H. V. *Analyst* **2012**, *137*, 4564-4570.
(96) Kollner, T. G.; Schnee, C.; Gershenzon, J.; Degenhardt, J. *Plant Cell* **2004**, *16*, 1115-1131.
(97) Srivastava, P. L., University of Pune, 2014.
(98) O' Maille, P. E.; Chappell, J.; Noel, J. P. *Arch. Biochem. Biophys.* **2006**, *448*, 73-82.
(99) Corey, E. J.; Kim, C. U.; Takeda, M. *Tetrahedron Lett.* **1972**, *13*, 4339-4342.
(100) Davisson, V. J.; Woodside, A. B.; Poulter, C. D. *Method. Enzymol.* **1985**, *110*, 130-144.
(101) Trost, B. M.; Kunz, R. A. *J. Am. Chem. Soc.* **1975**, *97*, 7152-7157.
(102) Sallaud, C.; Rontein, D.; Onillon, S.; Jabes, F.; Duffe, P.; Giacalone, C.; Thoraval, S.; Escoffier, C.; Herbette, G.; Leonhardt, N.; Causse, M.; Tissier, A. *The Plant Cell Online* **2009**, *21*, 301-317.
(103) Schalk, M.; Firmenich Sa; Schalk M; Firmenich&Cie: 2009.
(104) Schalk, M.; Firmenich Sa; Firmenich&Cie: 2011.
(105) Jones, C. G.; Moniodis, J.; Zulak, K. G.; Scaffidi, A.; Plummer, J. A.; Ghisalberti, E. L.; Barbour, E. L.; Bohlmann, J. *J. Biol. Chem.* **2011**, *286*, 17445-17454.
(106) Cleland, W. W. *Arch. Biochem. Biophys.* **2005**, *433*, 2-12.
(107) Cleland, W. W. *Bioorg. Chem.* **1987**, *15*, 283-302.
(108) Oldfield, E. *Accounts Chem. Res.* **2010**, *43*, 1216-1226.
(109) Kollner, T. G.; Schnee, C.; Gershenzon, J.; Degenhardt, J. *Plant Cell* **2004**, *16*, 1115-1131.
(110) Peralta-Yahya, P. P.; Ouellet, M.; Chan, R.; Mukhopadhyay, A.; Keasling, J. D.; Lee, T. S. *Nat. Commun.* **2011**, *2*.
(111) Crock, J.; Wildung, M.; Croteau, R. *Proc. Natl. Acad. Sci. U.S.A.* **1997**, *94*, 12833-12838.
(112) Beale, M. H.; Birkett, M. A.; Bruce, T. J. A.; Chamberlain, K.; Field, L. M.; Huttly, A. K.; Martin, J. L.; Parker, R.; Phillips, A. L.; Pickett, J. A.; Prosser, I. M.; Shewry, P. R.; Smart, L. E.; Wadhams, L. J.; Woodcock, C. M.; Zhang, Y. *Proc. Natl. Acad. Sci. U.S.A.* **2006**, *103*, 10509-10513.
(113) Faraldos, J. A.; Gonzalez, V.; Li, A.; Yu, F.; Koksal, M.; Christianson, D. W.; Allemann, R. K. *J. Am. Chem. Soc.* **2012**, *134*, 20844-20848.

Erratum

Erratum

Erratum